AD NUMBER
ADC002497
CLASSIFICATION CHANGES
TO: unclassified
FROM: confidential
LIMITATION CHANGES
TO: Approved for public release, distribution unlimited
FROM: Distribution authorized to U.S. Gov't. agencies and their contractors; Administrative/Operational Use; DEC 1974. Other requests shall be referred to Office of Naval Research, Arlington, VA 22217.
AUTHORITY
31 Dec 1980, per document marking; CNO/N772 ltr N772A/6U875630 20 Jan 2006 & ONR ltr 31 Jan 2006

APPLIED RESEARCH LABORATORIES
THE UNIVERSITY OF TEXAS AT AUSTIN

ARL-TR-74-53
December 1974

Copy No. 46

CHURCH ANCHOR EXPLOSIVE SOURCE (SUS) PROPAGATION MEASUREMENTS (U)

edited by
Aubrey L. Anderson

OFFICE OF NAVAL RESEARCH
Contract N00014-70-A-0166, Task 0023

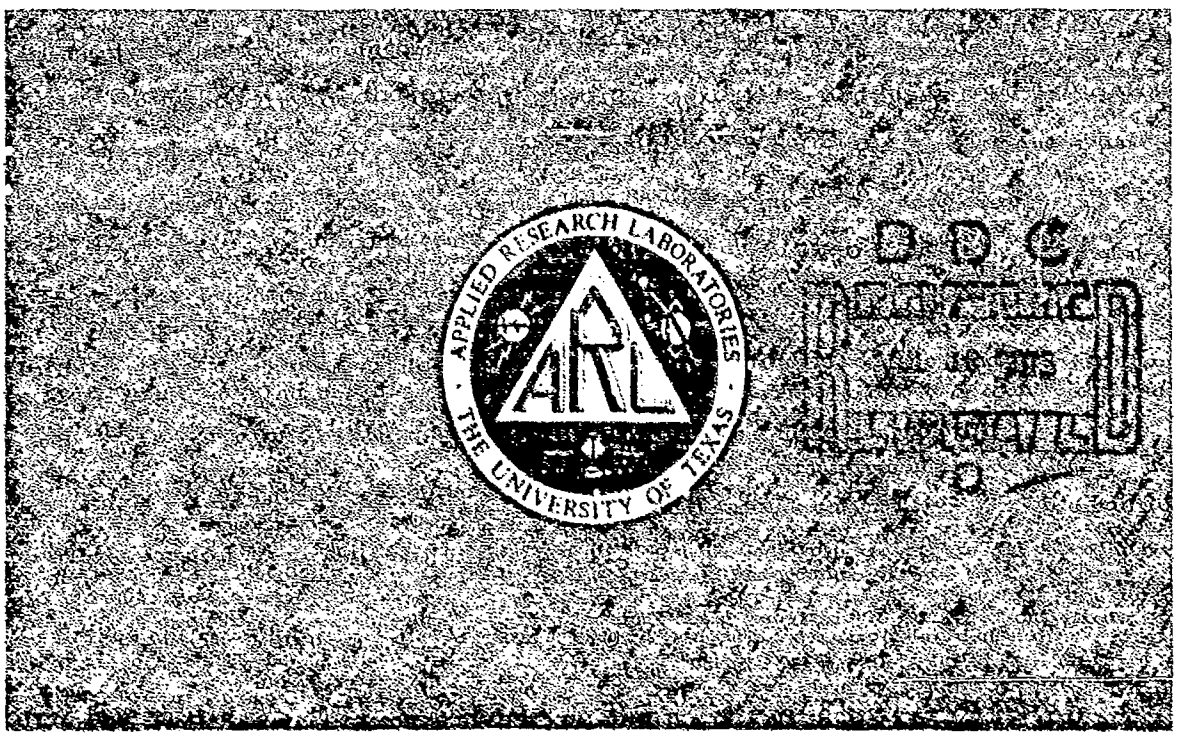

ARL-TR-74-53
December 1974

CHURCH ANCHOR EXPLOSIVE SOURCE (SUS) PROPAGATION MEASUREMENTS (U)

edited by

Aubrey L. Anderson

This work sponsored by
OFFICE OF NAVAL RESEARCH
Contract N00014-70-A-0166, Task 0023

APPLIED RESEARCH LABORATORIES
THE UNIVERSITY OF TEXAS AT AUSTIN
AUSTIN, TEXAS 78712

CONTRIBUTORS

(U) Many persons at ARL/UT and other organizations contributed to the planning, data processing, analysis, and interpretation which has resulted in this compilation of results. Most of these are listed below. The planning and execution of the exercise were carried out by an even larger group.

Contributors from ARL/UT

Analysis and Interpretation

A. L. Anderson
S. K. Mitchell
T. D. Plemons

Data Processing

N. R. Bedford
K. C. Focke
J. A. Shooter
S. L. Watkins

Planning and Coordination

G. E. Ellis
L. D. Hampton

Non-ARL Contributors

Naval Oceanographic Office -
Environmental Data, Source-to-Receiver Ranges

Defence Research Establishment, Pacific -
MESA Data Processing

Texas Instruments, Inc. -
ACODAC Operations

Underwater Systems, Inc. -
SUS Quality Control

(The reverse of this page is blank.)

ABSTRACT

(U) The received energy of sound waves generated by underwater explosive sources (SUS) was recorded during August and September 1973 as part of the CHURCH ANCHOR Exercise conducted in the central Northeastern Pacific Ocean. The analog and digital magnetic tape recordings of these data have been analyzed by digital hardware/software processing techniques including automatic shot detection, shot length estimation, and fast Fourier transform (FFT) spectrum analysis. Results of these analyses are plotted as propagation loss versus range, for ranges up to 1200 nm; for frequencies of 25, 50, and 158 Hz, with limited data for 100 and 250 Hz; for source depths of 18 m and 91 m; and for receiver depths near the sound channel axis, near the critical depth, and near the ocean bottom. Sound propagation characteristics were examined as a function of source-to-receiver range, source depth, receiver depth, frequency, and bathymetry.

(C) Often no source depth dependence is evident; however, in some cases propagation loss from the deep (91 m) source is as much as 15 dB less than from the shallow (18 m) source. Minimum propagation loss was always observed at the sound channel axis, with up to 10 dB higher loss at the critical depth and as much as 50 dB higher loss (at 1000 nm range) below the critical depth and near the ocean bottom. Only slight frequency dependence is exhibited and it is interrelated with source depth. Propagation across seamounts blocking 25% of the sound channel introduced as much as 10 dB additional loss over clear channel propagation. Beyond a range of about 175 nm, signal-to-noise ratio (S/N) decreases with increasing receiver depth, the rate of decrease being greater below critical depth. For ranges less than 175 nm, the S/N was greatest at the deepest (near bottom) hydrophones. The S/N at 50 Hz was usually lower than S/N at either 25 Hz or 158 Hz.

(The reverse of this page is blank.)

TABLE OF CONTENTS

TABLE OF CONTENTS (Cont'd)

I.a. INTRODUCTION

(U) The CHURCH ANCHOR Exercise, which was conducted in the central Northeastern Pacific Ocean during August and September 1973, included concurrent measurements of underwater acoustical propagation and ocean environmental parameters. Objectives of this Long Range Acoustic Propagation Project (LRAPP) exercise are described in Refs. 1 and 2 and details of the several types of data to be acquired are given. This report describes results of the analysis of propagation data obtained during the exercise from measurements with underwater explosive (SUS) sound sources. Receivers for these data included three Acoustic Data Capsules (ACODAC) and one Multi-Element Super-directive Array (MESA). Hydrophones were located at depths near the deep sound channel axis, the critical depth, and the ocean bottom. The SUS explosive sources were detonated at depths of 18 m and 91 m. Section II, Data Acquisition, describes this portion of the exercise in more detail.

(U) Signals received by the ACODAC arrays were recorded on analog magnetic tape recorders, whereas MESA array data were recorded in part by digital recorders and in part by analog recorders. The analog tapes were duplicated and the data were digitized. Subsequent processing included automatic shot detection, shot length estimation, shot and noise energy estimation using a fast Fourier transform over the frequency band from 10 to 300 Hz, propagation loss and signal-to-noise ratio calculation, plotting, and editing results. This processing is described in detail in Section III, Data Analysis.

(U) Portions of the propagation data, selected from the complete data set in the appendices, are used in Section IV to illustrate important

(U) features of underwater sound propagation in the exercise area. Similar illustrations of signal-to-noise ratio are given in Section V. In Sections IV and V, propagation loss and signal-to-noise ratios are examined as functions of receiver depth, source depth, frequency, and source-to-receiver range.

(U) Plots of propagation loss versus range for all SUS source events and ACODAC receiver depths for which recorded data were processed are shown in Appendix A for frequencies of 25, 50, and 158 Hz. Appendix B contains propagation loss versus range plots derived from MESA data for frequencies of 25, 50, 100, 158, and 251 Hz. Error estimates for the ACODAC data analysis techniques are described in Appendix C.

I.b. SUMMARY OF RESULTS

(U) Summarized below are observations of propagation loss and signal-to-noise ratio characteristics and dependencies. These are discussed in detail in Sections IV and V.

A. Propagation Loss Summary

1. Source Depth Dependence

(C) Propagation loss frequently exhibits no source depth dependence. When a dependence is observed, loss from the deep source (91 m) is as much as 15 dB less than for the shallow source (18 m). This is particularly evident in the MESA data (receiver at axis depth).

2. Receiver Depth Dependence

(C) Minimum propagation loss is always observed at the sound channel axis. For ranges beyond 200 nm north of a receiver, near axis depth propagation loss increases only very slowly with increasing range--even decreasing with increasing range at site C for the lower frequencies and deeper source.

(C) Hydrophones at depths within 160 m of the critical depth exhibit higher propagation loss than axis depth hydrophones. The difference increases with range and averages 5 dB for the 18 m source depth and 10 dB for the 91 m source depth. The rate of increase of propagation loss with increasing receiver depth is large for depth increments near and below critical depth with 2 to 5 dB higher loss at 194 m below critical depth than at 162 m above critical depth.

(C) Propagation loss to receivers beneath the sound channel and near the sea floor exhibits a much more rapid increase with range than would result from simple cylindrical spreading. For ranges on the order of 1000 nm, the propagation loss difference between sound channel axis and near bottom receivers is greater than 35 dB and can be as large as 50 dB.

3. Frequency Dependence

(C) For frequencies between 25 and 158 Hz, there is often no indication of frequency dependence of propagation loss; especially between 25 Hz and 50 Hz. When a frequency dependence is exhibited, propagation loss decreases with increasing frequency for the 10 m source depth and increases with increasing frequency for the 91 m source depth. Frequency dependence is most often exhibited by axis depth receivers.

4. Bathymetry Dependence

(C) Bathymetry and/or sound speed profile changes near Pathfinder Seamount introduced as much as 10 dB additional propagation loss at receiver locations south of the seamount when the sources were deployed north of the seamount. The presence of Kermit-Roosevelt Seamount, extending 800 m into the sound channel between the source and receiver, also increased propagation loss by about 10 dB. Propagation across the seamount results in a convergence zone-like structure in the propagation loss versus range plots.

B. Signal-to-Noise (S/N) Summary

1. Receiver Depth Dependence

(C) For ranges out to 175 nm at site C, the S/N is larger near the sea floor (1700 m below critical depth) than near the sound channel axis.

(C) For ranges greater than 175 nm, the S/N is larger near the sound channel axis than at other depths. At receivers separated in depth by 300 m, in the vicinity of critical depth, the S/N values are essentially equal. Beneath the deep sound channel, S/N decreases with increasing depth for source-to-receiver ranges beyond 175 nm.

2. Frequency Dependence

(C) At 50 Hz the S/N is consistently less than that at 25 Hz for all sites and almost all ranges, the difference being greater for the 91 m source depth than for the 18 m source depth. At 50 Hz the S/N is frequently less than that at 158 Hz, although it is equal to or greater than that at 158 Hz for some range intervals south of site C, and for ranges greater than 400 nm north of site C. S/N is usually higher at 158 Hz than at 251 Hz.

(The reverse of this page is blank.)

II. DATA ACQUISITION

(C) The CHURCH ANCHOR Exercise was conducted in August and September 1973 in that region of the Northeastern Pacific Ocean shown in Fig. II-1. During the exercise, acoustic energy from underwater explosive (SUS) sources was recorded with two types of receiving systems: Acoustic Data Capsules (ACODACs) located at sites A, C, and D, and a Multielement Super-directive Array (MESA) located at site E. The primary source track for the data, as shown in Fig. II-1, was the south-to-north line (longitude 143°30'W) passing through sites A, C, D, and E and extending from 150 nm south of site A to the beginning of the Alaskan Slope (about 850 nm north of site D). Also shown in Fig. II-1 is the secondary source track, a 90 nm segment of the radial line from Kermit-Roosevelt Seamount to site A, centered on the seamount.

(U) Two source detonation depths were used for each SUS run: 18 m and 91 m. The SUS charges were deployed by USNS SILAS BENT (T-AGS 26) along the primary track from 28°30'N to 46°30'N and subsequently by aircraft flying from 46°30'N to 59°30'N along the northern portion of the track (see Fig. II-1 for track segments and Table II-1 for deployment times). For the secondary track passing over Kermit-Roosevelt Seamount, the SUS charges were deployed by USNS BARTLETT (T-AGOR 13). Nominal range intervals between shots at each depth were 1 nm for the ship runs and 8 nm for the aircraft source run. Various receiving systems were used during the exercise to record sound energy received from SUS charges and CW sources and to record ambient noise energy. Because of this variety of tasks, the ACODAC 10-day recording interval at site A expired before the BENT and aircraft source runs were completed. The other two ACODACs and the MESA array at site E recorded data throughout each of the SUS runs. Receiver recording time intervals and source event time intervals are summarized in Table II-1.

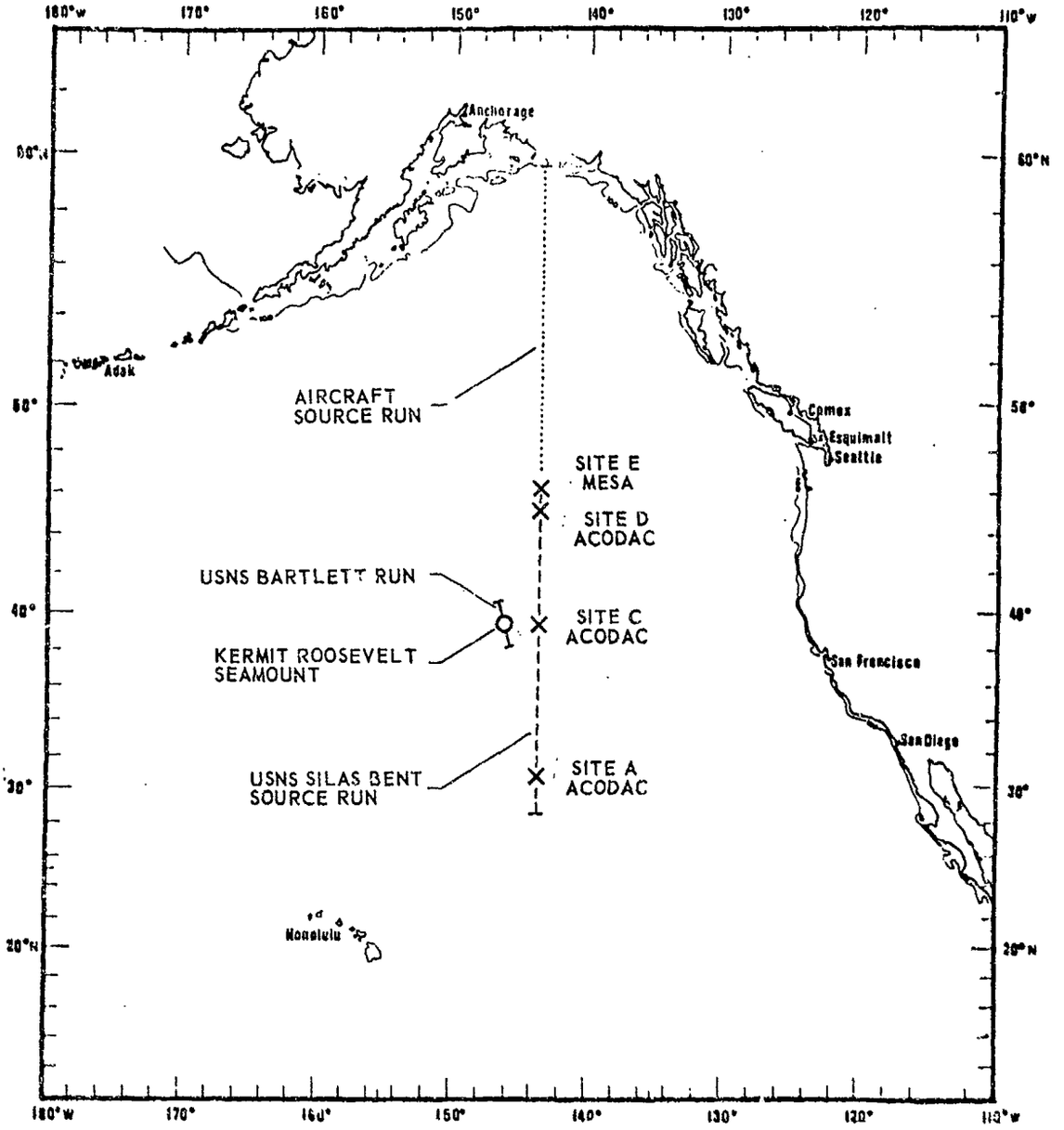

FIGURE II-1
EXERCISE AREA SHOWING SOURCE TRACKS
AND RECEIVER LOCATIONS

ARL-UT
AS-74-1000
ALA-DR
10-7-74

CONFIDENTIAL

TABLE II-1

(C) a. Source Information (U)

Event*	Source Vessel	Begin Deployment	End Deployment
30	BARTLETT	1900Z,21 Sept. 39° 55.0'N 146° 24.9'W	0346Z,22 Sept. 38° 37.8'N 145° 58.0'W
31	BENT	†0400Z,22 Sept. 28° 31.5'N	2147Z,25 Sept. 46° 28.5'N
32	AIRCRAFT	2200, 25 Sept. 46° 36'N	0114Z,26 Sept. 59° 28.9'N
For Events 31 and 32, Source Track Latitude = 143° 30'W			

†Data not processed for segment from 28° 31.5'N to 33° 25'N (0115Z, 25 Sept.)

(C) b. Receiver Information (U)

Site	Position	System Type	Hydrophone Depths (m)	Bottom Depth (m)	Begin Recording	End Recording
A	30° 31.9'N 143° 30.0'W	ACODAC	749, 4046, 4353, 4659	5091	0600 Z 13 Sept.	1400 Z 24 Sept.
C	39° 13.3'N 143° 28.1'W	ACODAC	696, 4055, 4361, 5521	5555	0022 Z 16 Sept.	0313 Z 27 Sept.
D	45° 05.1'N 143° 30.5'W	ACODAC	**3325, 3625, 3925, 4225, 4520, 4610	4646	0730 Z 18 Sept.	1730 Z 28 Sept.
E	46° 30'N 143° 30'W	MESA	400		1900 Z 21 Sept.	0100 Z 26 Sept.

**Data not processed for depths of 3325, 4225, and 4520 m.

(C) c. Source Deployment and Receiver Recording Time Intervals (U)

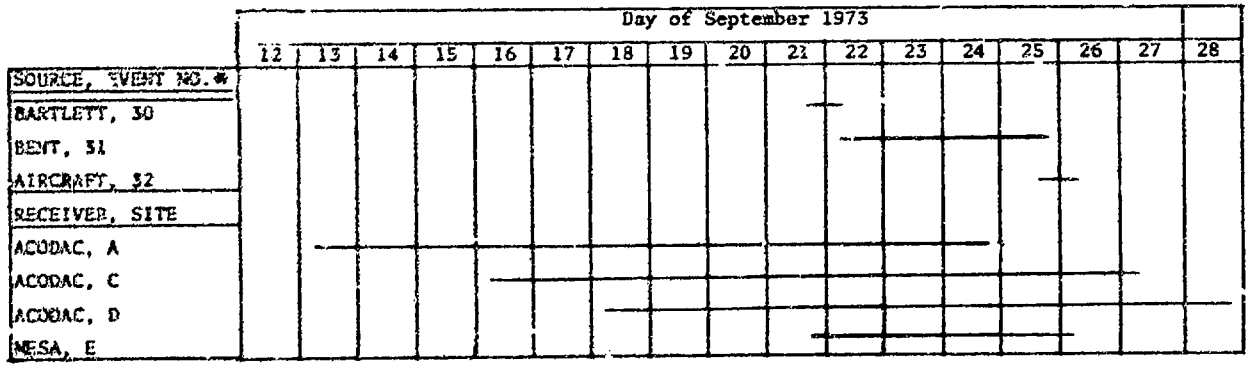

*Indicated Event Numbers are those assigned in the Church Anchor Data Analysis Plan.

CONFIDENTIAL

(U) The ACODAC systems have six hydrophones distributed vertically in the water column. The hydrophone depths at each ACODAC site and the MESA at site E are shown in Table II-1. Two midwater ACODAC hydrophones at sites A and C did not function and are not included in Table II-1. Receiving system locations and hydrophone depths are also indicated in Fig. II-2 on a cross section showing the bathymetry along the primary source track. Sound speed profiles based on data obtained during the Exercise are shown in Fig. II-2, together with indications of the deep sound channel axis and the critical depth.

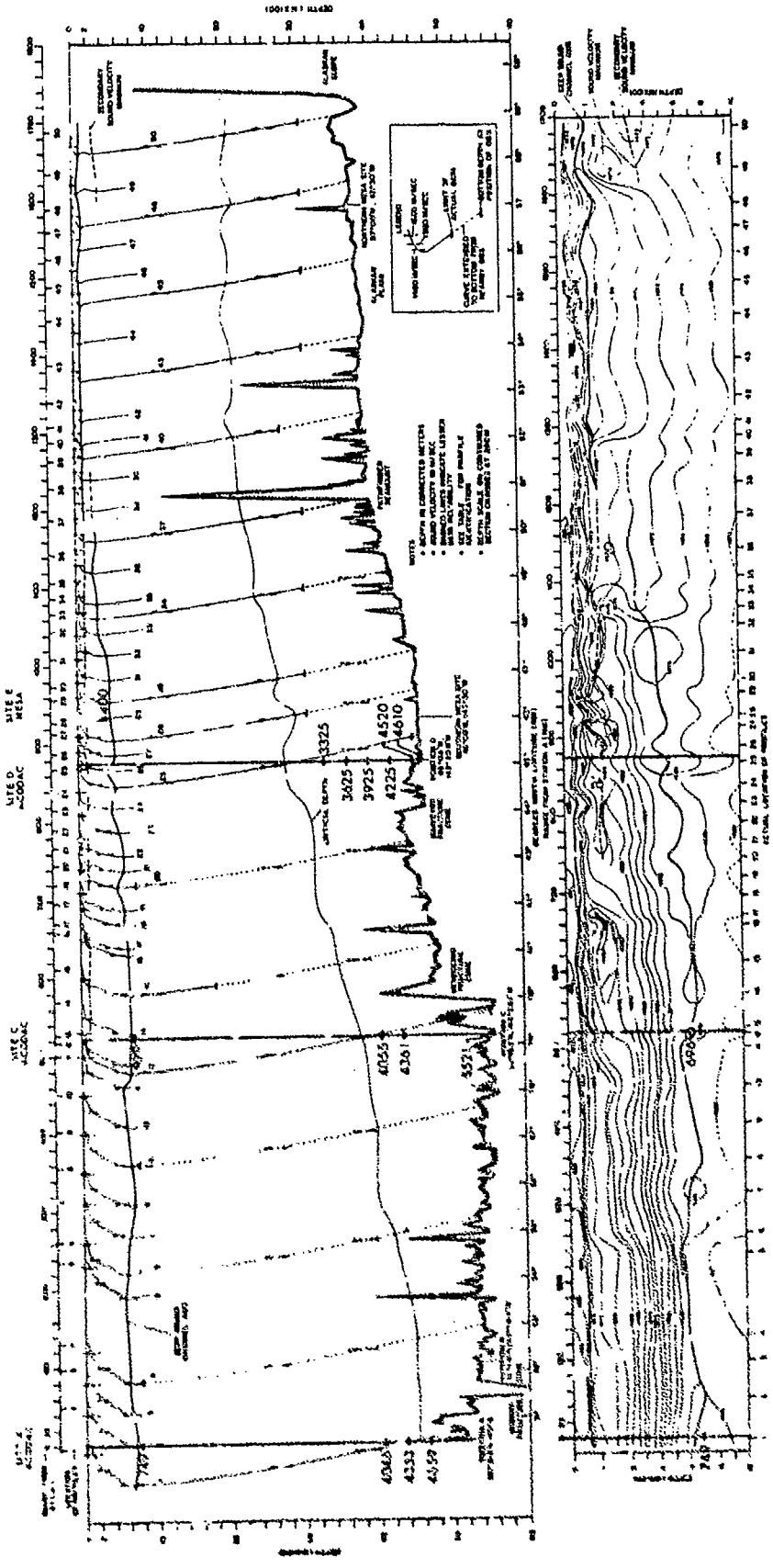

FIGURE 8-2
CROSS SECTION OF PRIMARY SOURCE TRACK SHOWING RECEIVER LOCATIONS, HYDROPHONE DEPTHS, BATHYMETRY, AND SOUND SPEED STRUCTURE

(The reverse of this page is blank.)

III. DATA ANALYSIS

(U) SUS signals received by the ACODAC and MESA sensor systems were recorded on magnetic tape in analog and digital format, respectively. The processing of data from both systems is described in this section.

A. ACODAC Data Processing

1. Outline of ACODAC Data Processing

(U) The following is a listing of the steps performed in processing the data. Each step is described in detail in the subsections which follow.

Tape Duplication
Preprocessing Edit
Analog-to-Digital Conversion
Multichannel Shot Detection
Shot Length Estimation
Shot and Noise Energy Estimation
Propagation Loss and Signal-to-Noise Calculations
Plotting of Analyzed Data
Final Editing

2. Tape Duplication

(U) The ACODAC analog tapes were duplicated by Texas Instruments, Dallas, Texas. After duplication, the original tape was archived for preservation and subsequent analysis was performed only on the duplicates.

3. Preprocessing Edit

(U) Prior to processing, each analog tape was edited for quality and completeness of data recorded during each exercise event of interest. The edit checks included data quality, time code consistency, tape speed consistency, overload density, and the quality of the internal and external calibration signals.

4. Analog-to-Digital (A/D) Conversion

(U) The edited analog data from three channels (hydrophones) are played back at a speed-up of 20:1, bandpass filtered (10 to 300 Hz) to minimize strumming and aliasing effects, and simultaneously sampled at a rate of 600 Hz. The 50 Hz carrier of the time code is extracted and multiplied to 600 Hz using a phase-lock loop frequency multiplier. This 600 Hz signal is used to control the A/D conversion process in order to minimize the errors due to mechanical variations in the analog record/playback systems. The digital samples are continuously stored on digital magnetic tape in blocks of 10 sec (ACODAC time).

(U) The digital data for one or more events are stored in a temporary tape library for processing with a CDC 3200 digital computer.

5. Shot Detection

(U) An important aspect of the hardware/software system used in the processing of SUS data is the automatic detection of shot energy arrivals. The leading edge of an arrival on each of three channels is located by continuously comparing a short time average of the recorded signal to a longer time average. The short time average value E_s will be larger than the longer time average E_l when a shot signal is present in the time interval of the short time average. Recursive filtering techniques are used to obtain E_s and E_l. Whenever E_s exceeds a threshold level of $2E_l$, the arrival of shot energy on the channel of interest

(U) is hypothesized and this portion of the record is selected for further processing.

(U) The probability of processing false detections is reduced by requiring that E_s exceed $2E_\ell$ simultaneously on two or three channels, and that the detection be within a few seconds of a possible shot energy arrival time determined by the times of previous detections and the shot deployment schedule. Nominal shot detonation depth is identified by comparing the arrival time with previous arrivals for the different depths and the known shot deployment pattern. Exact deployment times or source-to-receiver ranges are not known; however, it is assumed that the planned schedule of deployment and ship/aircraft speed was approximately adhered to. Reference arrival times for processing purposes are initially obtained from plots of the signal envelope.

6. Shot Length Estimation

(U) To ensure that all the significant multipath energy is included in the time interval used to estimate shot energy, the shot duration must be estimated. Simply using a very long signal segment results in unnecessary measurement errors due to statistical fluctuations of the noise.

(U) To ensure precision and repeatability in the shot length estimate, a recursive filter is used to automatically update the shot length estimate on each channel. In this process, the signal energy is measured in time intervals Δt before and after the current estimate of signal end time. The two energies are respectively designated E_L and E_R. The time interval Δt is the greater of 1 sec or one-tenth of the signal length. A noise reference energy E_N in a time segment Δt is computed from the background level. If $E_R > E_N$ and $E_L > 1.1\ E_N$, then the signal length estimate is increased by 9%; otherwise it is decreased by 10%. A minimum shot length of 2 sec is imposed. If either E_L or E_R exceeds $2E_N$, then the signal length estimate is increased by 20% to reduce convergence time of the length estimation process.

(U) In addition to the attention given to the shot termination, two steps are taken to ensure that all of the initial shot energy is included: 1) shot integration for energy estimation begins before the indicated detection time (normal lead is 0.5 sec) and 2) the beginning of shot integration for all channels is set by the earliest detection time over the three channels.

7. Shot and Noise Energy Estimation

(U) For each SUS signal detected, the SUS signal plus noise energy is estimated using 2048 spectral energy levels computed by a fast Fourier transform (FFT) over the frequency band from 10 to 300 Hz with 0.146 Hz resolution. Noise spectral energy is similarly estimated for a 13 sec segment of noise data ending 2.5 sec before the shot detection time. The total received shot energy plus noise energy and total noise energy in 1-octave and 1/3-octave bands centered on frequencies of interest are then computed by summing the individual spectral energy levels. The received SUS energy estimate is determined by subtracting the noise energy estimate from the SUS signal-plus-noise energy estimate.

8. Propagation Loss and Signal-to-Noise Calculations

(U) The output of the energy estimation process is combined with source-to-receiver range information (from a digital range tape supplied by the Naval Oceanographic Office) and with sensor system response parameters to determine the propagation loss and signal-to-noise ratio for each shot.

(U) The ACODAC external and internal calibration signals are converted to digital representation at the same time as the shot data. These calibration data are processed and used to correct the results for the recording and playback system frequency response.

(U) Other parameters used for propagation loss and signal-to-noise ratio calculation include the hydrophone sensitivity, acoustical impedance of the water at the hydrophone, source level, and source detonation depth.

(U) Explosive source levels for 1.8 lb SUS charges detonated at 18 and 91 m depth were obtained from Gaspin and Shuler (Ref. 3). The source levels used are shown in Table III-1 in ergs/cm^2/Hz at 100 yd.

TABLE III-1

Shot Energy by Gaspin and Shuler

Source Depth m	Frequency				
	25 Hz		50 Hz		160 Hz
	1 octave	1/3 octave	1 octave	1/3 octave	1/3 octave
18	18.6	20.0	15.8	14.9	10.3
91	19.9	20.7	15.6	15.7	11.5

(U) Corrections were made to the source levels in Table III-1 because of variations in actual detonation depth of the SUS charges. True detonation depth was determined by measurement of the period of the first bubble pulse (Underwater Systems, Inc., 1974). Approximately 10% of the shot signals were discarded because of excessive depth deviations (from the nominal detonation depth).

9. Plotting of Processed Data

(U) The propagation loss, signal-to-noise ratio (S/N), and noise estimate for each shot is plotted as a function of frequency, source depth, and receiver depth. Symbols used to plot the propagation loss for each shot are coded to indicate the signal-to-noise ratio of the received signal (see Appendix A for code). Range of detection (but not propagation loss) is indicated for overloaded shots and for shots with S/N < -3 dB.

10. Final Editing

(U) The propagation loss and signal-to-noise ratio data are subjected to a final editing for quality control. For ranges that exhibit extreme noise estimates, the narrowband spectra for the shot signal detected in those ranges are inspected to determine the quality of the data. Presumed signals which did not show the characteristic bubble pulse pattern were rejected as being noise contaminated.

B. MESA Data Processing

1. System Description

(U) The data from a single MESA hydrophone were recorded in digital format for the BENT SUS run and in analog format for the aircraft SUS run. The processing of all SUS data is with the fast Fourier transform (FFT) method (Ref. 4) utilizing Hewlett-Packard hardware. For SUS signals covering time periods longer than 6.55 sec, additional consecutive transforms are taken and added to obtain total energy. The energy for the SUS signal-plus-noise and the noise estimate are calculated in 1/3-octave bands from higher resolution energy spectra. The 1/3-octave bands are weighted with a sixth-order Butterworth filter function. From these energy estimates, the SUS signal energy, propagation loss, and signal-to-noise ratios are calculated as a function of source depth and source-to-receiver range.

2. Processing Parameters

(U) The parameters relevant to the SUS processing are

A/D rate:	2500 Hz
Data window:	6.55 sec (16,384 points)
FFT bandwidth:	0.153 Hz

IV. DISCUSSION OF PROPAGATION LOSS

(U) Propagation loss is examined in this section as a function of source-to-receiver range, receiver site, receiver depth, source depth, frequency, and bathymetry. An inventory of the data examined is included in Table IV-1. Propagation loss is plotted, in Appendix A for ACODAC data and in Appendix B for MESA data, as a function of range for each source depth, frequency, and receiver depth. Selected plots of these data are combined in some of the illustrations of this section. A description of the symbols used in these plots is given in Appendix A.

(U) The data for each receiver site are discussed below on an individual basis. Observations based on data from all four receiver sites are combined in the Summary of Results (Section I.b).

(U) Because the source-to-receiver ranges varied from less than one nautical mile to over 1200 nautical miles, the received signals were sometimes so large that they overloaded the receiving systems, and at other times they were of such low level that the resultant low signal-to-noise ratio precluded accurate propagation loss calculation. Thus, in some range segments either the low propagation loss (high signal level) or the high propagation loss (low signal-to-noise ratio) data are missing and the fine structure of the propagation loss versus range plots is lost. Overloaded and low signal-to-noise ratio signals are indicated on the ACODAC data plots in the manner described in Appendix A.

A. ACODAC, Site A

(U) At site A the sound channel axis depth was 670 m and the critical depth was 4515 m. Propagation loss data are available for the EXNT SUS run over the range interval from 200 to 550 nm north of site A for two

(U)

TABLE IV-1

Inventory of SUS Data Processed and Plotted

Source Depths	18 m and 91 m	
Frequencies and Bandwidths Analyzed	† ACODAC	25 and 50 Hz at 1 octave 158 Hz at 1/3 octave
	MESA	25, 50, 100, 158, and 251 Hz at 1/3 octave

† In addition to these frequencies, propagation analyses were performed, with the results now stored on digital magnetic tape, for the ACODAC data at the following frequencies (all 1/3 octave): 25, 50, 100, and 250 Hz.

RECEIVER				SOURCE			
Site	Type	Hydrophone Depth (m)	Relation to Other Features (Distances in meters)	Event 30 BARTLETT	Event 31, USNS SILAS BENT South of C	Event 31, USNS SILAS BENT North of C	Event 32 AIRCRAFT
A	ACODAC	749	79 below sound channel axis.	*	x		x
		4353	162 above critical depth.	*	*		x
		4659	144 below critical depth, and 432 above sea floor.	*	*		x
C	ACODAC	696	41 below sound channel axis.	*	*	*	*
		4055	195 below critical depth.	*	*	*	*
		5521	1661 below critical depth, and 34 above sea floor.	*	*	*	*
D	ACODAC	3625	785 below critical depth.	*	*		*
		3925	1085 below critical depth.	0	0		0
		4612	1770 below critical depth, and 34 above sea floor.	*	*		*
E	MESA	400	10 above sound channel axis.	x	*		*

* Data Analyzed and Plotted.
x No Data
0 Data Analyzed and Plotted, but Overload Detector in ACODAC Not Working

(U) hydrophone depths: 1) 4353 m (162 m above critical depth) and 2) 4659 m (144 m below critical depth). These data are shown in Appendix A, Figs. A19 through A30.

(C) Data for the 4353 m hydrophone depth are combined in Fig. IV-1 and for the 4659 m hydrophone depth in Fig. IV-2. These two illustrations show the dependence of propagation loss on source depth. At 25 Hz for both receiver depths, propagation loss is greater for the 18 m source depth (although the large number of overloaded shots preclude detailed comparisons). At 50 Hz, the shallower (18 m) source similarly exhibits greater propagation loss to the hydrophone 144 m below critical depth while, for a receiver 162 m above critical depth, the loss is approximately the same for each source depth. Source depth appears to have little influence on propagation loss at 158 Hz for either hydrophone depth.

(C) Propagation loss to the hydrophone 144 m below critical depth is consistently greater than propagation loss to the hydrophone 162 m above critical depth. This is illustrated in Fig. IV-3 where the difference in propagation loss for the two hydrophone depths is shown for each shot having greater than 0 dB signal-to-noise ratio at both hydrophones. Though the hydrophones are only separated by about 300 m, the signals arriving at the hydrophone above the critical depth are, at all three frequencies, 2 to 5 dB higher, on the average, than those arriving at the hydrophone below the critical depth, i.e., propagation loss is consistently greater to the deeper phone.

(C) The frequency dependence of propagation loss is illustrated in Figs. IV-4 and IV-5, where the difference in propagation loss computed at two different frequencies is plotted versus range. The data indicate that propagation loss is almost independent of frequency for both source depths from 25 to 50 Hz. However, the 158 Hz propagation loss is consistently different from the lower frequency data and the difference

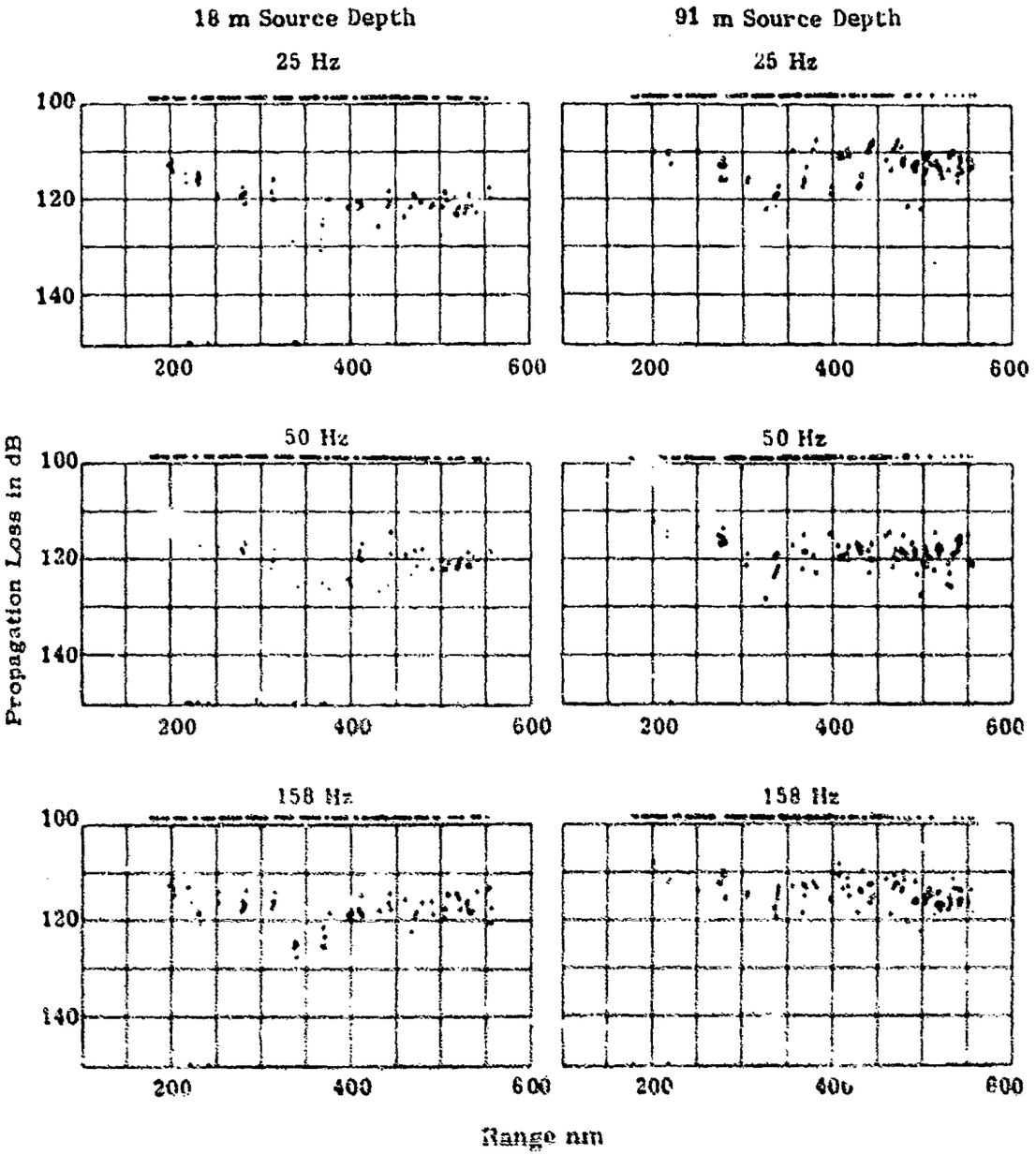

FIGURE IV-1

PROPAGATION LOSS AT SITE A FOR TWO SOURCE DEPTHS, THREE FREQUENCIES, AND RECEIVER DEPTH OF 4353 m

AS-74-1375

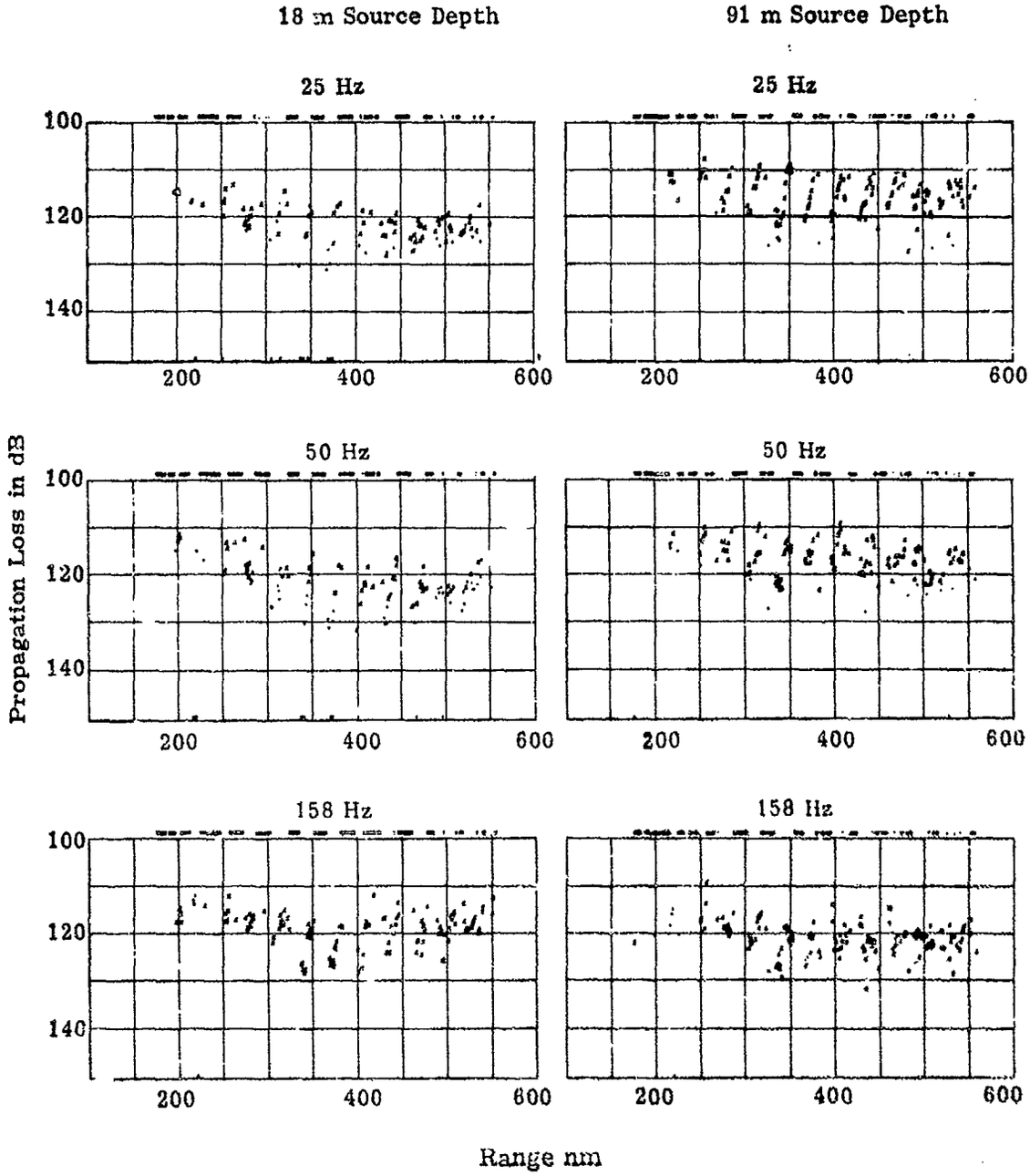

FIGURE IV-2

PROPAGATION LOSS AT SITE A FOR TWO SOURCE DEPTHS, THREE FREQUENCIES, AND RECEIVER DEPTH OF 4659 m

AS-74-1376

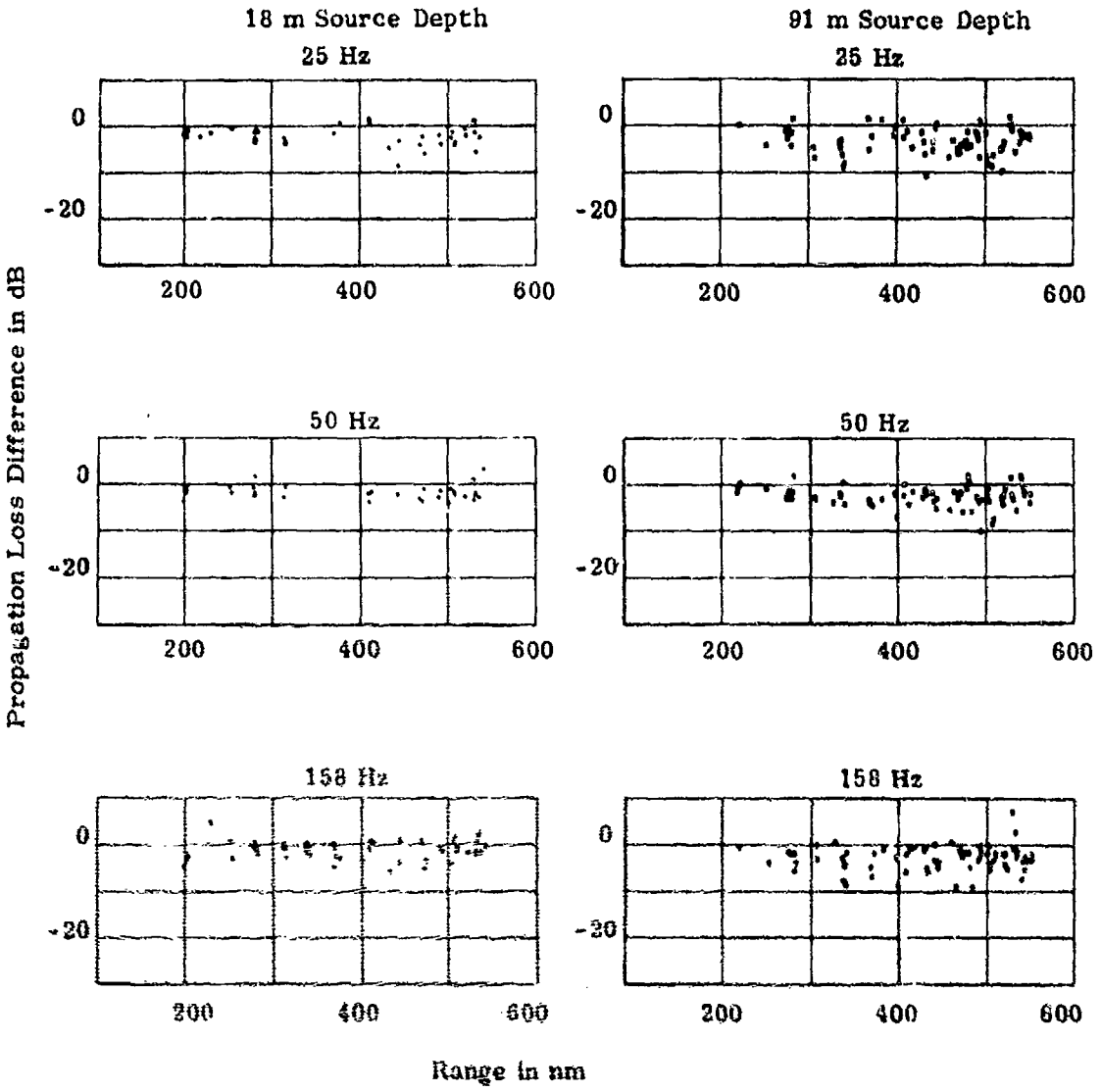

FIGURE IV-3

PROPAGATION LOSS DIFFERENCE BETWEEN
TWO RECEIVER DEPTHS (4353 m minus 4659 m) AT SITE A

AS-74-1377

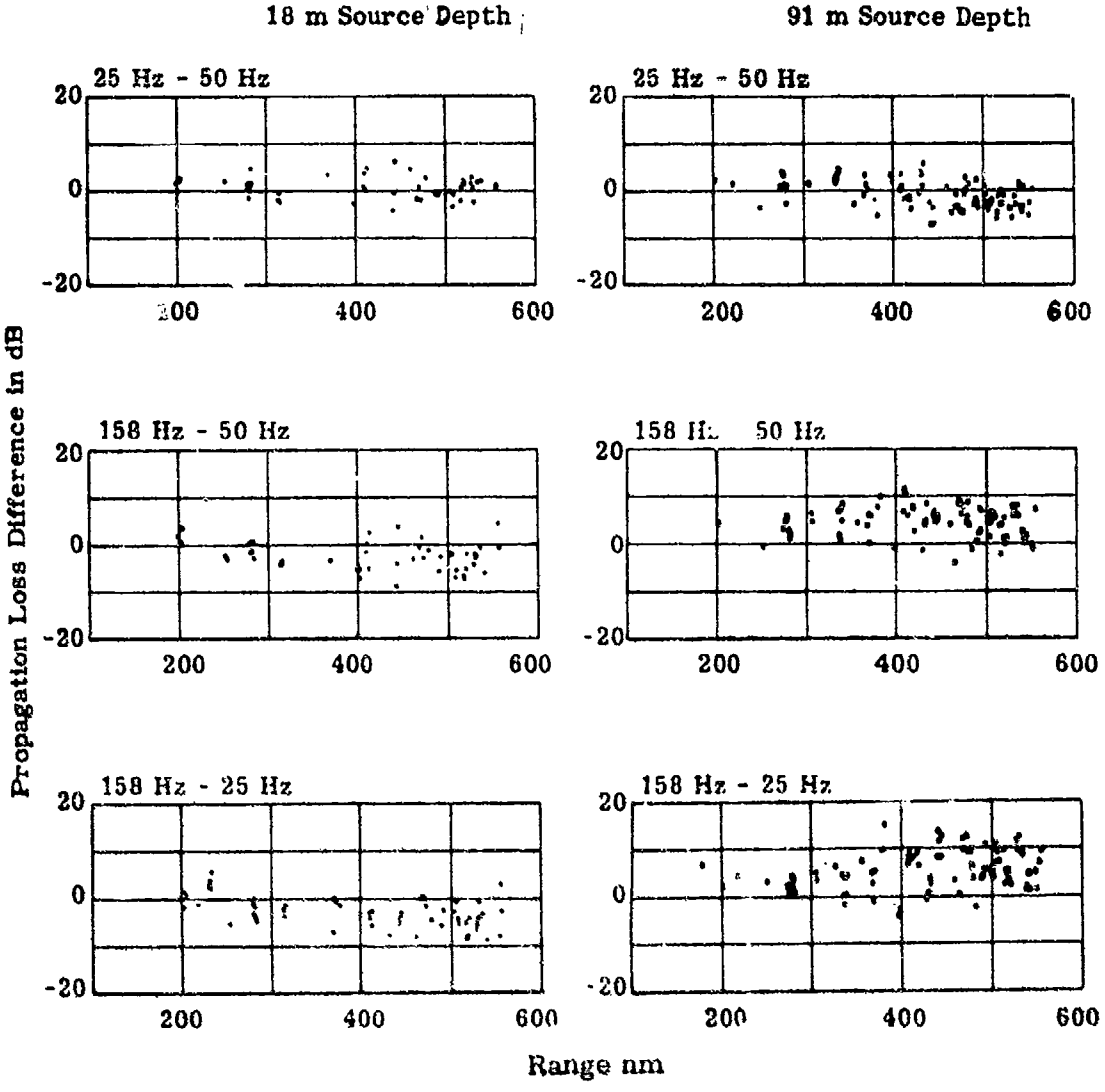

FIGURE IV-4

PROPAGATION LOSS DIFFERENCE BETWEEN
THREE FREQUENCIES AT SITE A RECEIVER DEPTH OF 4353 m

AS-74-1378

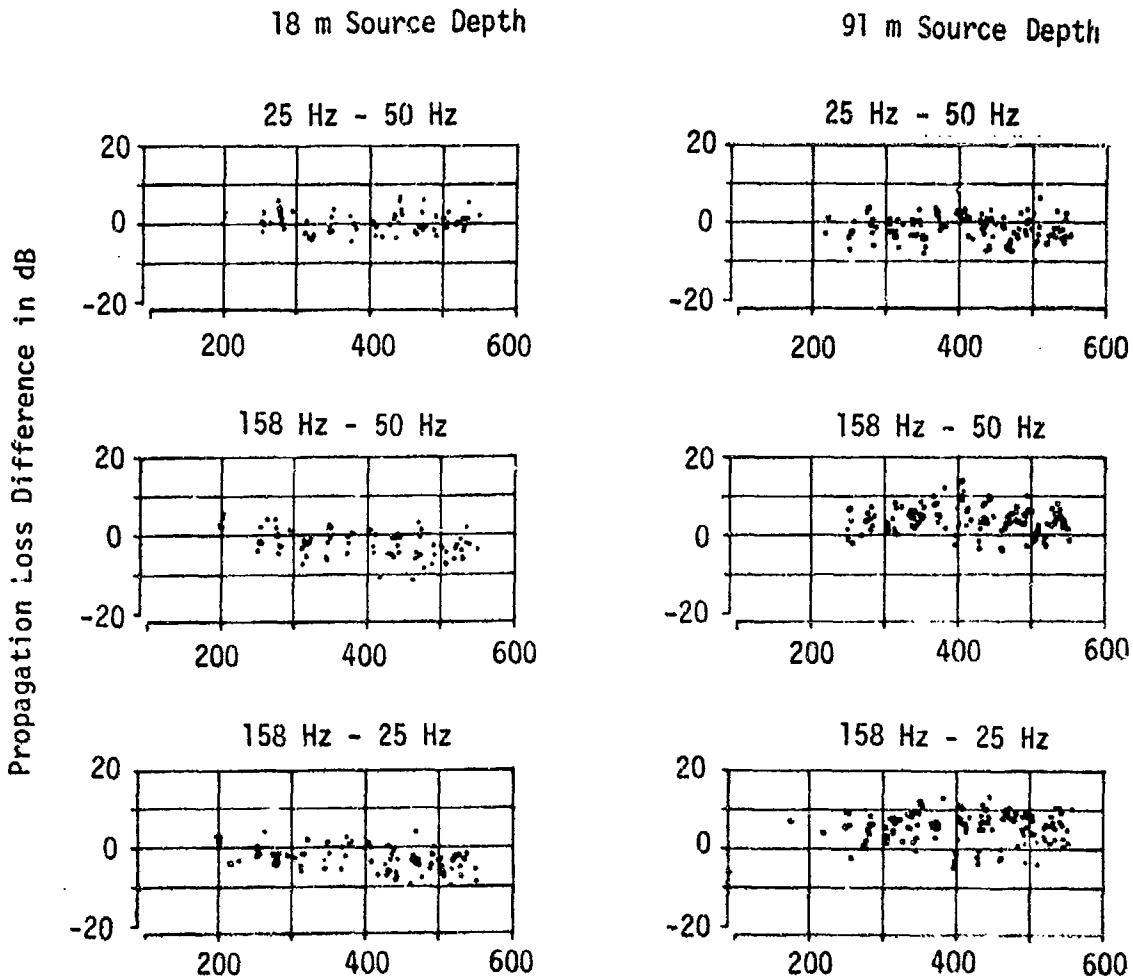

FIGURE IV-5

PROPAGATION LOSS DIFFERENCE BETWEEN
THREE FREQUENCIES AT SITE A RECEIVER DEPTH OF 4659 m

AS-74-1379

(C) is dependent on source depth: the 91 m source depth data indicates that propagation loss increases between 50 and 158 Hz while the 18 m source depth data shows that propagation loss decreases between 50 and 158 Hz.

(U) The secondary source track passes over the Kermit-Roosevelt Seamount approximately 540 nm from site A. On this track, which is radial to site A, USNS BARTLETT deployed SUS charges over the range interval from 500 to 580 nm from site A. Propagation loss measured at site A for this source run is shown in Appendix A, Figs. A1 through A18.

(C) The BARTLETT SUS run data provide an indication of the influence of topographic blockage on propagation loss. The Kermit-Roosevelt Seamount rises 3000 m above the sea floor; approximately 800 m above critical depth (i.e., into the deep sound channel). Propagation loss data at 50 Hz are summarized in Fig. IV-6 for both source depths. Beyond 540 nm range (i.e., beyond the seamount), two characteristics are shown by the data. First, the slope of the propagation loss versus range is greater and the overloading of the receiver abruptly decreases or ceases for most receiver depths. Second, a convergence zone-like fine structure appears in the data (for ranges less than 540 nm the fine structure may exist, but be obscured by overloading). As indicated by Fig. IV-6, the topographic effects are greater for the shallower (18 m) source depth. For the near axis depth receiver (749 m), the deep source (91 m) data overloads continue beyond the seamount range.

(C) Figure IV-6 indicates that at 50 Hz, for the BARTLETT SUS run, propagation loss increases with receiver depth, especially for ranges beyond the seamount. This fact is further borne out in Figs. IV-7 and IV-8, which show data for frequencies of 25, 50, and 158 Hz. In Fig. IV-7, the propagation loss for the 18 m source depth shows almost no frequency dependence, perhaps decreasing slightly with increasing frequency for ranges less than 540 nm. For the 91 m source depth,

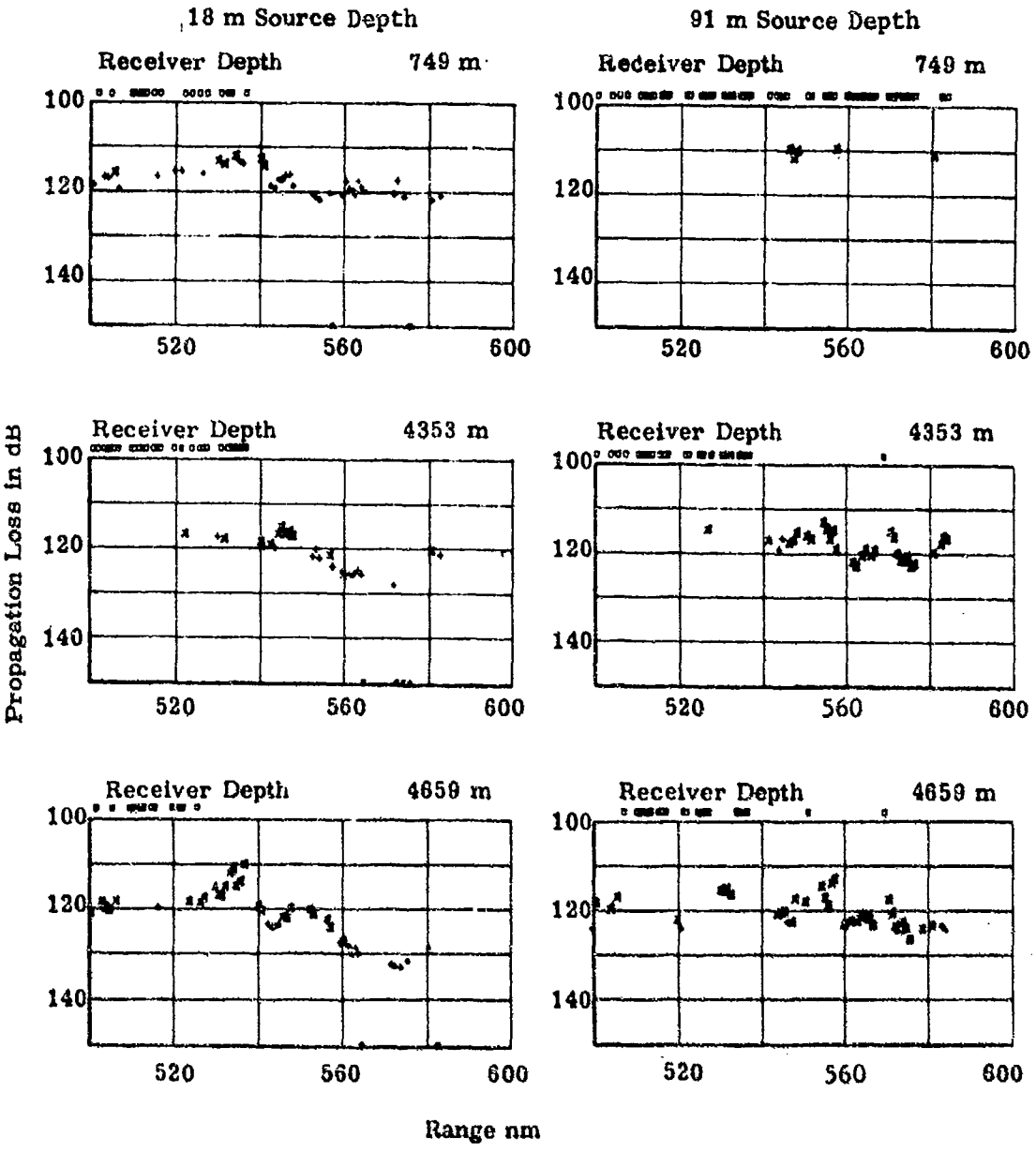

FIGURE IV-6

50 Hz PROPAGATION LOSS AT SITE A FOR
18 m AND 91 m SOURCE DEPTHS AND THREE RECEIVER DEPTHS

AS-74-1380

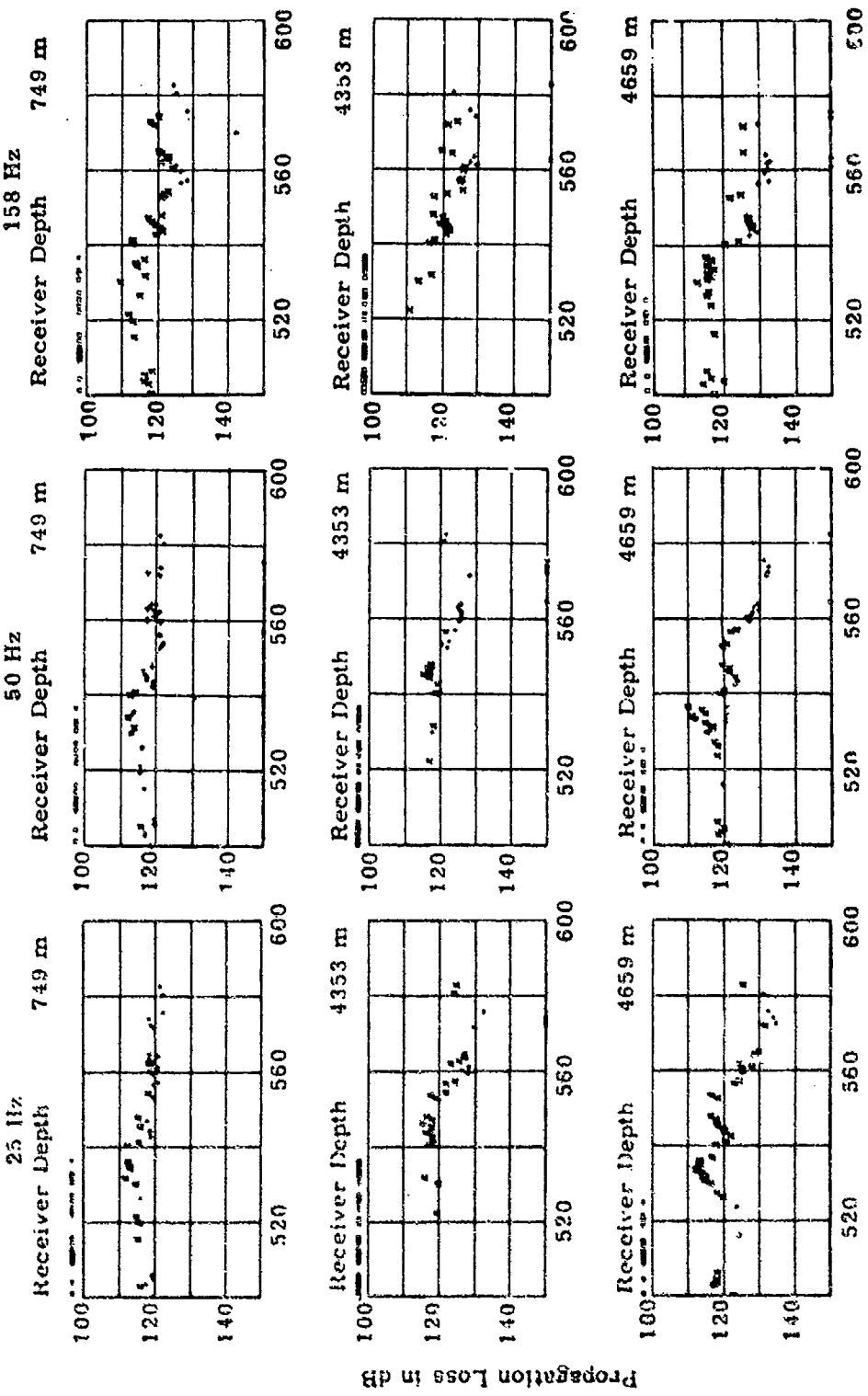

FIGURE IV-7

PROPAGATION LOSS AT SITE A FOR 18 m SOURCE DEPTH AND THREE RECEIVER DEPTHS - KERMIT ROOSEVELT SEAMOUNT EXTENDING 800 m INTO THE SOUND CHANNEL AT 540 nm RANGE

AS-74-1381

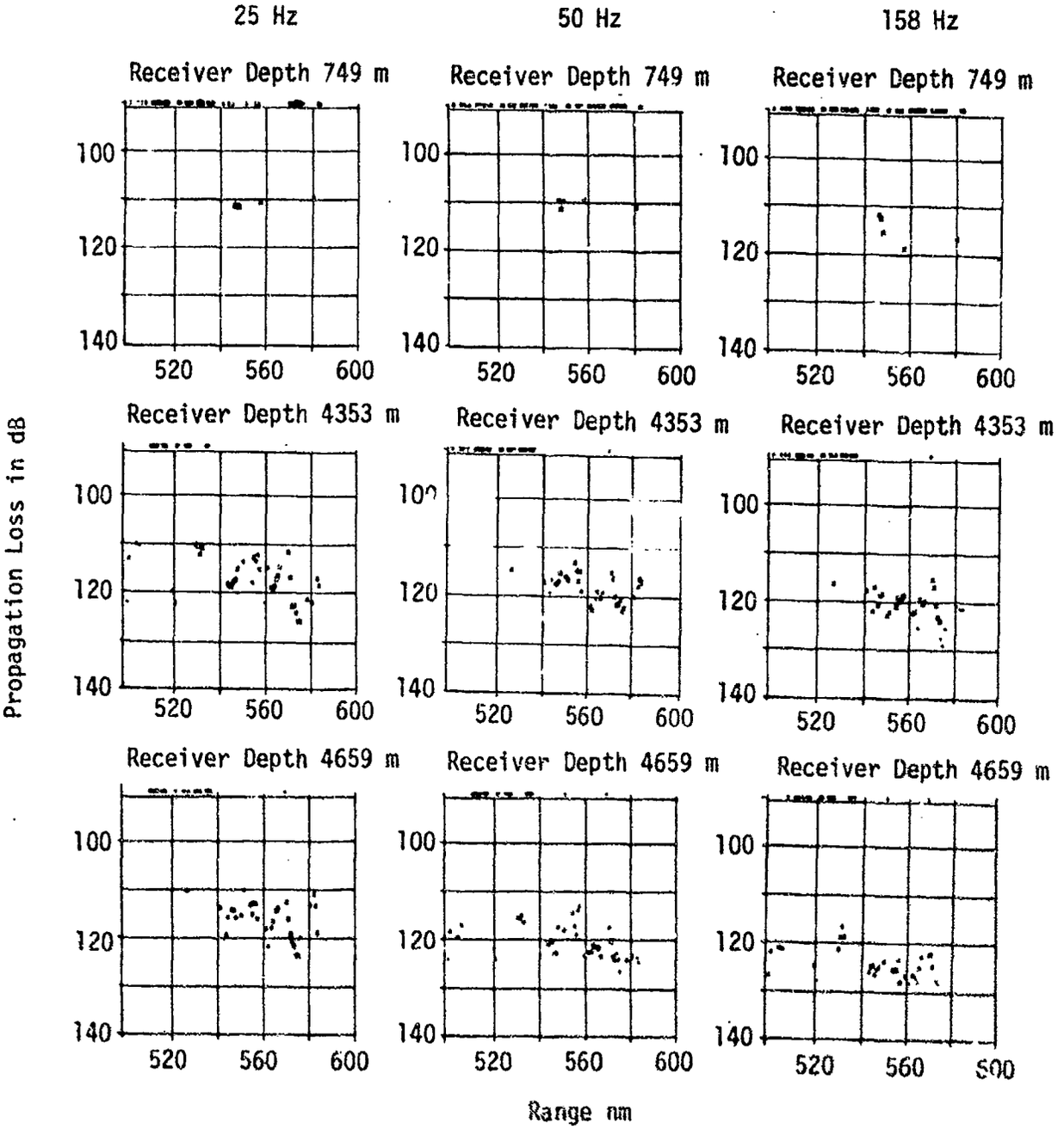

FIGURE IV-8

PROPAGATION LOSS AT SITE A FOR 91 m SOURCE DEPTH AND THREE RECEIVER DEPTHS - KERMIT ROOSEVELT SEAMOUNT EXTENDING 800 m INTO THE SOUND CHANNEL

AS-74-1382

(C) Fig. IV-8, propagation loss increases with increasing frequency. Thus, the frequency dependence behavior is consistent with that measured during the BENT SUS run.

B. ACODAC, Site C

(U) The BENT SUS run passed northward over site C. Thus, data are available for a range interval from 0 to 350 nm south of site C (northward propagation) and for a range interval from 0 to 440 nm north of the site (southward propagation). Additional data for sources from 440 nm to 1220 nm north of site C are provided by the aircraft SUS run. Data for these three range segments are included in Appendix A, Figs. A49 through A102.

(U) Propagation loss from these SUS runs is examined below for hydrophone depths of 696 m, 4055 m, and 5521 m. At site C, the sound channel axis depth was 655 m, the critical depth was 3860, and the sea floor depth is 5555 m. This information is summarized in Table IV-1.

(C) Propagation loss data at 25 Hz are shown in Fig. IV-9 for the three source-to-receiver range segments, both source depths, and the 696 m hydrophone depth. The range segments are combined to provide a continuous indication of propagation loss from 350 nm south of site C to 1200 nm north of site C. Similar data for 50 Hz and 158 Hz are shown in Figs. IV-10 and IV-11, respectively. These illustrations show a greater propagation loss for the shallow (18 m) source. They also indicate decreasing or constant propagation loss with range for the deep source at ranges beyond 200 nm north of site C. This decreasing loss with range results from shoaling of the sound channel axis and consequently better coupling of energy from the sources north of site C (see Fig. II-2). Minimum loss occurs when both source and receiver are near the axis depth. An abrupt increase in loss at 158 Hz from the shallow source, at a range of 700 nm north of site C, results from partial blockage of the channel by Pathfinder Seamount (Fig. II-2).

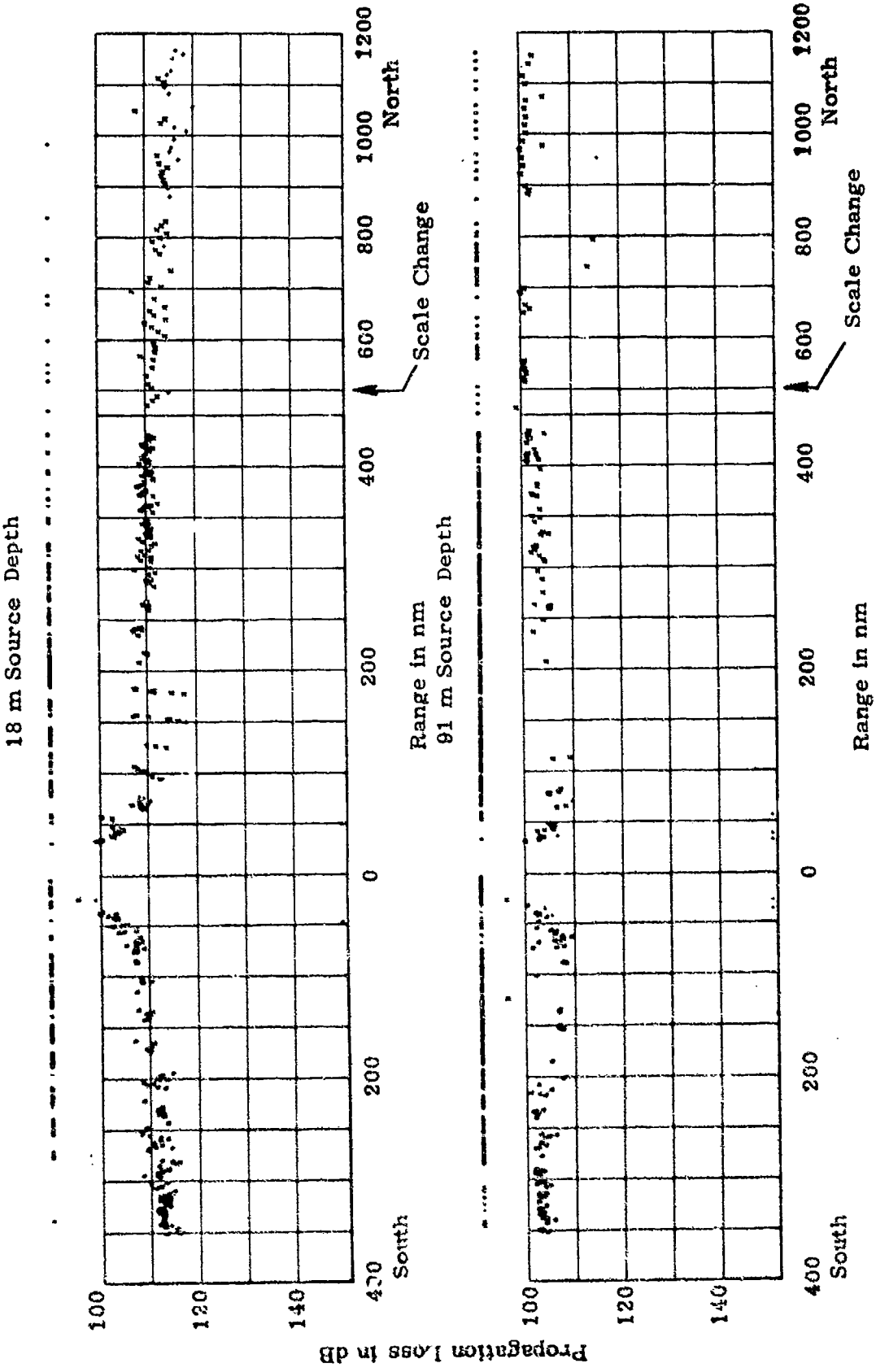

FIGURE IV-9

PROPAGATION LOSS NORTH AND SOUTH OF SITE C AT 25 Hz
FROM 18 m and 91 m SOURCE TO A RECEIVER AT 696 m

AS-74-1383

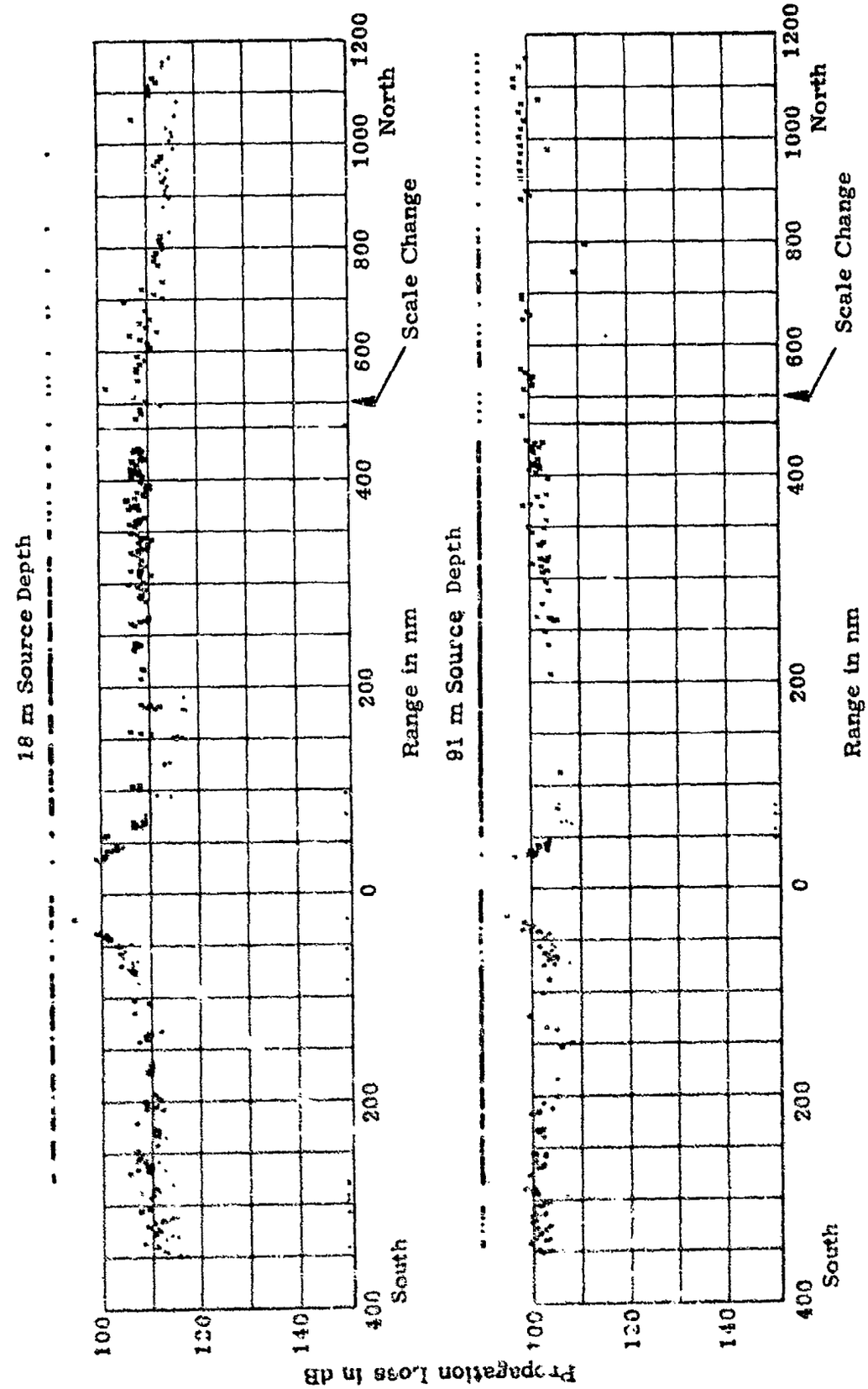

FIGURE IV-10

PROPAGATION LOSS NORTH AND SOUTH OF SITE C AT 50 Hz
FROM 18 m AND 91 m SOURCE TO A RECEIVER AT 696 m

AS-74-1384

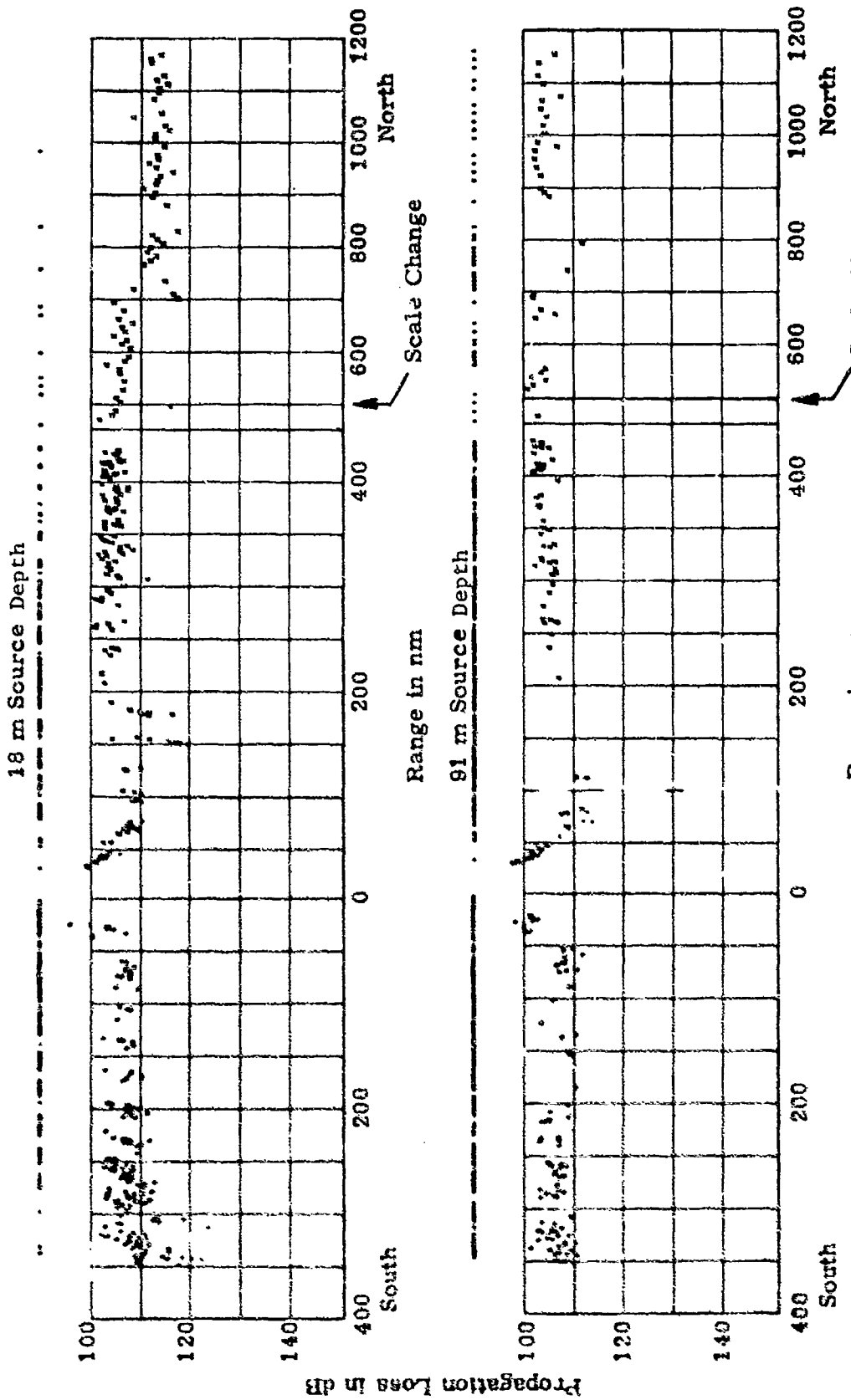

FIGURE IV-11

PROPAGATION LOSS NORTH AND SOUTH OF SITE C AT 158 Hz
FROM 18 m AND 91 m SOURCE TO A RECEIVER AT 696 m

AS-74-1385

(C) Propagation loss to the 5521 m (near bottom) hydrophone depth is illustrated in Figs. IV-12, IV-13, and IV-14. For all frequencies and source depths, the loss increases more rapidly with range than it does at the channel axis. For the initial 200 nm range segment, the loss to the near bottom hydrophone increases more rapidly with range north of site C than south of site C. This greater loss may be due to partial blockage of the near bottom hydrophone by the Mendocino Escarpment, which rises 1500 m above the sea floor about 50 nm north of site C (Fig. II-2).

(C) All of the very short range data were overloaded. In some cases, processing of the signals was started at about 25 nm range, which is why the overload indications do not occur continuously across zero range in Figs. IV-9 through IV-14.

(C) Receiver depth dependence of propagation loss is indicated by comparing Figs. IV-9, IV-10, and IV-11 with Figs. IV-12, IV-13, and IV-14. For all three frequencies and both source depths the loss is always greater for the near bottom depth than for the near axis depth. This difference in propagation loss increases with range until it exceeds 50 dB beyond about 800 nm. Receiver depth dependence is further illustrated in Figs. IV-15, IV-16, and IV-17 where the difference in propagation loss between the axis depth and the other two depths (near critical depth and near bottom) is shown. In Fig. IV-15 and IV-16, for the portion of the BENT SUS run south of site C and for both source depths and all three frequencies, the loss near the bottom is shown to be consistently larger than near the axis and the difference increases with increasing range. This same type of behavior is exhibited by the data for the range segments north of site C. Figure IV-15 shows that, for the 18 m source depth and for all three frequencies, the propagation loss is, on the average, slightly larger (perhaps 5 dB) for the near critical depth (4055 m) than for the axis depth (696 m) and the difference does not exhibit any consistent change with range. Figure IV-16 exhibits similar behavior for the 91 m source depth except that the average difference

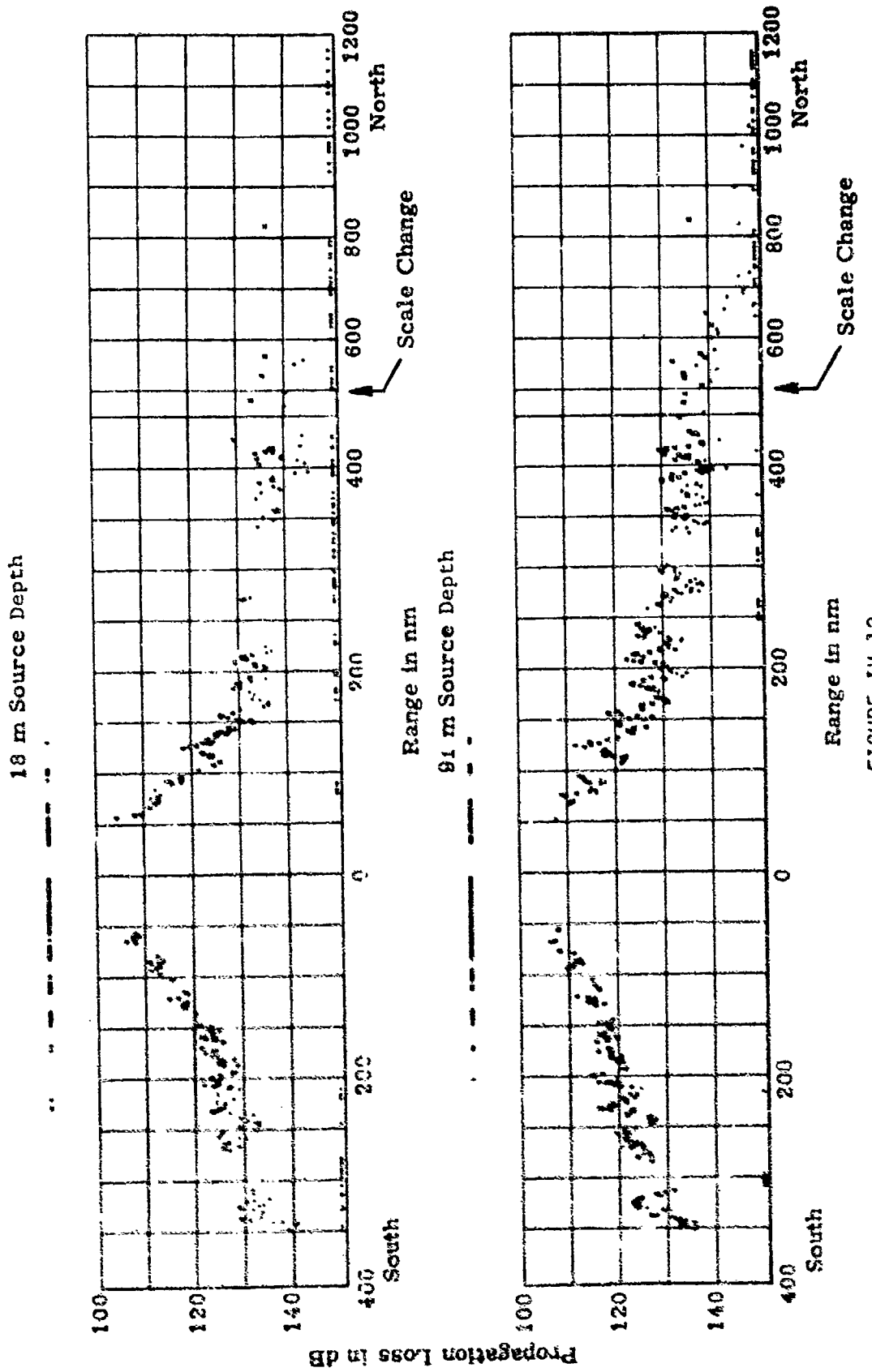

FIGURE IV-12

PROPAGATION LOSS NORTH AND SOUTH OF SITE C AT 25 Hz
FROM 18 m AND 91 m SOURCE TO A RECEIVER AT 5521 m

AS-74-1386

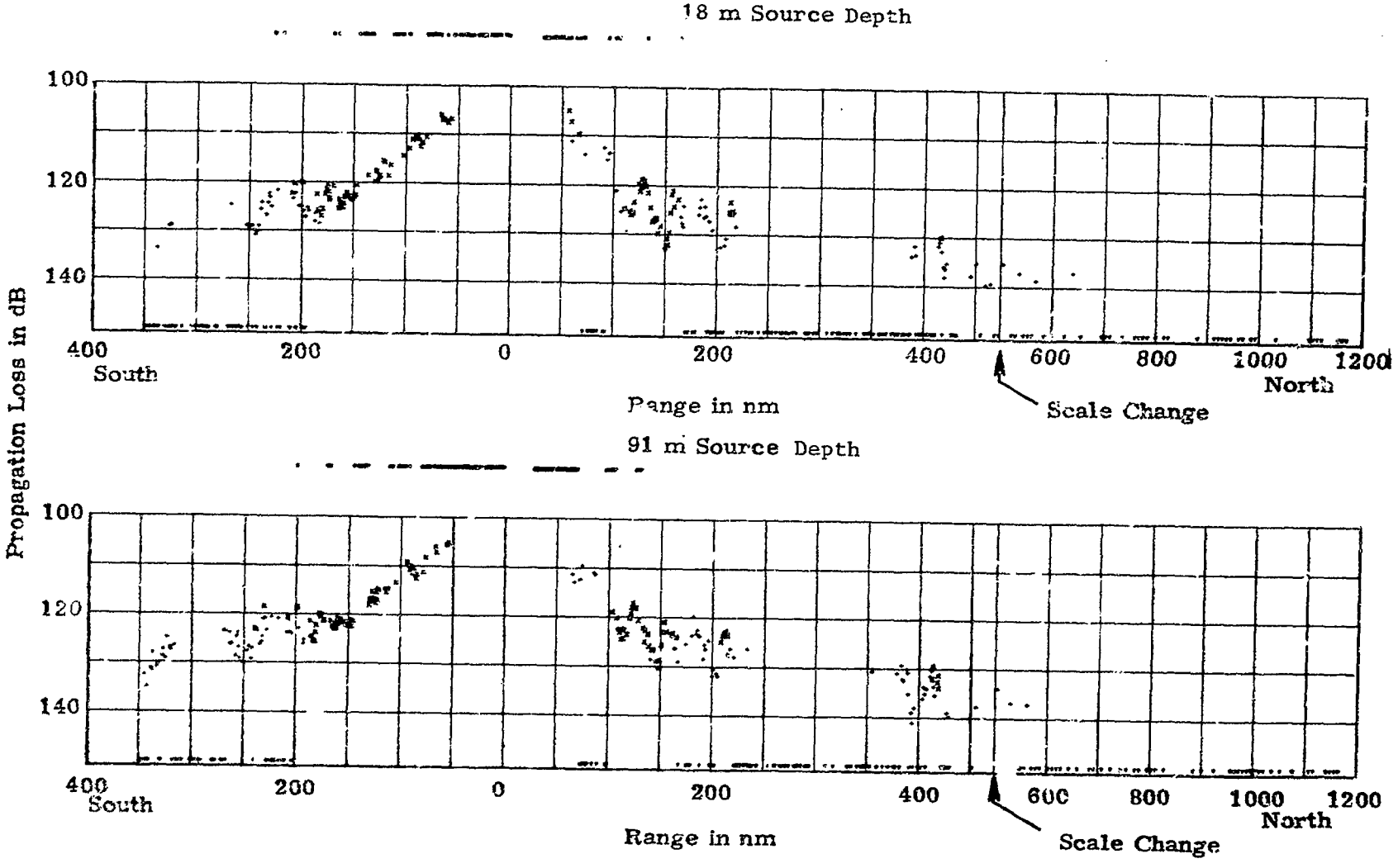

FIGURE IV-13

PROPAGATION LOSS NORTH AND SOUTH OF SITE C AT 50 Hz
FROM 18 m AND 91 m SOURCE TO A RECEIVER AT 5521 m

AS-74-1387

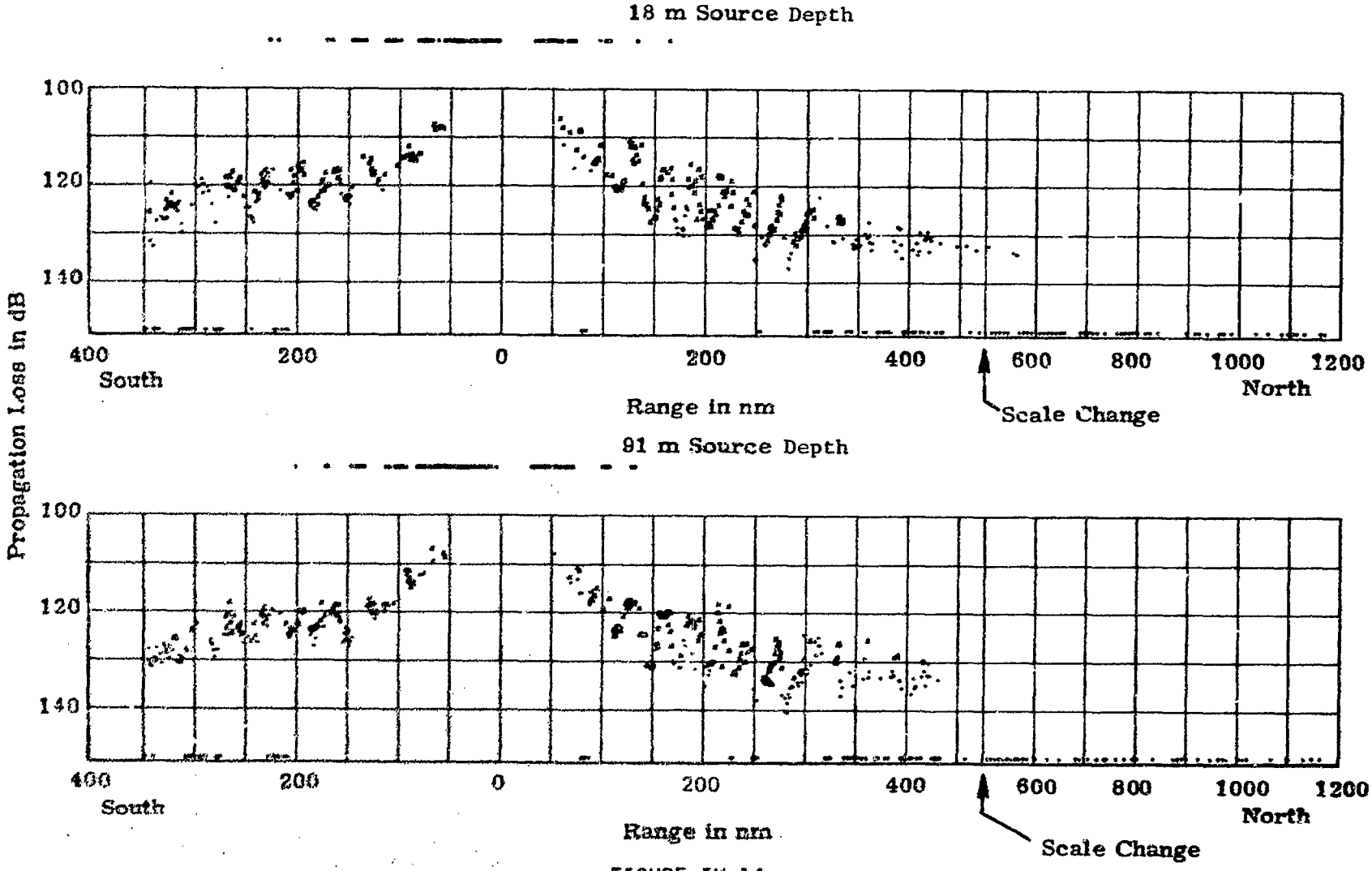

FIGURE IV-14

PROPAGATION LOSS NORTH AND SOUTH OF SITE C AT 158 Hz
FROM 18 m AND 91 m SOURCE TO A RECEIVER AT 5521 m

AS-74-1388

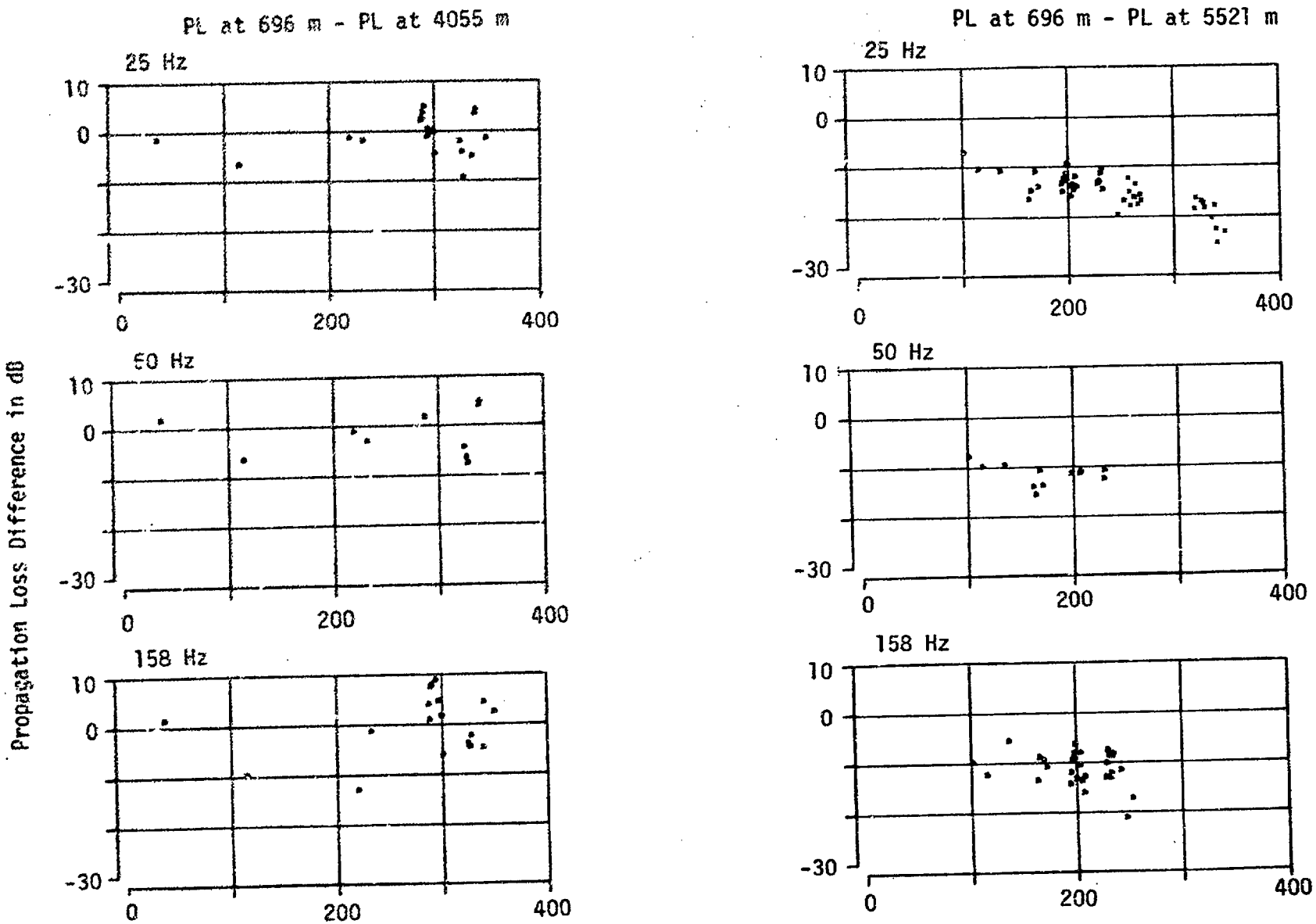

FIGURE IV-15

DIFFERENCE BETWEEN PROPAGATION LOSS TO DIFFERENT RECEIVER DEPTHS
BENT SOURCE RUN SOUTH OF SITE C, 18 m SOURCE DEPTH

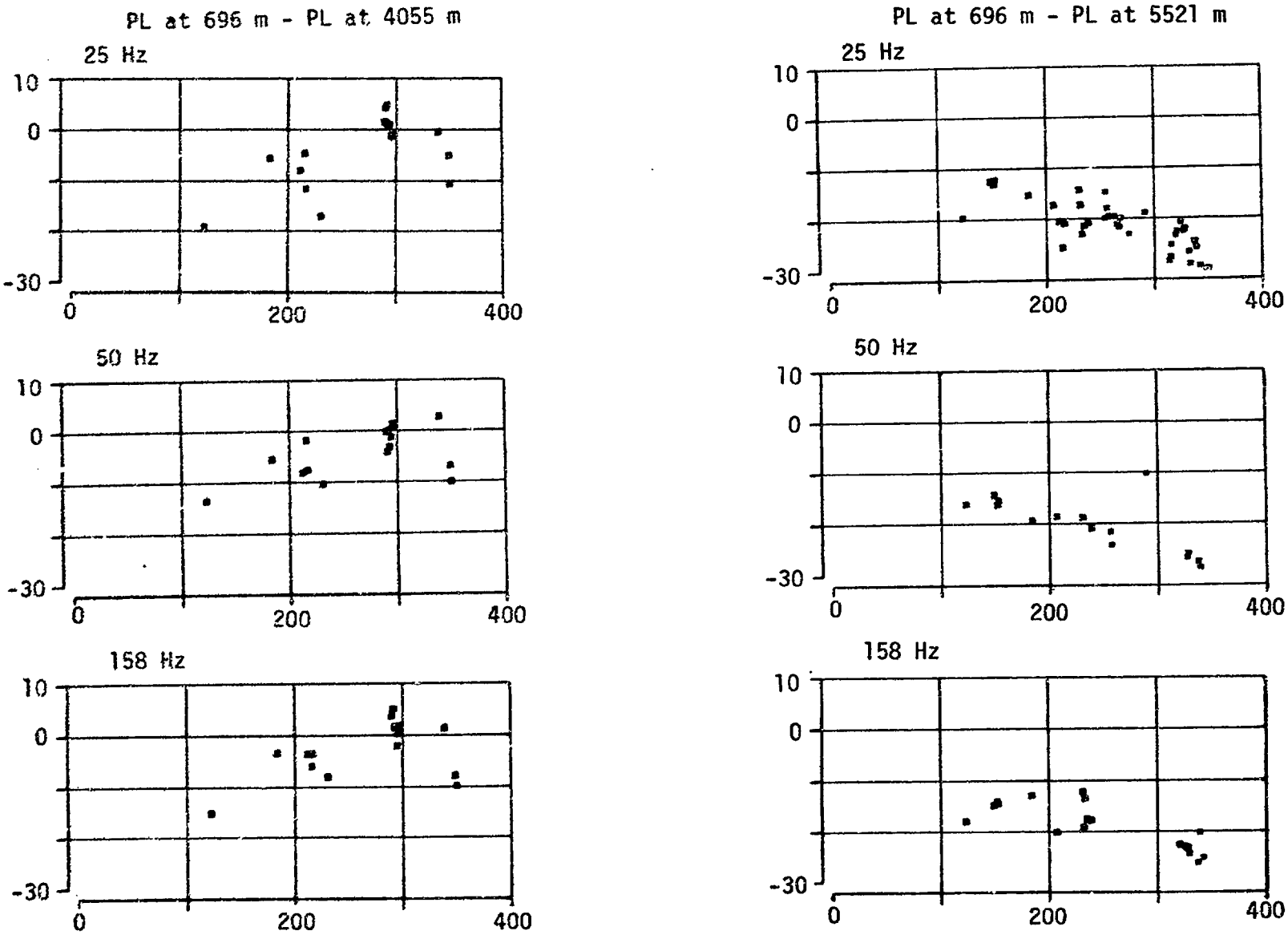

FIGURE IV-16

DIFFERENCE BETWEEN PROPAGATION LOSS TO DIFFERENT RECEIVER DEPTHS
BENT RUN, SOUTH OF SITE C, 91 m SOURCE DEPTH

AS-74-1390

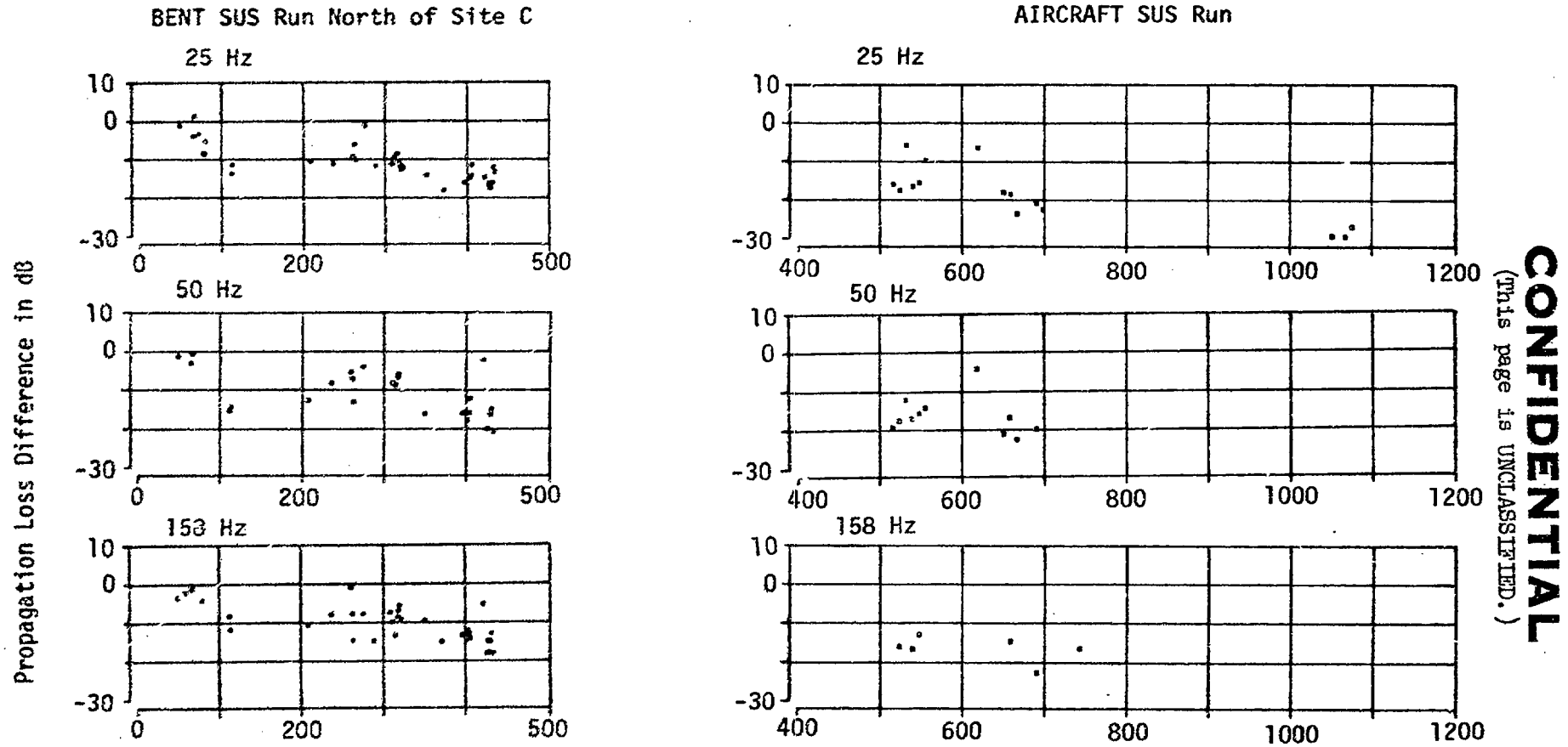

FIGURE IV-17

DIFFERENCE BETWEEN PROPAGATION LOSS AT TWO HYDROPHONES:
PROPAGATION LOSS AT 696 m MINUS PROPAGATION LOSS AT 4055 m
PROPAGATION TO SITE C FROM THE NORTH, 91 m SOURCE DEPTH

AS-74-1391

(C) is larger, the loss being about 10 dB higher at 4055 m than at 696 m. The same general pattern of receiver depth dependence is exhibited by the data for sources north of site C as shown in Fig. IV-17, except that a gradual increase in the difference with range is shown for ranges beyond 300 nm.

(C) The frequency dependence of propagation loss at site C is shown, for the 18 m source depth, in Fig. IV-18 for the 696 m receiver depth and in Fig. IV-19 for the 4055 m receiver depth. Consistent with findings at site A, for the axis depth, loss tends to decrease with increasing frequency for the 18 m source depth both north and south of site C (Fig. IV-18). Loss also decreases with increasing frequency at 4055 m for sources north of site C (Fig. IV-19); however, no consistent difference in loss with frequency is exhibited by the data for sources south of site C. For the 91 m source depth, propagation loss increases with increasing frequency at all receiver depths.

C. ACODAC, Site D

(U) At site D, the sound channel axis depth was 478 m, the critical depth was 2840 m, and the ocean bottom depth is 4646 m. All of the hydrophones at this site are deeper than critical depth, ranging from 3325 m to 4612 m deep. As indicated in Table IV-1, data are described for the hydrophones at depths of 3625, 3925, and 4612 m; these represent distances below the critical depth of 785, 1085, and 1770 m, respectively, with the deepest receiver (4612 m) only 34 m above the sea floor. The overload detector was not working for the hydrophone at 3925 m depth; therefore some of the high level signals probably overloaded the ACODAC system and the data plots are useful for only the high propagation loss data.

(U) The BENT SUS run passed northward over site D and propagation data are available for a range from 0 to 700 nm south of site D and from 0 to 83 nm north of site D. Most of the signals received from north of site D were large enough to overload the ACODAC receiver. The aircraft SUS run

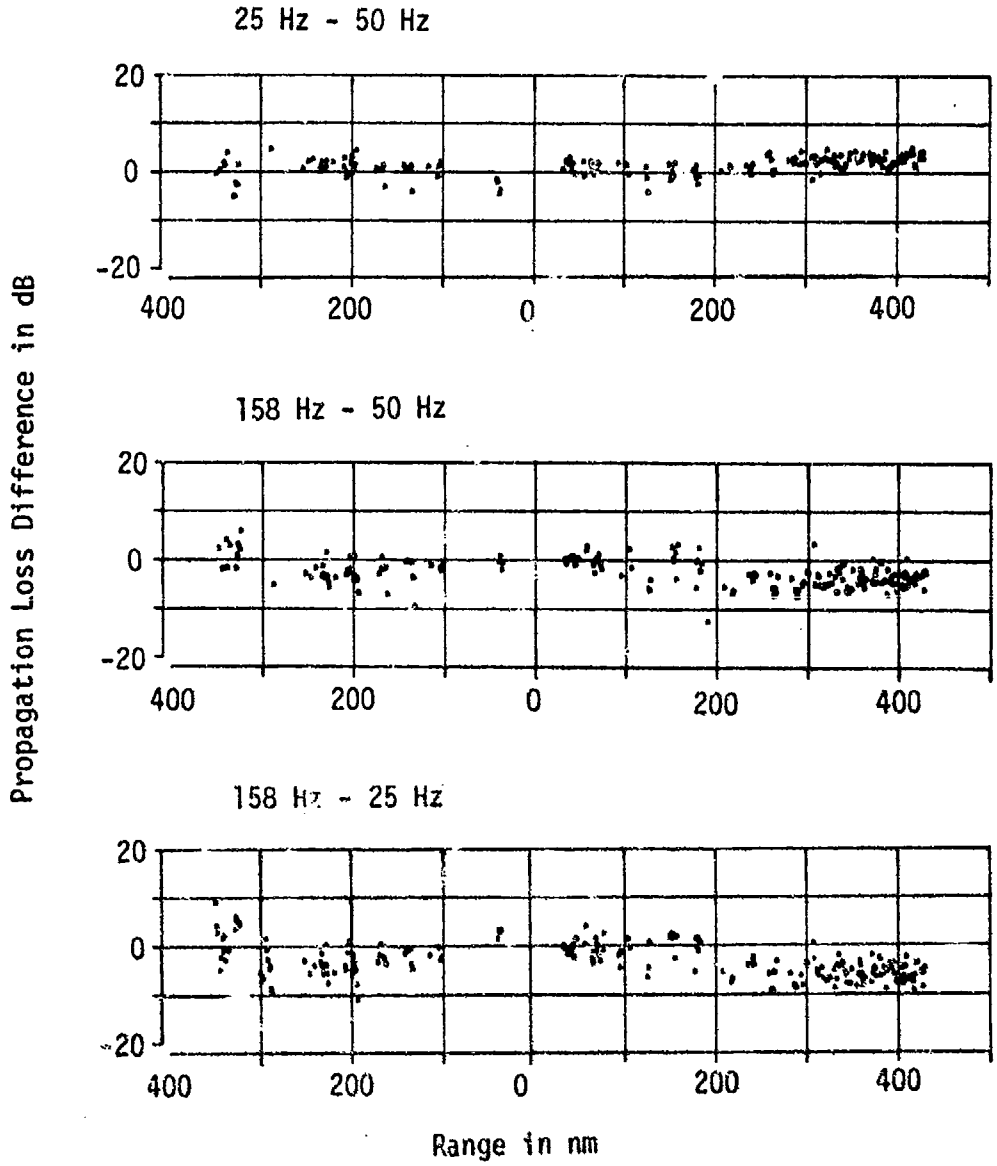

FIGURE IV-18

PROPAGATION LOSS DIFFERENCES BETWEEN THREE FREQUENCIES AT SITE C FOR SOURCE DEPTH OF 18 m AND RECEIVER DEPTH OF 696 m

AS-74-1392

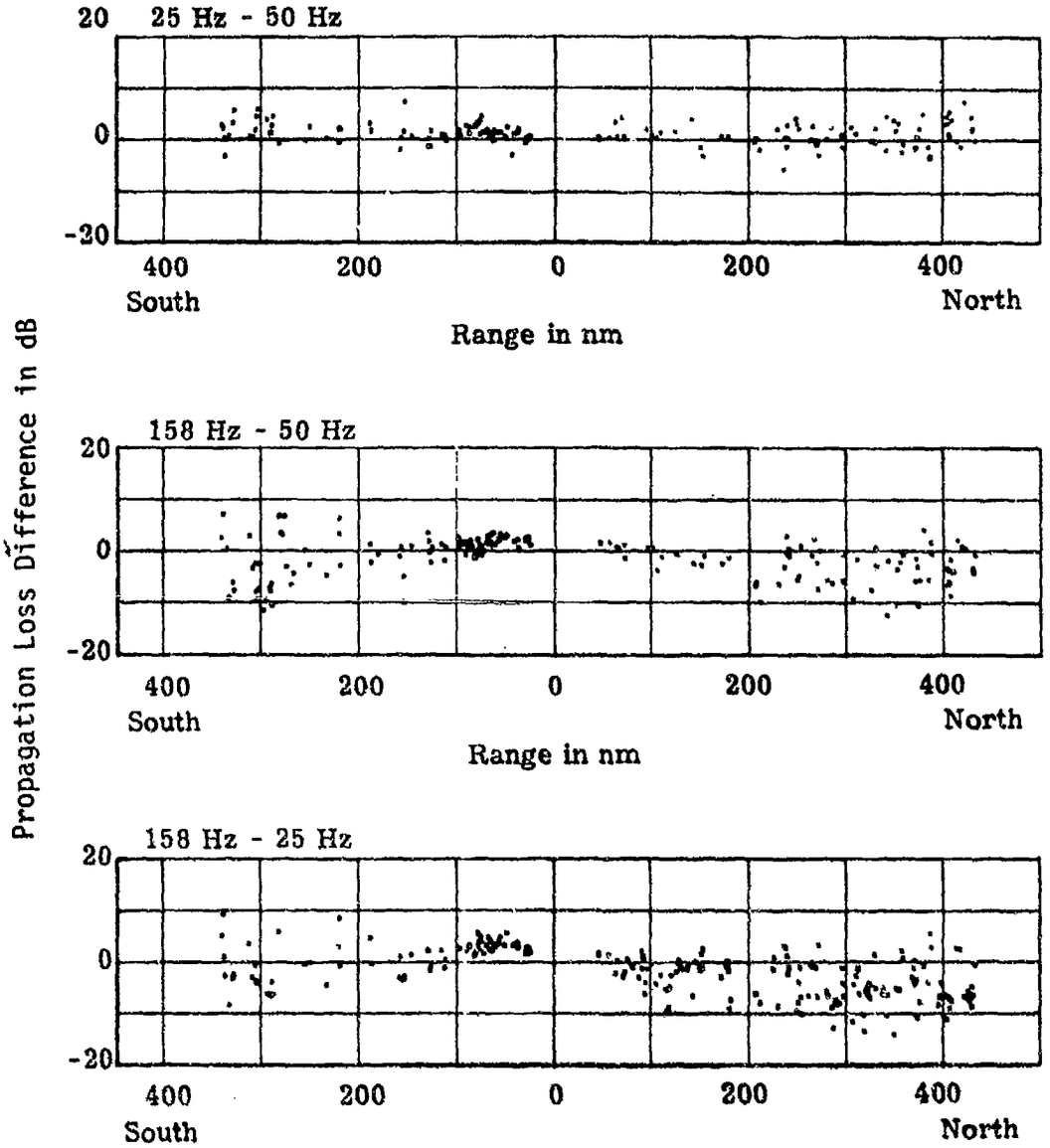

FIGURE IV-19

PROPAGATION LOSS DIFFERENCES BETWEEN
THREE FREQUENCIES AT SITE C FOR SOURCE
DEPTH OF 18 m AND RECEIVER DEPTH OF 4055 m

AS-74-1393

(U) provides propagation data for ranges north of site D from about 90 to 900 nm. The propagation loss to site D from these SUS runs is shown in Appendix A, Figs. A-121 through A-156.

(C) The general nature of the propagation loss versus range at site D is illustrated in Fig. IV-20, which combines data for propagation from south and north of site D for the 91 m source depth and the 4612 m receiver depth at 25 Hz. The 4 nm nominal spacing between shots for the aircraft SUS run (north) provides lower density sampling. Processing of the aircraft run data began at 150 nm range because of overloaded data at shorter ranges. The rapid increase in propagation loss at about 350 nm north and continued low signal levels beyond this range are typical of the data for propagation from north of site D and probably result from partial blockage by Pathfinder Seamount (Fig. II-2).

(C) Figure IV-21 illustrates that at 50 Hz the propagation loss is, in general, higher for the 18 m source depth than for the 91 m source depth; this is also true at 25 Hz. However, as shown in Fig. IV-22, for 158 Hz at the near bottom hydrophone, for ranges less than 300 nm, the maximum signal levels are as much as 8 dB higher for the 18 m source depth than for the 91 m source depth, minimum signal levels being about the same for both source depths. Beyond about 400 nm, the 158 Hz data are similar to those for 25 Hz and 50 Hz in that the 18 m source depth propagation loss is somewhat higher than is the 91 m source depth loss (note the higher incidence of low signal-to-noise ratio for the 18 m source depth). Another notable feature of the 18 m source depth 158 Hz data, for this near bottom receiver, is the large span of values for propagation loss over range intervals of less than 50 nm (convergence zone structure).

(C) For ranges greater than about 200 nm, the propagation loss increases significantly with receiver depth, as shown in Fig. IV-23. This is also evidenced by the higher incidence of overloads at 3625 m and the higher incidence of low signal-to-noise ratios at 4612 m (Fig. IV-23).

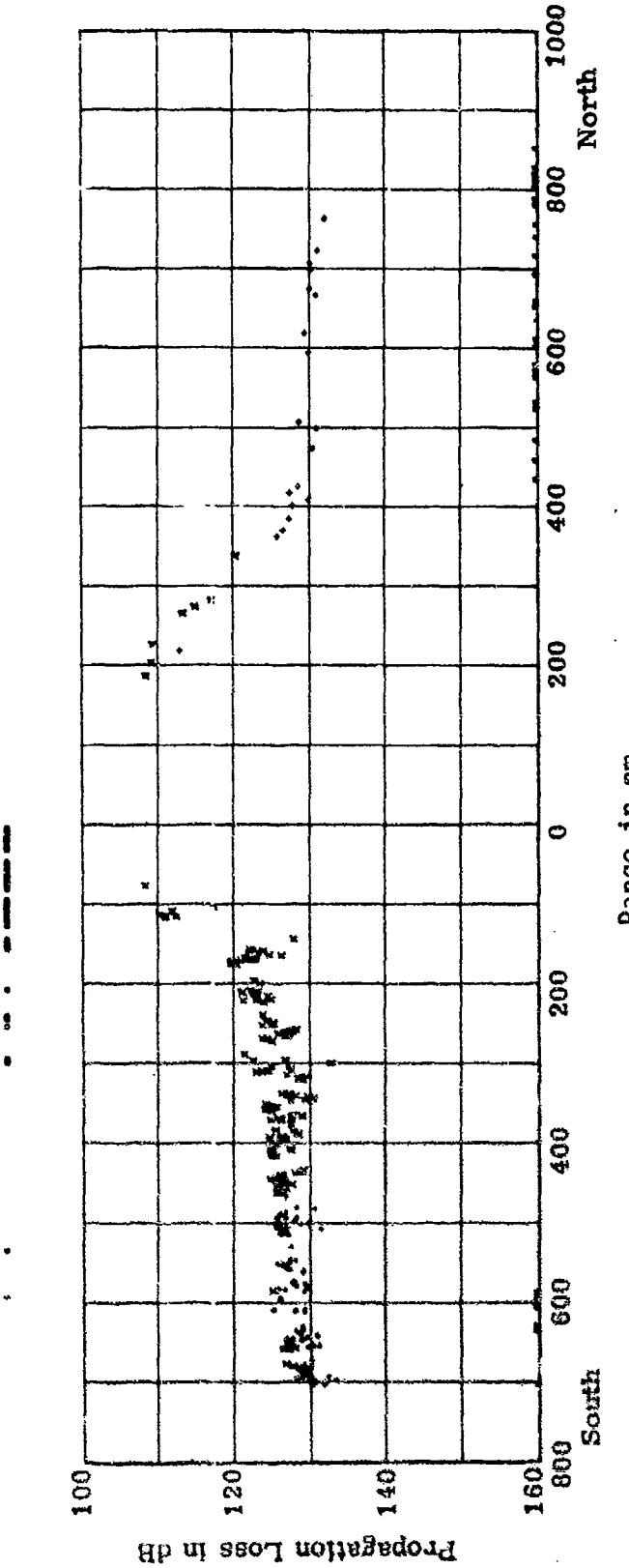

FIGURE IV-20

PROPAGATION LOSS NORTH AND SOUTH OF SITE D AT 25 Hz
FROM 91 m SOURCE TO A RECEIVER AT 4612 m

AS-74-1394

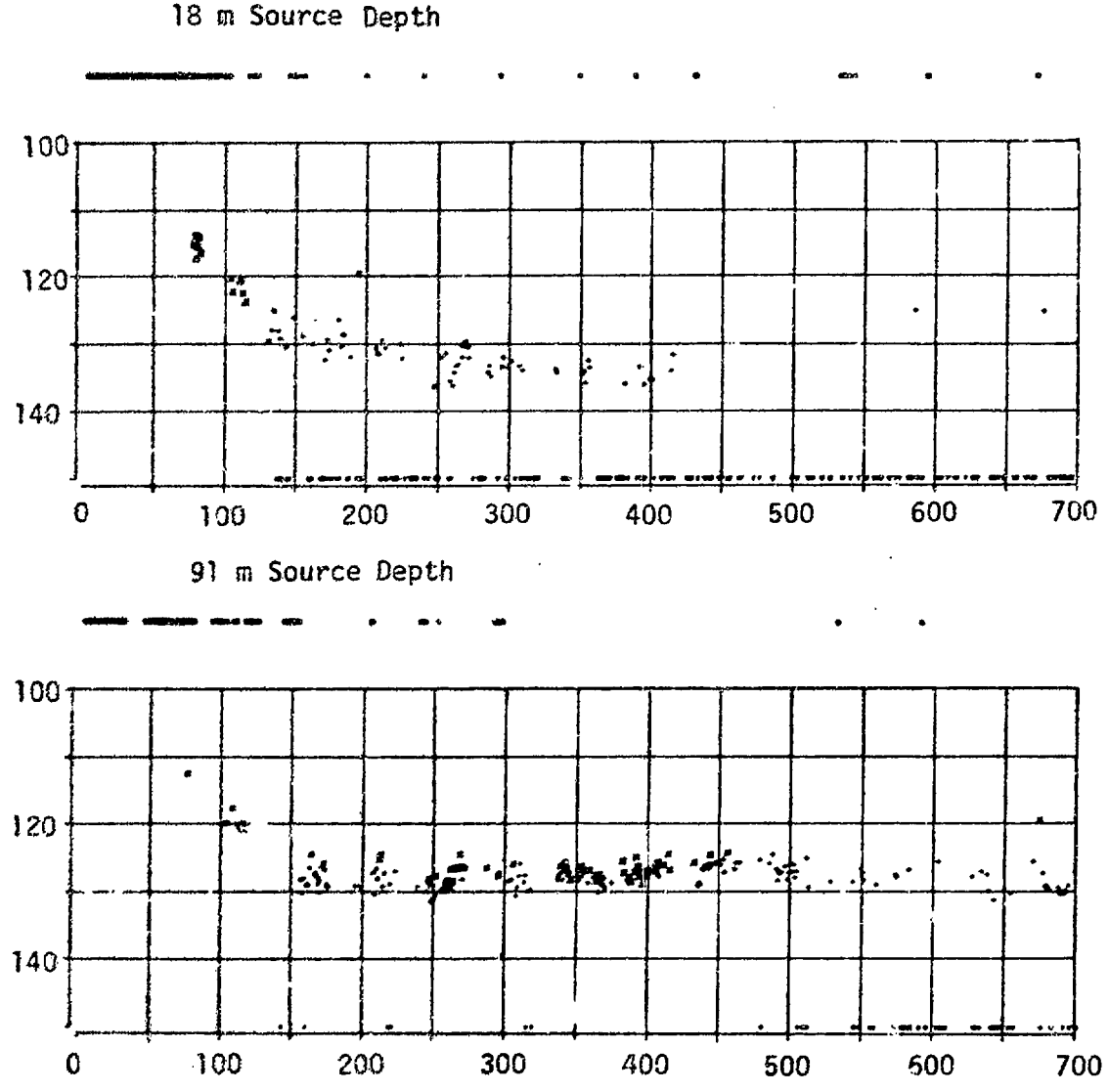

FIGURE IV-21

PROPAGATION LOSS SOUTH OF SITE D AT 50 Hz
FROM AN 18 m AND 91 m SOURCE TO A RECEIVER AT 4612 m

AS-74-1395

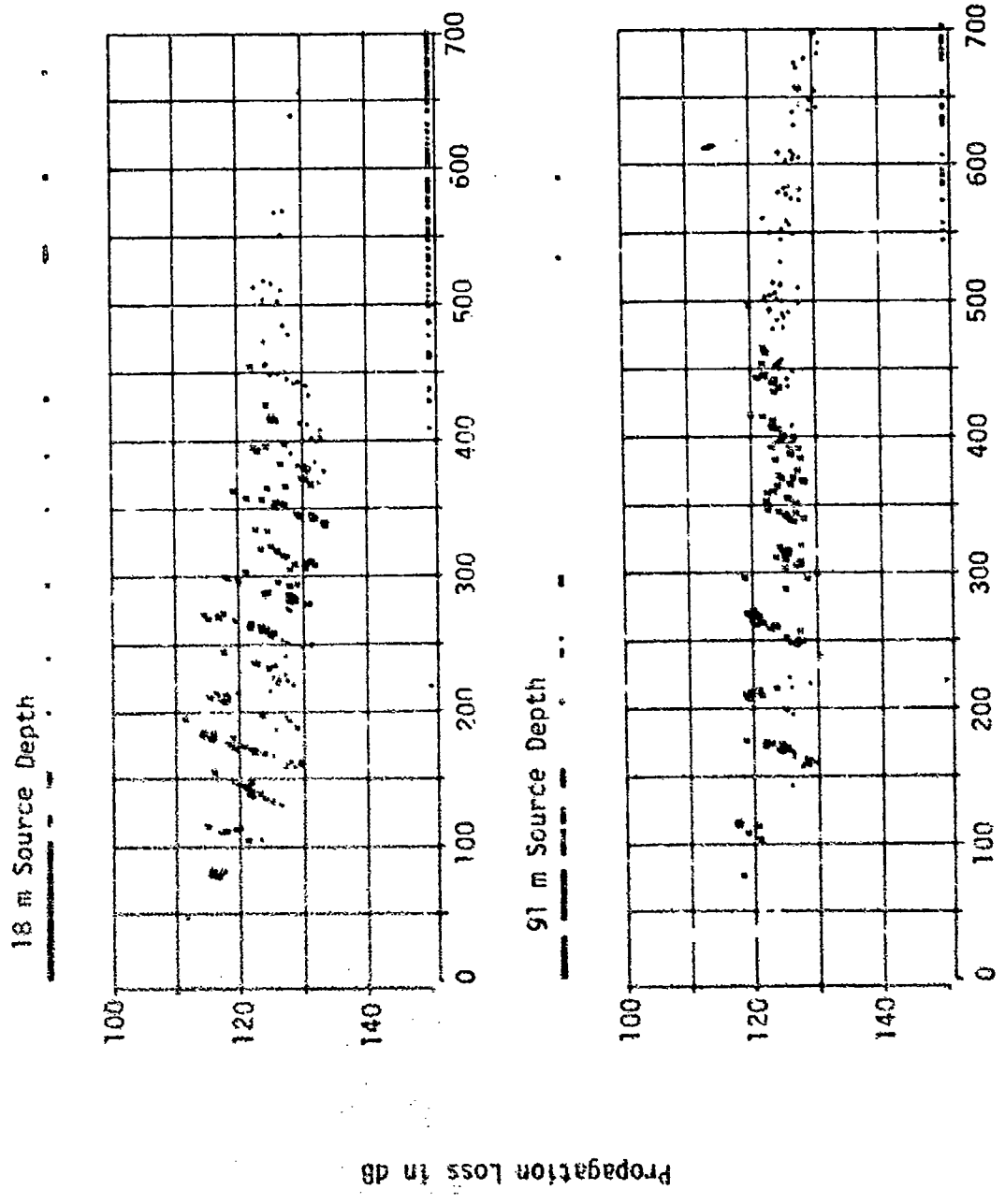

PROPAGATION LOSS SOUTH OF SITE D AT 158.5 Hz FROM
AN 18 m AND 91 m SOURCE TO A RECEIVER AT 4612 m

FIGURE IV-22

AS-74-1396

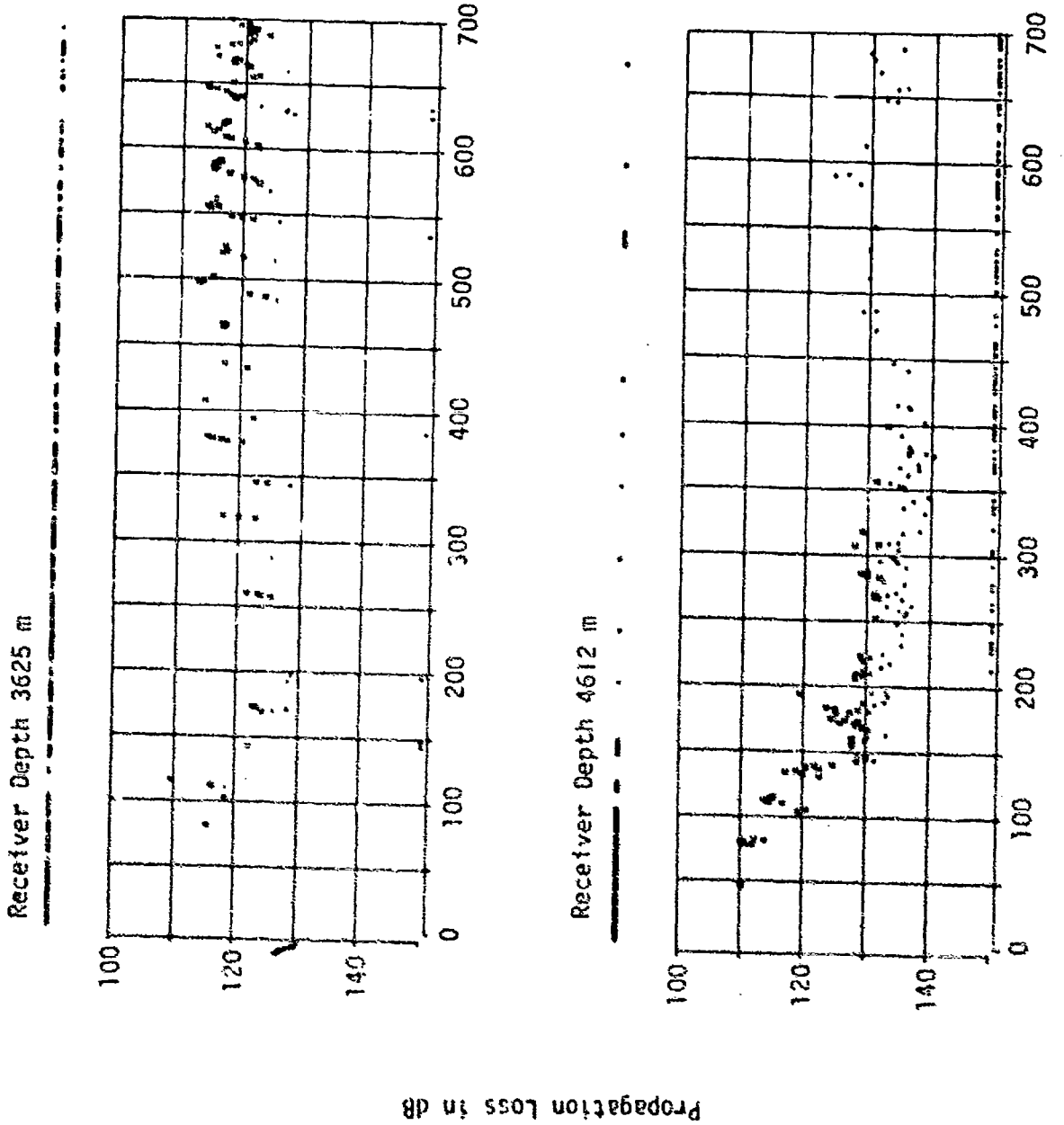

FIGURE IV-23

PROPAGATION LOSS SOUTH OF SITE D AT 25 Hz FROM AN 18 m SOURCE TO TWO RECEIVER DEPTHS

AS-74-1397

(C) With the exception of the previously noted lower minimum propagation loss values for short ranges at 158 Hz for the 18 m source depth and 4612 m receiver depth (Fig. IV-23), no significant frequency dependence is exhibited by the data for site D. An example of this is shown in Fig. IV-24.

D. MESA, Site E

(C) At site E, the MESA hydrophone was at 400 m depth; 10 m above the sound channel axis and 4200 m above the sea floor. Similar to the other receiver locations, site E is on the primary source track (Fig. II-1). The BENT SUS run northward ended at site E and the aircraft source run began near site E. Thus, source-to-receiver ranges vary from 0 to 967 nm south and from 0 to 780 nm north of site E. Propagation loss versus range plots are shown in Appendix B. Figure IV-25 combines the data south of site E for both source depths and frequencies of 25, 50, and 158 Hz. These data, and those for the aircraft run north of site E, illustrate that propagation loss is greater at all frequencies for the 18 m source depth than for the 91 m source depth. The data also indicate that the 18 m source depth propagation loss shows a decrease with increasing frequency while the 91 m source depth propagation loss increases with increasing frequency; however, the difference in propagation loss for the different frequencies is small. This behavior is consistent with ACODAC results for near axis hydrophones

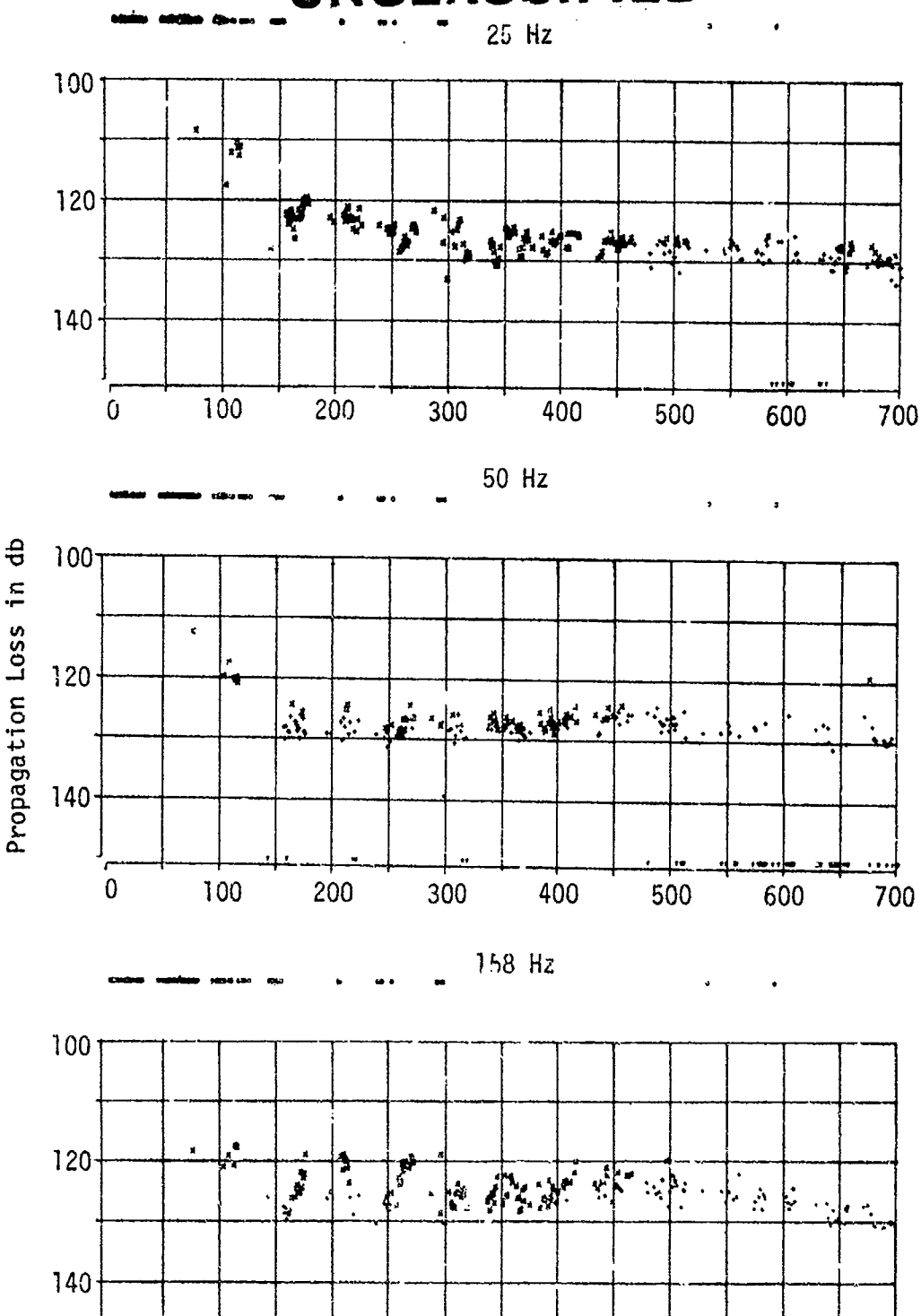

FIGURE IV-24

PROPAGATION LOSS SOUTH OF SITE D AT
THREE FREQUENCIES FROM A 91 m
SOURCE TO RECEIVER AT 4612 m

AS-74-1398

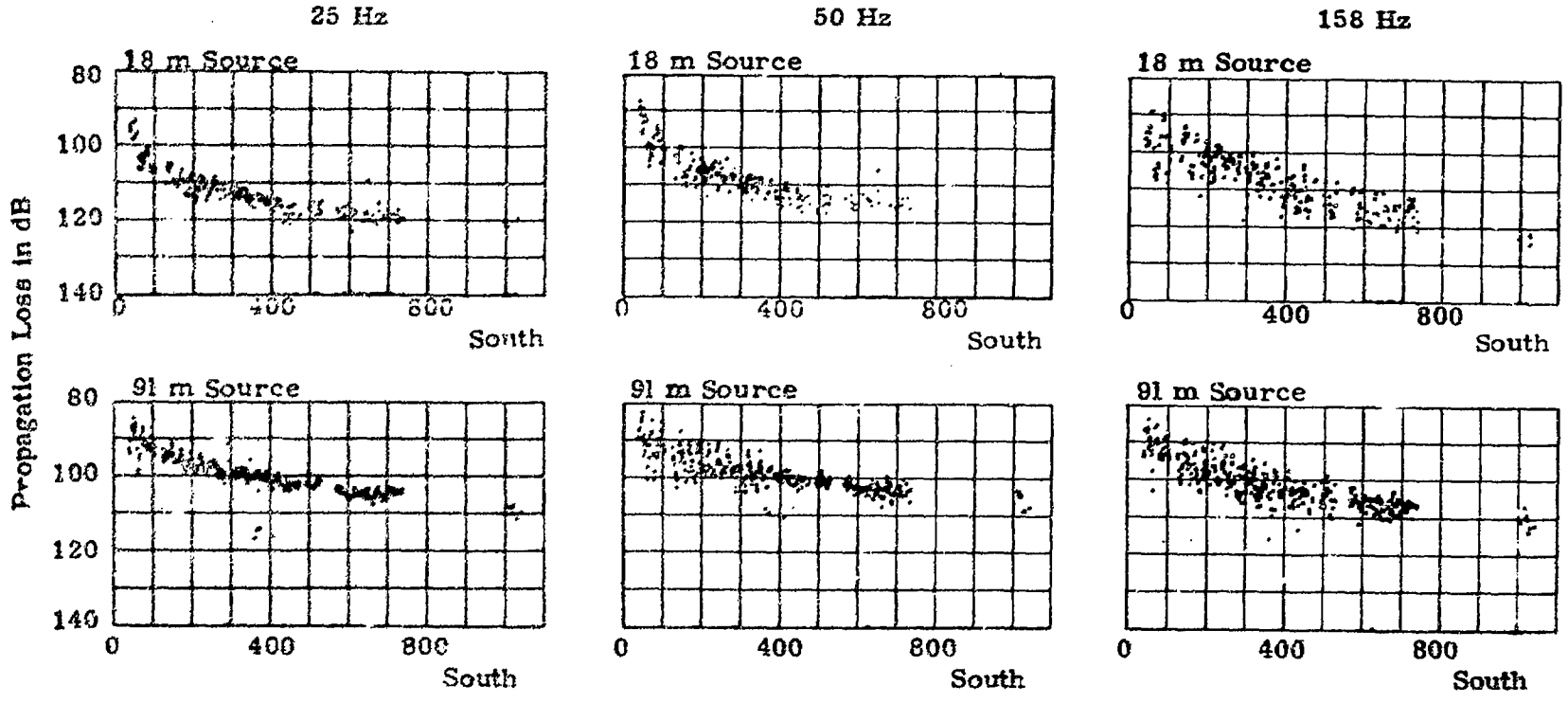

FIGURE IV-25

PROPAGATION LOSS SOUTH OF SITE E AT
THREE FREQUENCIES FROM AN 18 m AND 91 m
SOURCE TO A RECEIVER AT 400 m

V. DISCUSSION OF SIGNAL-TO-NOISE RATIO (S/N)

(U) For the ACODAC data, signal-to-noise ratio (S/N) was computed by dividing the energy in the received SUS signal, within a given frequency band (1 octave at 25 and 50 Hz, 1/3 octave at 158 Hz), by the noise energy within the same band as measured over a 13 sec interval ending 2.5 sec before the SUS signal arrival. Signal-to-noise ratio differences between the signal at the same frequency received at two different hydrophones and between different frequencies for the signal received at the same hydrophone have been computed on a shot-by-shot basis and plotted as a function of range. These are used below to examine the variation of S/N with receiver depth and with frequency. The data shown have all been smoothed by averaging over 10 nm range increments.

(U) The signal-to-noise ratio for the MESA data was computed using 1/3 octave signal-plus-noise and noise only segments of 6.55 sec length (see Section III-I). This S/N has been plotted versus range and composite illustrations of this are used below to examine the variation of S/N with frequency.

A. Variation of Signal-to-Noise Ratio with Receiver Depth

(C) As previously described in Section IV, the signal level generally decreases with increasing receiver depth for a given source depth and range (i.e., propagation loss increases with increasing receiver depth). As described in Ref. 5, the ambient noise intensity level also decreases with increasing receiver depth, but not necessarily at the same rate as the signal level. Consequently, S/N does not necessarily increase or decrease monotonically with depth for a given source-to-receiver geometry. In addition, the ambient noise intensity level at a given depth is nonstationary. Variations in S/N with range can therefore be attributed to variations in propagation loss, variations in noise intensity,

(C) or combinations of these. Computing the S/N difference tends to reduce these variations. The resulting S/N difference curves are useful for noting major trends in the S/N data.

(C) Figure V-1 shows S/N differences between hydrophones located at depths of 4363 m and 4659 m at site A. These data correspond to the 1-octave band centered at 50 Hz and are for the BENT SUS run. As the figure illustrates, S/N difference varies with range, but with no obvious deterministic behavior. The average S/N difference is approximately zero for both the 18 m and 91 m source depth, i.e., on the average the S/N is the same for these two hydrophone depths and for both source depths.

(C) In Fig. V-2, curves of S/N difference versus hydrophone depth are plotted for the three frequency bands centered on 25 Hz (1 octave), 50 Hz (1 octave), and 158 Hz (1/3 octave) for site C where data were processed for hydrophone depths of 696 m, 4055 m, and 5521 m. The data are for an 18 m source depth and they have been smoothed over a 10 nm range increment. For propagation to ranges less than 175 nm (except for a short range segment near 100 nm) S/N at the deeper depth of 5521 m is greater than at the other two depths of 4055 m and 696 m. Beyond 175 nm range, this situation is reversed and S/N is higher for the two shallower hydrophones indicating that the acoustic propagation at long ranges to 5521 m depth is not as efficient as to the depths of 696 m and 4055 m. This same S/N behavior is exhibited at 25 Hz and at 50 Hz at site C for propagation from the 91 m source depth as Fig. V-3 illustrates. Also, for ranges beyond 175 nm, S/N at 696 m is greater than at 4055 m. Thus, for ranges less than the transition range of about 175 nm, the S/N is usually highest for the deepest (near bottom, 5521 m) hydrophone. For longer ranges, S/N decreases with increasing depth from the axis to the critical depth and continues to decrease with depth to the near bottom hydrophone. This is in agreement with the observation of a generally increasing transmission loss with depth for site C as discussed in Section IV. A similar range dependence of the S/N difference with

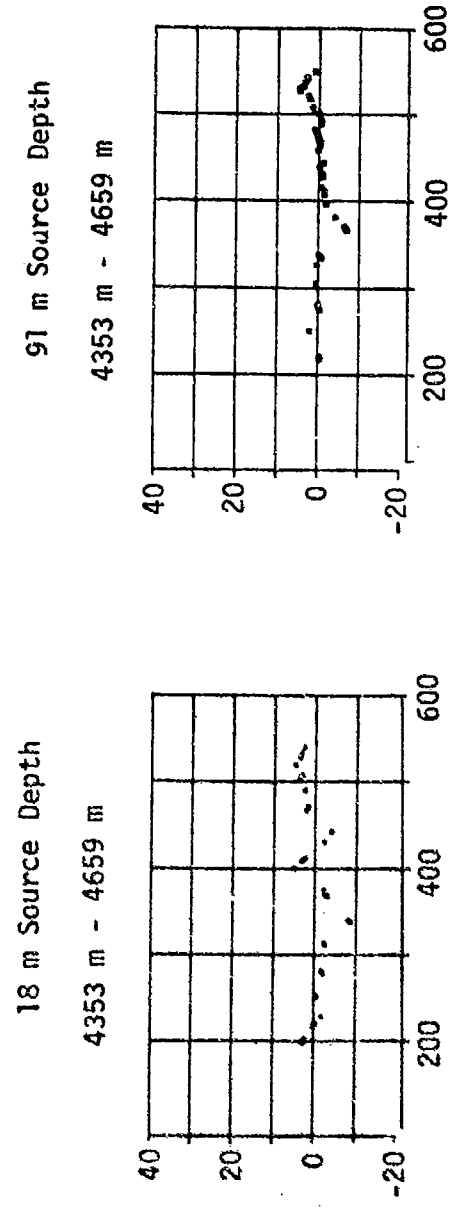

FIGURE V-1

DIFFERENCE IN S/N BETWEEN RECEIVER DEPTHS
SITE A (BENT)
50 Hz

AS-74-1400

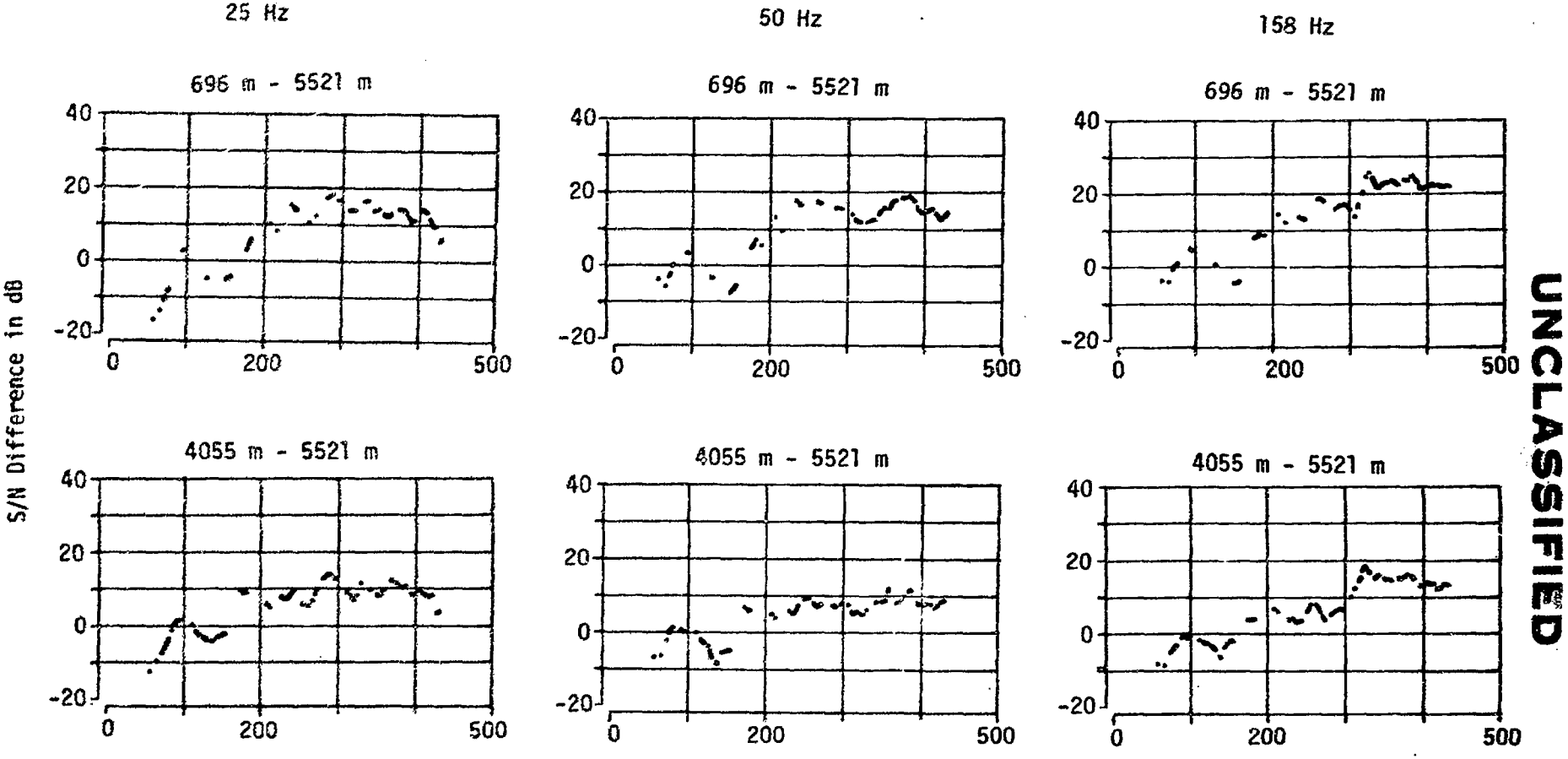

FIGURE V-2

DIFFERENCE IN S/N BETWEEN RECEIVER DEPTHS
SITE C NORTH (BENT)
18 m SOURCE DEPTH

AS-74-1401

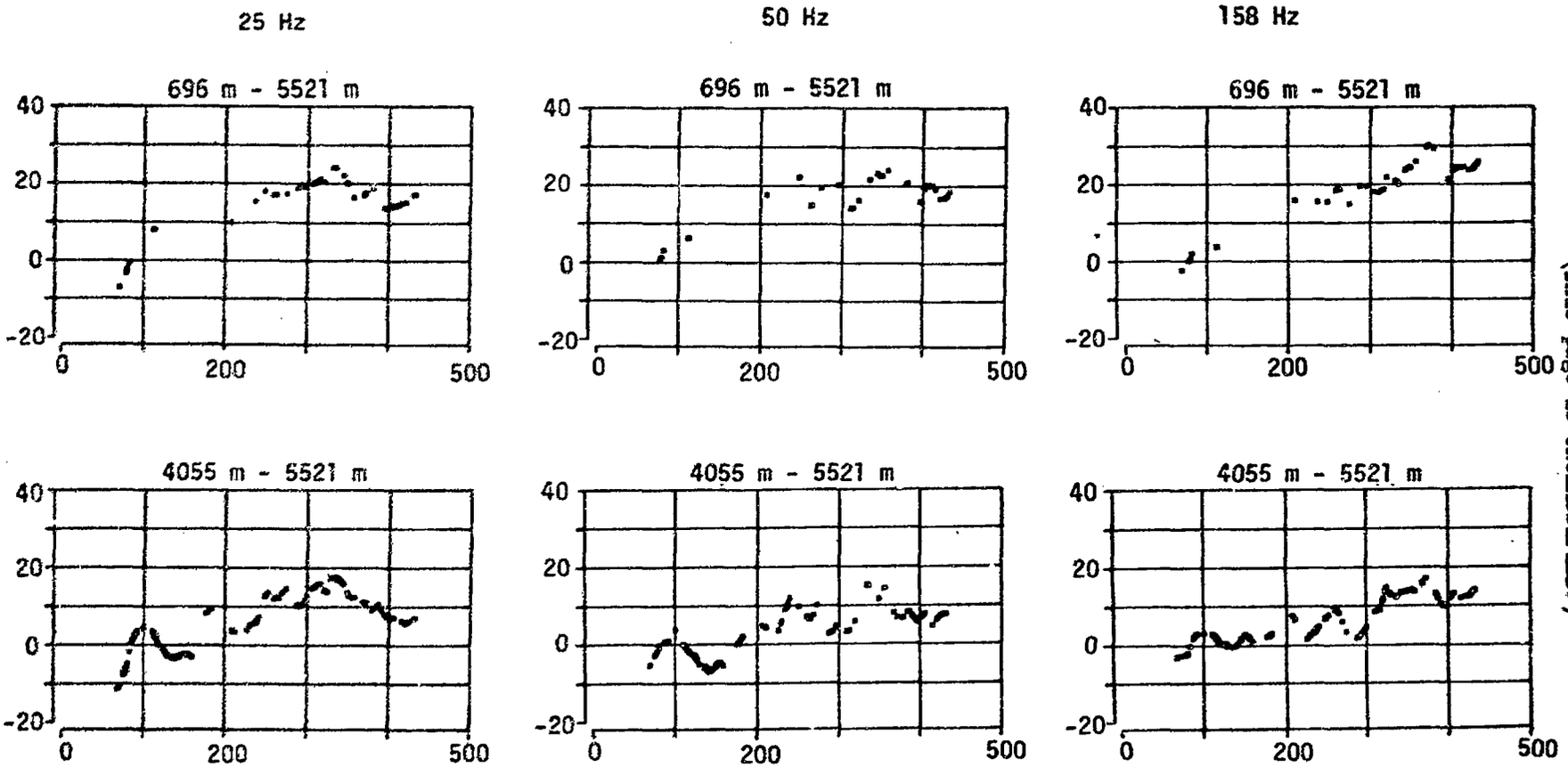

FIGURE V-3

DIFFERENCE IN S/N BETWEEN RECEIVER DEPTHS
SITE C NORTH (BENT)
91 m SOURCE DEPTH

AS-74-1402

CONFIDENTIAL

CONFIDENTIAL
(This page is UNCLASSIFIED.)

(C) depth is exhibited for the BENT run segment south of site C, as shown in Fig. V-4.

(C) For ranges beyond 400 nm north of site C, S/N differences with depth for some of the aircraft SUS run data are shown in Fig. V-5. For the initial range segment, these data support the conclusions previously stated. The leveling off of the S/N difference between the 696 m and 5521 m depth hydrophones corresponds to the observed leveling off of propagation loss at very long ranges for the 5521 m hydrophone depth (the 696 m hydrophone depth propagation loss is almost constant with range, see Section IV). This behavior of the propagation loss at the 5521 m hydrophone depth probably results from reduction of the continually decreasing received SUS signal energy level below the ACODAC receiving system noise. Note, in Section IV and in Appendix A, that for ranges beyond 600 nm north, the signals received on the 5521 m hydrophone at 50 Hz are all rejected because S/N is less than -3 dB. For long ranges, the apparent decrease in S/N difference between that at 4055 m depth and that at 5521 m depth also results from the propagation loss at the deeper hydrophone bottoming out in the system noise while the 4055 m depth propagation loss continues to increase with range.

(C) At site D, the three hydrophones at depths of 3625 m, 3925 m, and 4612 m are all below the critical depth. As Fig. V-6 illustrates, the deepest hydrophone always has the lowest S/N and the difference becomes more significant with increased range. The data suggest the possibility of a transition range of about 100 nm with S/N increasing with depth below critical for shorter ranges. There is not sufficient data for a definitive statement, but such behavior would be consistent with the observations at site C. There is no significant difference in S/N between 3625 m and 3925 m for ranges up to 400 nm for both the 18 m and 91 m source depths. Between 400 and 700 nm range, the S/N at 3625 m depth becomes greater than at 3925 m by as much as 10 dB. For ranges beyond 400 nm, these conclusions are supported by data from site D for the aircraft SUS run as shown by Fig. V-7.

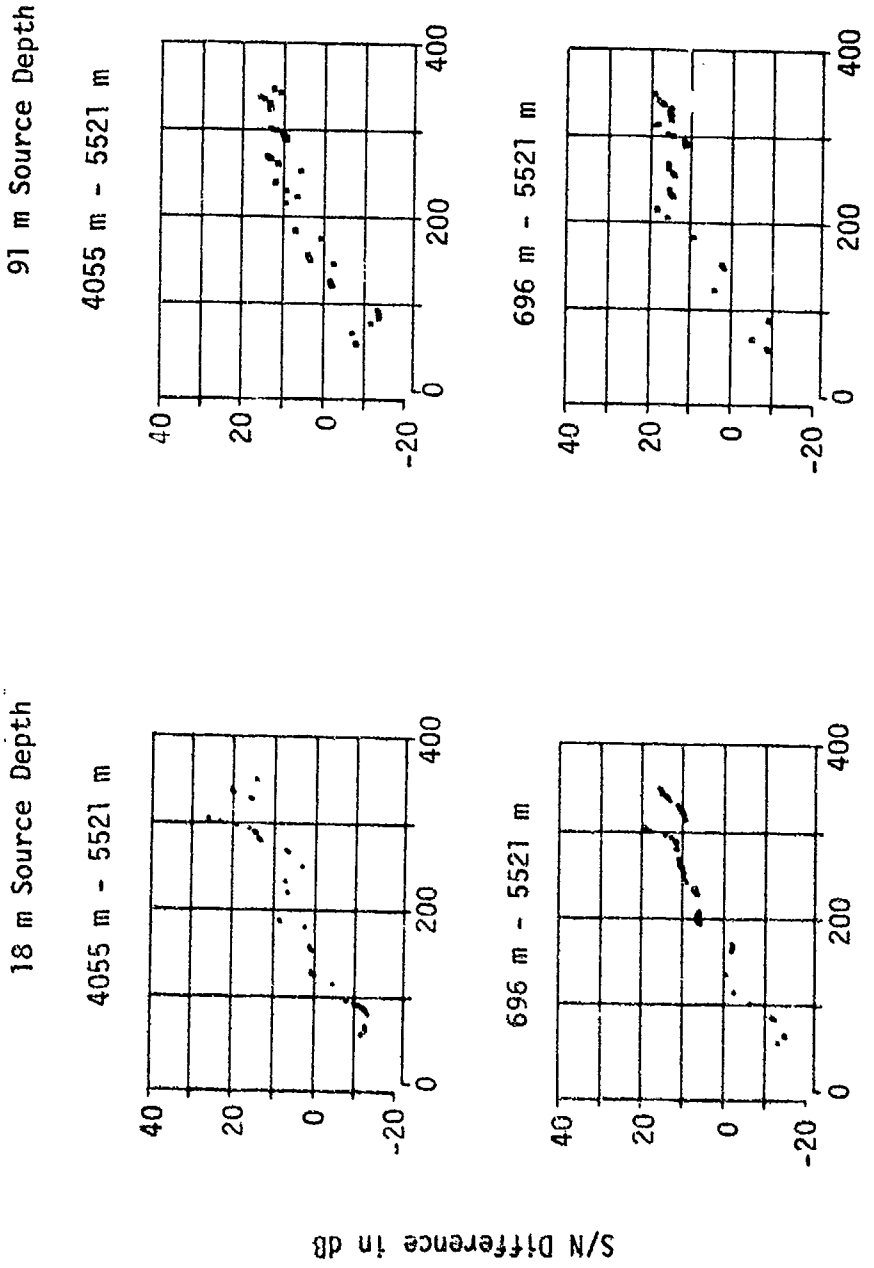

FIGURE V-4

DIFFERENCE IN S/N BETWEEN RECEIVER DEPTHS
SITE C SOUTH (BENT)
50 Hz

AS-74-1403

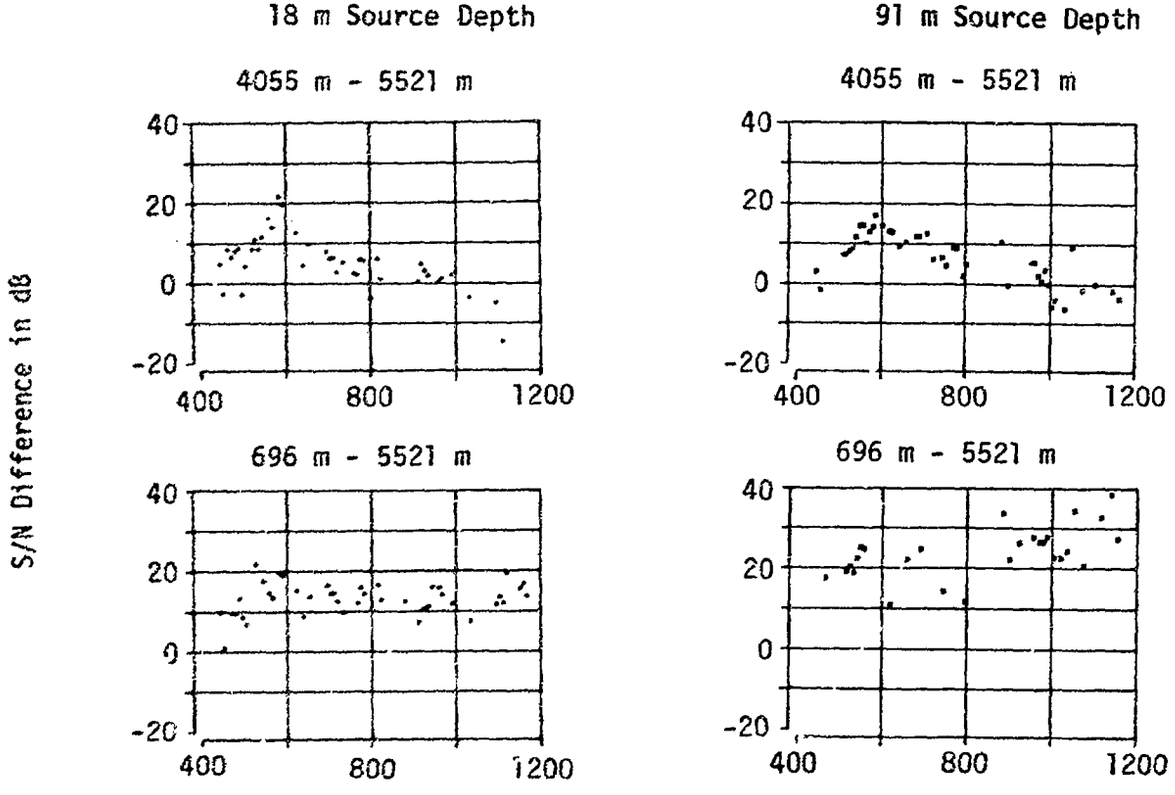

FIGURE V-5

DIFFERENCE IN S/N BETWEEN RECEIVER DEPTHS
SITE C (AIRCRAFT)
50 Hz

AS-74-1404

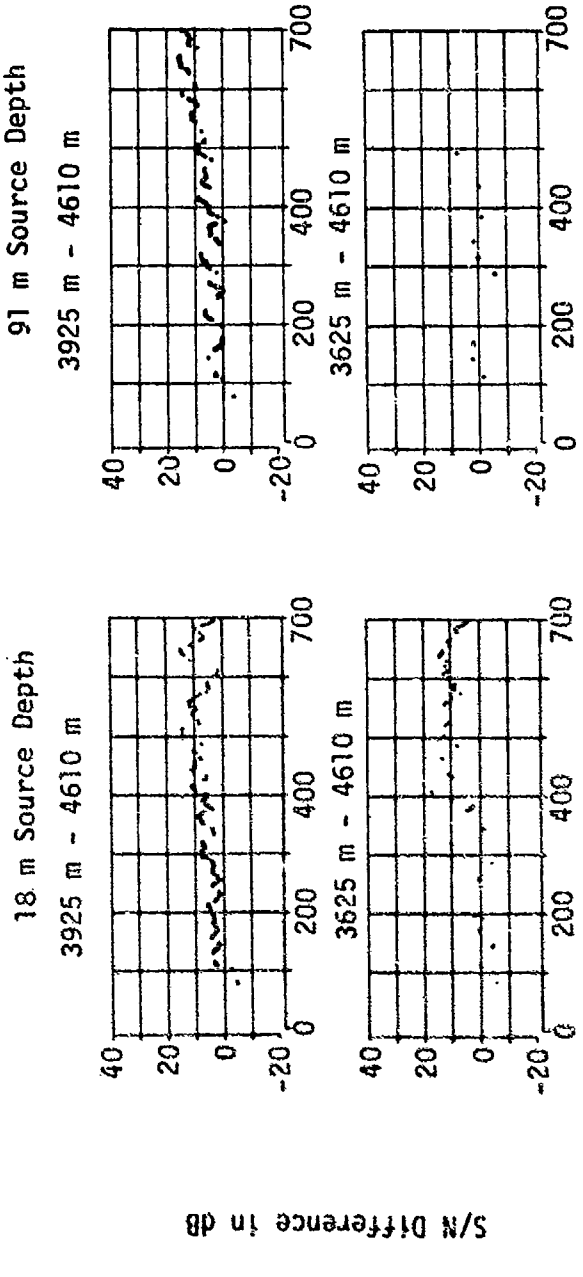

FIGURE V-6

DIFFERENCE IN S/N BETWEEN RECEIVER DEPTHS
SITE D (BENT)
50 Hz

AS-74-1405

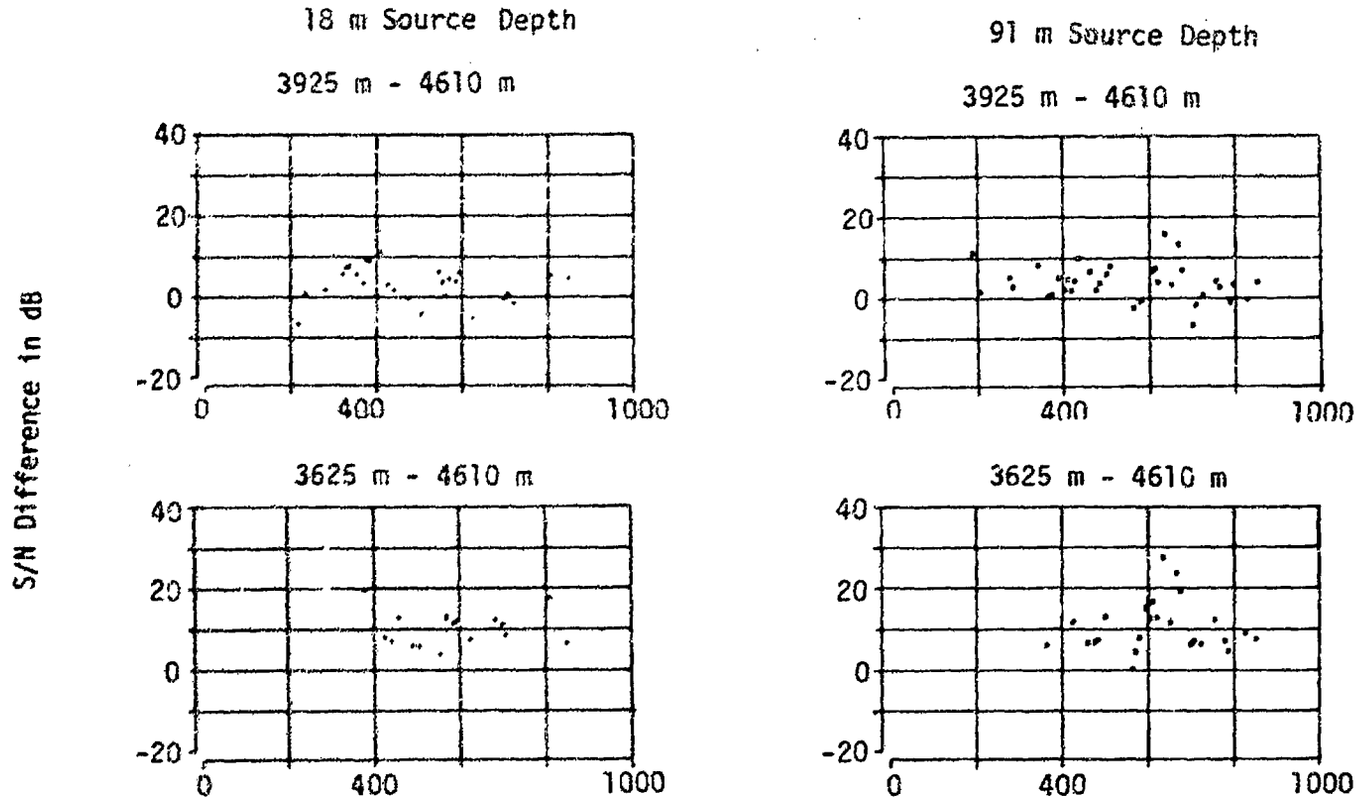

FIGURE V-7

DIFFERENCE IN S/N BETWEEN RECEIVER DEPTHS
SITE D (AIRCRAFT)
50 Hz

AS-74-1406

B. Variation of Signal-to-Noise Ratio with Frequency

(C) The frequency dependence of S/N is illustrated by plotting, versus range, the difference between S/N for two frequencies for given source and receiver depths. For a source at 18 m depth and a receiver at 4659 m depth at site A, the difference between S/N at 25 and 50 Hz and at 158 and 50 Hz is shown in Fig. V-8. The lowest S/N occurs consistently at 50 Hz. At 158 Hz, for the 18 m source depth, S/N is 7 to 10 dB larger than at 50 Hz, while at 25 Hz S/N is only 2 to 3 dB larger. For the 91 m source, the difference between the 25 Hz and 50 Hz S/N, and variability of the difference, increases with range. Similar frequency dependence of S/N is exhibited by the data for other receiver depths at site A.

(C) Frequency dependence of S/N for both source depths and for the 5521 m hydrophone depth at site C is illustrated in Figs. V-9 through V-11. For the deep (91 m) sources, S/N at 25 Hz always exceeds S/N at 50 Hz. For most range segments, this is also true for the shallow (18 m) sources.

(C) At site C, the difference between S/N at 158 Hz and 50 Hz exhibits a similar range dependence for both source depths. For sources south of site C, Fig. V-9 shows that S/N is higher at 50 Hz for ranges less than 175 nm, but S/N at 158 Hz is higher for ranges in excess of 175 nm. Figures V-10 and V-11 show that, for propagation from sources north of site C, S/N at 158 Hz is higher for ranges out to 400 nm beyond which S/N at 50 Hz exceeds that at 158 Hz on the average.

(U) Figures V-12 and V-13 show the frequency dependence of S/N for the 4612 m depth at site D. For propagation from south of the site (Fig. V-12) S/N is almost always less at 50 Hz than at either 25 Hz or 158 Hz. For propagation from the north (Fig. V-13), large fluctuations

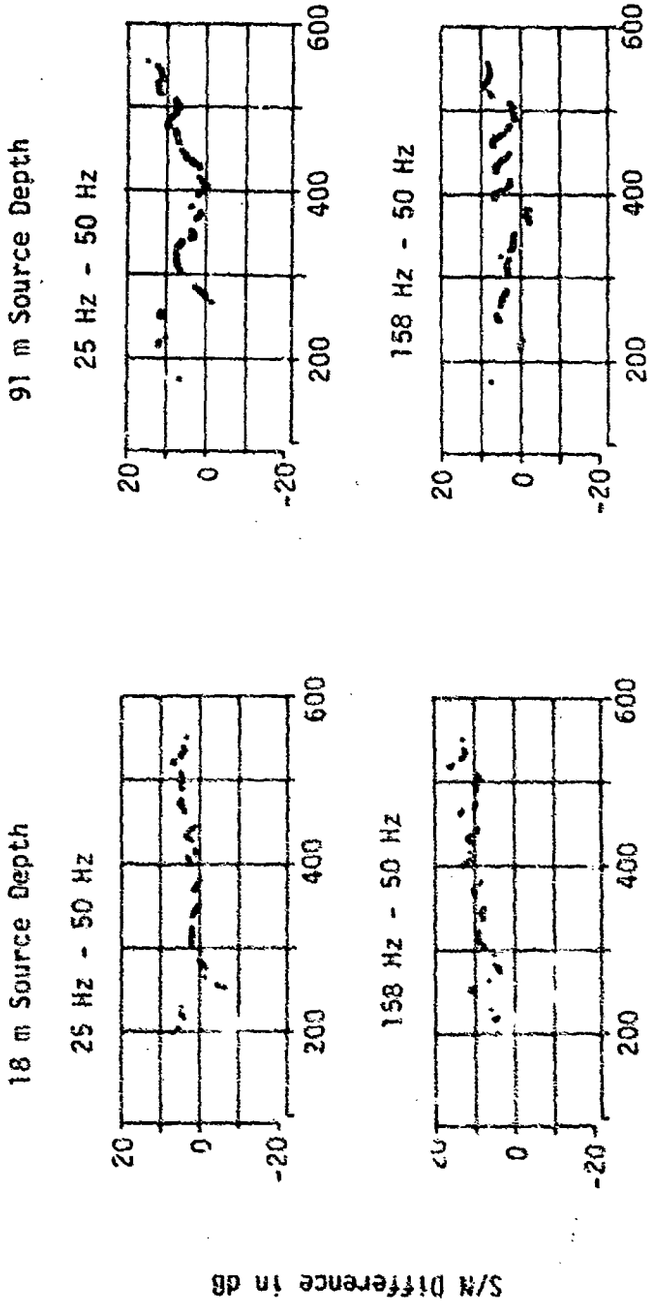

FIGURE V-8

DIFFERENCE IN S/N BETWEEN FREQUENCIES
SITE A (BENT)
RECEIVER DEPTH 4659 m

AS-74-1407

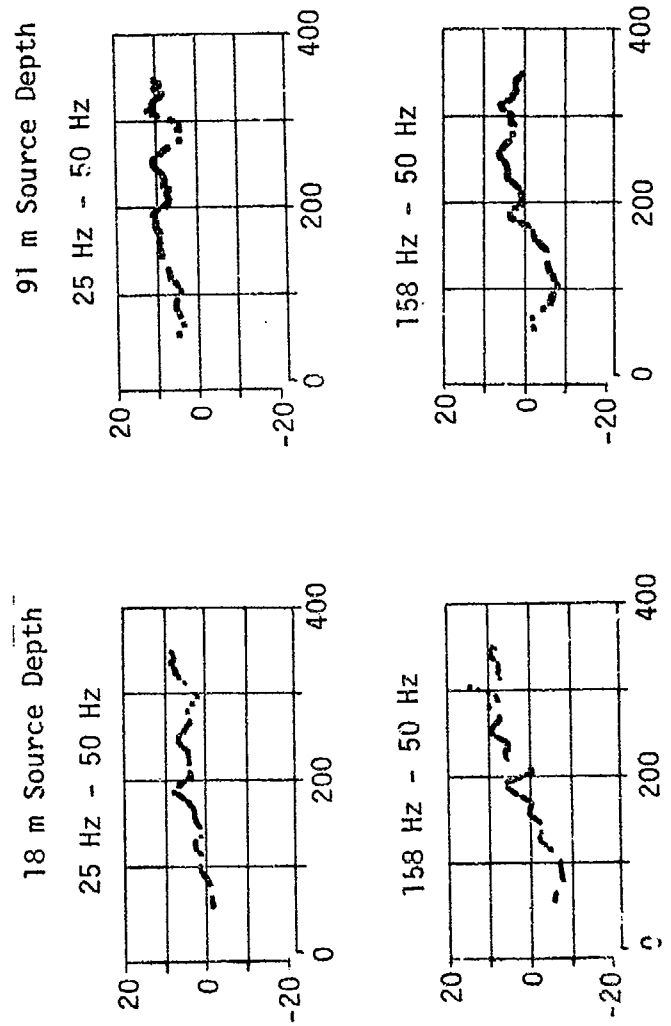

FIGURE V-9

DIFFERENCE IN S/N BETWEEN FREQUENCIES
SITE C SOUTH (BENT)
RECEIVER DEPTH 5521 m

AS-74-1408

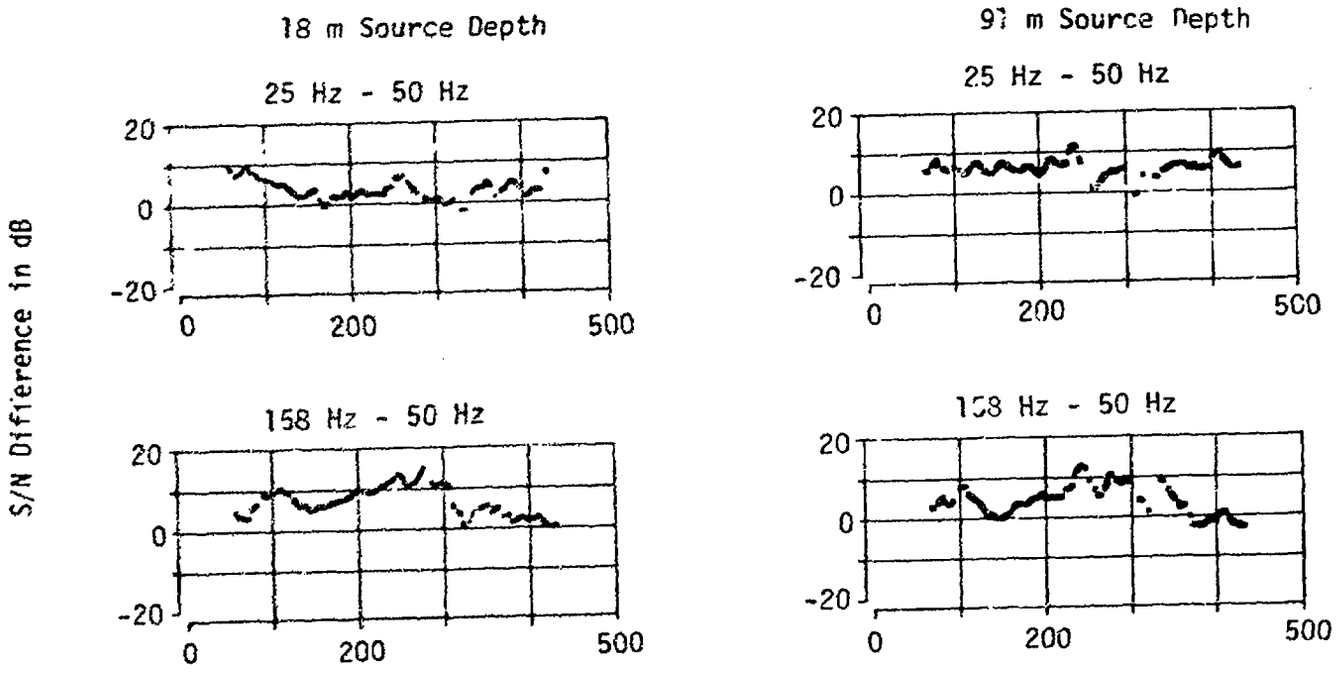

FIGURE V-10

DIFFERENCE IN S/N BETWEEN FREQUENCIES
SITE C NORTH (BENT)
RECEIVER DEPTH 5521 m

AS-74-1409

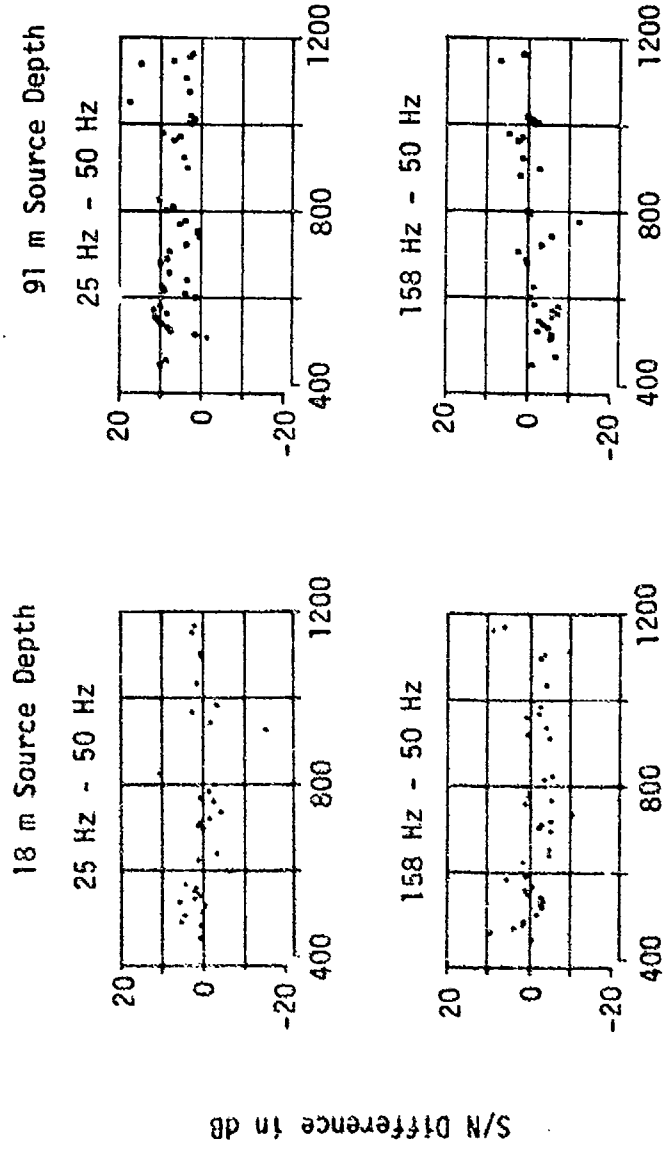

FIGURE V-11

DIFFERENCE IN S/N BETWEEN FREQUENCIES
SITE C (AIRCRAFT)
RECEIVER DEPTH 5521 m

AS-74-1410

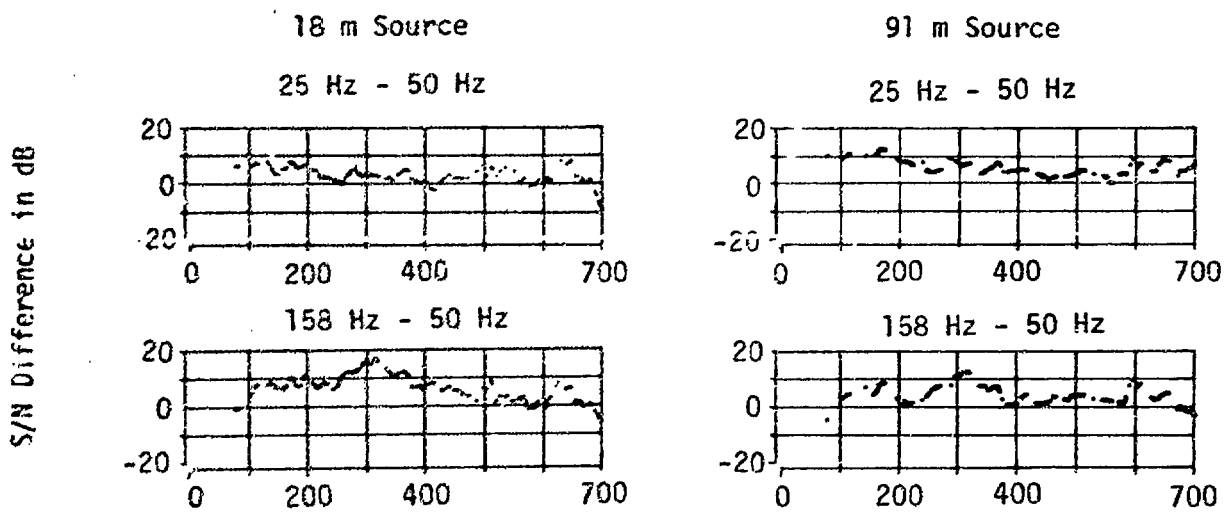

FIGURE V-12

DIFFERENCE IN S/N BETWEEN FREQUENCIES
SITE D (BENT)
RECEIVER DEPTH 4612 m
PROPAGATION FROM SOUTH OF SITE D

AS-74-1411

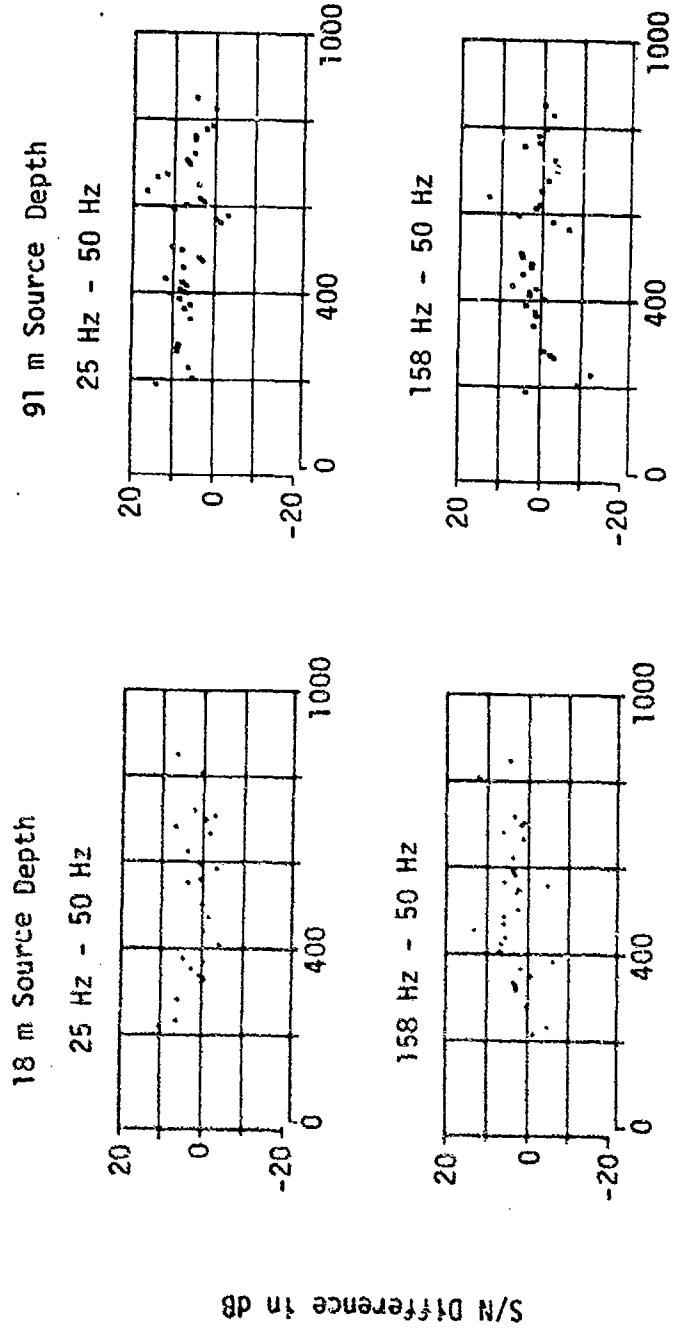

FIGURE V-13

DIFFERENCE IN S/N BETWEEN FREQUENCIES
SITE D (AIRCRAFT)
RECEIVER DEPTH 4610 m
PROPAGATION FROM NORTH OF SITE D

AS-74-1412

(U) in the S/N difference are exhibited, but generally S/N is minimum at 50 Hz.

(C) In agreement with ACODAC results, the MESA data given in Figs. V-14 and V-15 indicate that S/N is minimum at 50 Hz. S/N at 25 Hz and 50 Hz are approximately equal with the exception of the 91 m source depth of the BENT SUS run, for which S/N at 25 Hz is about 5 dB higher than S/N at 50 Hz. For all the MESA data, S/N increases with increasing frequency between 50 and 158 Hz, but decreases with increasing frequency between 158 and 251 Hz. Thus, the maximum S/N occurs at 158 Hz.

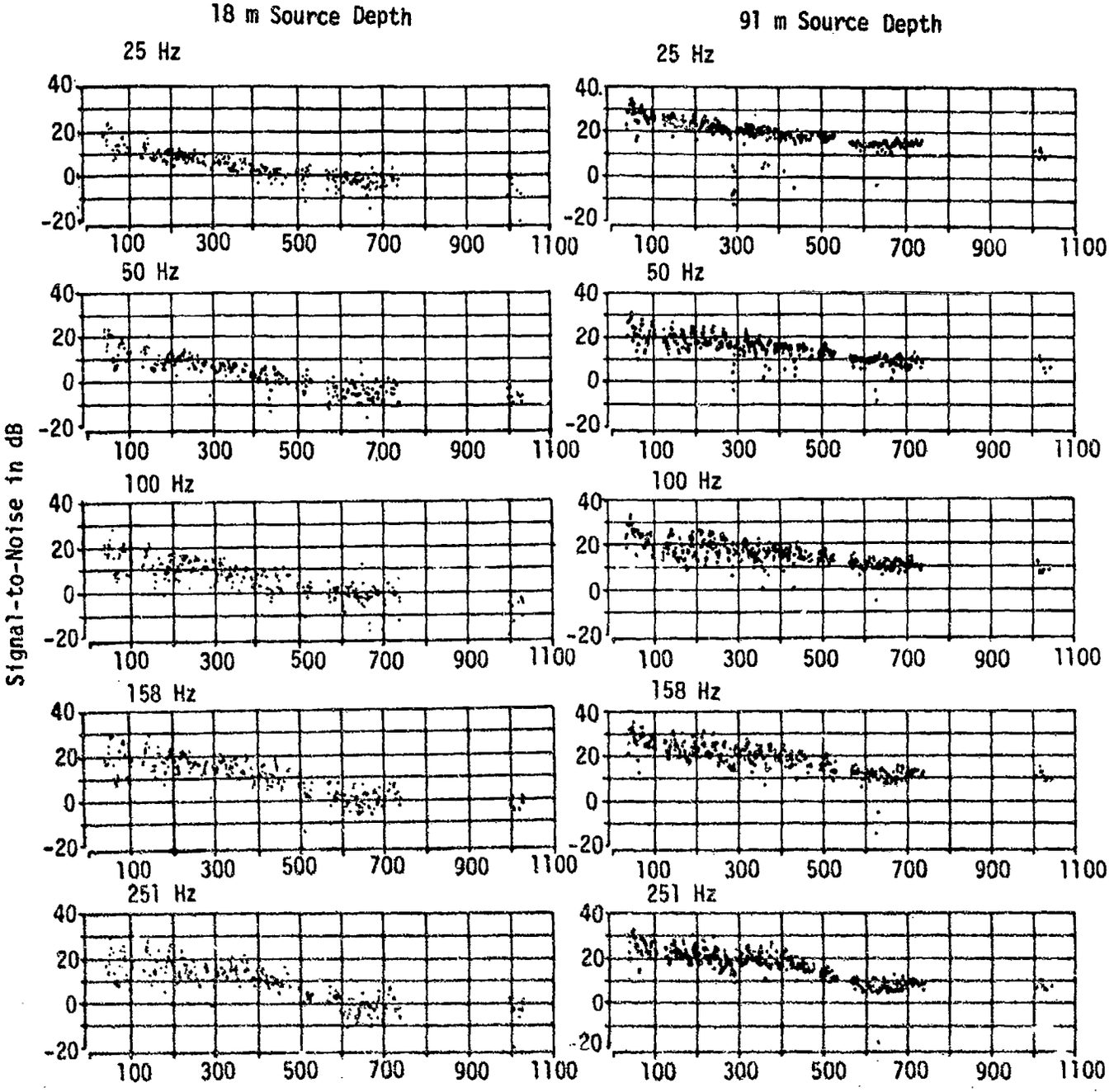

FIGURE V-14

SIGNAL-TO-NOISE RATIO AT SITE E
AT FIVE FREQUENCIES FROM AN 18 m AND 91 m
SOURCE TO A RECEIVER OF 400 m DURING BENT RUN

AS-74-1422

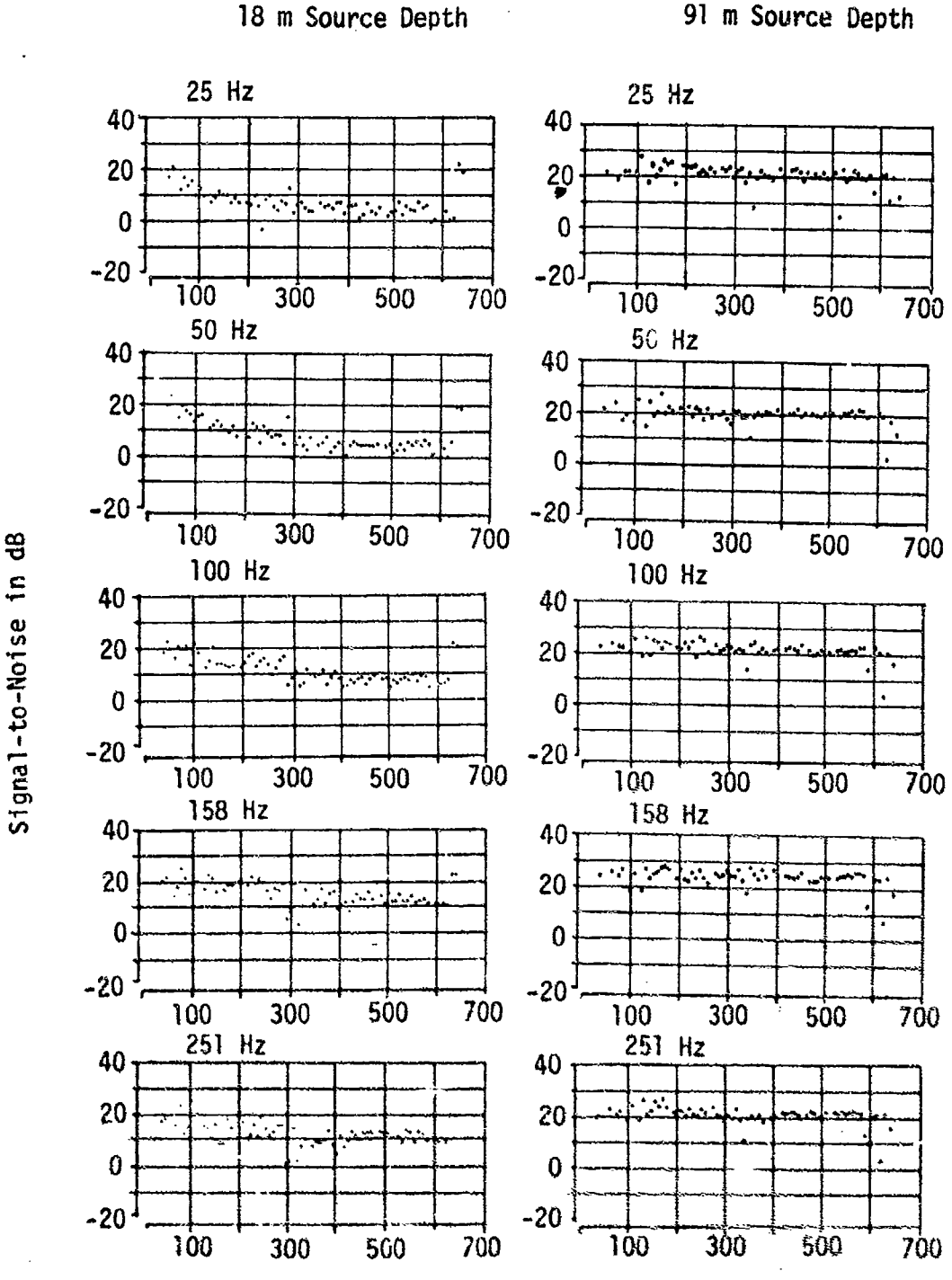

FIGURE V-15

SIGNAL-TO-NOISE RATIO AT SITE E
AT FIVE FREQUENCIES FROM AN 18 m AND 91 m
SOURCE TO A RECEIVER OF 400 m DURING AIRCRAFT RUN

AS-74-1423

(U) REFERENCES

1. "CHURCH ANCHOR Exercise Plan" (U), Long Range Acoustic Propagation Project, Ocean Science Program, Maury Center for Ocean Science, Department of the Navy, Washington, D.C., June 1973. (CONFIDENTIAL)

2. "CHURCH ANCHOR Synopsis Report" (U), Long Range Acoustic Propagation Project, Ocean Science Program, Maury Center for Ocean Science, Department of the Navy, Washington, D.C., December 1973. (SECRET)

3. J. B. Gaspin, and V. K. Shuler, "Source Levels of Shallow Underwater Explosions," NOLTR-71-160, Naval Ordnance Laboratory, White Oak, Silver Spring, Maryland, 1971.

4. "CHURCH ANCHOR Data Analysis Plan" (U). Long Range Acoustic Propagation Project, Ocean Science Program, Maury Center for Ocean Science, Department of the Navy, Washington, D.C., October 1974. (CONFIDENTIAL)

5. J. Hoffman, "CHURCH ANCHOR Ambient Noise Report" (U), Texas Instruments, Dallas, Texas, May 1974. (CONFIDENTIAL)

6. "SUS Quality Assessment," Underwater Systems Inc., Silver Spring, Maryland, December 1973 (revised June 1974).

(The reverse of this page is blank.)

APPENDIX A

ACODAC PROPAGATION LOSS DATA

(U) The propagation loss, computed as described in section III, is shown versus range in nautical miles in Figs. A1 through A156. Different symbols are used to indicate the signal-to-noise ratio (S/N) for each data point:

the symbol ✕ indicates that S/N exceeds +3 dB, but the signal is not overloaded;

the symbol + indicates that S/N is less than +3 dB but greater than 0 dB; and

the symbol • indicates that S/N is less than 0 dB but greater than -3 dB.

The range of detection for signals detected with S/N less than -3 dB is shown by plotting the symbol ∇ on the bottom of the figure. Similarly, a shot which triggered the overload signal is indicated by plotting the symbol 0 at the top of the figure at the range of detection.

(U) The following three pages each contain a table for one of the ACODAC sites indicating the figure number assigned in this appendix to the propagation loss plot for each source event, hydrophone depth, frequency, and source depth.

(U) Though not shown in this appendix, analyzed propagation data are available on digital magnetic tape for 1/3 octave band analysis at frequencies of 25, 50, 100, and 250 Hz.

The data presented in this appendix are
UNCLASSIFIED

TABLE A1

SITE A, ACODAC

Figure Number for Source Depth 18 m, 91 m

Source Event	Hydrophone Depth (m)	Center Frequency (Hz)//Bandwidth (octave)		
		25//1	50//1	158//1/3
30 Bartlett Source Run	749	A1, A2	A7, A8	A13, A14
	4353	A3, A4	A9, A10	A15, A16
	4659	A5, A6	A11, A12	A17, A18
31 BENT Source Run	4353	A19, A20	A23, A24	A27, A28
	4659	A21, A22	A25, A26	A29, A30

TABLE A2

SITE C, ACODAC

Figure Number for Source Depth 18 m, 91 m

Source Event	Hydrophone Depth (m)	Center Frequency (Hz)// Bandwidth (octave)		
		25//1	50//1	158//1/3
30 BARTLETT Source Run	696	A31, A32	A37, A38	A43, A44
	4055	A33, A34	A39, A40	A45, A46
	5521	A35, A36	A41, A42	A47, A48
31 BENT RUN South of Site C	696	A49, A50	A55, A56	A61, A62
	4055	A51, A52	A57, A58	A63, A64
	5521	A53, A54	A59, A60	A65, A66
31 BENT RUN North of Site C	696	A67, A68	A73, A74	A79, A80
	4055	A69, A70	A75, A76	A81, A82
	5521	A71, A72	A77, A78	A83, A84
32 AIRCRAFT Source Run	696	A85, A86	A91, A92	A97, A98
	4055	A87, A88	A93, A94	A99, A100
	5521	A89, A90	A95, A96	A101, A102

TABLE A3

SITE D, ACODAC

Figure Number for Source Depth 18 m, 91 m

Source Event	Hydrophone Depth (m)	Center Frequency (Hz)// Bandwidth (octave)		
		25//1	50//1	158//1/3
30 BARTLETT Source Run	3625	A103, A104	A109, A110	A115, A116
	*3925	A105, A106	A111, A112	A117, A118
	4612	A107, A108	A113, A114	A119 A120
31 BENT Source Run	3625	A121, A122	A127, A128	A133, A134
	*3925	A123, A124	A129, A130	A135, A136
	4612	A125, A126	A131, A132	A137, A138
32 AIRCRAFT Source Run	3625	A139, A140	A145, A146	A151, A152
	*3925	A141, A142	A147, A148	A153, A154
	4612	A143, A144	A149, A150	A155, A156

*The ACODAC overload detector was not working on this channel; therefore the low propigation loss data points in these plots may include distorted (overloaded) signals.

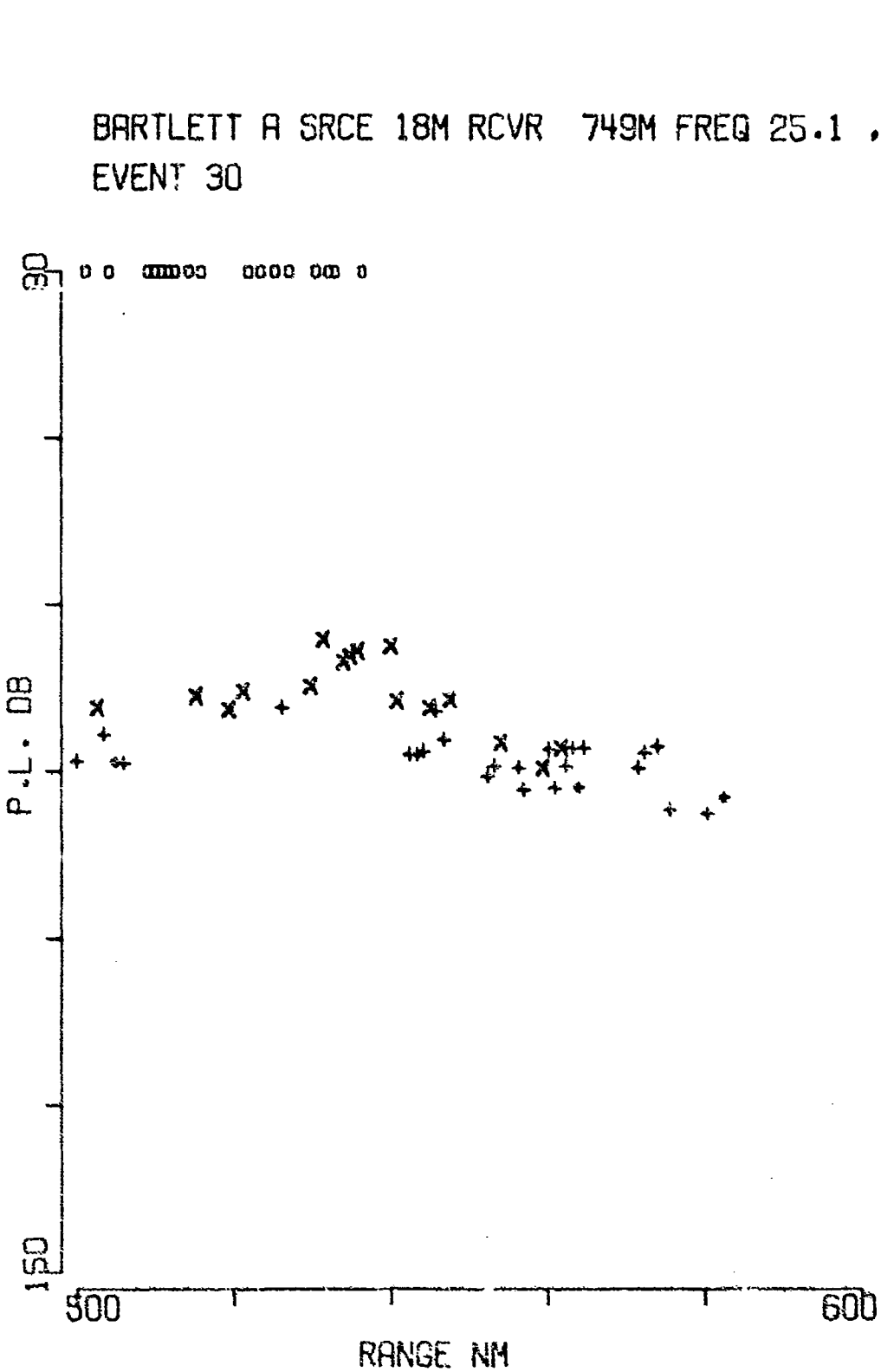
BARTLETT A SRCE 18M RCVR 749M FREQ 25.1 .1 OCT
EVENT 30
30
150
P.L. DB
500
600
RANGE NM

FIGURE A-1

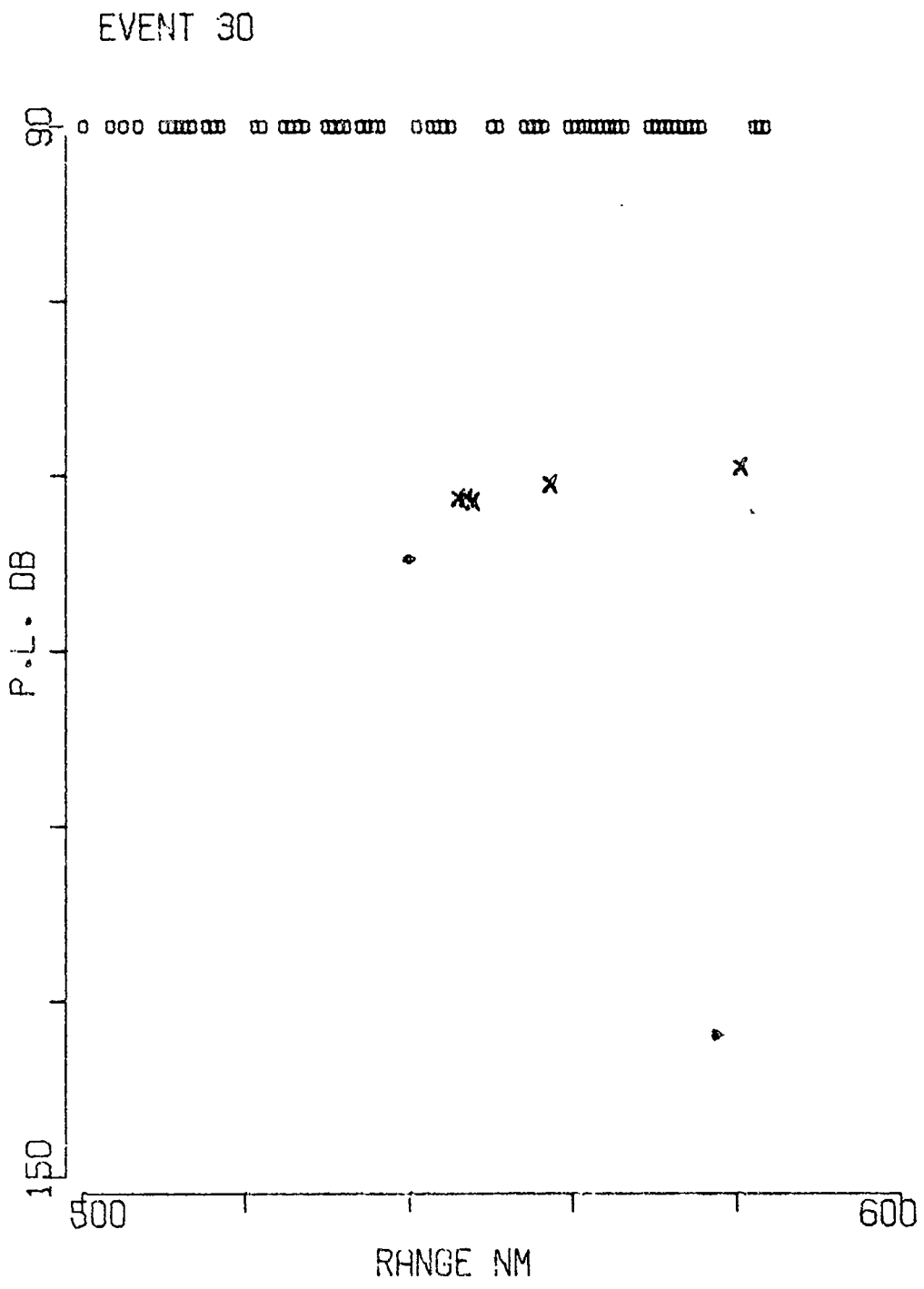
BARTLETT A SRCE 91M RCVR 749M FREQ 25.1 ,1 OCT
EVENT 30
90
150
P.L. DB
500
600
RANGE NM

FIGURE A-2

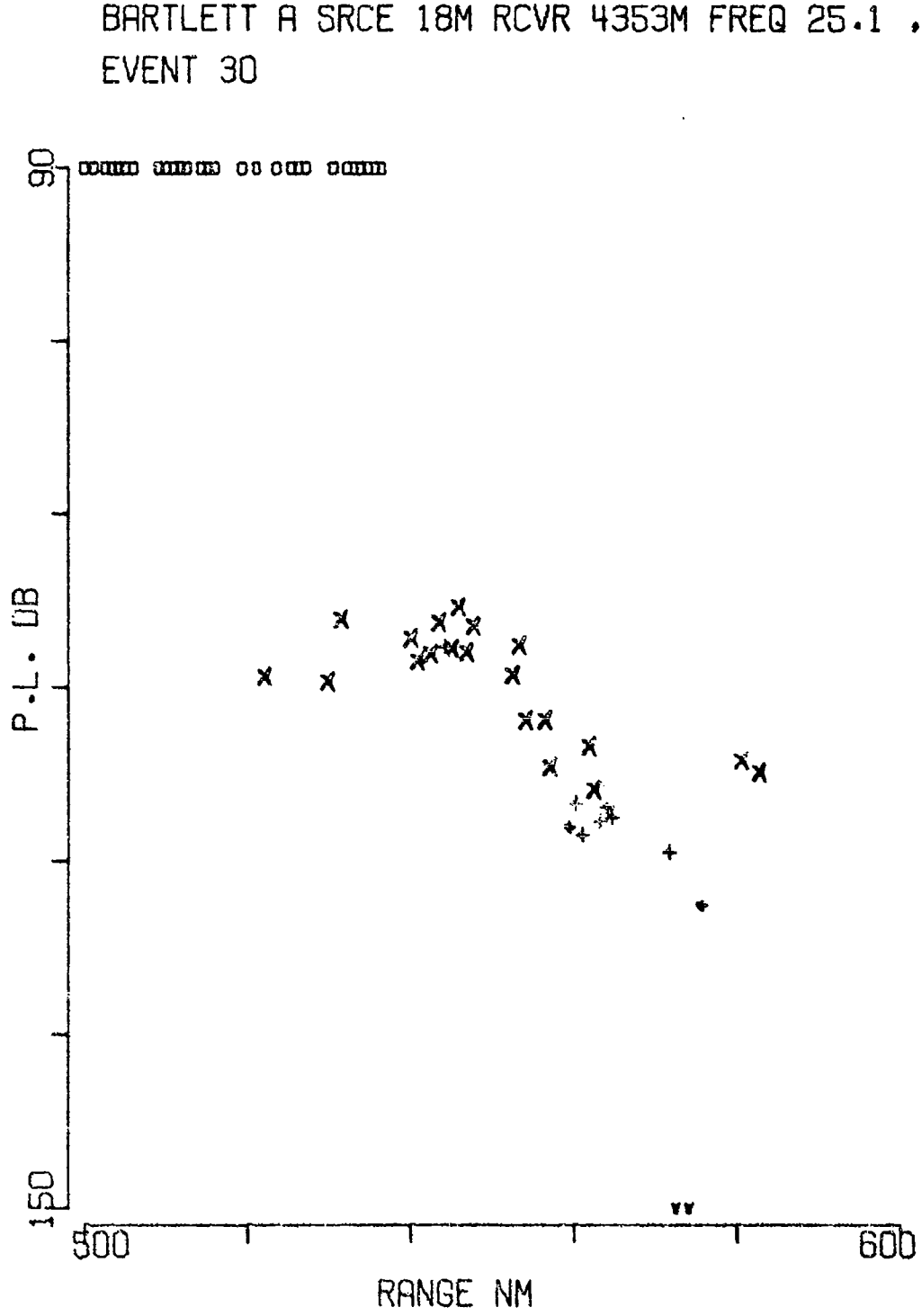
BARTLETT A SRCE 18M RCVR 4353M FREQ 25.1 .1 OCT
EVENT 30
90
150
P.L. DB
500
600
RANGE NM

FIGURE A-3

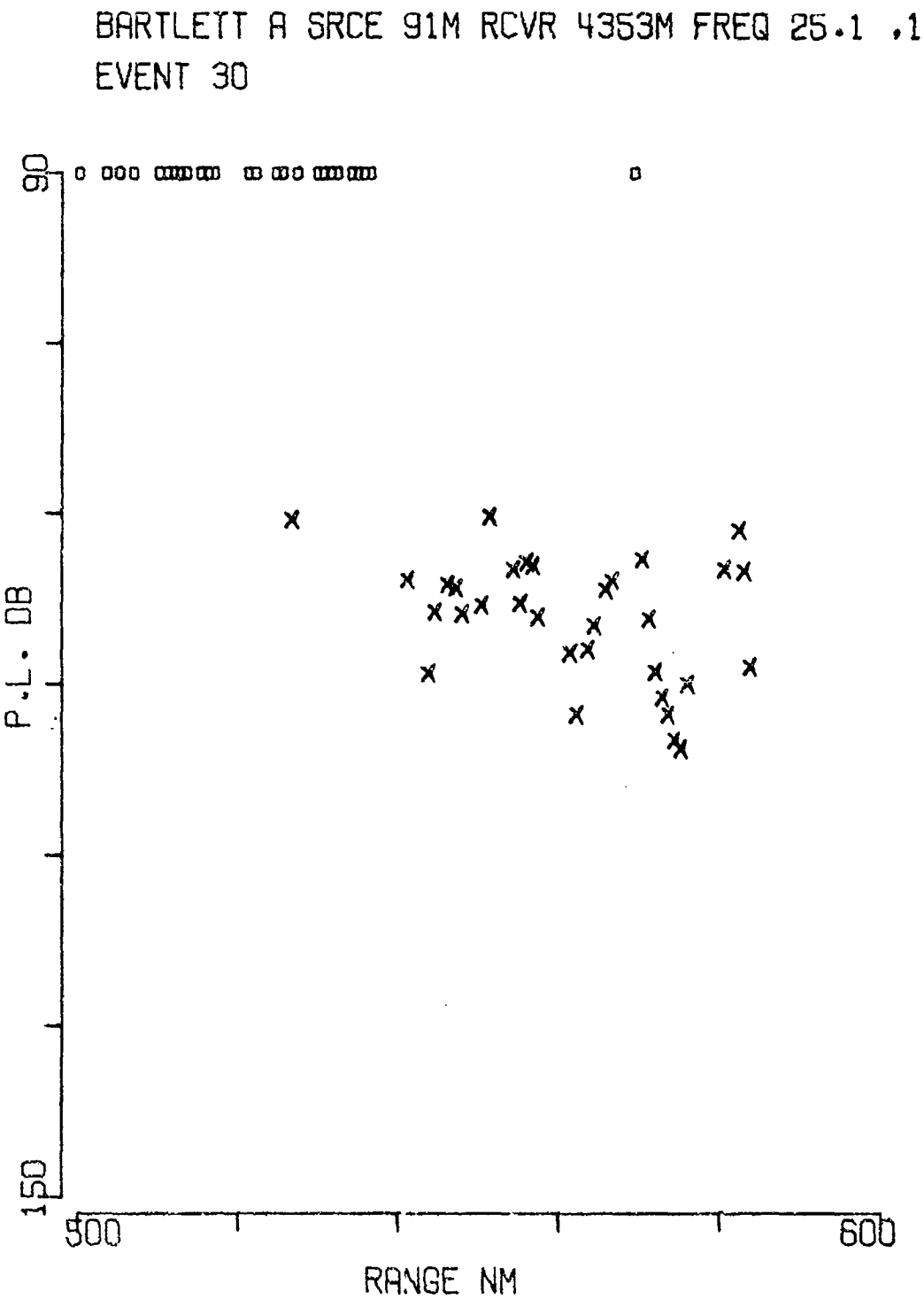
BARTLETT A SRCE 91M RCVR 4353M FREQ 25.1 .1 OCT
EVENT 30
90
150
P.L. DB
500
600
RANGE NM

FIGURE A-4

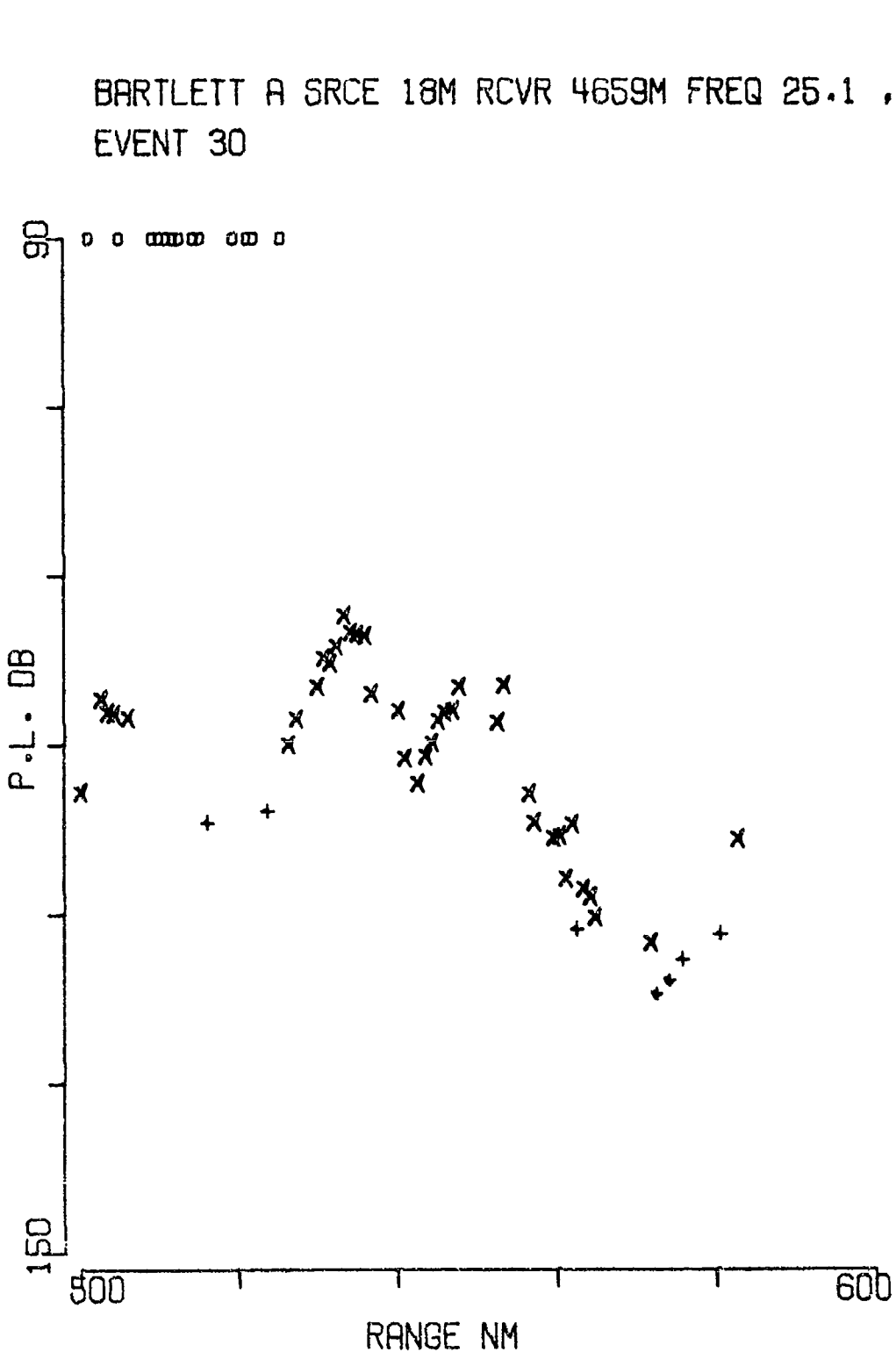
BARTLETT A SRCE 18M RCVR 4659M FREQ 25.1 .1 OCT
EVENT 30
90
150
P.L. DB
500
600
RANGE NM

FIGURE A-5

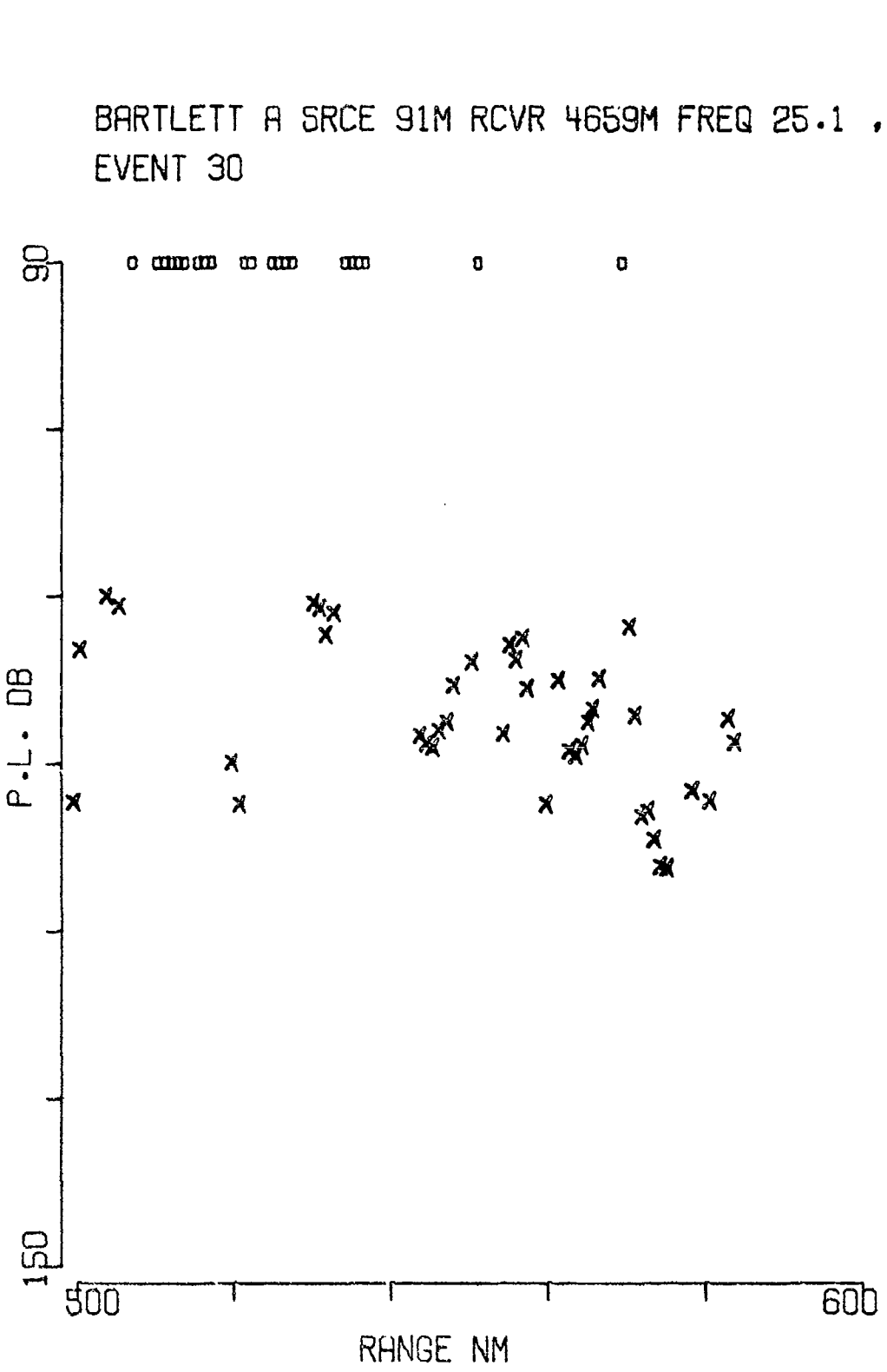
BARTLETT A SRCE 91M RCVR 4659M FREQ 25.1 .1 OCT
EVENT 30
90
150
P.L. DB
500
600
RANGE NM

FIGURE A-6

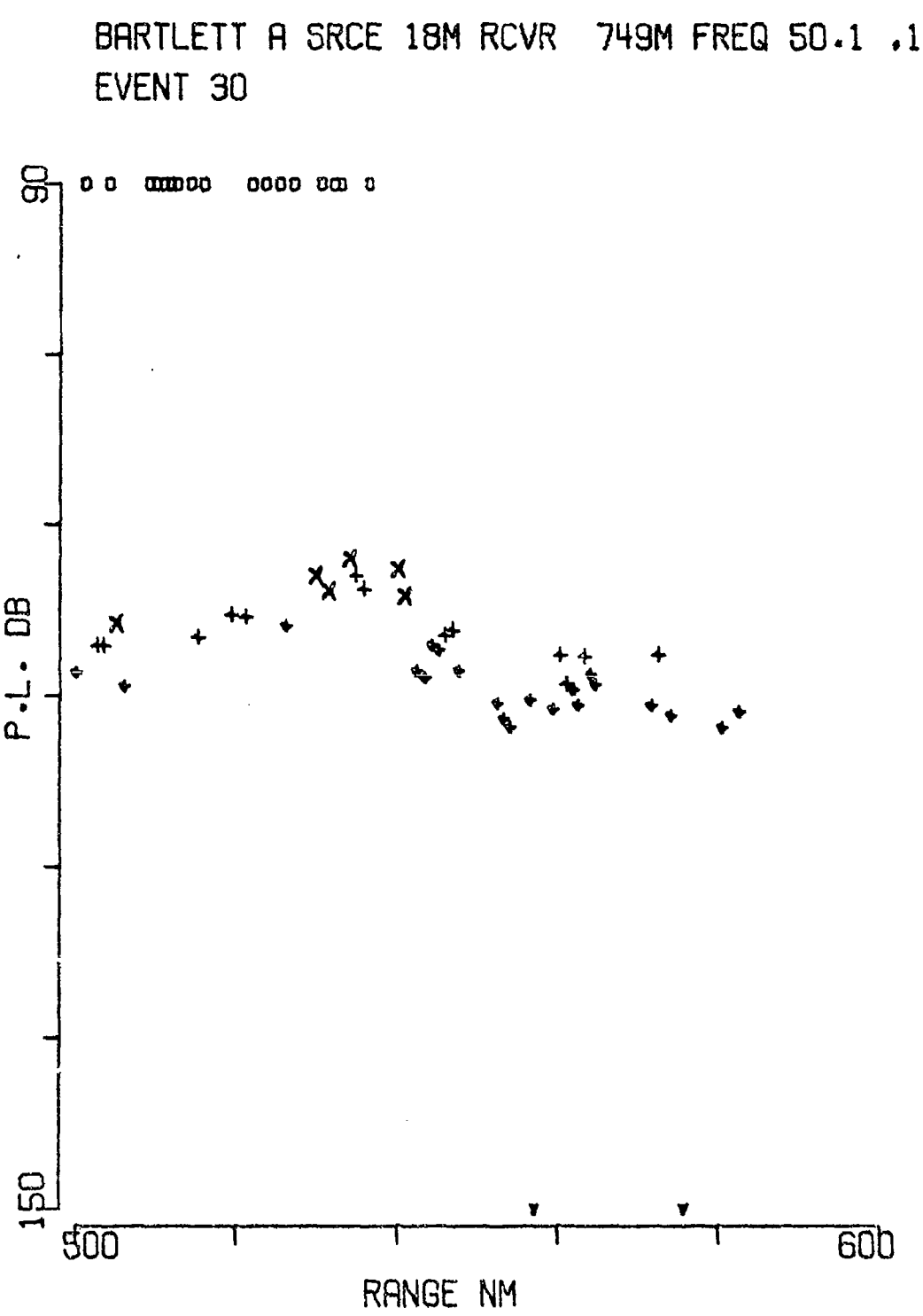
BARTLETT A SRCE 18M RCVR 749M FREQ 50.1 .1 OCT
EVENT 30
90
150
P.L. DB
500
600
RANGE NM

FIGURE A-7

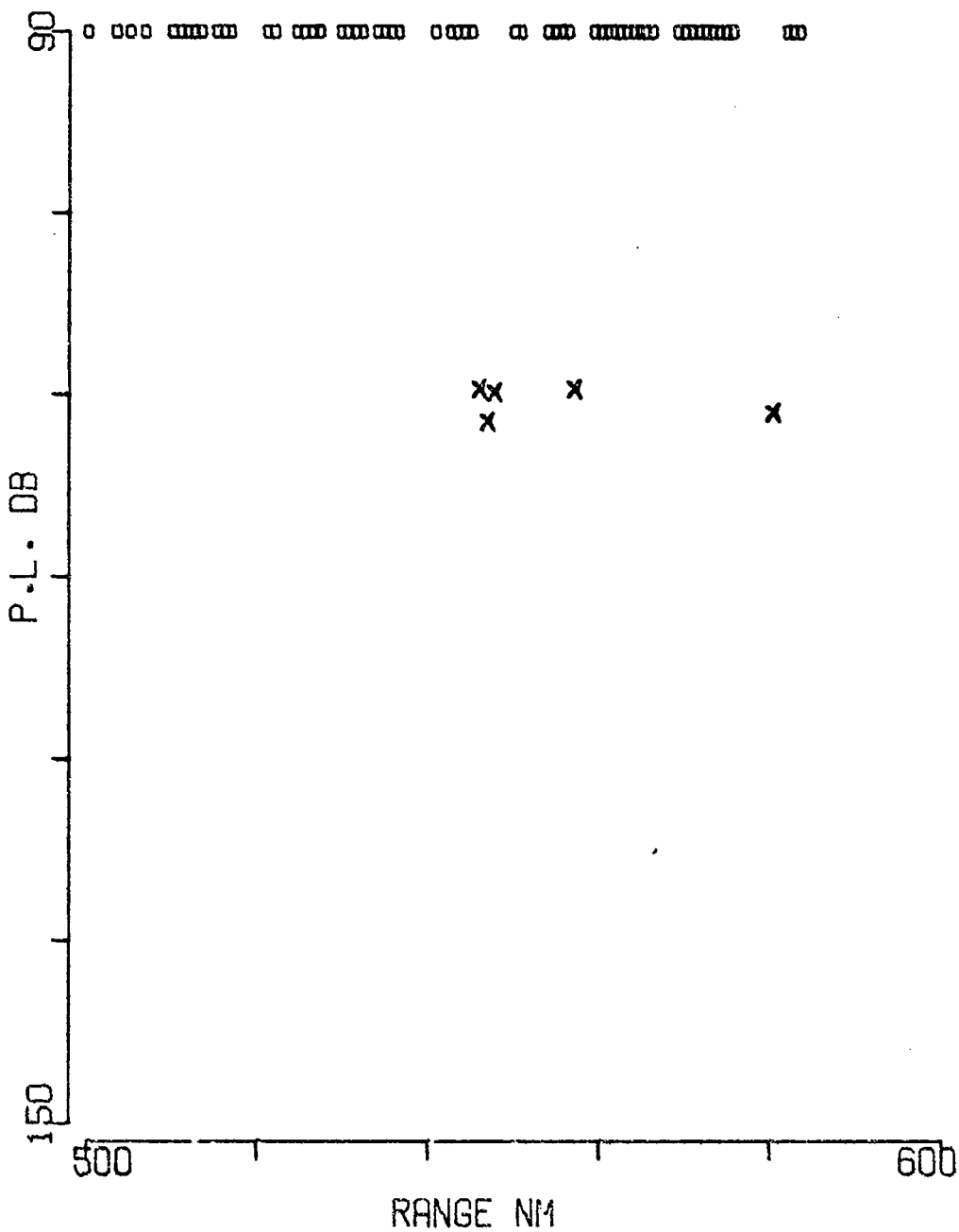
BARTLETT A SRCE 91M RCVR 749M FREQ 50.1 ,1 OCT
EVENT 30
90
150
P.L. DB
500
600
RANGE NM

FIGURE A-8

BARTLETT A SRCE 18M RCVR 4353M FREQ 50.1 ,1 OCT
EVENT 30

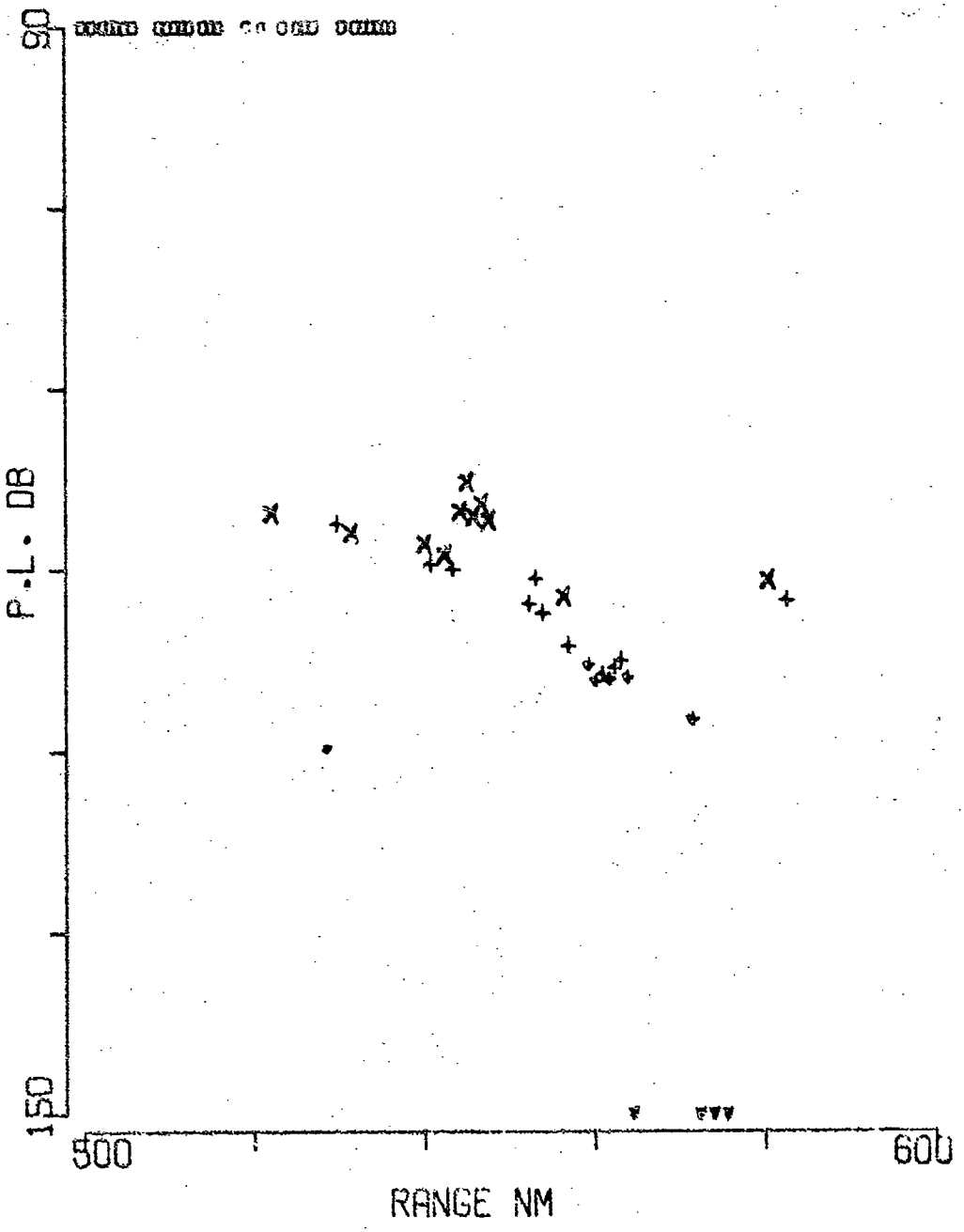

FIGURE A-9

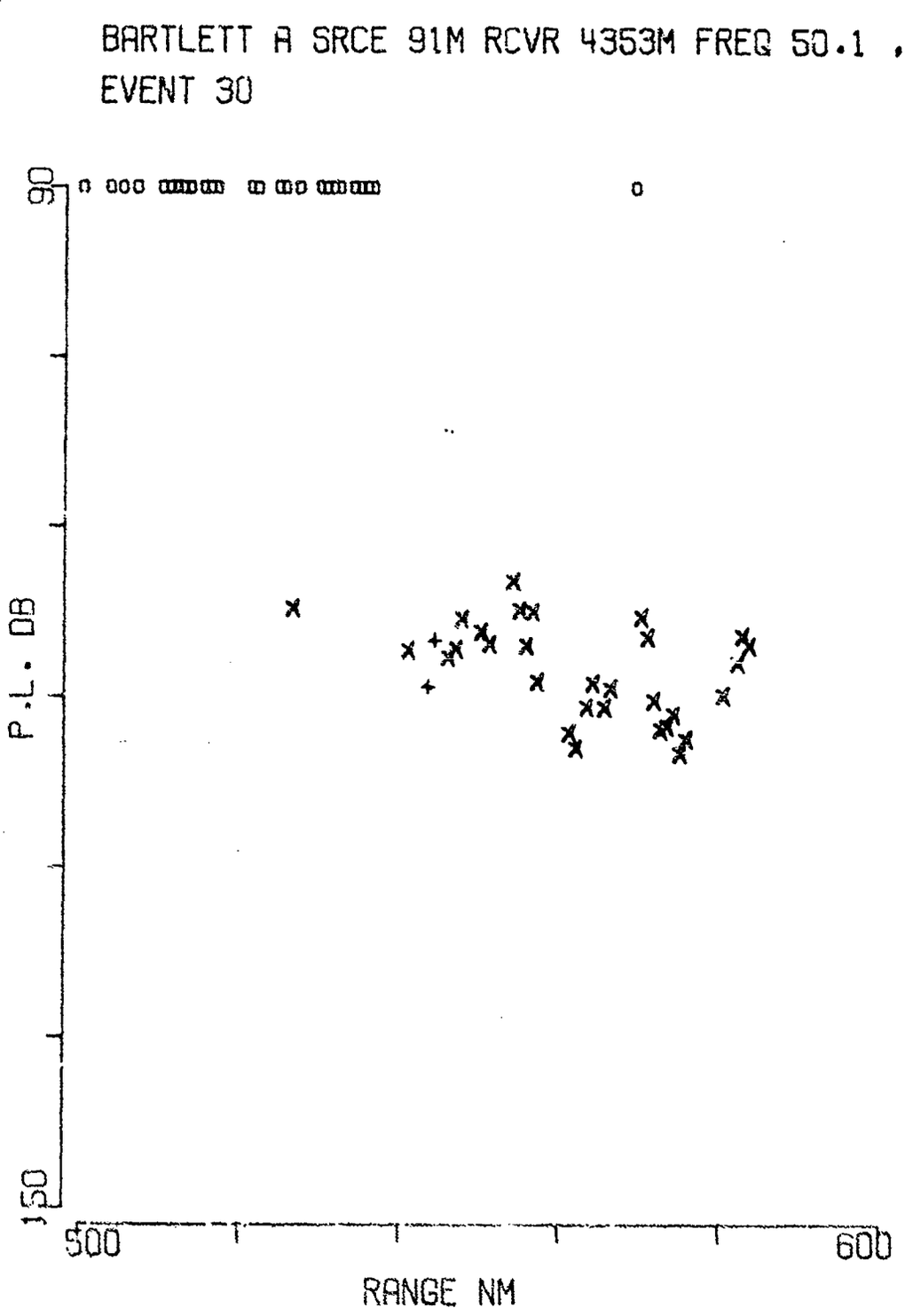
BARTLETT A SRCE 91M RCVR 4353M FREQ 50.1 ,1 OCT
EVENT 30
90
150
P.L. DB
500
600
RANGE NM

FIGURE A-10

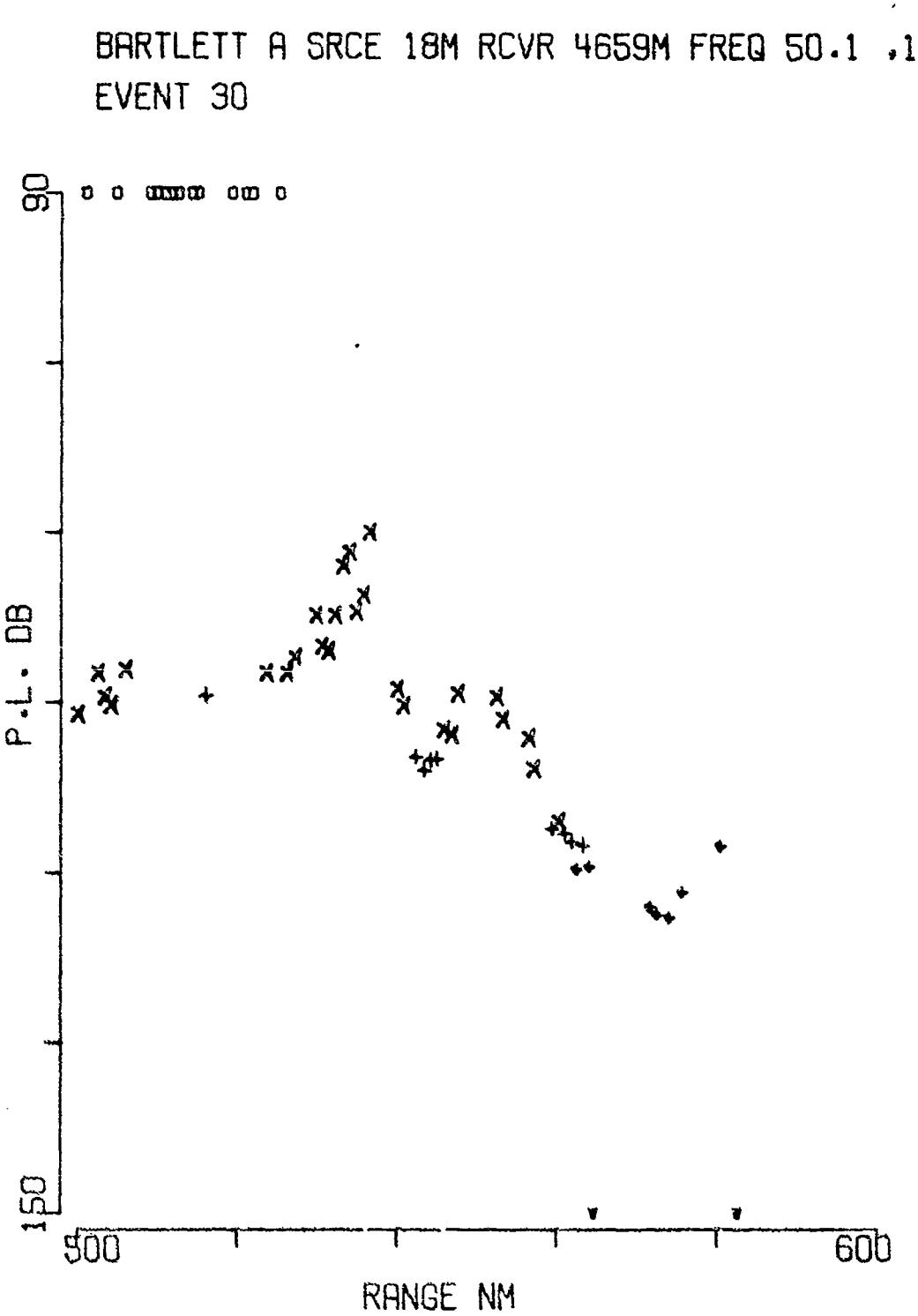
BARTLETT A SRCE 18M RCVR 4659M FREQ 50.1 .1 OCT
EVENT 30
90
150
P.L. DB
500
600
RANGE NM

FIGURE A-11

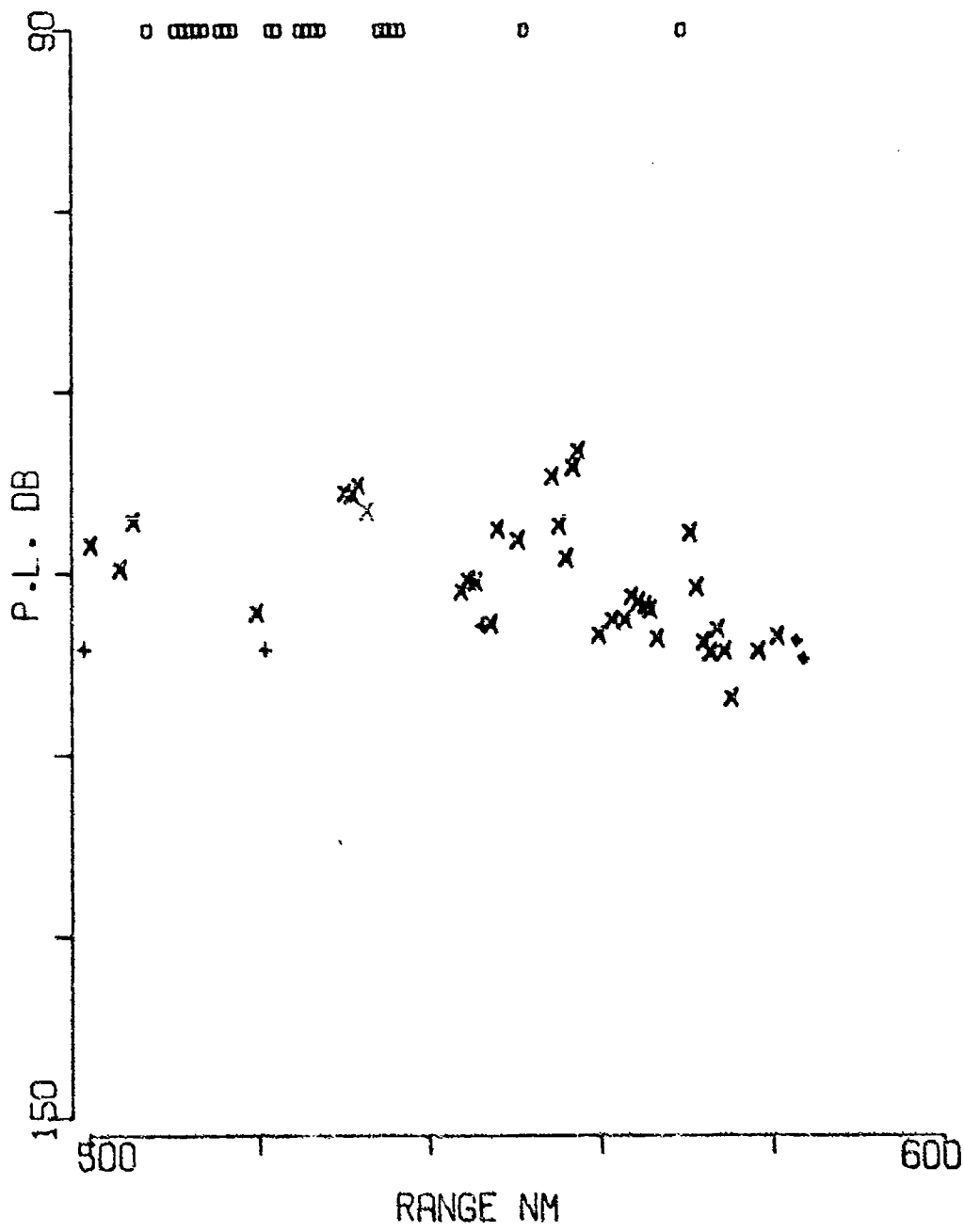
BARTLETT A SRCE 91M RCVR 4659M FREQ 50.1 ,1 OCT
EVENT 30
90
150
P.L. DB
500
600
RANGE NM

FIGURE A-12

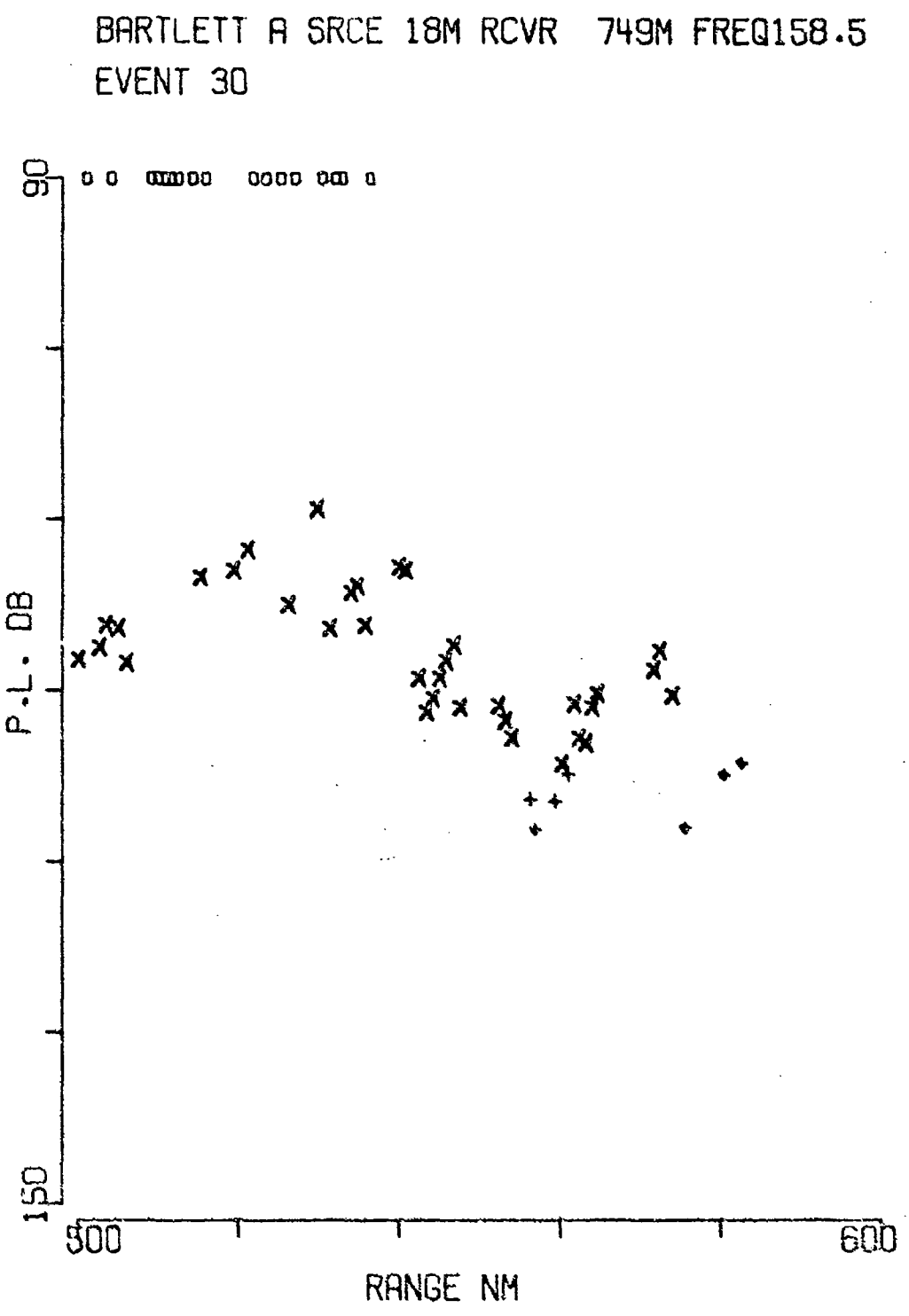
BARTLETT A SRCE 18M RCVR 749M FREQ158.5
EVENT 30
90
150
P.L. DB
300
600
RANGE NM

FIGURE A-13

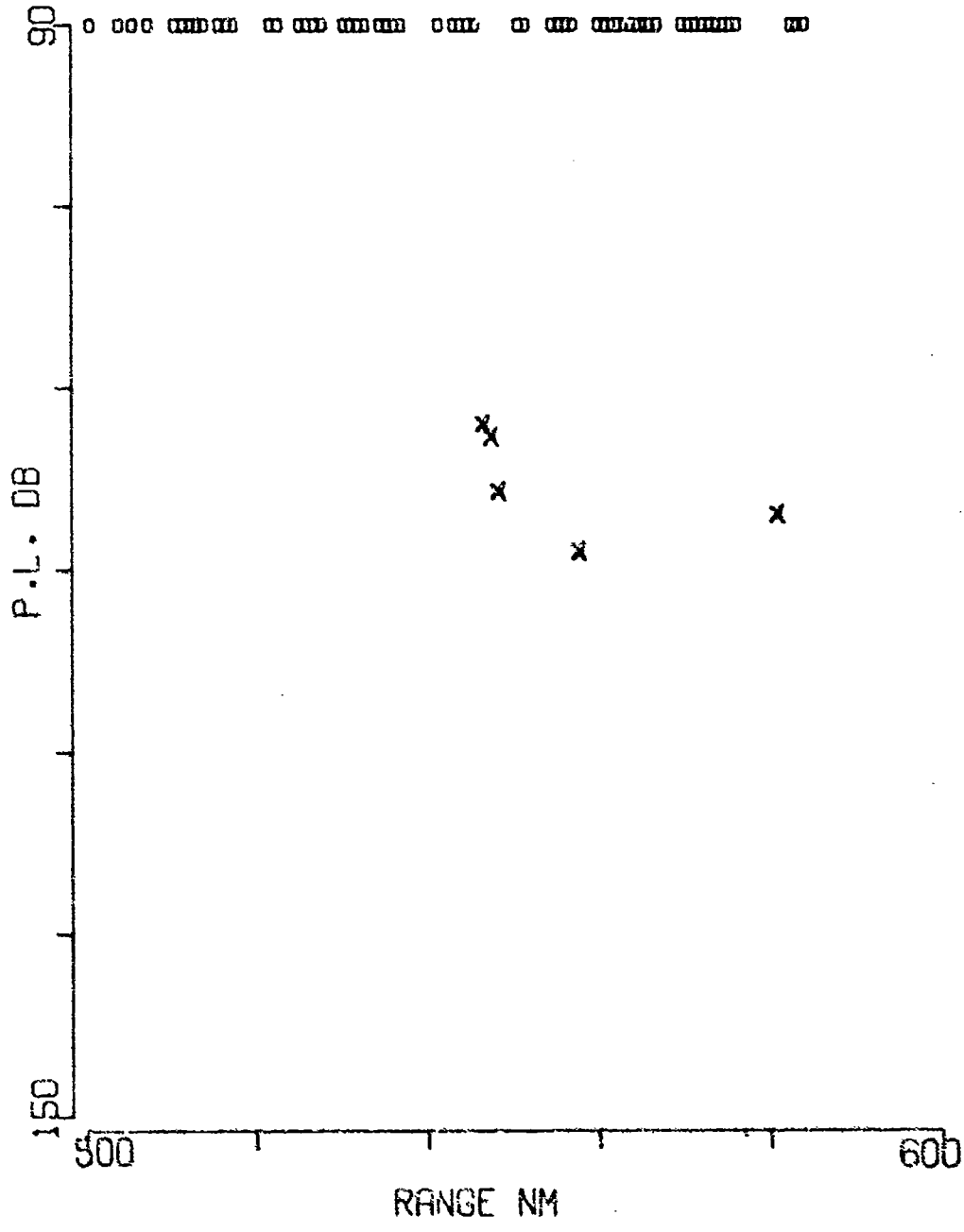
BARTLETT A SRCE 91M RCVR 749M FREQ158.5
EVENT 30
90
150
P.L. DB
500
600
RANGE NM

FIGURE A-14

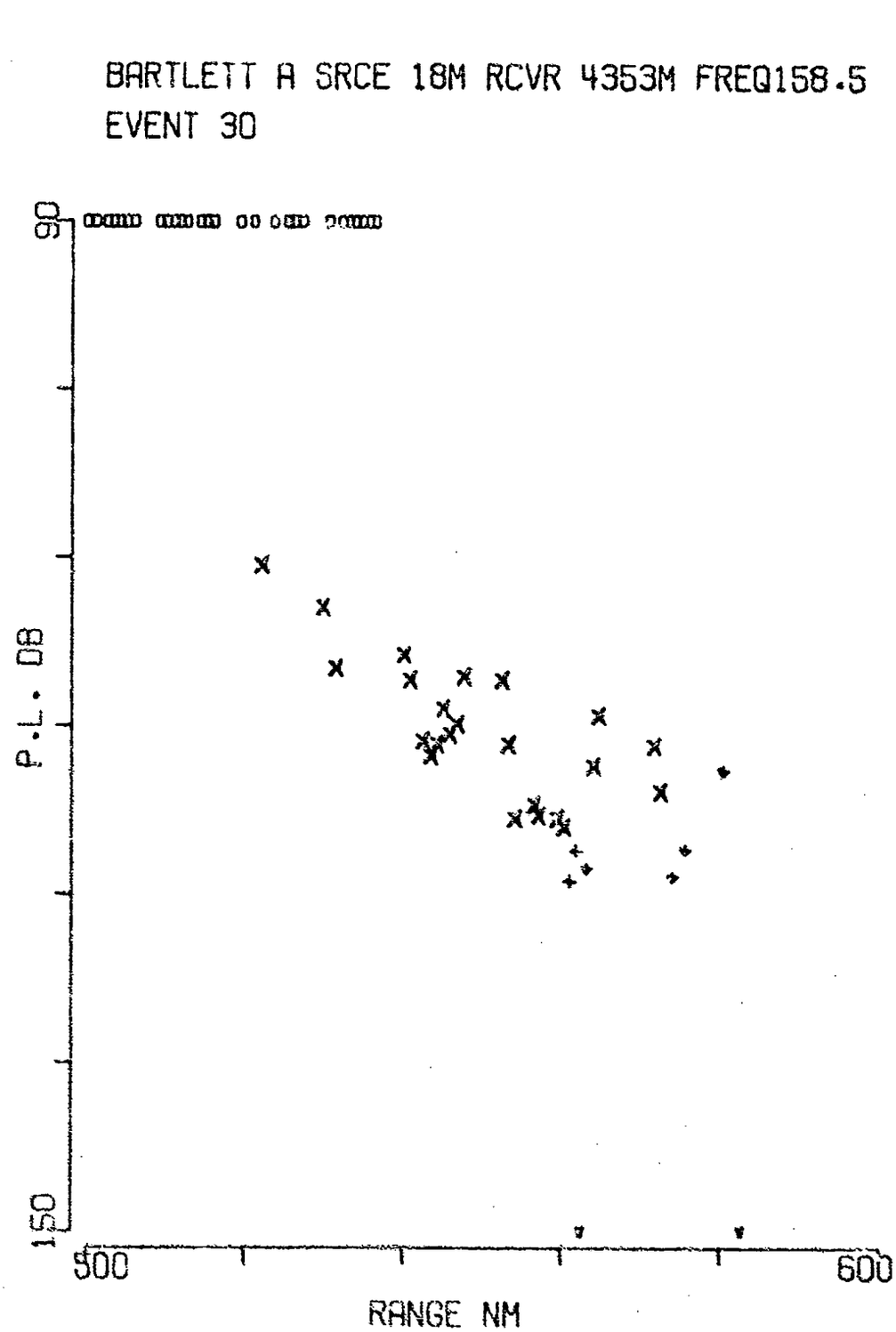
BARTLETT A SRCE 18M RCVR 4353M FREQ158.5
EVENT 30
60
150
P.L. DB
500
600
RANGE NM

FIGURE A-15

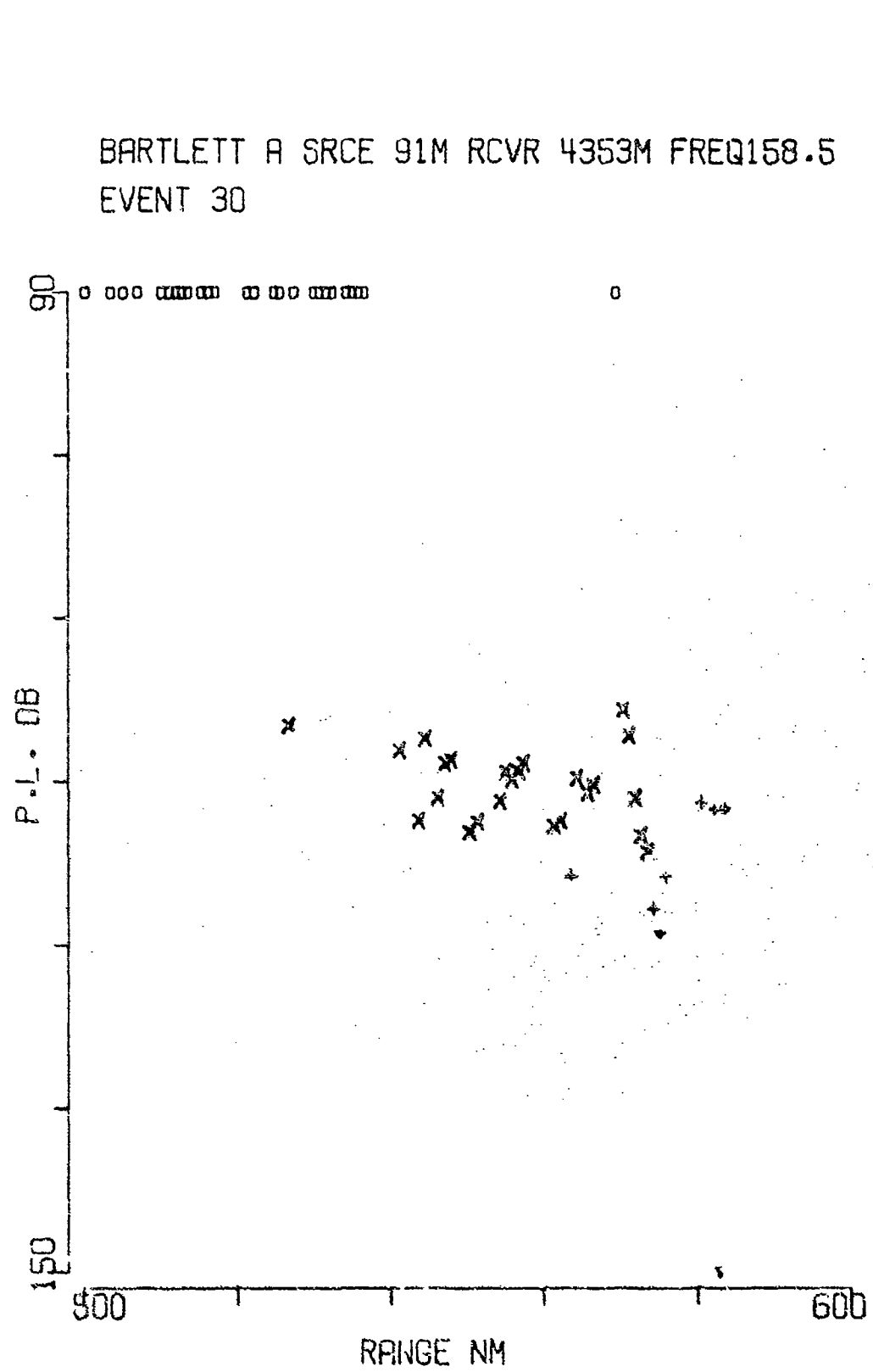
BARTLETT A SRCE 91M RCVR 4353M FREQ158.5
EVENT 30
90
150
P.L. DB
500
600
RANGE NM

FIGURE 3-16

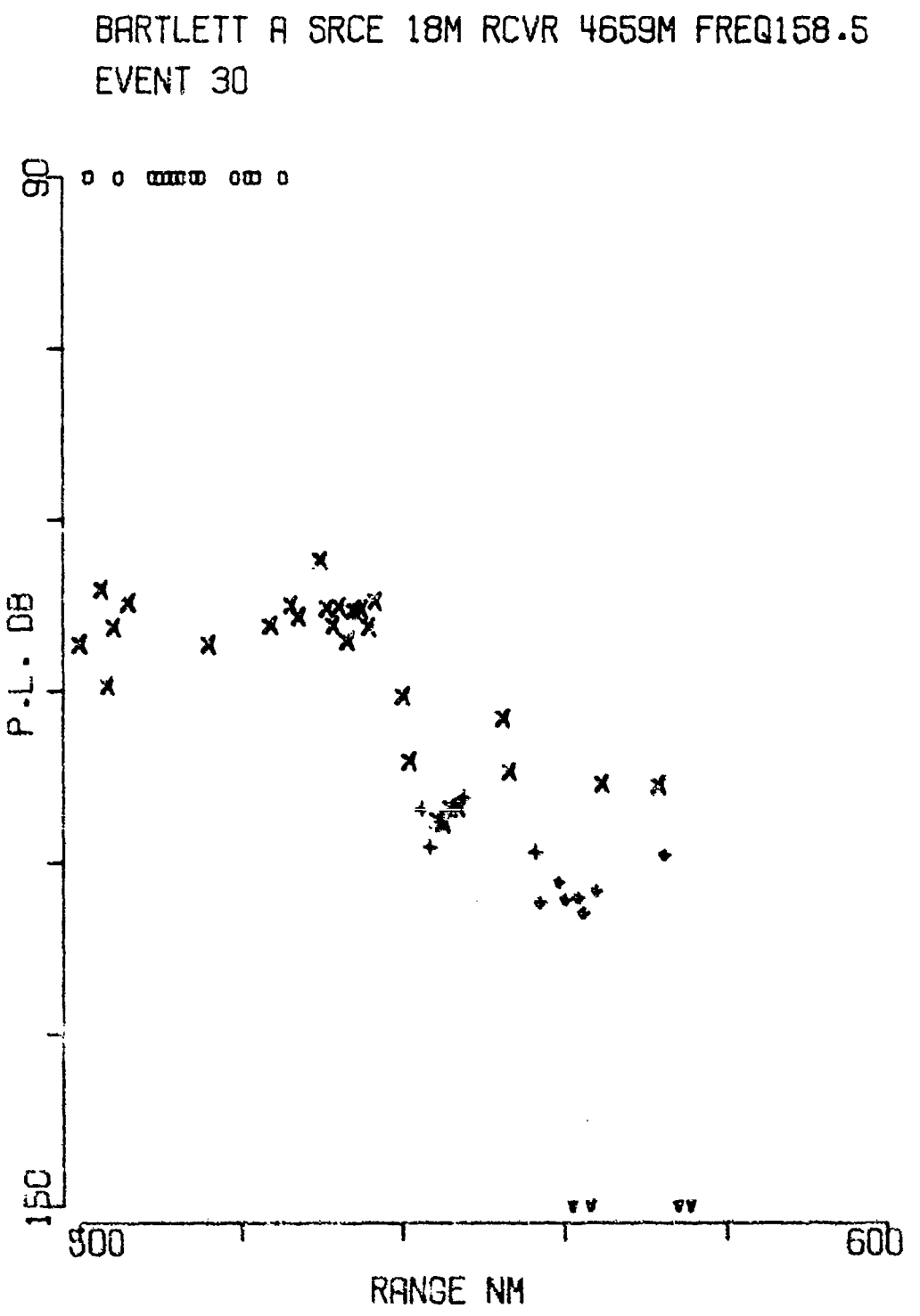
BARTLETT A SRCE 18M RCVR 4659M FREQ158.5
EVENT 30
90
150
P.L. DB
900
600
RANGE NM

FIGURE A-17

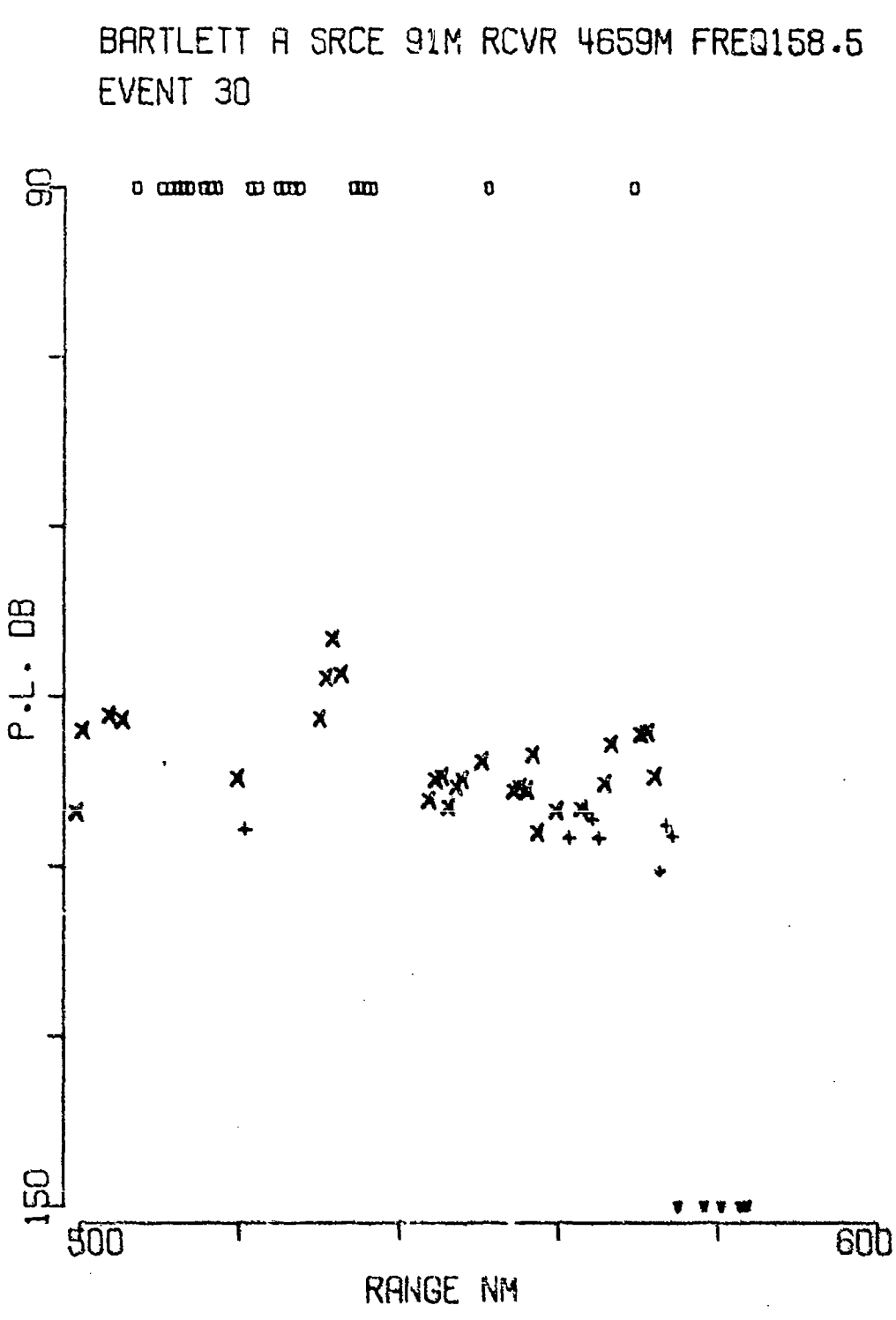
BARTLETT A SRCE 91M RCVR 4659M FREQ158.5
EVENT 30
90
150
P.L. DB
500
600
RANGE NM

FIGURE A-18

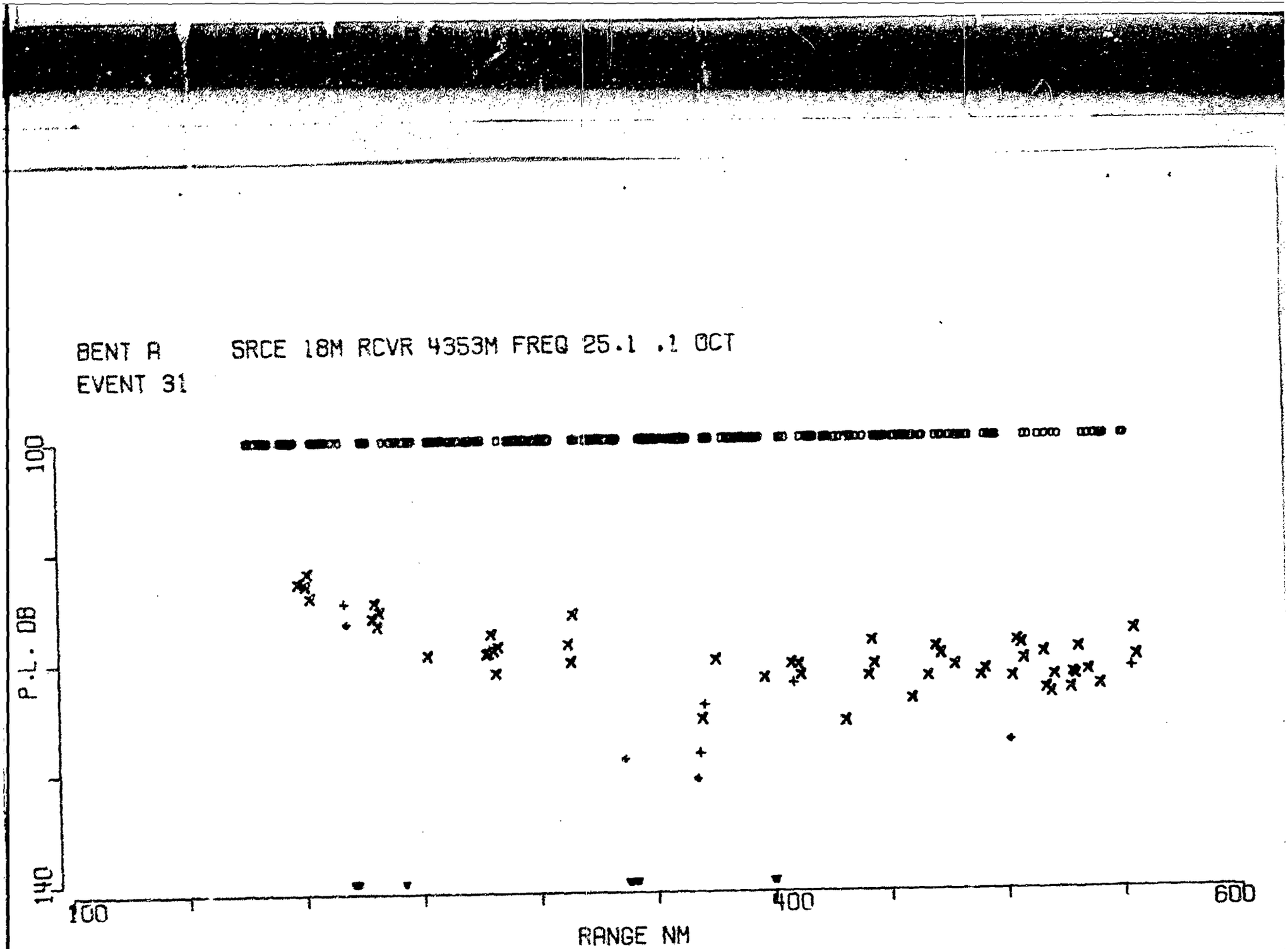
BENT A SRCE 18M RCVR 4353M FREQ 25.1 .1 OCT
EVENT 31
P.L. DB
100
140
100
400
600
RANGE NM

FIGURE A-19

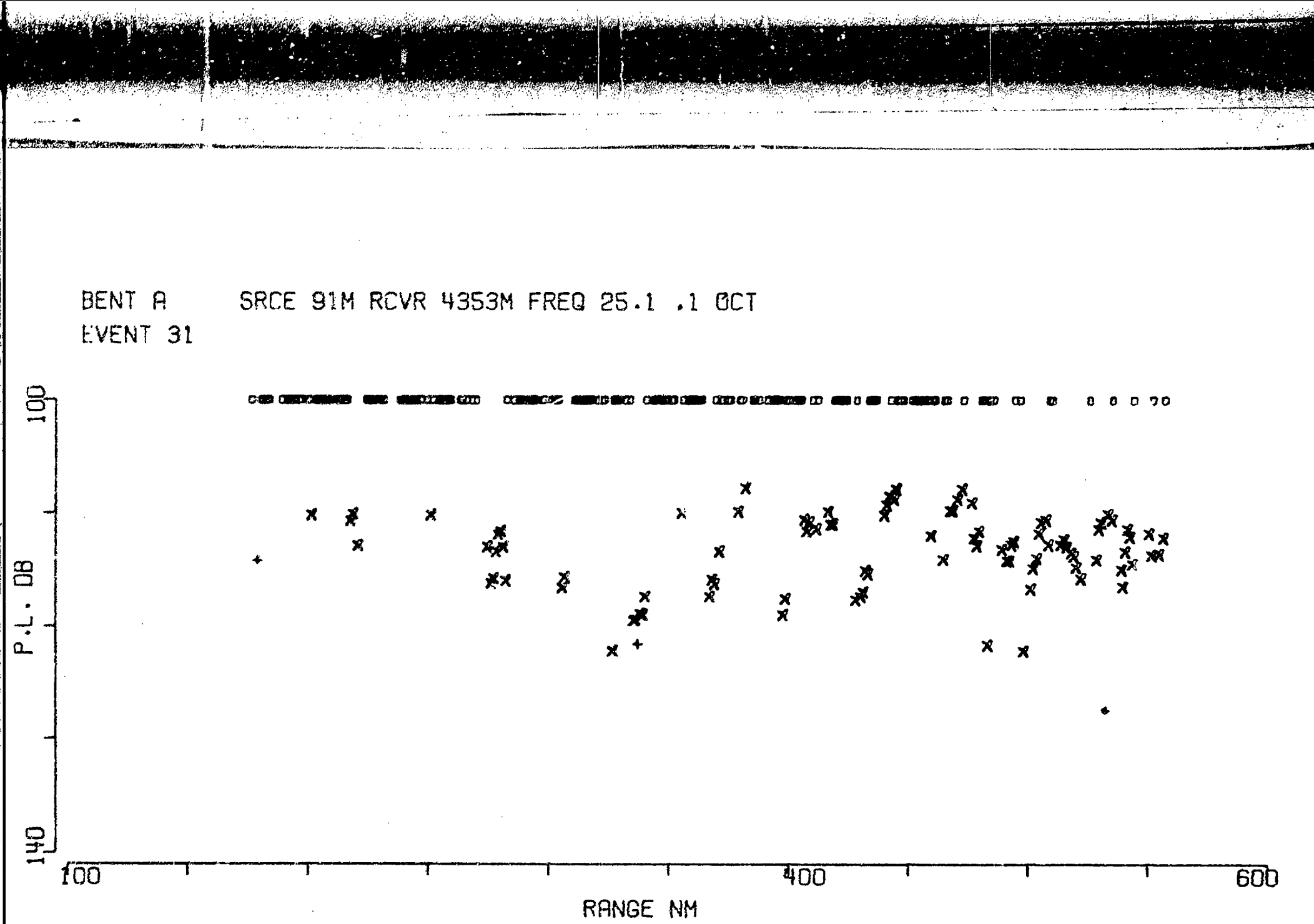
BENT A SRCE 91M RCVR 4353M FREQ 25.1 .1 OCT
EVENT 31
P.L. DB
100
140
100
400
600
RANGE NM

FIGURE A-20

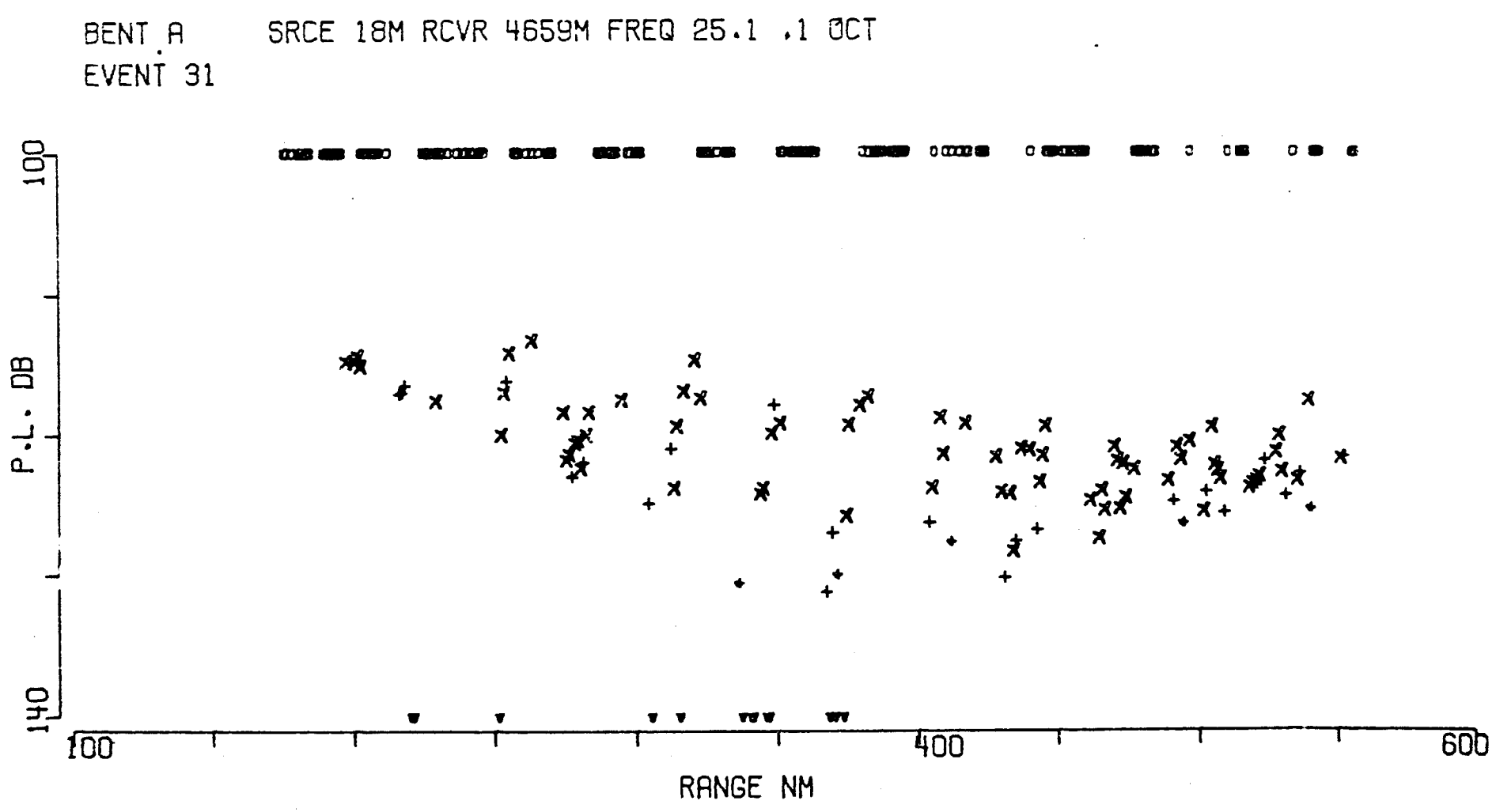
BENT A SRCE 18M RCVR 4659M FREQ 25.1 .1 OCT
EVENT 31
100
140
P.L. DB
100
400
600
RANGE NM

FIGURE A-21

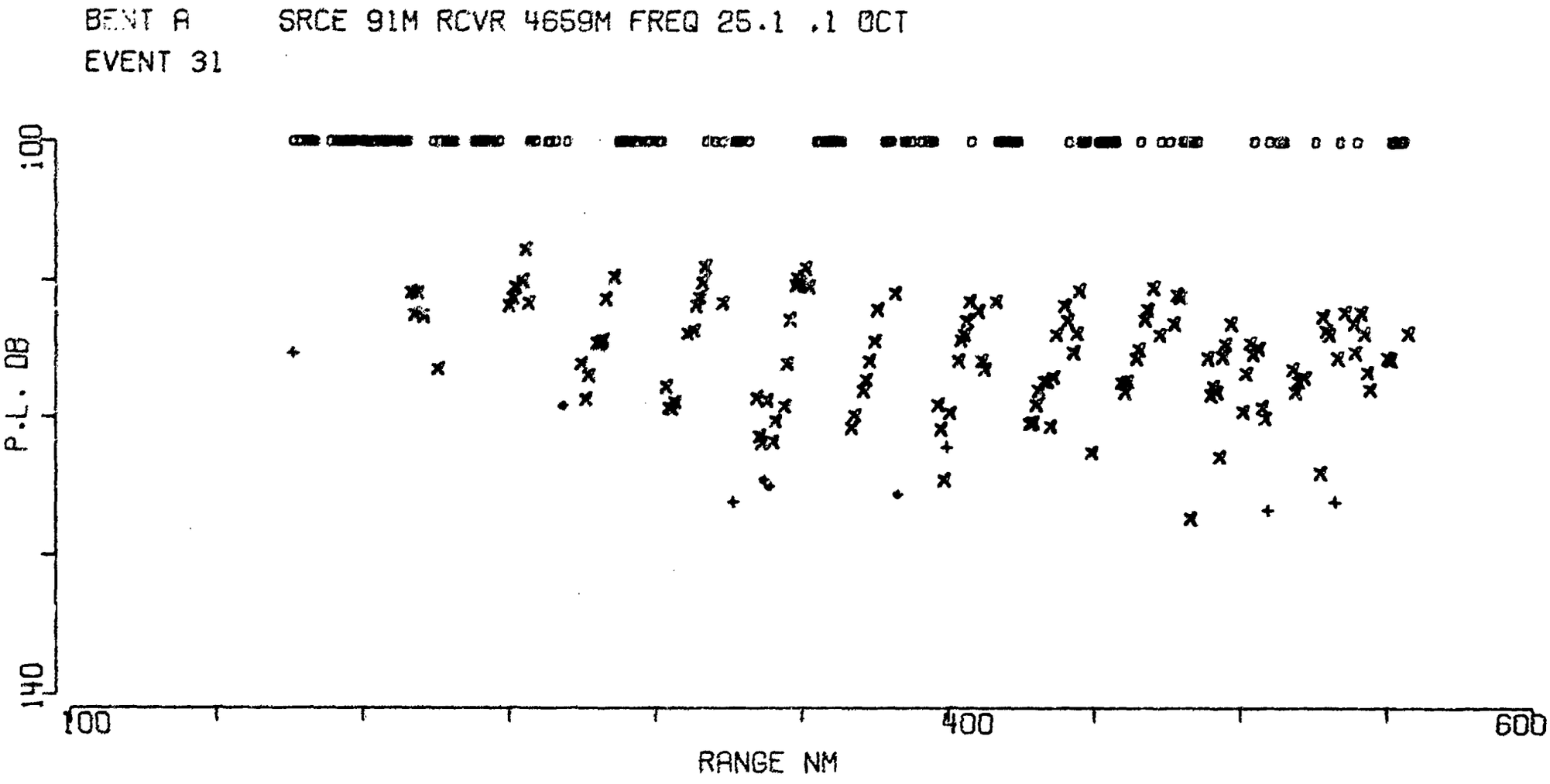
BENT A SRCE 91M RCVR 4659M FREQ 25.1 .1 OCT
EVENT 31
100
P.L. DB
140
100
400
600
RANGE NM

FIGURE A-22

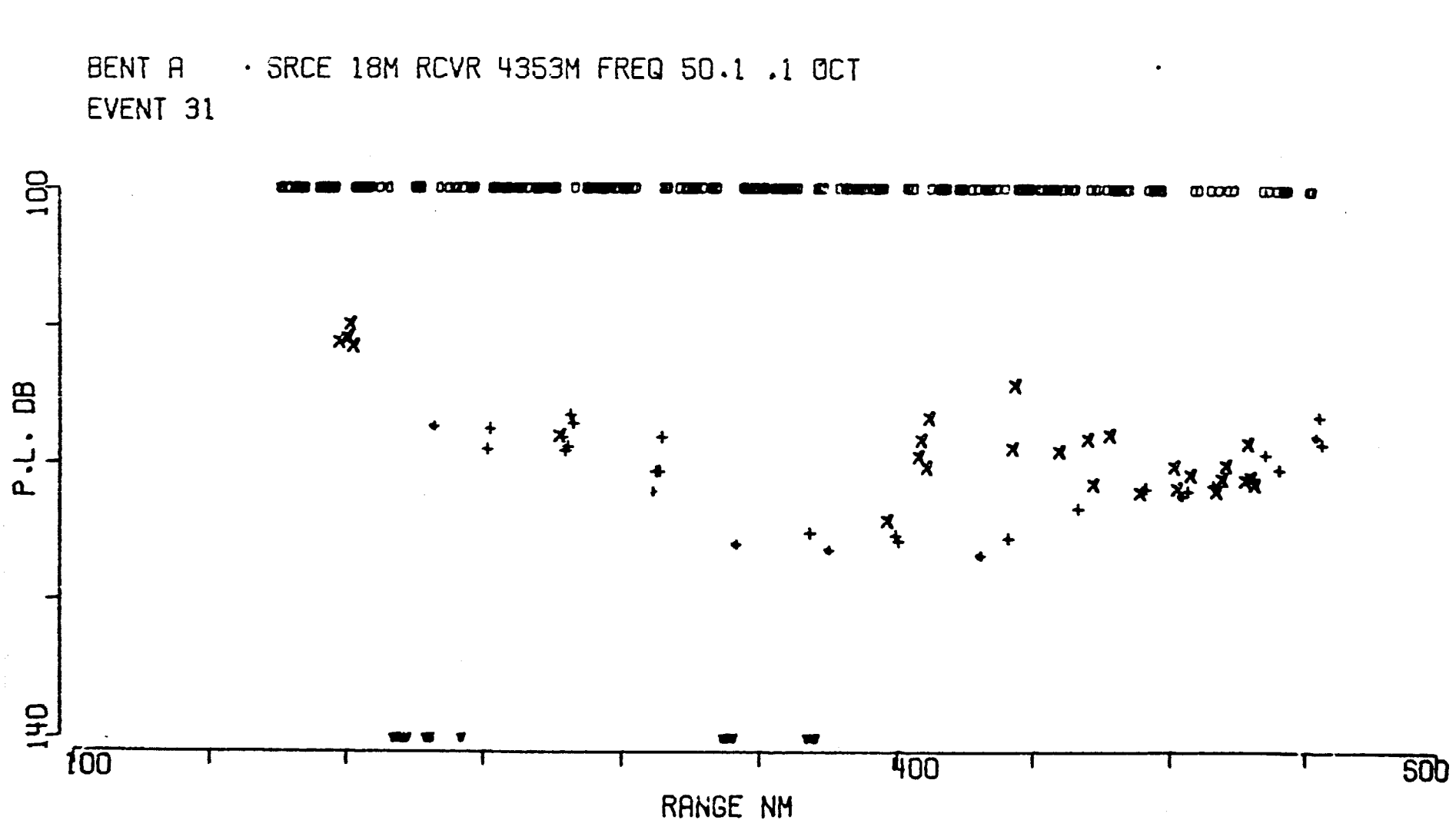
BENT A · SRCE 18M RCVR 4353M FREQ 50.1 .1 OCT
EVENT 31
100
140
P.L. DB
100
400
500
RANGE NM

FIGURE A-23

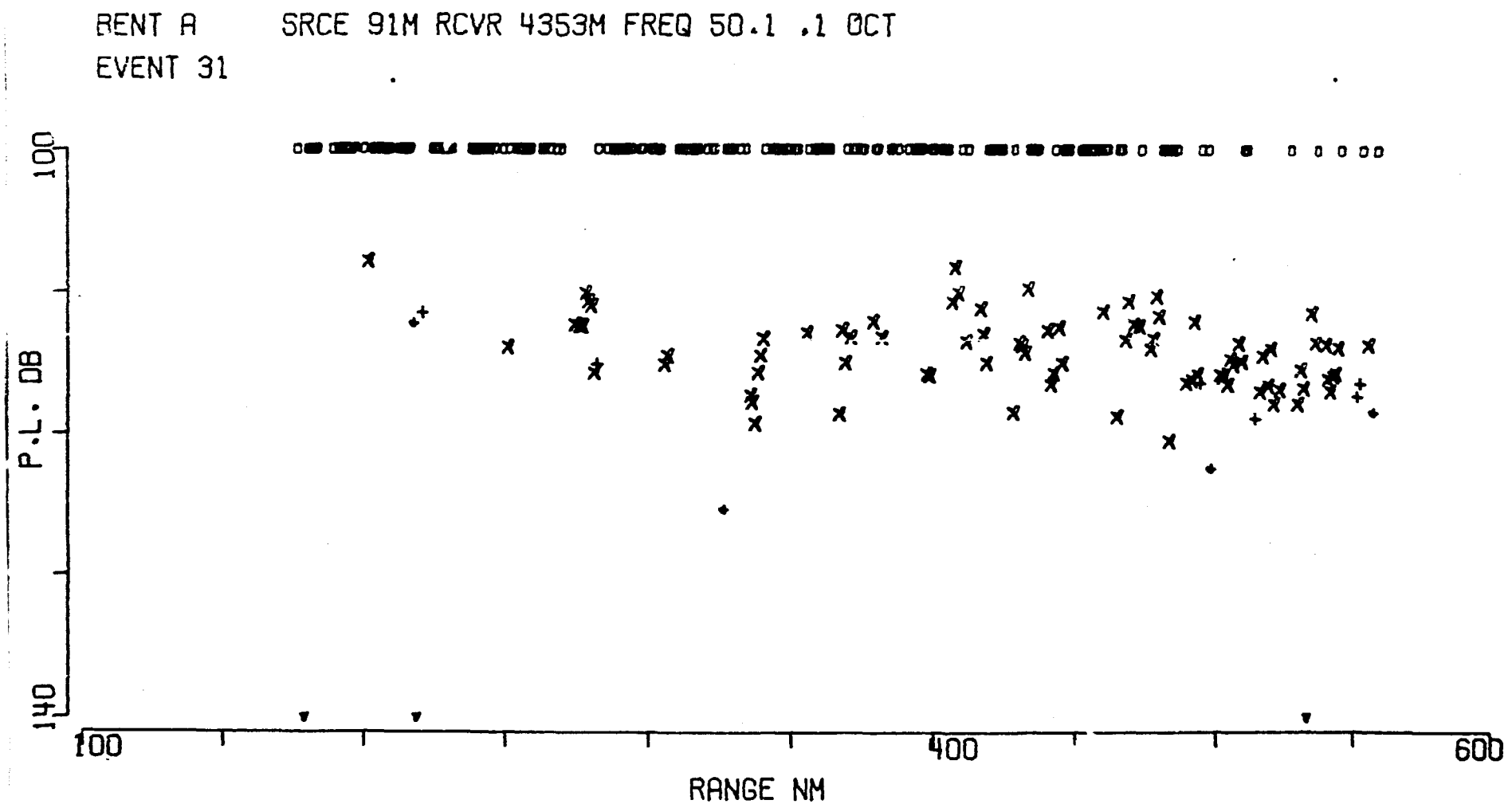
RENT A SRCE 91M RCVR 4353M FREQ 50.1 .1 OCT
EVENT 31
100
P.L. DB
140
100
400
600
RANGE NM

FIGURE A-24

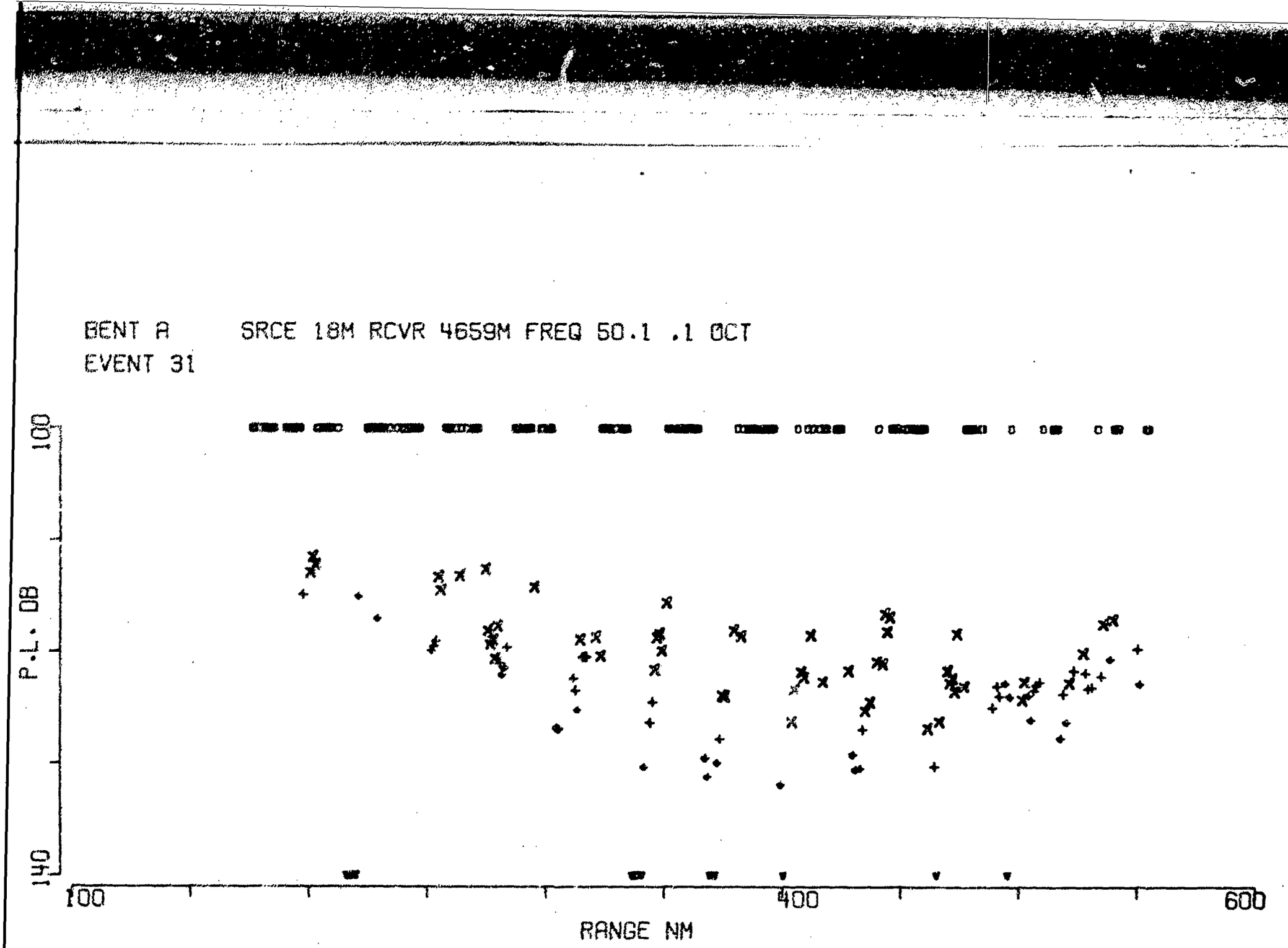
BENT A SRCE 18M RCVR 4659M FREQ 50.1 .1 OCT
EVENT 31
100
140
P.L. DB
100
400
600
RANGE NM

FIGURE A-25

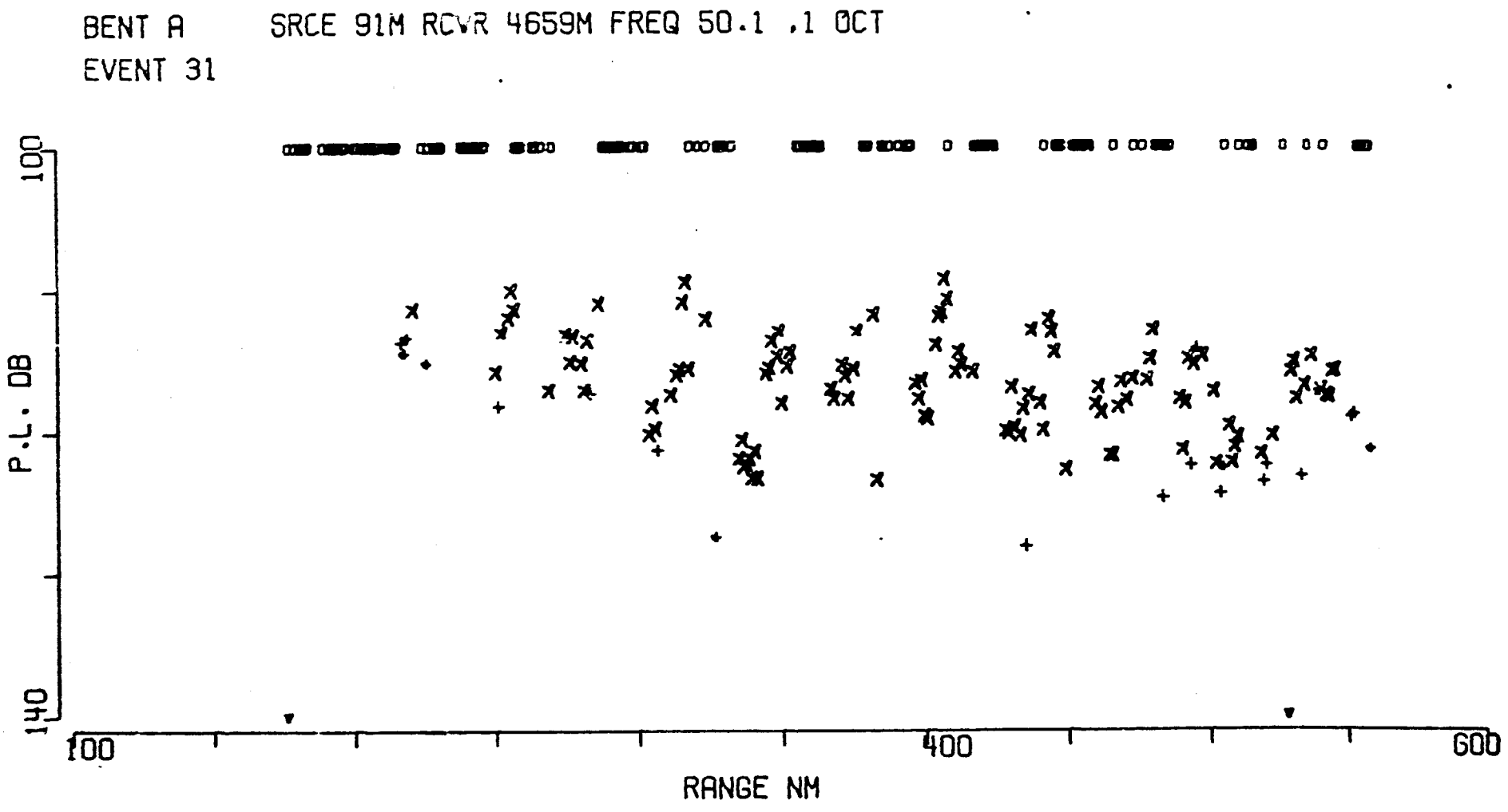
BENT A SRCE 91M RCVR 4659M FREQ 50.1 .1 OCT
EVENT 31
100
140
P.L. DB
100
400
600
RANGE NM

FIGURE A-26

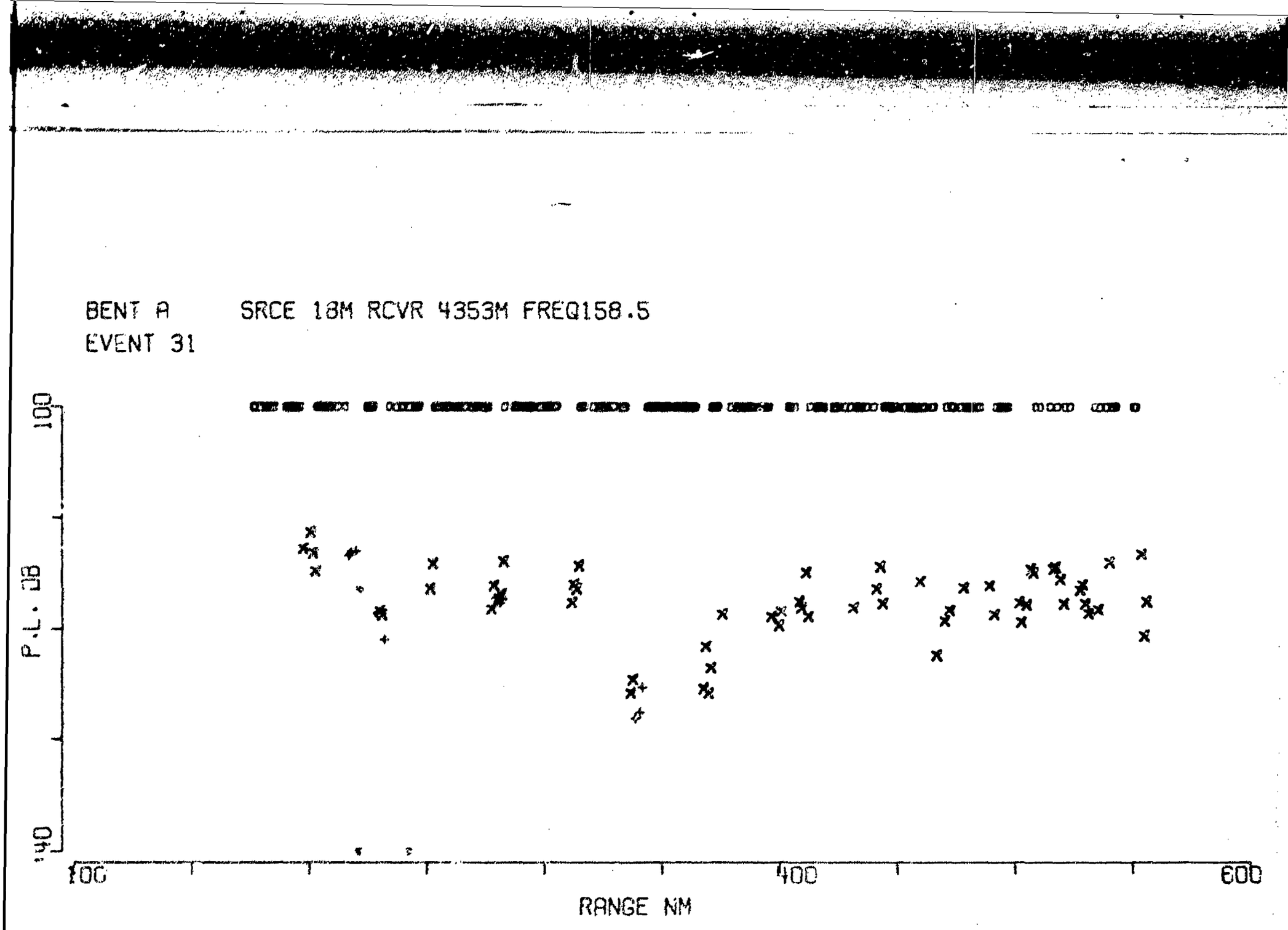
BENT A SRCE 18M RCVR 4353M FREQ158.5
EVENT 31
P.L. DB
100
RANGE NM
400
600

FIGURE A-27

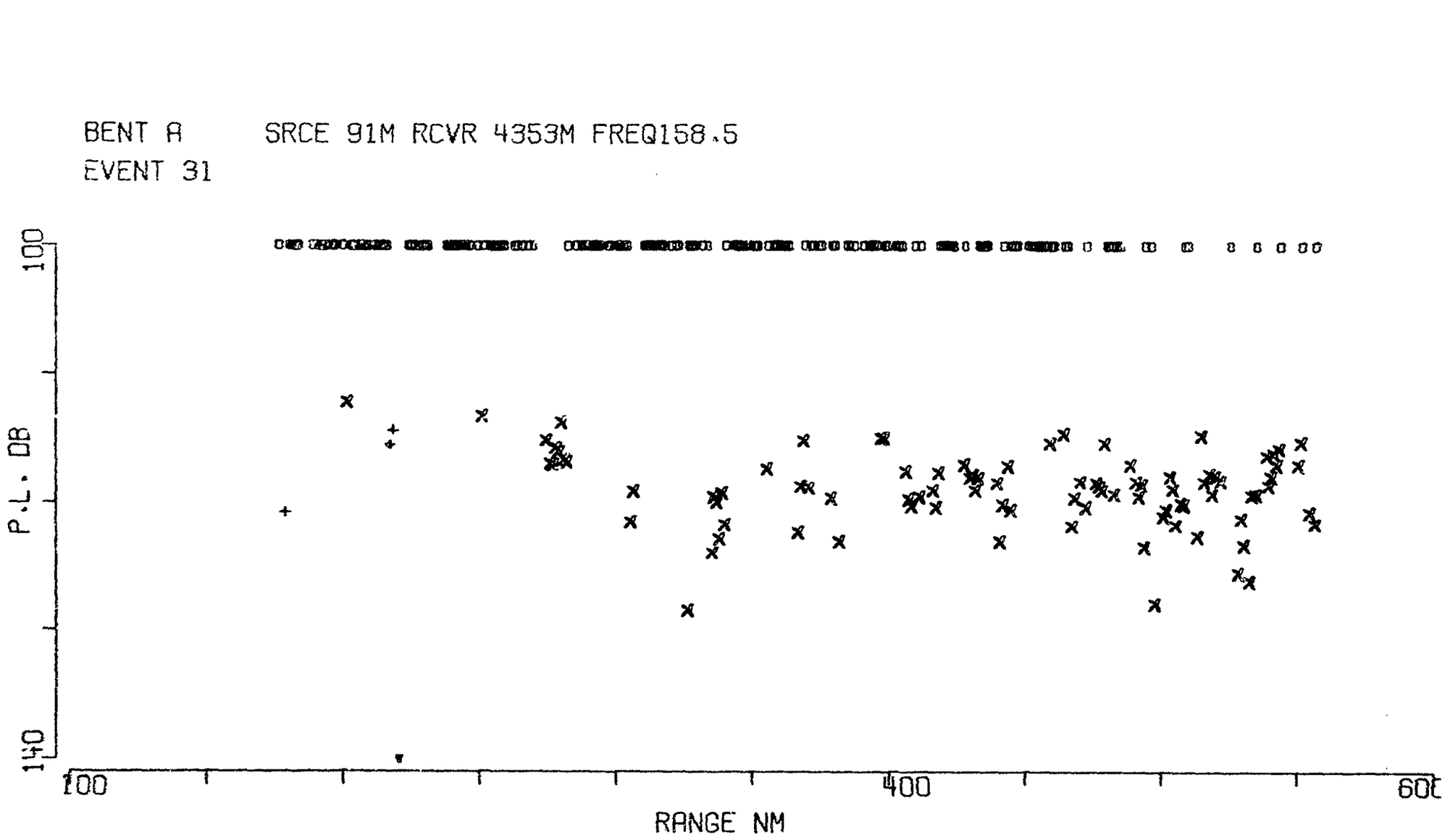
BENT A SRCE 91M RCVR 4353M FREQ158.5
EVENT 31
100
P.L. DB
140
100
400
600
RANGE NM

FIGURE A-28

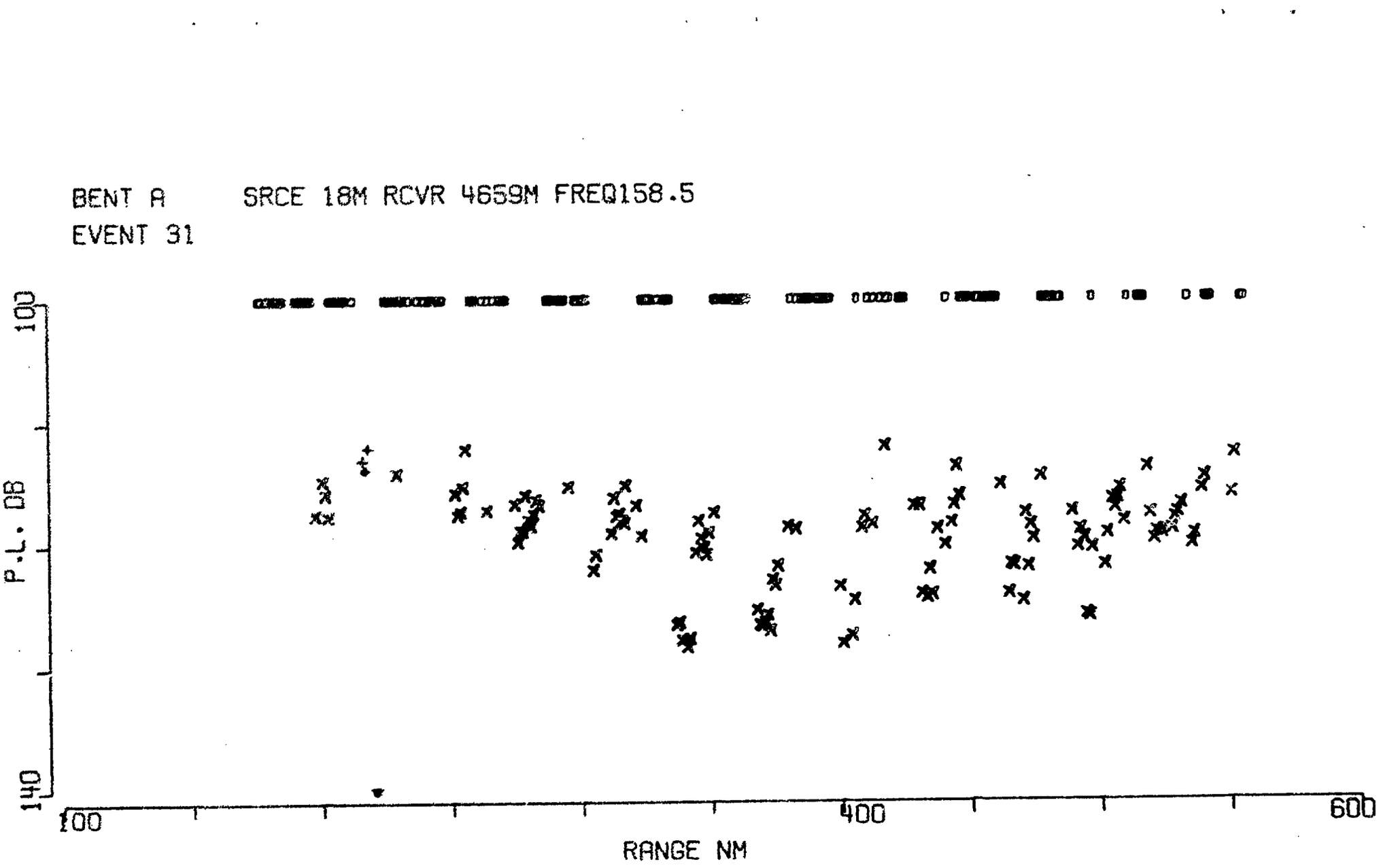
BENT A SRCE 18M RCVR 4659M FREQ158.5
EVENT 31
100
140
P.L. DB
100
400
600
RANGE NM

FIGURE A-29

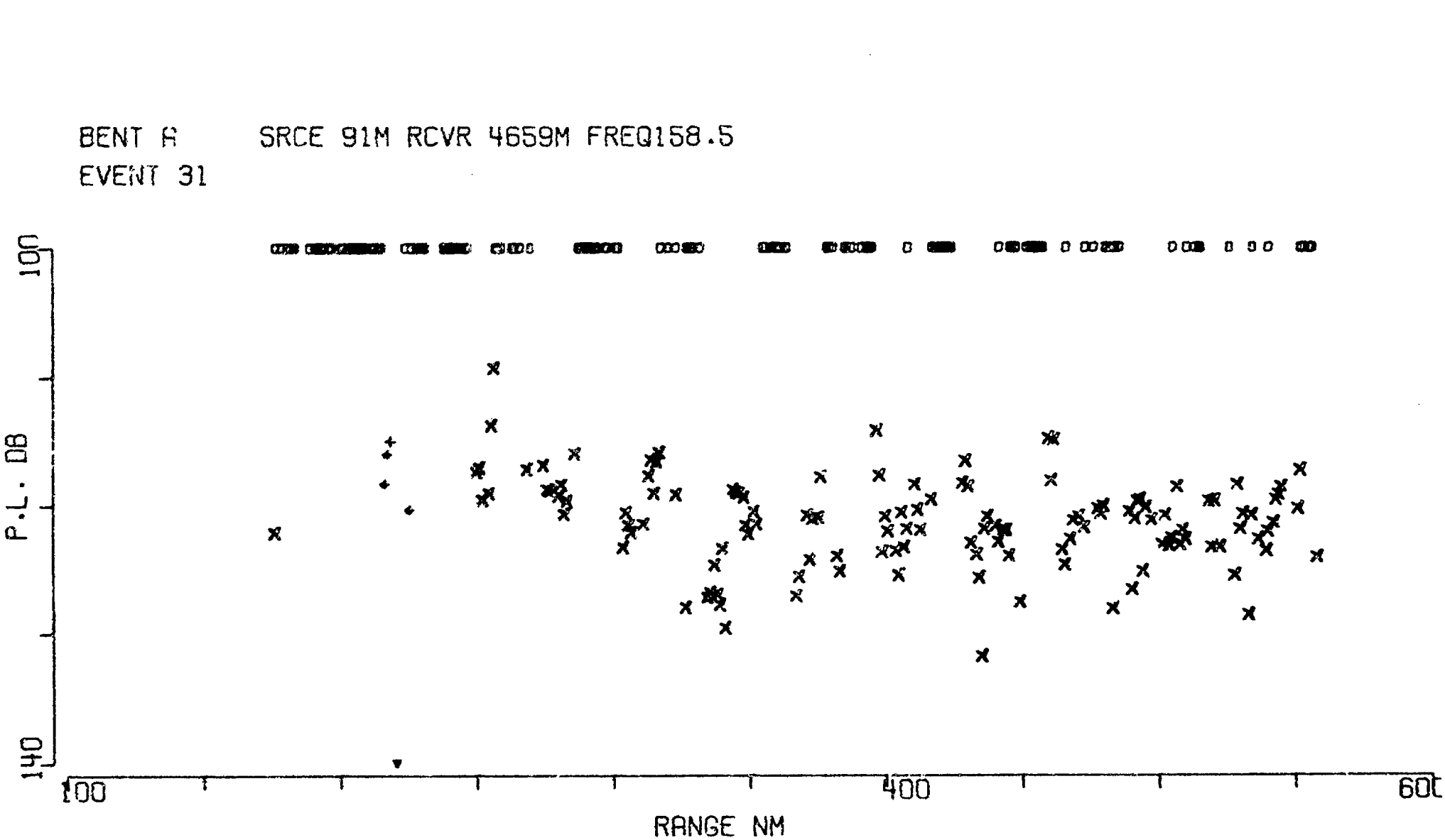
BENT A SRCE 91M RCVR 4659M FREQ158.5
EVENT 31
100
140
P.L. DB
100
400
600
RANGE NM

FIGURE A-30

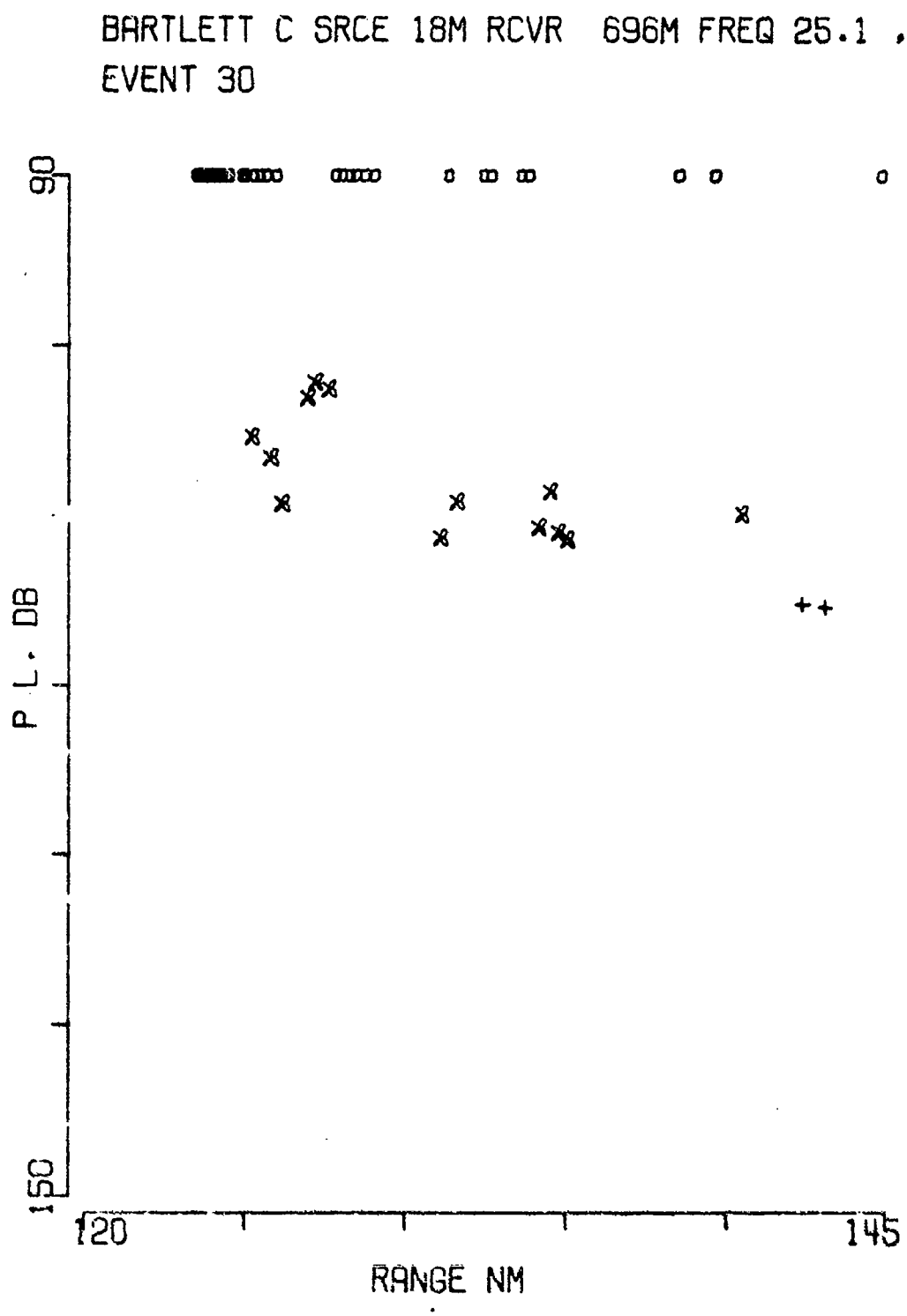
BARTLETT C SRCE 18M RCVR 696M FREQ 25.1 ,1 OCT
EVENT 30
90
150
P L. DB
120
145
RANGE NM

FIGURE A-51

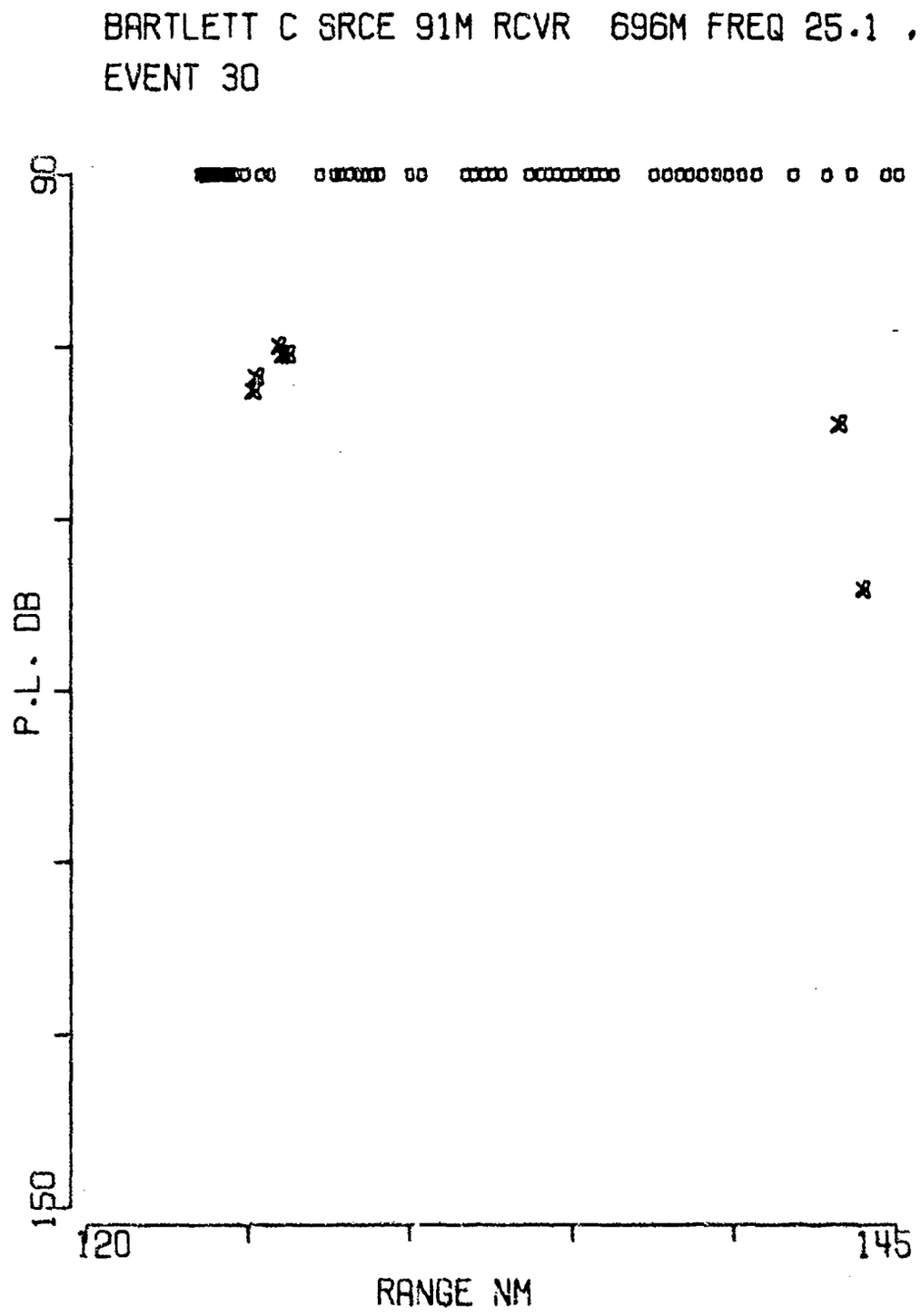
BARTLETT C SRCE 91M RCVR 696M FREQ 25.1 .1 OCT
EVENT 30
90
150
P.L. DB
120
145
RANGE NM

FIGURE A-32

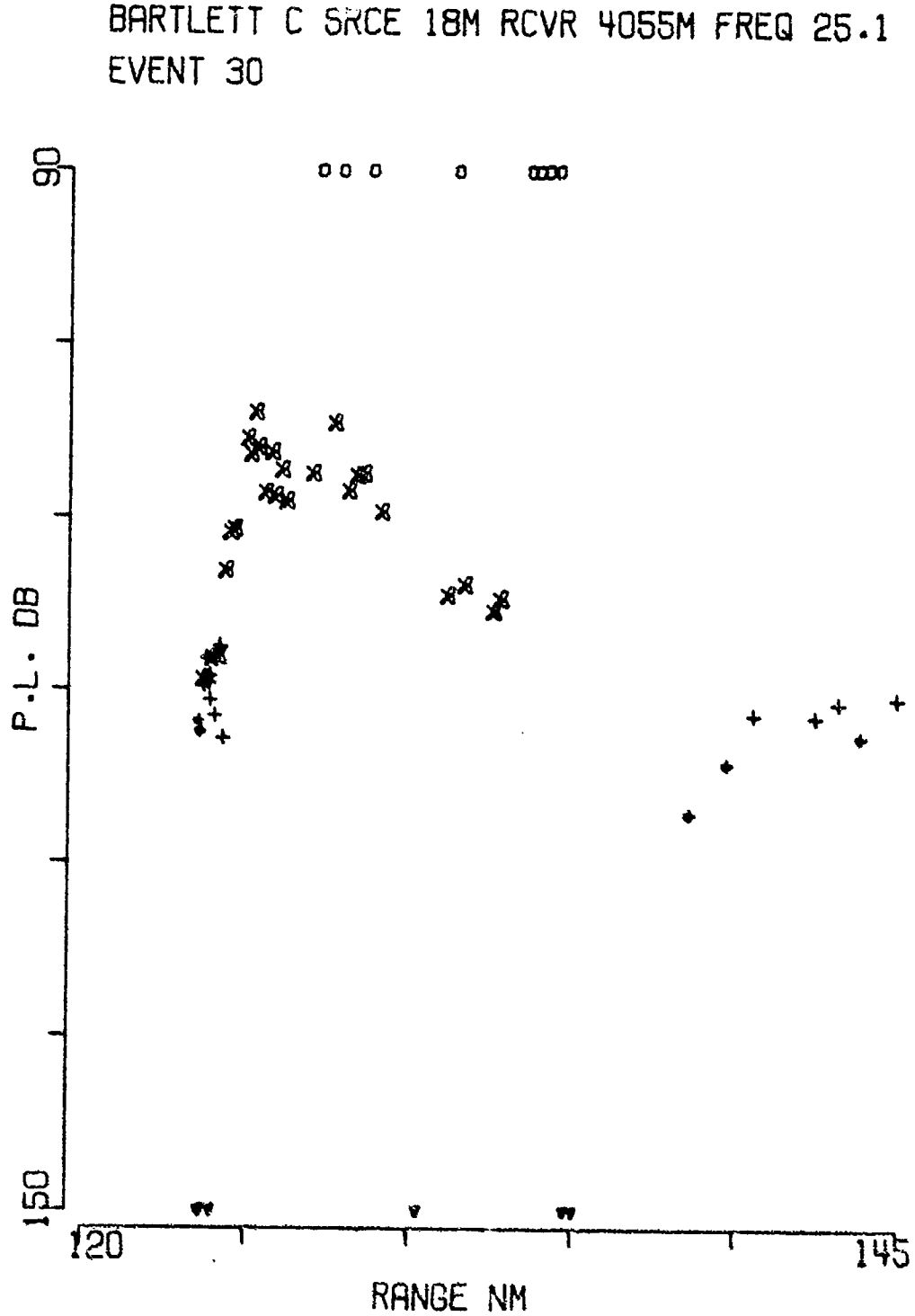
BARTLETT C SRCE 18M RCVR 4055M FREQ 25.1 .1 OCT
EVENT 30
90
150
P.L. DB
120
145
RANGE NM

FIGURE A-33

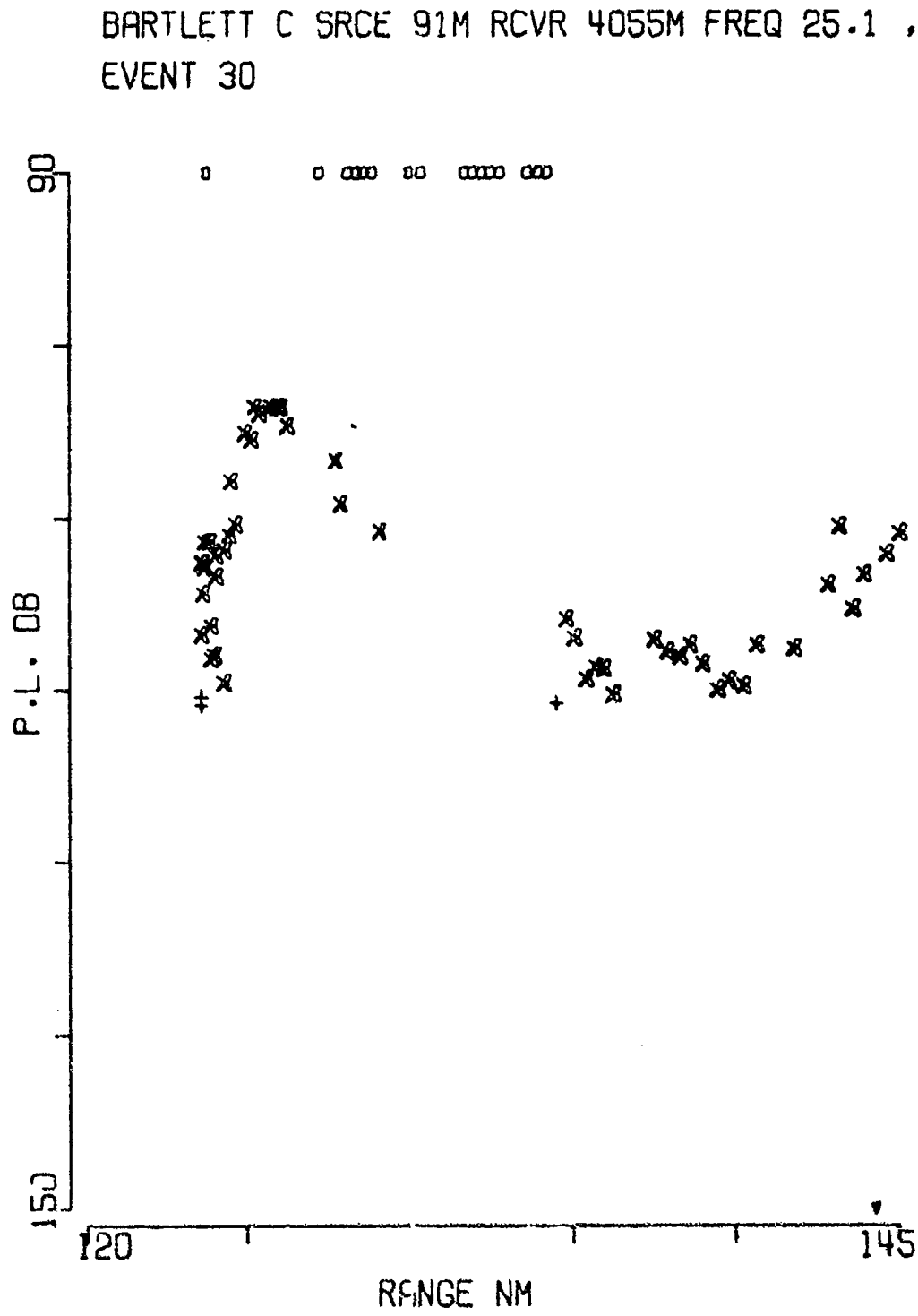
BARTLETT C SRCE 91M RCVR 4055M FREQ 25.1 ,1 OCT
EVENT 30
90
150
P.L. DB
120
145
RANGE NM

FIGURE A-34

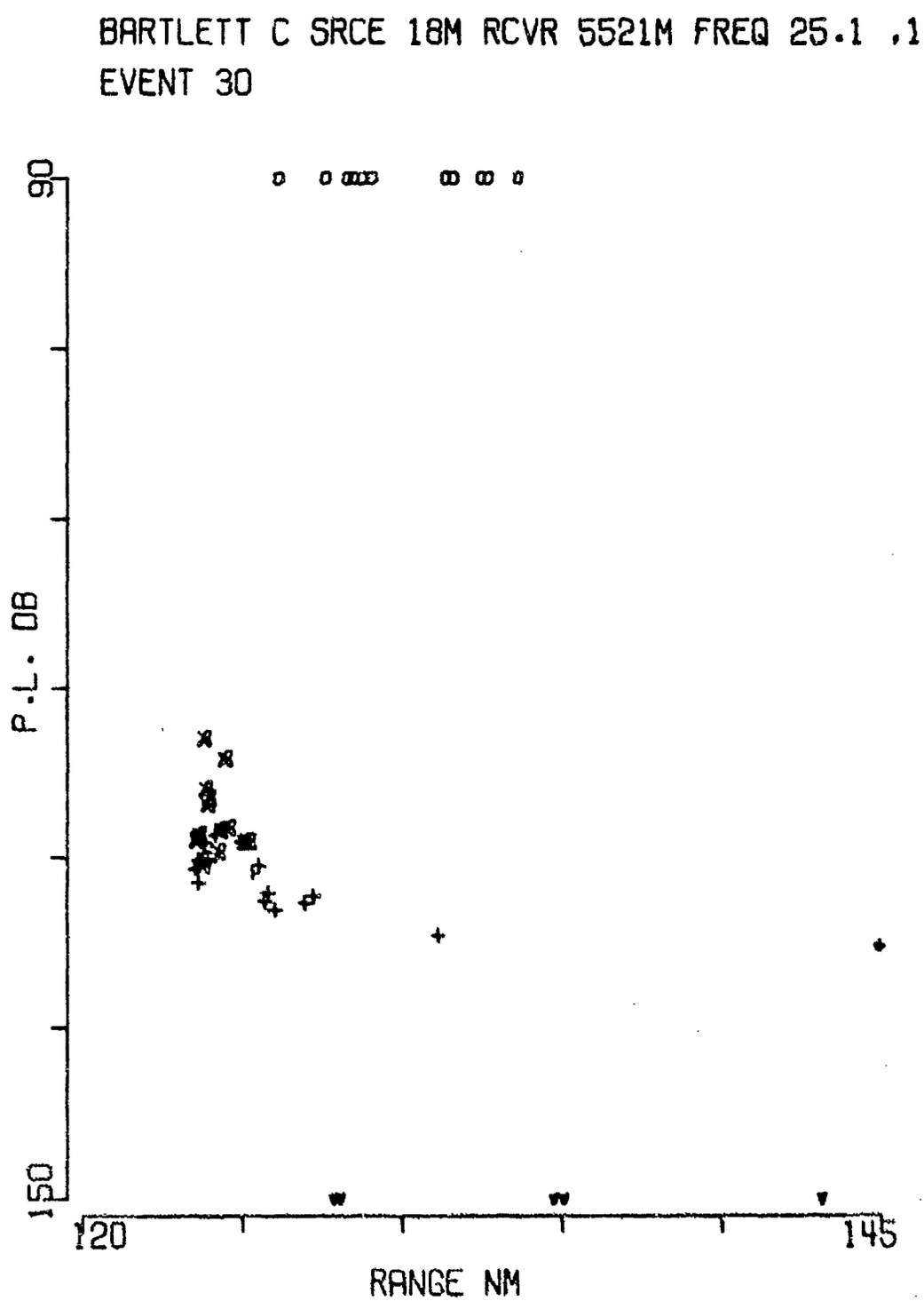
BARTLETT C SRCE 18M RCVR 5521M FREQ 25.1 .1 OCT
EVENT 30
90
150
P.L. DB
120
145
RANGE NM

FIGURE A-35

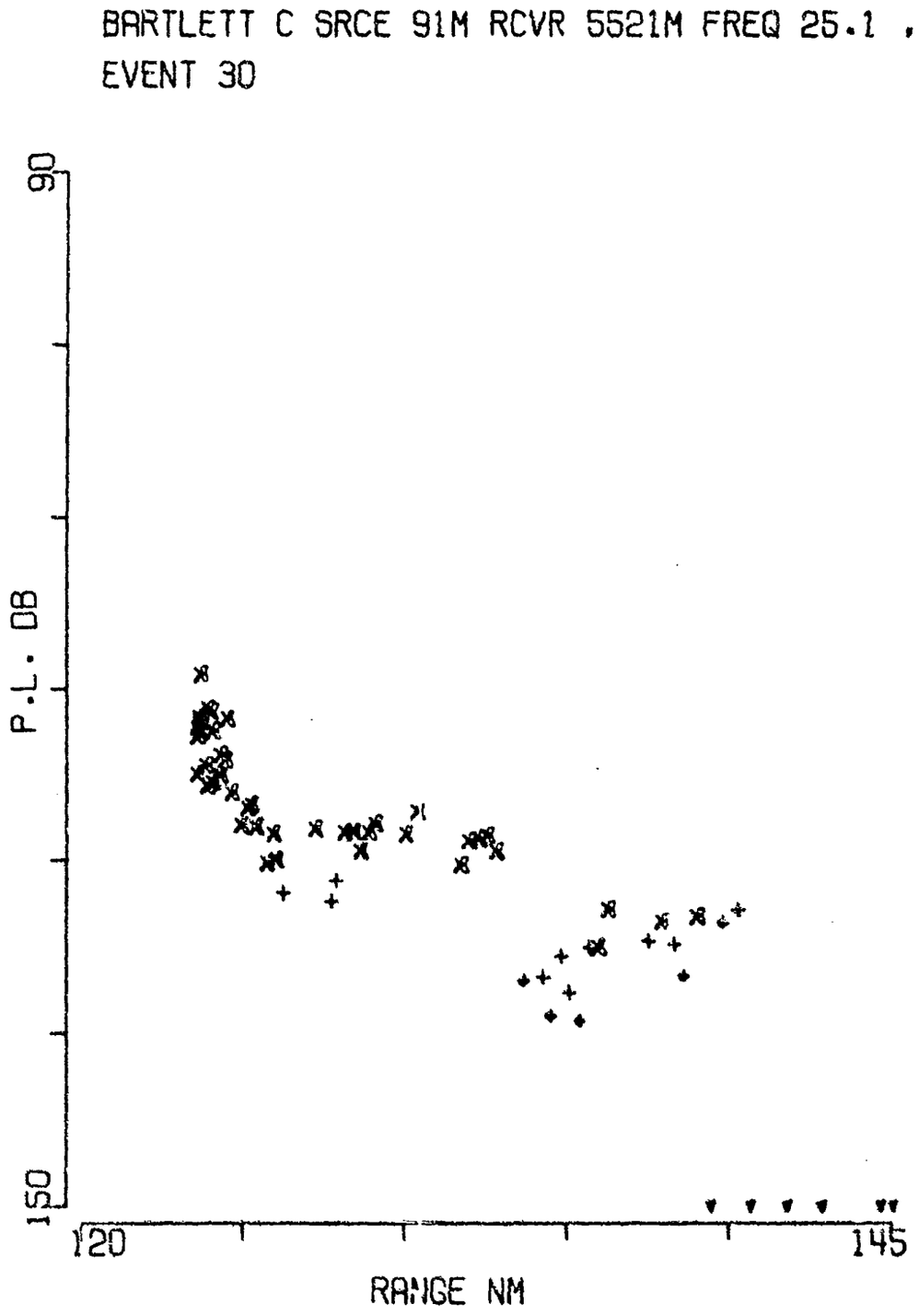
BARTLETT C SRCE 91M RCVR 5521M FREQ 25.1 .1 OCT
EVENT 30
90
150
P.L. DB
120
145
RANGE NM

FIGURE A-36

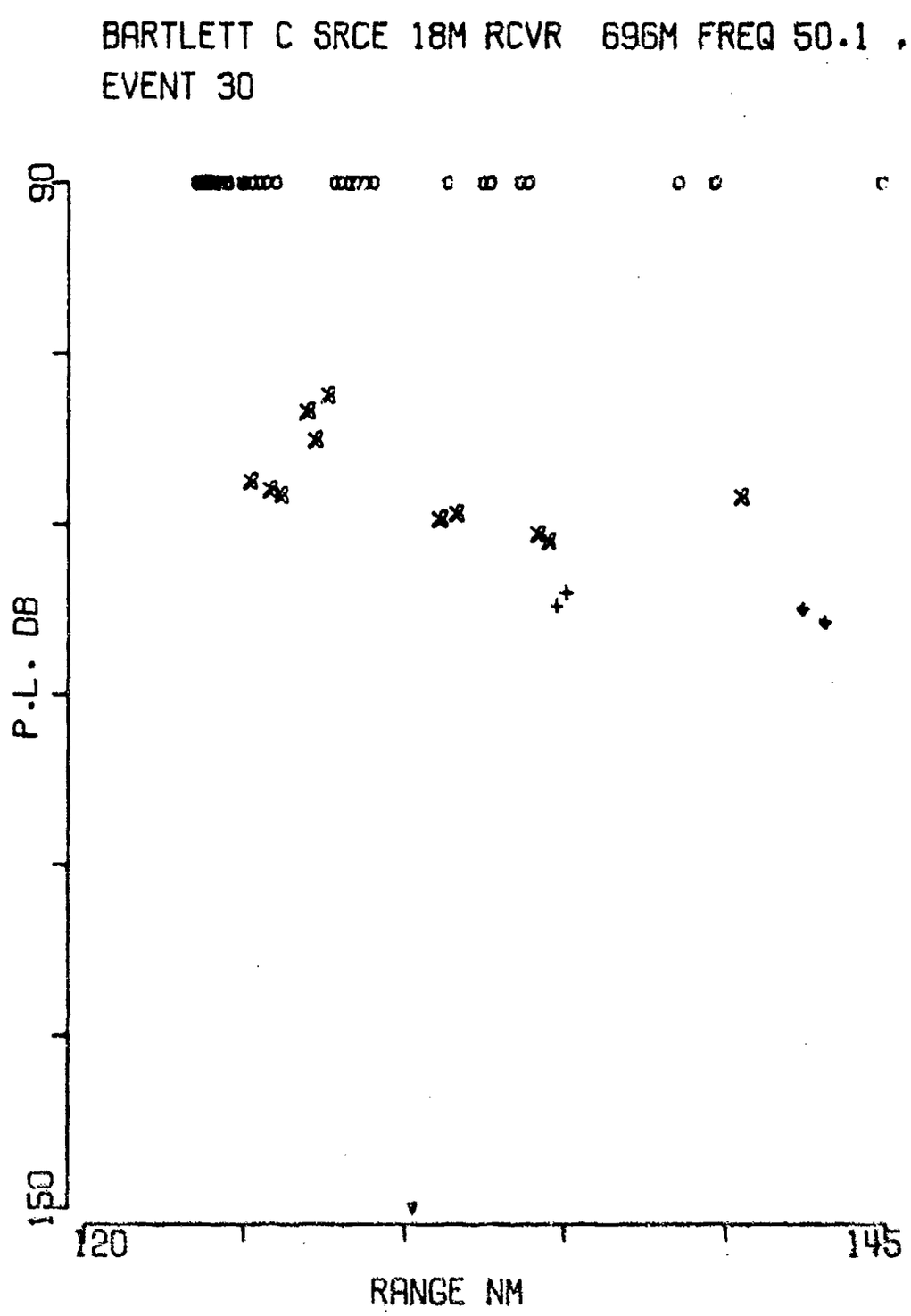
BARTLETT C SRCE 18M RCVR 696M FREQ 50.1 .1 OCT
EVENT 30
90
150
P.L. DB
120
145
RANGE NM

FIGURE A-37

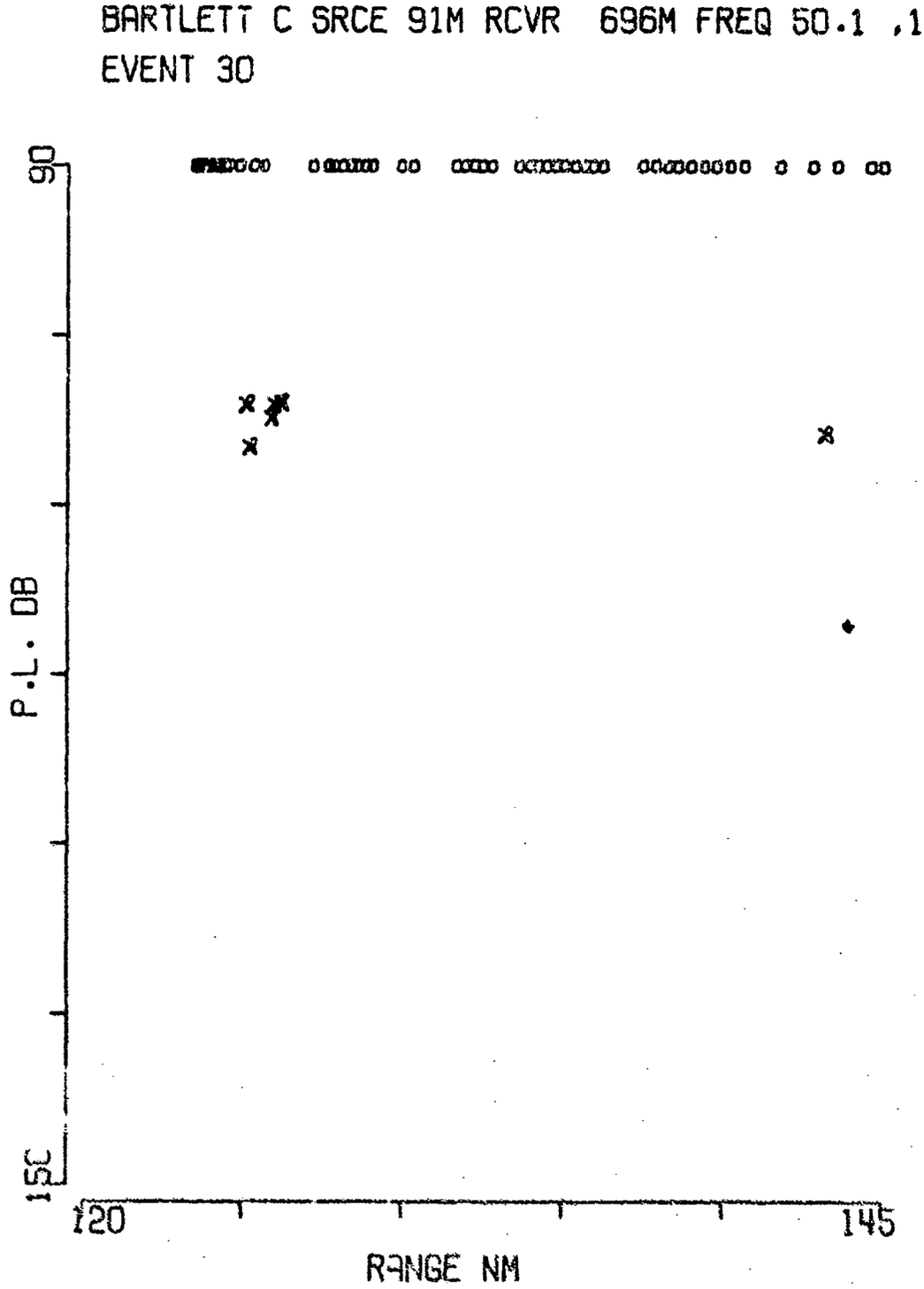
BARTLETT C SRCE 91M RCVR 696M FREQ 50.1 ,1 OCT
EVENT 30
90
150
P.L. DB
120
145
RANGE NM

FIGURE A-38

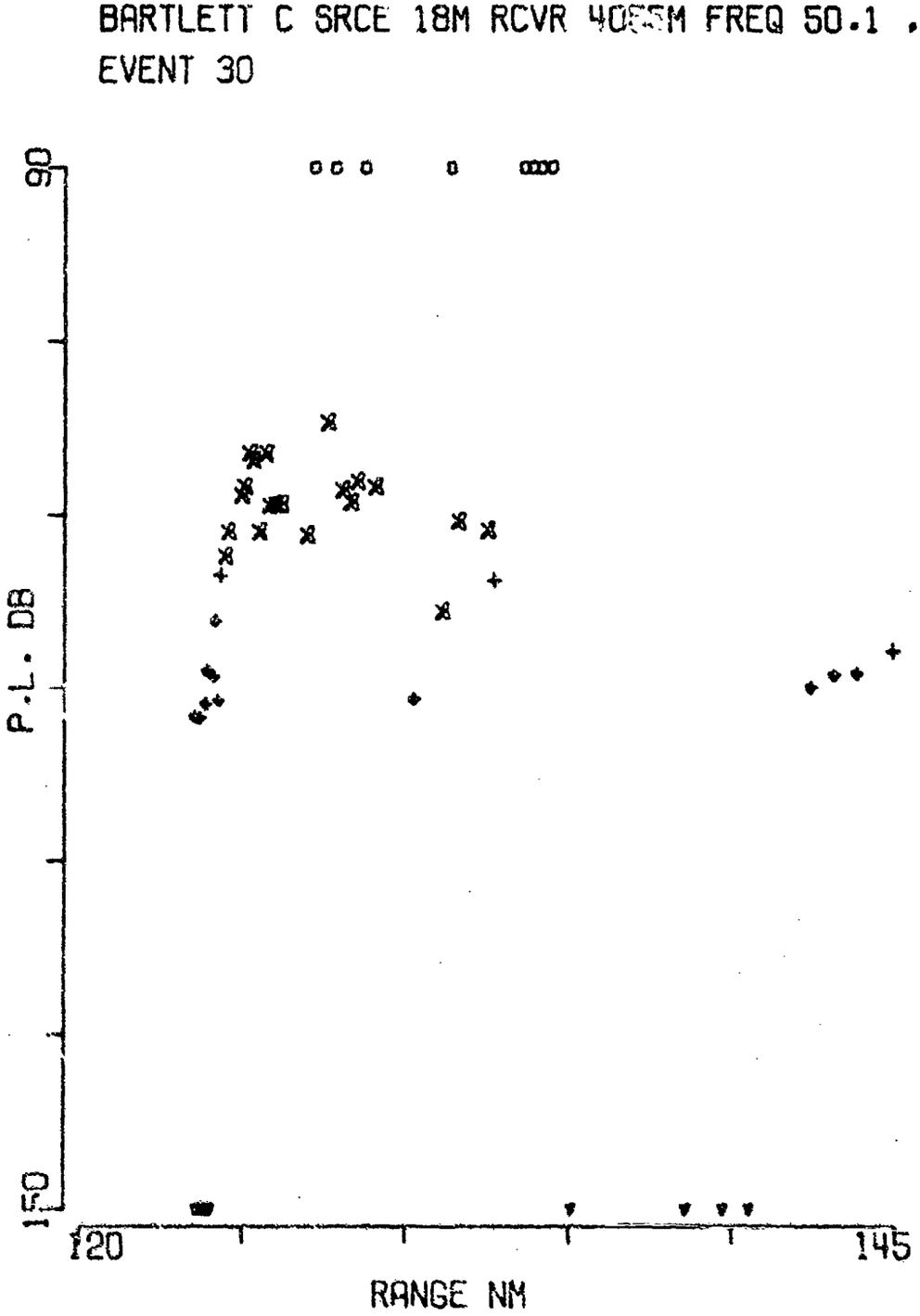
BARTLETT C SRCE 18M RCVR 40[illegible]M FREQ 50.1 .1 OCT
EVENT 30
90
150
P.L. DB
120
145
RANGE NM

FIGURE A-39

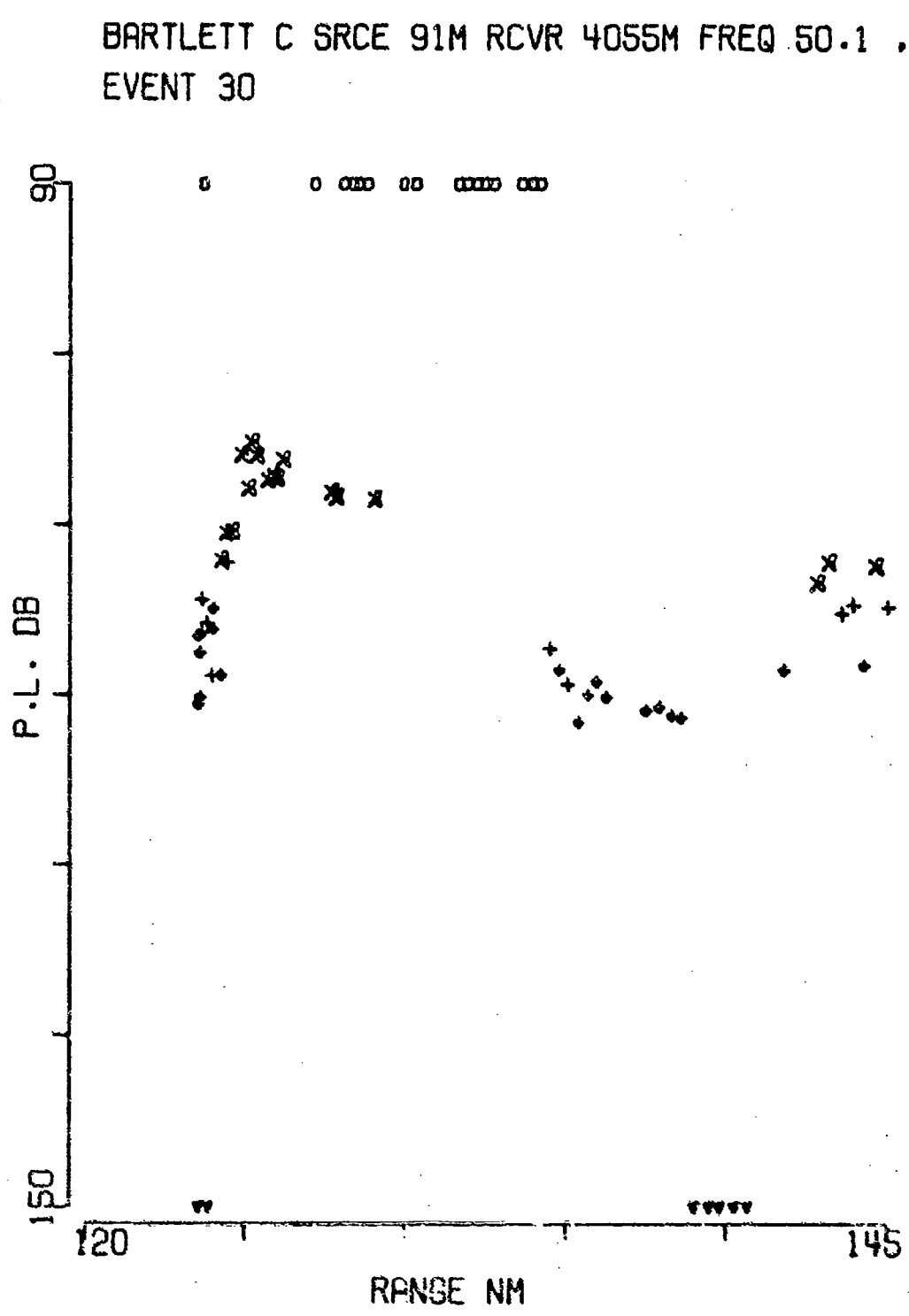
BARTLETT C SRCE 91M RCVR 4055M FREQ 50.1 .1 OCT
EVENT 30
90
150
P.L. DB
120
145
RANGE NM

FIGURE A-40

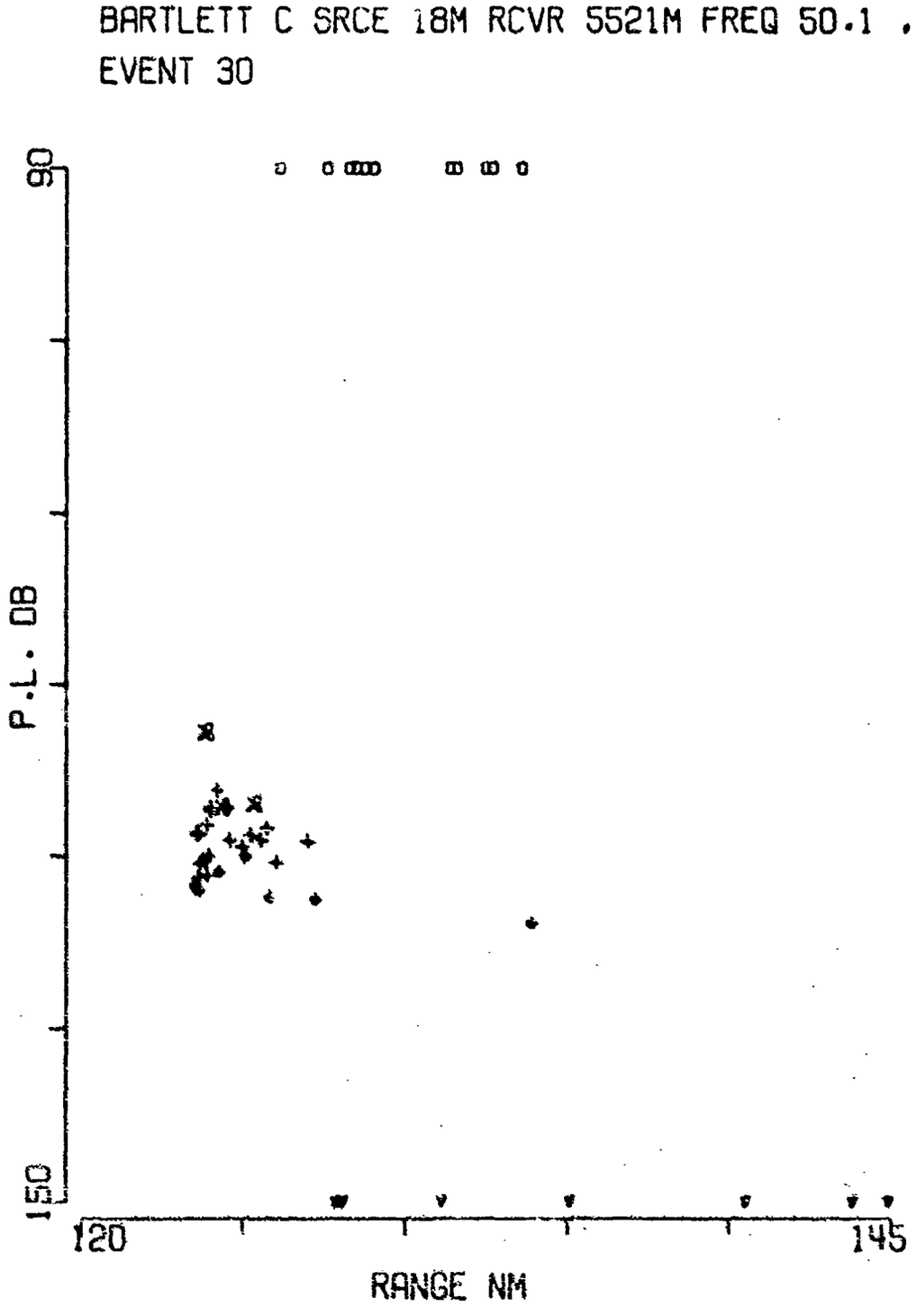
BARTLETT C SRCE 18M RCVR 5521M FREQ 50.1 .1 OCT
EVENT 30
90
150
P.L. DB
120
145
RANGE NM

FIGURE A-41

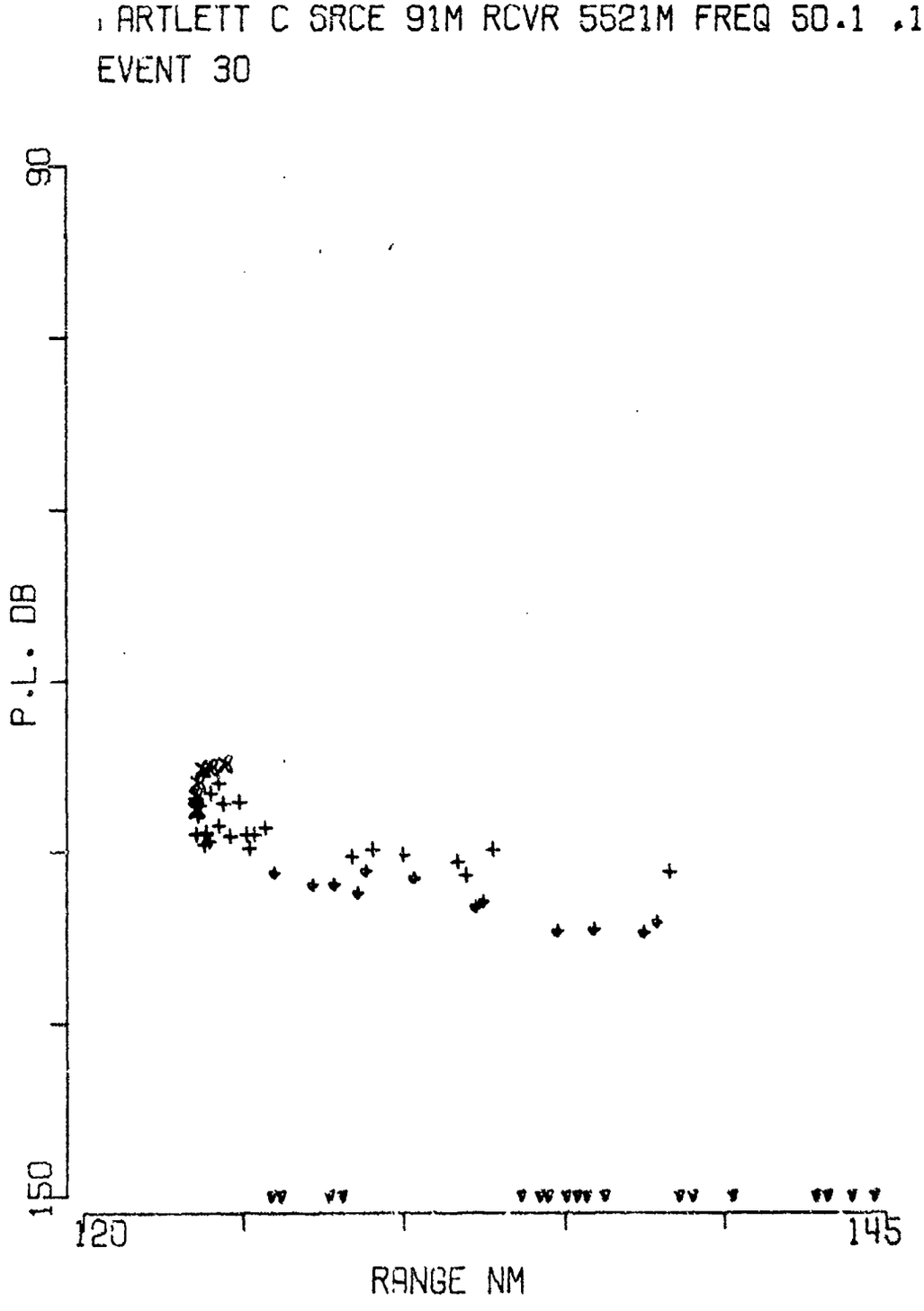
, ARTLETT C SRCE 91M RCVR 5521M FREQ 50.1 .1 OCT
EVENT 30
90
P.L. DB
150
120
145
RANGE NM

FIGURE A-42

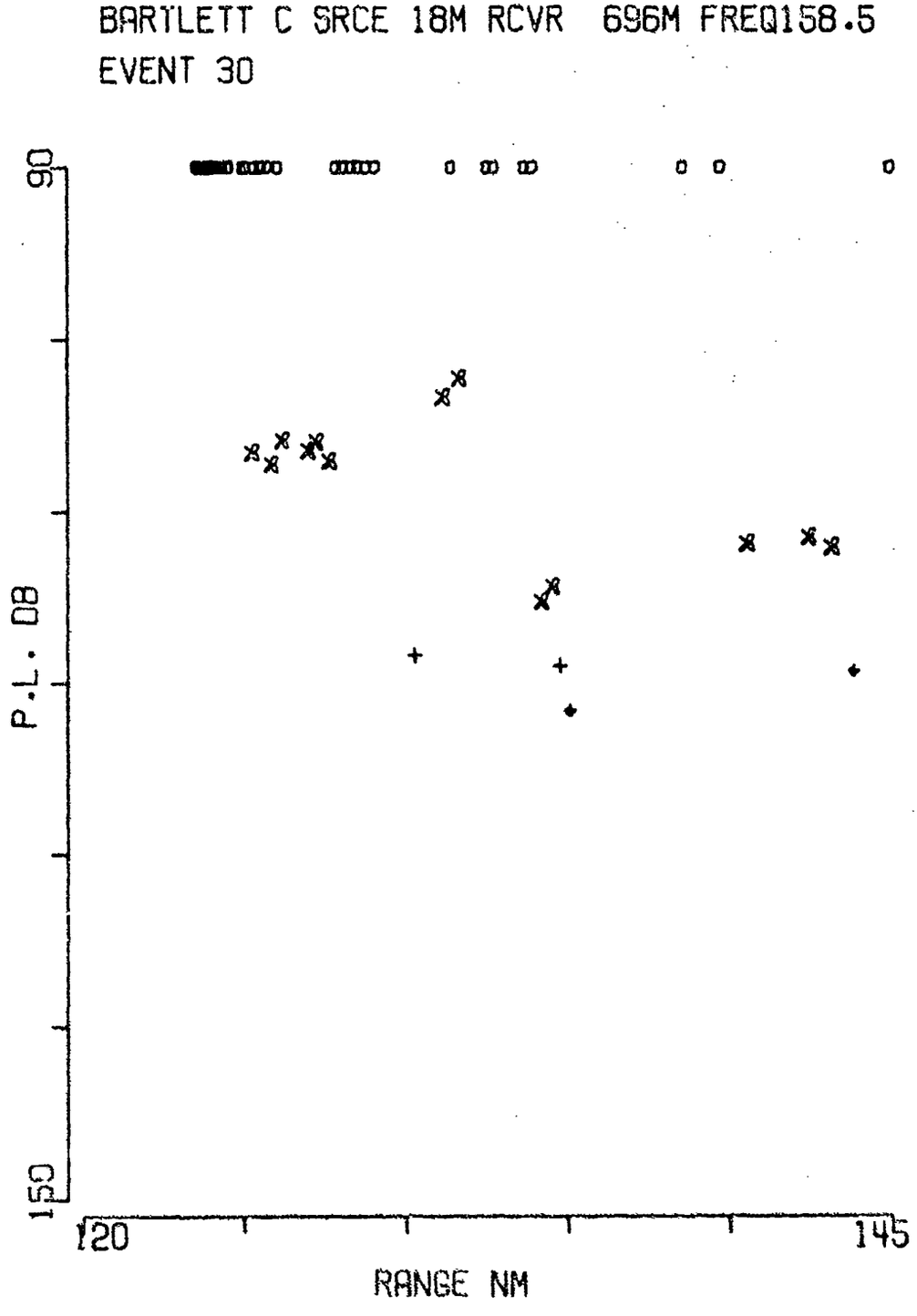
BARTLETT C SRCE 18M RCVR 696M FREQ158.5
EVENT 30
90
150
P.L. DB
120
145
RANGE NM

FIGURE A-43

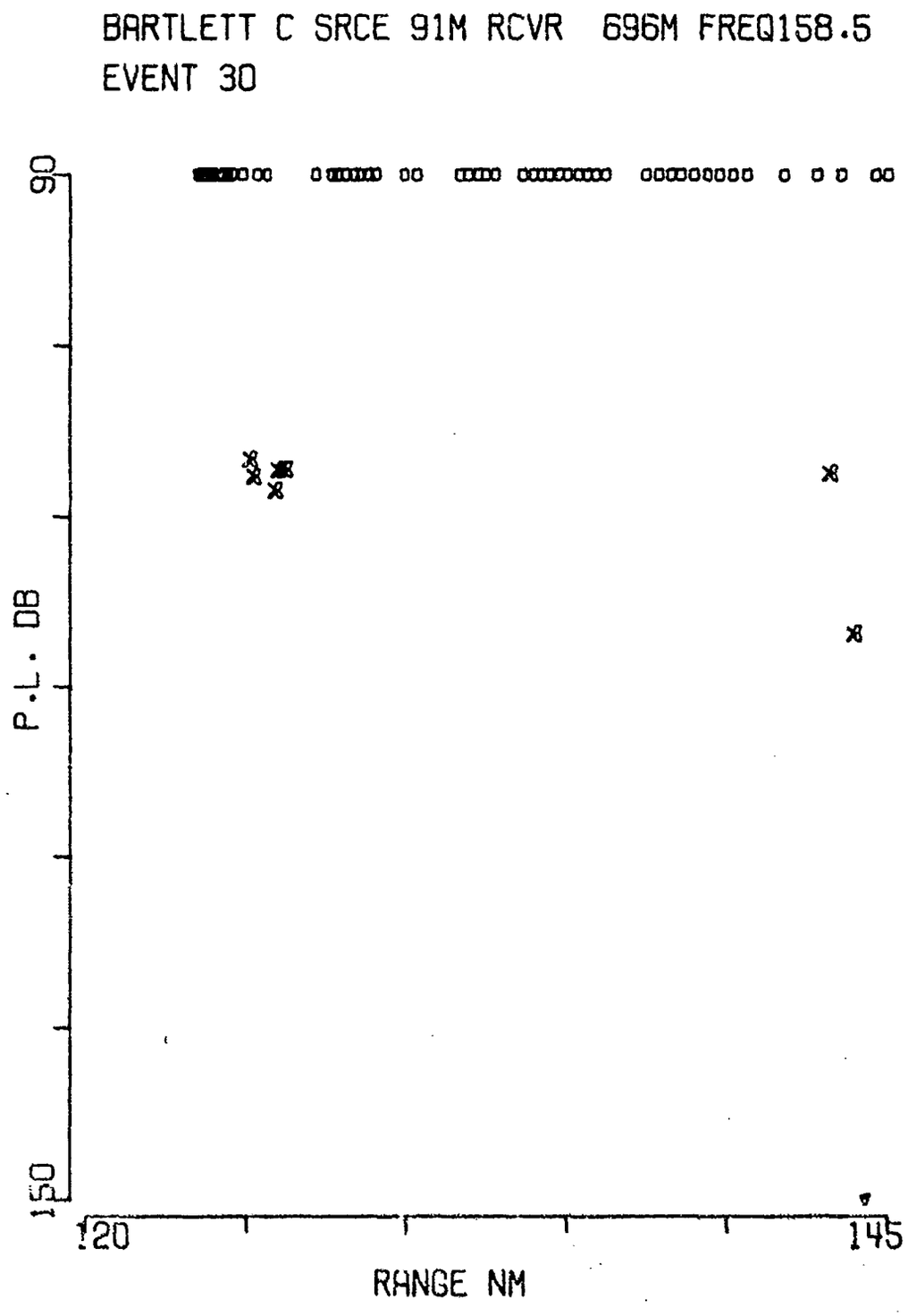
BARTLETT C SRCE 91M RCVR 696M FREQ158.5
EVENT 30
90
150
P.L. DB
120
145
RANGE NM

FIGURE A-44

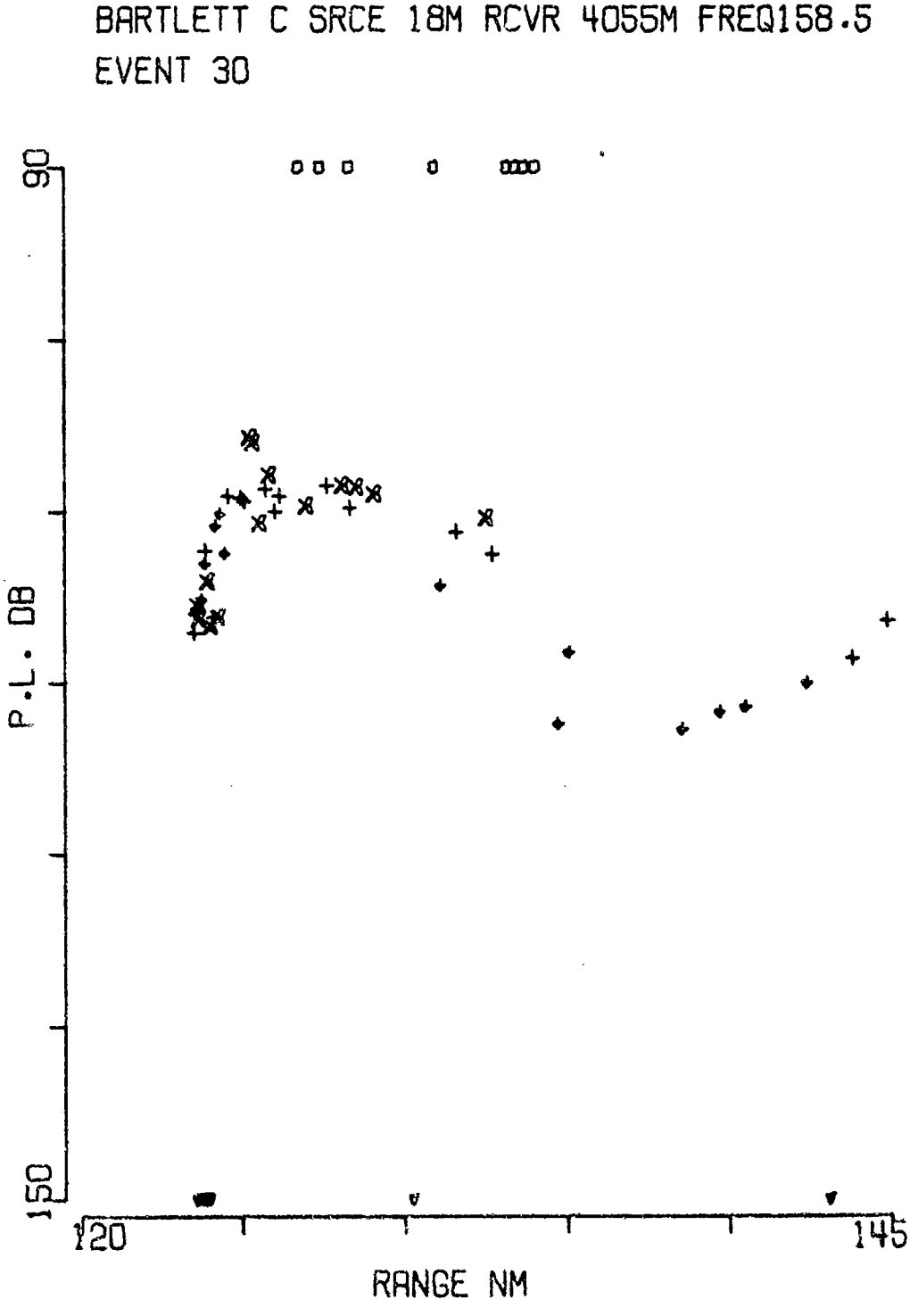
BARTLETT C SRCE 18M RCVR 4055M FREQ158.5
EVENT 30
90
150
P.L. DB
120
145
RANGE NM

FIGURE A-45

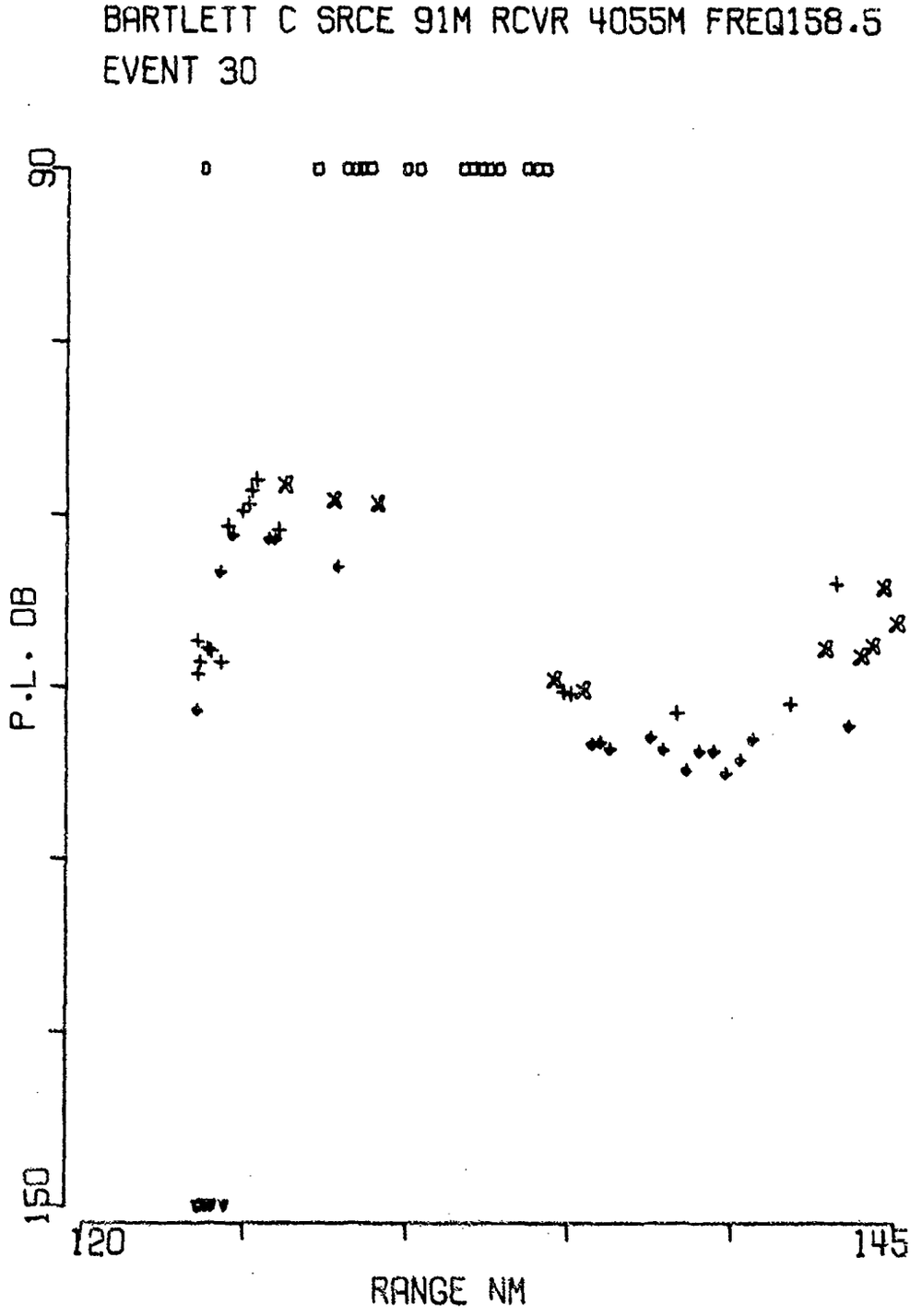
BARTLETT C SRCE 91M RCVR 4055M FREQ158.5
EVENT 30
90
150
P.L. DB
120
145
RANGE NM

FIGURE A-46

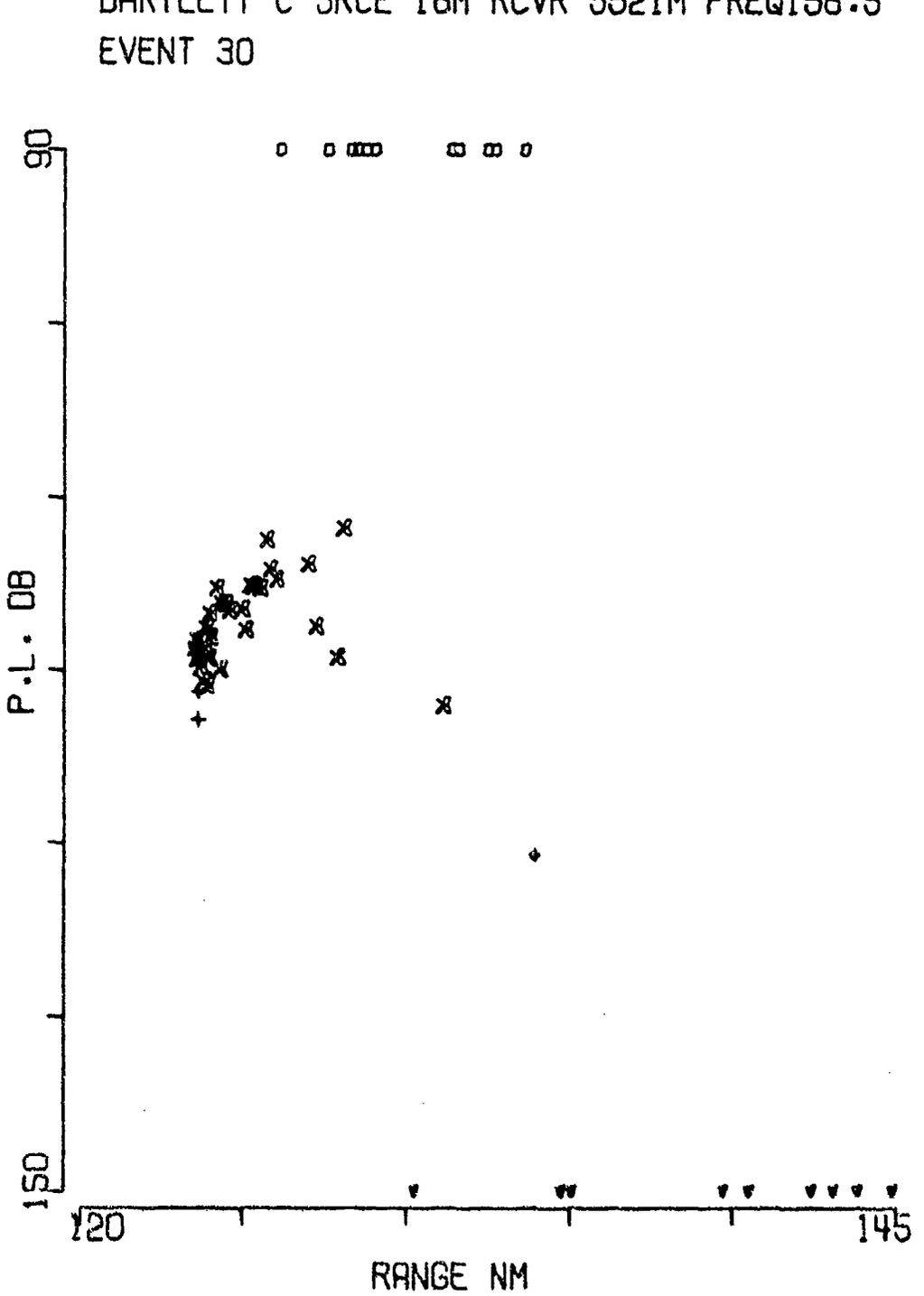
BARTLETT C SRCE 18M RCVR 5521M FREQ158.5
EVENT 30
90
150
P.L. DB
120
145
RANGE NM

FIGURE A-47

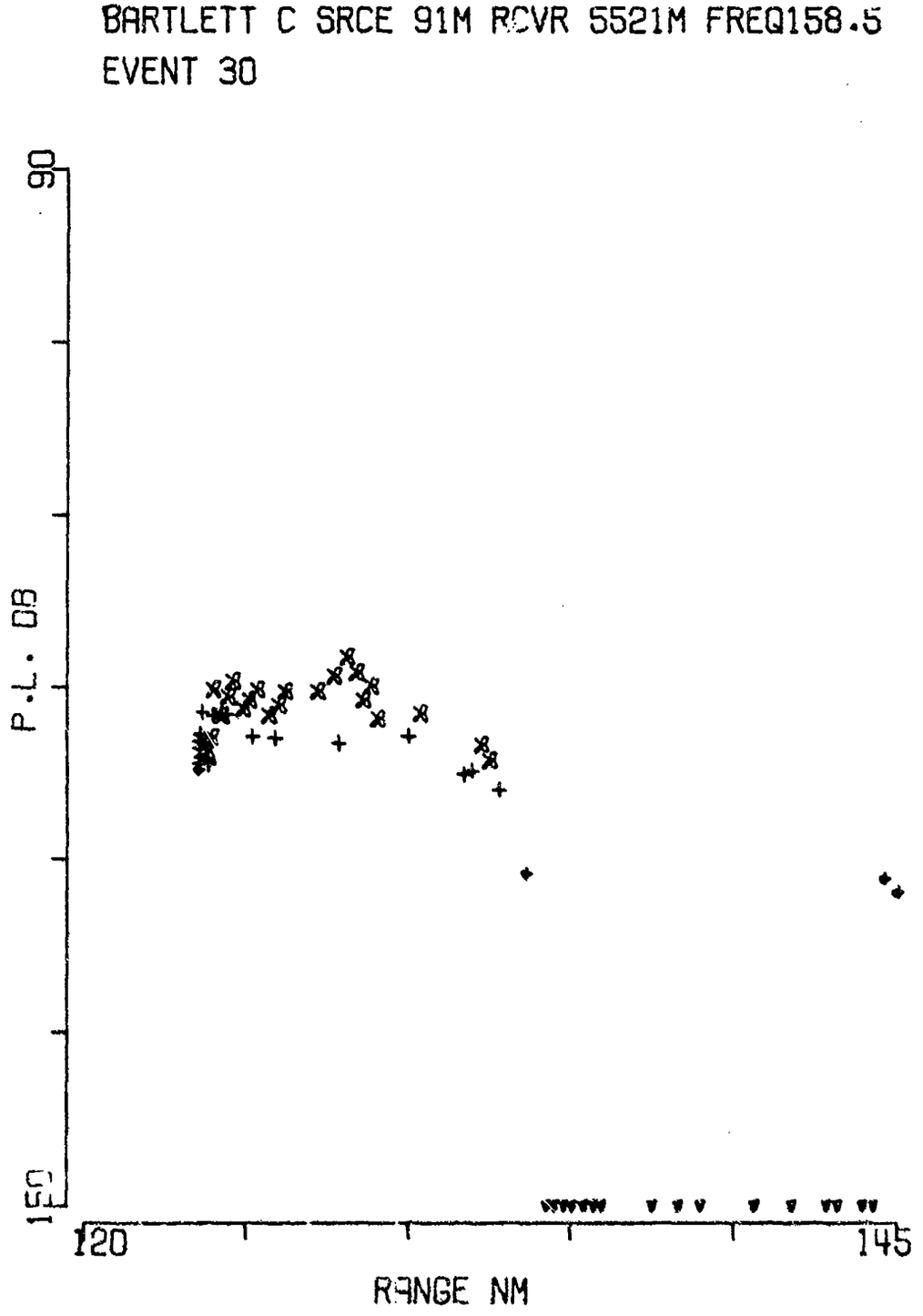
BARTLETT C SRCE 91M RCVR 5521M FREQ158.5
EVENT 30
90
P.L. DB
150
120
145
RANGE NM

FIGURE A-48

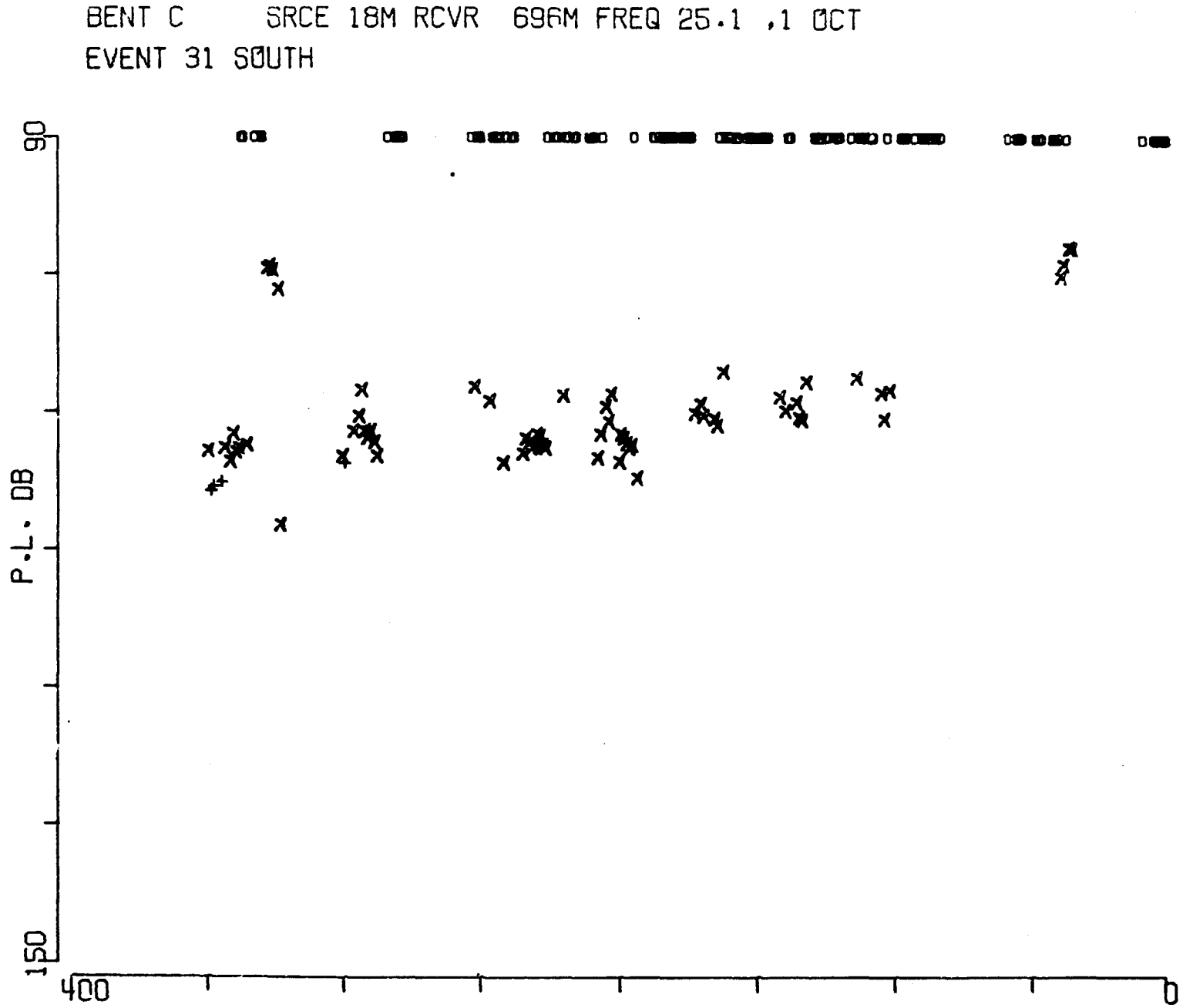
BENT C SRCE 18M RCVR 696M FREQ 25.1 ,1 OCT
EVENT 31 SOUTH
90
150
P.L. DB
400
0
RANGE NM

FIGURE A-49

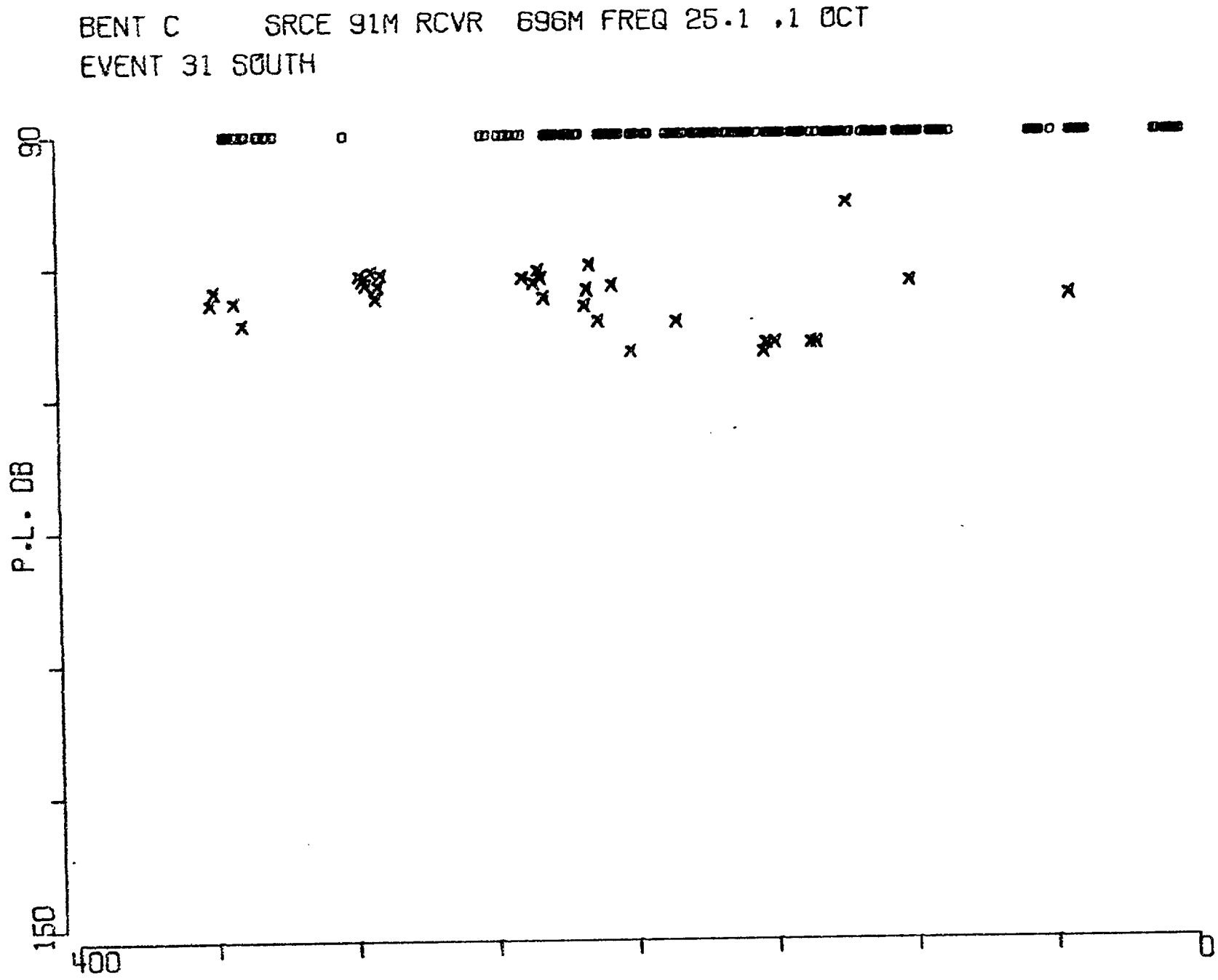
BENT C SRCE 91M RCVR 696M FREQ 25.1 .1 OCT
EVENT 31 SOUTH
90
150
P.L. DB
400
0
RANGE NM

FIGURE A-50

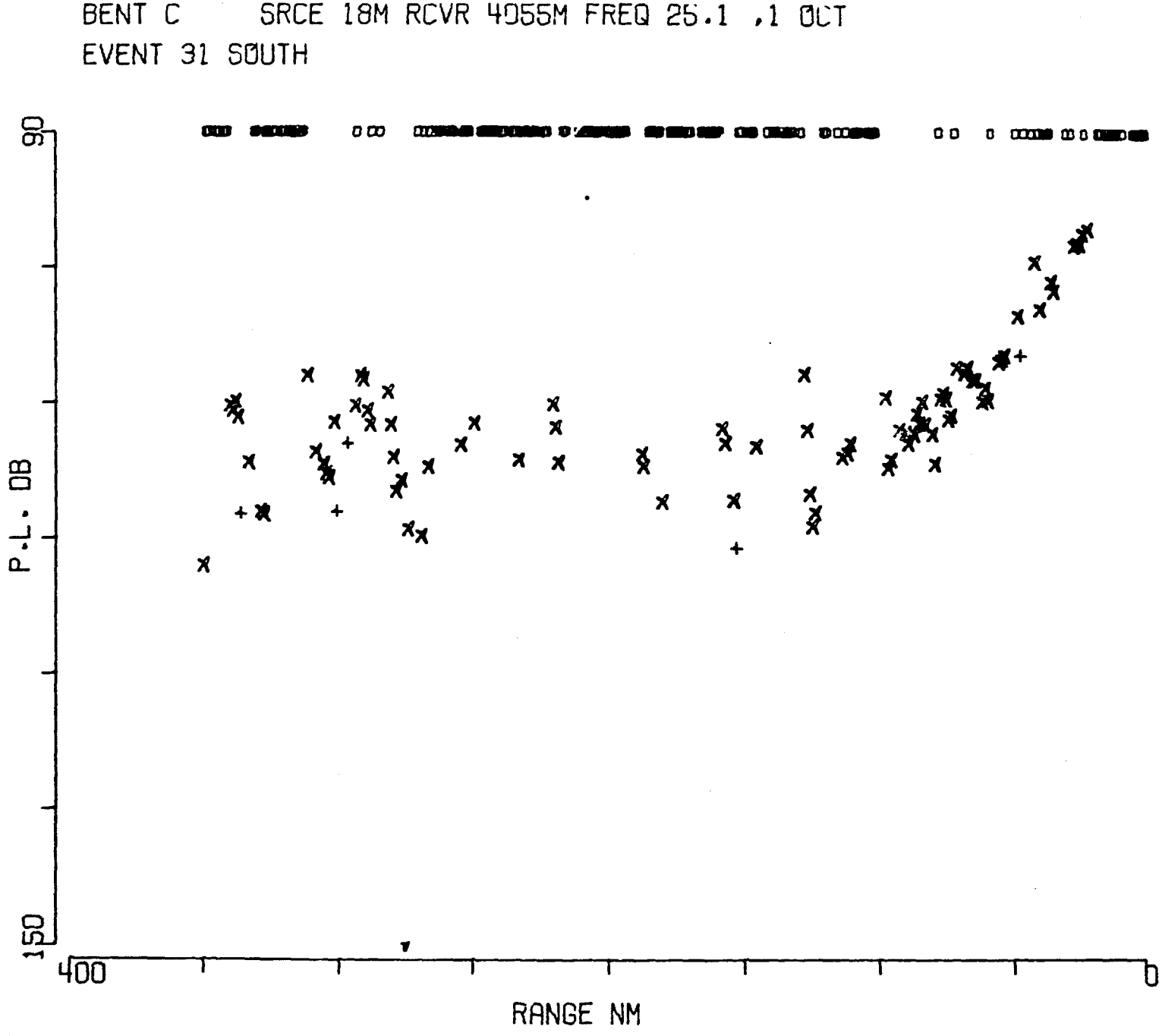
BENT C SRCE 18M RCVR 4055M FREQ 25.1 ,1 OCT
EVENT 31 SOUTH
90
150
P.L. DB
400
0
RANGE NM

FIGURE A-51

BENT C SRCE 91M RCVR 4055M FREQ 25.1 ,1 OCT
EVENT 31 SOUTH

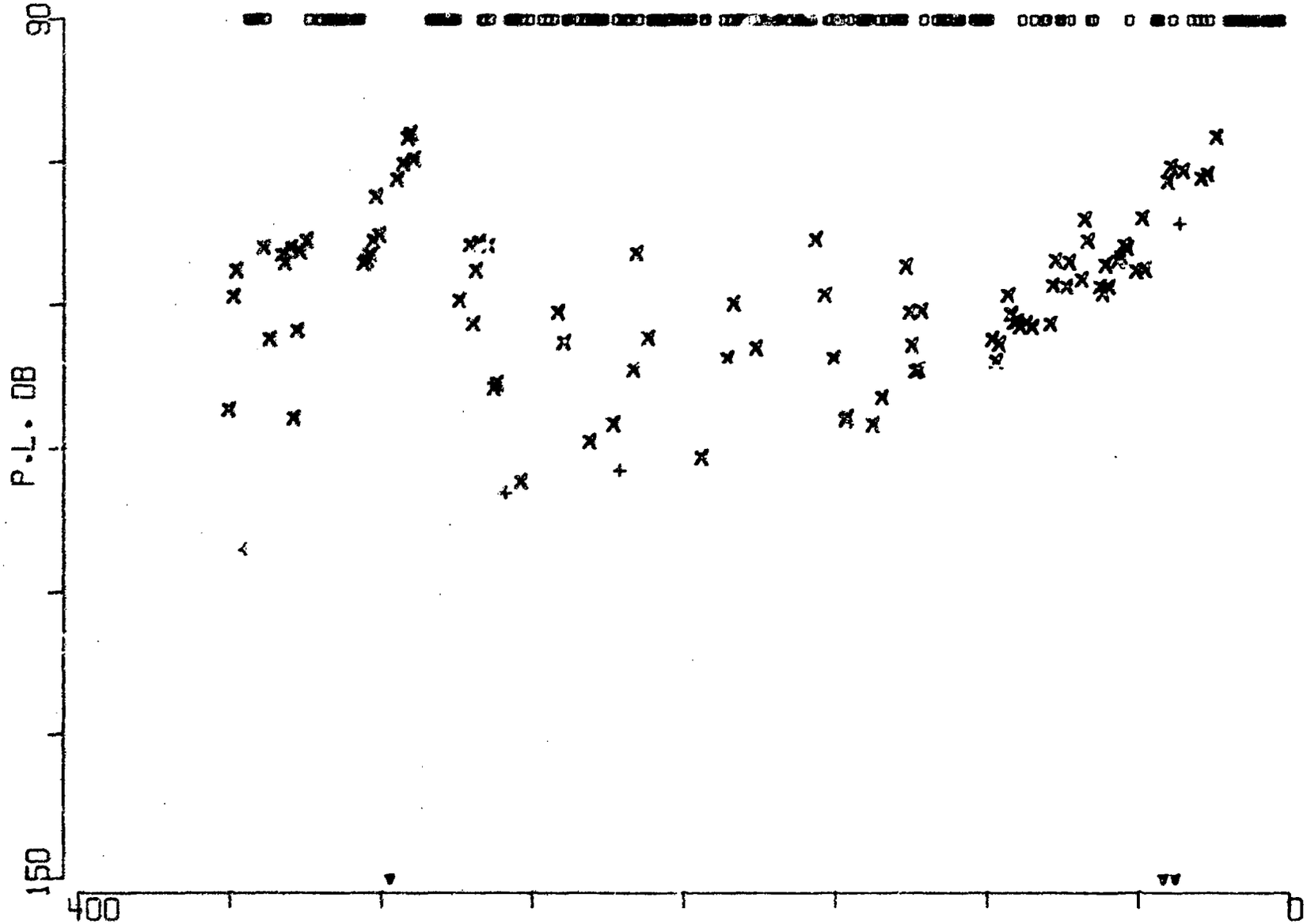

FIGURE A-52

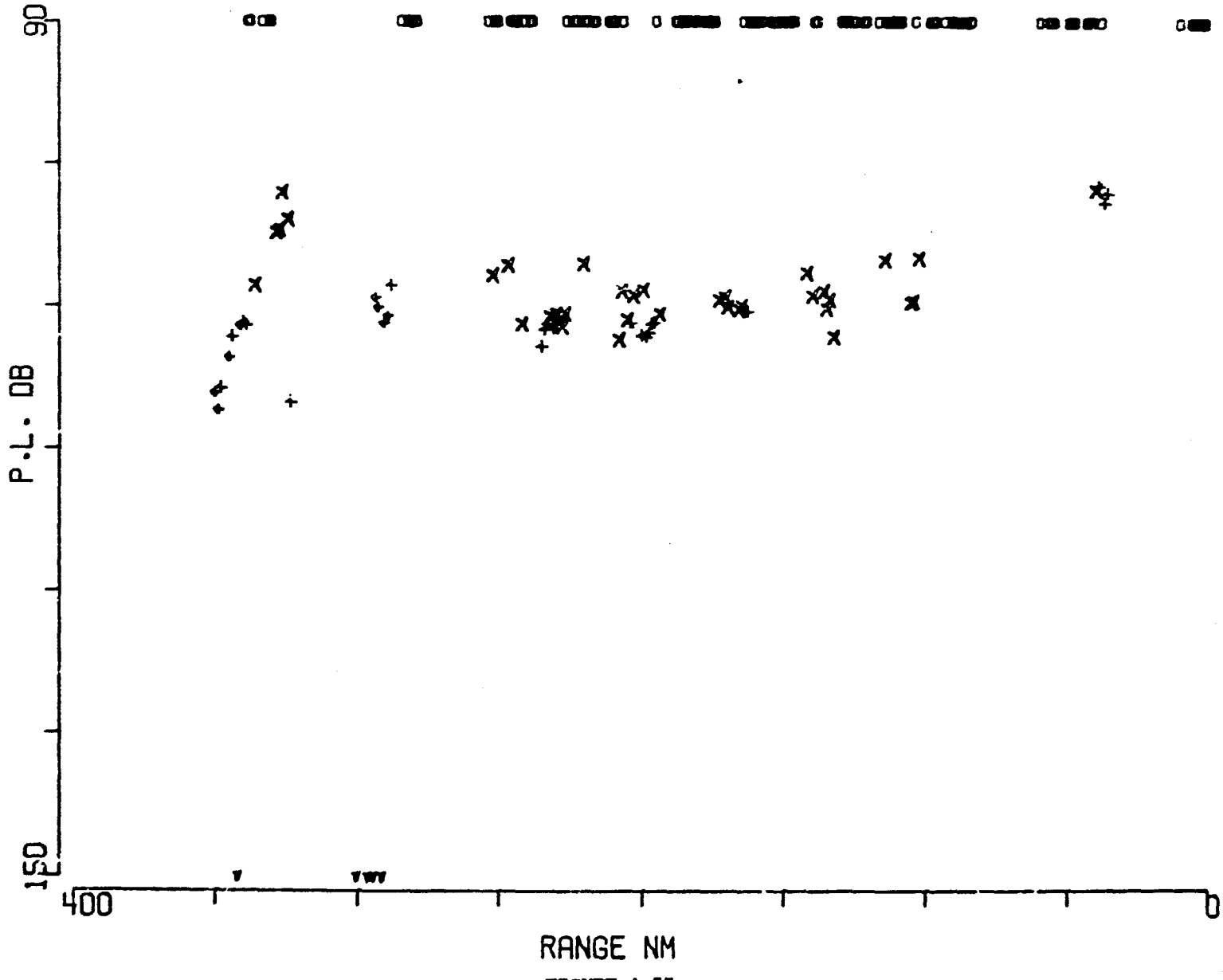
BENT C SRCE 18M RCVR 696M FREQ 50.1 ,1 OCT
EVENT 31 SOUTH
90
150
P.L. DB
400
0
RANGE NM

FIGURE A-35

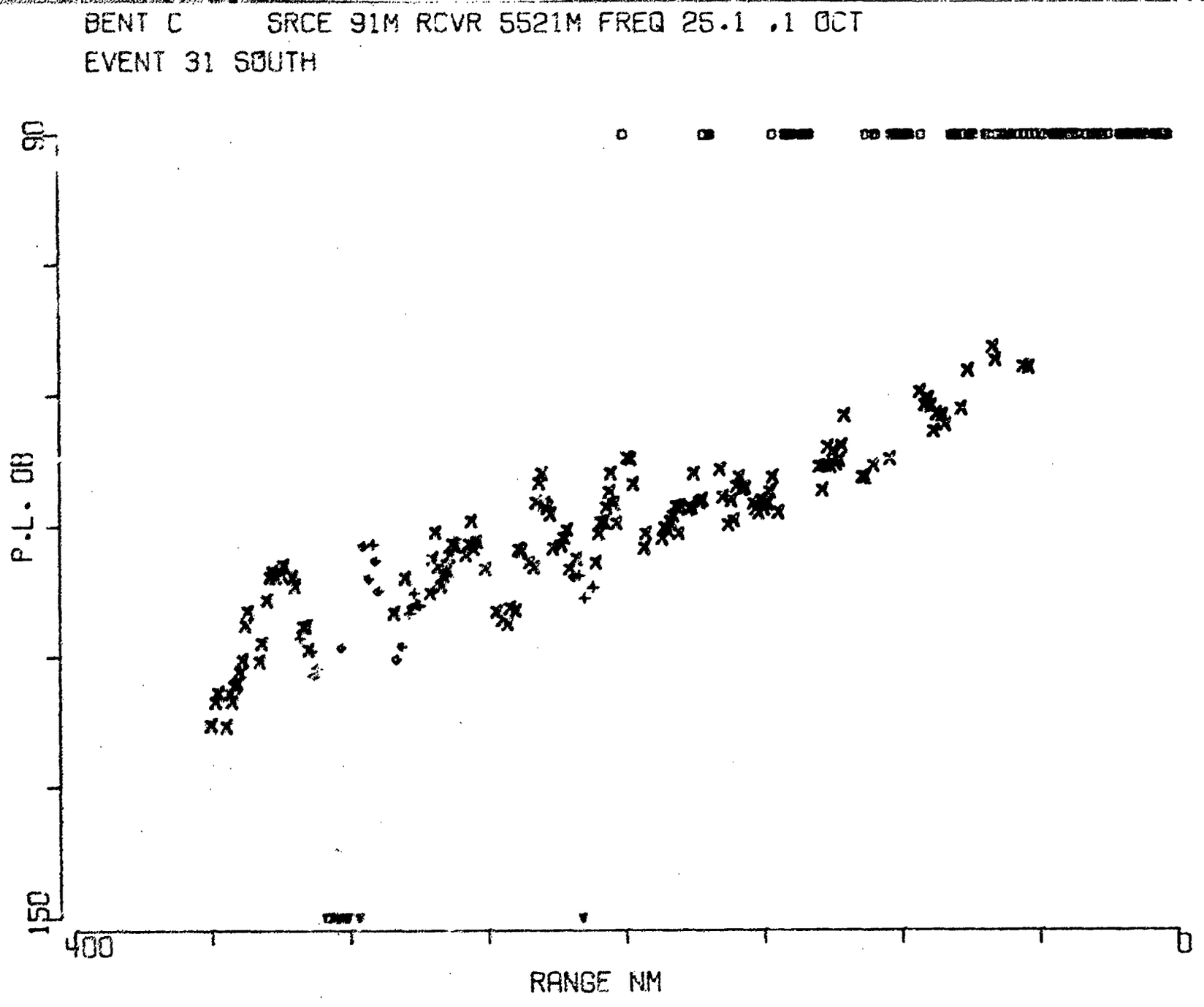
BENT C SRCE 91M RCVR 5521M FREQ 25.1 ,1 OCT
EVENT 31 SOUTH
90
P.L. DB
150
400
0
RANGE NM

FIGURE A-54

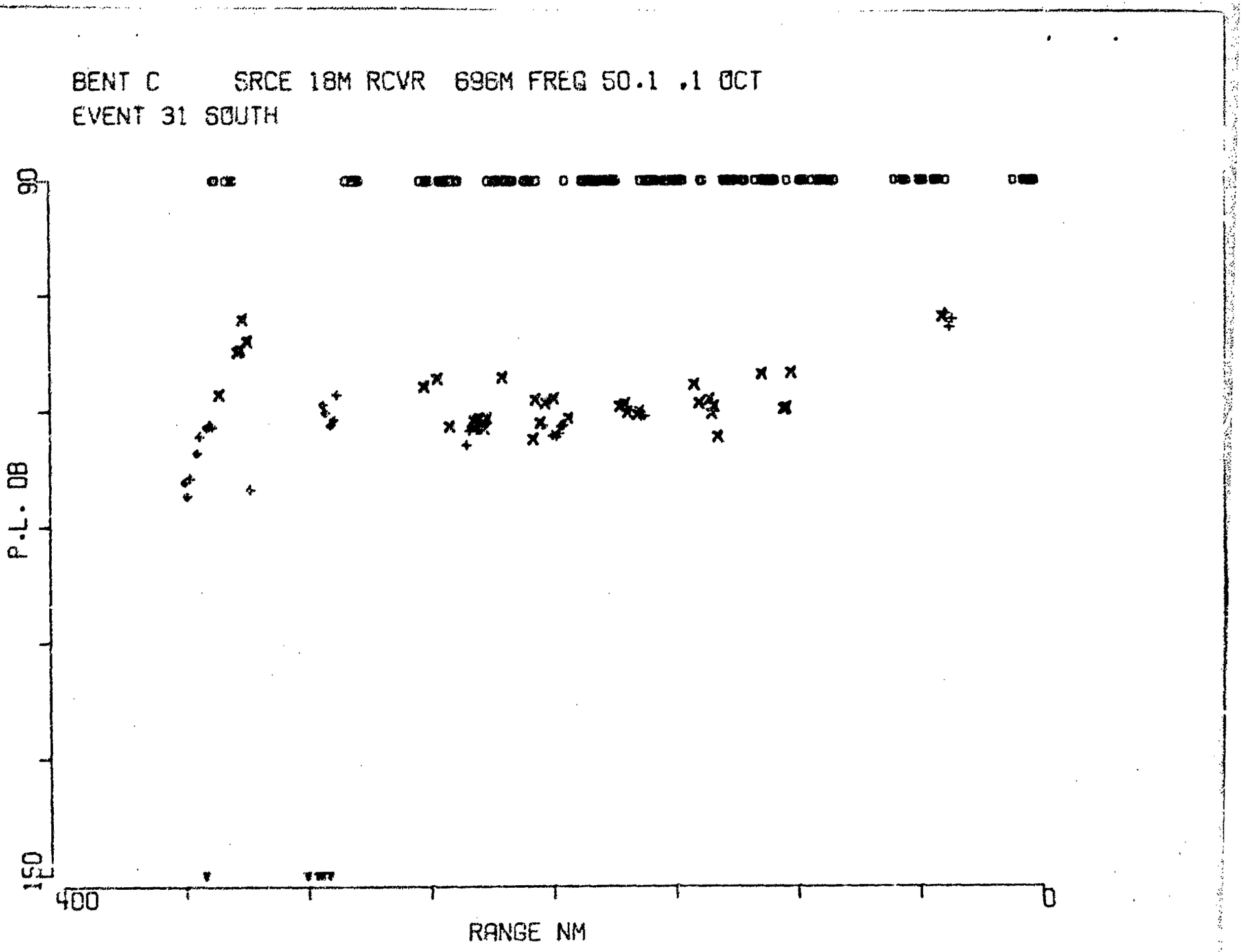
BENT C SRCE 18M RCVR 696M FREQ 50.1 .1 OCT
EVENT 31 SOUTH
90
150
P.L. DB
400
0
RANGE NM

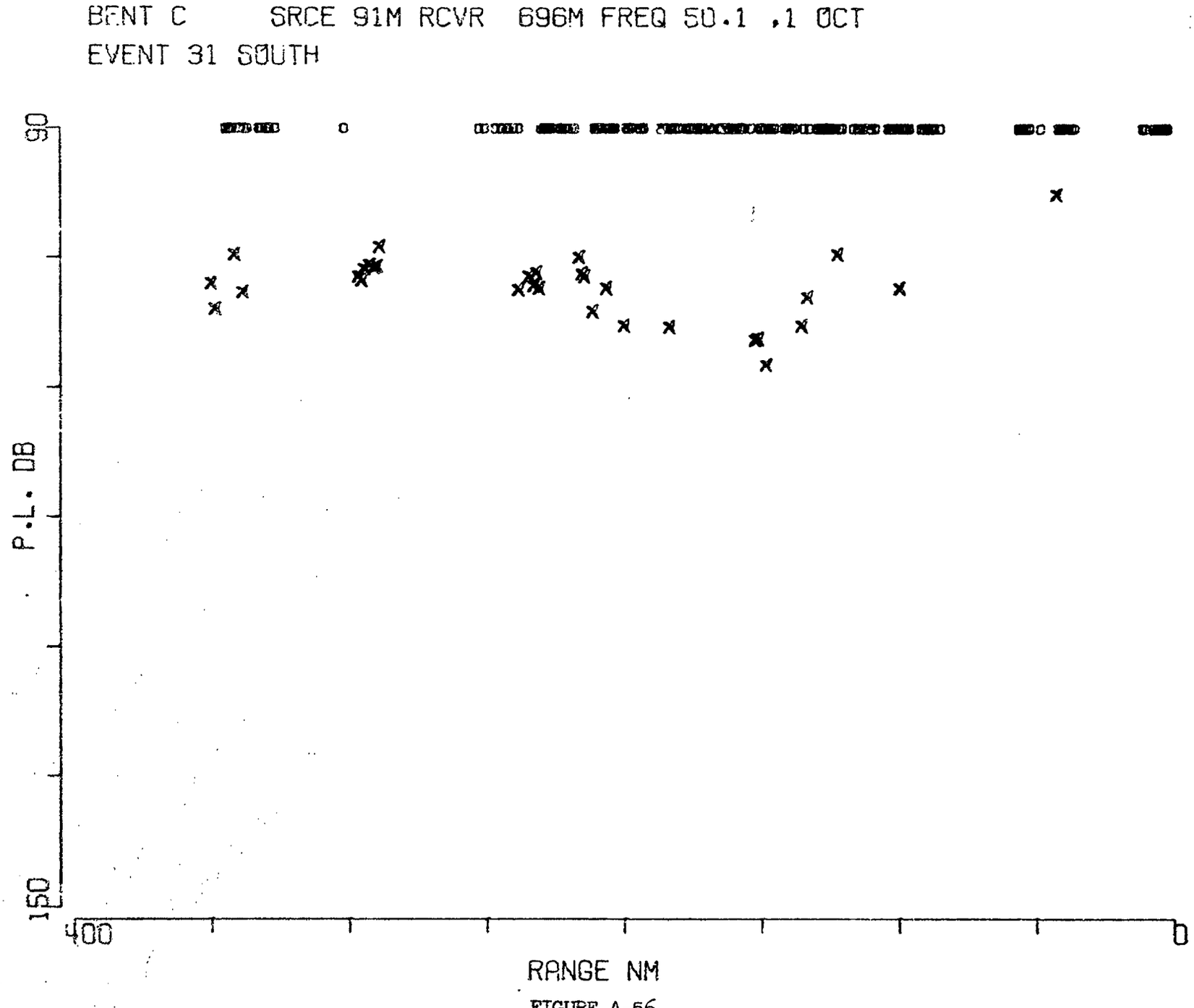
BENT C SRCE 91M RCVR 696M FREQ 50.1 ,1 OCT
EVENT 31 SOUTH
90
150
P.L. DB
400
0
RANGE NM

FIGURE A-56

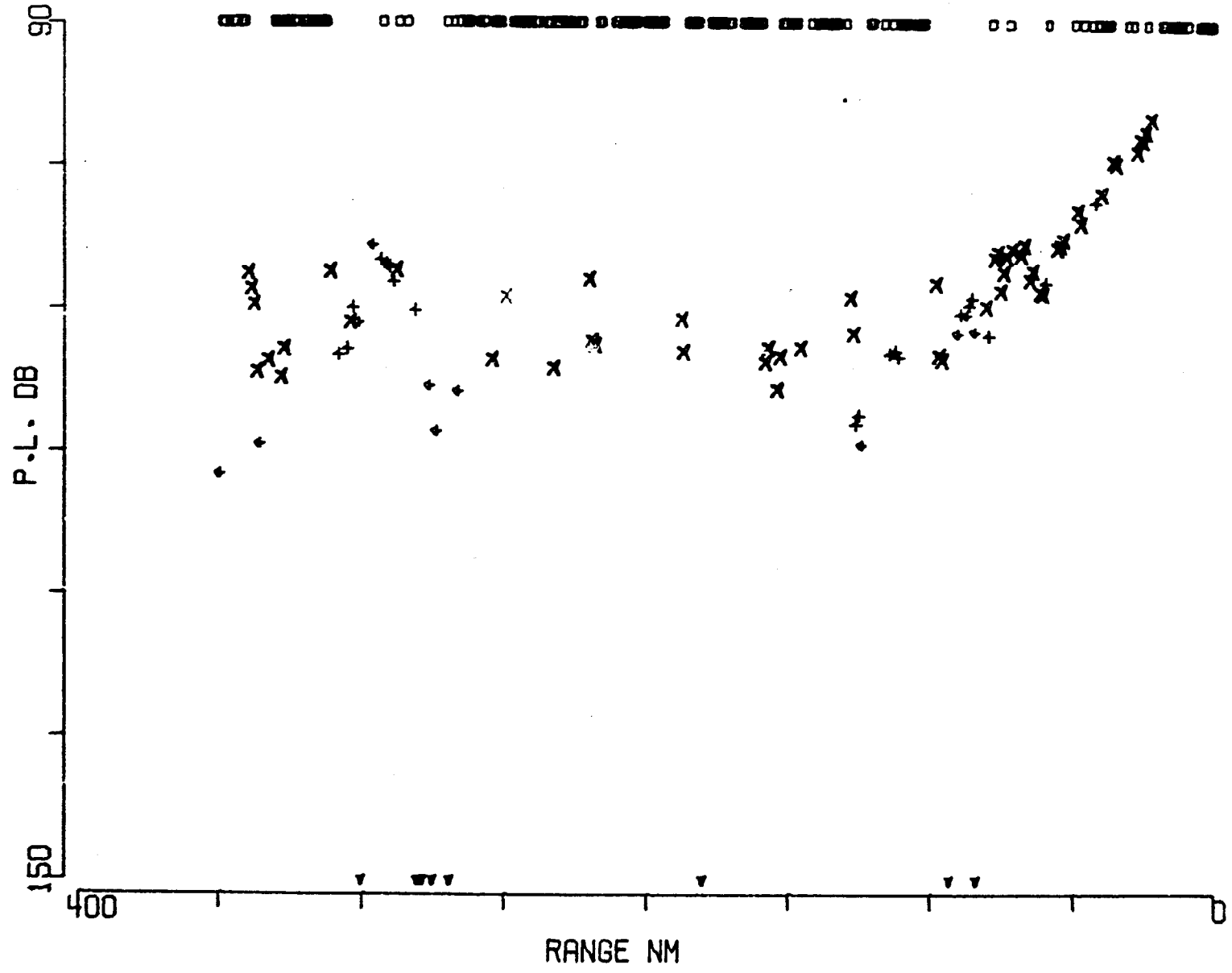
BENT C SRCE 16M RCVR 4055M FREQ 50.1 ,1 OCT
EVENT 31 SOUTH
90
150
P.L. DB
400
0
RANGE NM

FIGURE A-57

FIGURE A-57

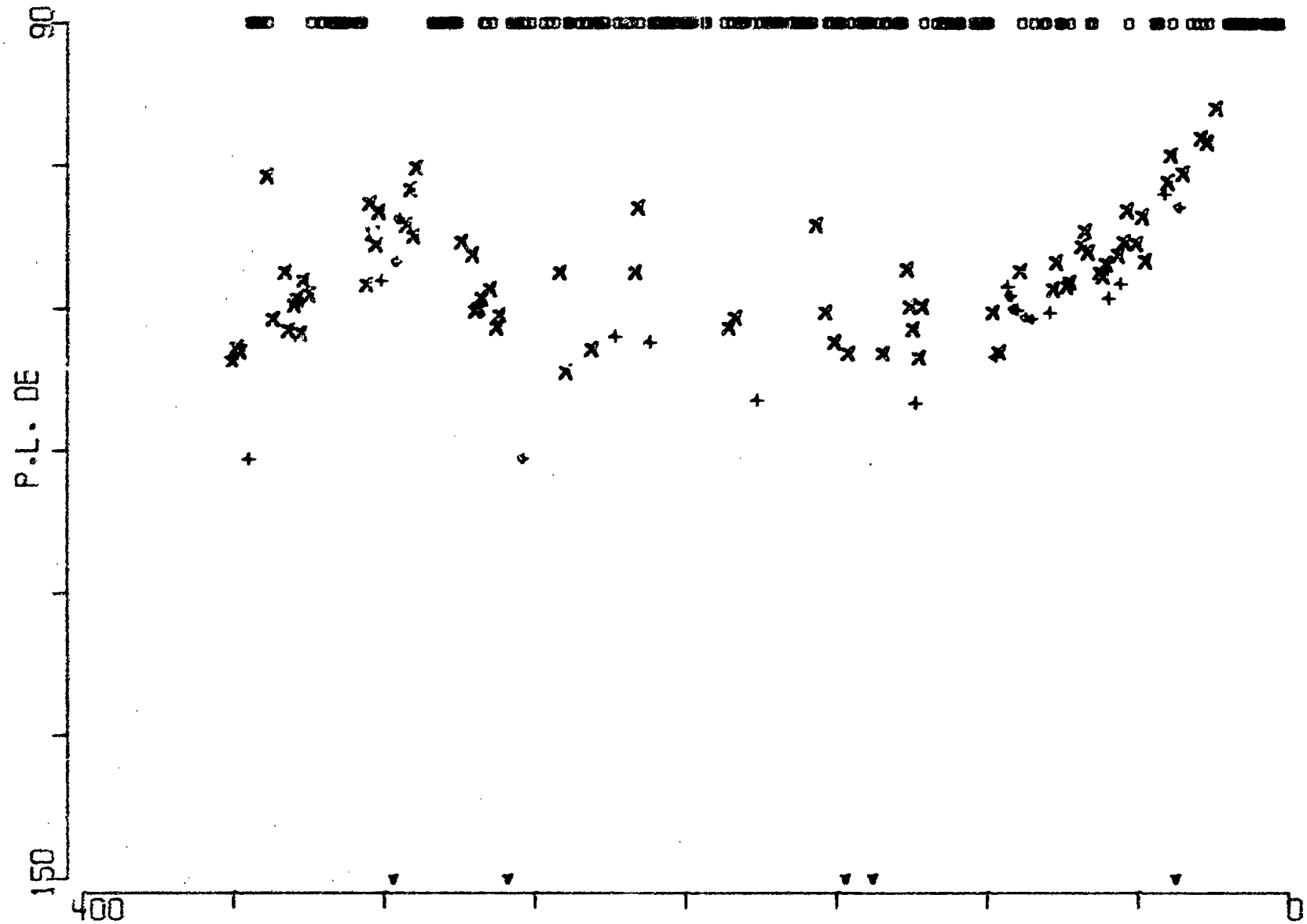

FIGURE A-58

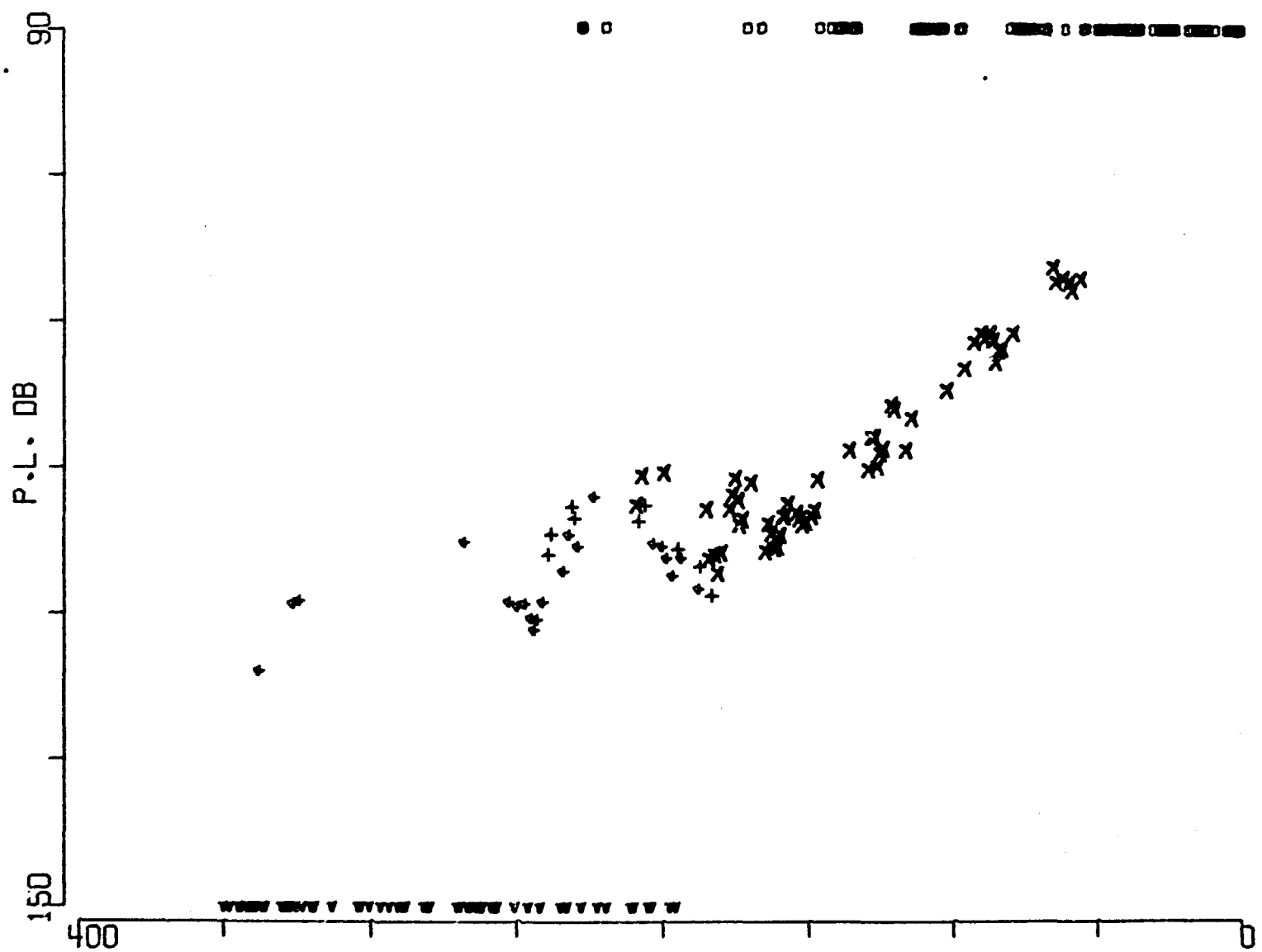
BENT C SRCE 18M RCVR 5521M FREQ 50.1 ,1 OCT
EVENT 31 SOUTH
90
150
P.L. DB
400
0
RANGE NM

FIGURE A-59

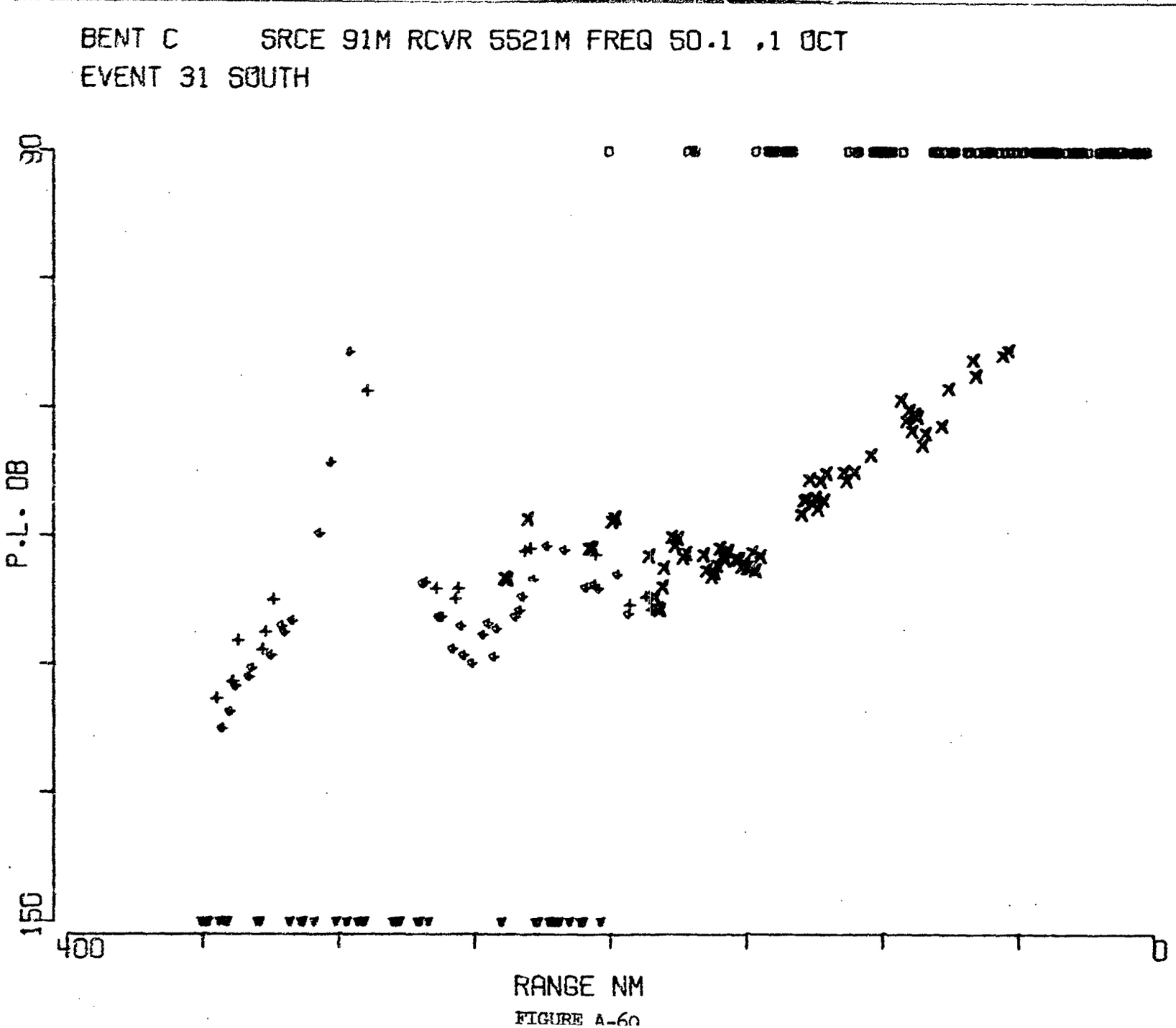
BENT C SRCE 91M RCVR 5521M FREQ 50.1 ,1 OCT
EVENT 31 SOUTH
90
150
P.L. DB
400
0
RANGE NM

FIGURE A-60

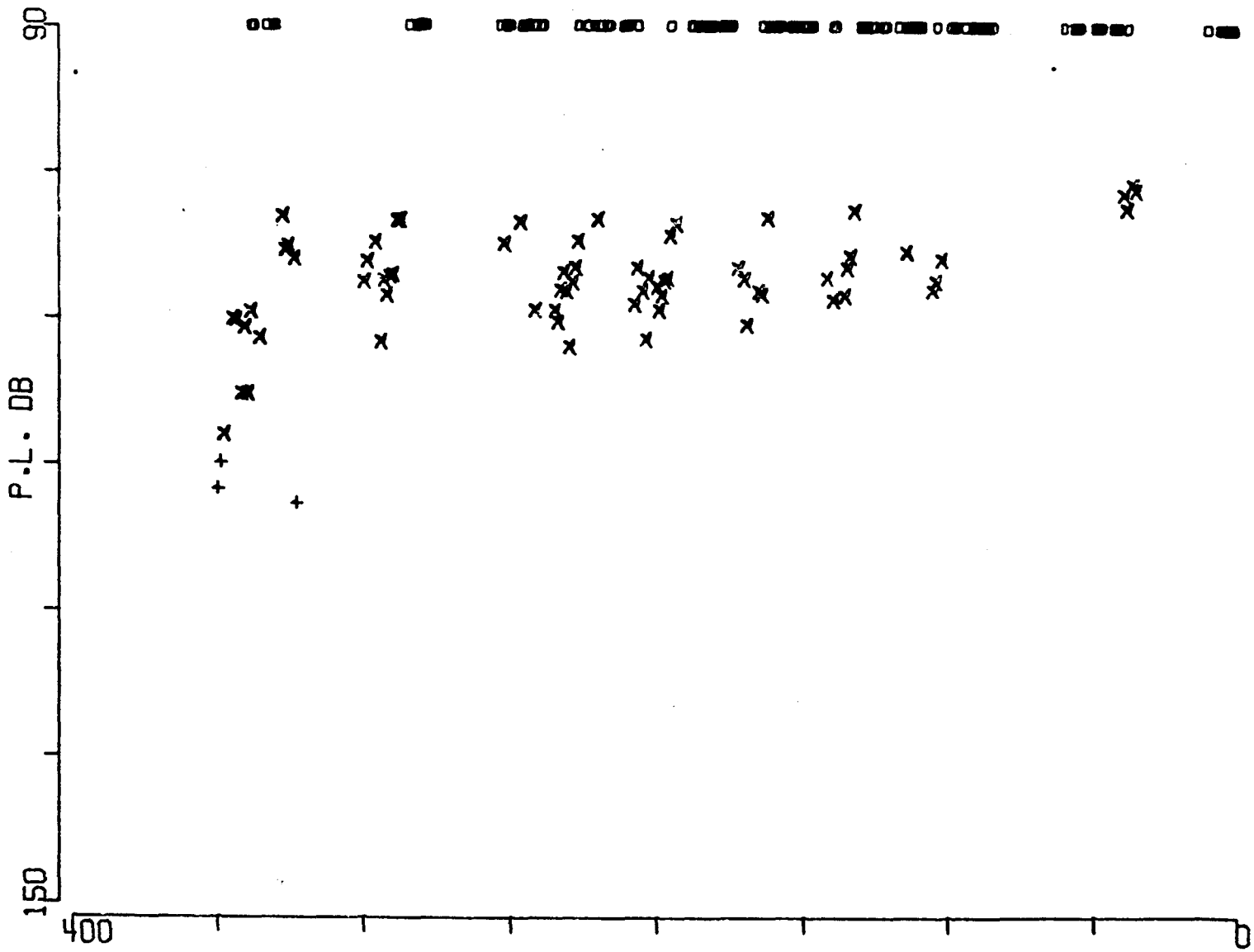
3ENT C SRCE 18M RCVR 696M FREQ158.5
EVENT 31 SØUTH
90
150
P.L. DB
400
0
RANGE NM

FIGURE A-61

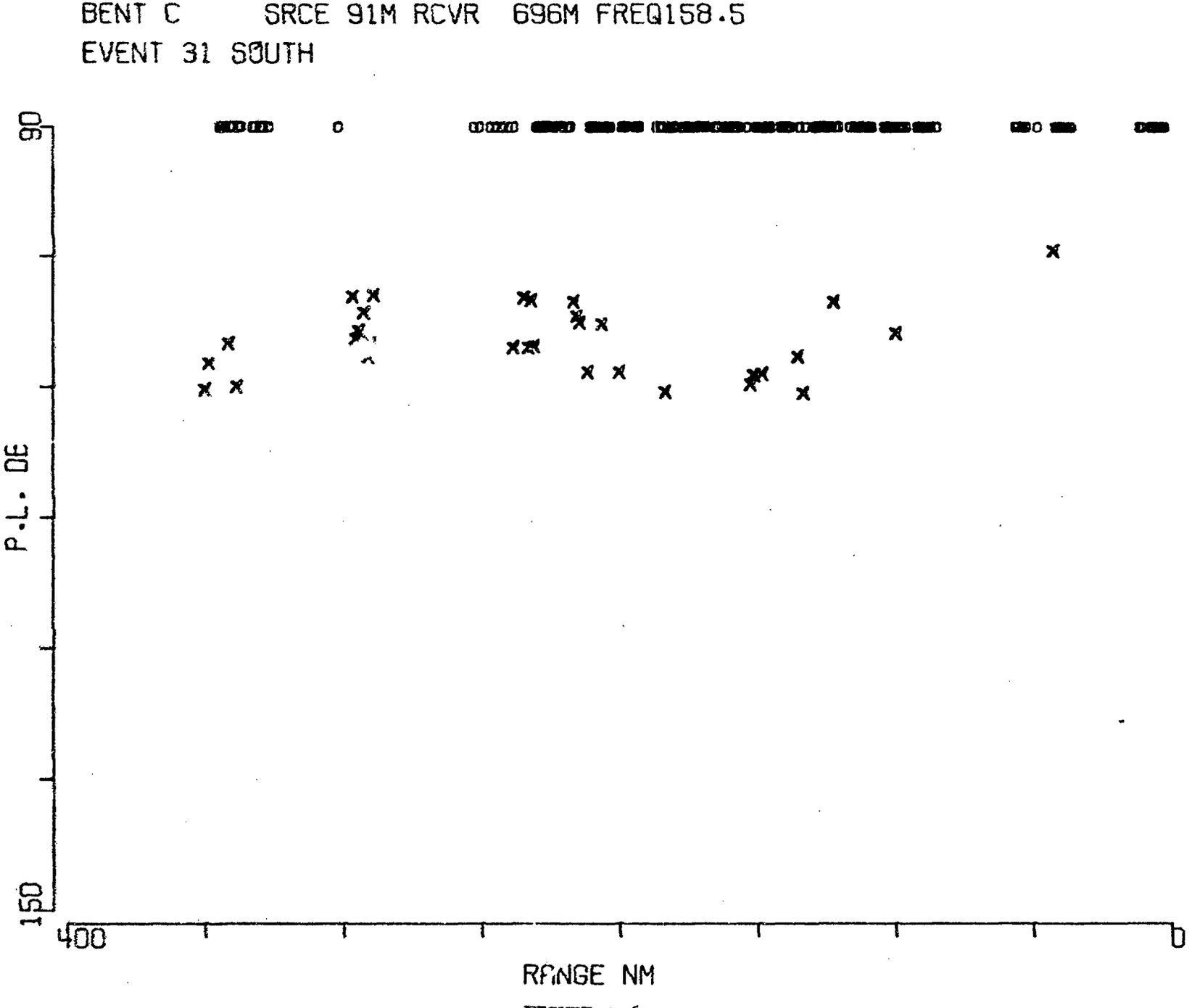
BENT C SRCE 91M RCVR 696M FREQ158.5
EVENT 31 SOUTH
90
150
P.L. DE
400
0
RANGE NM

FIGURE A-62

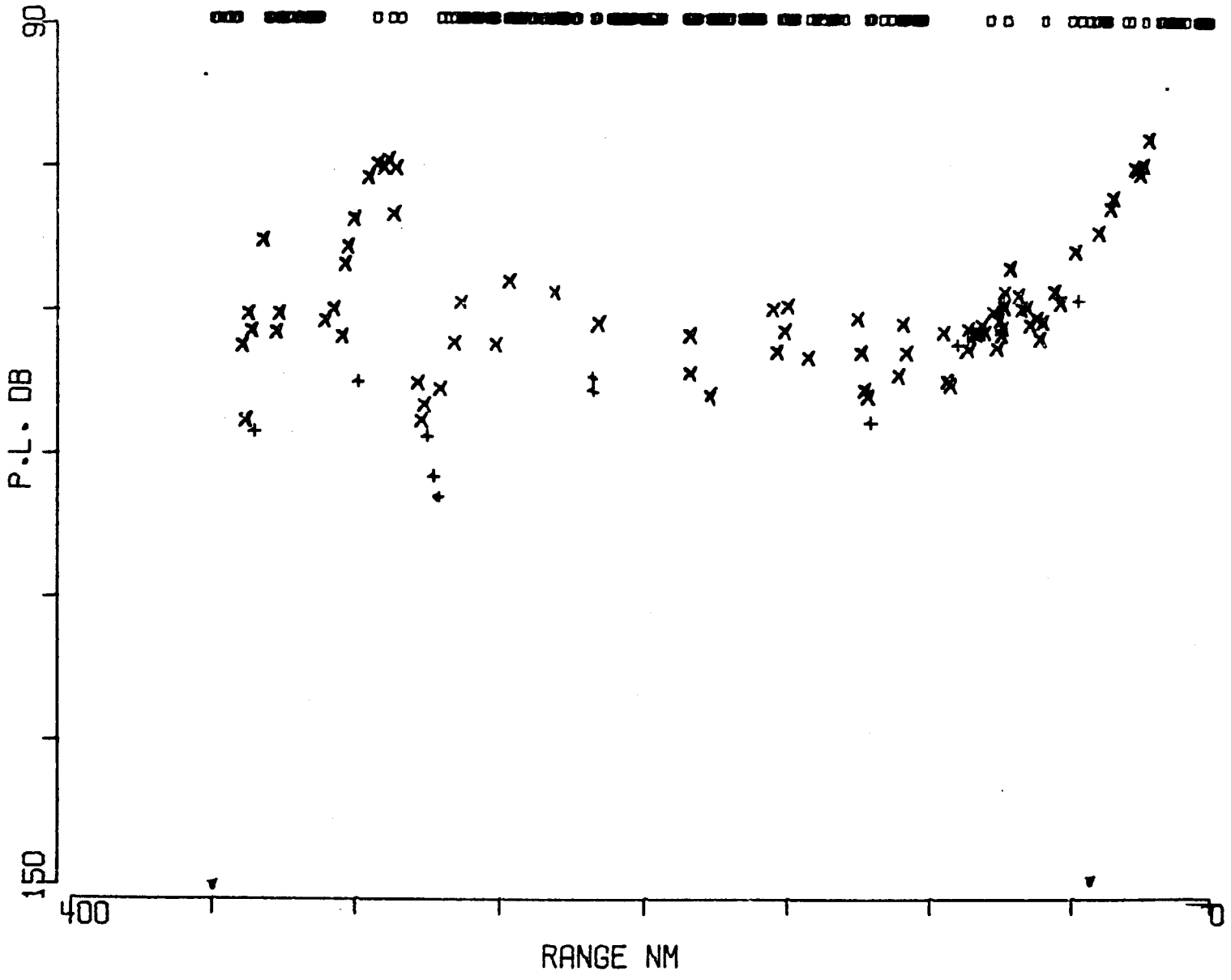
3ENT C SRCE 18M RCVR 4055M FREQ158.5
EVENT 31 SOUTH
90
P.L. DB
150
400
0
RANGE NM

FIGURE A-63

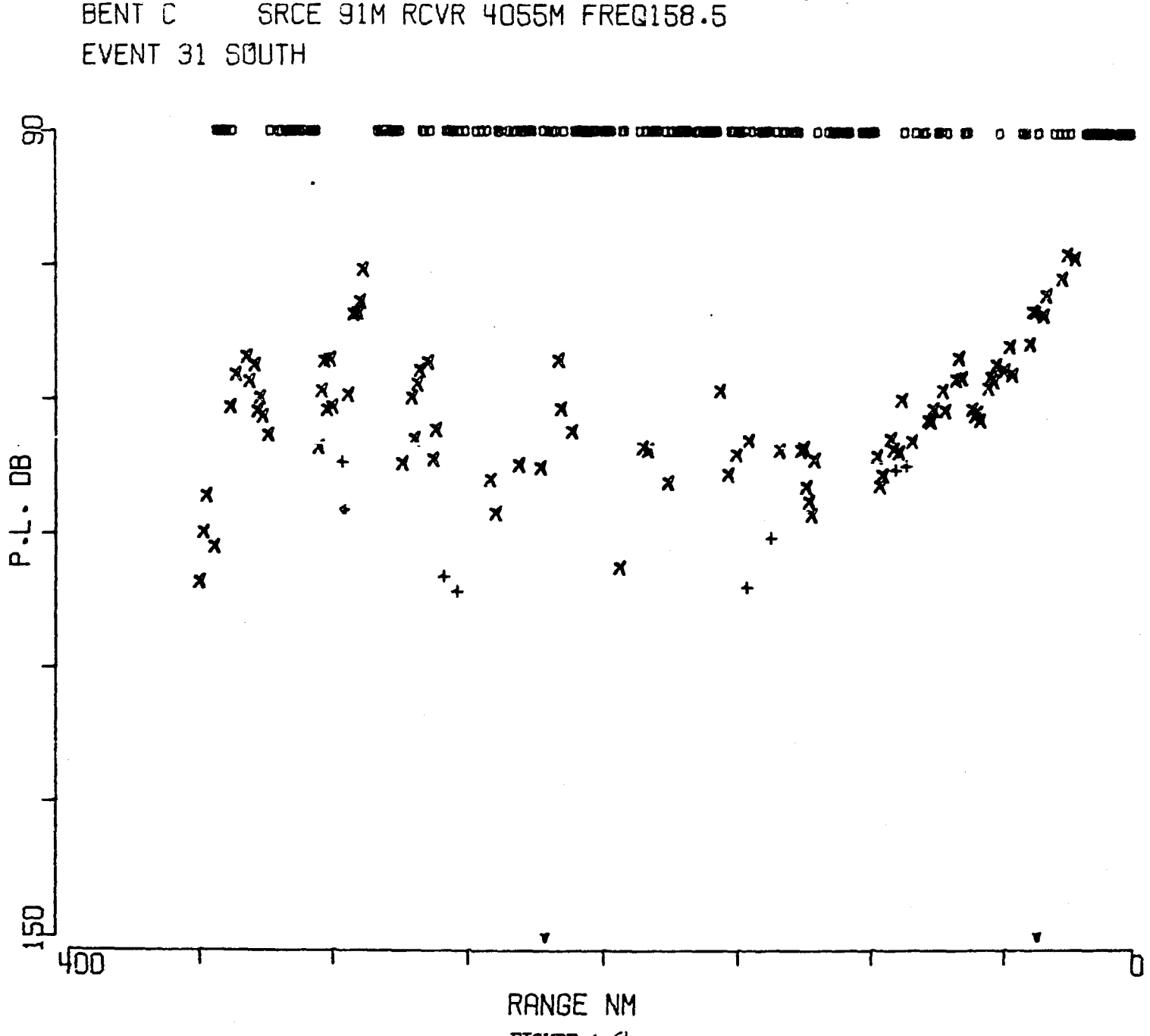
BENT C SRCE 91M RCVR 4055M FREQ158.5
EVENT 31 SOUTH
90
150
P.L. DB
400
0
RANGE NM

FIGURE A-64

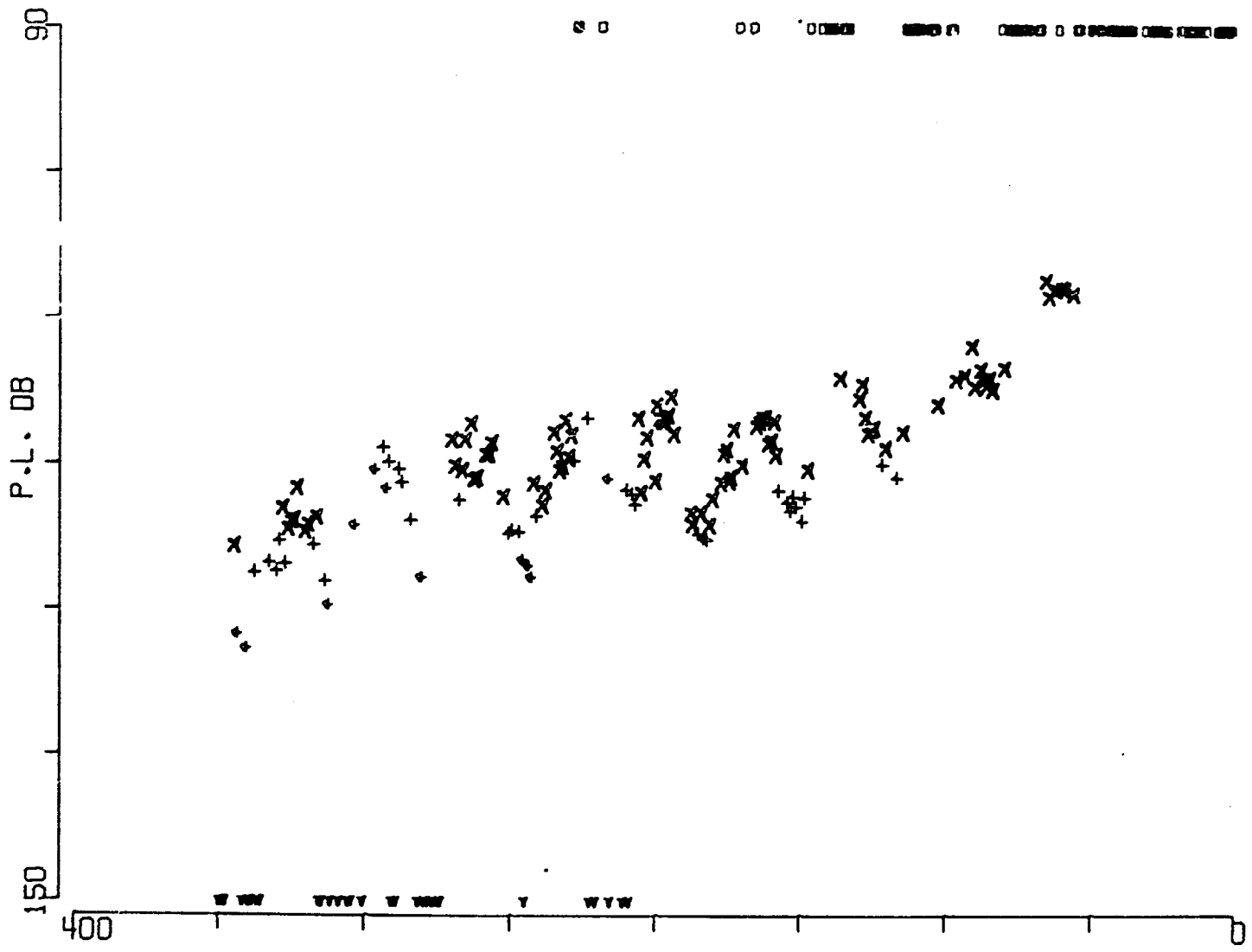
BENT C SRCE 18M RCVR 5521M FREQ158.5
EVENT 31 SOUTH
90
150
P.L. DB
400
0
RANGE NM

FIGURE A-65

FIGURE A-65

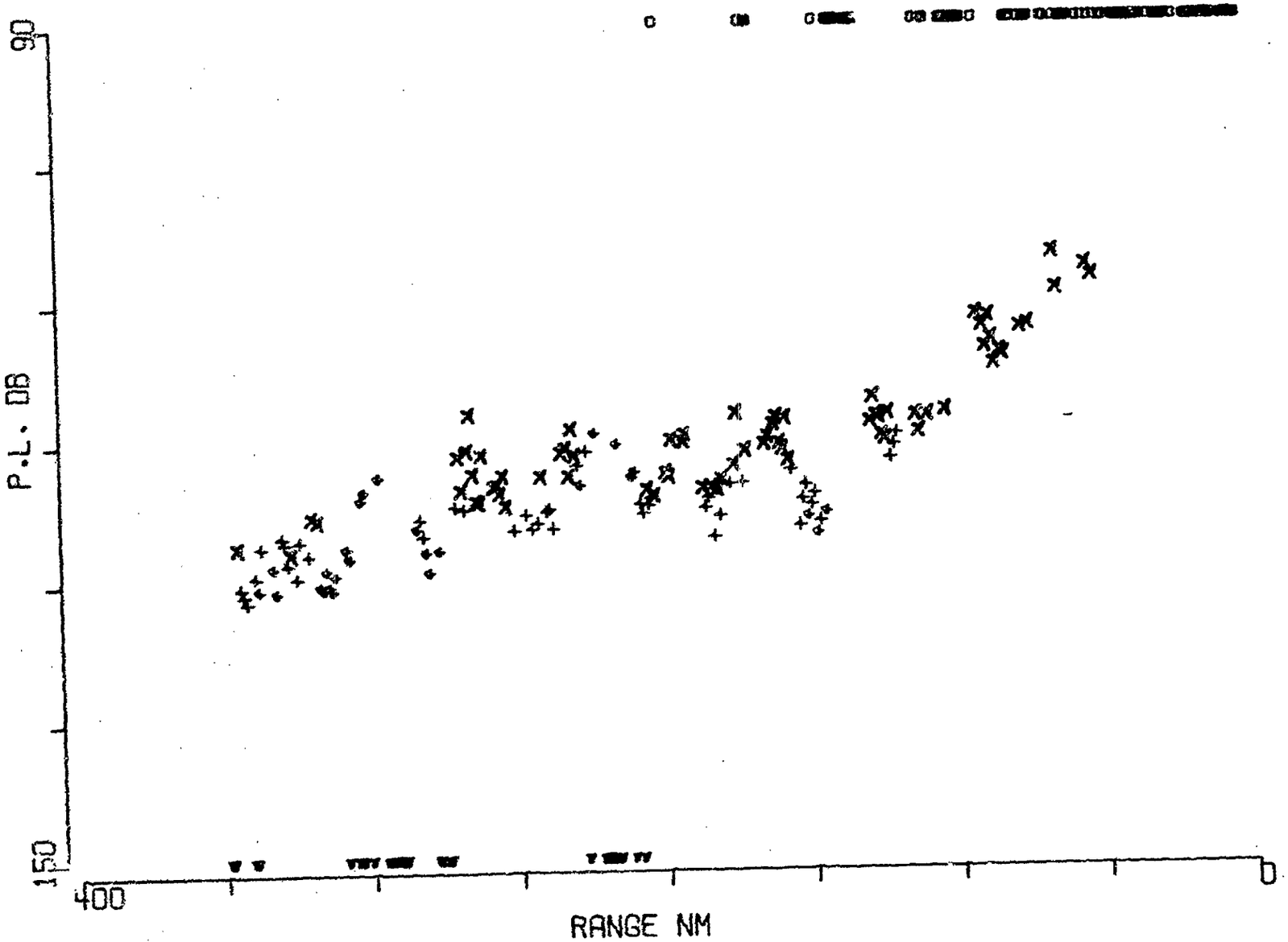

FIGURE A-66

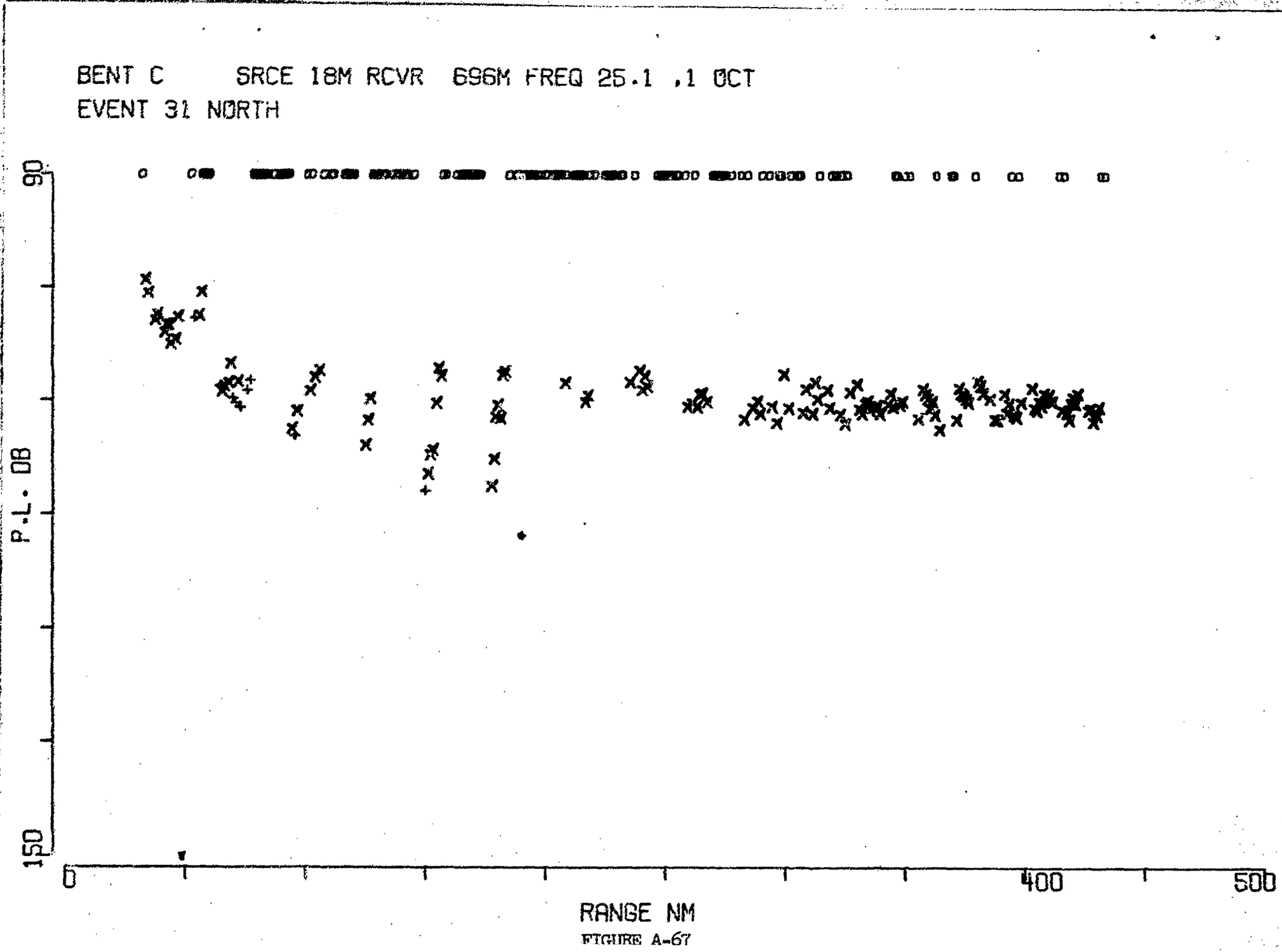
BENT C SRCE 18M RCVR 696M FREQ 25.1 ,1 OCT
EVENT 31 NORTH
90
150
P.L. DB
0
400
500
RANGE NM

FIGURE A-67

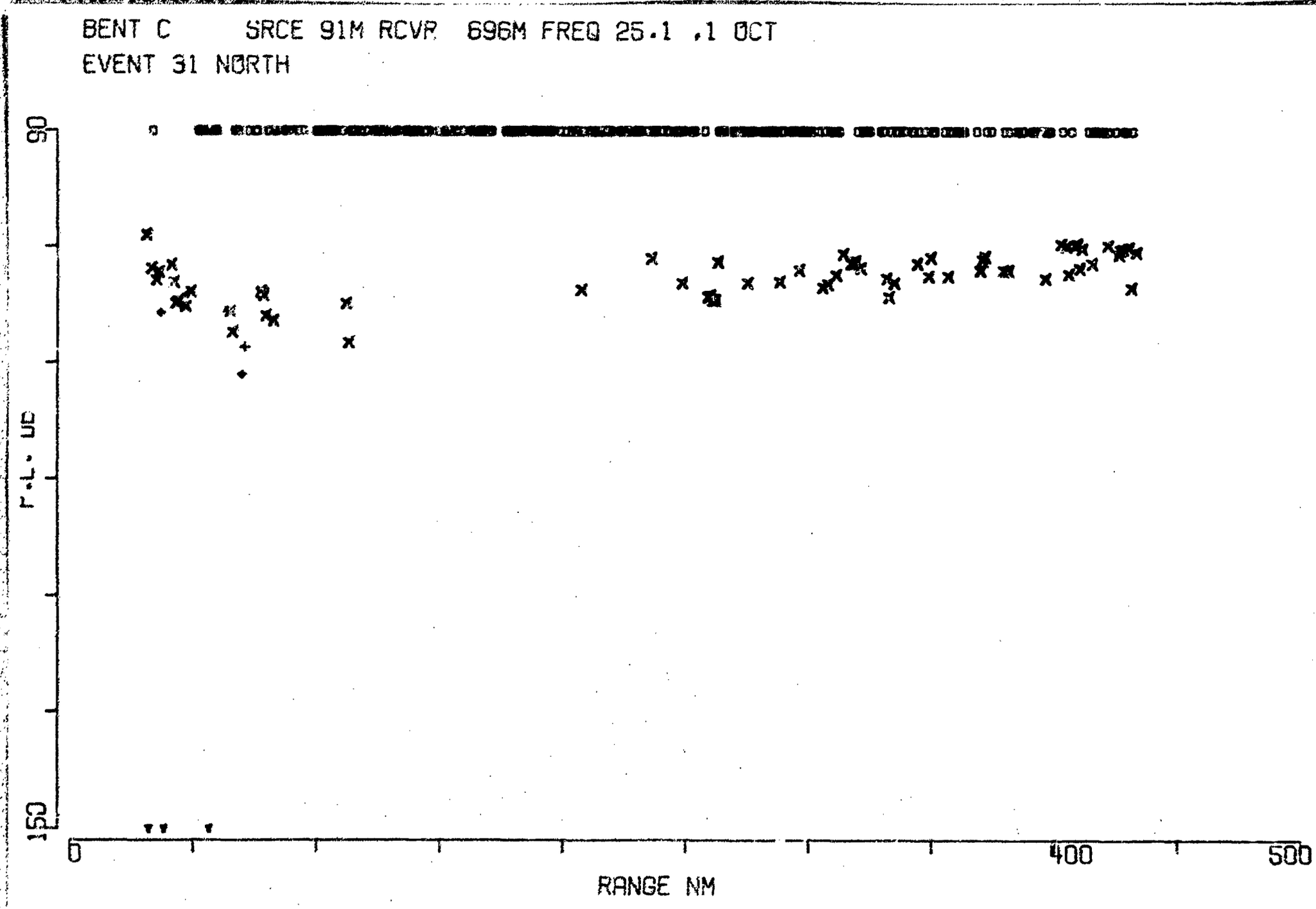
BENT C SRCE 91M RCVR 696M FREQ 25.1 ,1 OCT
EVENT 31 NORTH
90
150
P.L. dB
0
400
500
RANGE NM

FIGURE A-68

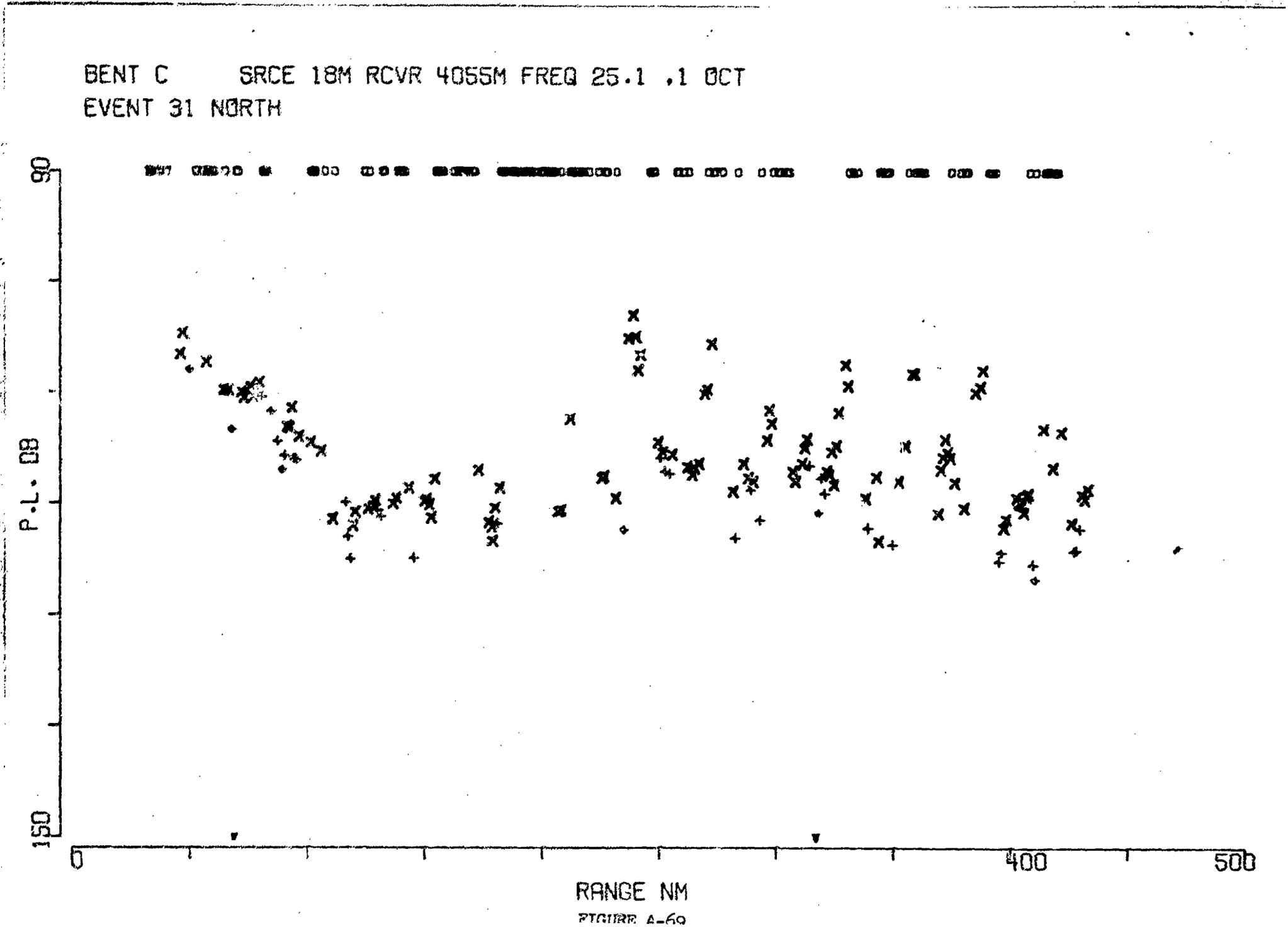
BENT C SRCE 18M RCVR 4055M FREQ 25.1 .1 OCT
EVENT 31 NORTH
90
150
P.L. DB
0
400
500
RANGE NM

FIGURE A-69

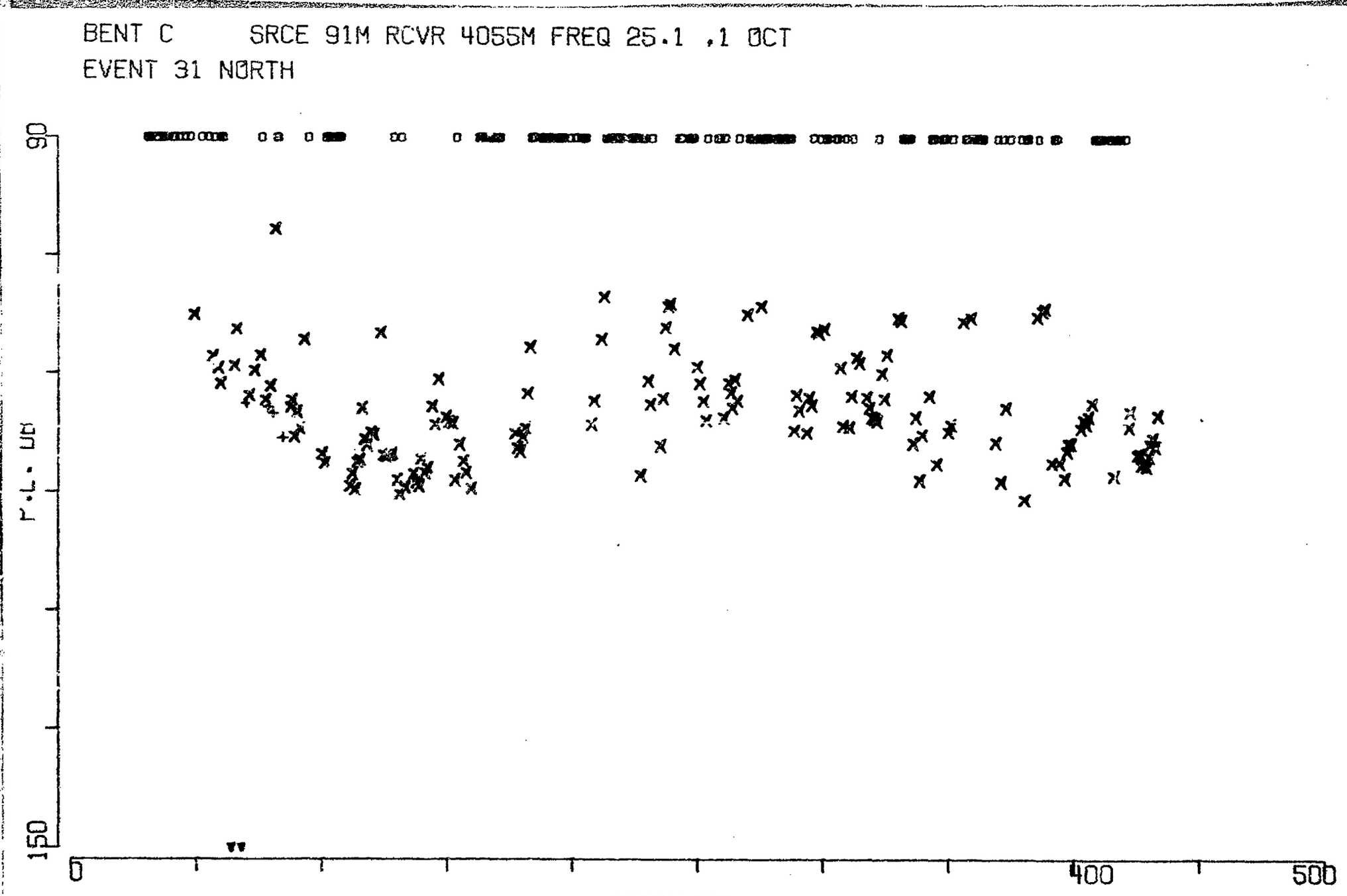
BENT C SRCE 91M RCVR 4055M FREQ 25.1 ,1 OCT
EVENT 31 NORTH
90
P.L. DB
150
0
400
500
RANGE NM

FIGURE A-70

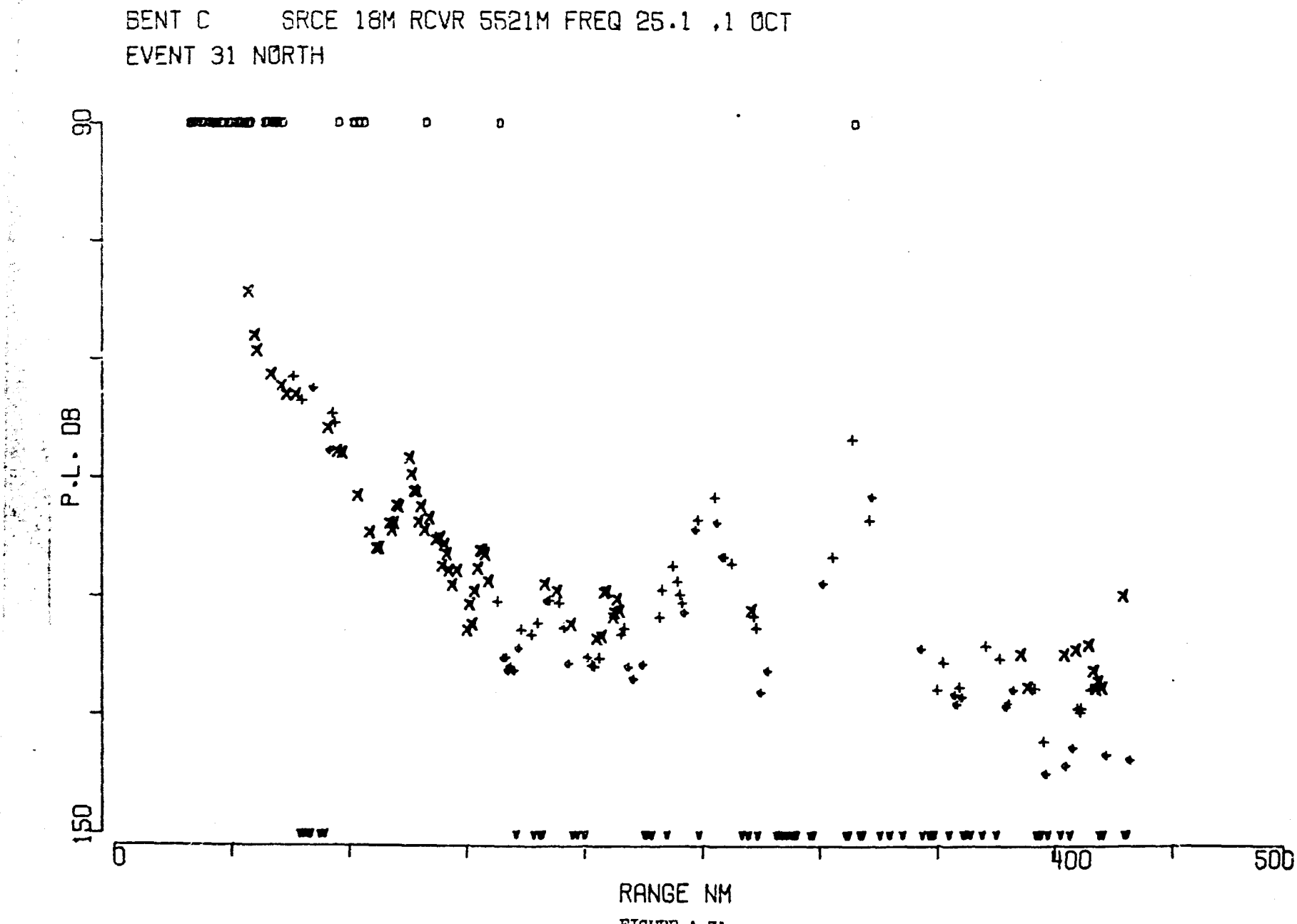
BENT C SRCE 18M RCVR 5521M FREQ 25.1 .1 OCT
EVENT 31 NORTH
90
150
P.L. DB
0
400
500
RANGE NM

FIGURE A-71

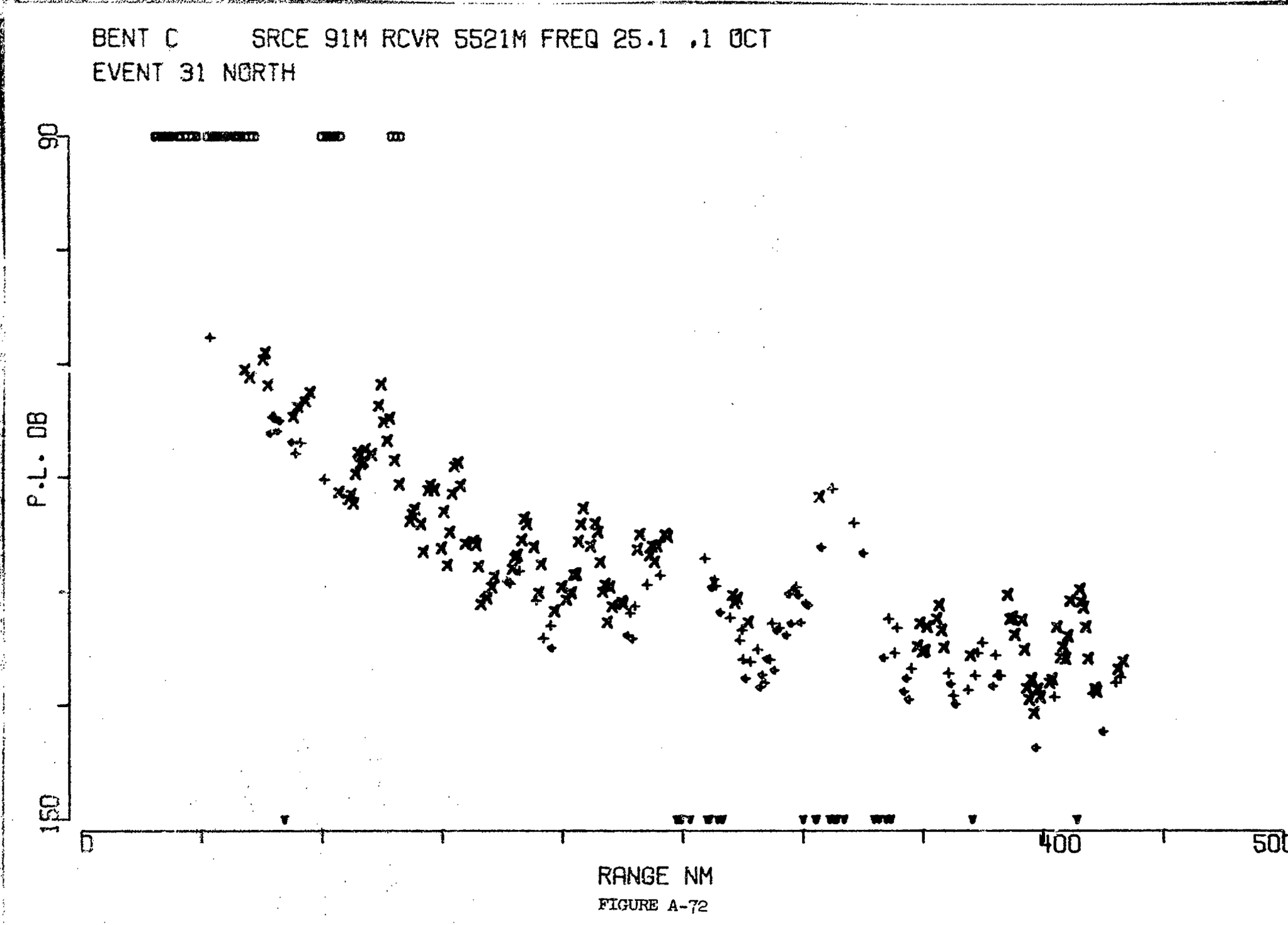
BENT C SRCE 91M RCVR 5521M FREQ 25.1 ,1 OCT
EVENT 31 NORTH
90
150
P.L. DB
0
400
500
RANGE NM

FIGURE A-72

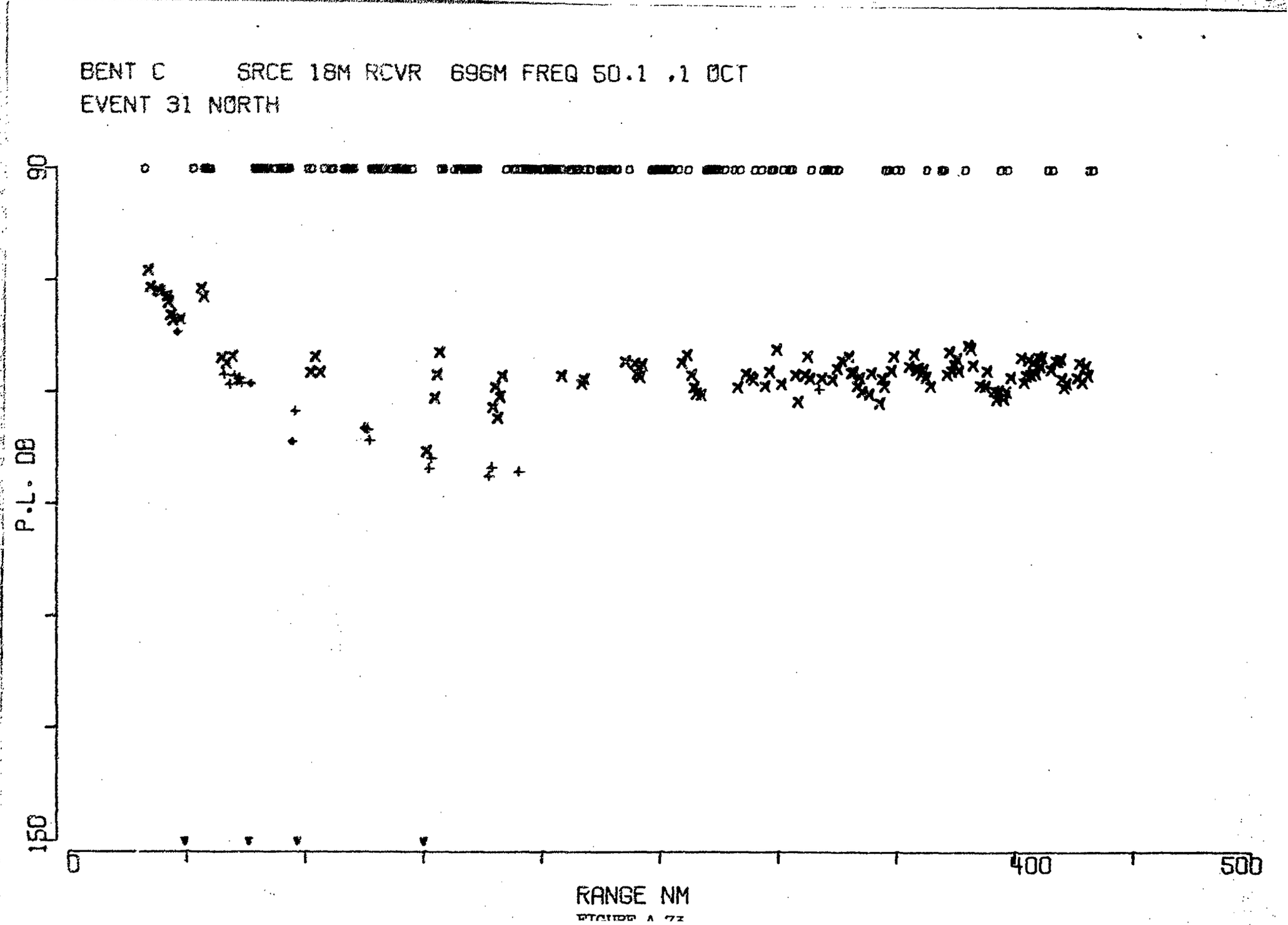
BENT C SRCE 18M RCVR 696M FREQ 50.1 ,1 OCT
EVENT 31 NORTH
90
P.L. DB
150
0
400
500
RANGE NM

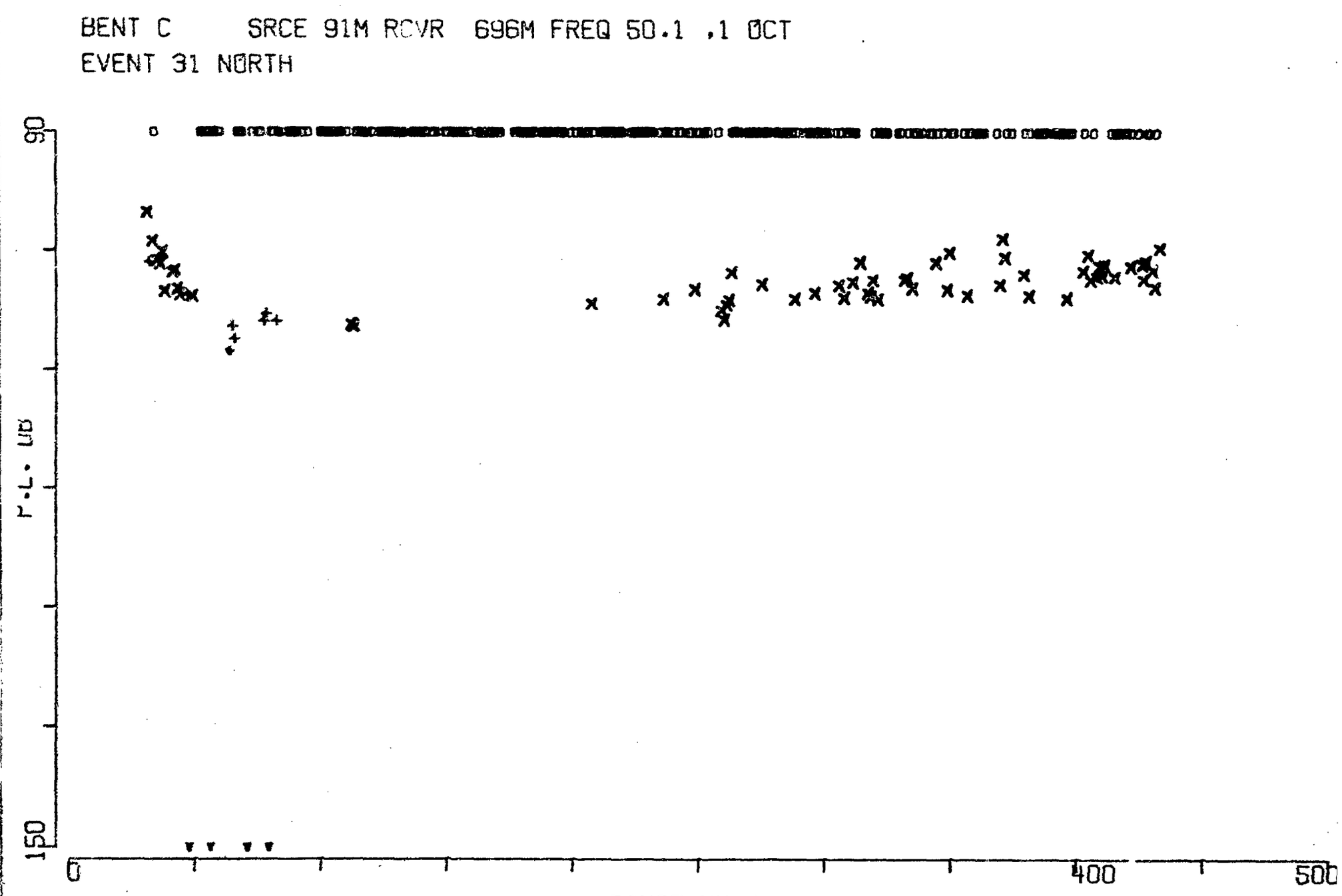
BENT C SRCE 91M RCVR 696M FREQ 50.1 ,1 OCT
EVENT 31 NORTH
90
150
P.L. dB
0
400
500
RANGE NM

FIGURE A-74

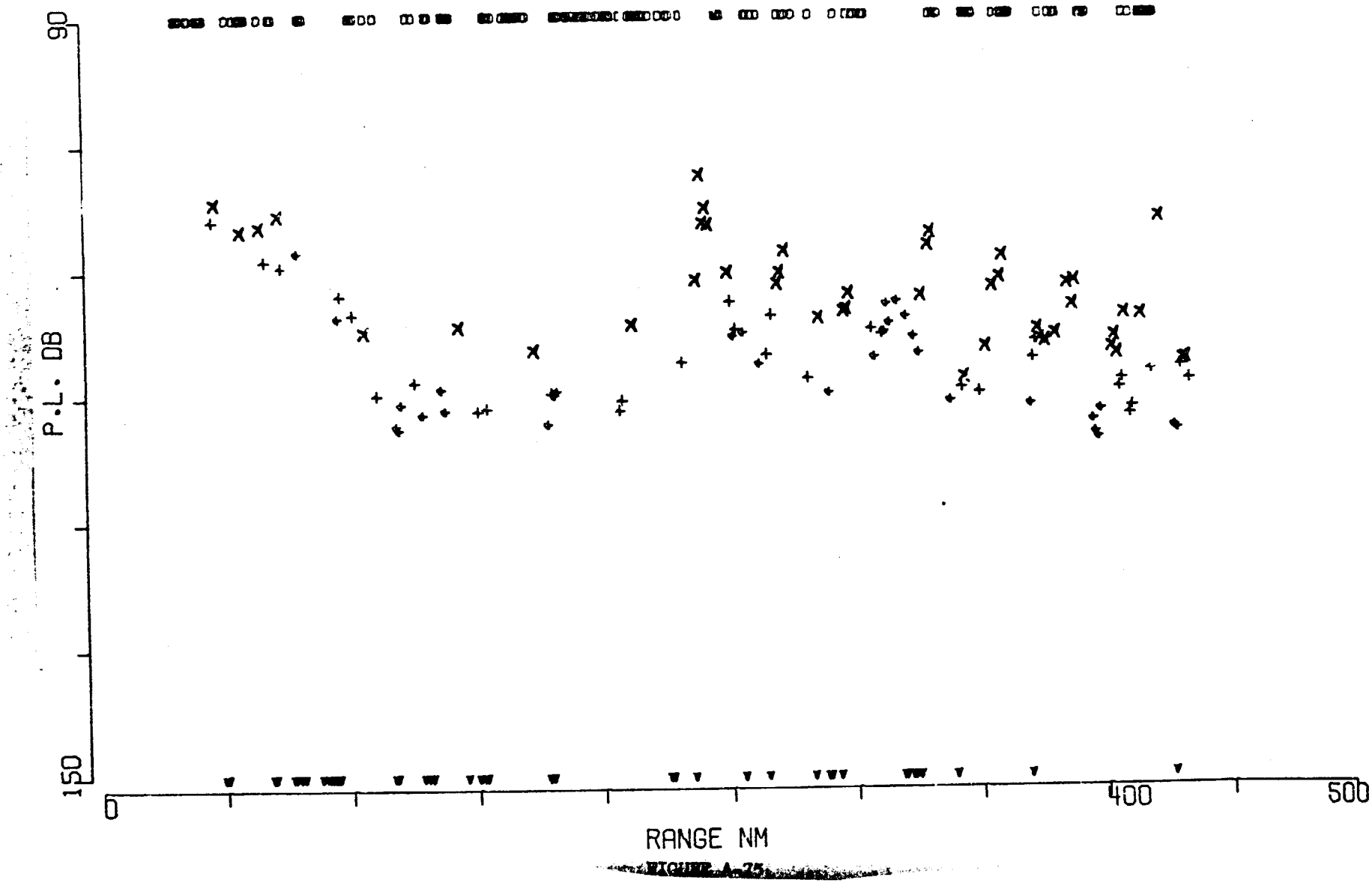
BENT C SRCE 18M RCVR 4055M FREQ 50.1 ,1 OCT
EVENT 31 NORTH
90
150
P.L. DB
0
400
500
RANGE NM

FIGURE A-75

BENT C SRCE 91M RCVR 4055M FREQ 50.1 ,1 OCT
EVENT 31 NORTH

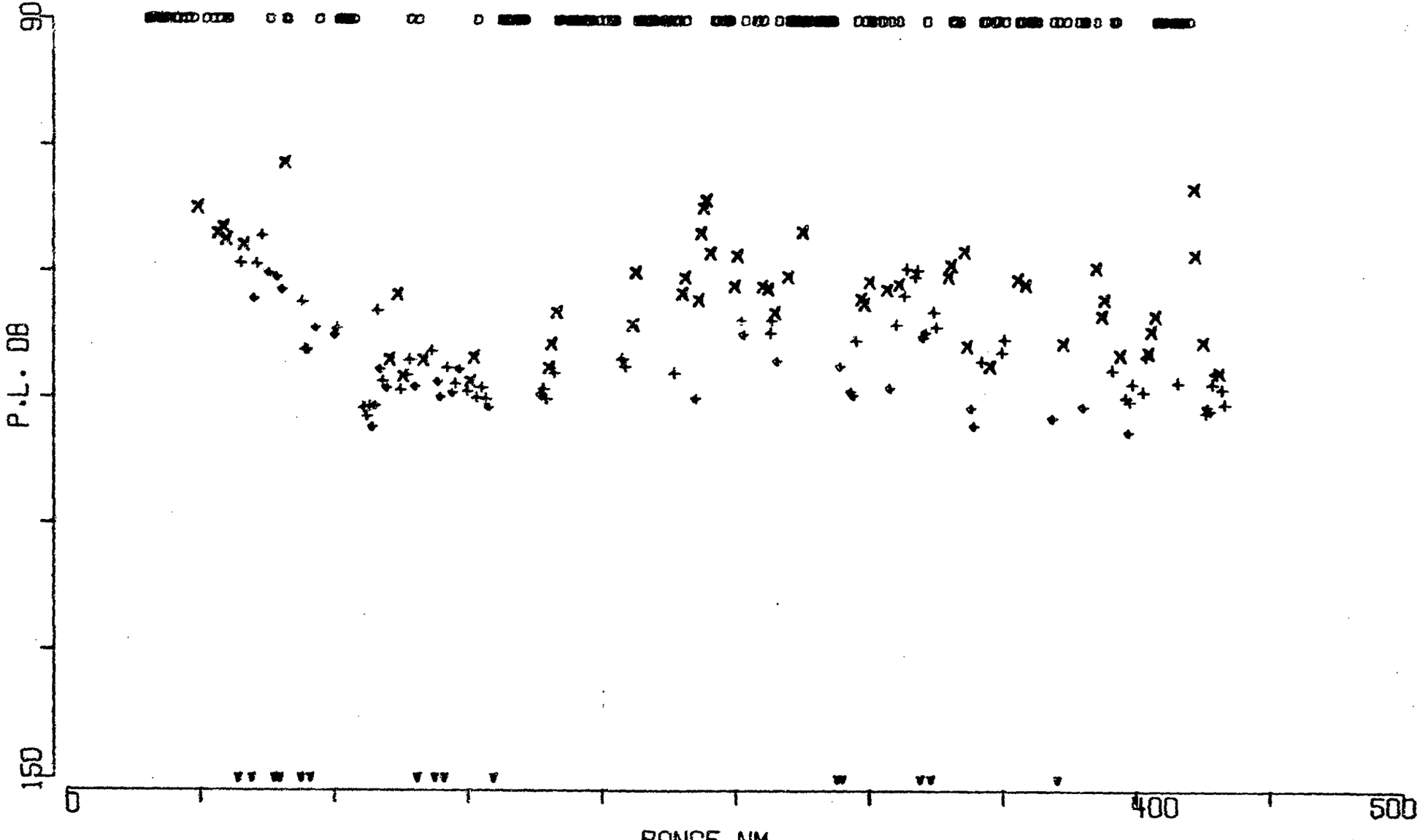

FIGURE A-76

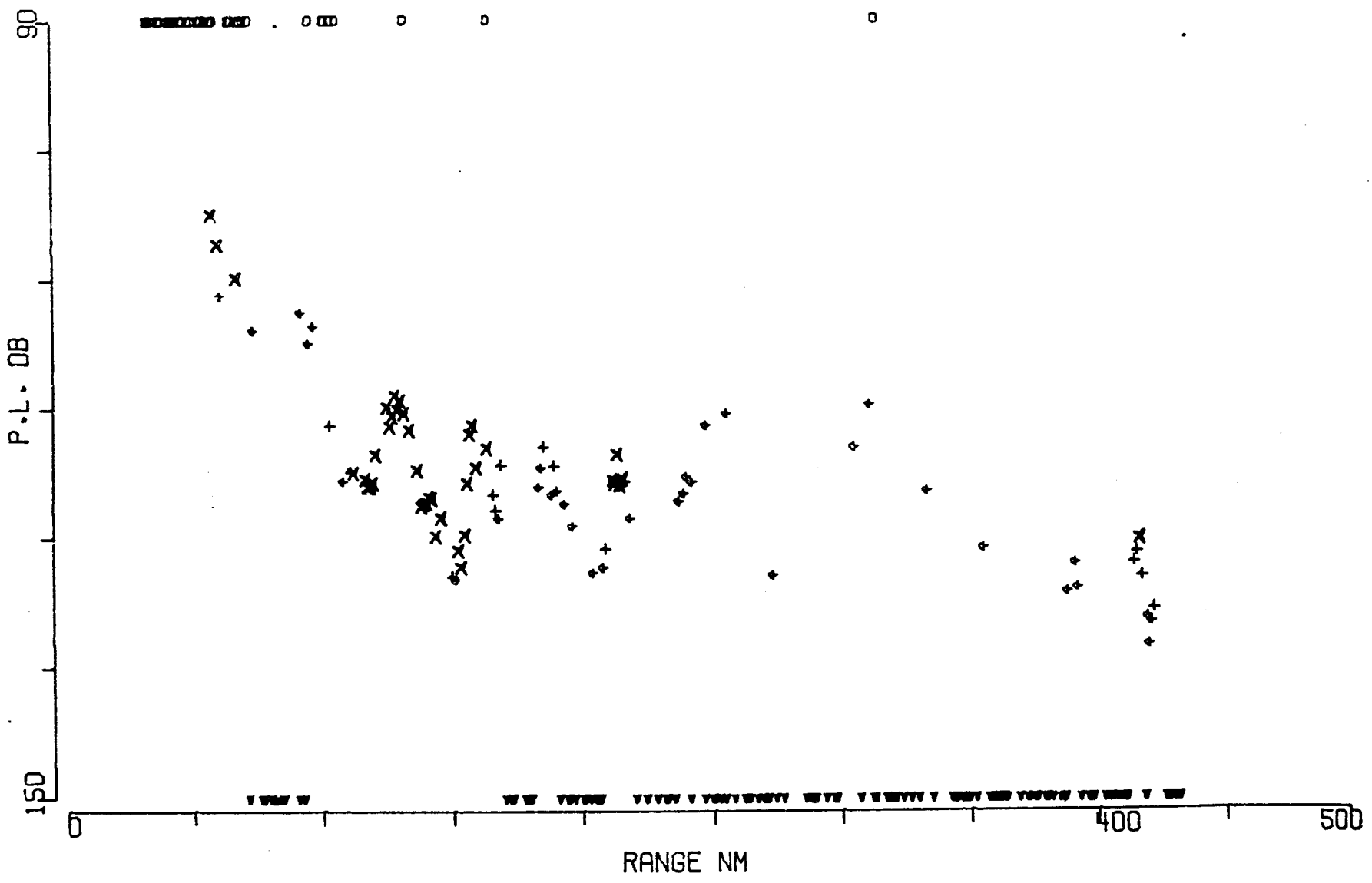
BENT C SRCE 18M RCVR 55211 FREQ 50.1 ,1 OCT
EVENT 31 NORTH
90
150
P.L. DB
0
400
500
RANGE NM

FIGURE A-77

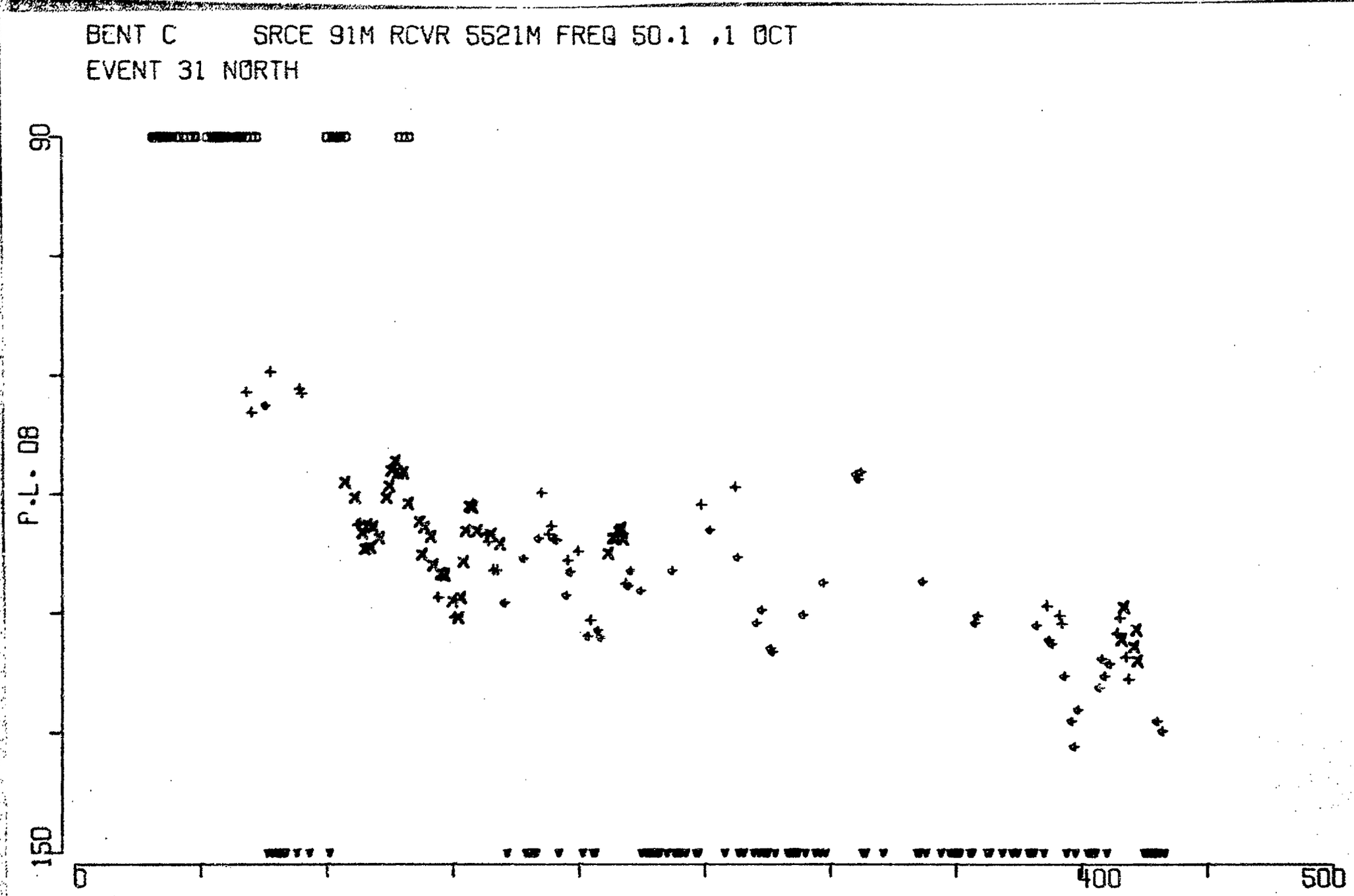
BENT C SRCE 91M RCVR 5521M FREQ 50.1 ,1 OCT
EVENT 31 NORTH
90
150
P.L. DB
0
400
500
RANGE NM

FIGURE A-78

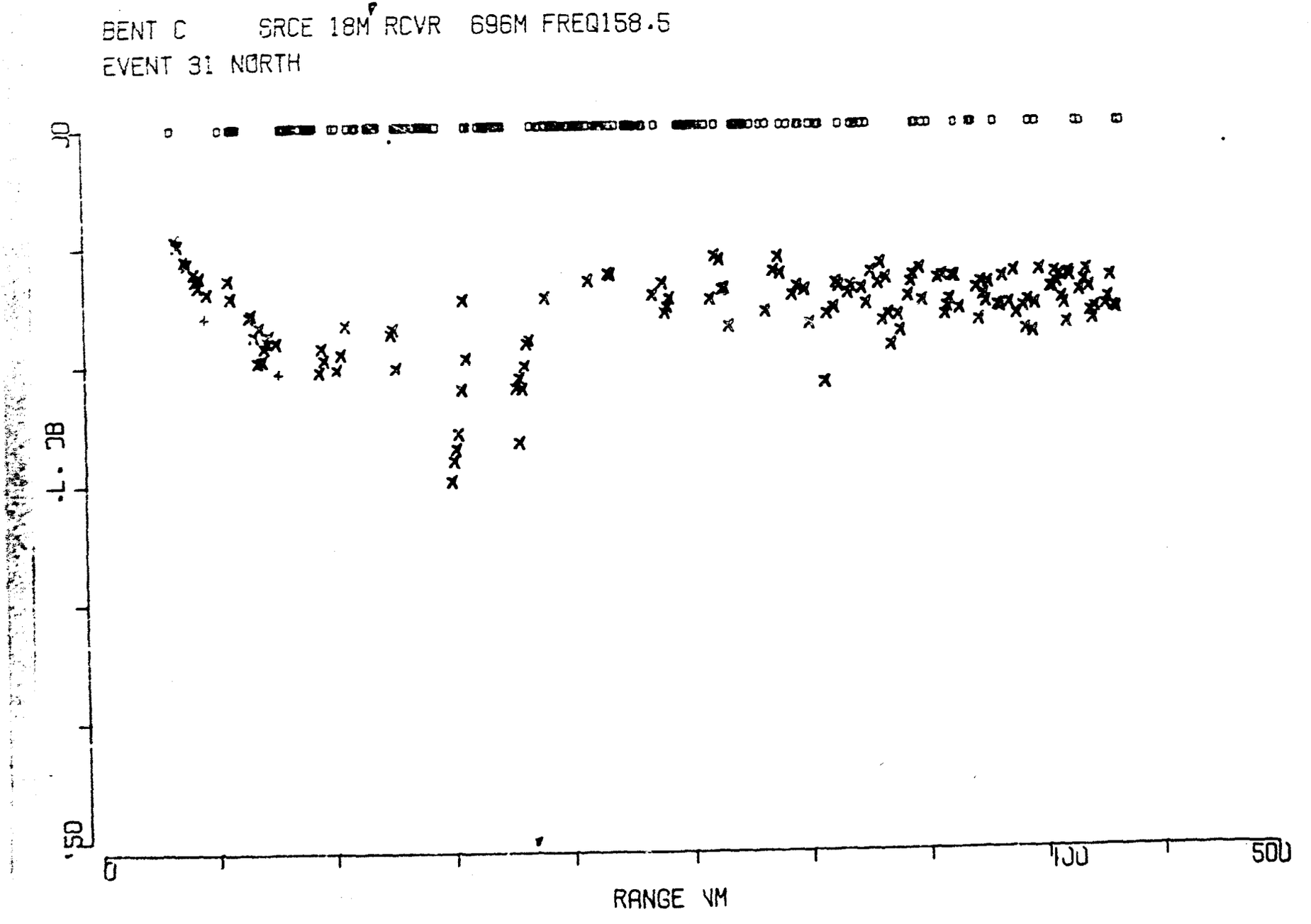
BENT C SRCE 18M RCVR 696M FREQ158.5
EVENT 31 NORTH
-50
-L. DB
0
100
500
RANGE YM

FIGURE A-79

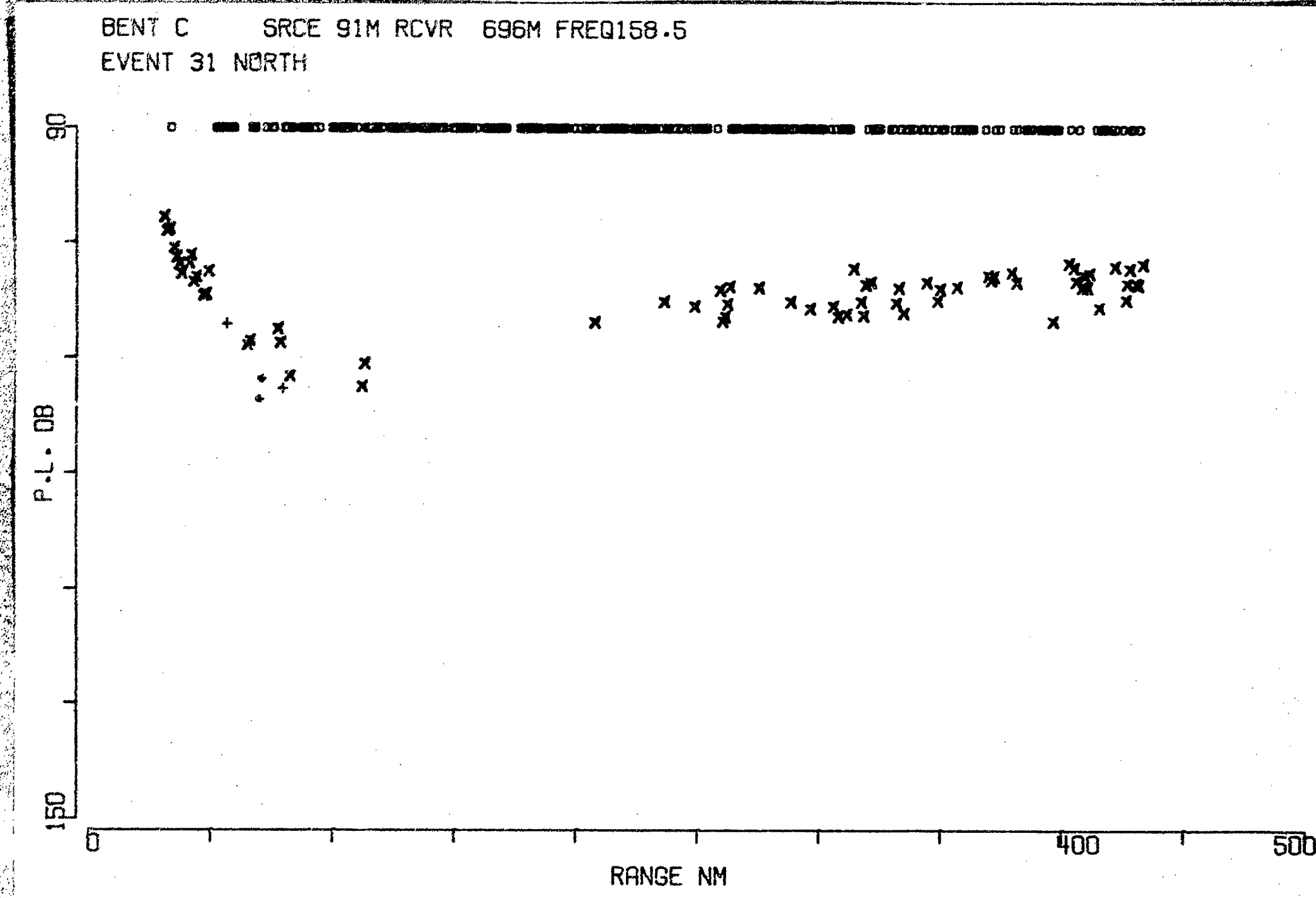
BENT C SRCE 91M RCVR 696M FREQ158.5
EVENT 31 NORTH
90
150
P.L. DB
0
400
500
RANGE NM

FIGURE A-80

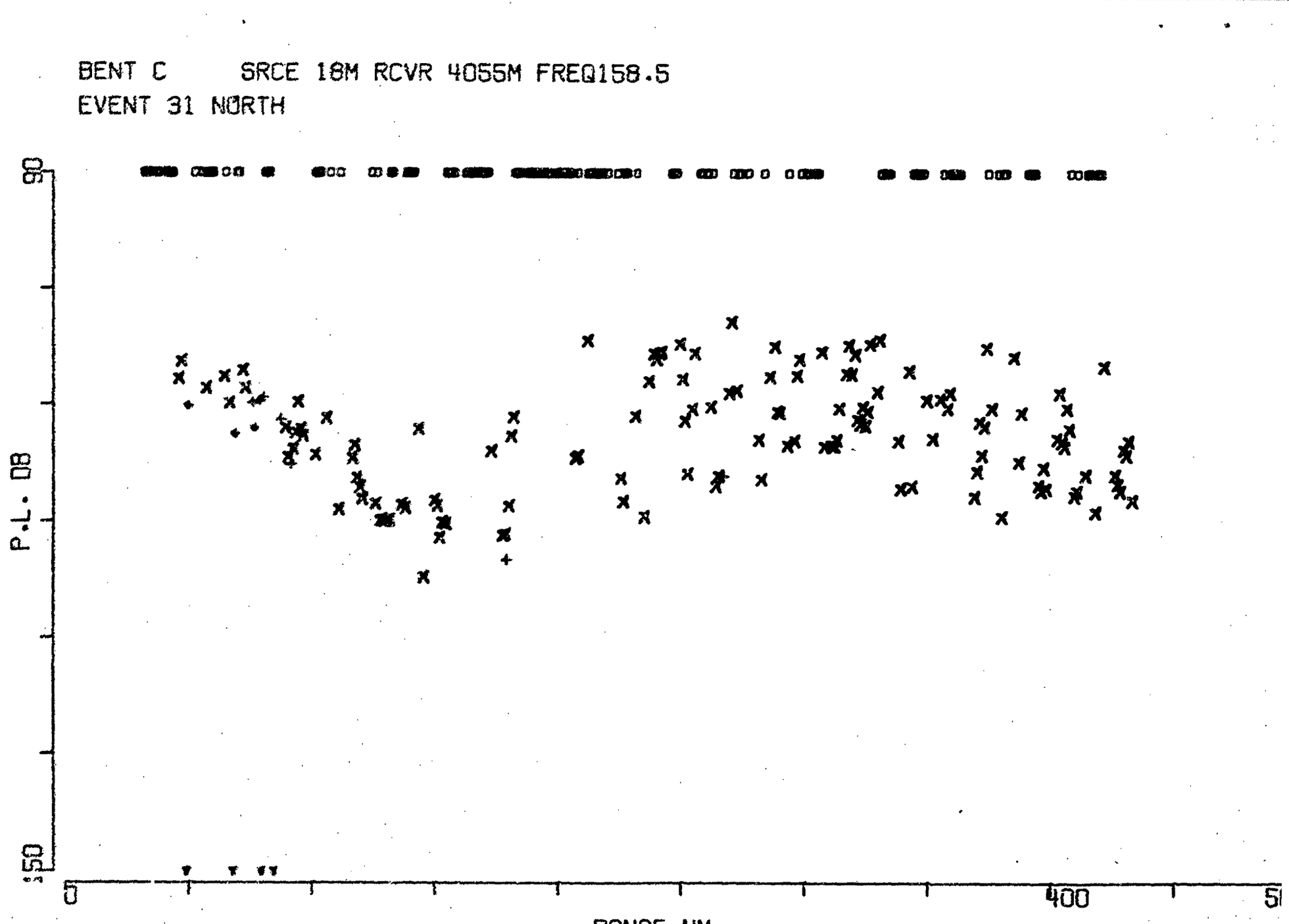
BENT C SRCE 18M RCVR 4055M FREQ158.5
EVENT 31 NORTH
90
P.L. DB
150
0
400
5
RANGE NM

FIGURE A-81

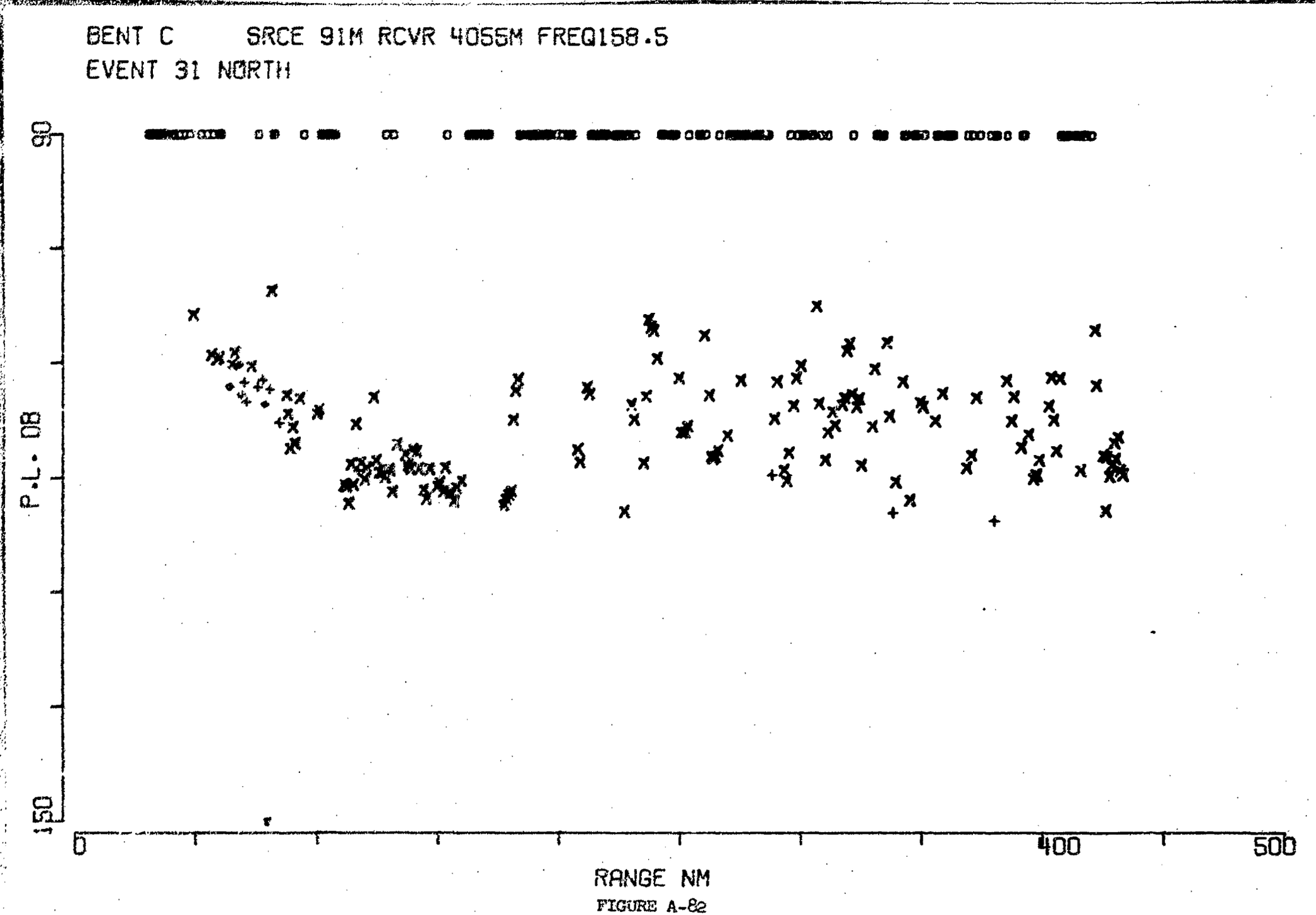
BENT C SRCE 91M RCVR 4055M FREQ158.5
EVENT 31 NORTH
90
150
P.L. DB
0
400
500
RANGE NM

FIGURE A-82

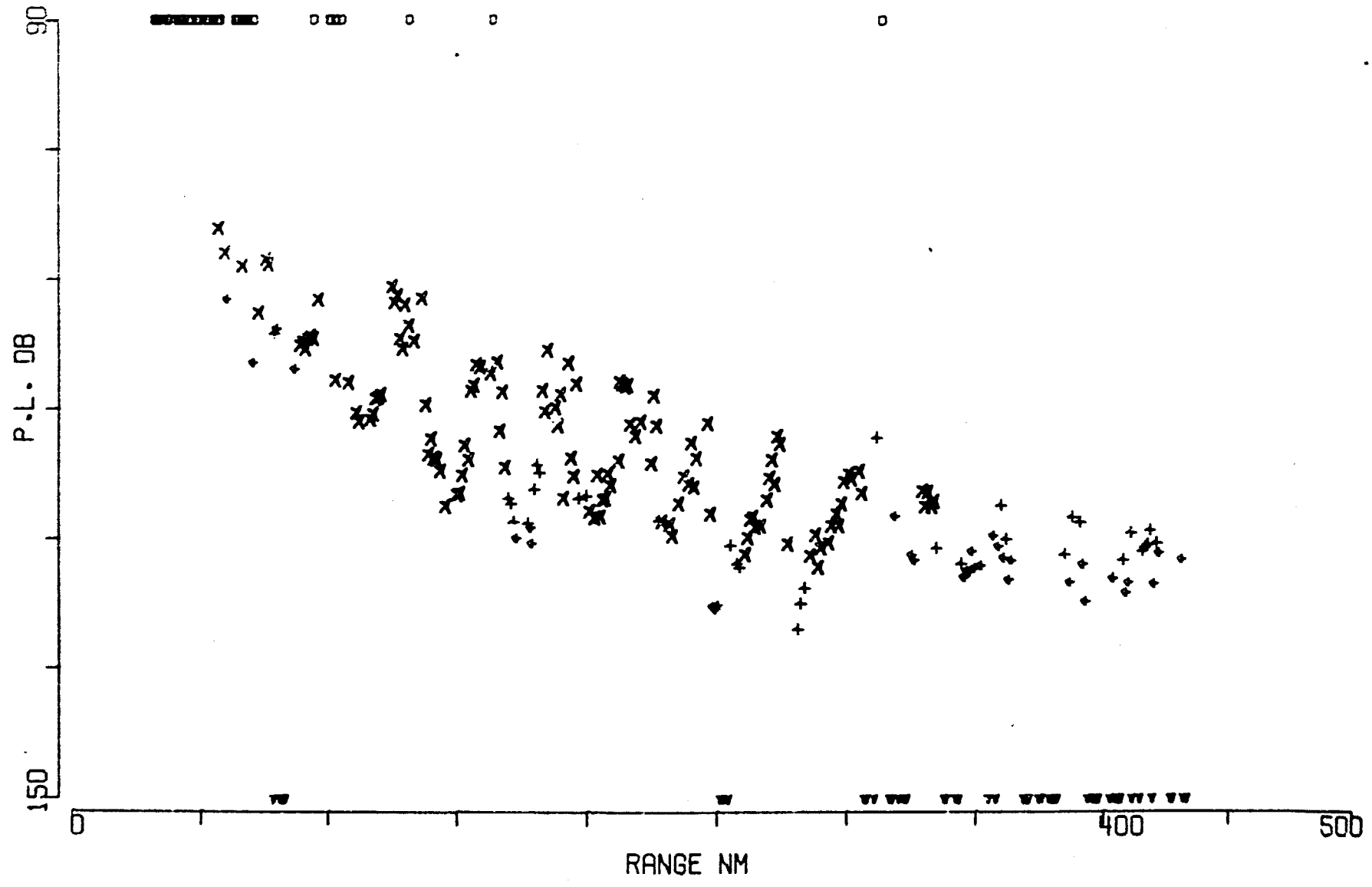
BENT C SRCE 18M RCVR 5521M FREQ158.5
EVENT 31 NORTH
90
150
P.L. DB
0
400
500
RANGE NM

FIGURE A-83

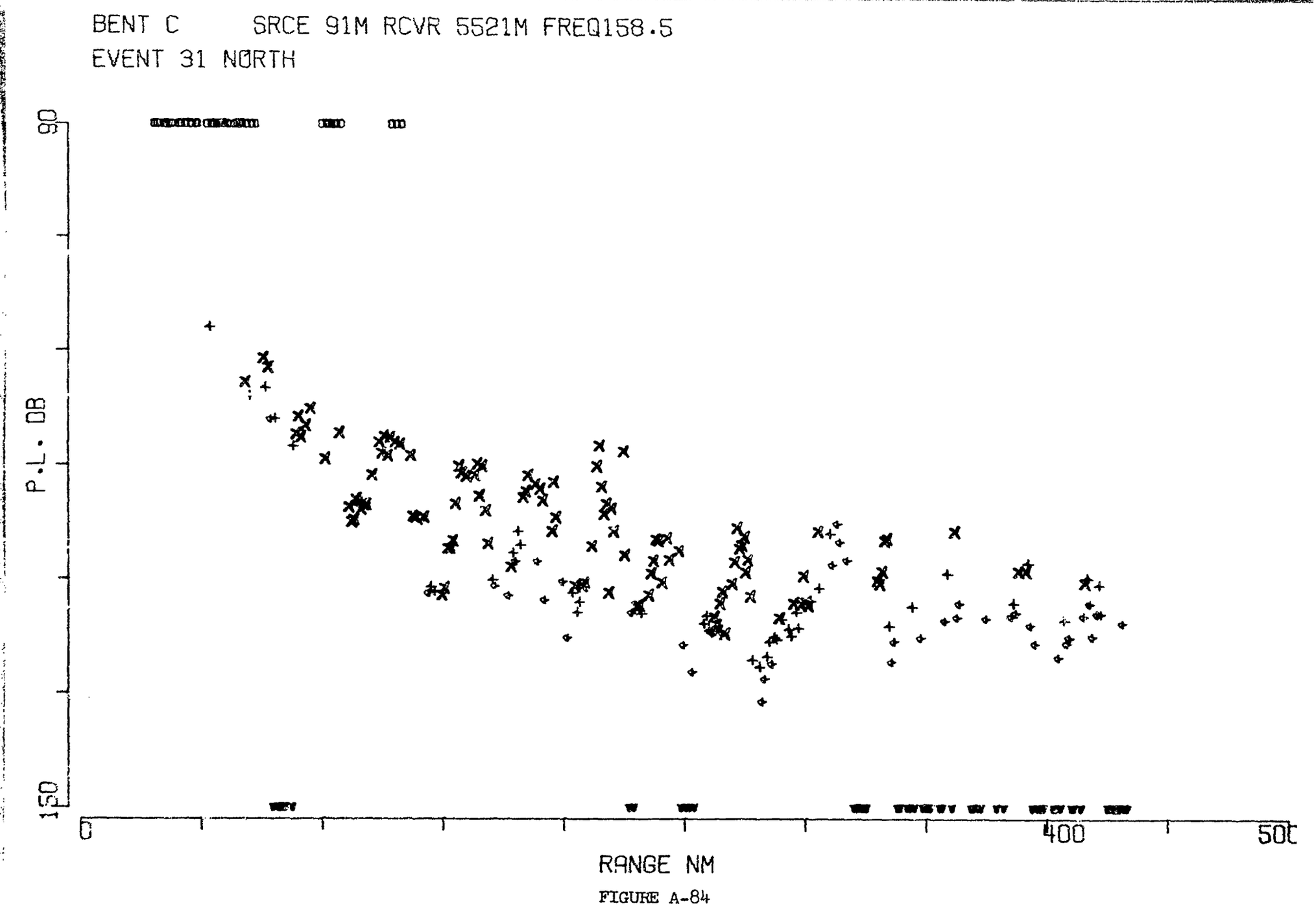
BENT C SRCE 91M RCVR 5521M FREQ158.5
EVENT 31 NORTH
90
150
P.L. DB
0
400
500
RANGE NM

FIGURE A-84

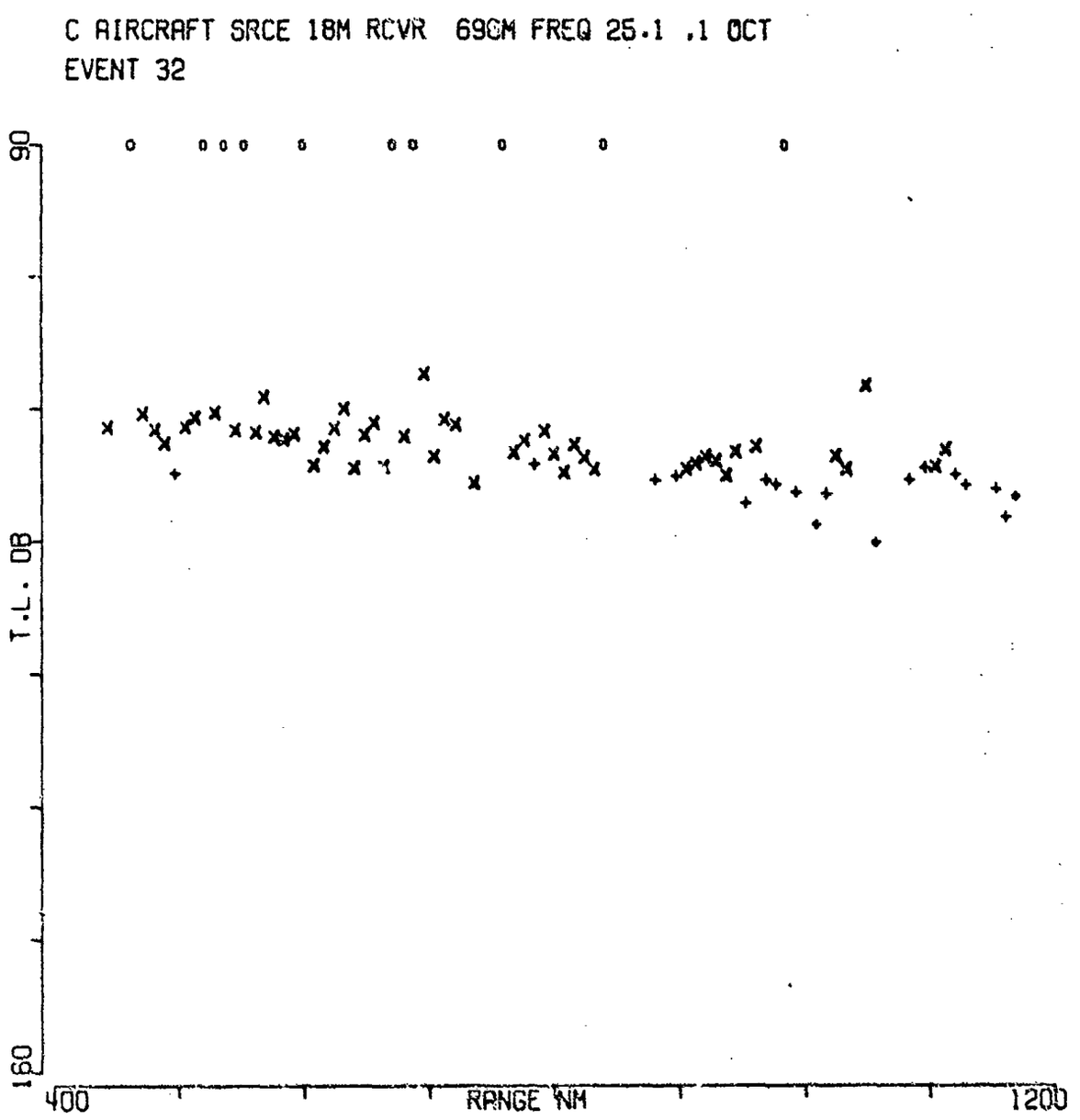
C AIRCRAFT SRCE 18M RCVR 69GM FREQ 25.1 .1 OCT
EVENT 32
90
160
T.L. DB
400
RANGE NM
1200

FIGURE A-85

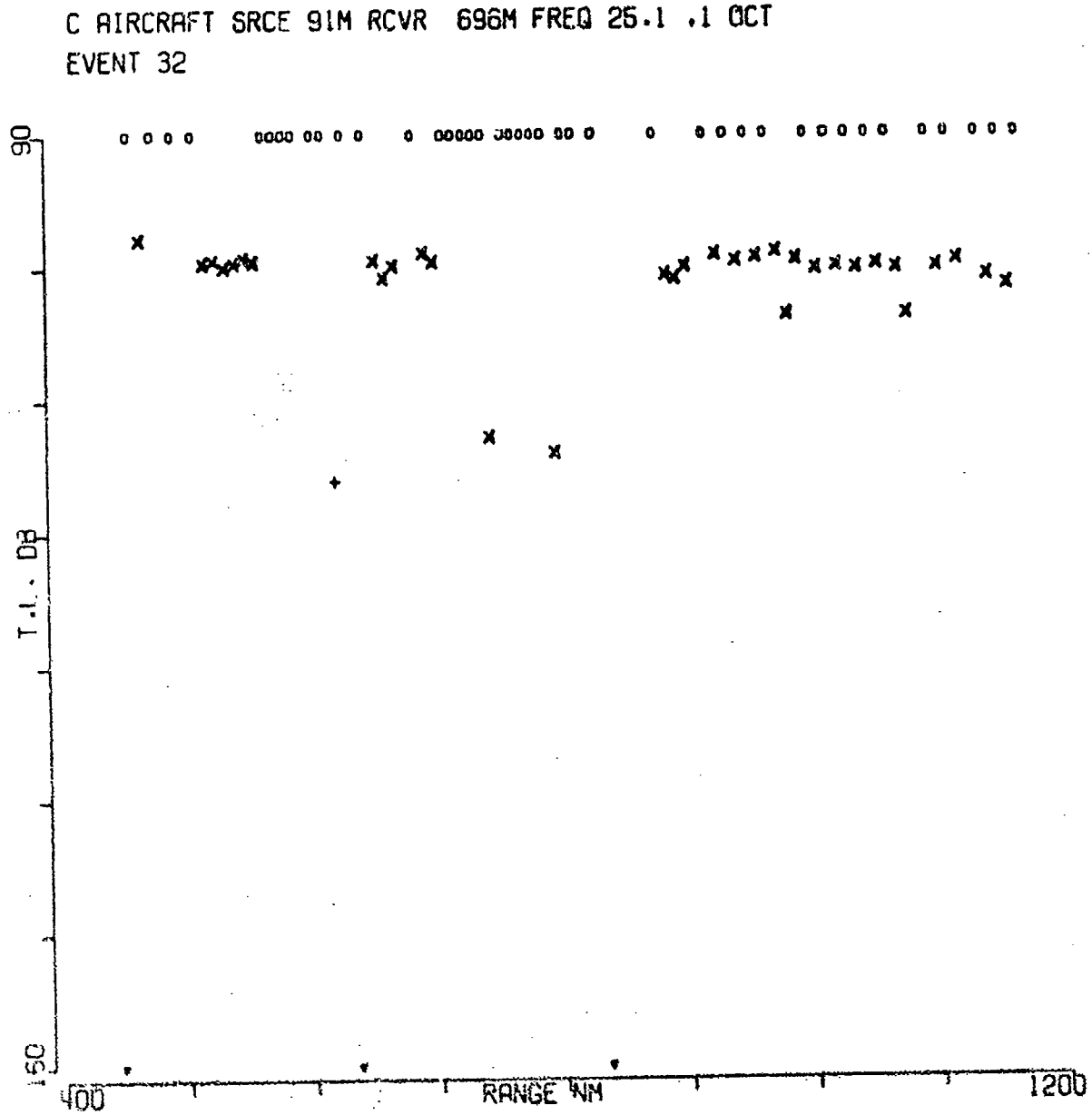
C AIRCRAFT SRCE 91M RCVR 696M FREQ 25.1 .1 OCT
EVENT 32
90
150
T.L. DB
400
RANGE NM
1200

FIGURE A-86

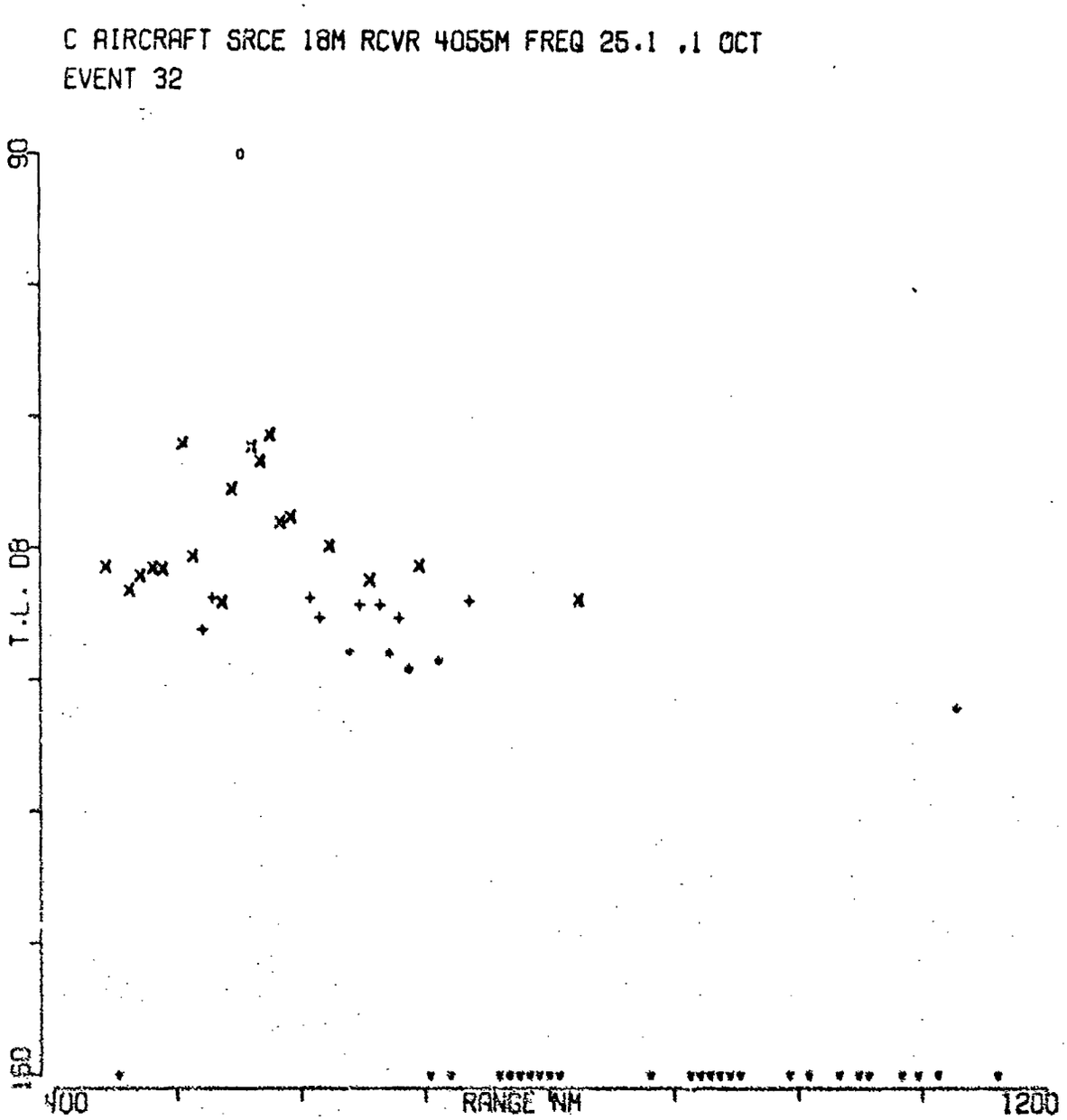
C AIRCRAFT SRCE 18M RCVR 4055M FREQ 25.1 .1 OCT
EVENT 32
90
T.L. DB
150
400
RANGE NM
1200

FIGURE A-87

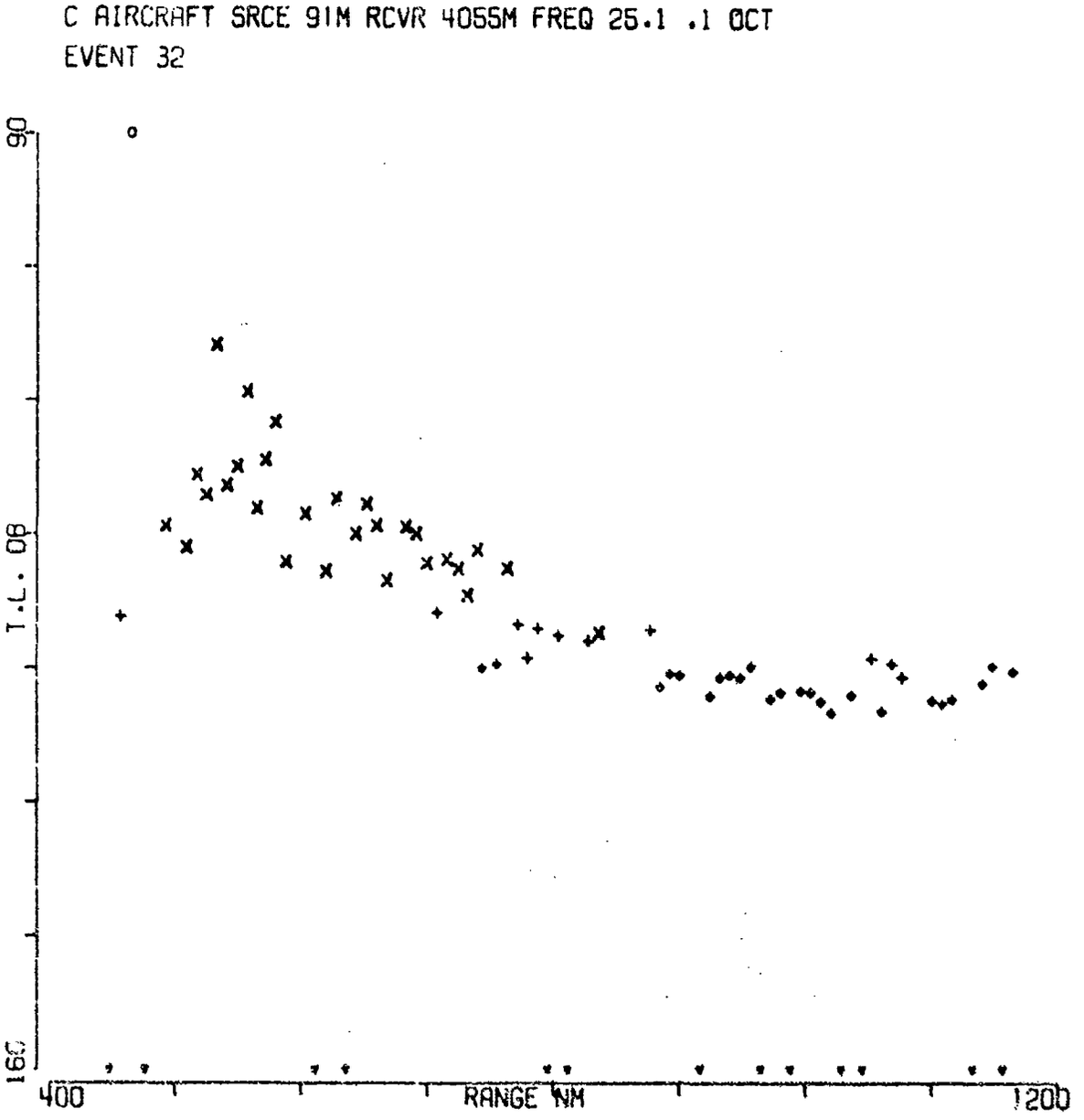
C AIRCRAFT SRCE 91M RCVR 4055M FREQ 25.1 .1 OCT
EVENT 32
90
T.L. DB
400
RANGE NM
1200

FIGURE A-88

C AIRCRAFT SRCE 18M RCVR 5221M FREQ 25.1 ,1 OCT
EVENT 32

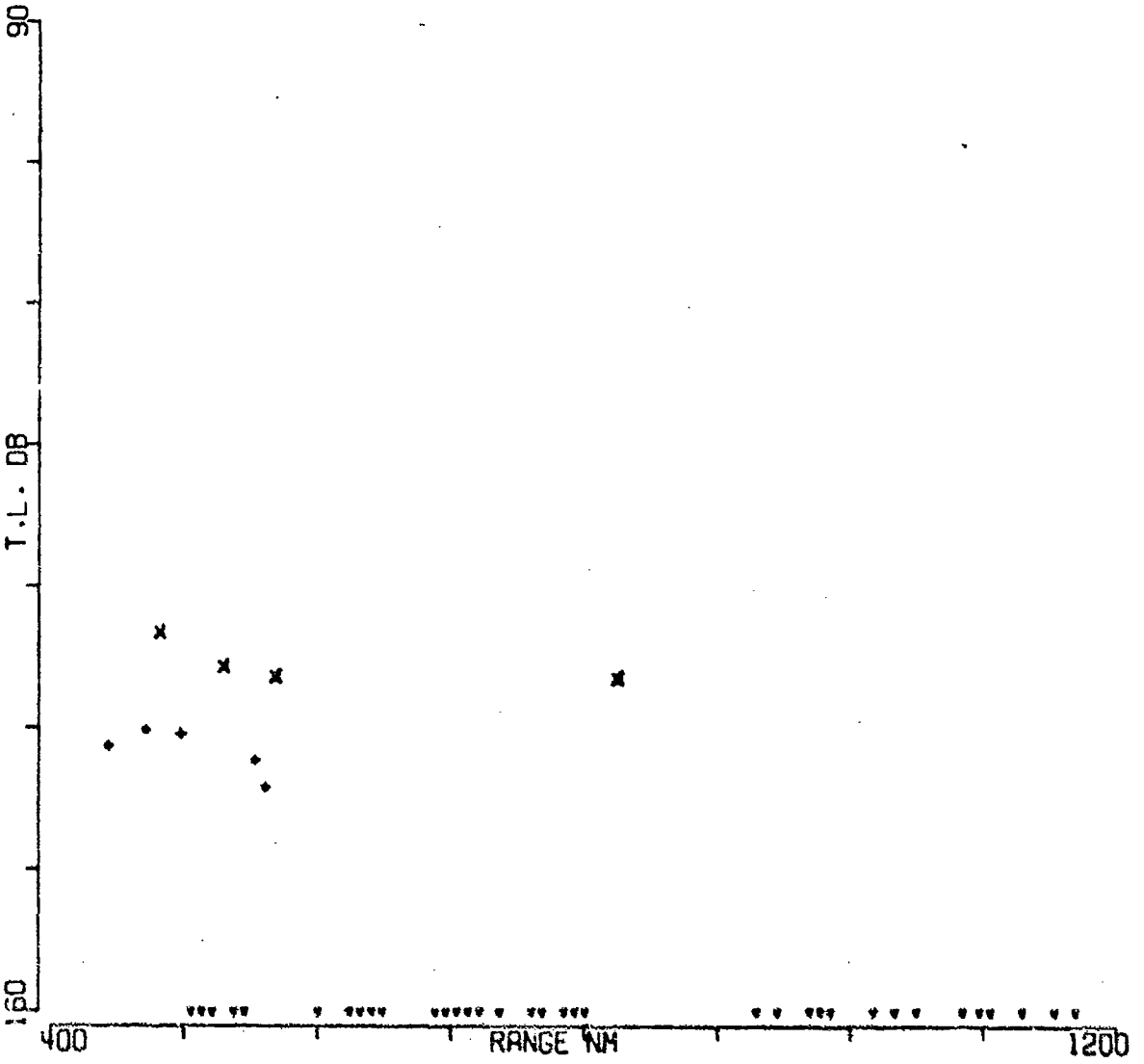

FIGURE A-89

C AIRCRAFT SRCE 91M RCVR 5221M FREQ 25.1 .1 OCT
EVENT 32

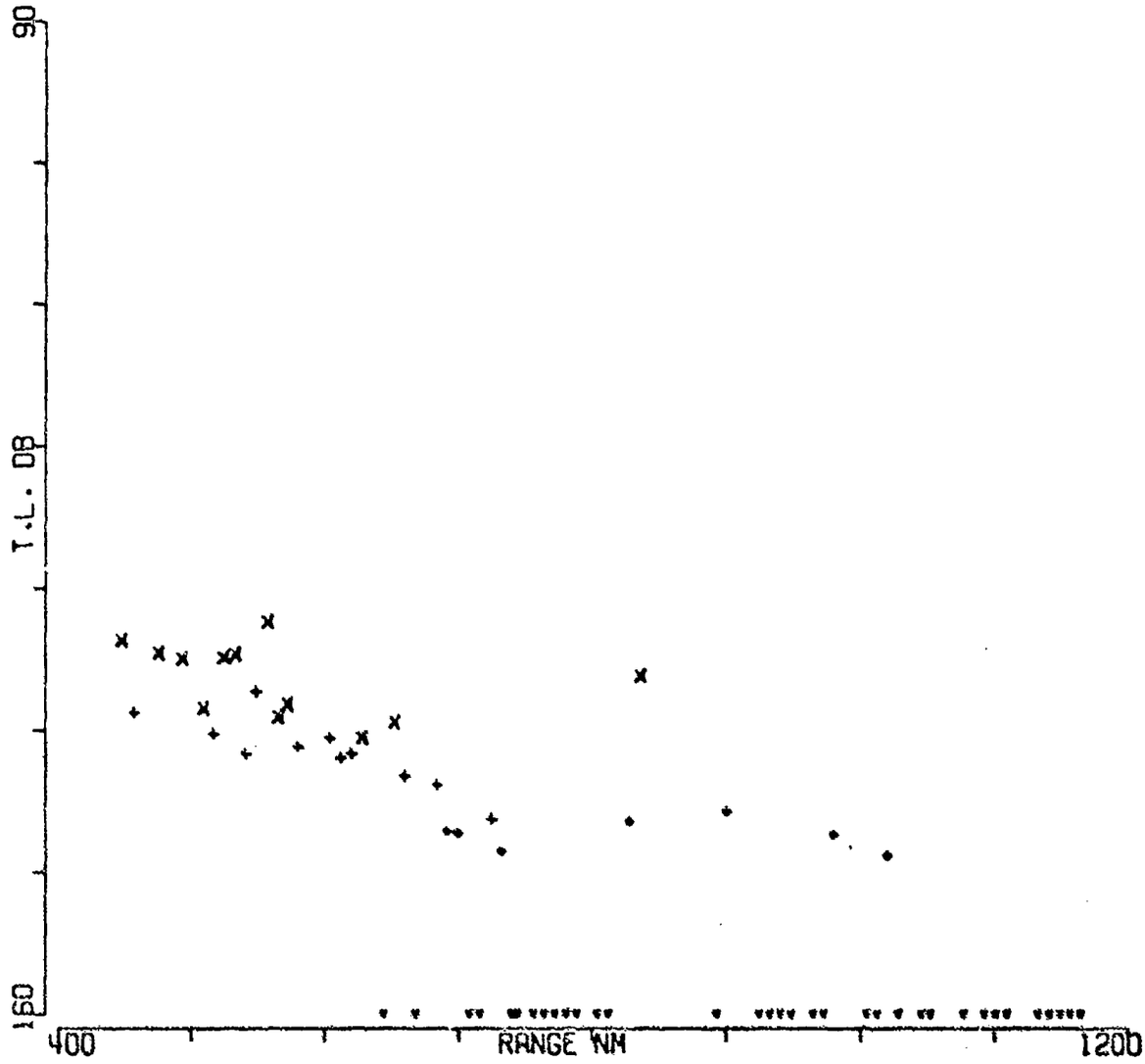

FIGURE A-90

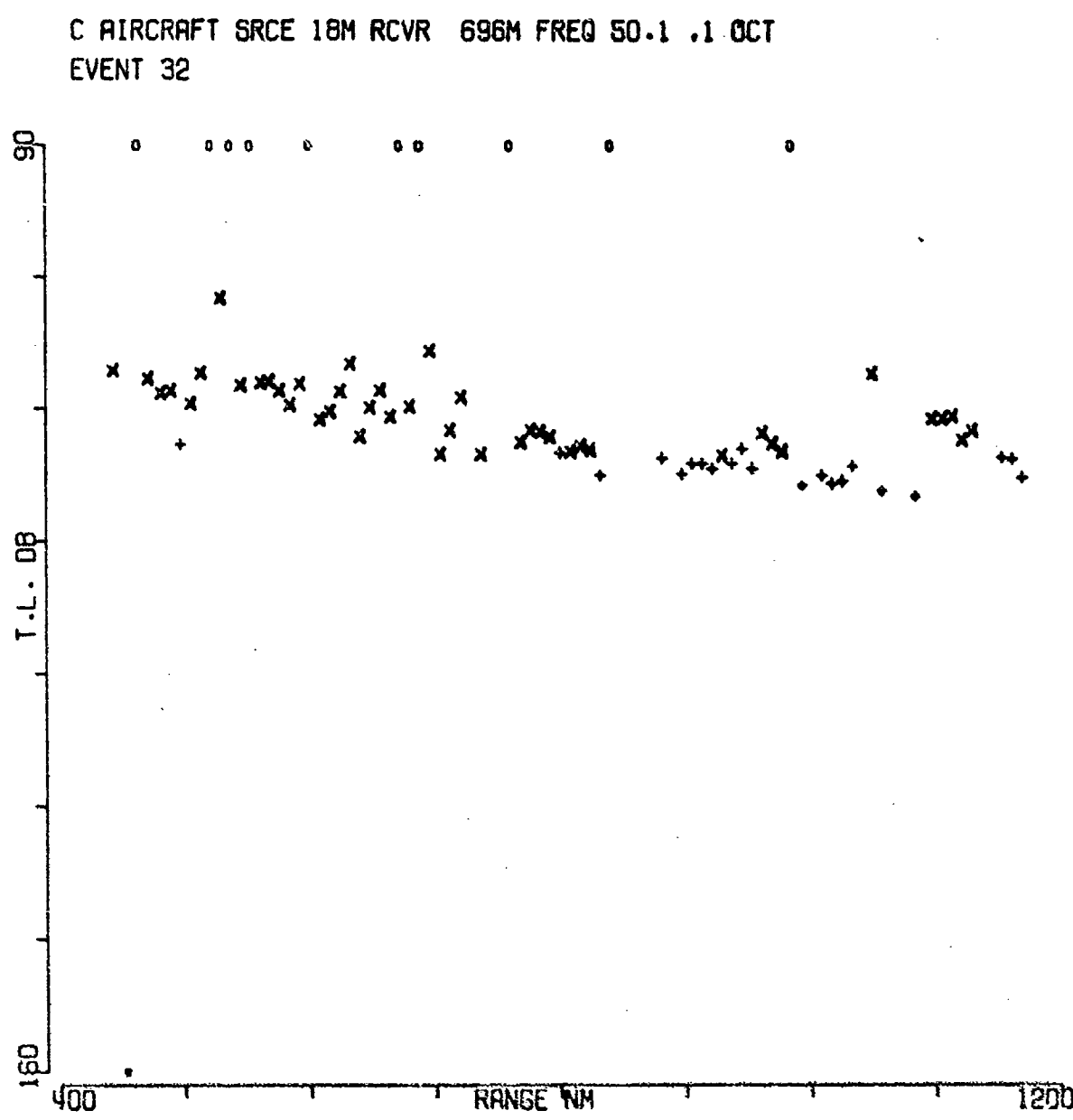
C AIRCRAFT SRCE 18M RCVR 696M FREQ 50.1 .1 OCT
EVENT 32
90
160
T.L. DB
400
RANGE NM
1200

FIGURE A-91

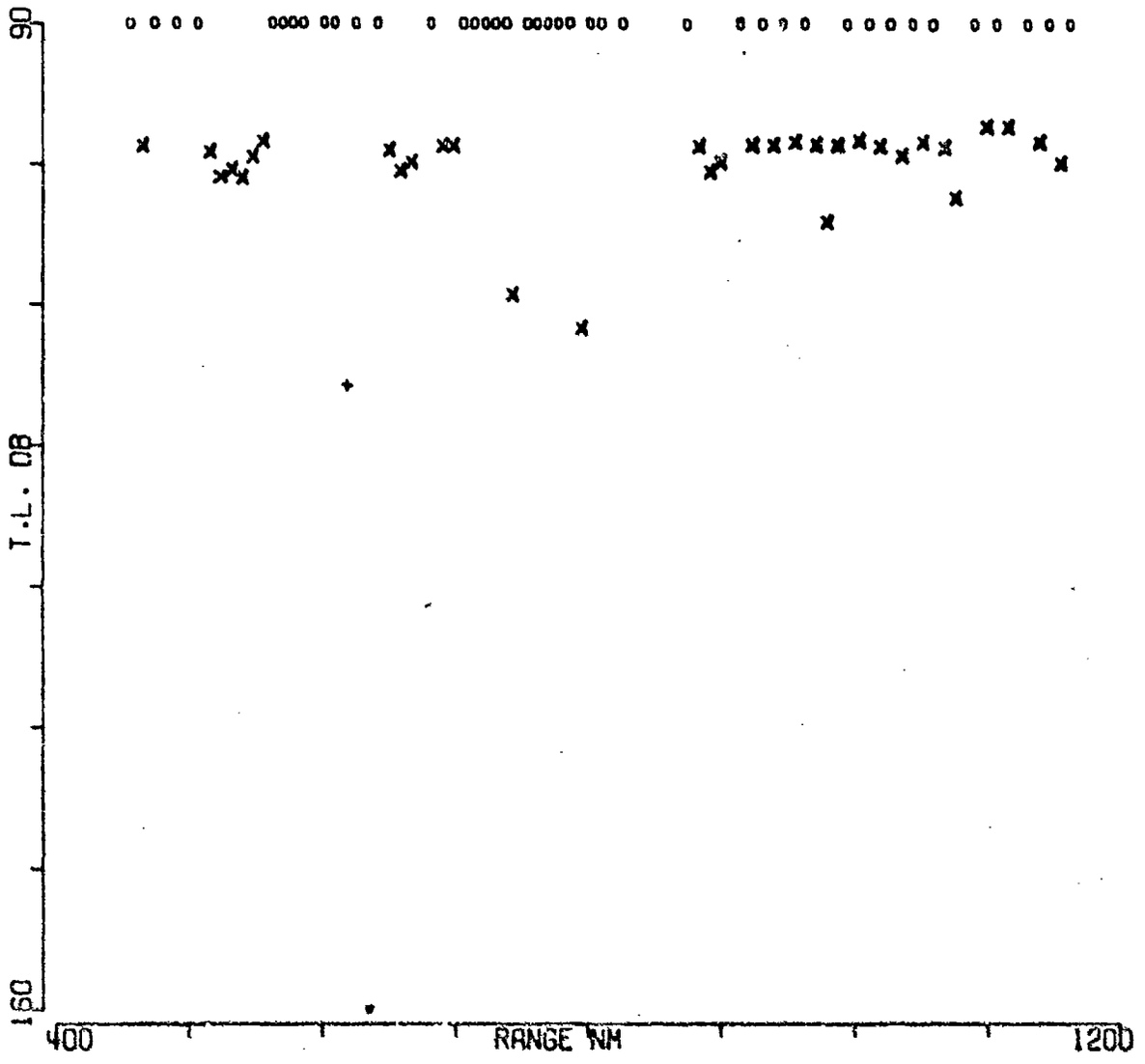
C AIRCRAFT SRCE 91M RCVR 696M FREQ 50.1 .1 OCT
EVENT 32
90
160
T.L. DB
400
RANGE NM
1200

FIGURE A-92

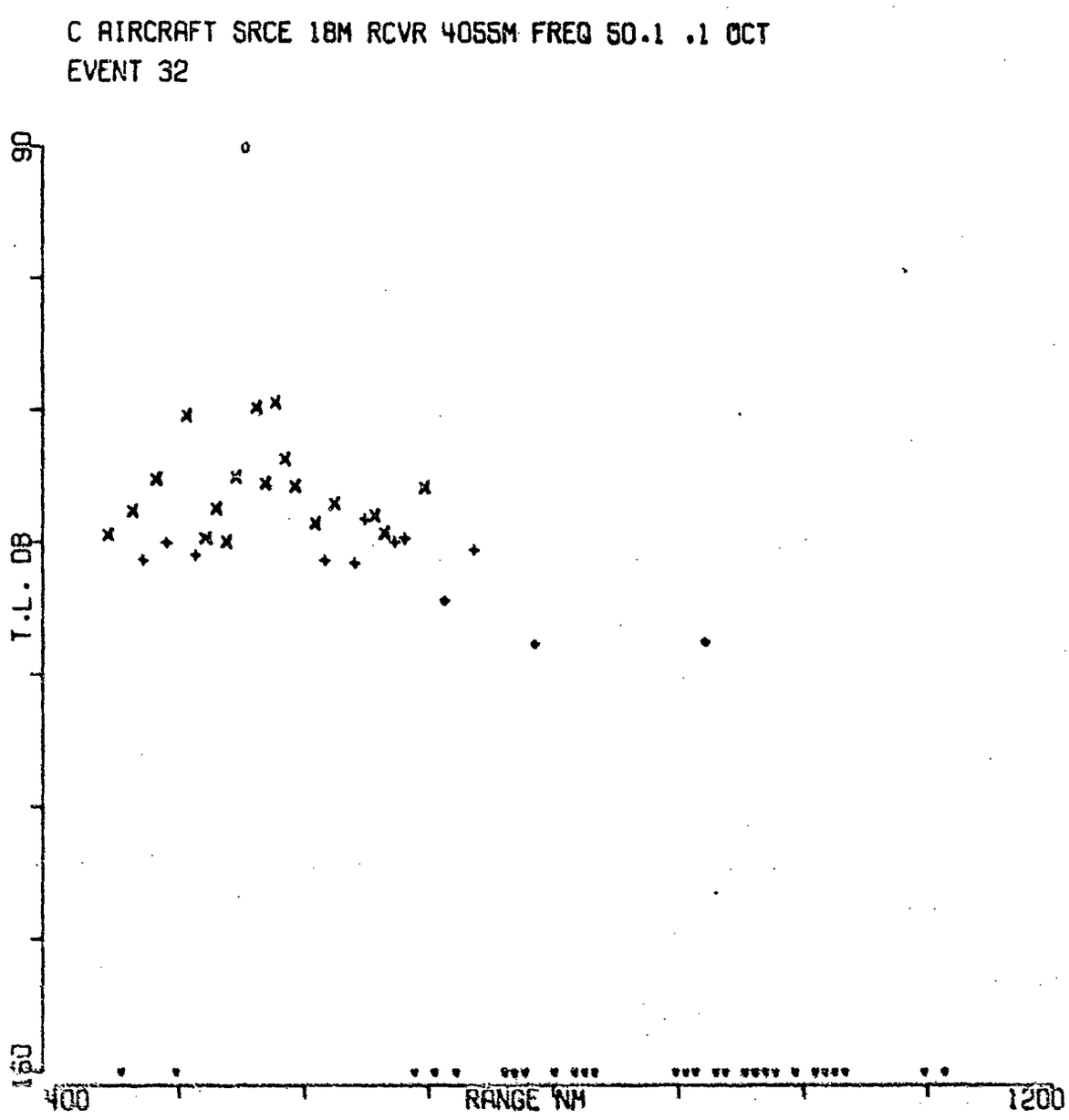
C AIRCRAFT SRCE 18M RCVR 4055M FREQ 50.1 .1 OCT
EVENT 32
90
T.L. DB
160
400
RANGE NM
1200

FIGURE A-93

C AIRCRAFT SRCE 91M RCVR 4055M FREQ 50.1 .1 OCT
EVENT 32

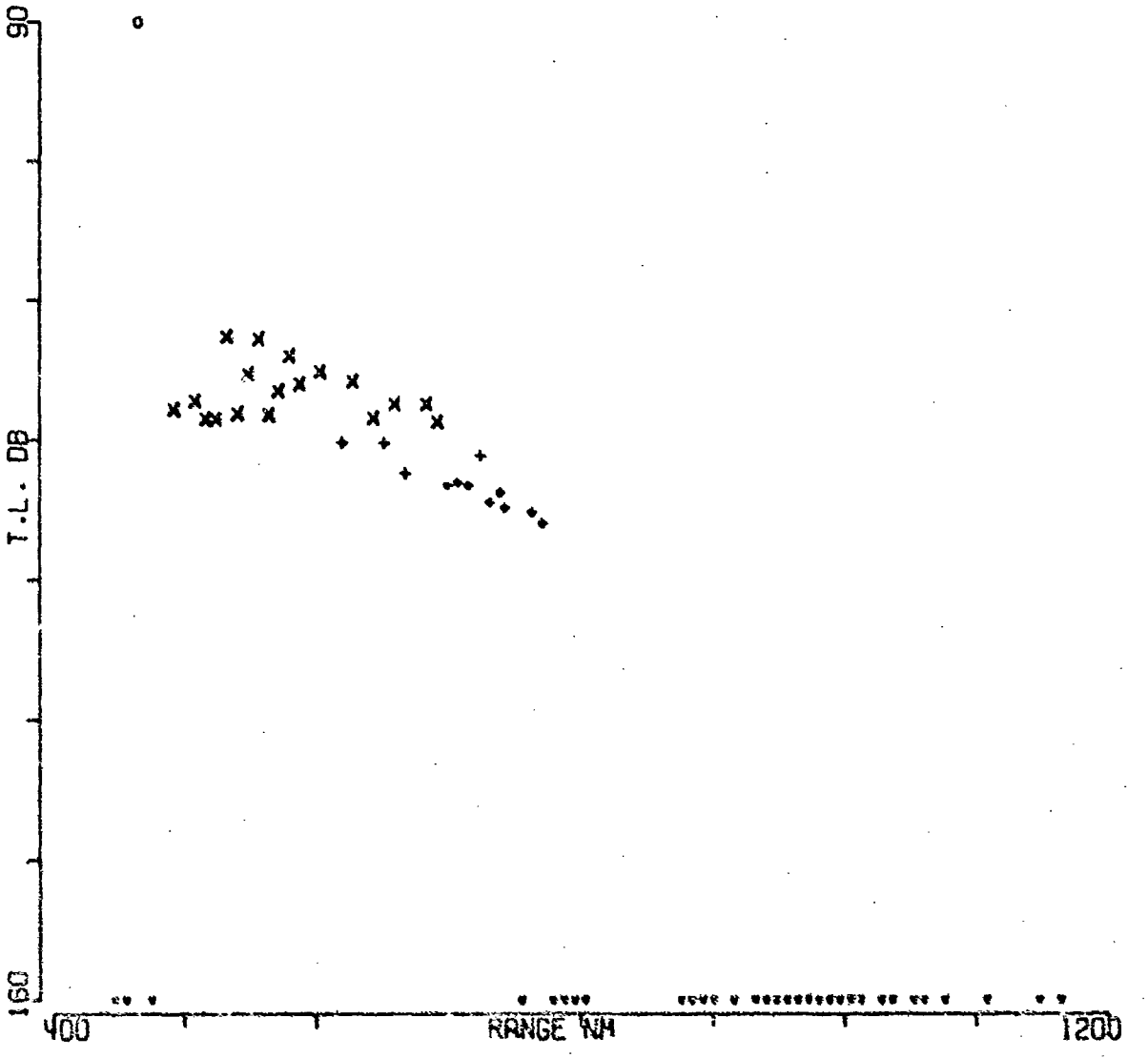

FIGURE A-94

C AIRCRAFT SRCE 16M RCVR 5221M FREQ 50.1 .1 OCT
EVENT 32

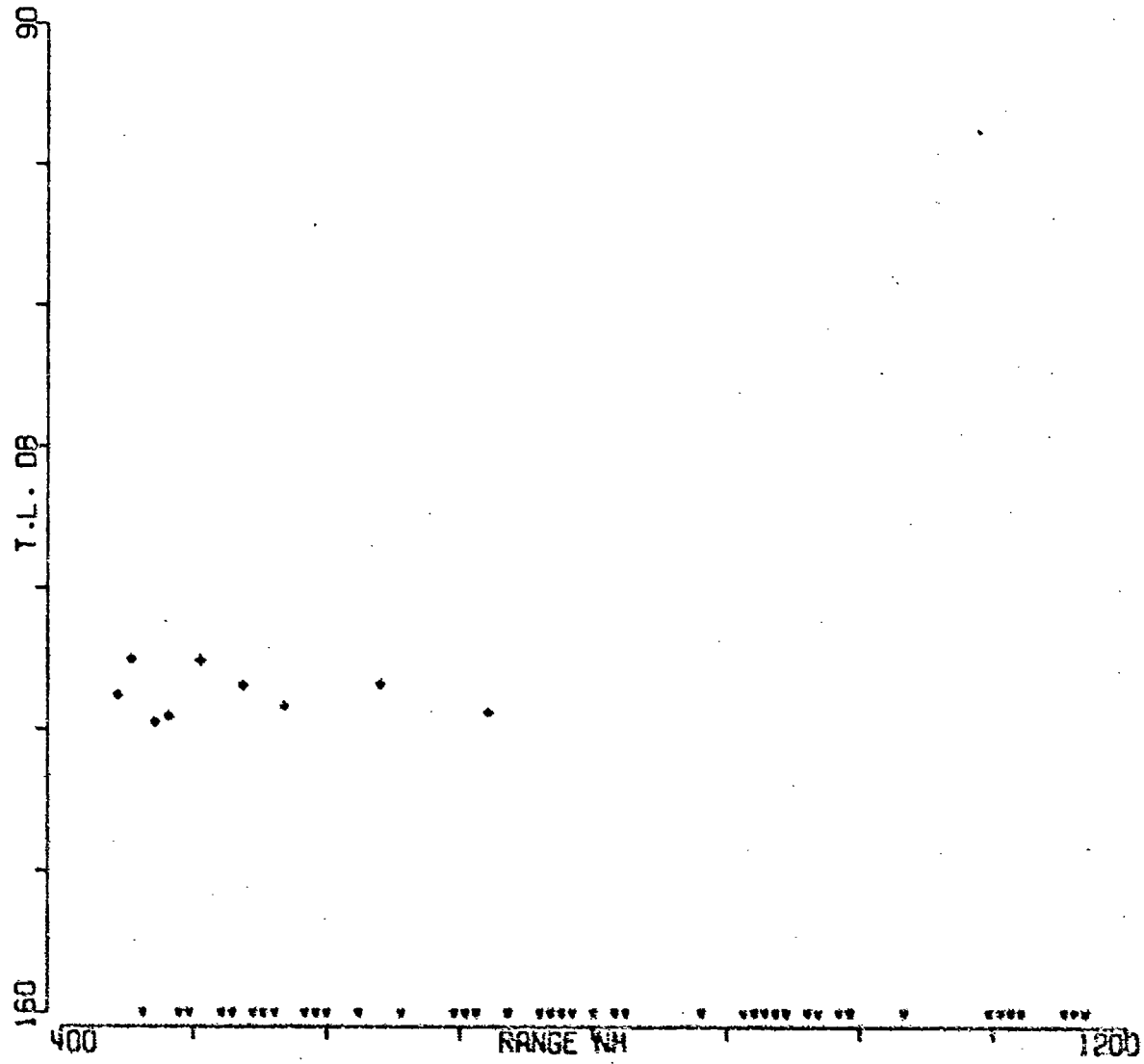

FIGURE A-95

C AIRCRAFT SRCE 91M RCVR 5221M FREQ 50.1 .1 OCT
EVENT 32

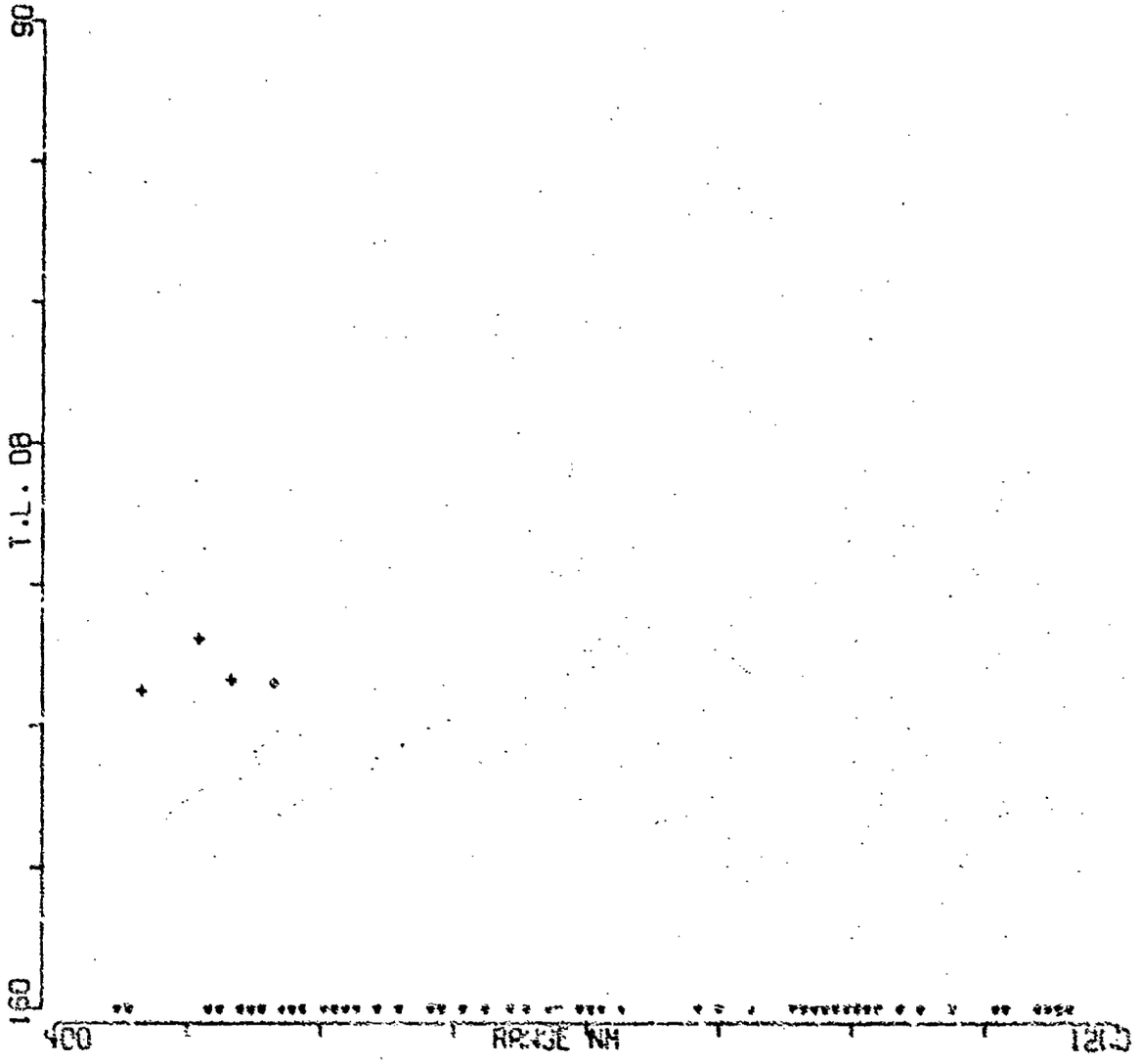

FIGURE A-96

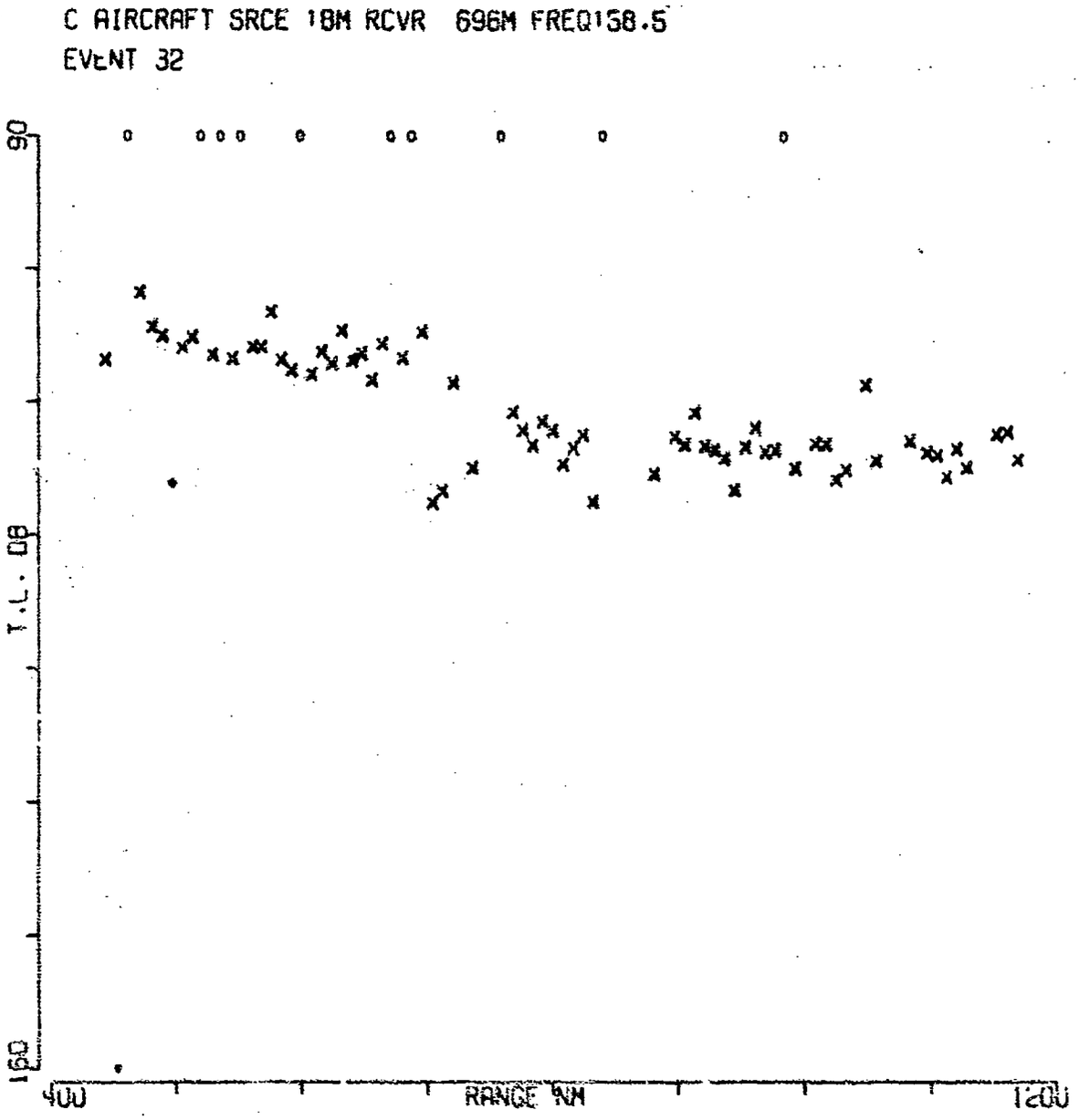
C AIRCRAFT SRCE 18M RCVR 696M FREQ158.5
EVENT 32
90
160
T.L. DB
400
RANGE NM
1200

FIGURE A-97

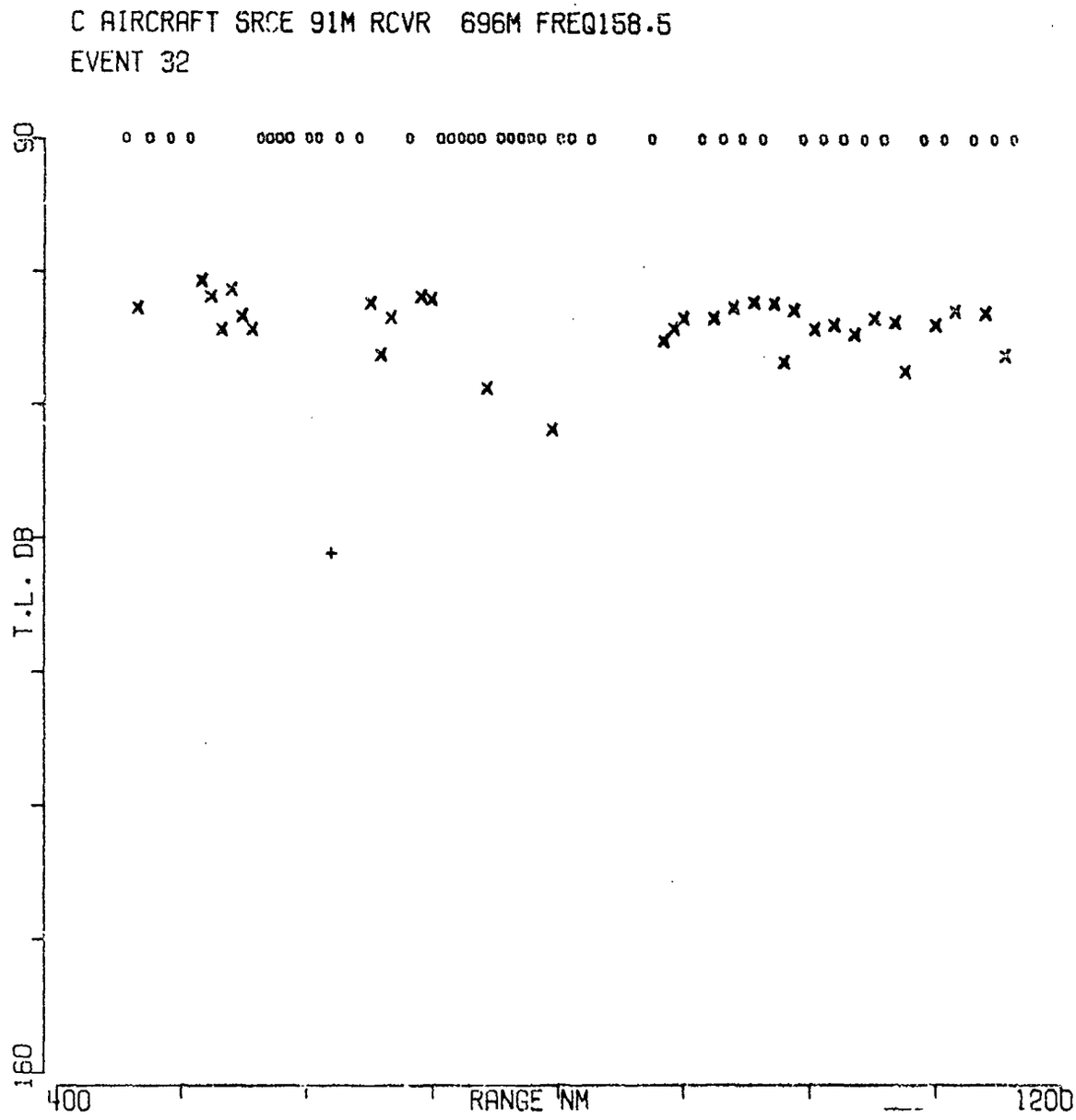
C AIRCRAFT SRCE 91M RCVR 696M FREQ158.5
EVENT 32
90
160
T.L. DB
400
RANGE NM
1200

FIGURE A-98

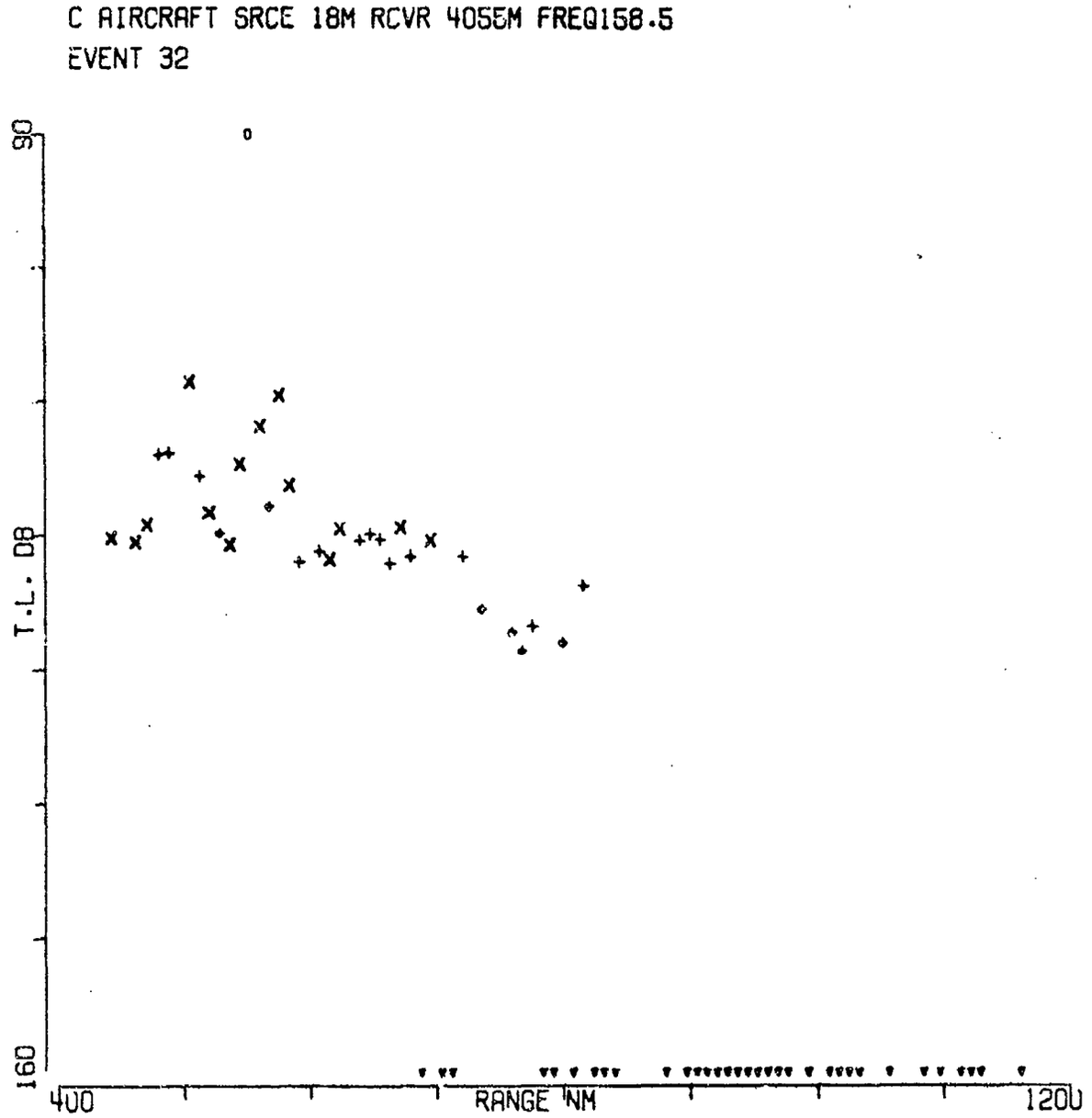
C AIRCRAFT SRCE 18M RCVR 4055M FREQ158.5
EVENT 32
90
160
T.L. DB
400
RANGE NM
1200

FIGURE A-99

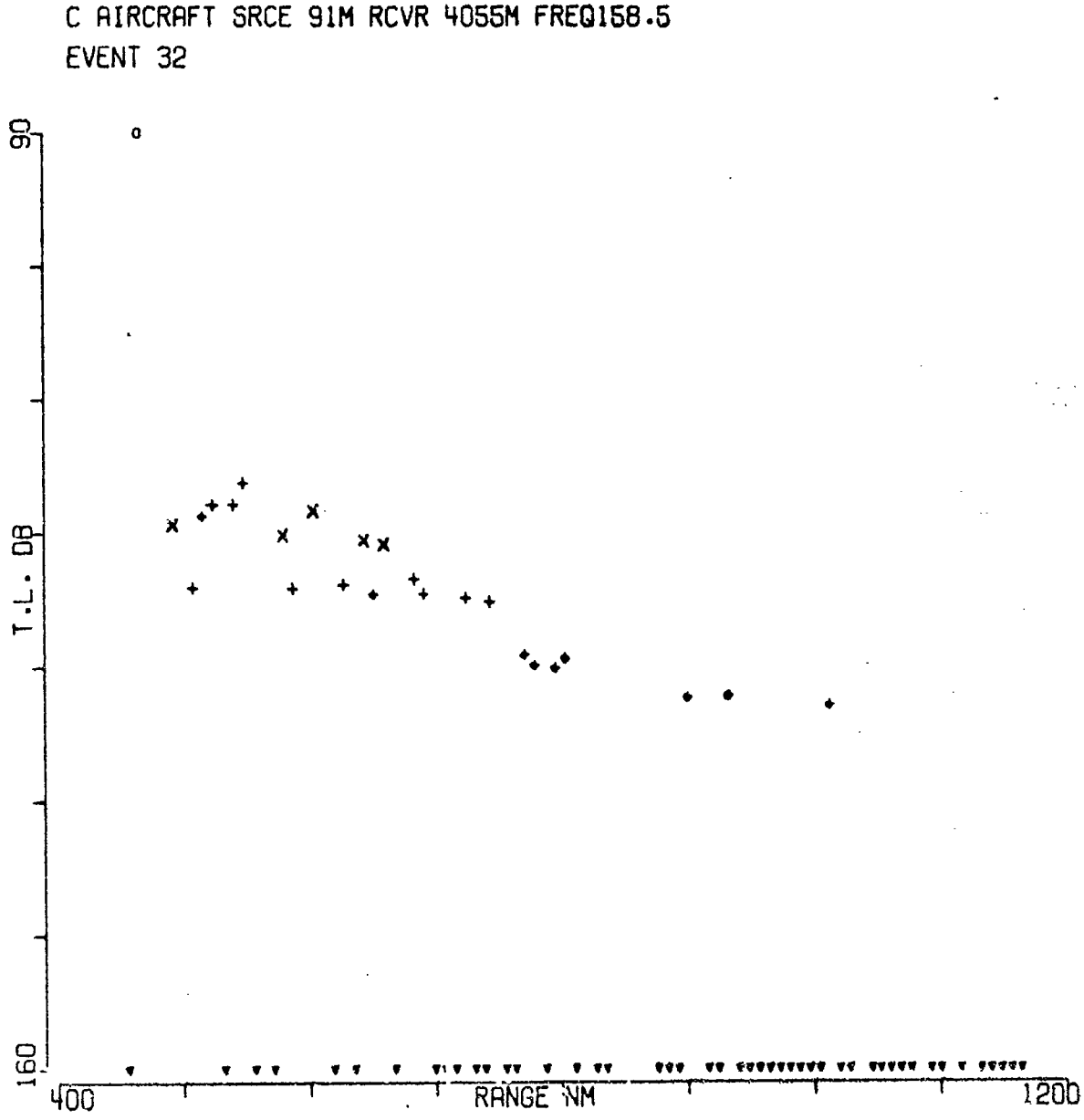
C AIRCRAFT SRCE 91M RCVR 4055M FREQ158.5
EVENT 32
90
T.L. DB
160
400
RANGE NM
1200

FIGURE A-100

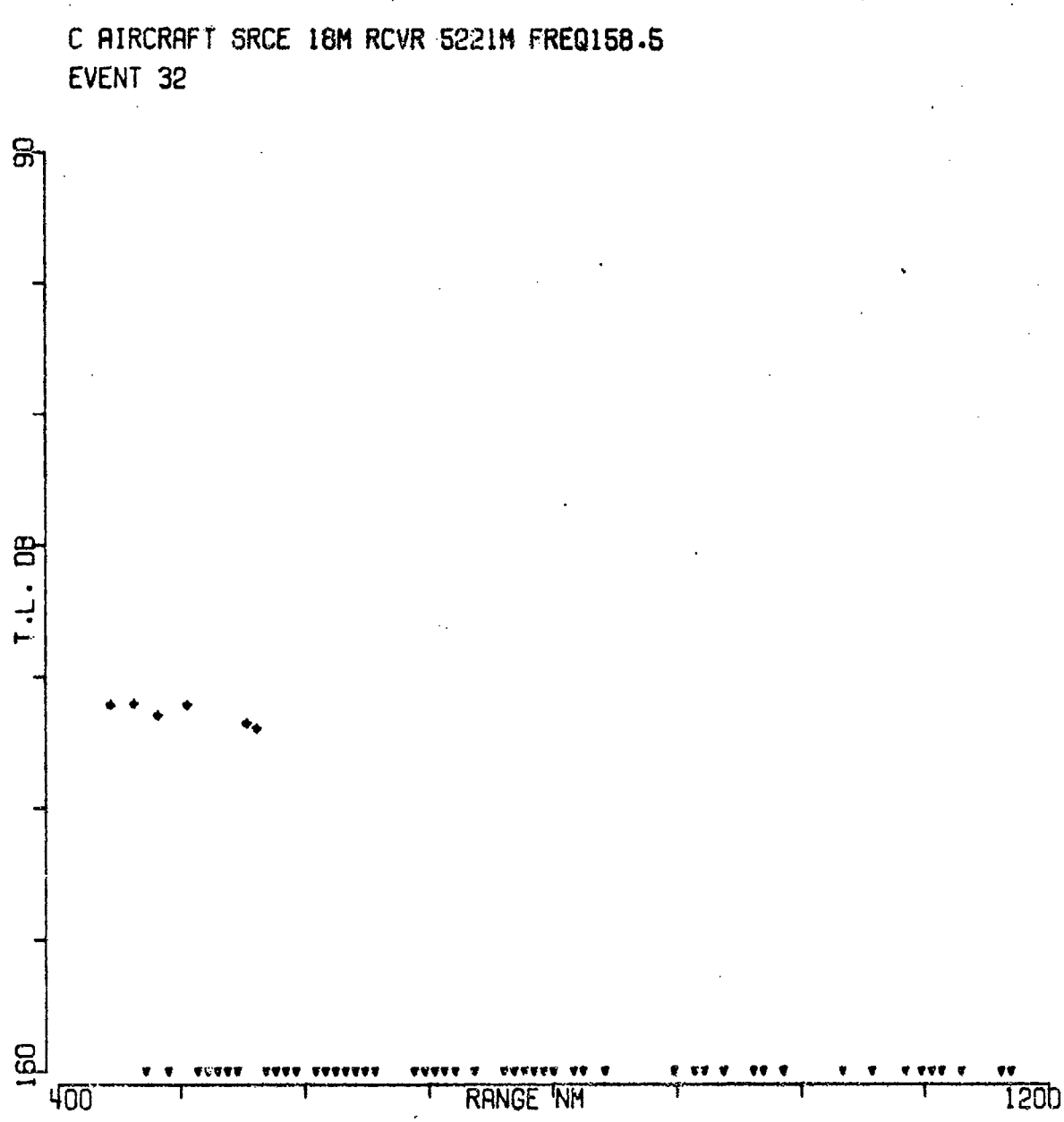
C AIRCRAFT SRCE 18M RCVR 5221M FREQ158.5
EVENT 32
90
T.L. DB
160
400
RANGE NM
1200

FIGURE A-101

C AIRCRAFT SRCE 91M RCVR 5221M FREQ158.5
EVENT 32

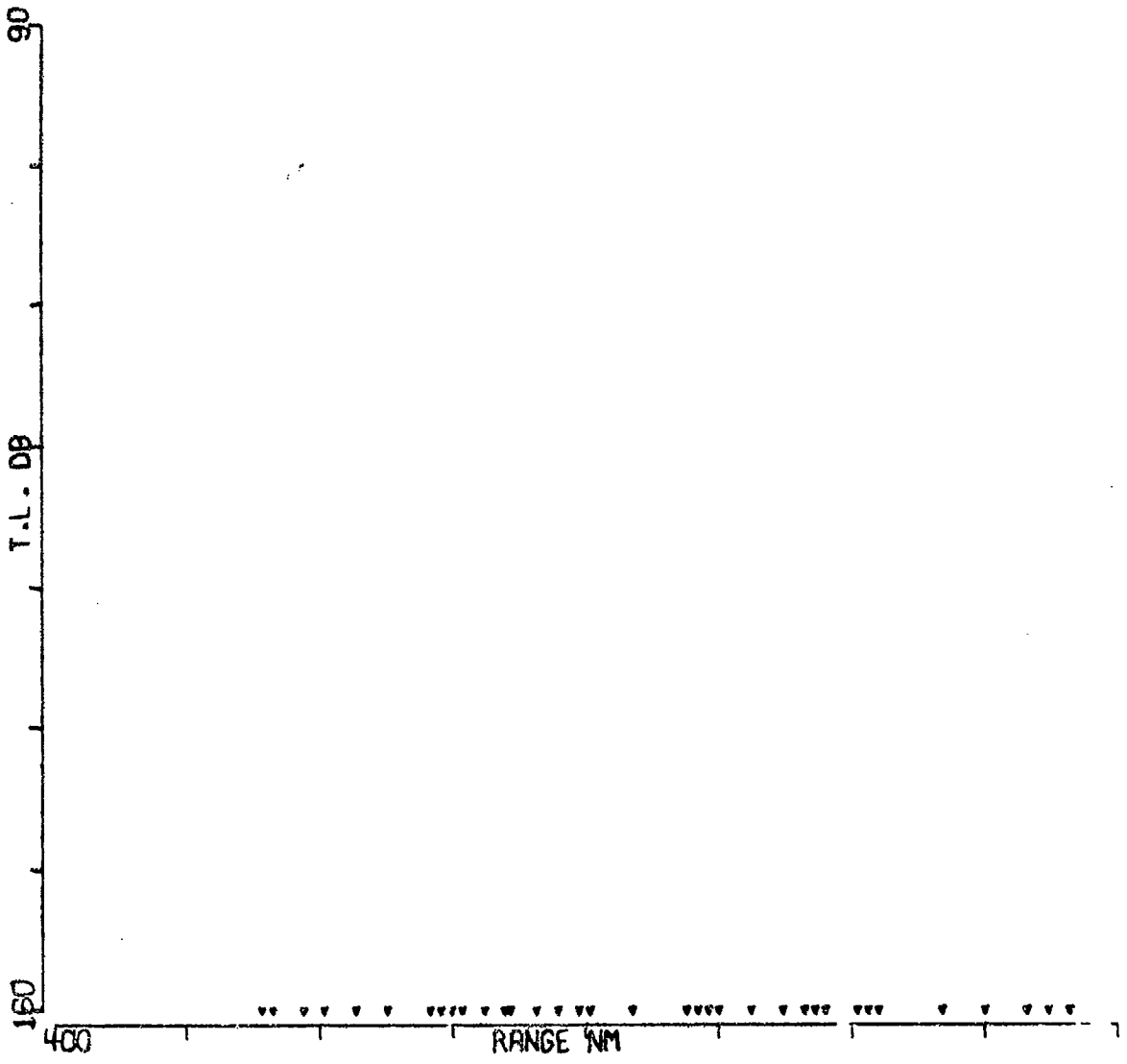

FIGURE A-102

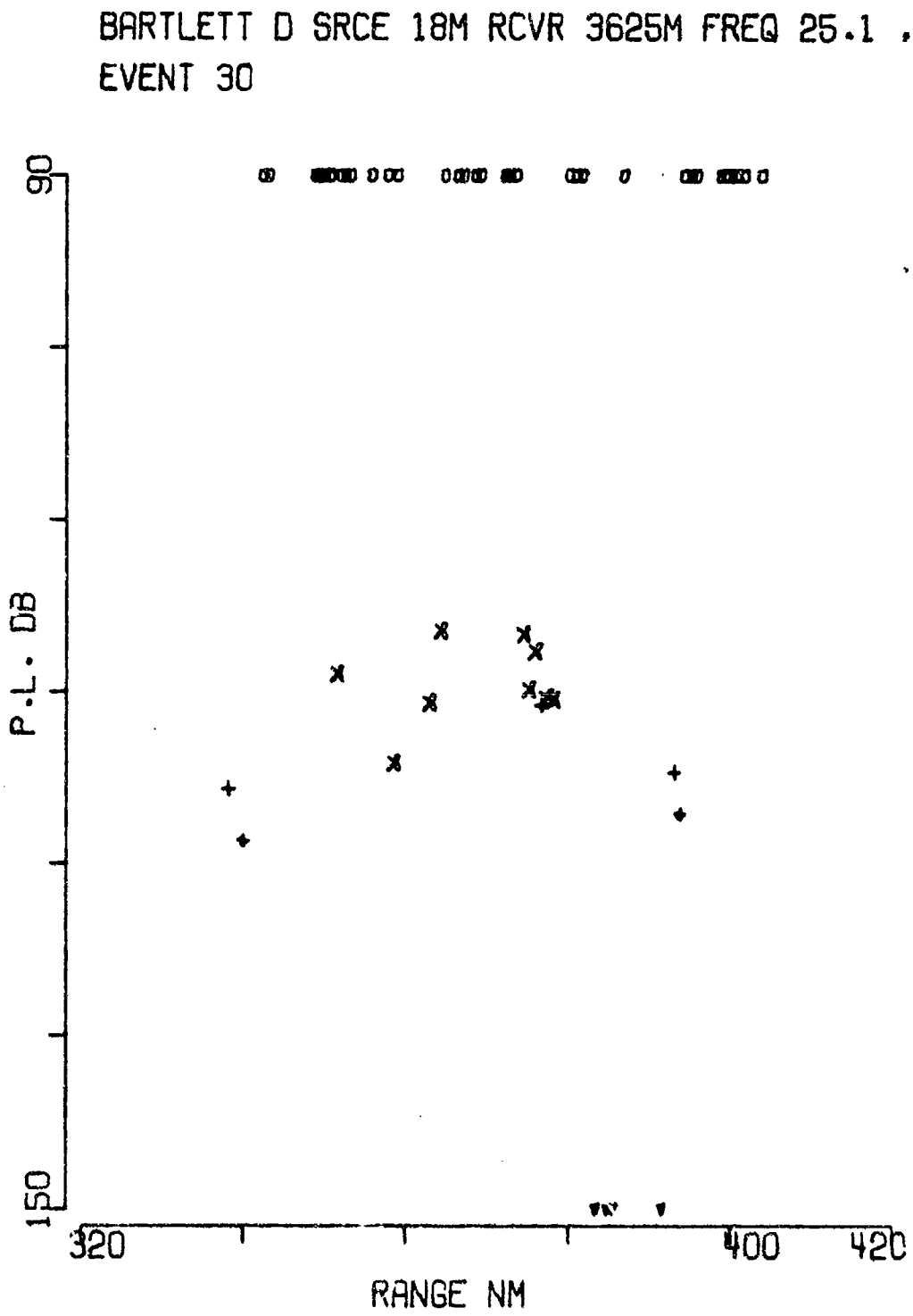
BARTLETT D SRCE 18M RCVR 3625M FREQ 25.1 .1 OCT
EVENT 30
90
150
P.L. DB
320
400
420
RANGE NM

FIGURE A-103

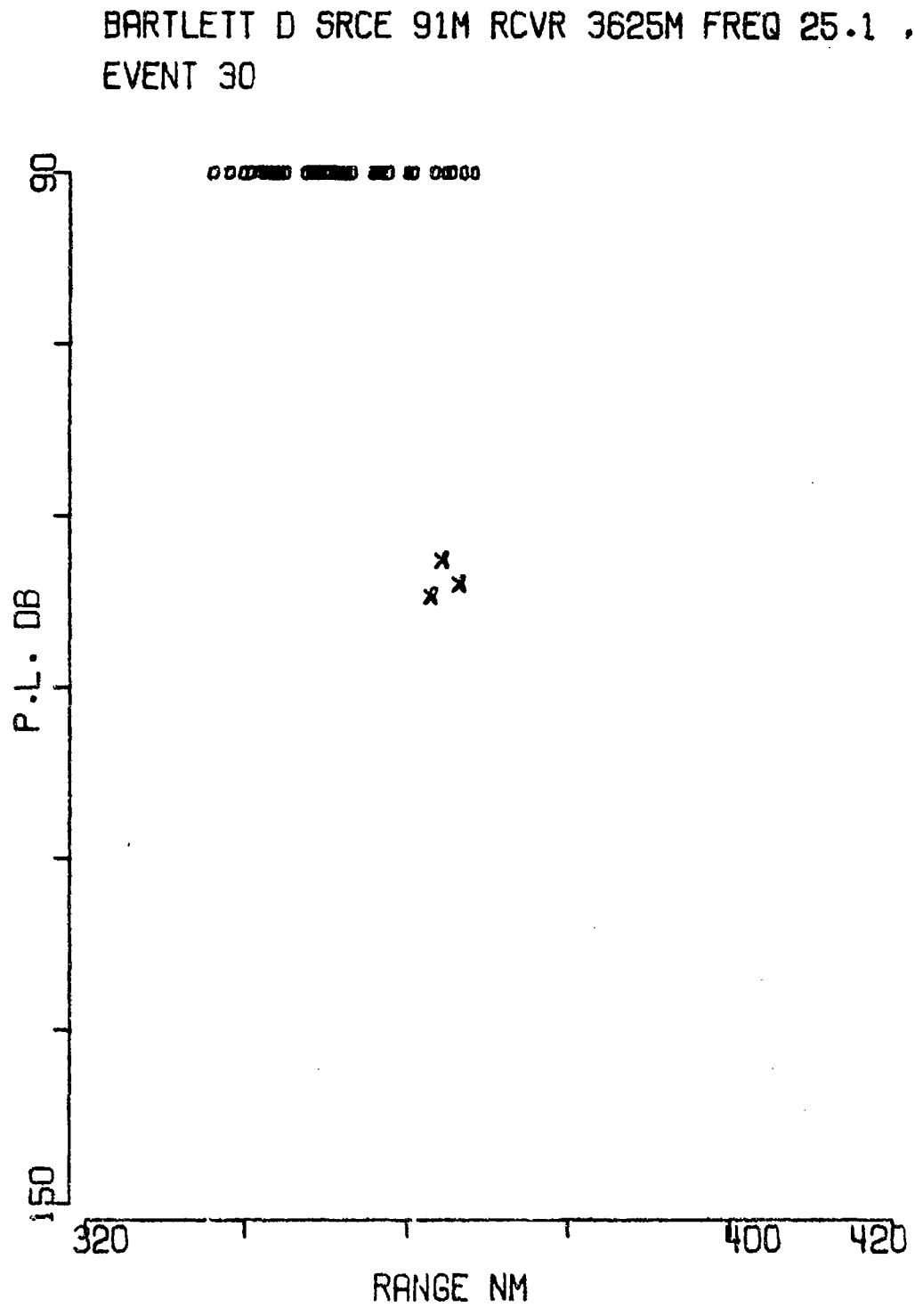
BARTLETT D SRCE 91M RCVR 3625M FREQ 25.1 .1 OCT
EVENT 30
90
150
P.L. DB
320
400
420
RANGE NM

FIGURE A-104

BARTLETT D SRCE 18M RCVR 3925M FREQ 25.1 .1 OCT
EVENT 30

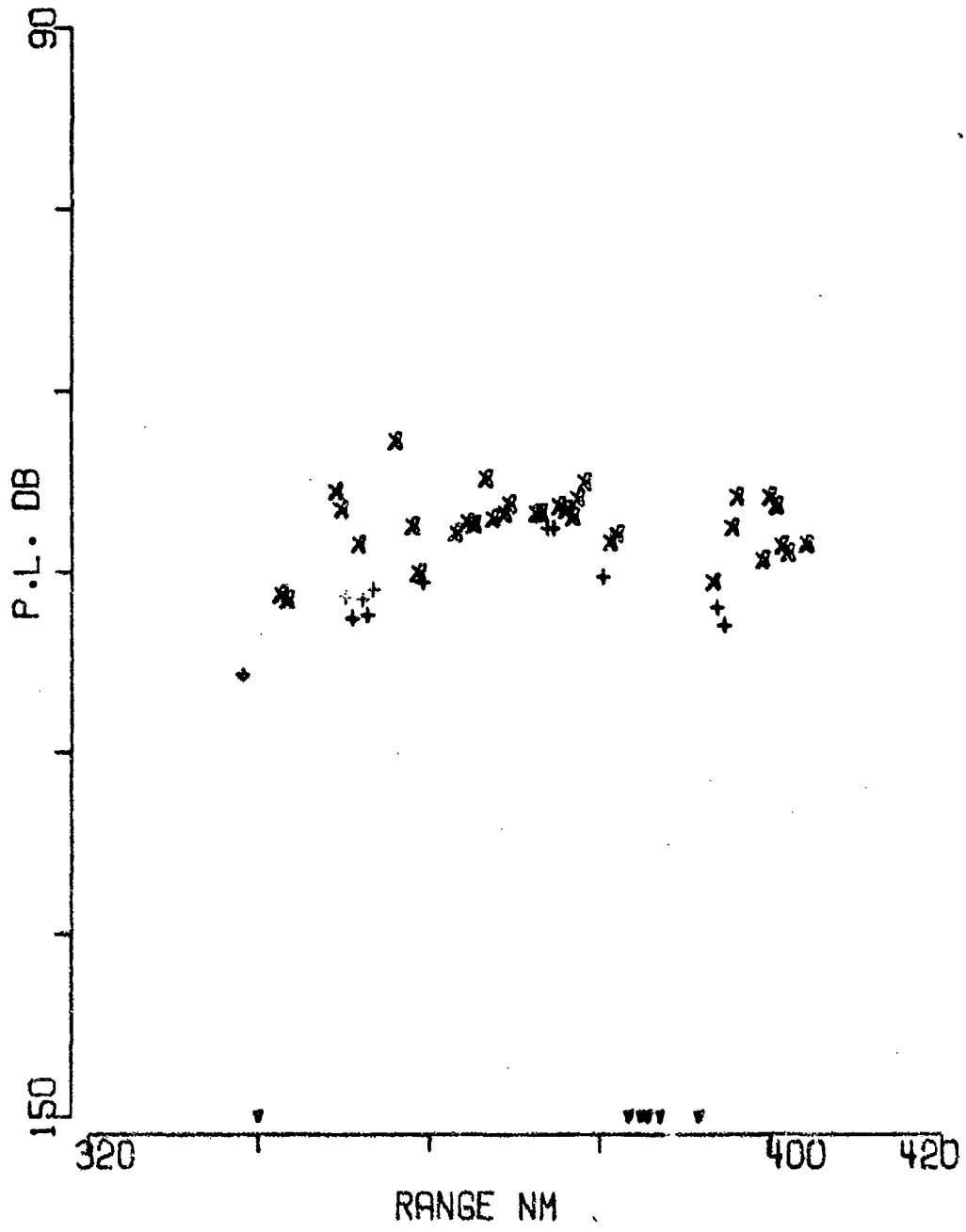

FIGURE A-105

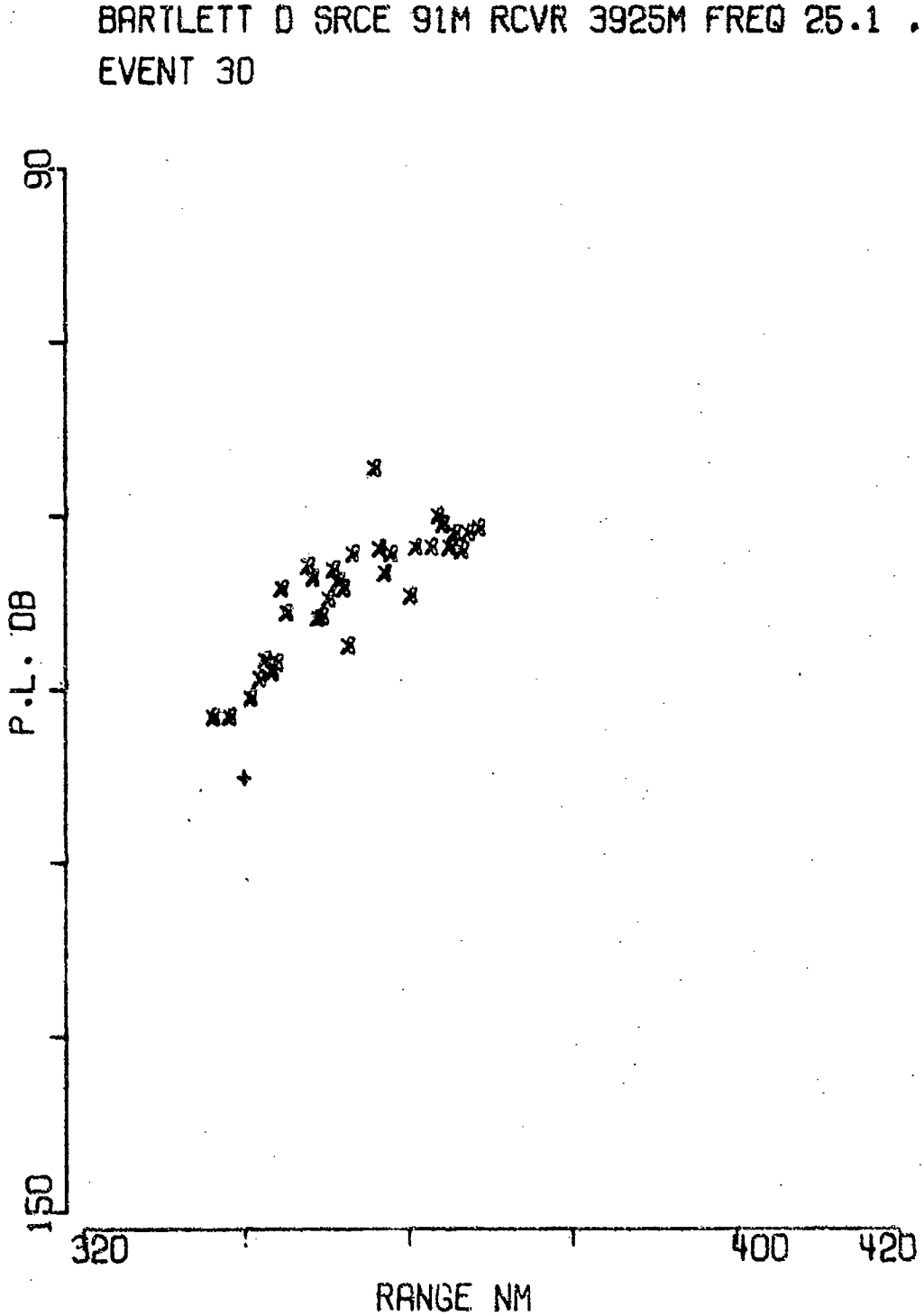
BARTLETT D SRCE 91M RCVR 3925M FREQ 25.1 .1 OCT
EVENT 30
90
150
P.L. DB
320
400
420
RANGE NM

FIGURE A-106

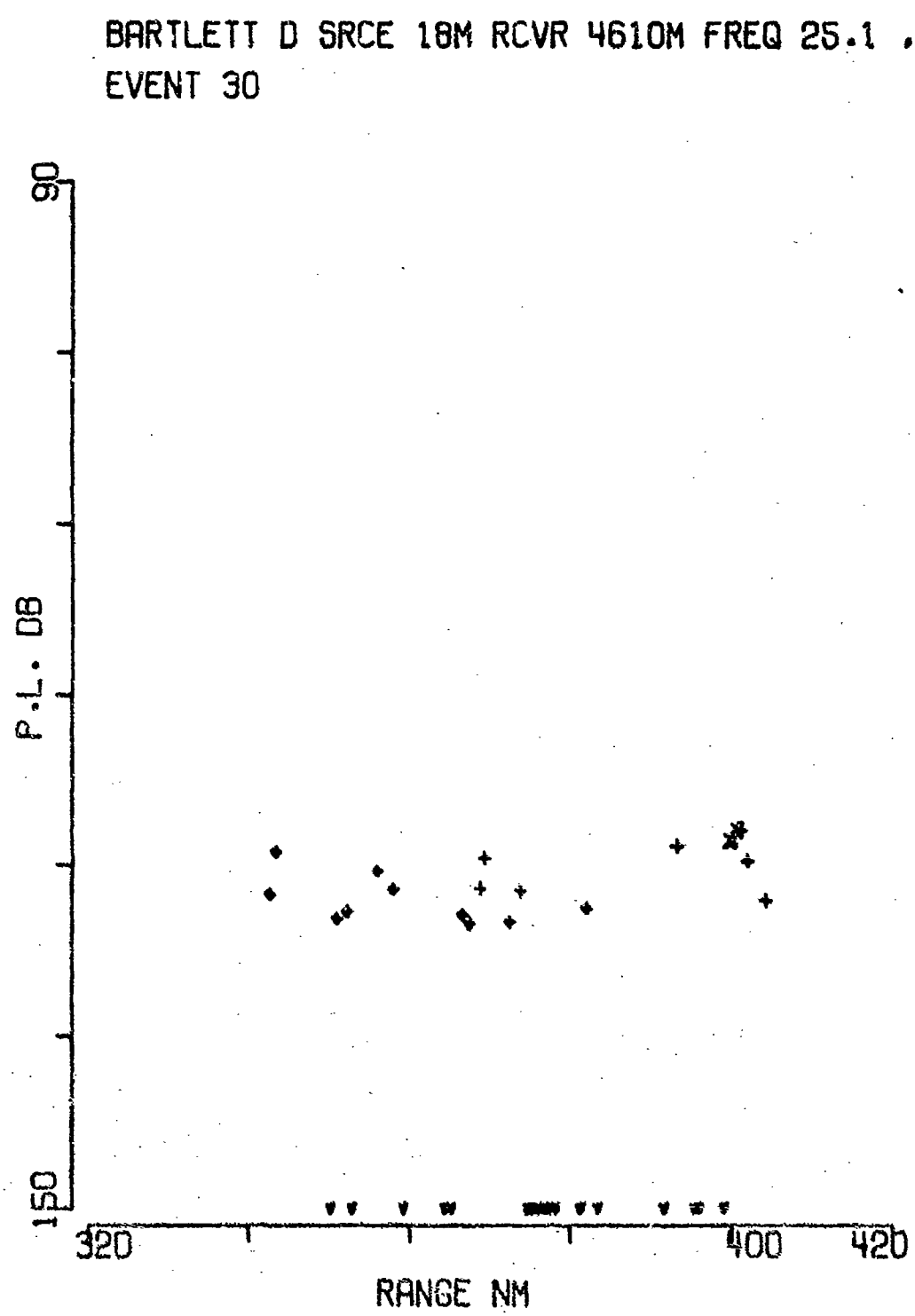
BARTLETT D SRCE 18M RCVR 4610M FREQ 25.1 .1 OCT
EVENT 30
90
150
P.L. DB
320
400
420
RANGE NM

FIGURE A-107

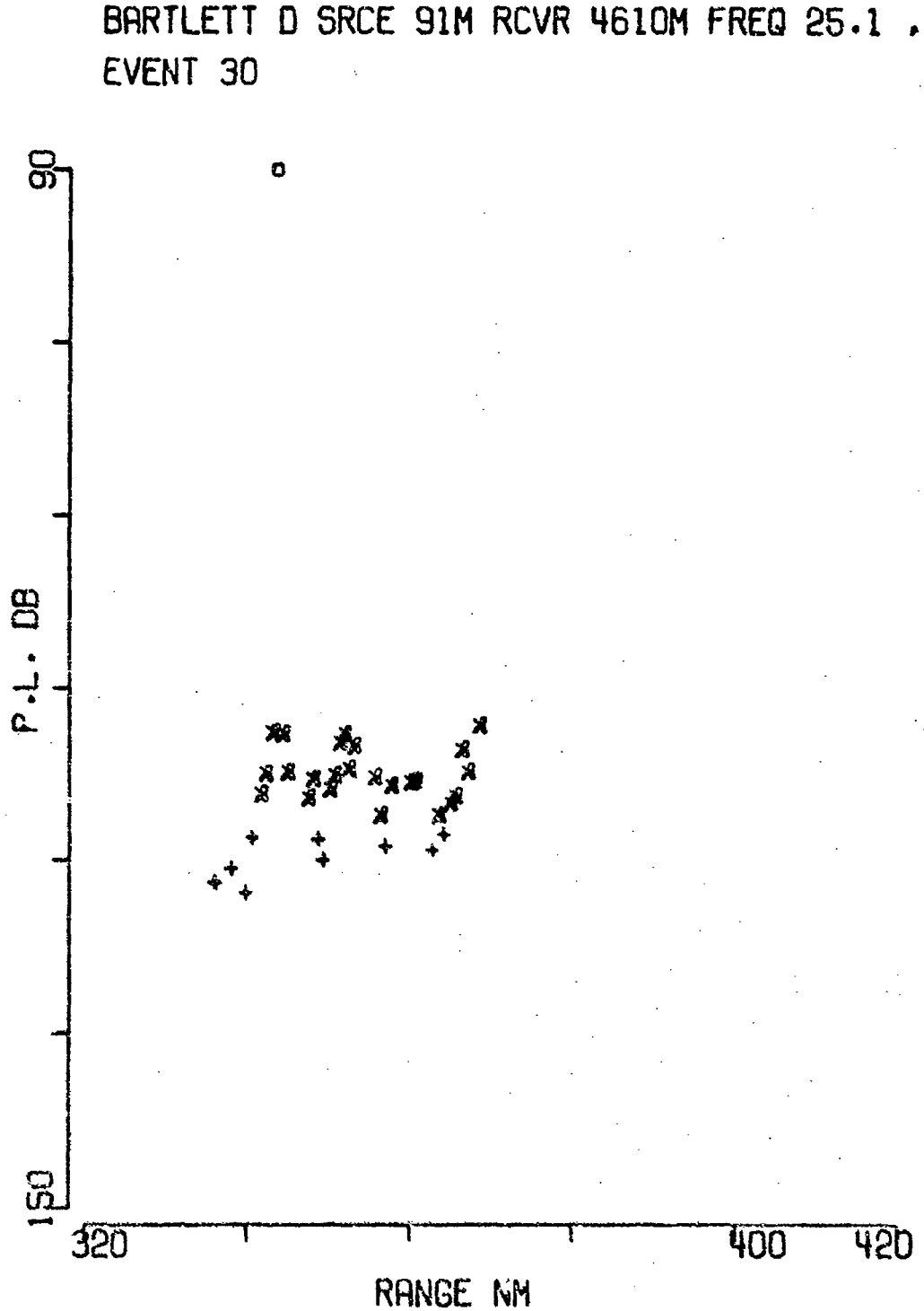
BARTLETT D SRCE 91M RCVR 4610M FREQ 25.1 .1 OCT
EVENT 30
90
150
P.L. DB
320
400
420
RANGE NM

FIGURE A-108

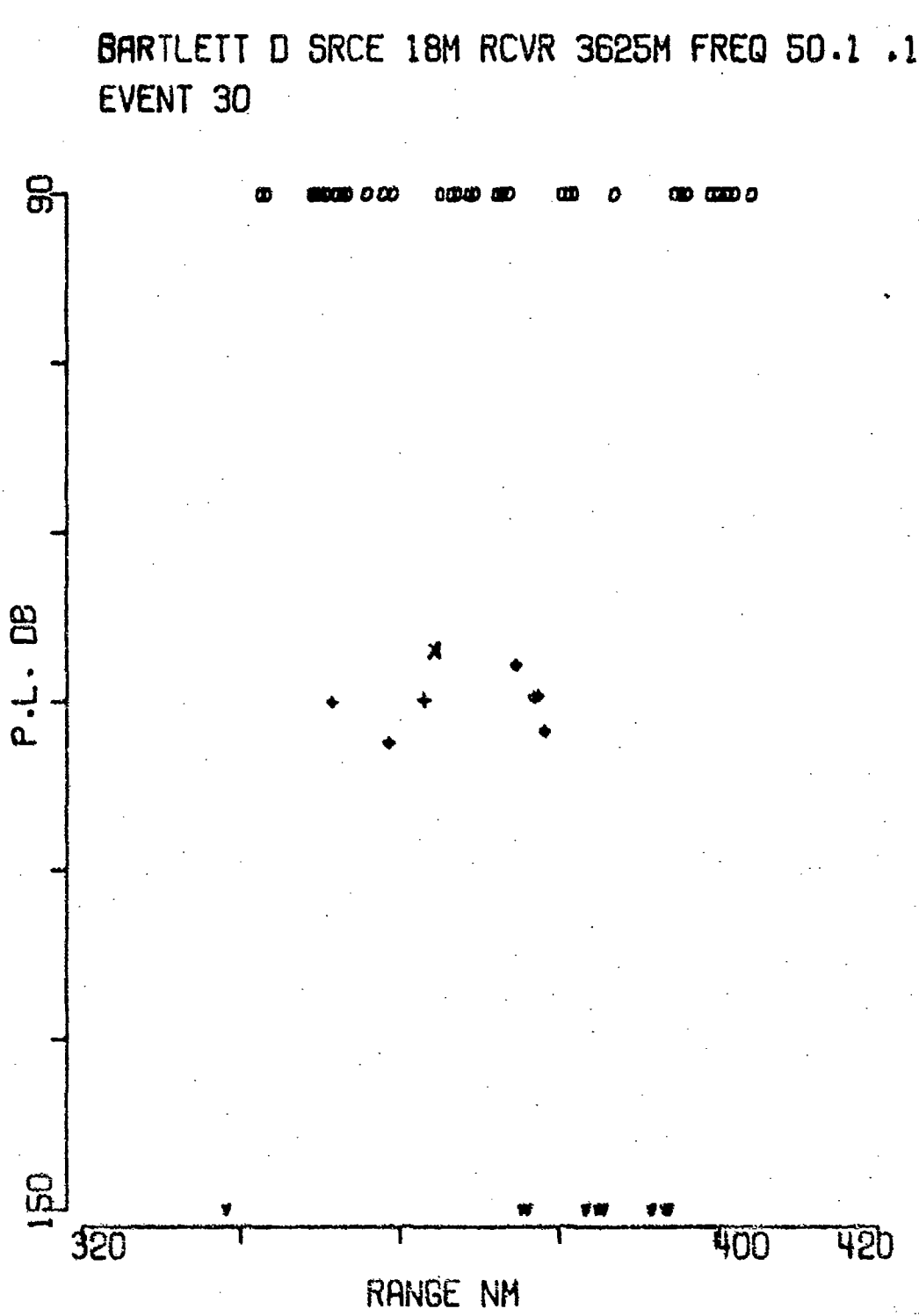
BARTLETT D SRCE 18M RCVR 3625M FREQ 50.1 .1 OCT
EVENT 30
90
150
P.L. DB
320
400
420
RANGE NM

FIGURE A-109

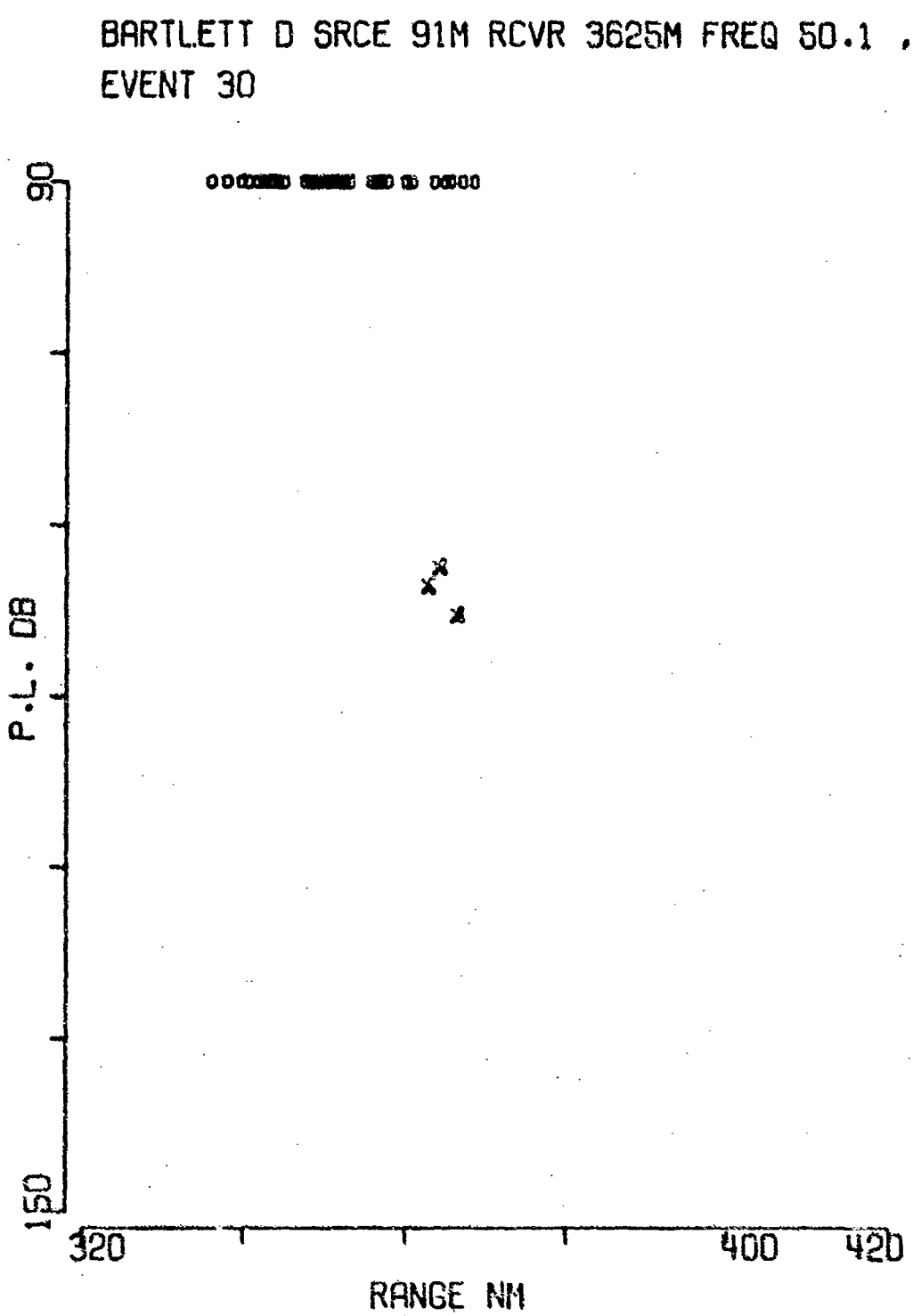
BARTLETT D SRCE 91M RCVR 3625M FREQ 50.1 .1 OCT
EVENT 30
90
150
P.L. DB
320
400
420
RANGE NM

FIGURE A-110

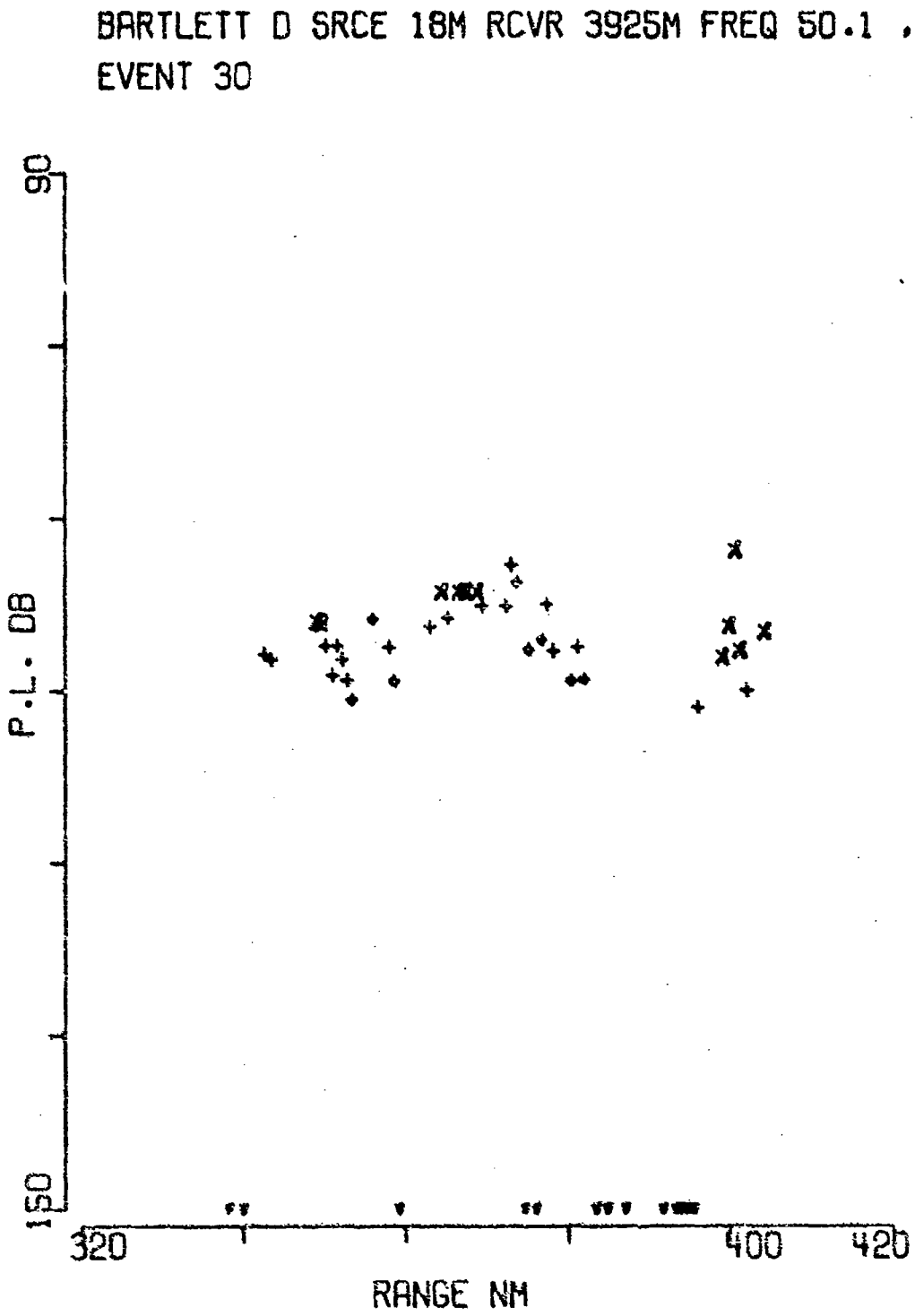
BARTLETT D SRCE 18M RCVR 3925M FREQ 50.1 .1 OCT
EVENT 30
90
150
P.L. DB
320
400
420
RANGE NM

FIGURE A-111

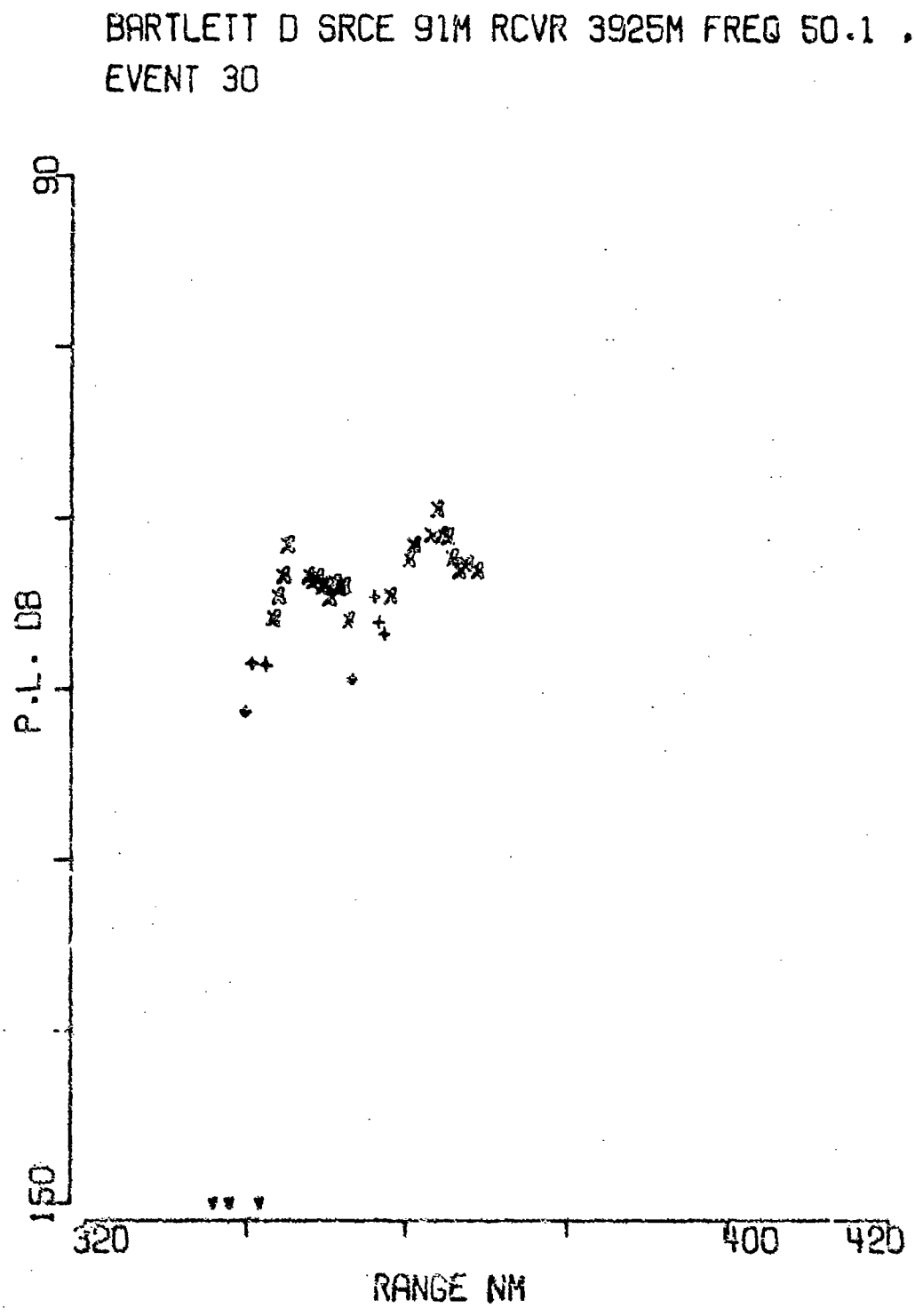
BARTLETT D SRCE 91M RCVR 3925M FREQ 50.1 .1 OCT
EVENT 30
90
150
P.L. DB
320
400
420
RANGE NM

FIGURE A-112

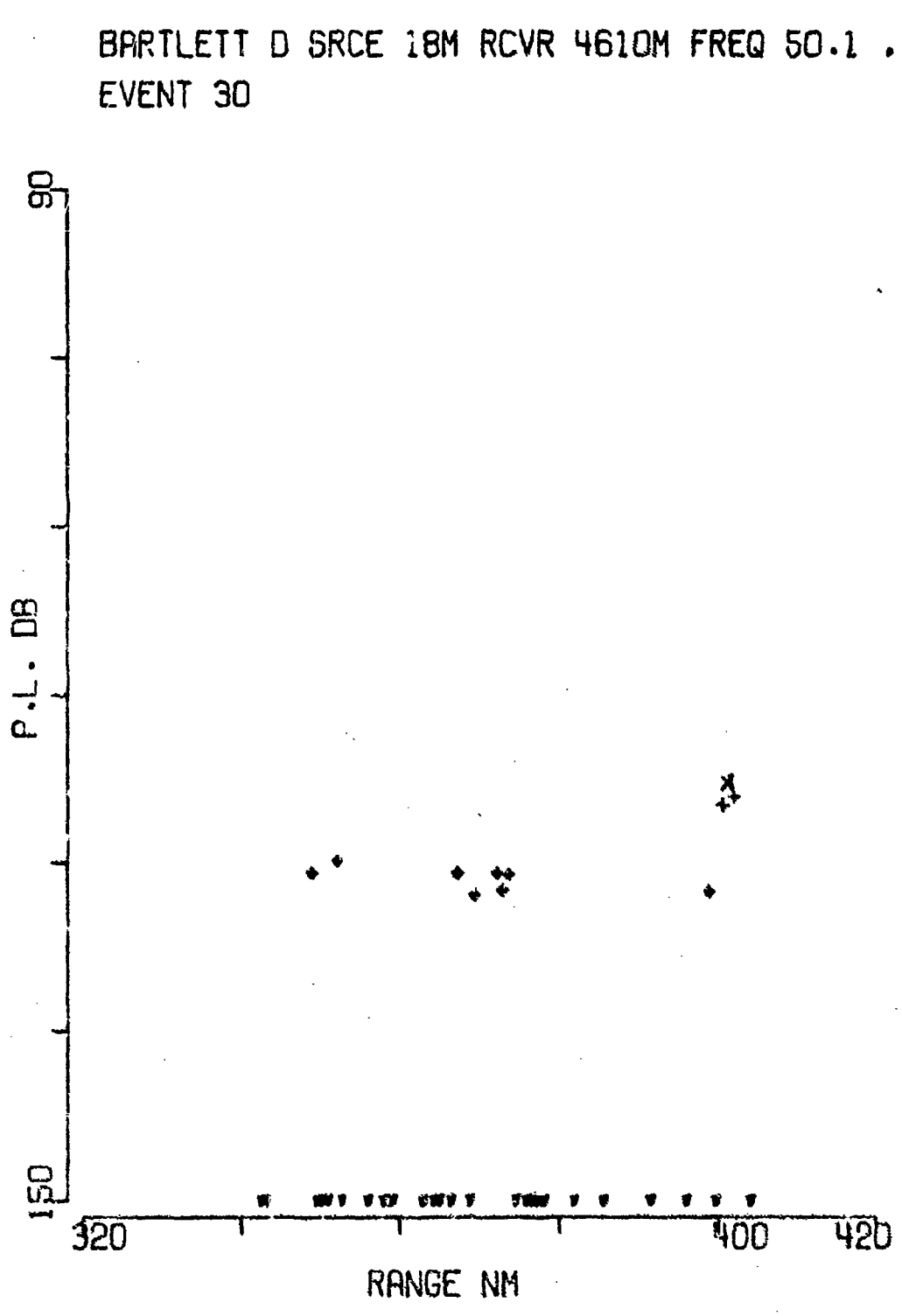
BARTLETT D SRCE 18M RCVR 4610M FREQ 50.1 .1 OCT
EVENT 30
90
150
P.L. DB
320
400
420
RANGE NM

FIGURE A-113

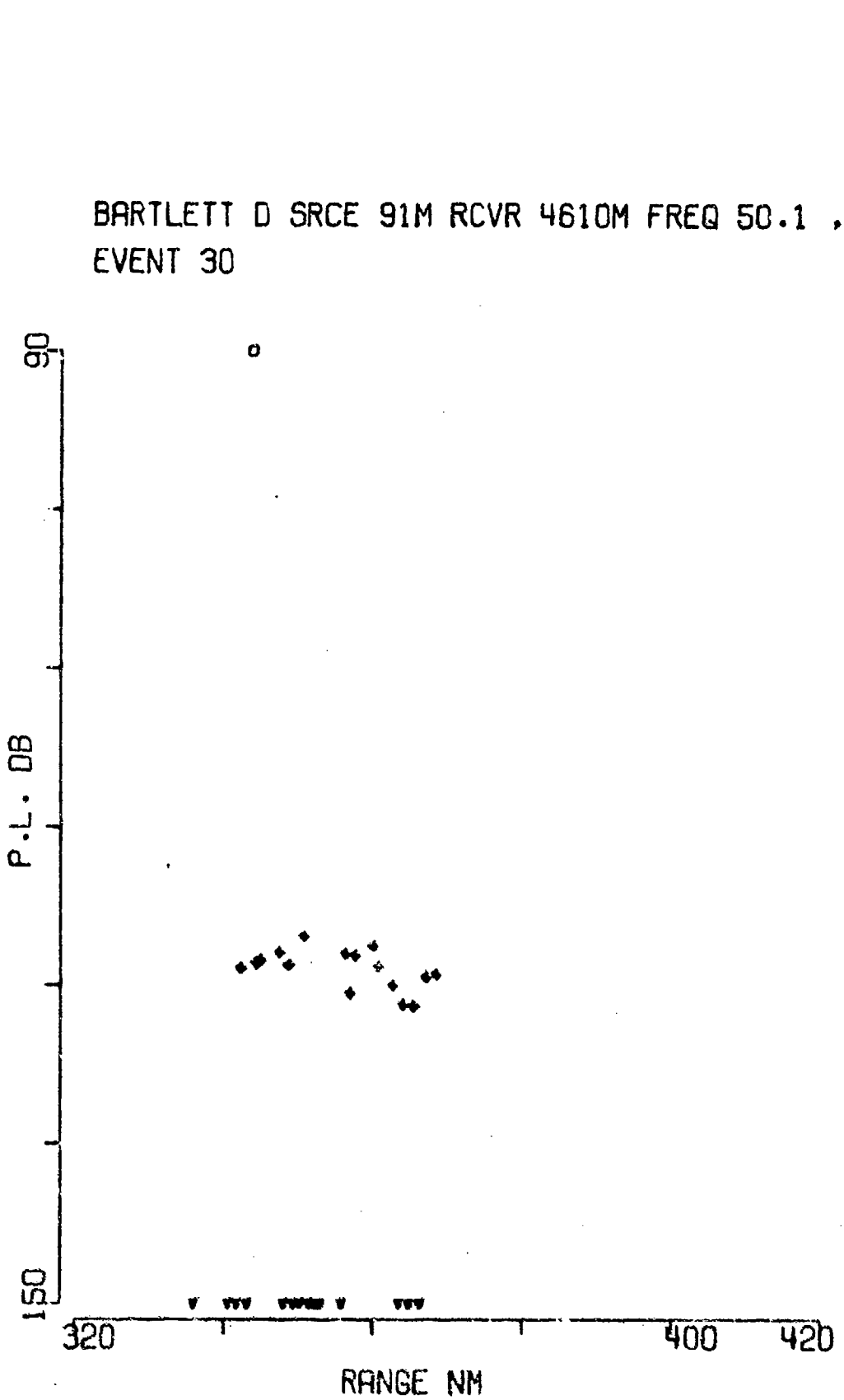
BARTLETT D SRCE 91M RCVR 4610M FREQ 50.1 .1 OCT
EVENT 30
60
150
P.L. DB
320
400
420
RANGE NM

FIGURE A-114

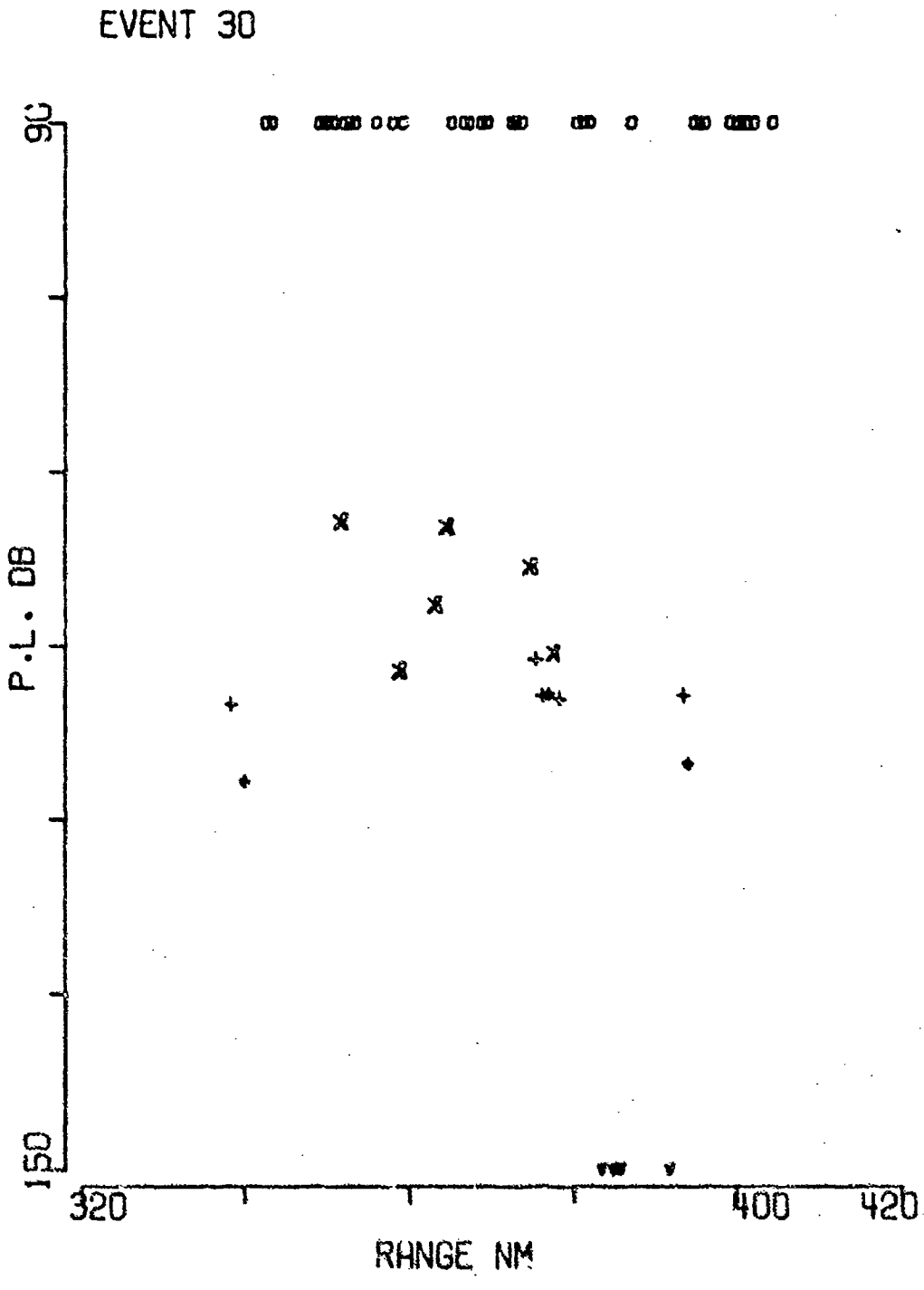
BARTLETT D SRCE 18M RCVR 3625M FREQ158.5
EVENT 30
90
150
P.L. DB
320
400
420
RANGE NM

FIGURE A-115

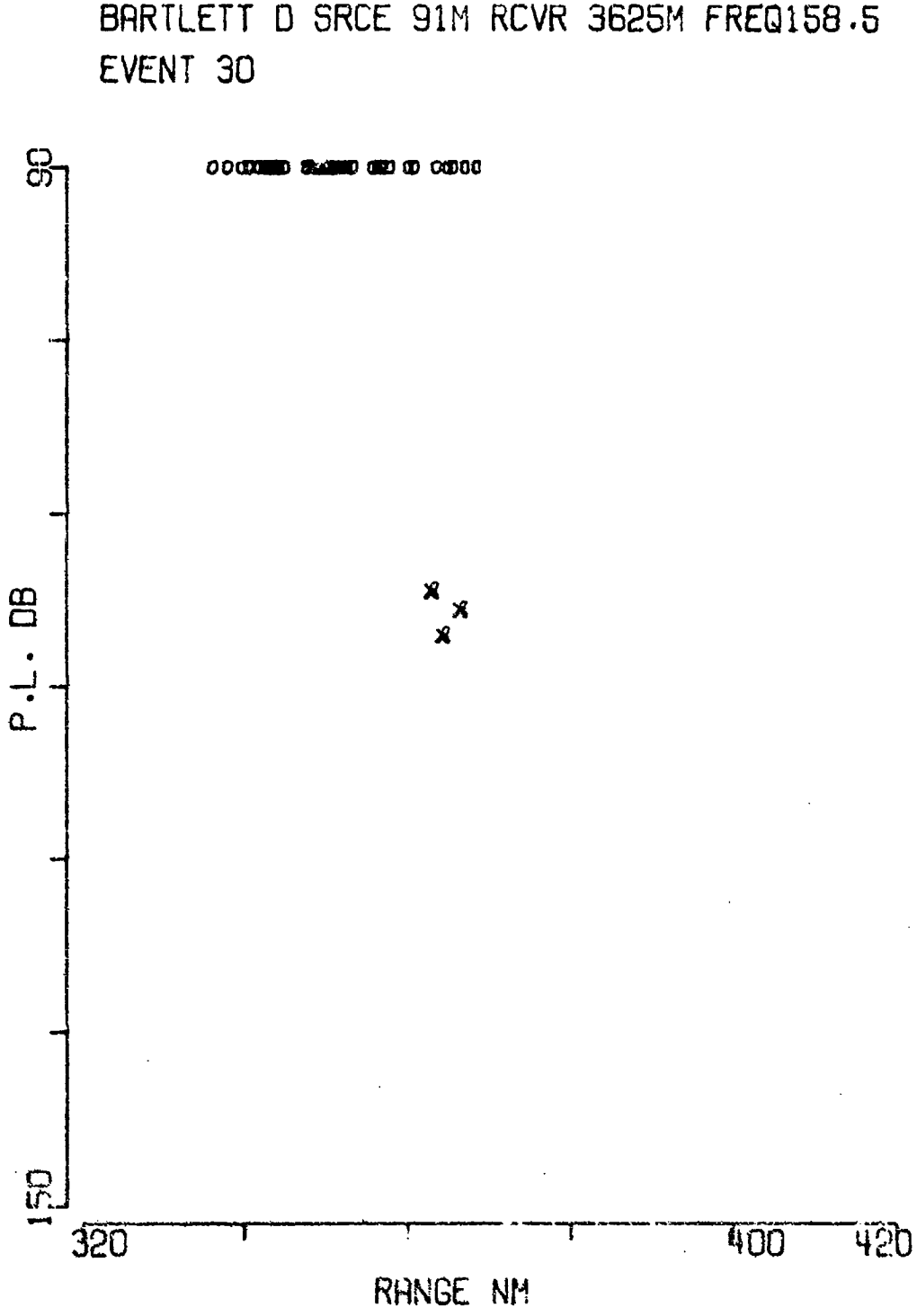
BARTLETT D SRCE 91M RCVR 3625M FREQ158.5
EVENT 30
90
150
P.L. DB
320
400
420
RANGE NM

FIGURE A-116

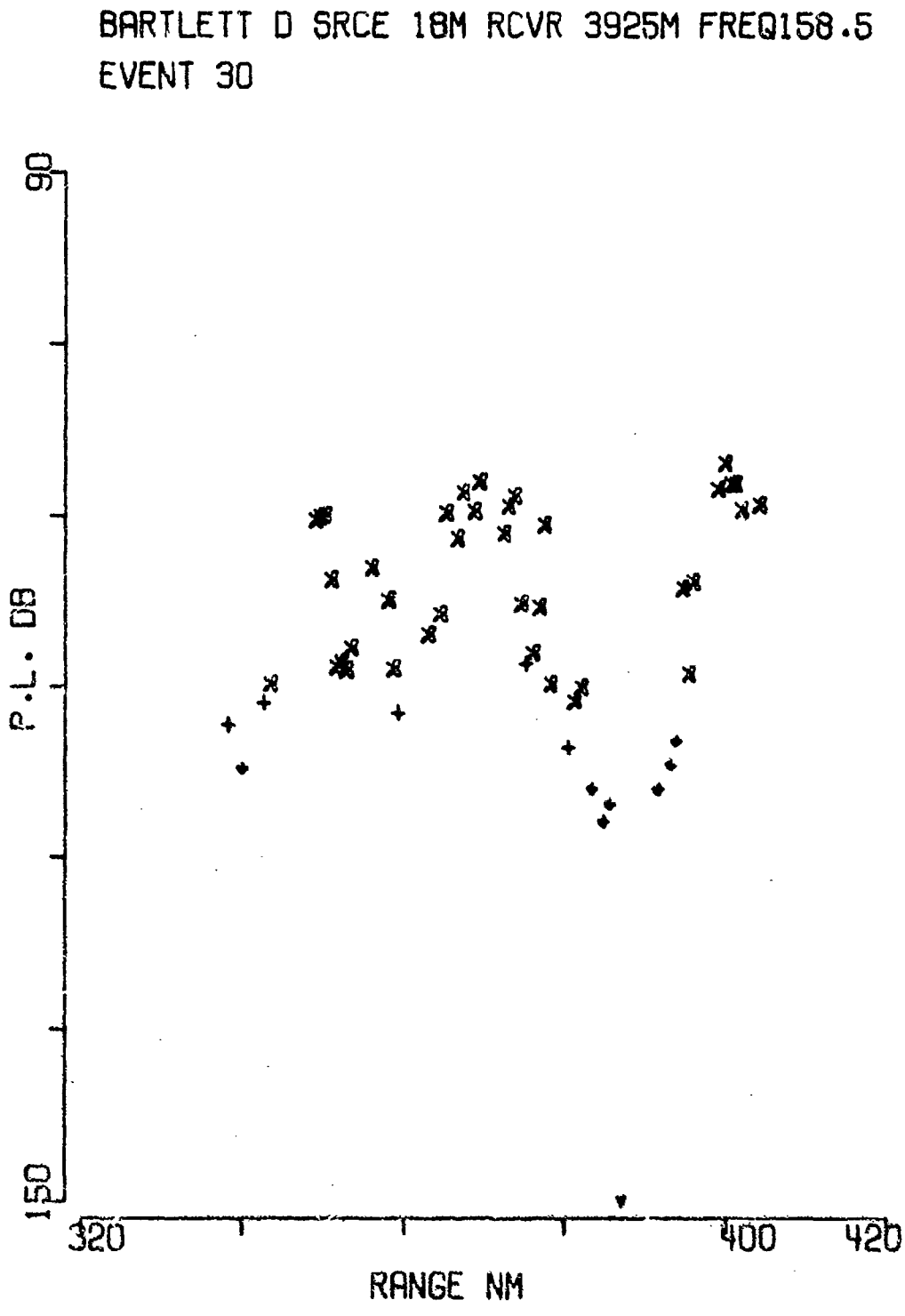
BARTLETT D SRCE 18M RCVR 3925M FREQ158.5
EVENT 30
90
150
P.L. DB
320
400
420
RANGE NM

FIGURE A-117

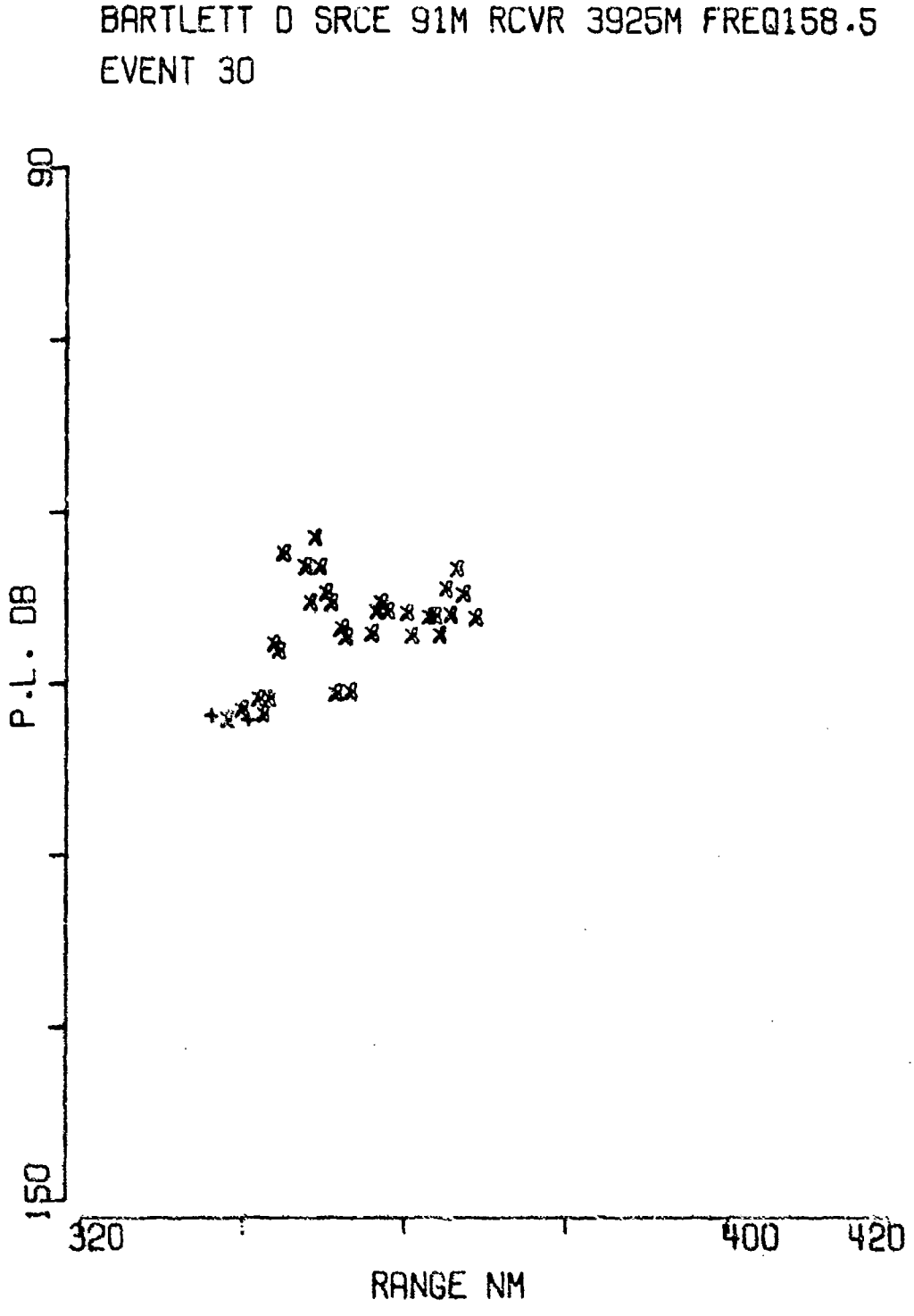
BARTLETT D SRCE 91M RCVR 3925M FREQ158.5
EVENT 30
90
150
P.L. DB
320
400
420
RANGE NM

FIGURE A-118

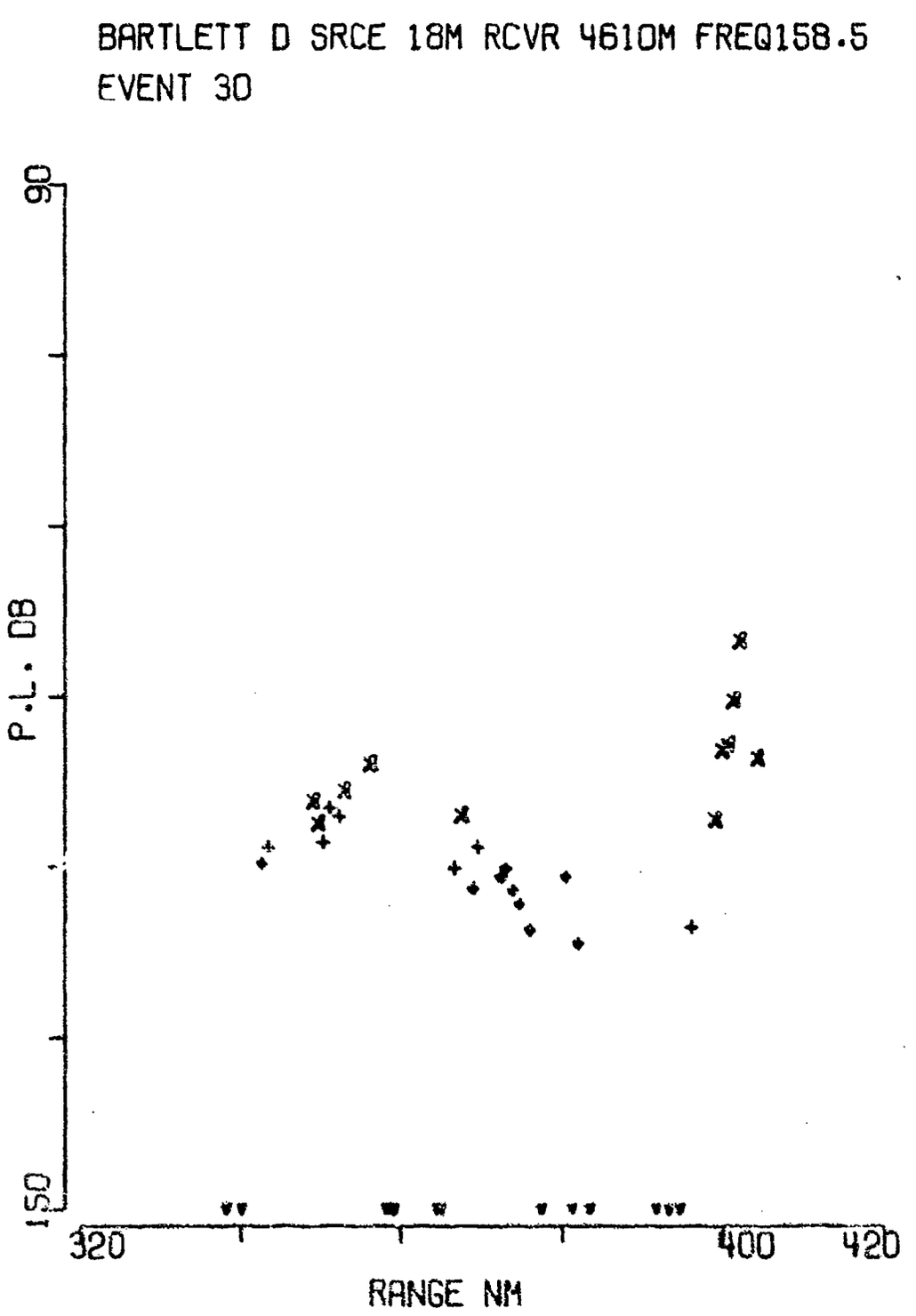
BARTLETT D SRCE 18M RCVR 4610M FREQ158.5
EVENT 30
90
150
P.L. DB
320
400
420
RANGE NM

FIGURE A-119

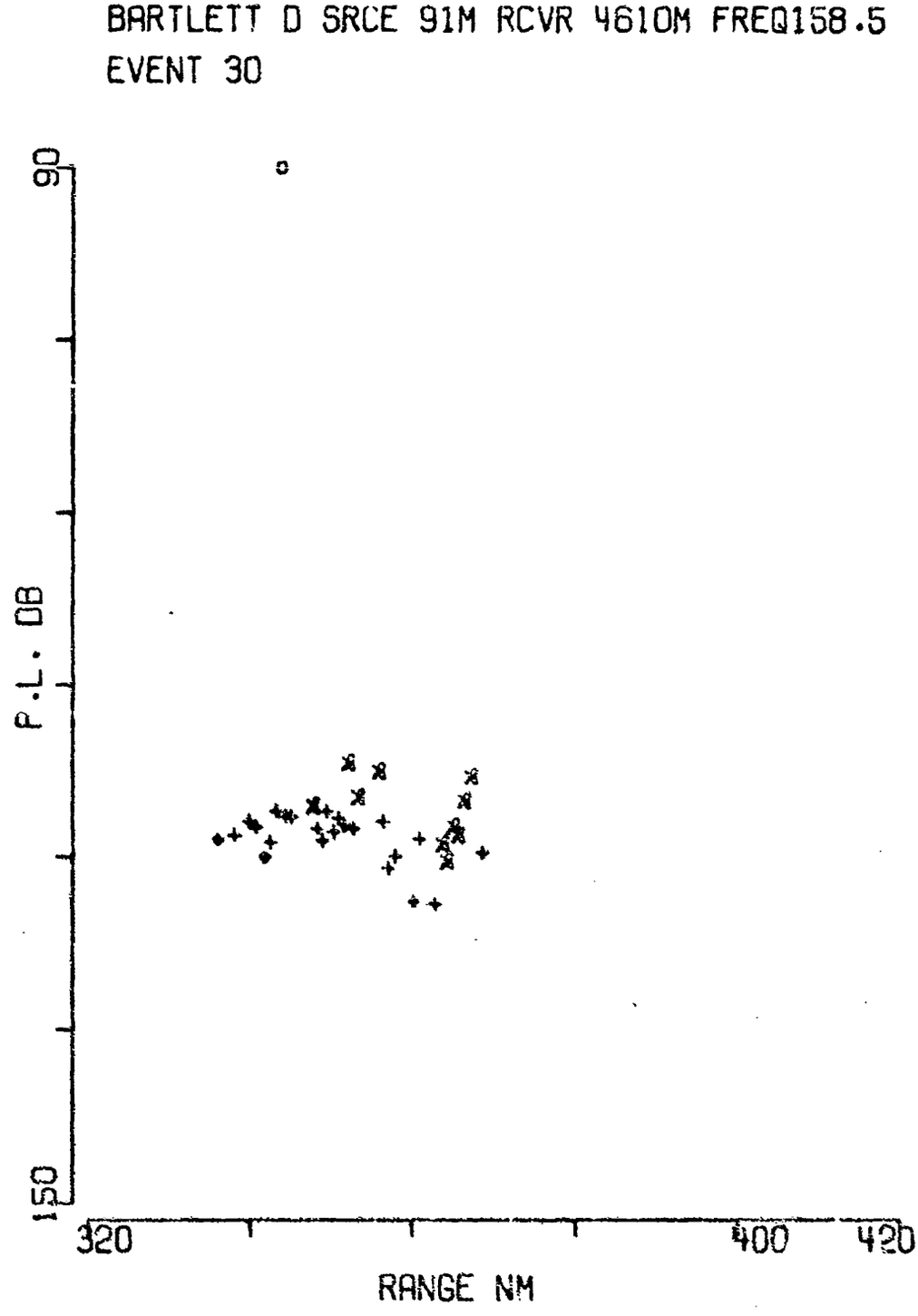
BARTLETT D SRCE 91M RCVR 4610M FREQ158.5
EVENT 30
90
150
P.L. DB
320
400
420
RANGE NM

FIGURE A-120

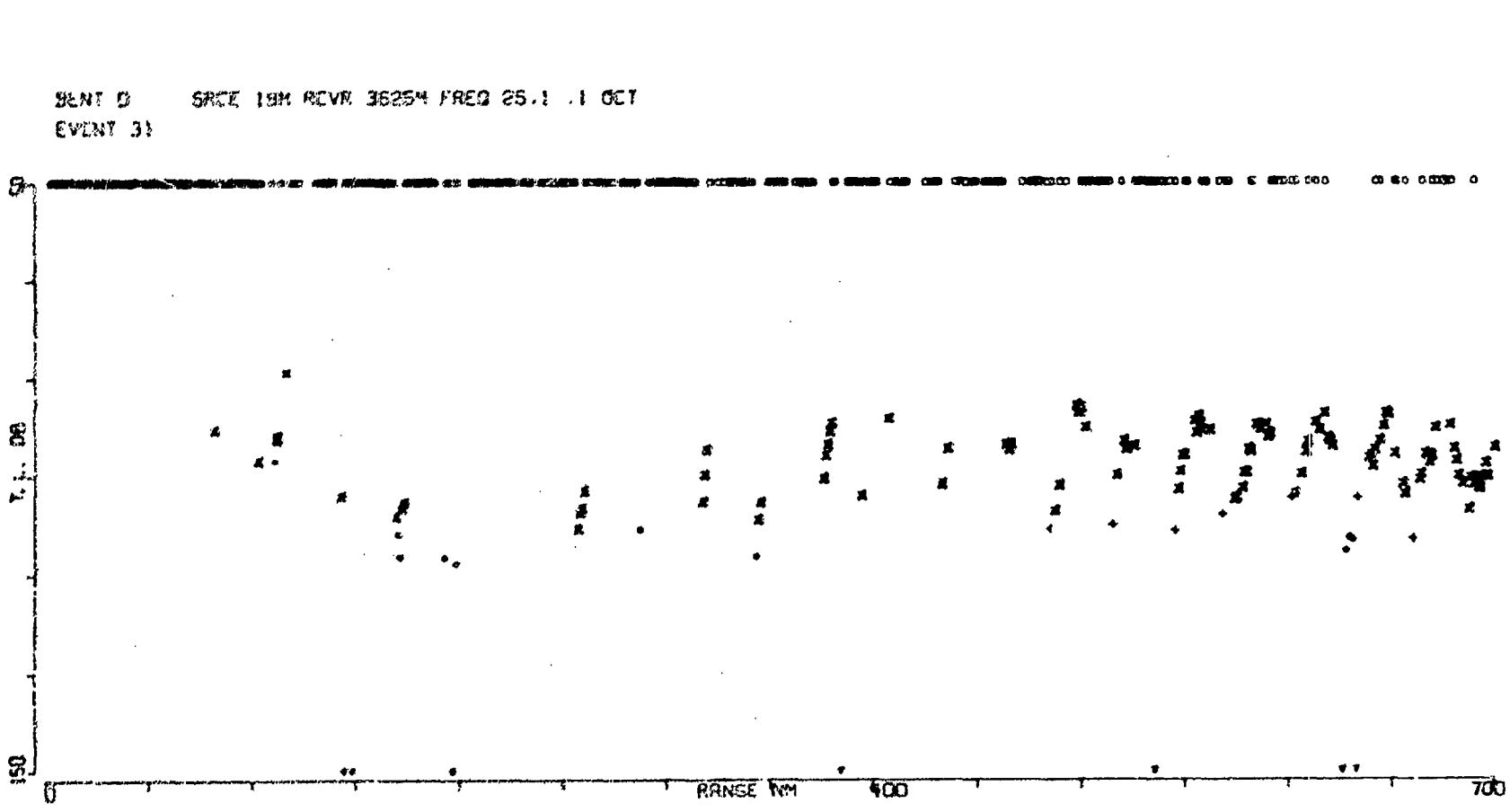
EVENT 0 SRCE 19M RCVR 36254 FREQ 25.1 .1 OCT
EVENT 31
0
150
RANGE NM
400
700

FIGURE A-121

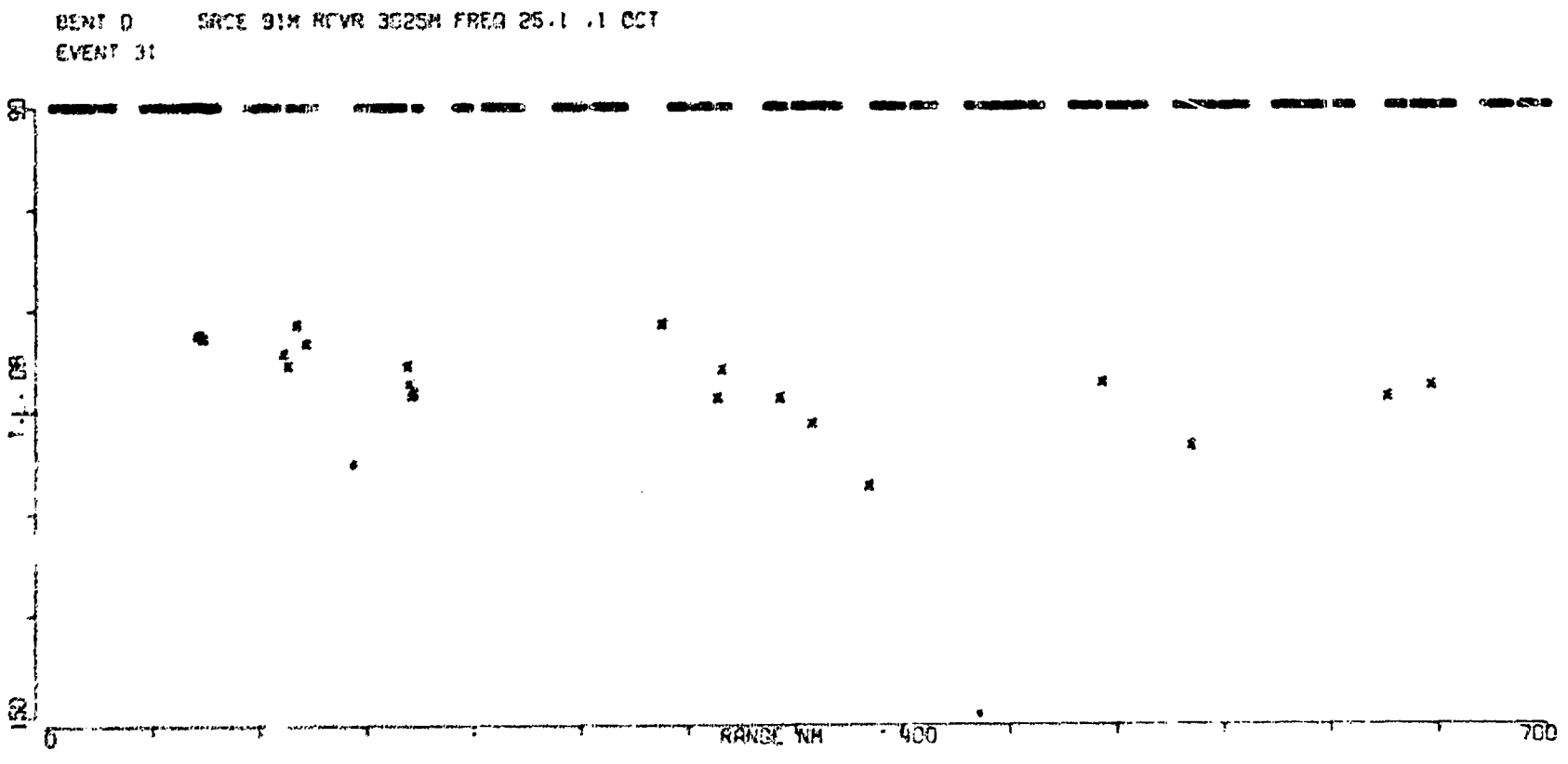
BENT 0 SRCE 91M RCVR 3025M FREQ 25.1 .1 OCT
EVENT 31
dB
-1.
-2
0
RANGE NM
400
700

FIGURE A-122

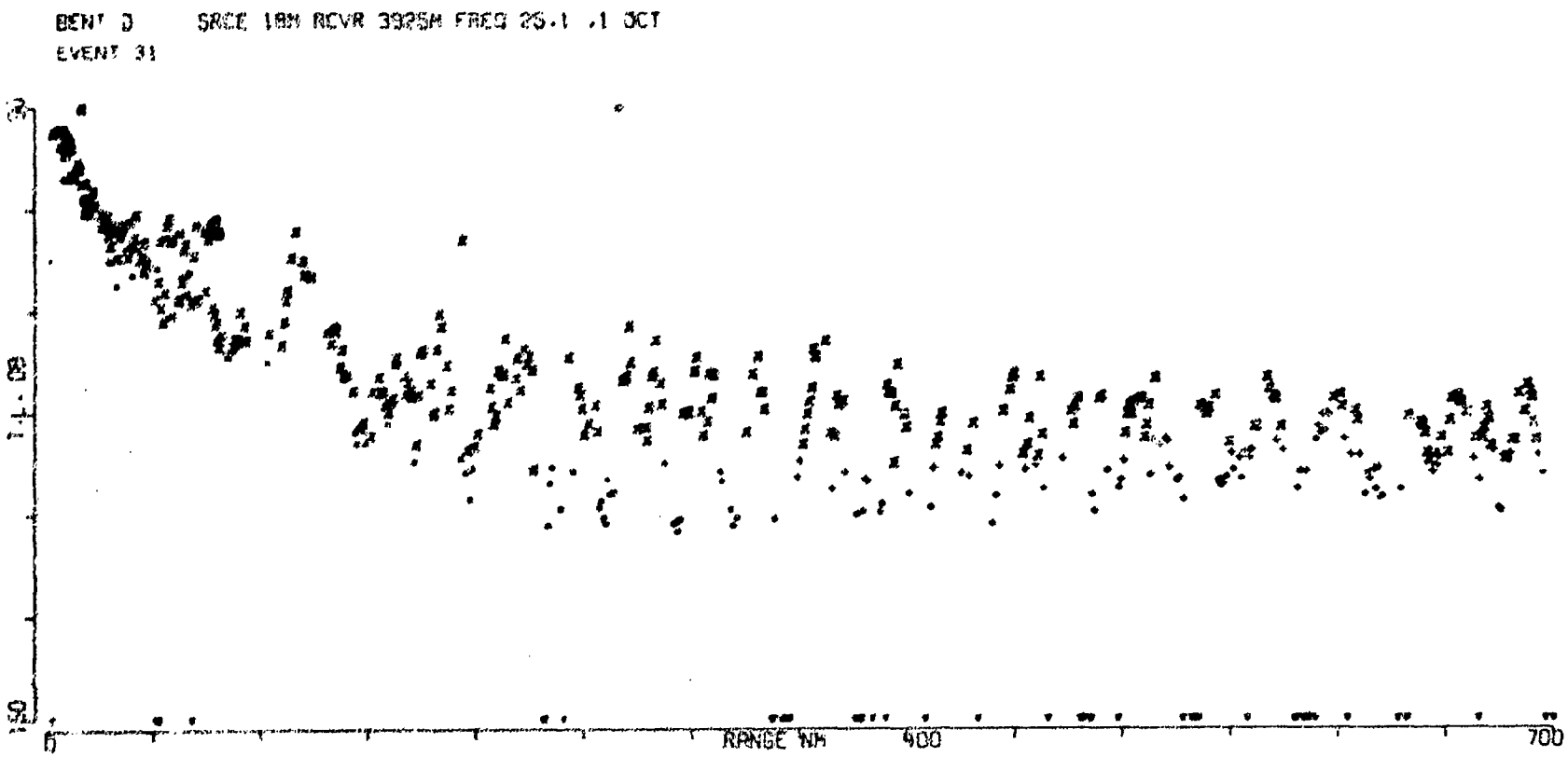
BENT 3 SRCE 18M RCVR 3325M FREQ 25.1 .1 OCT
EVENT 31
RANGE NM
400
700

FIGURE A-123

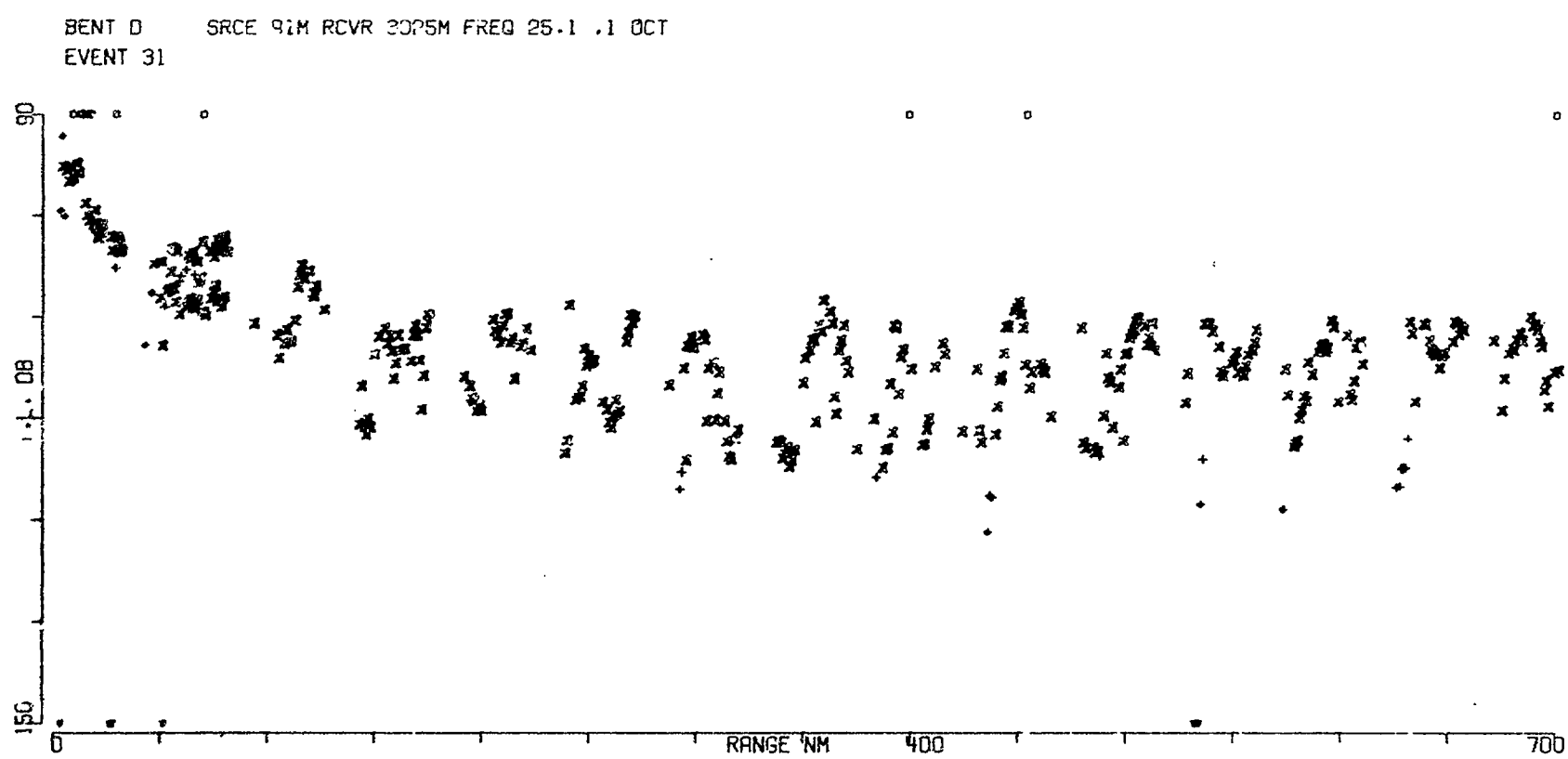
BENT D SRCE 91M RCVR 3025M FREQ 25.1 .1 OCT
EVENT 31
90
108
150
0
RANGE NM
400
700

FIGURE A-124

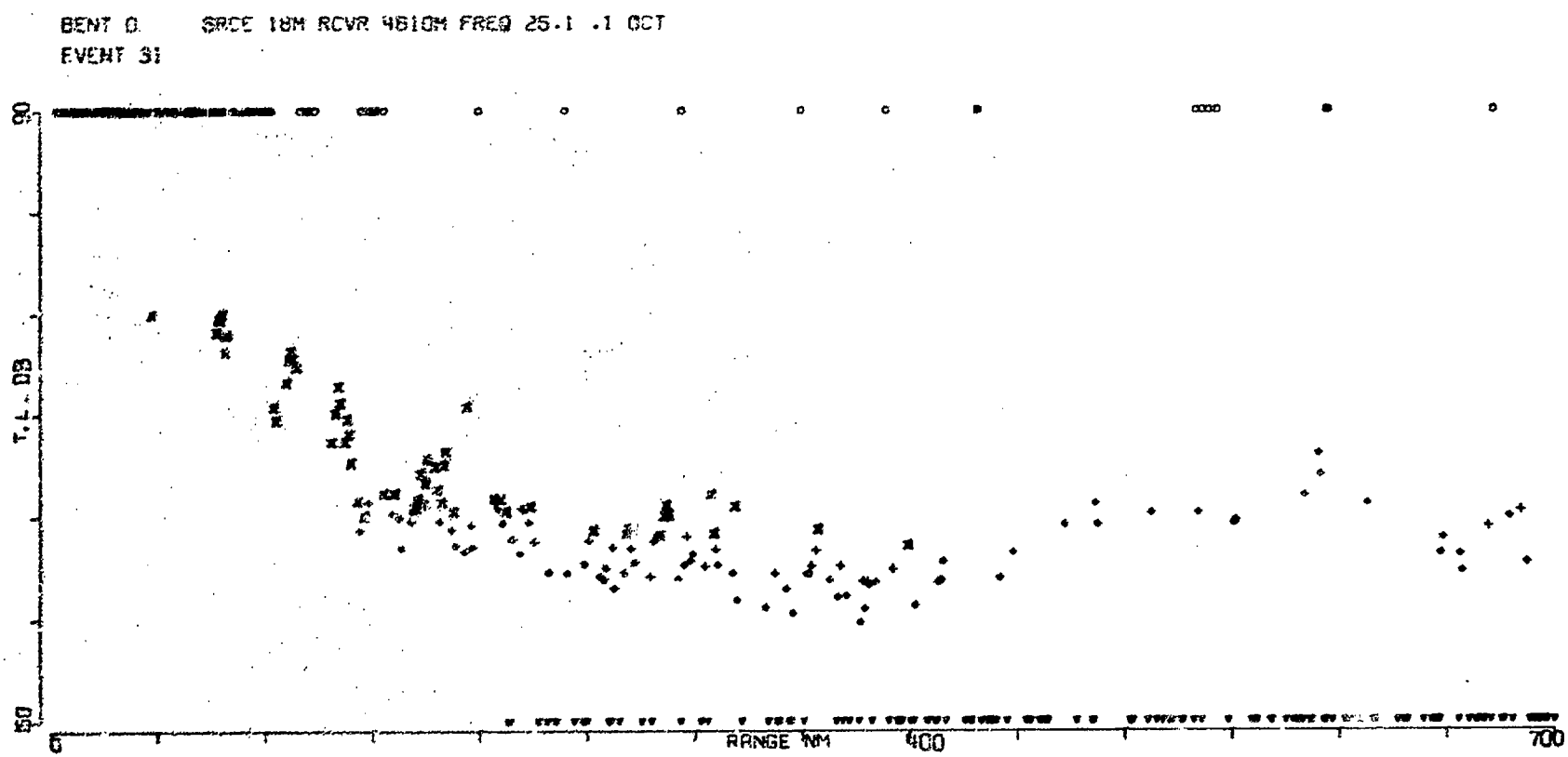
BENT 0 SRCE 18M RCVR 4810M FREQ 25.1 .1 OCT
EVENT 31
50
T.L. DB
80
0
RANGE NM
400
700

FIGURE A-125

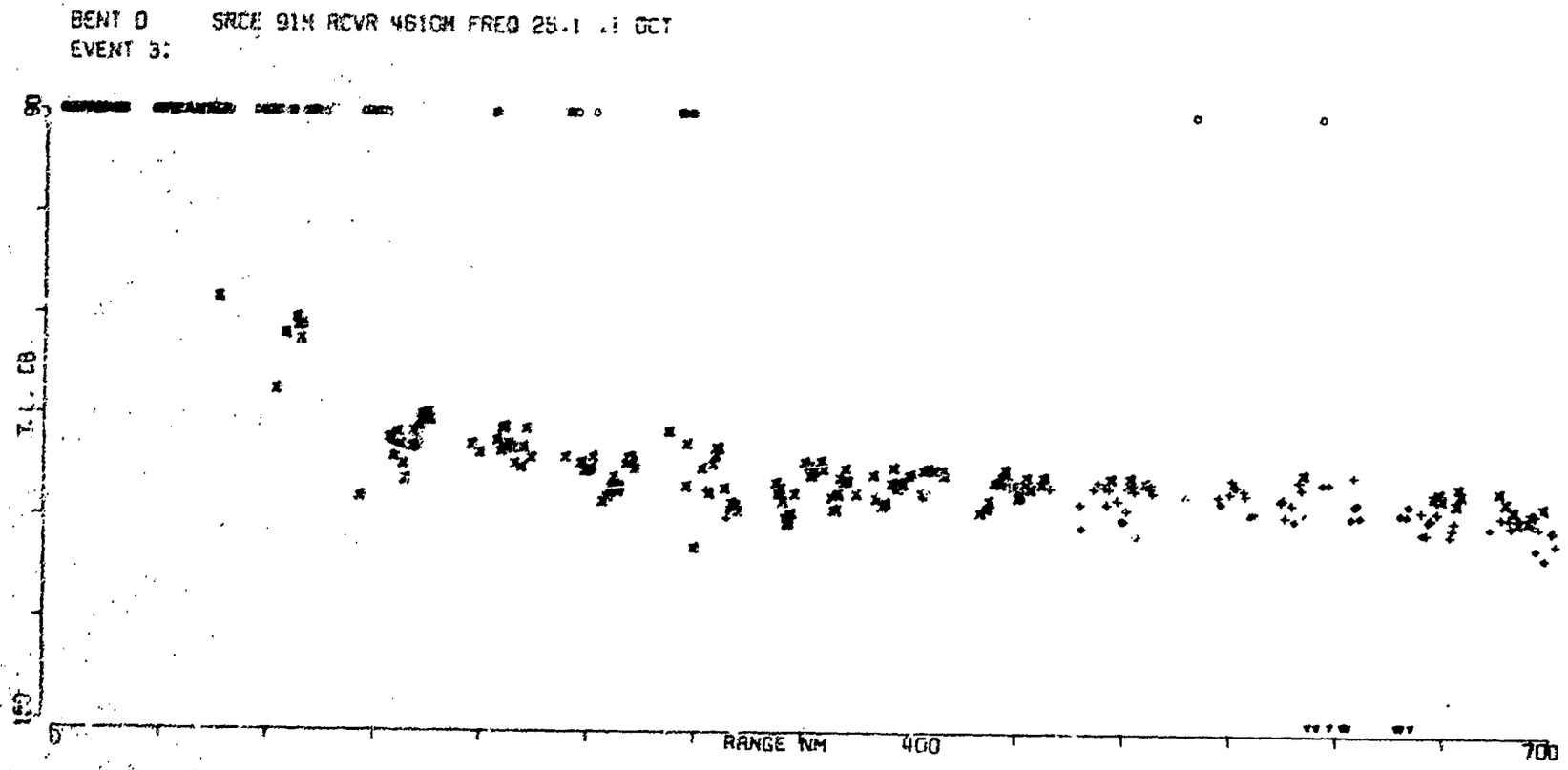
BENT D SRCE 91M RCVR 461CM FREQ 25.1 .I OCT
EVENT 3:
T.L. DB
RANGE NM
400
700

FIGURE A-126

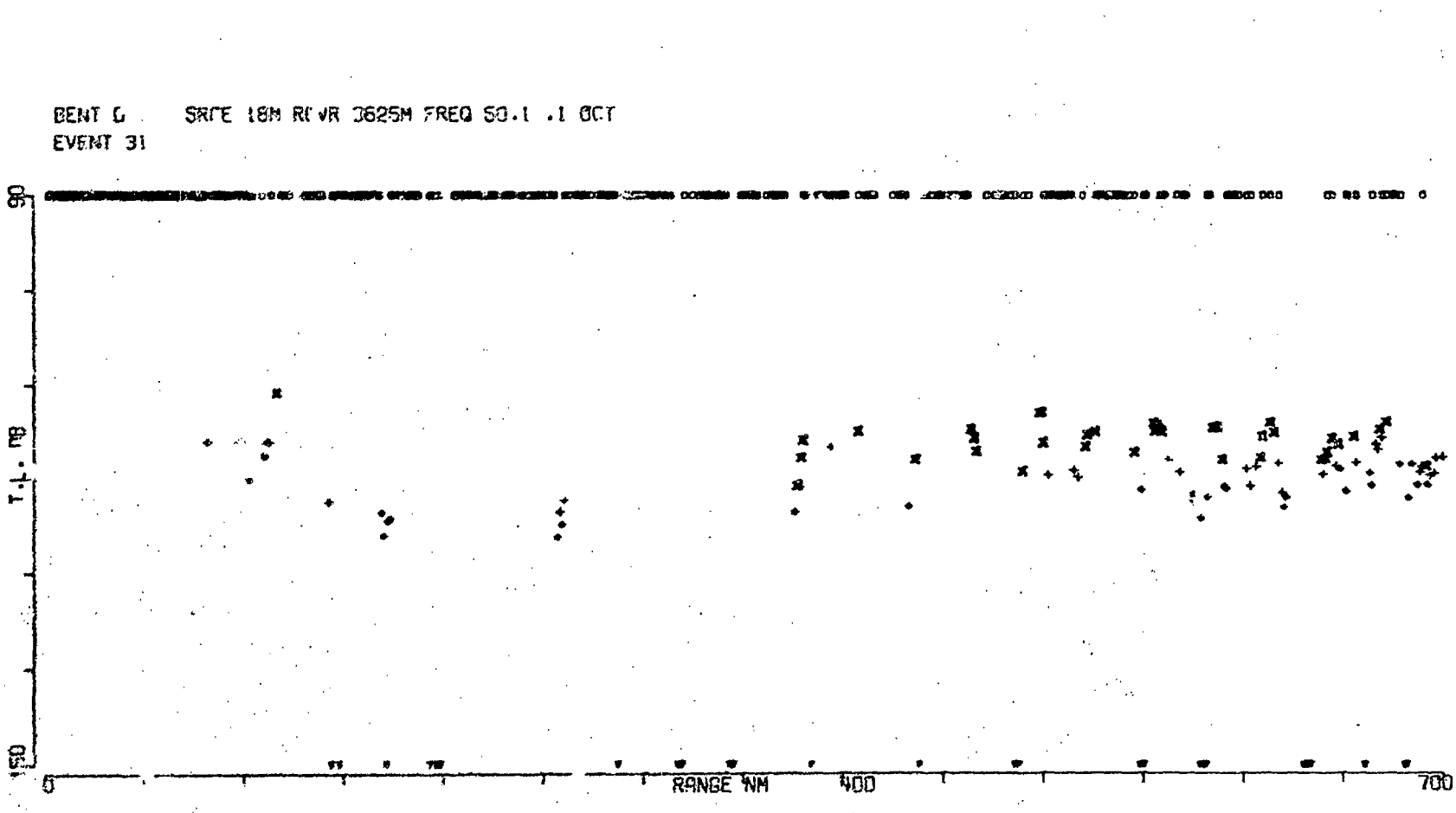
BENT G SRCE 18M RCVR 3625M FREQ 50.1 .1 OCT
EVENT 31
60
dB re 1 µPa
150
0
RANGE NM
400
700

FIGURE A-127

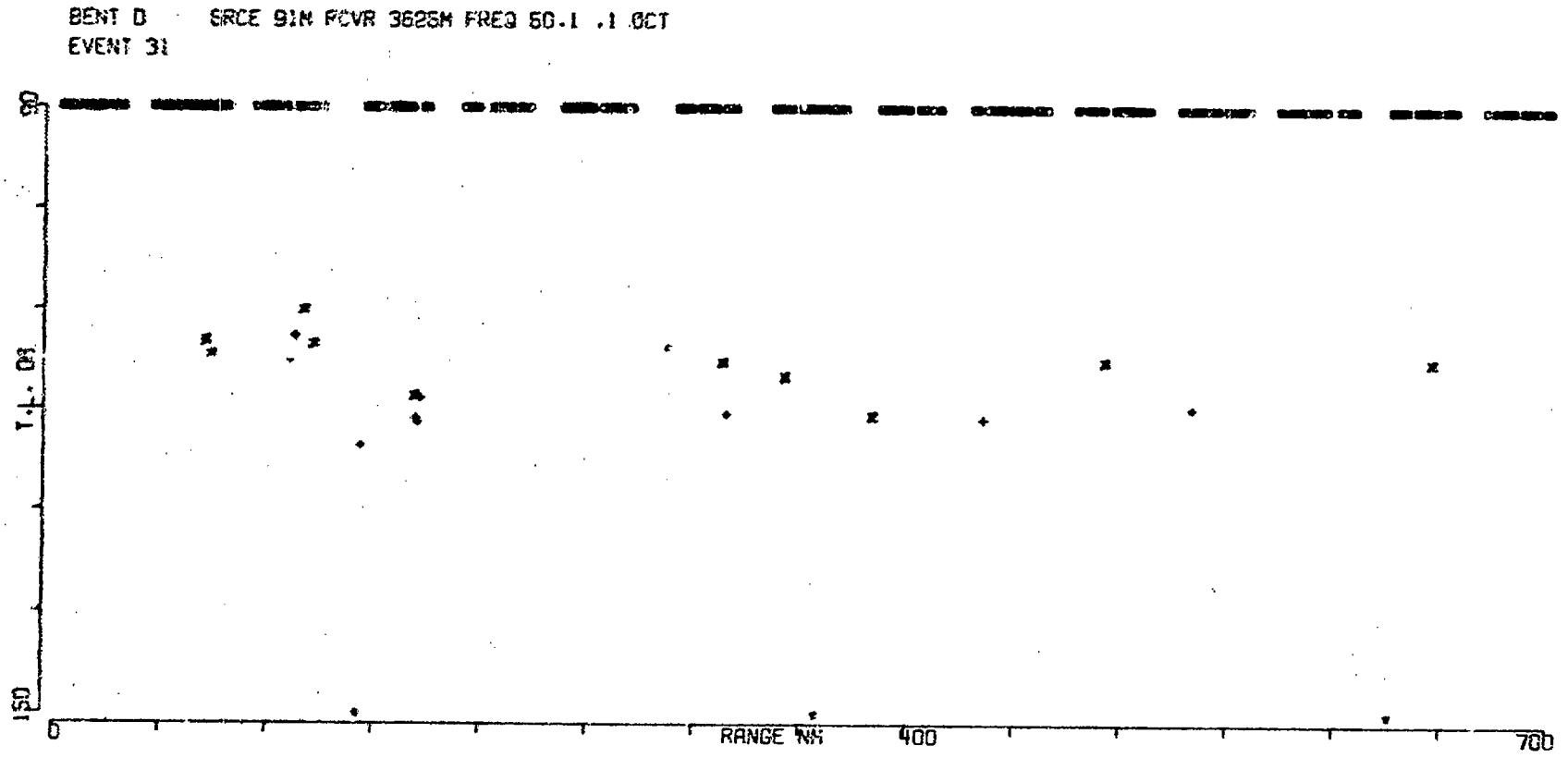
BENT D SRCE 91N RCVR 3628M FREQ 50.1 .1 OCT
EVENT 31
150
T.L. DB
0
RANGE NM
400
700

FIGURE A-128

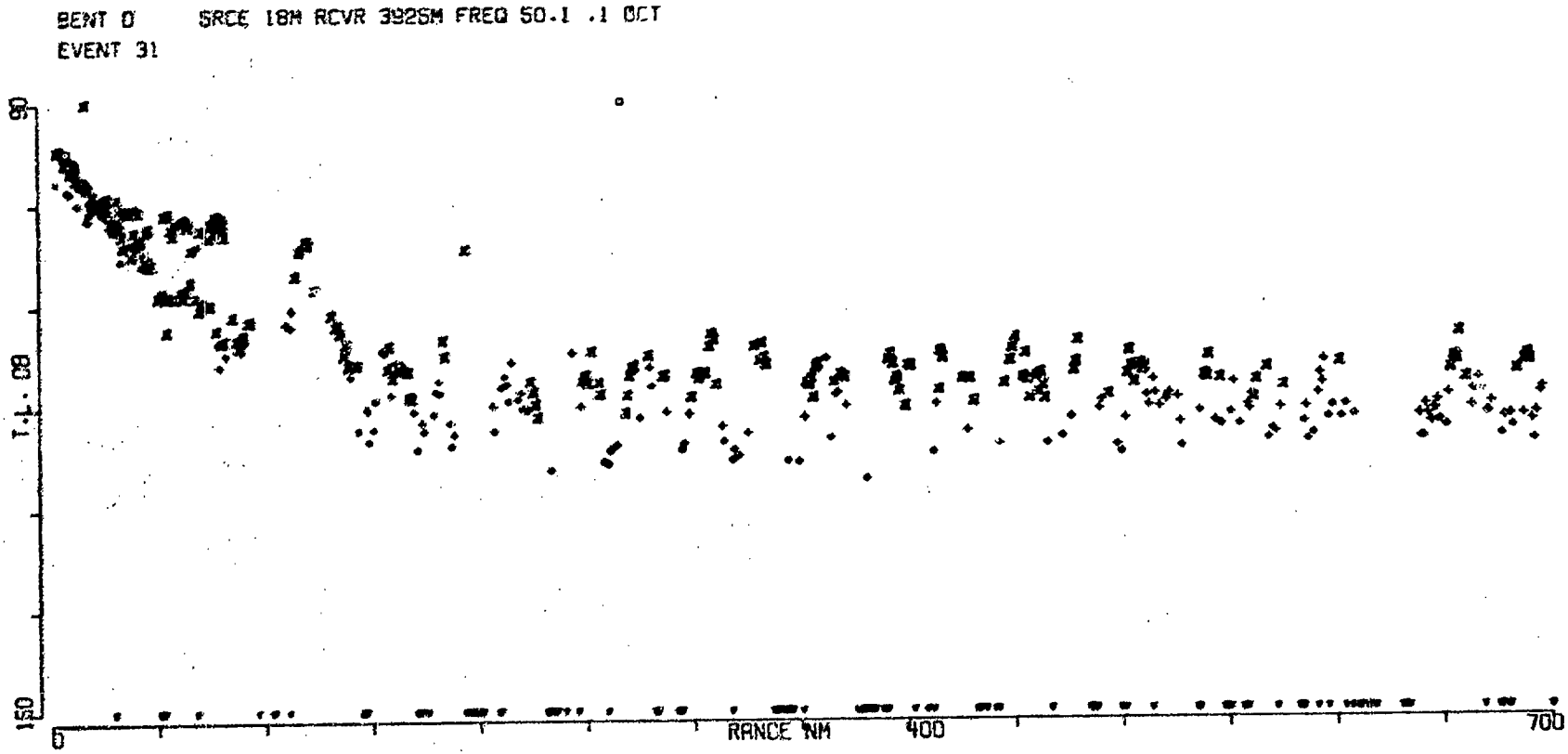
BENT 0 SRCE 18M RCVR 3925M FREQ 50.1 .1 OCT
EVENT 31
dB re 1 μ Pa
RANGE NM
0
400
700

FIGURE A-129

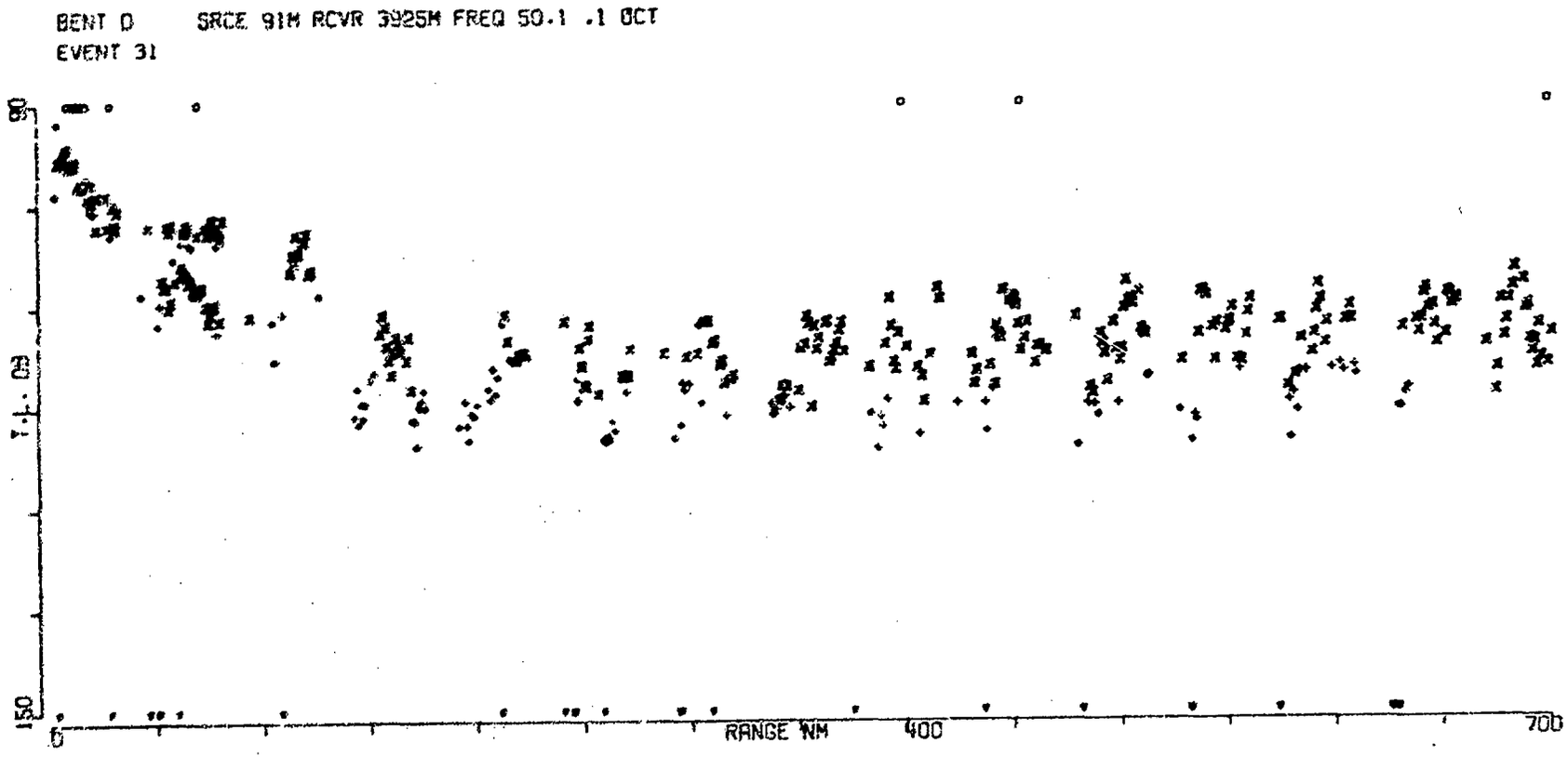
BENT D SRCE 91M RCVR 3925M FREQ 50.1 .1 OCT
EVENT 31
50
TL dB
150
0
RANGE NM
400
700

FIGURE A-130

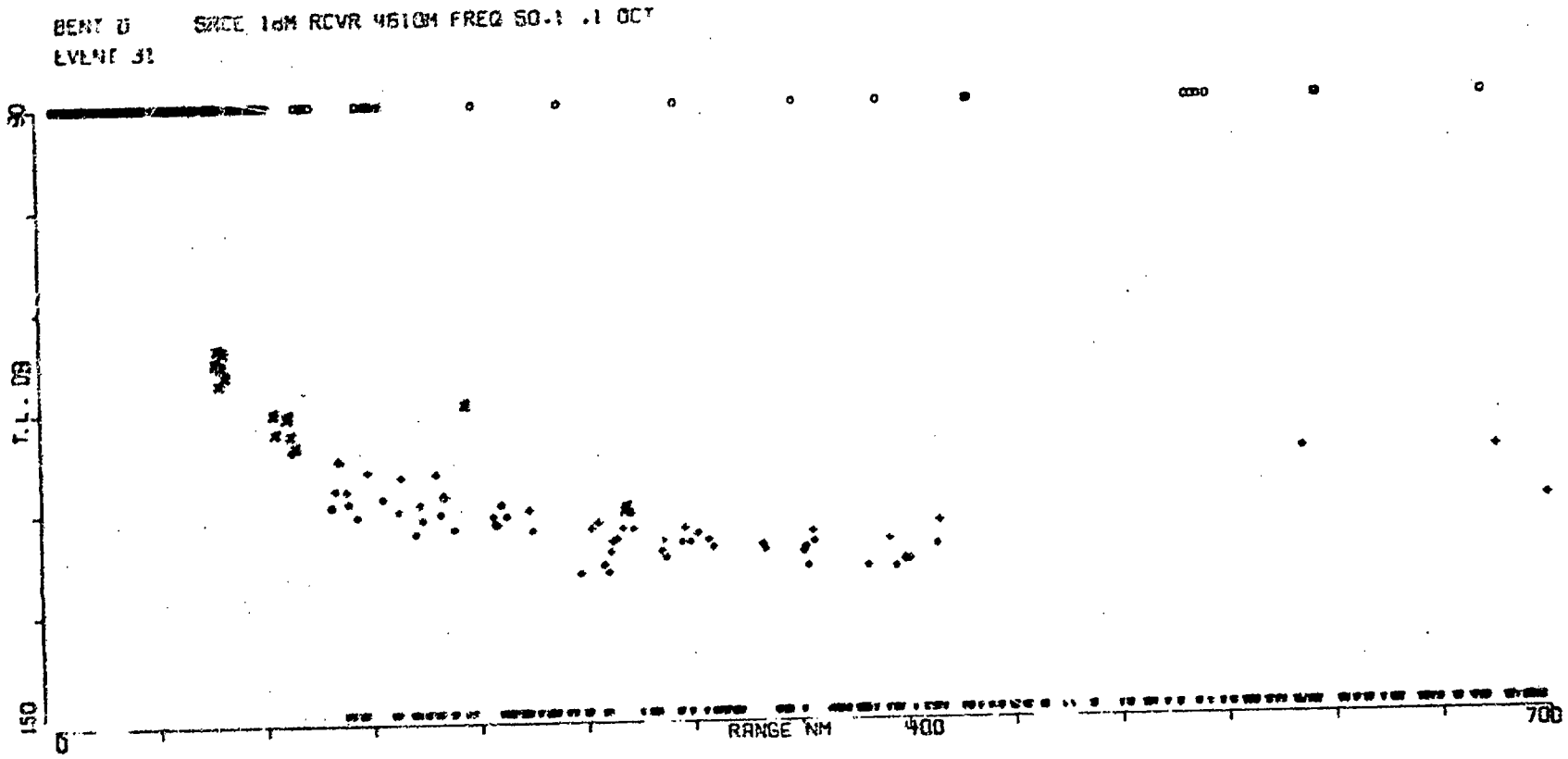
BENT 0
SRCE 1dM RCVR 4610M FREQ 50.1 .1 OCT
EVENT 31
T.L. DB
50
150
0
RANGE NM
400
700

FIGURE A-131

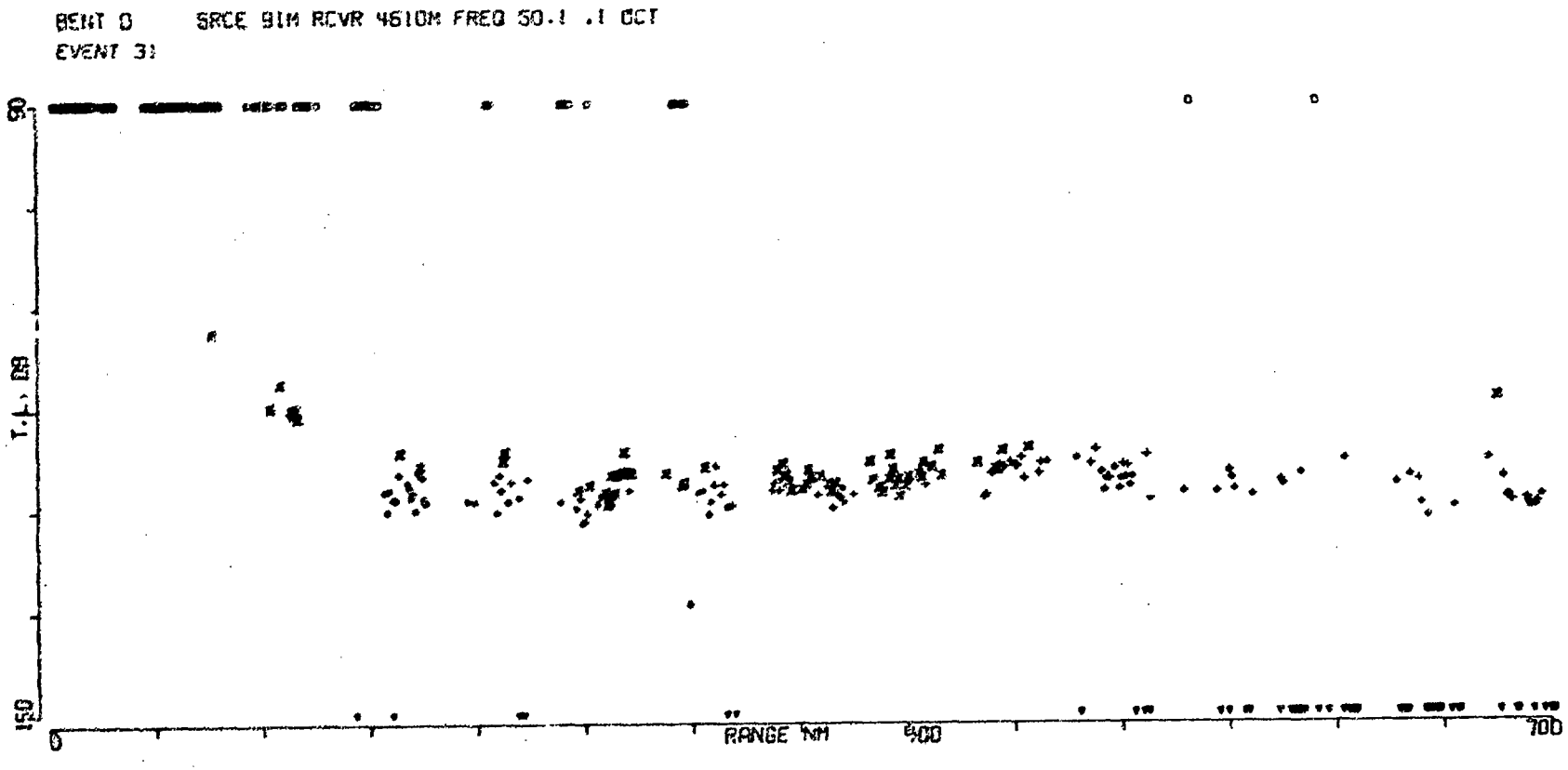
BENT 0 SRCE 91M RCVR 4610M FREQ 50.1 .1 OCT
EVENT 31
0
RANGE NM
400
700

FIGURE A-132

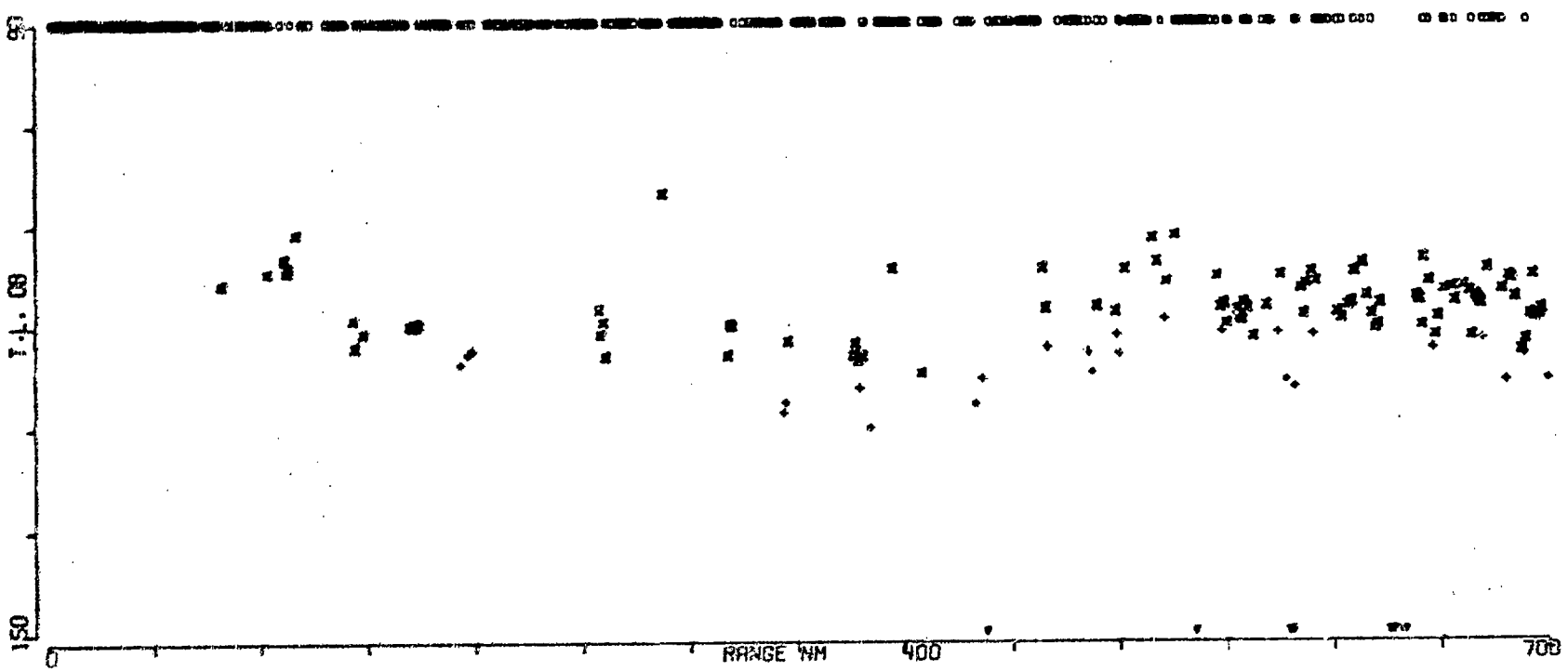

FIGURE A-133

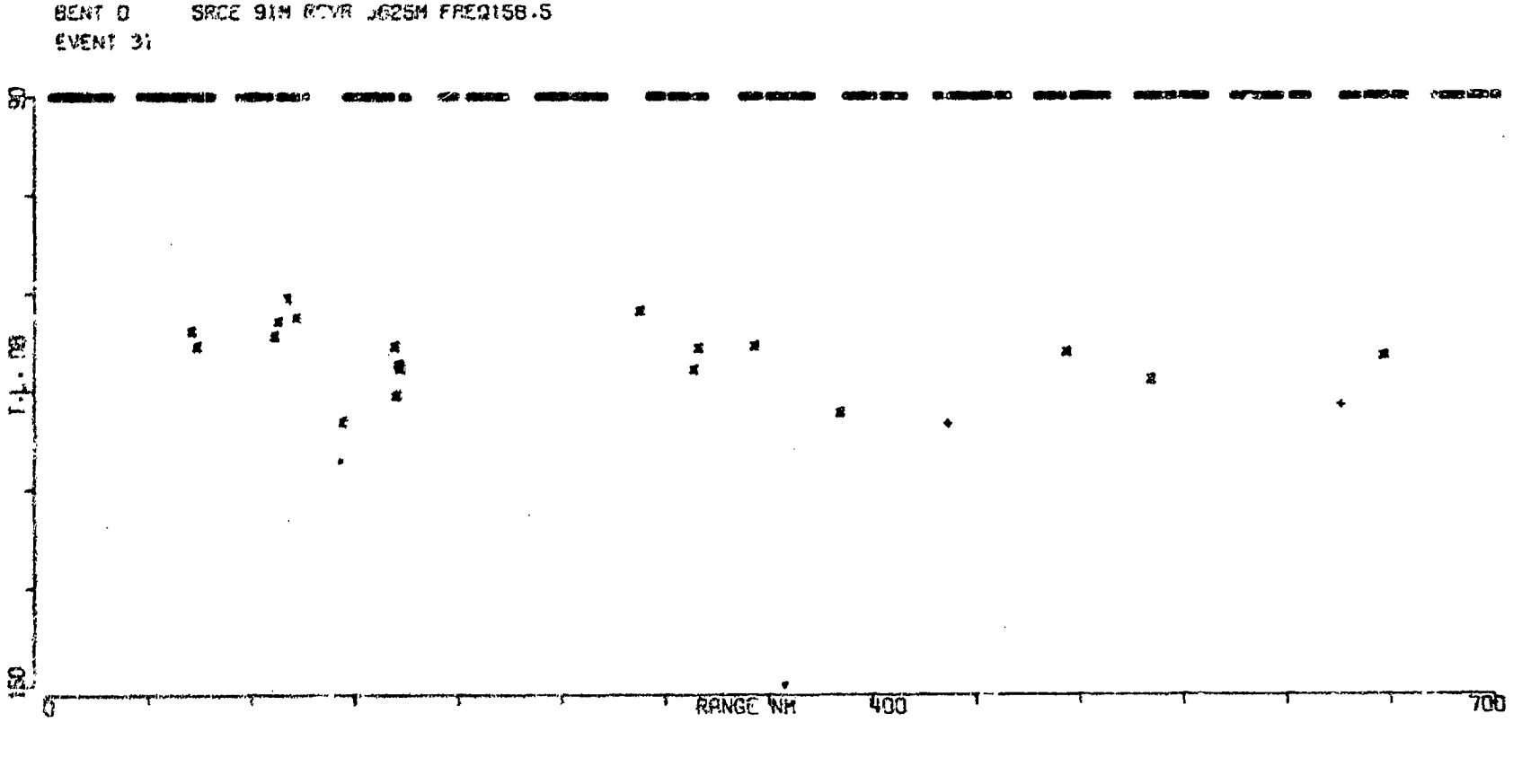
BENT 0 SRCE 91M RCVR 625M FREQ158.5
EVENT 31
50
150
dB re 1 μPa
0
RANGE NM
400
700

FIGURE A-134

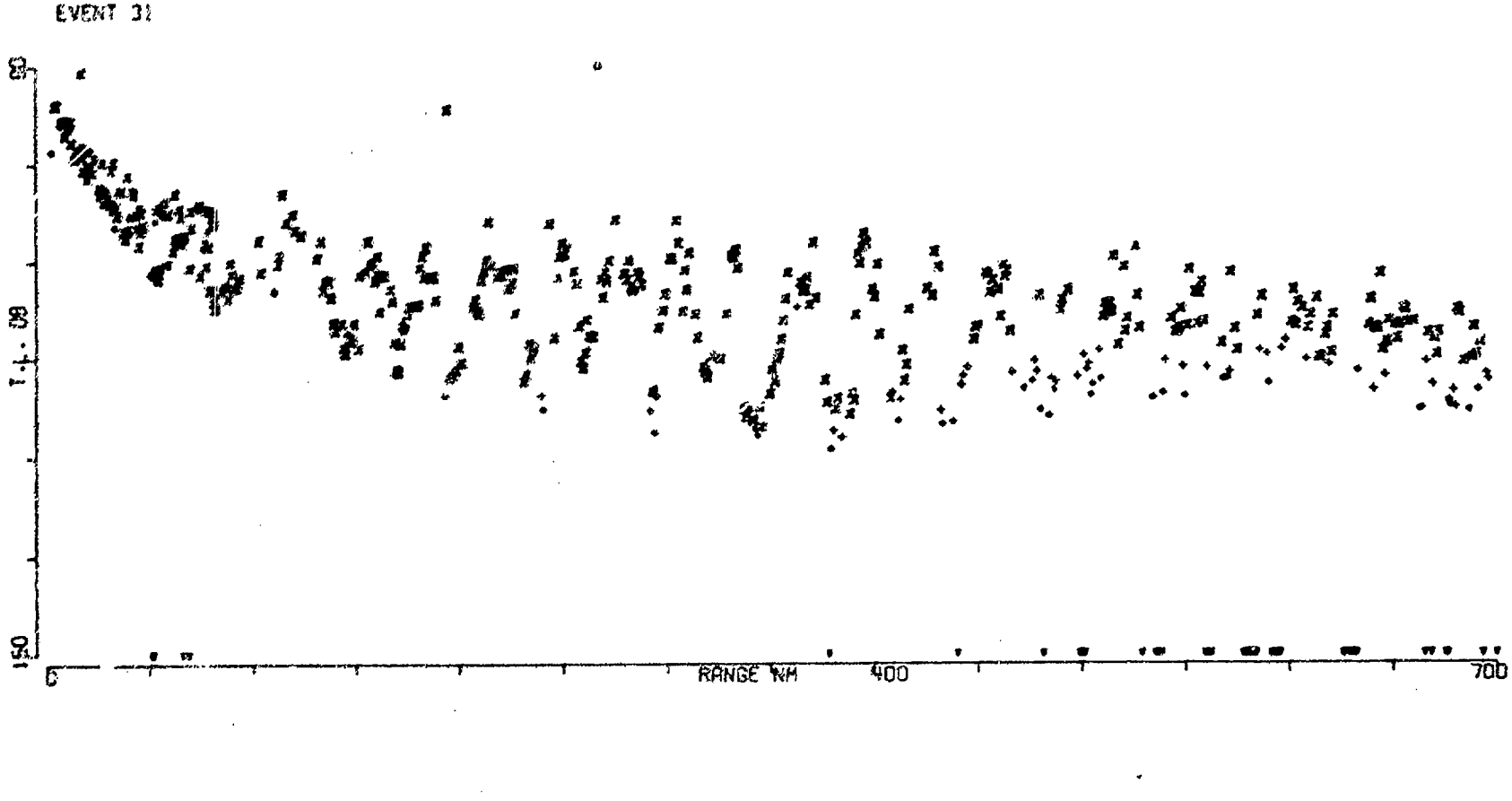
BENT D SRCE 10M RCVR 3925M FREQ158.5
EVENT 31
RANGE NM
0
400
700

FIGURE A-135

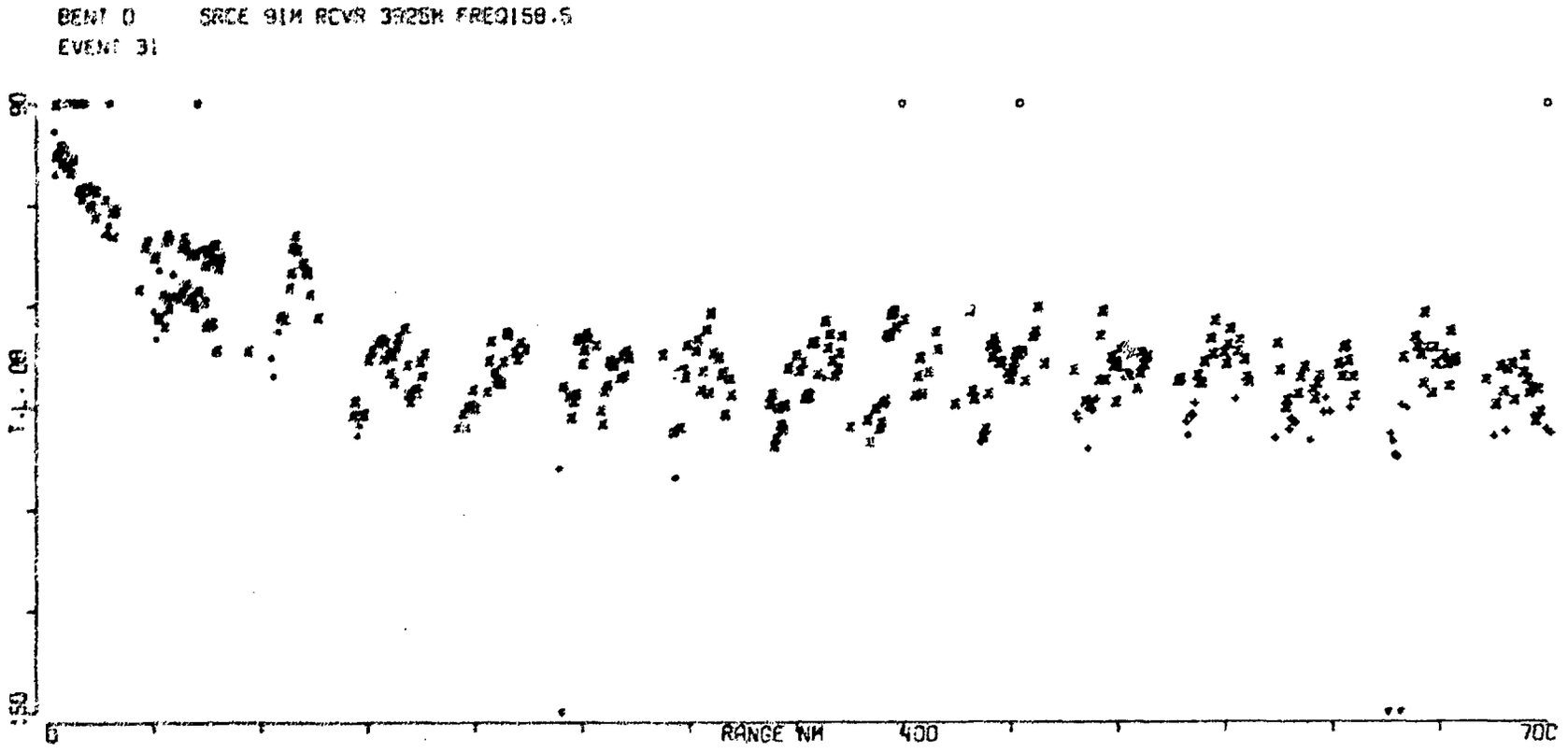
BENT 0 SRCE 91M RCVR 3925M FREQ158.5
EVENT 31
RANGE NM
0
400
700

FIGURE A-136

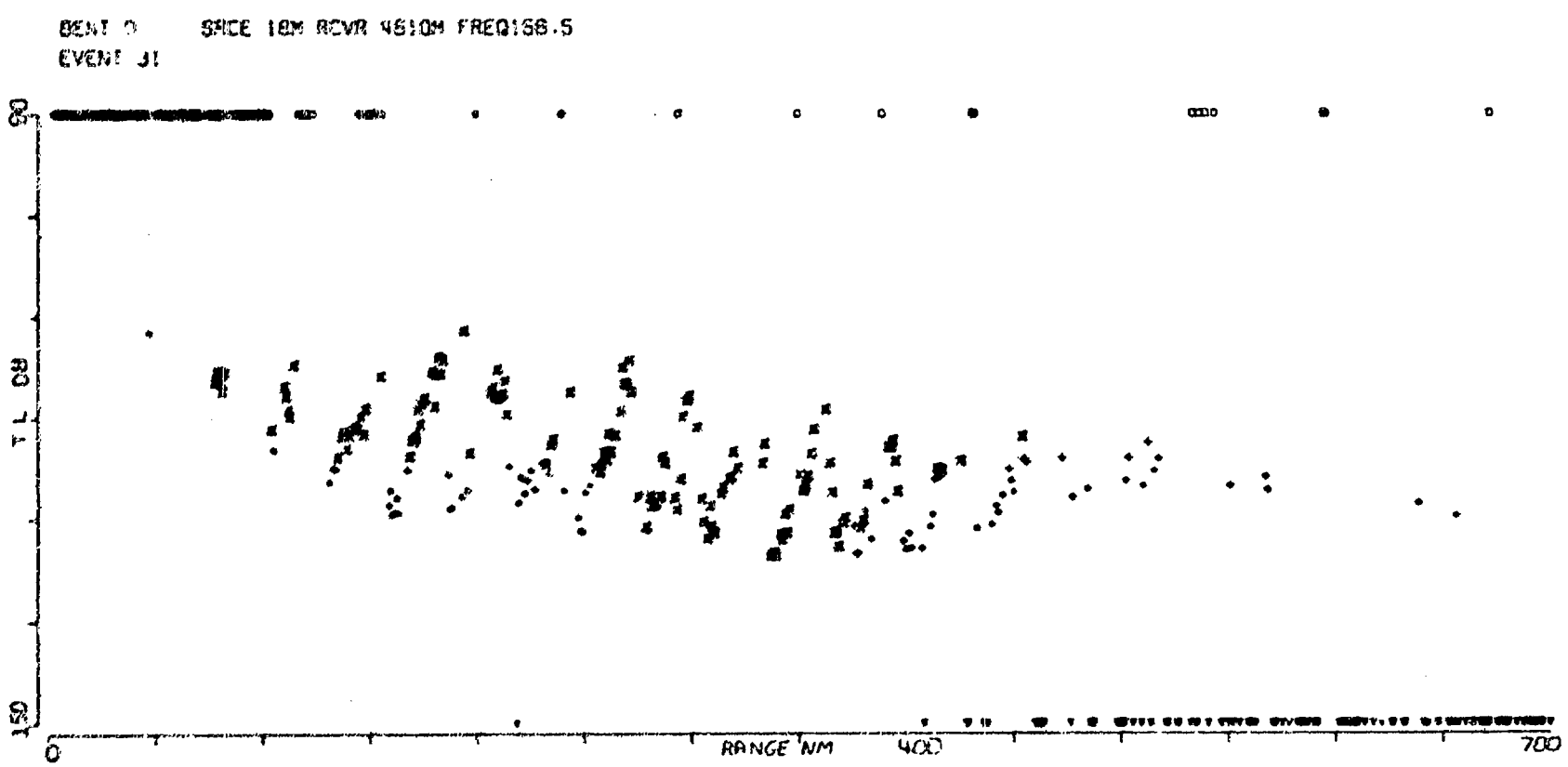
BENT 0 SRCE 18M RCVR 461.0M FREQ 168.5
EVENT 31
TL dB
80
150
0
RANGE NM
400
700

FIGURE A-137

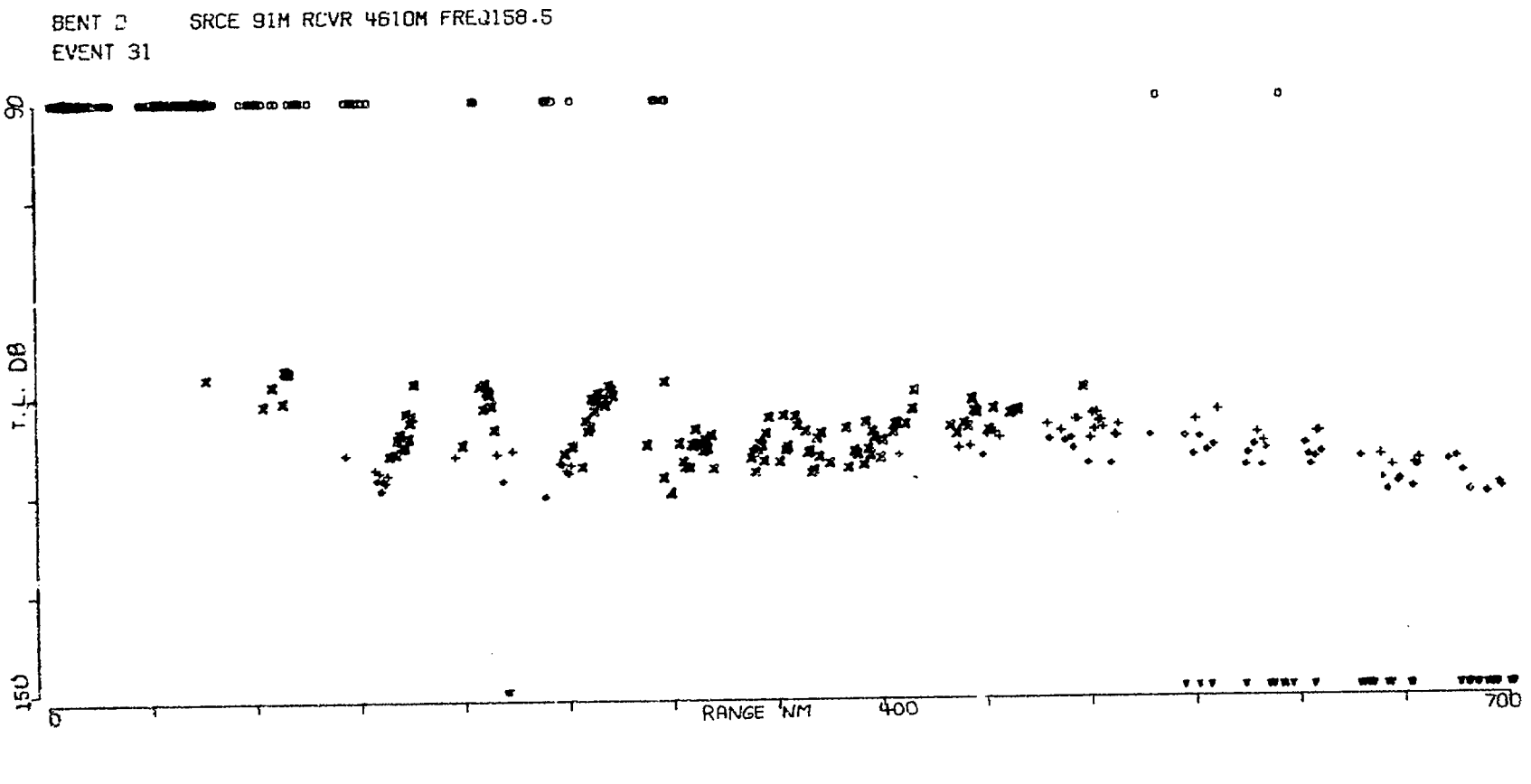
BENT 2 SRCE 91M RCVR 4610M FREQ158.5
EVENT 31
90
150
T.L. DB
0
RANGE NM
400
700

FIGURE A-138

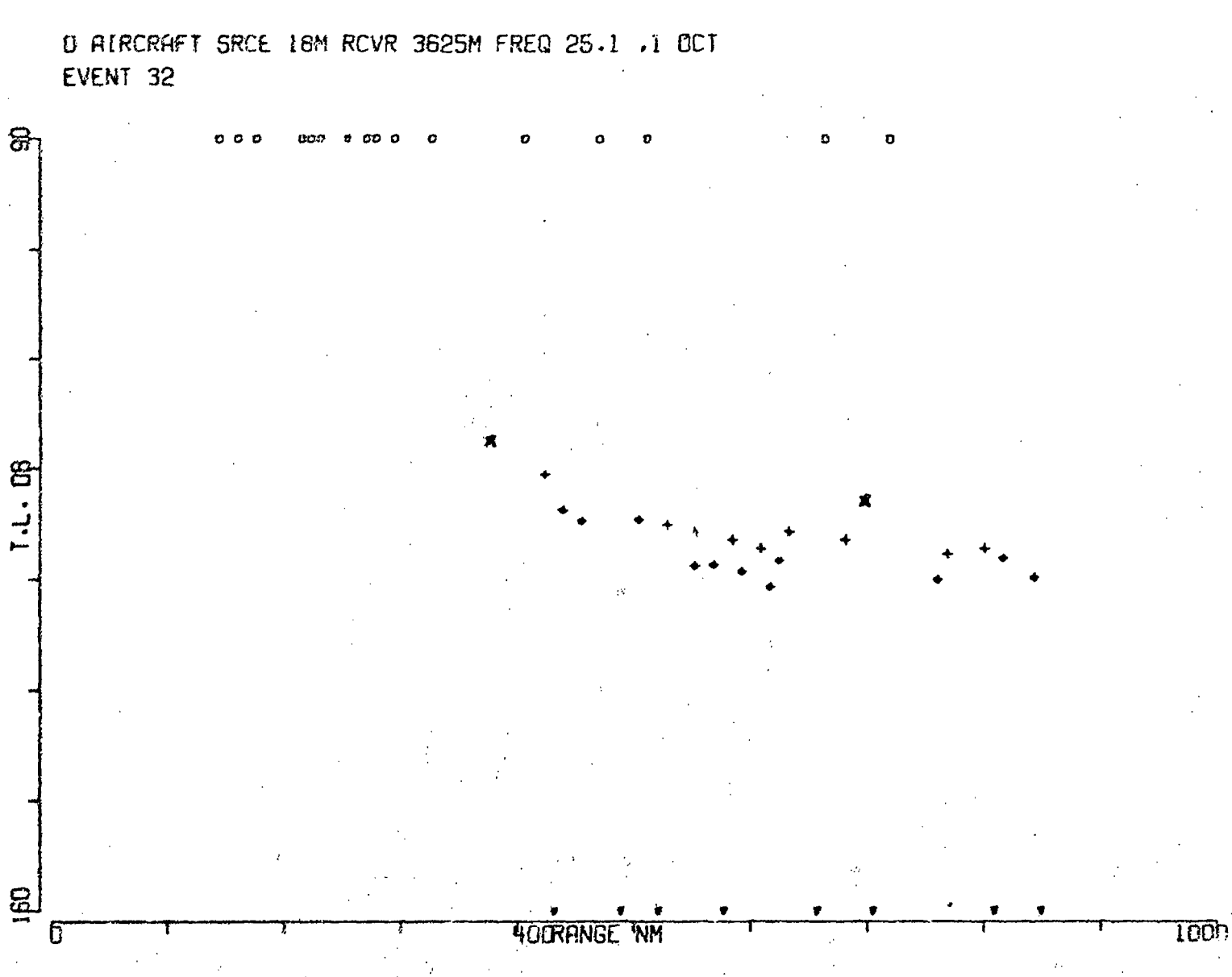
0 AIRCRAFT SRCE 18M RCVR 3625M FREQ 25.1 .1 OCT
EVENT 32
90
T.L. DB
160
0
400RANGE NM
100n

FIGURE A-139

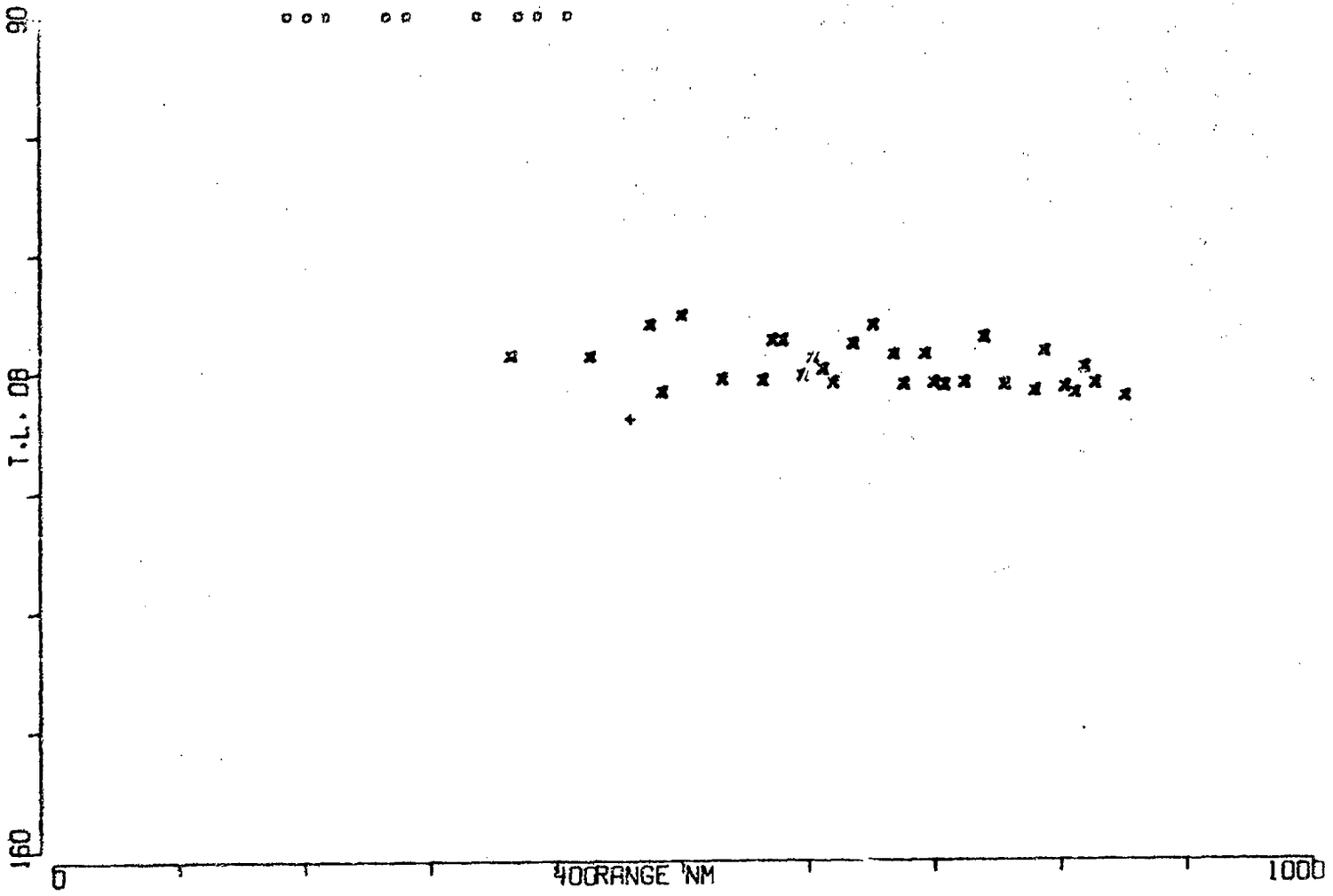
D AIRCRAFT SRCE 91M RCVR 362SM FREQ 25.1 .1 OCT
EVENT 32
90
T.L. DB
160
0
400RANGE NM
1000

FIGURE A-140

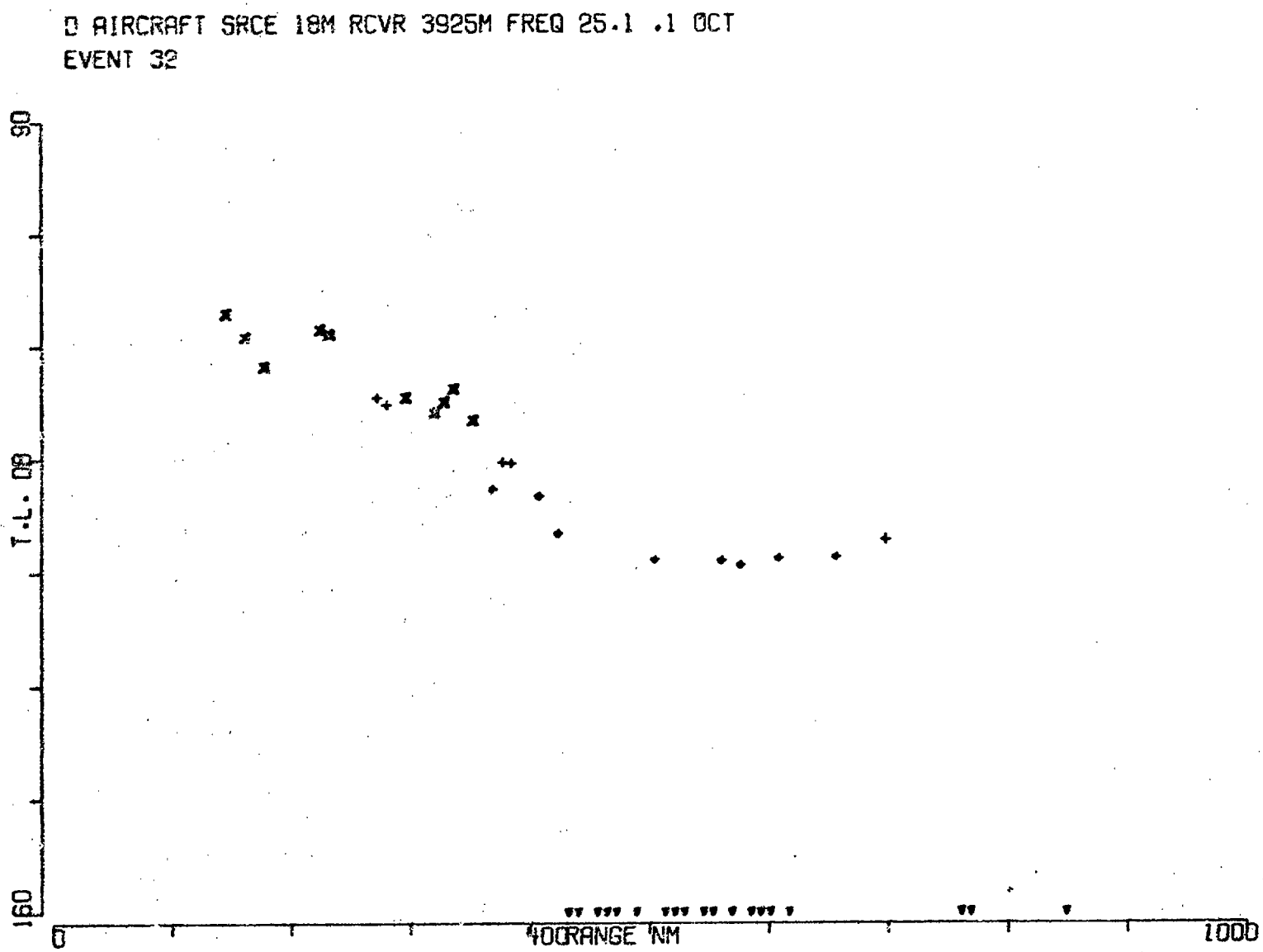
D AIRCRAFT SRCE 18M RCVR 3925M FREQ 25.1 .1 OCT
EVENT 32
90
T.L. DB
160
0
400RANGE NM
1000

FIGURE A-141

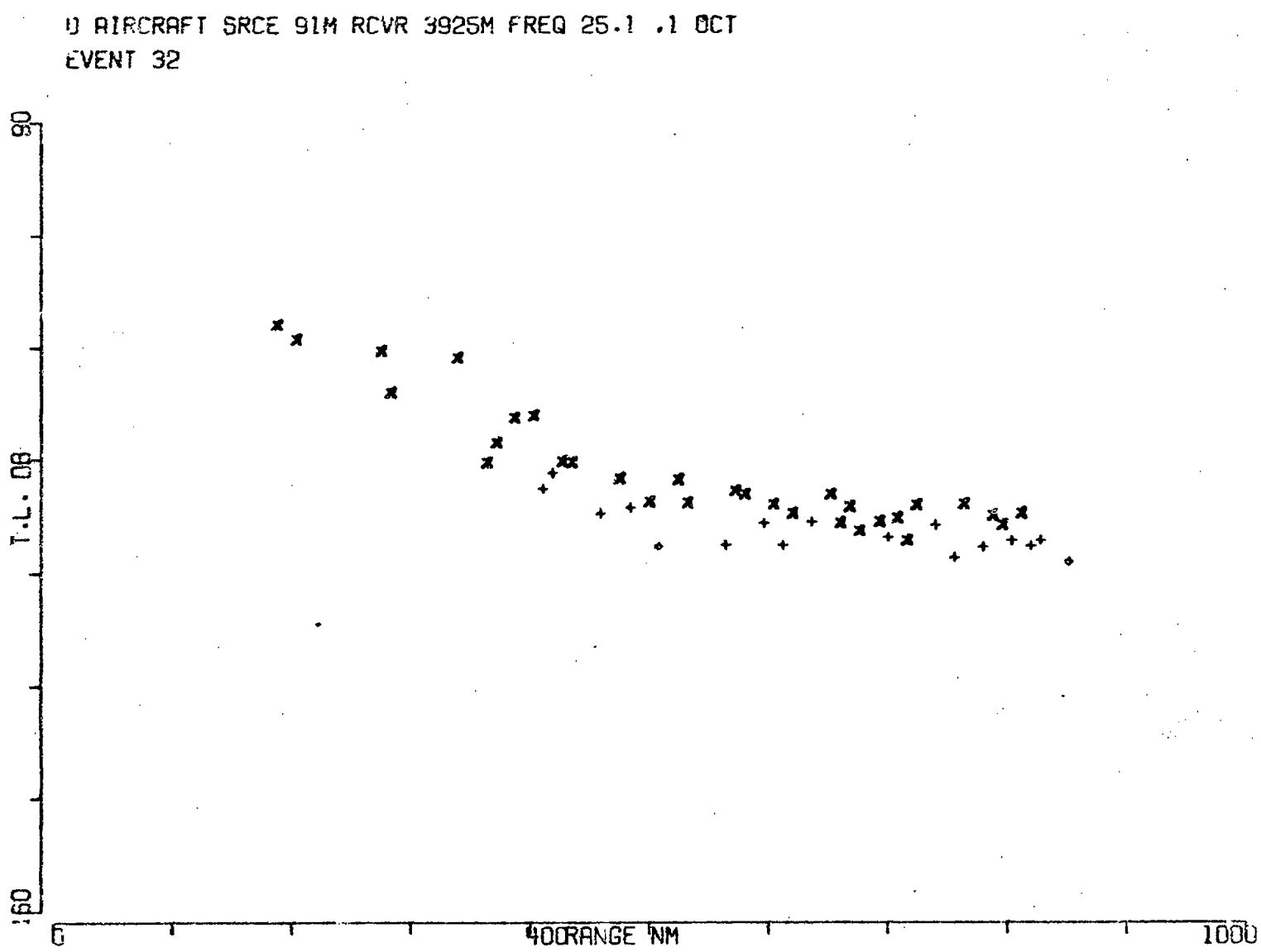
0 AIRCRAFT SRCE 91M RCVR 3925M FREQ 25.1 .1 OCT
EVENT 32
90
T.L. DB
160
0
400RANGE NM
1000

FIGURE A-142

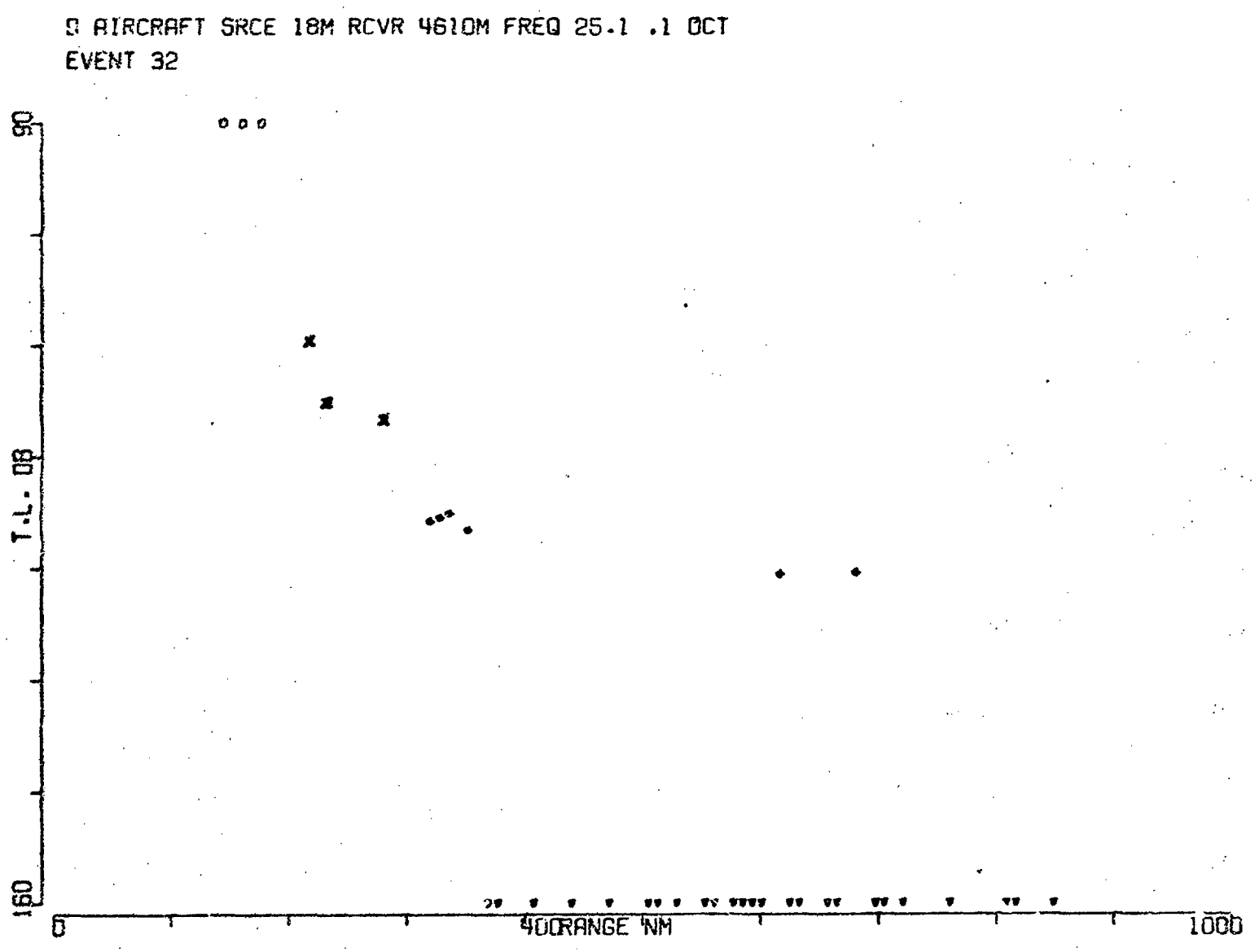
S AIRCRAFT SRCE 18M RCVR 4610M FREQ 25.1 .1 OCT
EVENT 32
90
T.L. DB
160
0
400RANGE NM
1000

FIGURE A-143

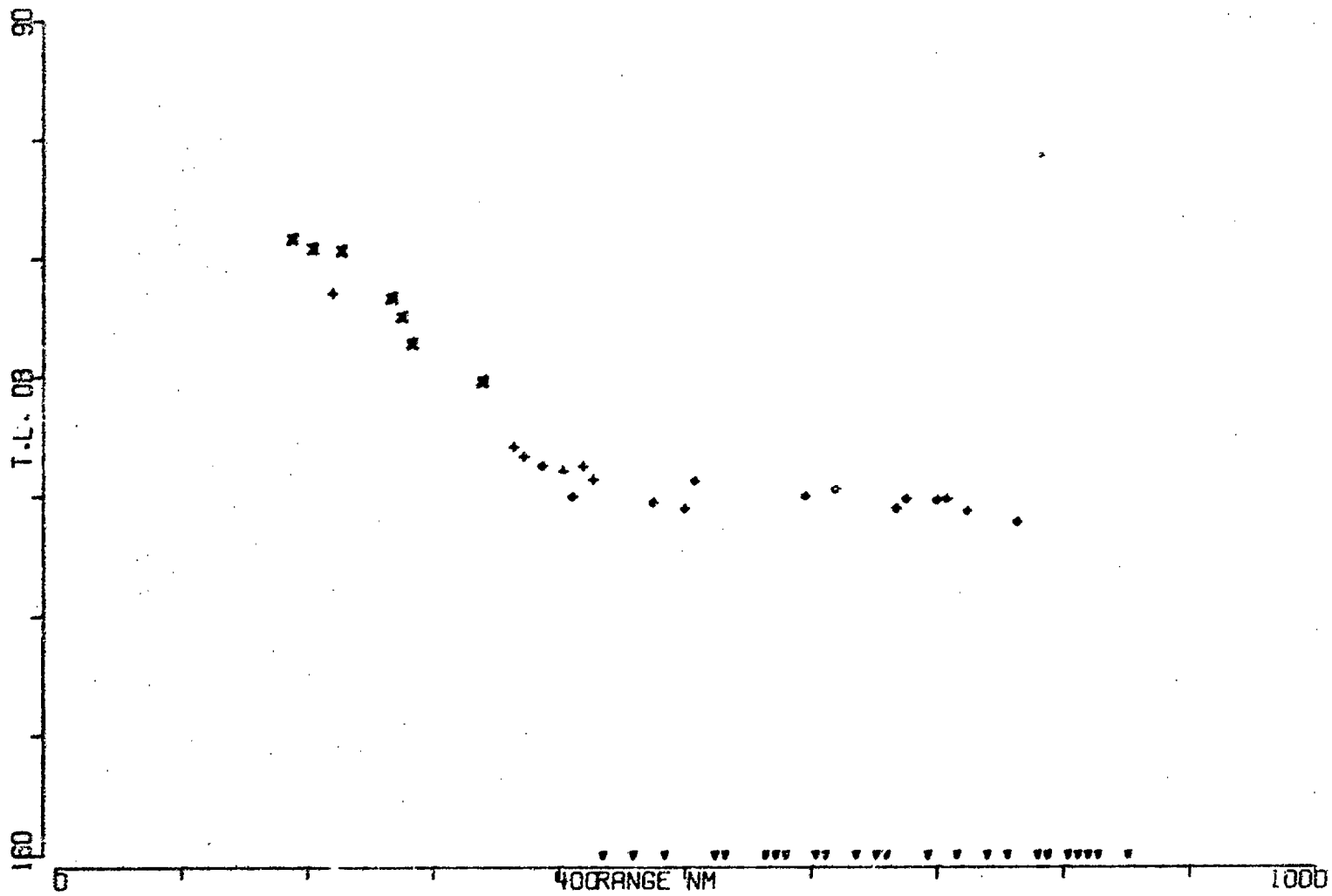
D AIRCRAFT SRCE 91M RCVR 4610M FREQ 25.1 .1 OCT
EVENT 32
60
T.L. DB
160
0
400RANGE NM
1000

FIGURE A-144

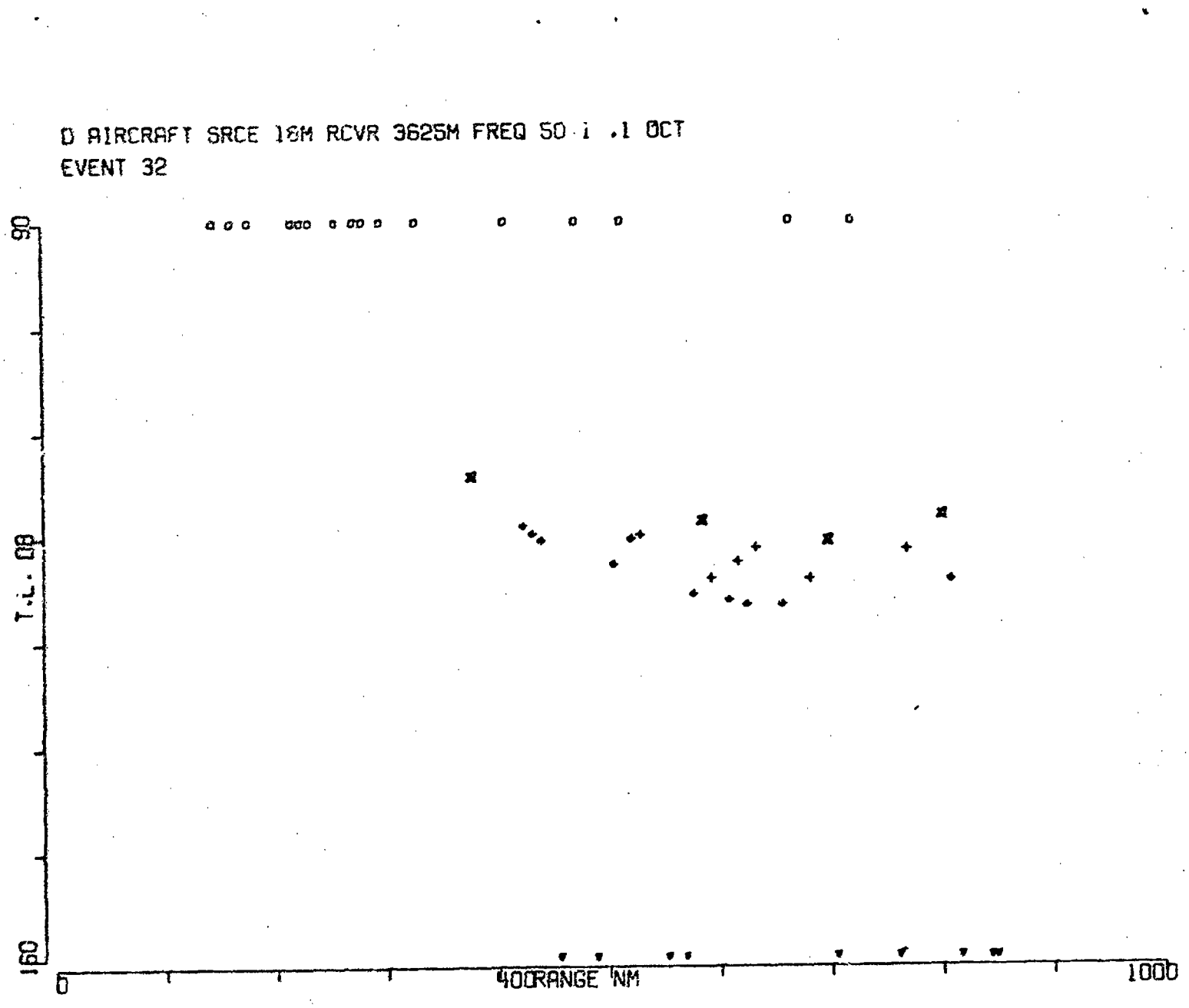
D AIRCRAFT SRCE 18M RCVR 3625M FREQ 50 i .1 OCT
EVENT 32
90
T.L. dB
160
0
400RANGE NM
1000

FIGURE A-145

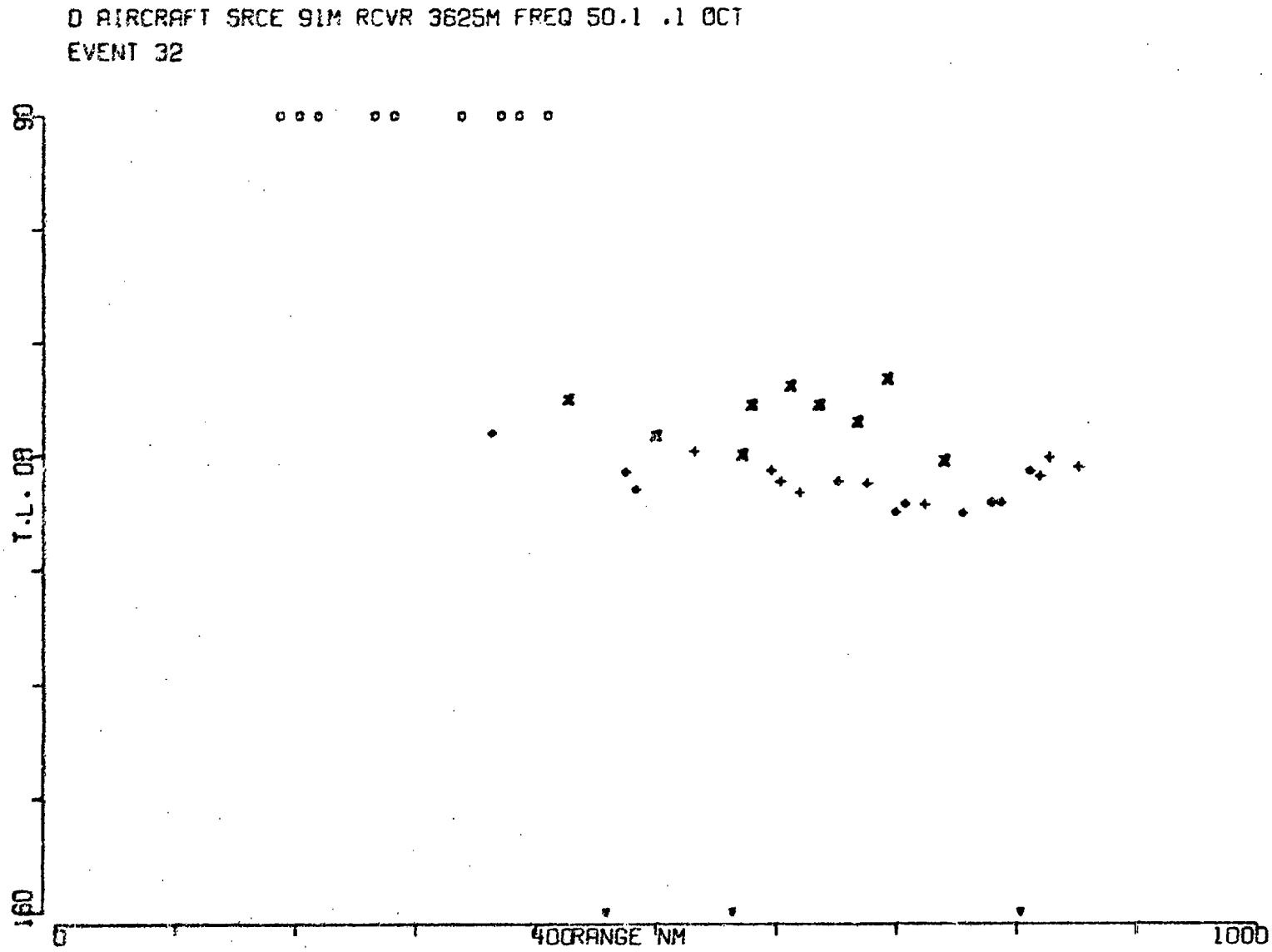
D AIRCRAFT SRCE 91M RCVR 3625M FREQ 50.1 .1 OCT
EVENT 32
60
T.L. DB
160
0
400RANGE NM
1000

FIGURE A-146

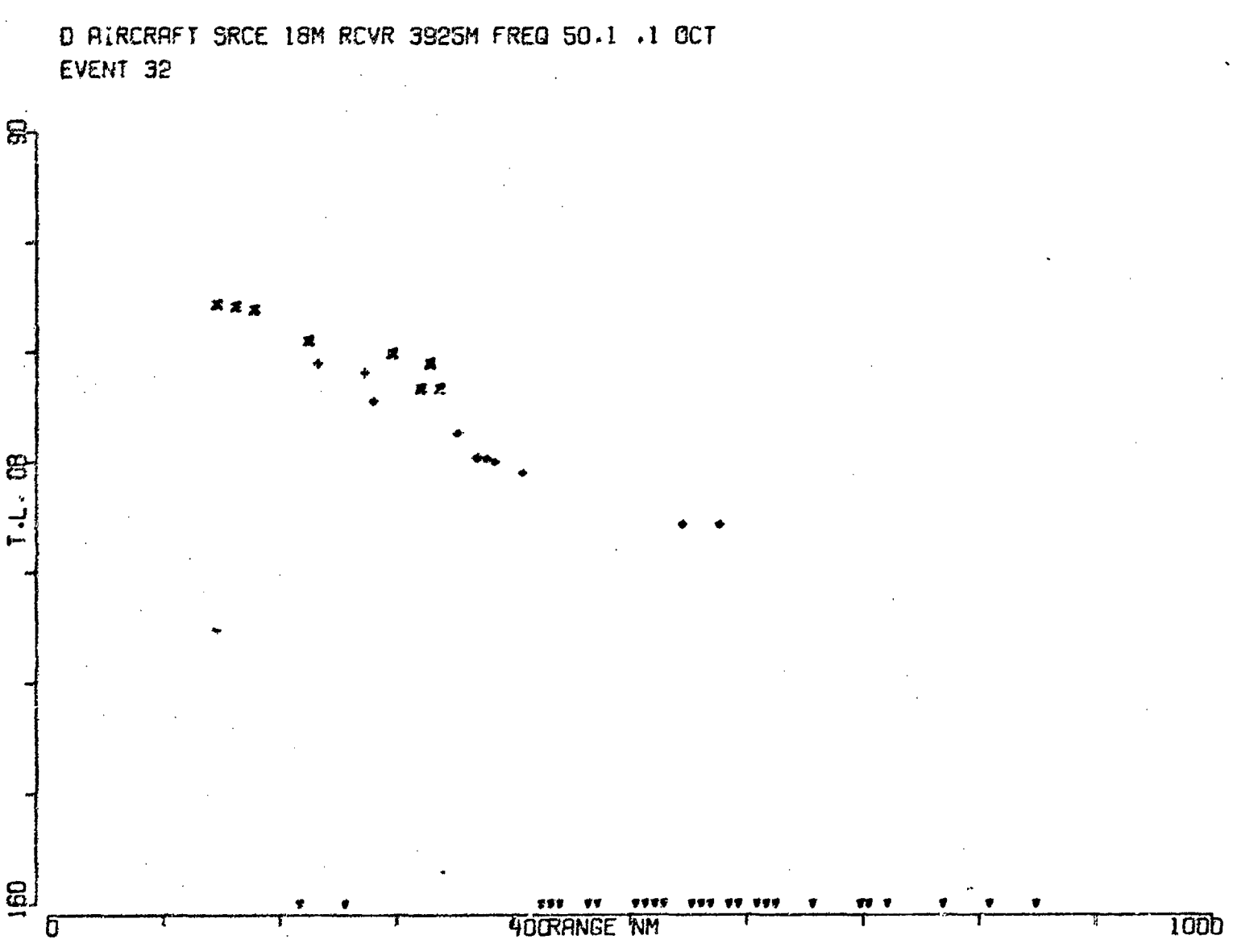
D AIRCRAFT SRCE 18M RCVR 3925M FREQ 50.1 .1 OCT
EVENT 32
60
80
160
T.L. DB
0
400RANGE NM
1000

FIGURE A-147

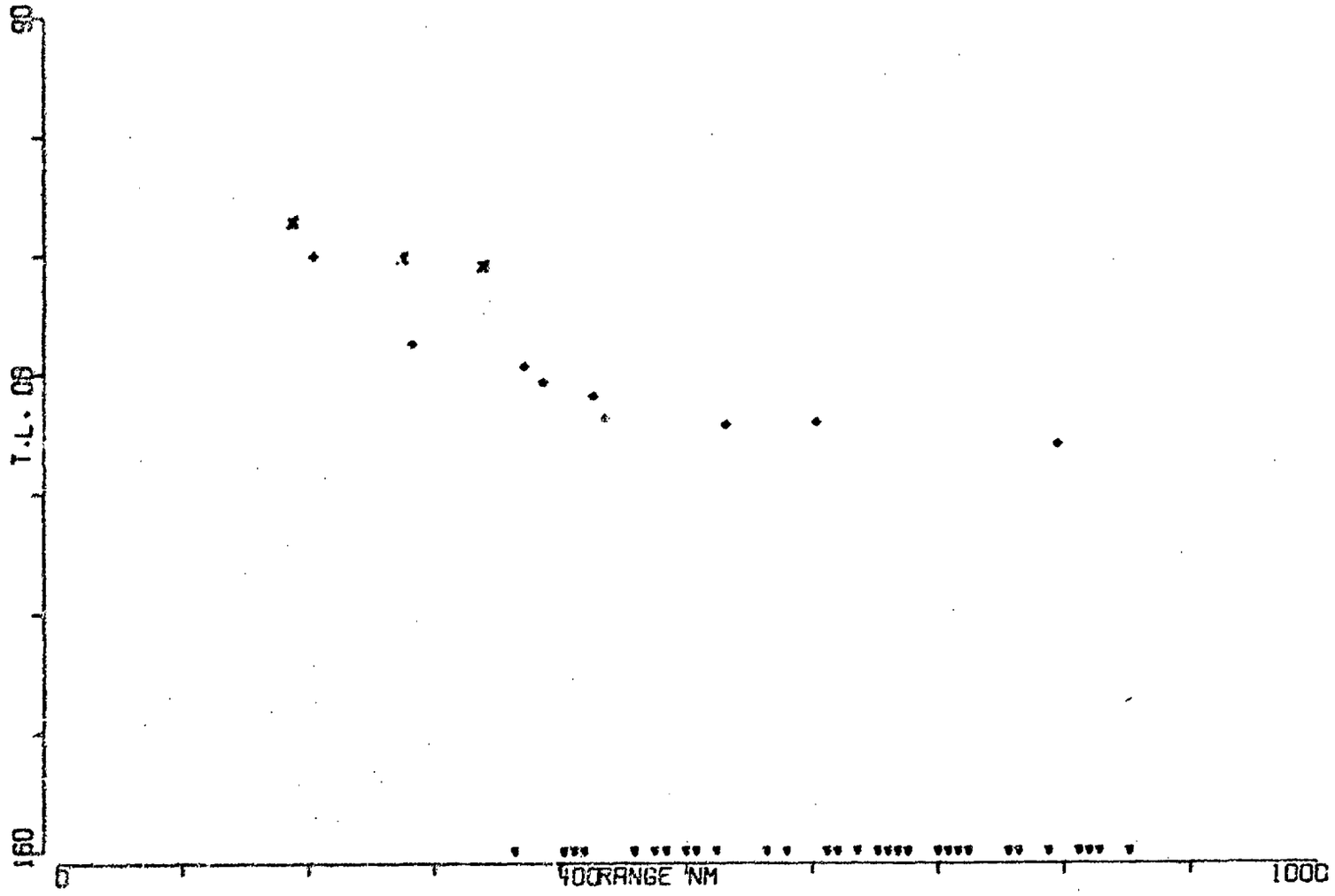
D AIRCRAFT SRCE 91M RCVR 3925M FREQ 50.1 .1 OCT
EVENT 32
60
T.L. DB
160
0
400RANGE NM
1000

FIGURE A-148

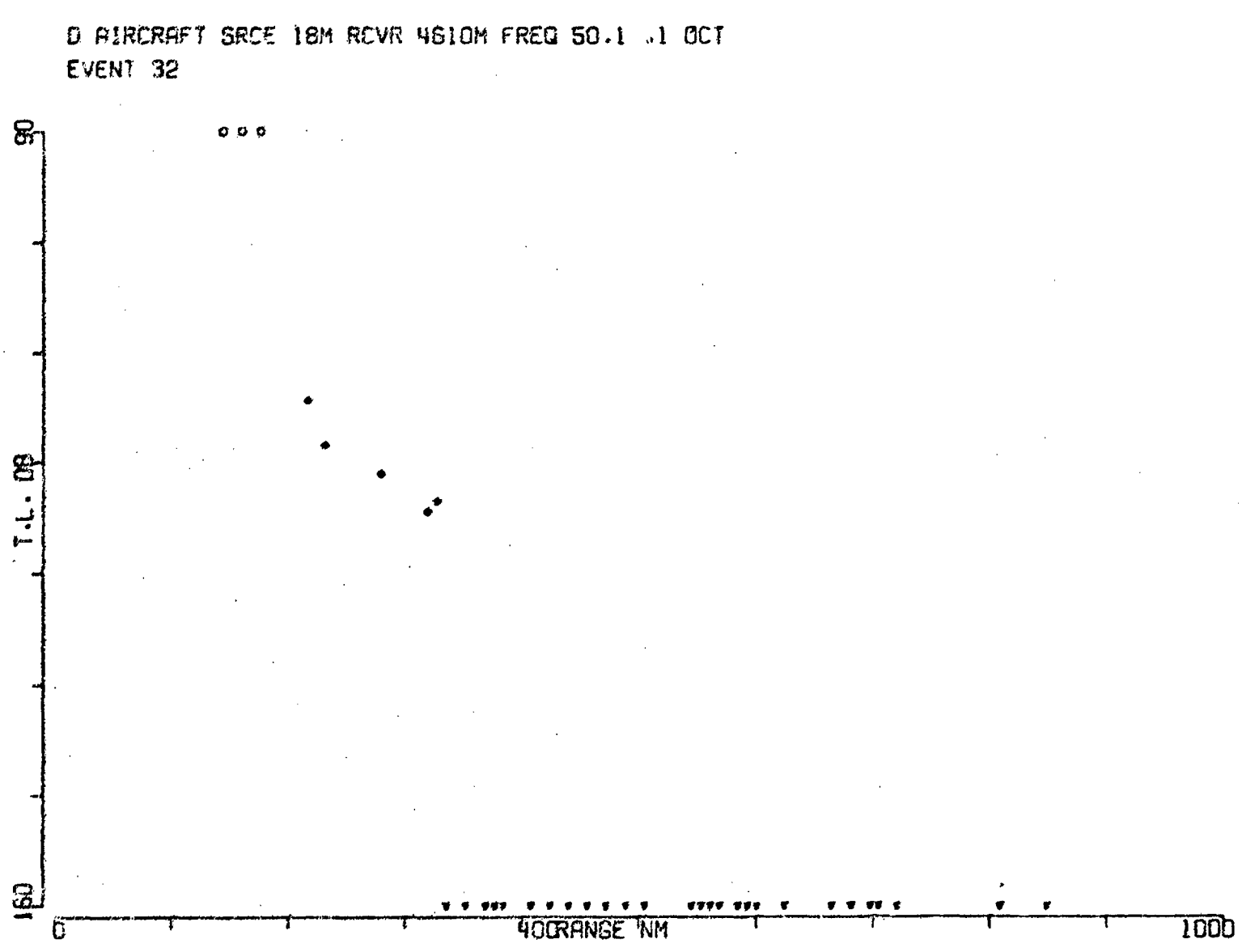
D AIRCRAFT SRCE 18M RCVR 4610M FREQ 50.1 .1 OCT
EVENT 32
80
T.L. DB
160
0
400RANGE NM
1000

FIGURE A-149

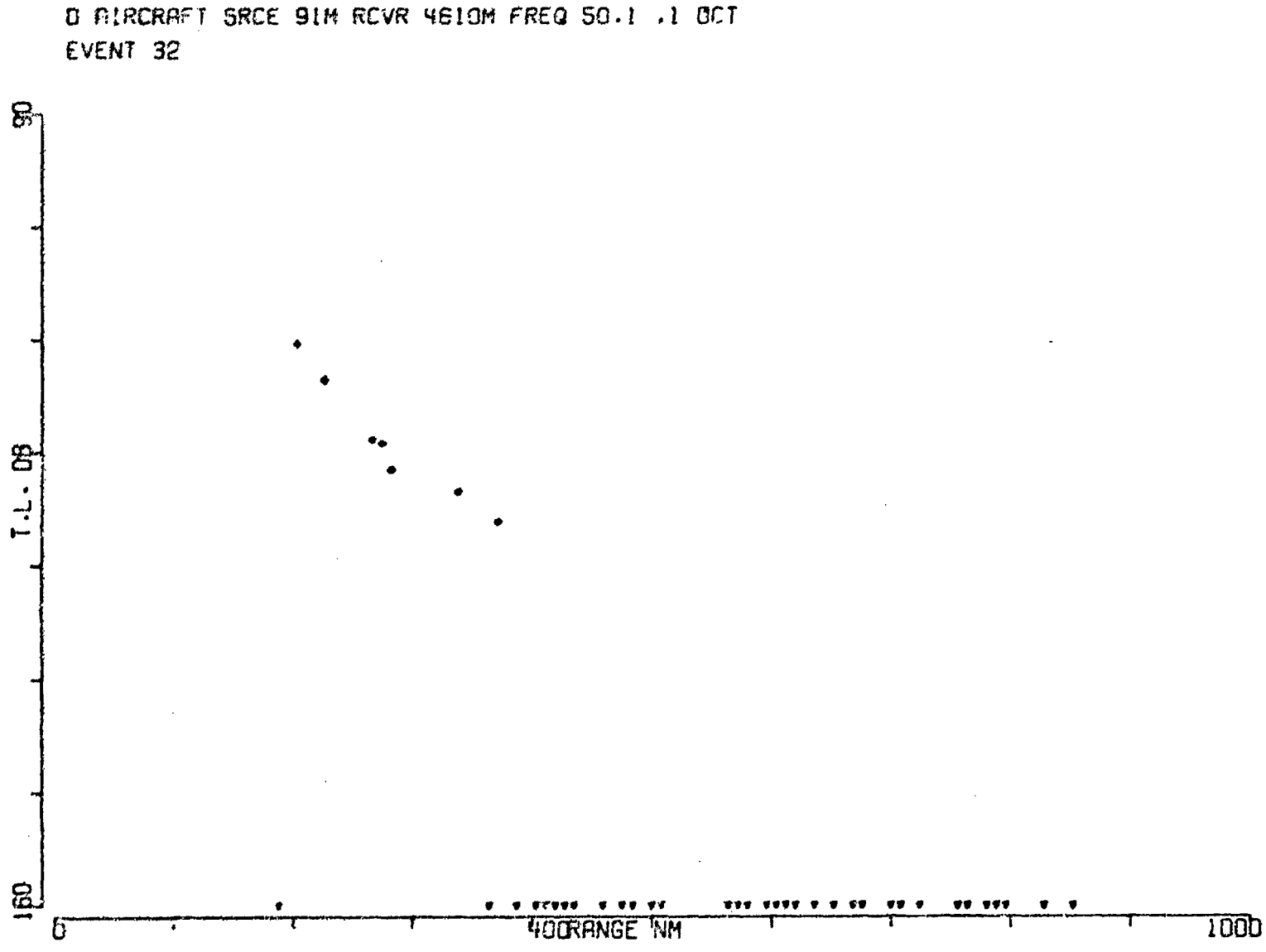
0 AIRCRAFT SRCE 91M RCVR 461OM FREQ 50.1 .1 OCT
EVENT 32
60
T.L. DB
160
0
400RANGE NM
1000

FIGURE A-15C

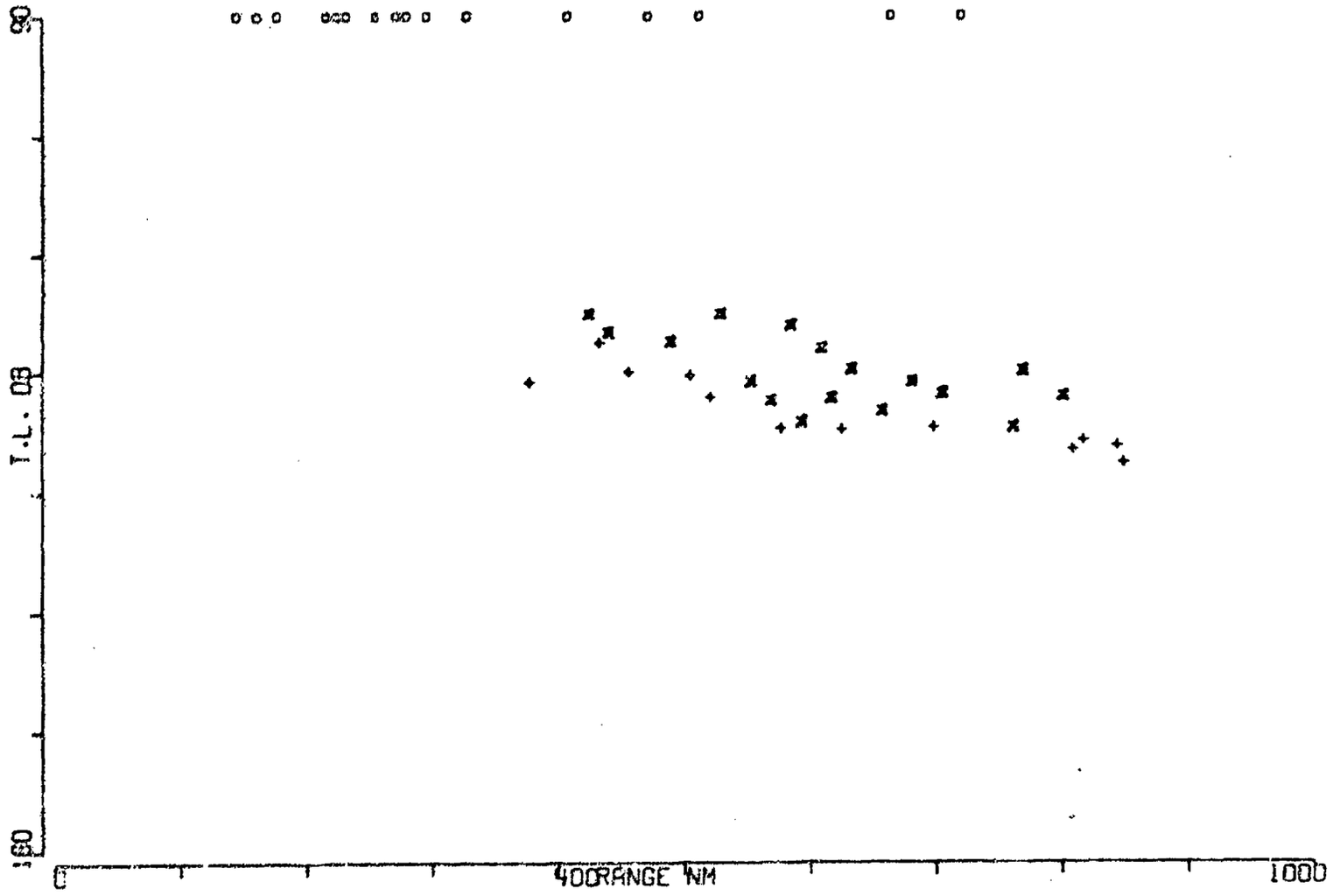
O AIRCRAFT SRCE 18M RCVR 3625M FREQ158.5
EVENT 32
80
T.L. DB
160
0
400RANGE NM
1000

FIGURE A-151

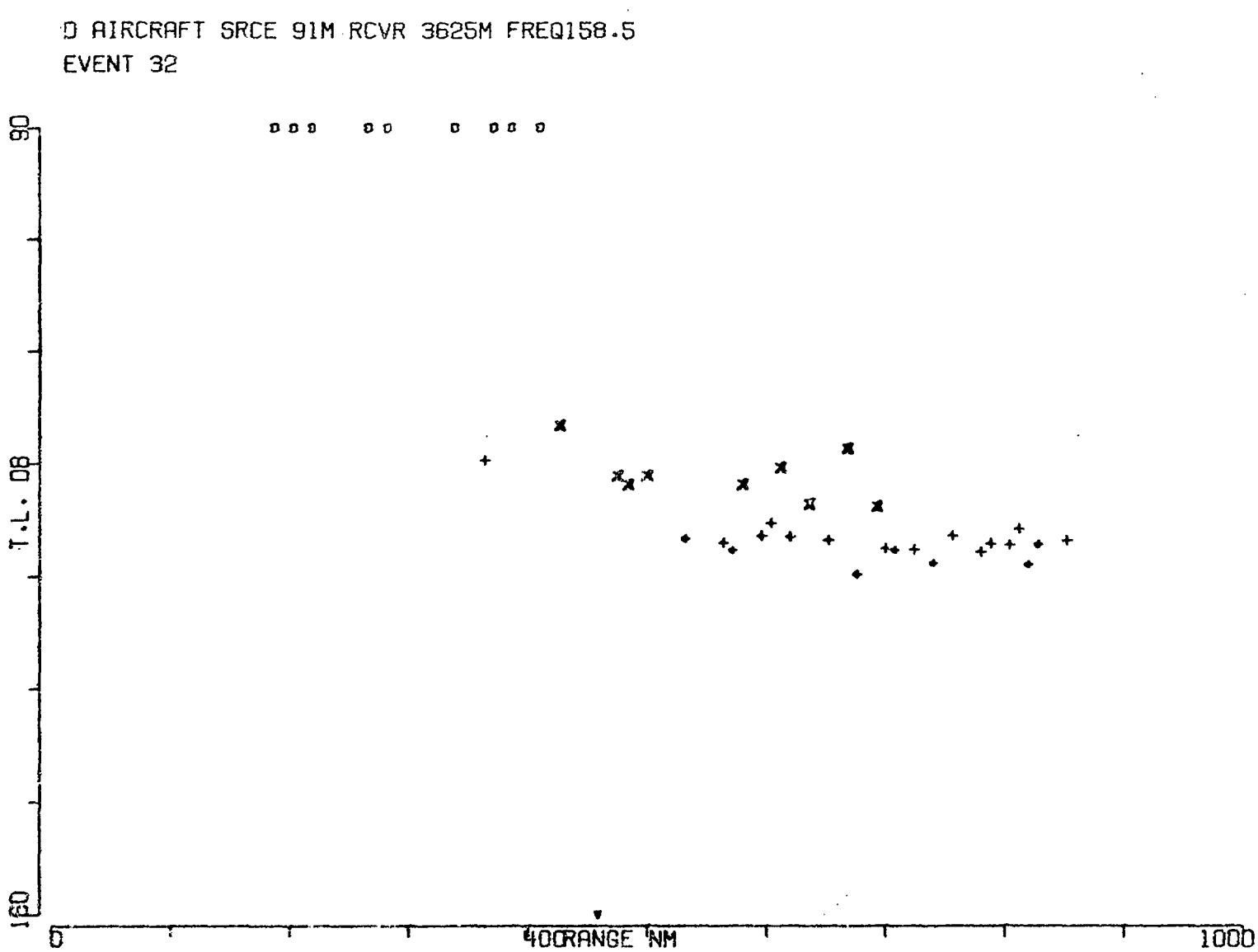
D AIRCRAFT SRCE 91M RCVR 3625M FREQ158.5
EVENT 32
90
T.L. DB
160
0
400RANGE NM
1000

FIGURE A-152

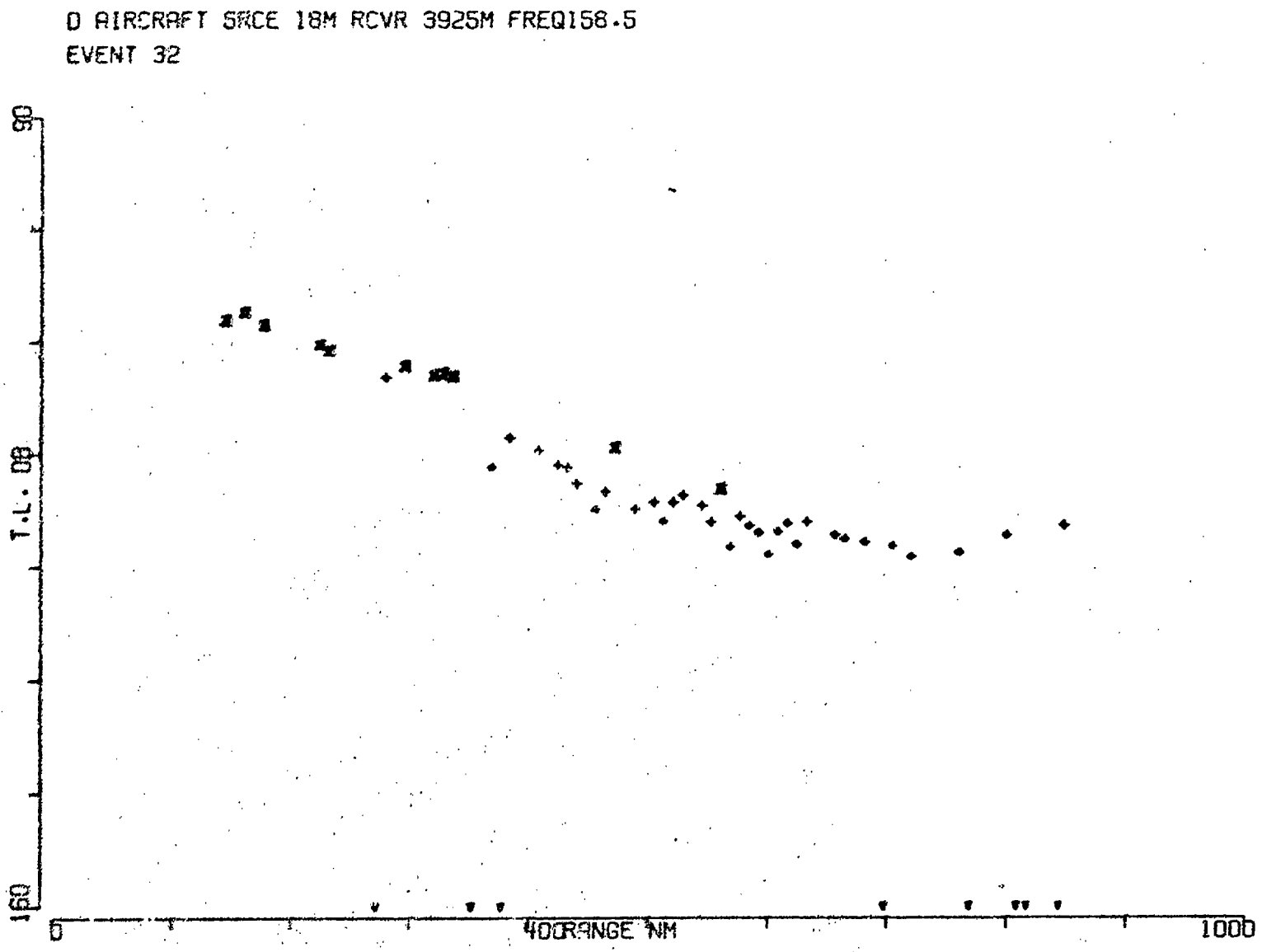
D AIRCRAFT SRCE 18M RCVR 3925M FREQ158.5
EVENT 32
60
T.L. DB
160
0
400RANGE NM
1000

FIGURE A-153

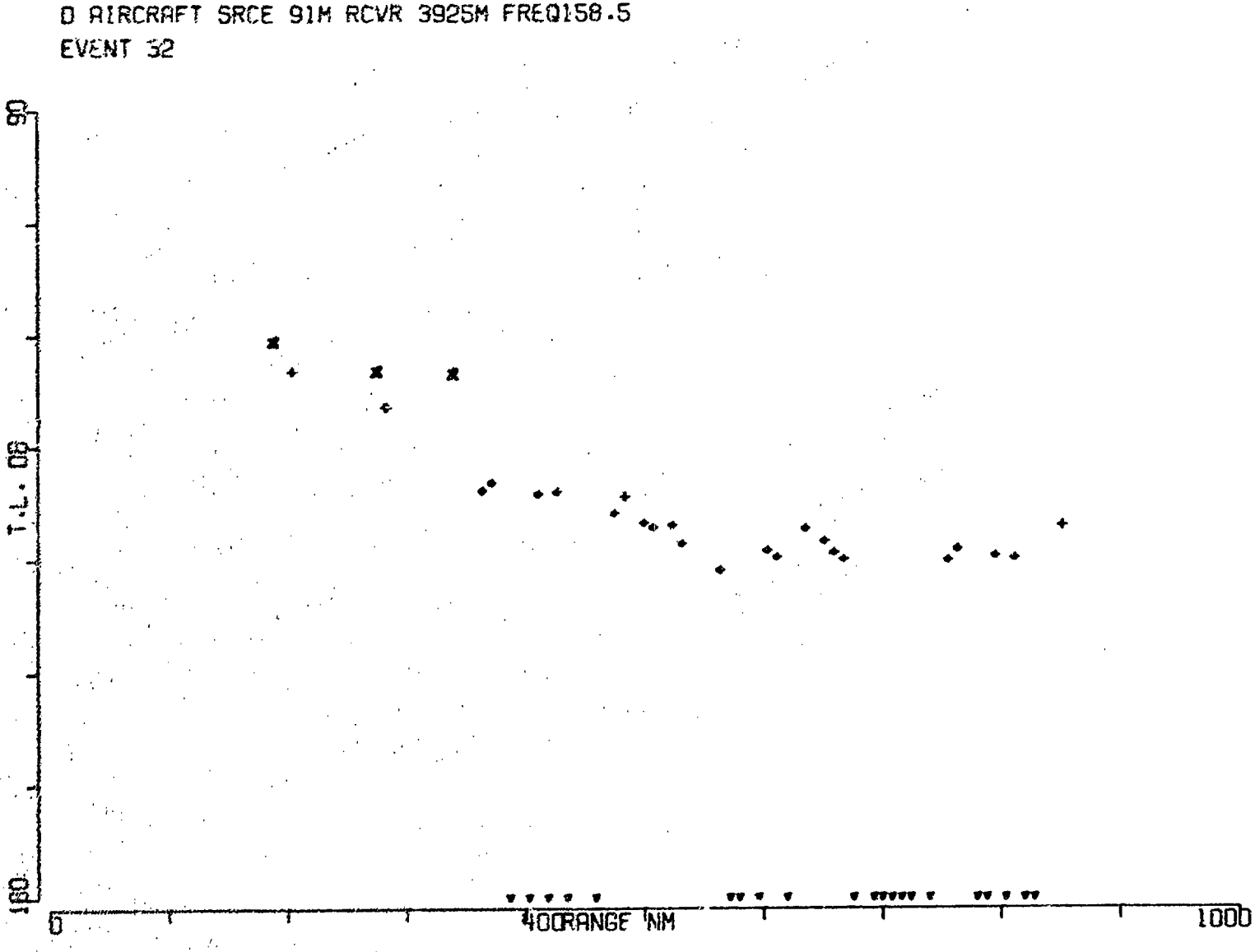
D AIRCRAFT SRCE 91M RCVR 3925M FREQ158.5
EVENT 32
60
T.L. DB
160
0
400RANGE NM
1000

FIGURE A-154

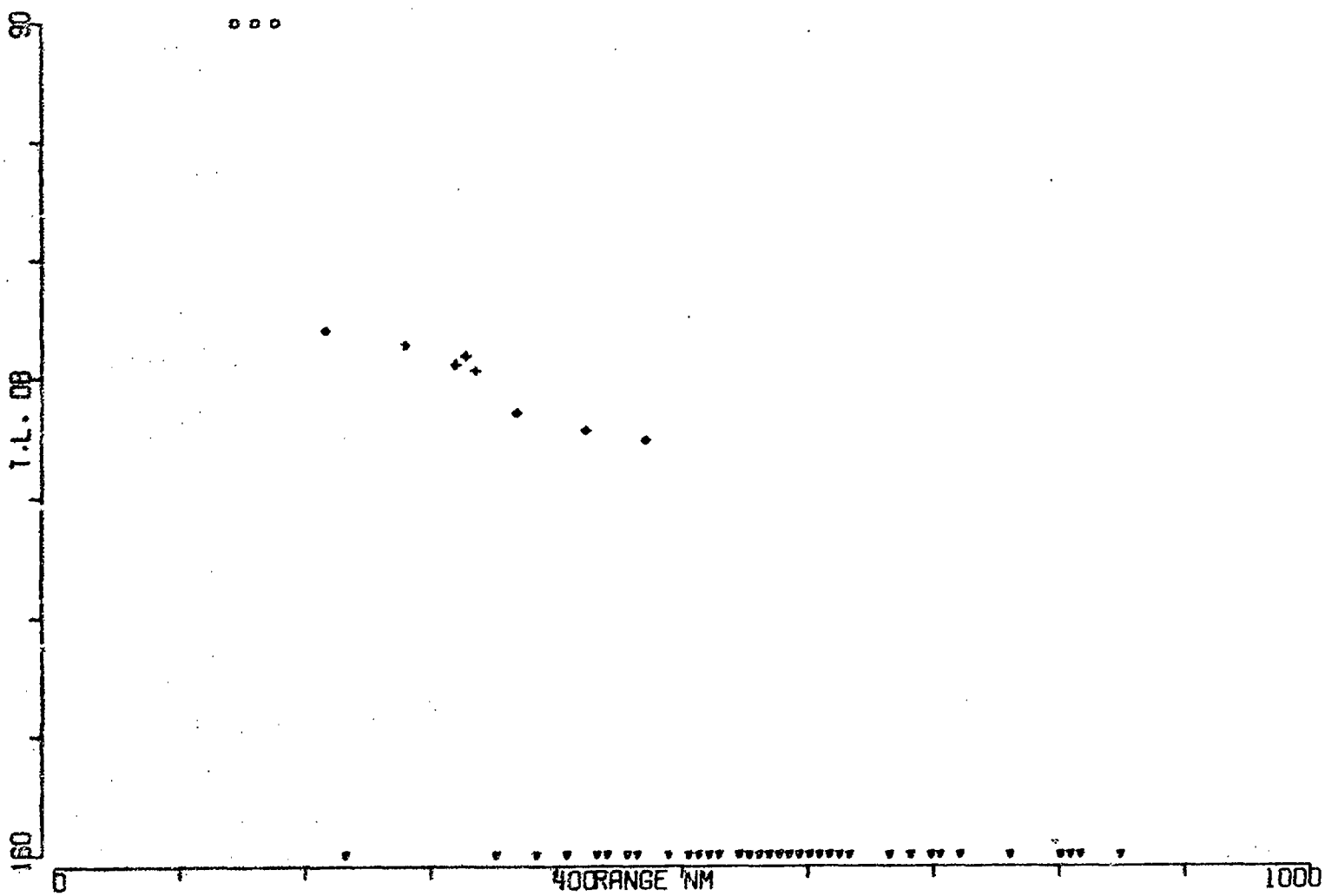
D AIRCRAFT SRCE 18M RCVR 4610M FREQ158.5
EVENT 32
80
T.L. dB
160
0
400RANGE NM
1000

FIGURE A-155

D AIRCRAFT SRCE 91M RCVR 4610M FREQ159.5
EVENT 32

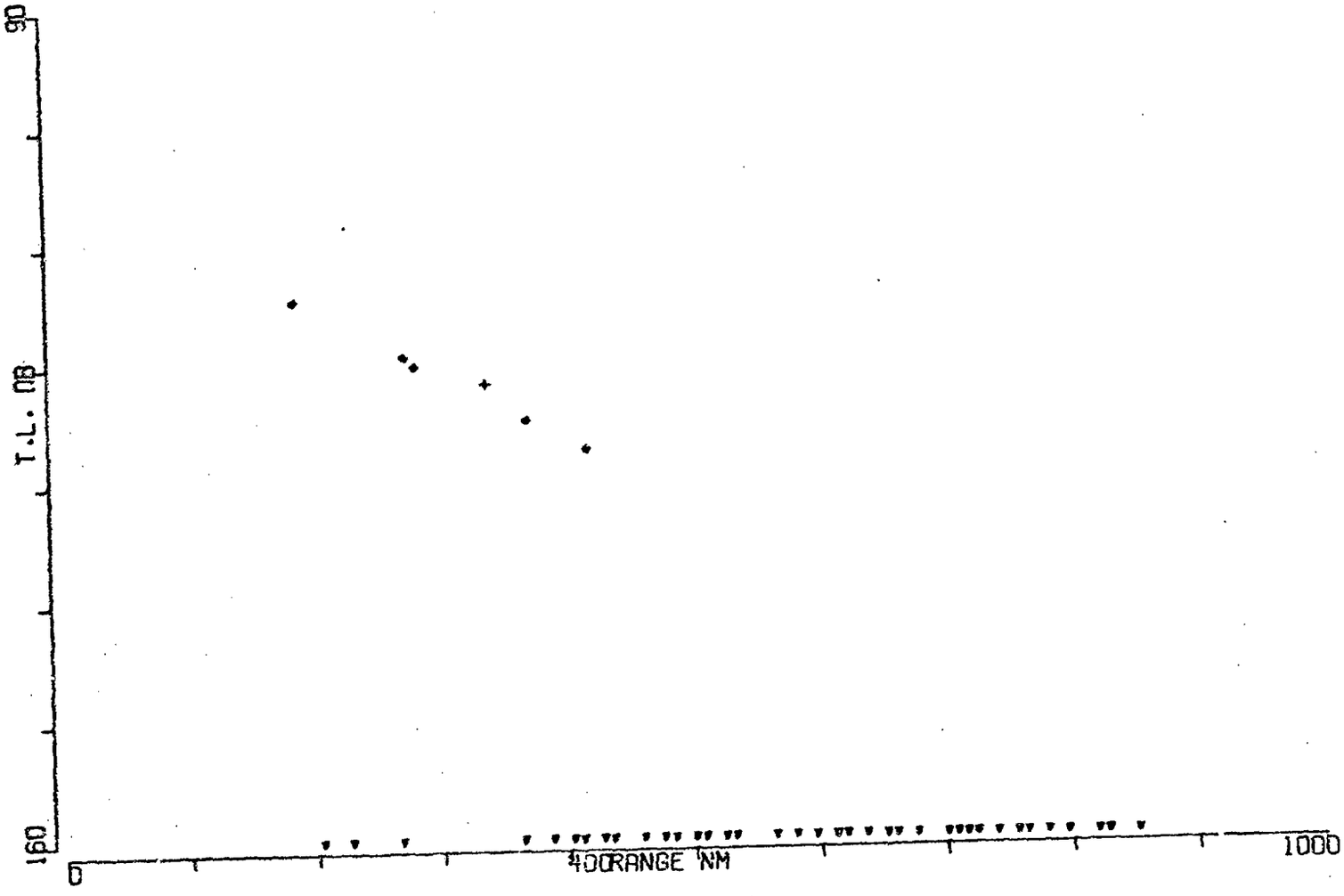

FIGURE A-156

APPENDIX B

MESA PROPAGATION LOSS DATA

(U) MESA array propagation loss data are shown in Figs. B1 through B20. The signal-to-noise ratio (S/N) for each shot is indicated by different symbols as explained in Appendix A. Table B-1 summarizes the figure numbers used in this appendix for each source event, frequency, and source depth.

The data presented in this appendix are
UNCLASSIFIED

TABLE B1

SITE E, MESA

Figure Number for Source Depth 18 m, 91 m
Hydrophone Depth 400 m

Source Event	Center Frequency (Hz) of 1/3 Octave Band				
	25	50	100	158	251
31 BENT Source Run	B1, B2	B3, B4	B5, B6	B7, B8	B9, B10
32 AIRCRAFT Source Run	B11, B12	B13, B14	B15, B16	B17, B18	B19, B20

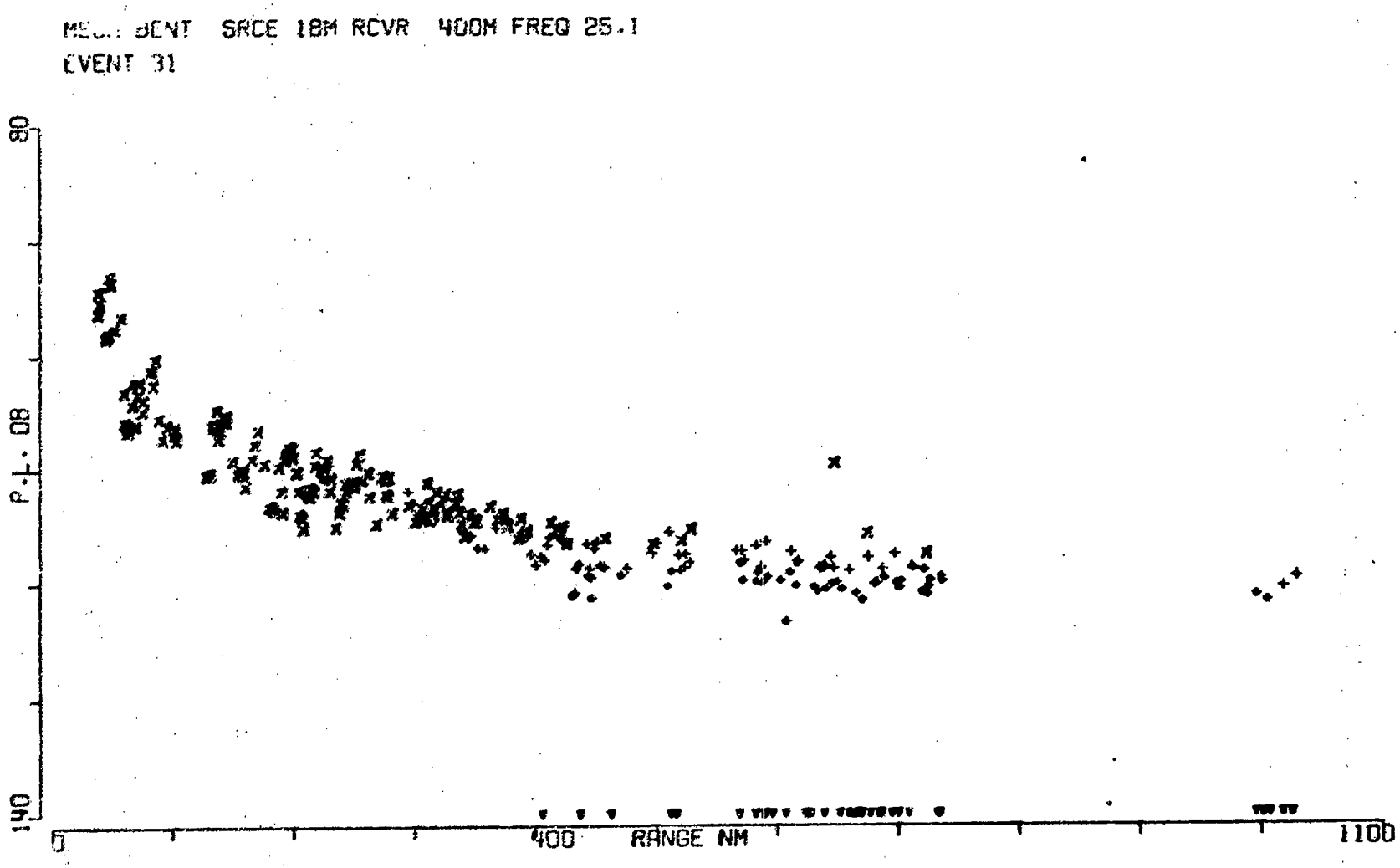
MEA... BENT SRCE 18M RCVR 400M FREQ 25.1
EVENT 31
60
140
P.L. DB
0
400
RANGE NM
1100

FIGURE B-1

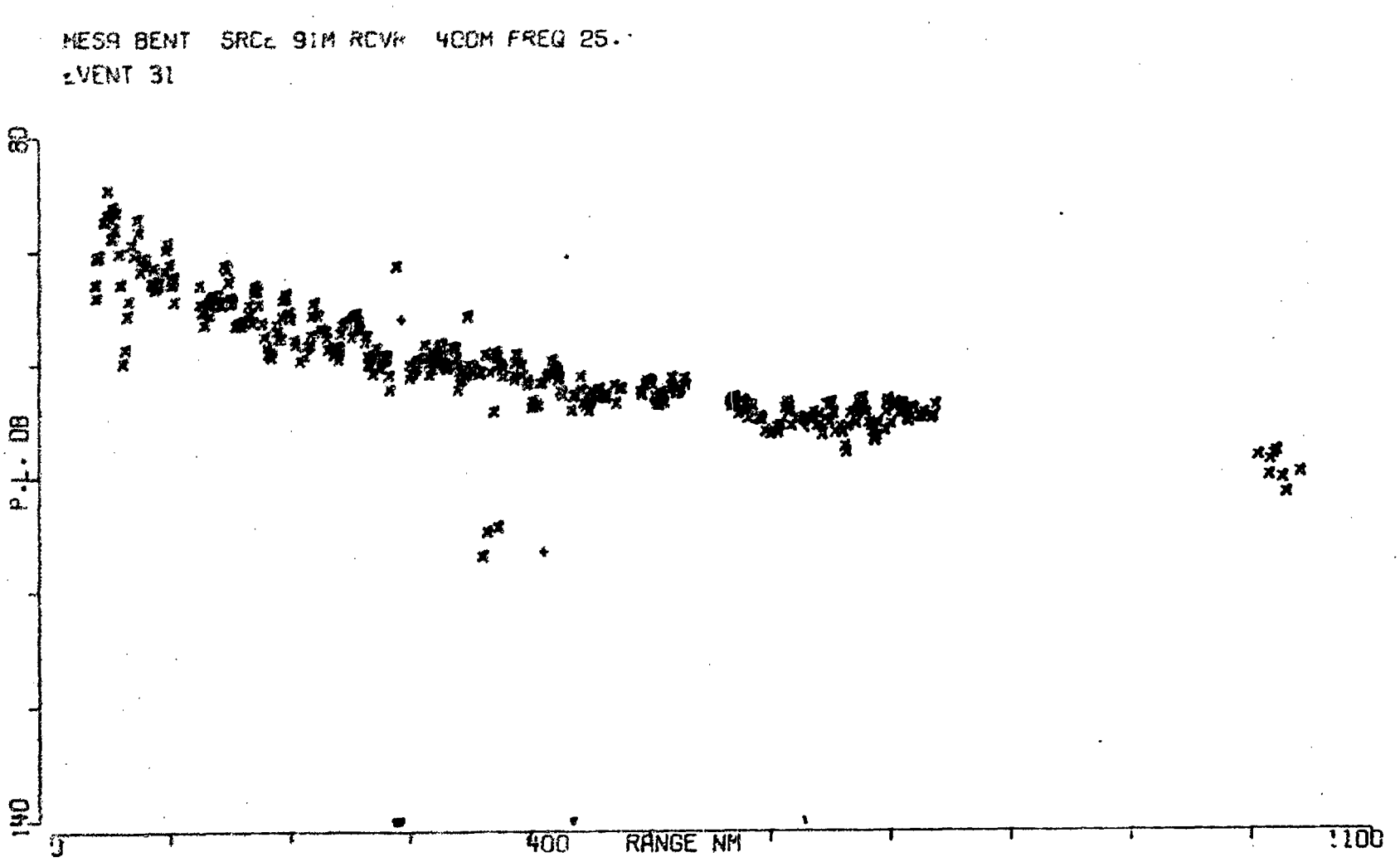
MESA BENT SRCE 91M RCVR 400M FREQ 25.
EVENT 31
60
P.L. DB
140
0
400
RANGE NM
1100

FIGURE B-2

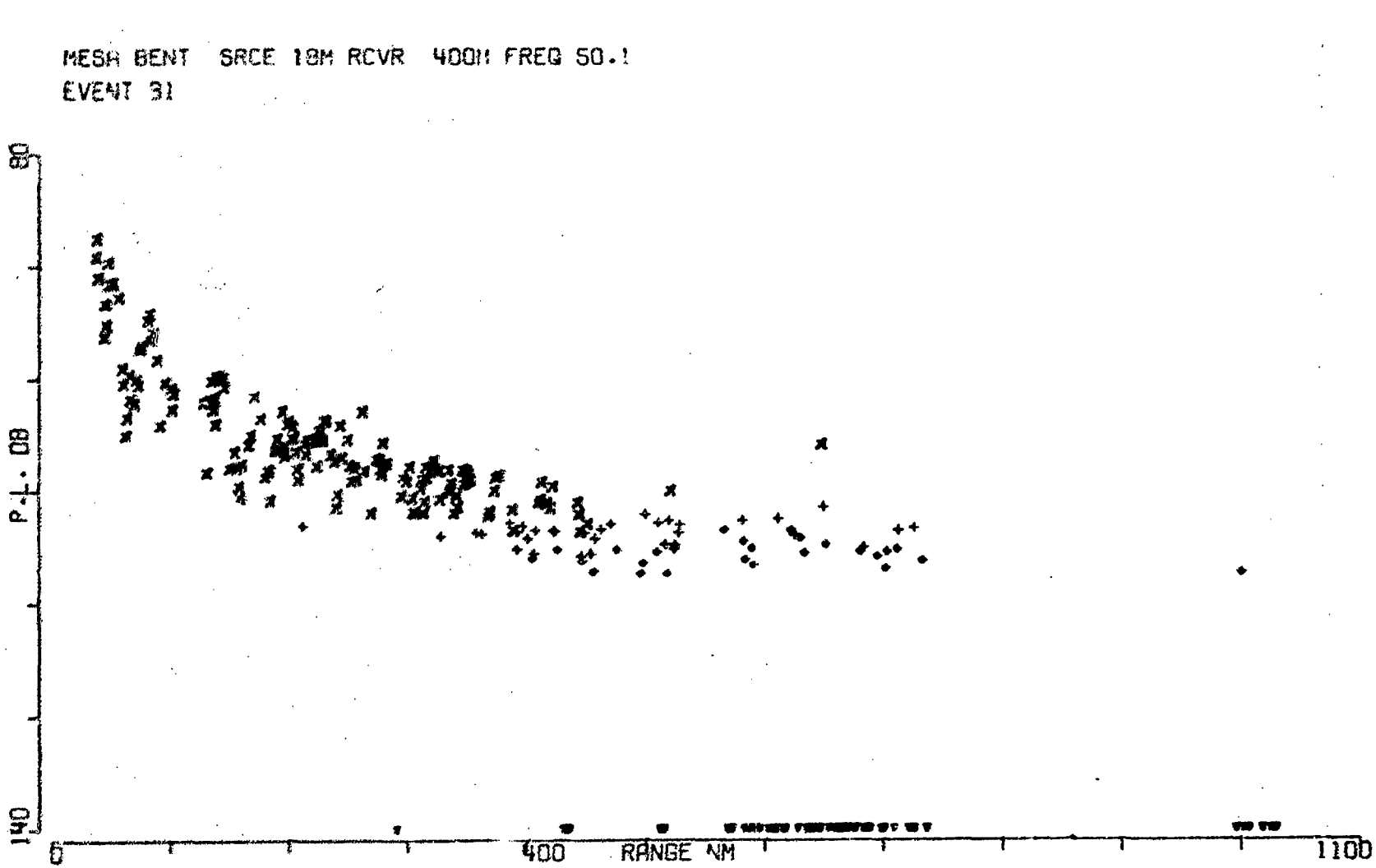
MESH BENT SRCE 10M RCVR 400M FREQ 50.1
EVENT 31
60
P.L. dB
140
0
400
RANGE NM
1100

FIGURE B-3

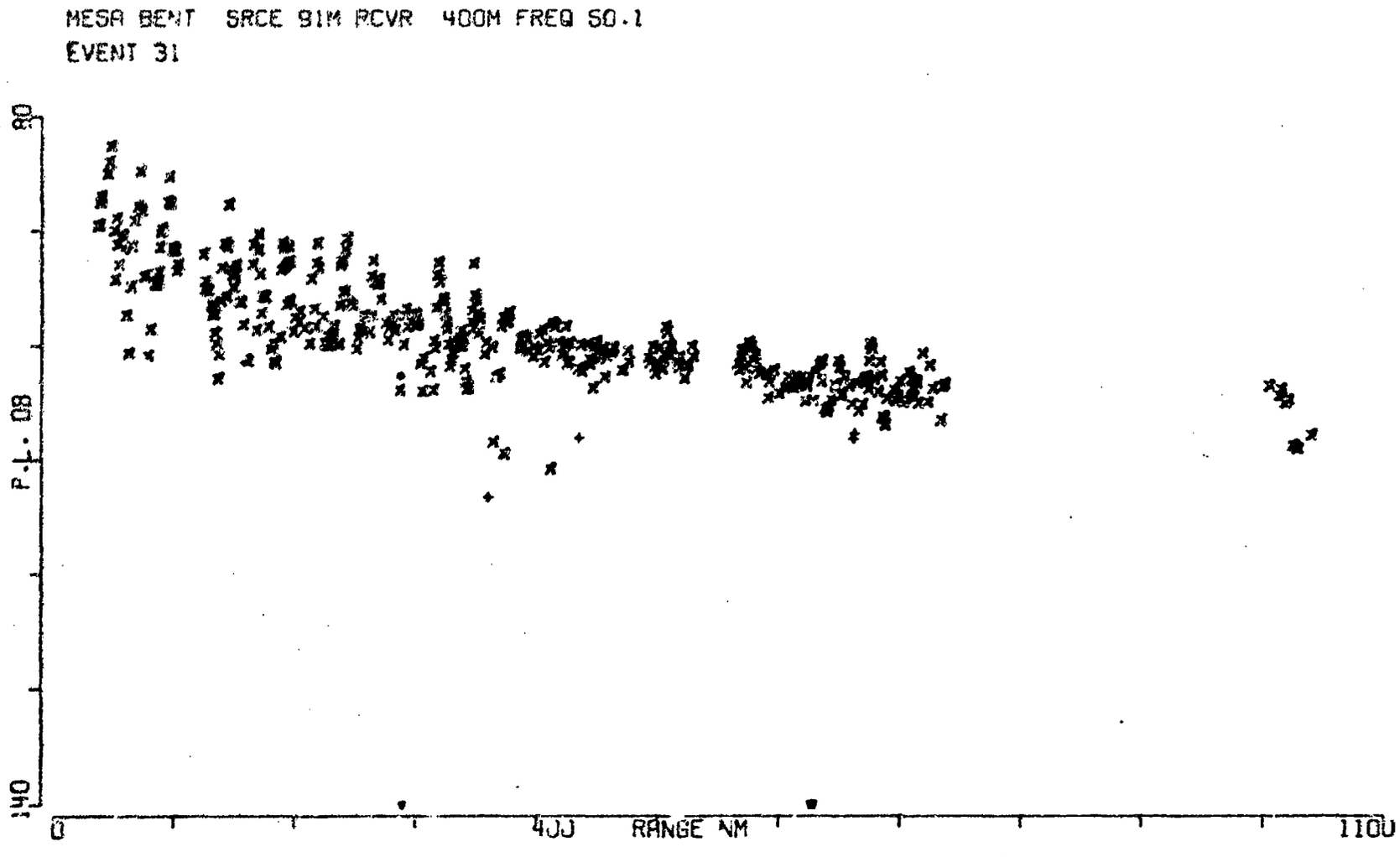
MESA BENT SRCE 91M RCVR 400M FREQ 50.1
EVENT 31
80
P.L. DB
140
0
400
RANGE NM
1100

FIGURE B-4

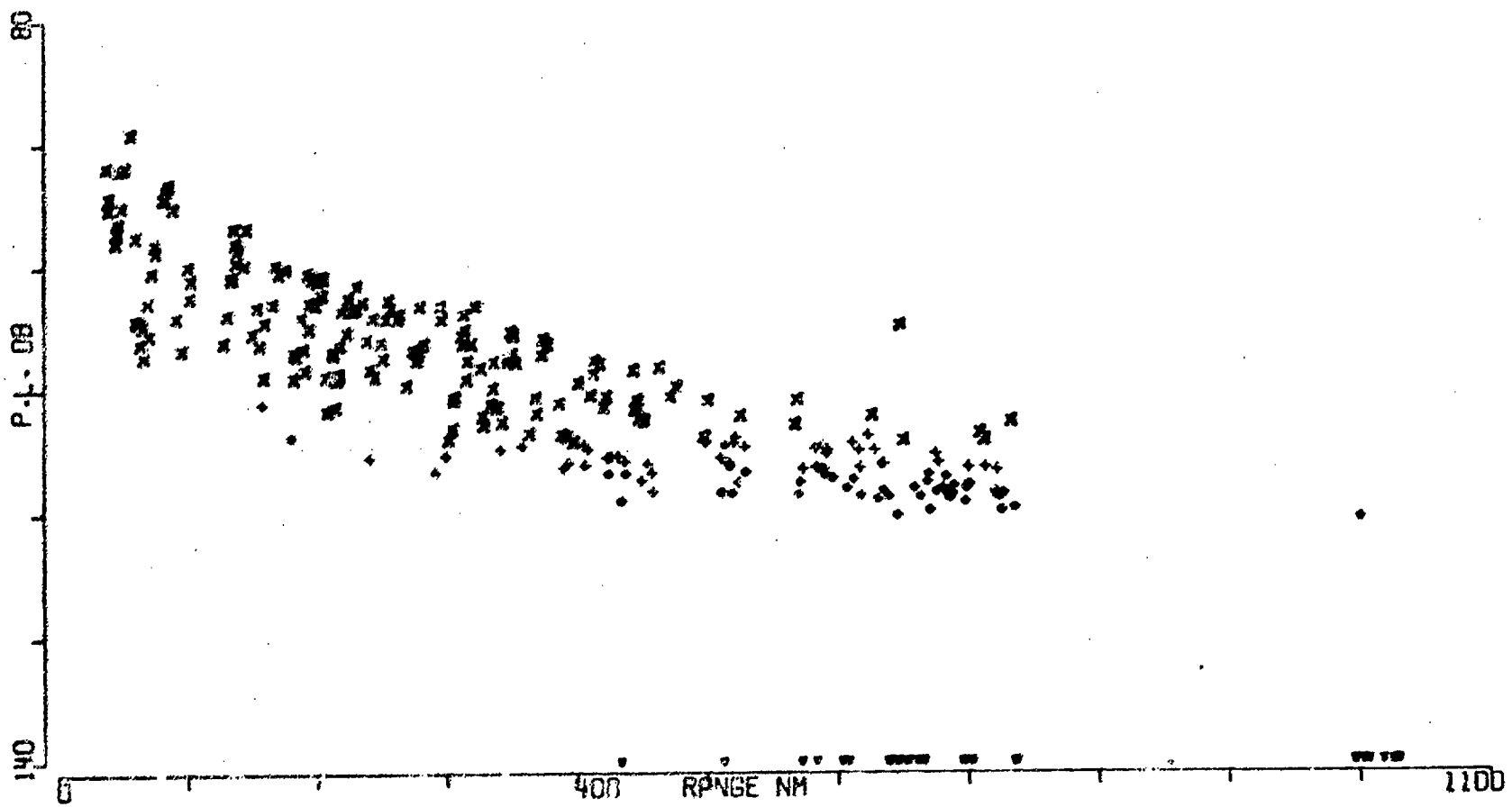
MESA BENT SRCE 18M RCVR 400M FREQ100.0
EVENT 31
80
P-L, DB
140
0
400
RANGE NM
1100

FIGURE B-5

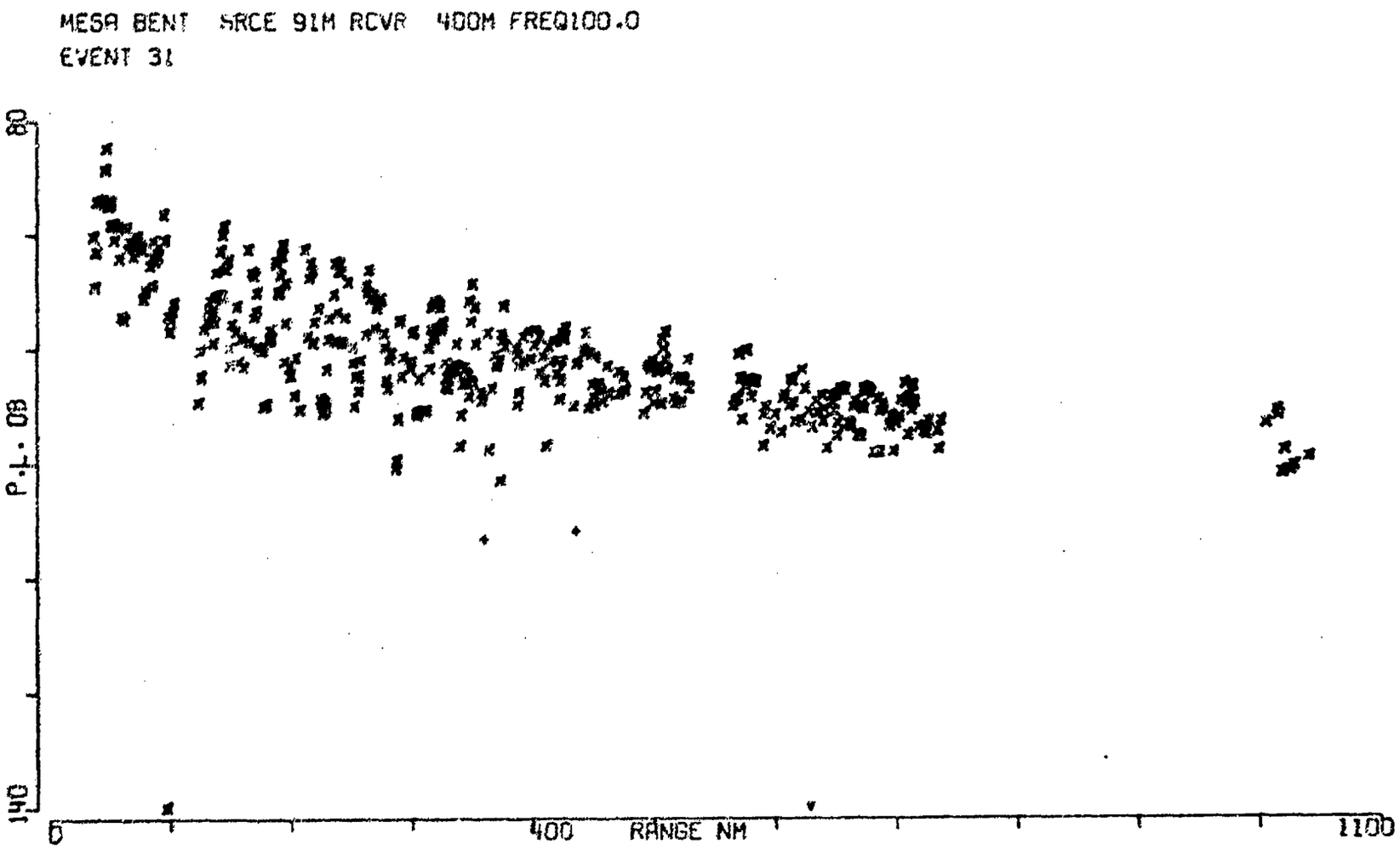
MESA BENT SRCE 91M RCVR 400M FREQ100.0
EVENT 31
80
P.L. dB
140
0
400
RANGE NM
1100

FIGURE B-6

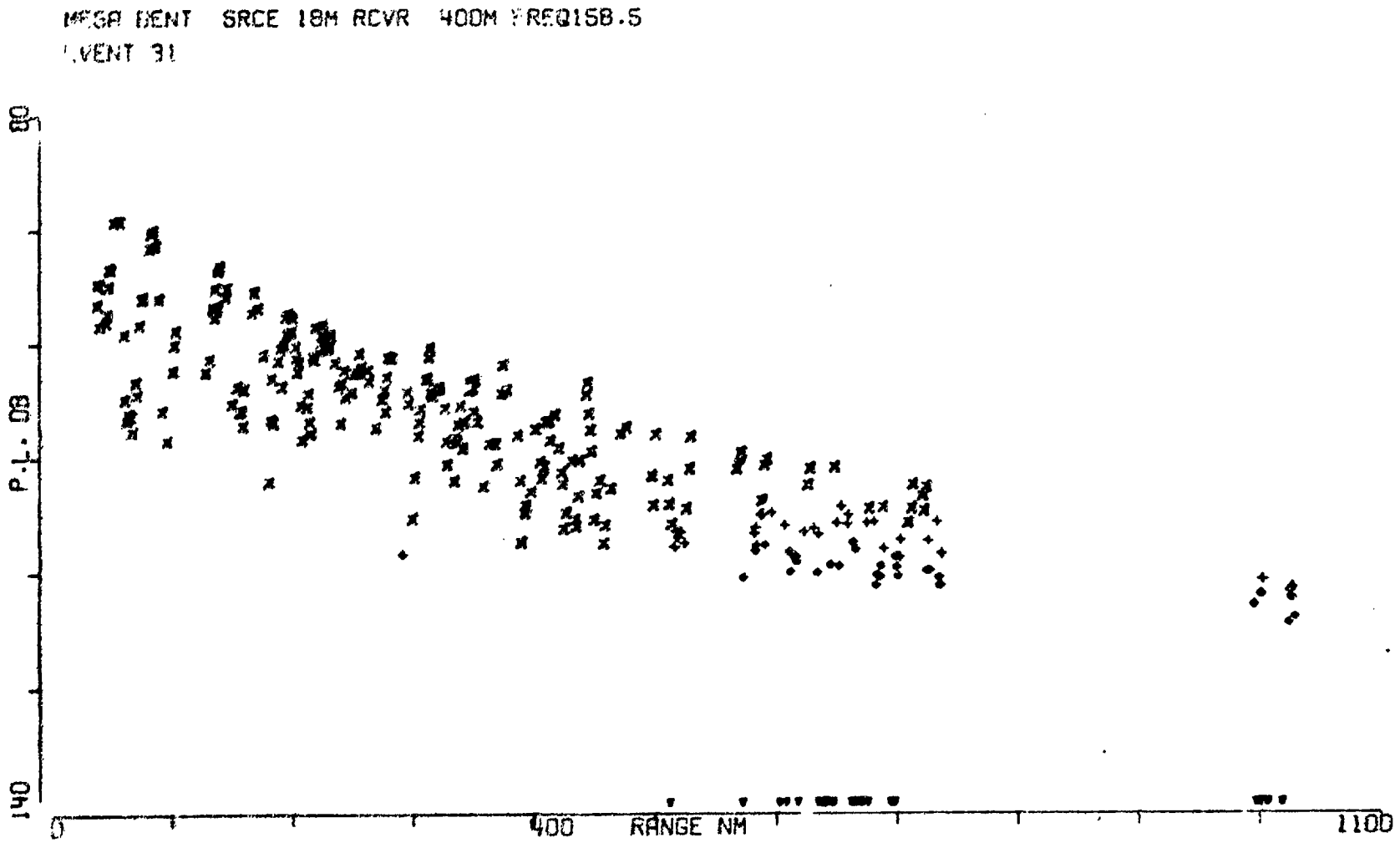
MEGA DENT SRCE 18M RCVR 400M FREQ158.5
EVENT 31
P.L. DB
60
140
0
400
RANGE NM
1100

FIGURE B-7

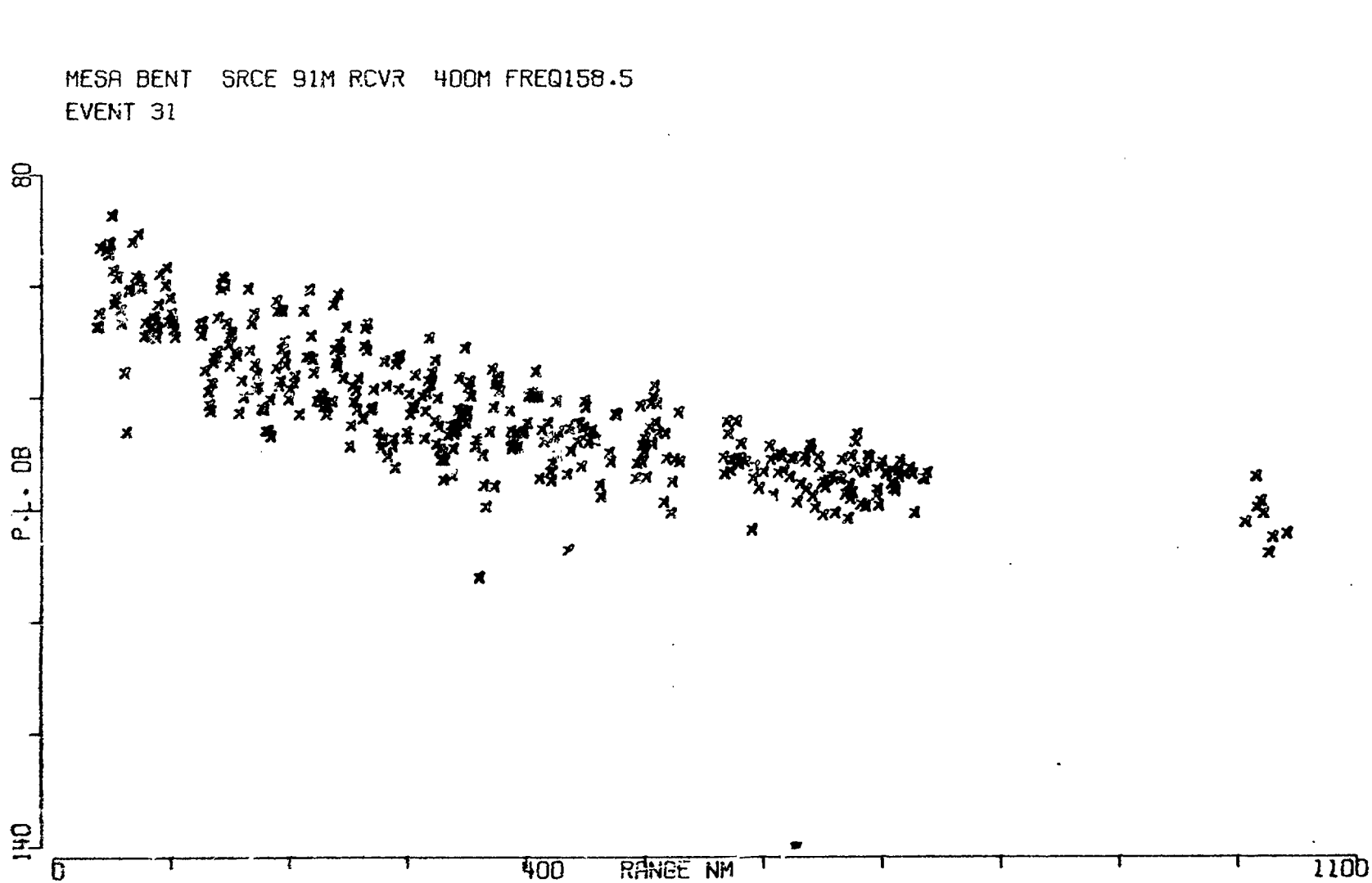
MESA BENT SRCE 91M RCVR 400M FREQ158.5
EVENT 31
80
140
P.L. DB
0
400
RANGE NM
1100

FIGURE B-8

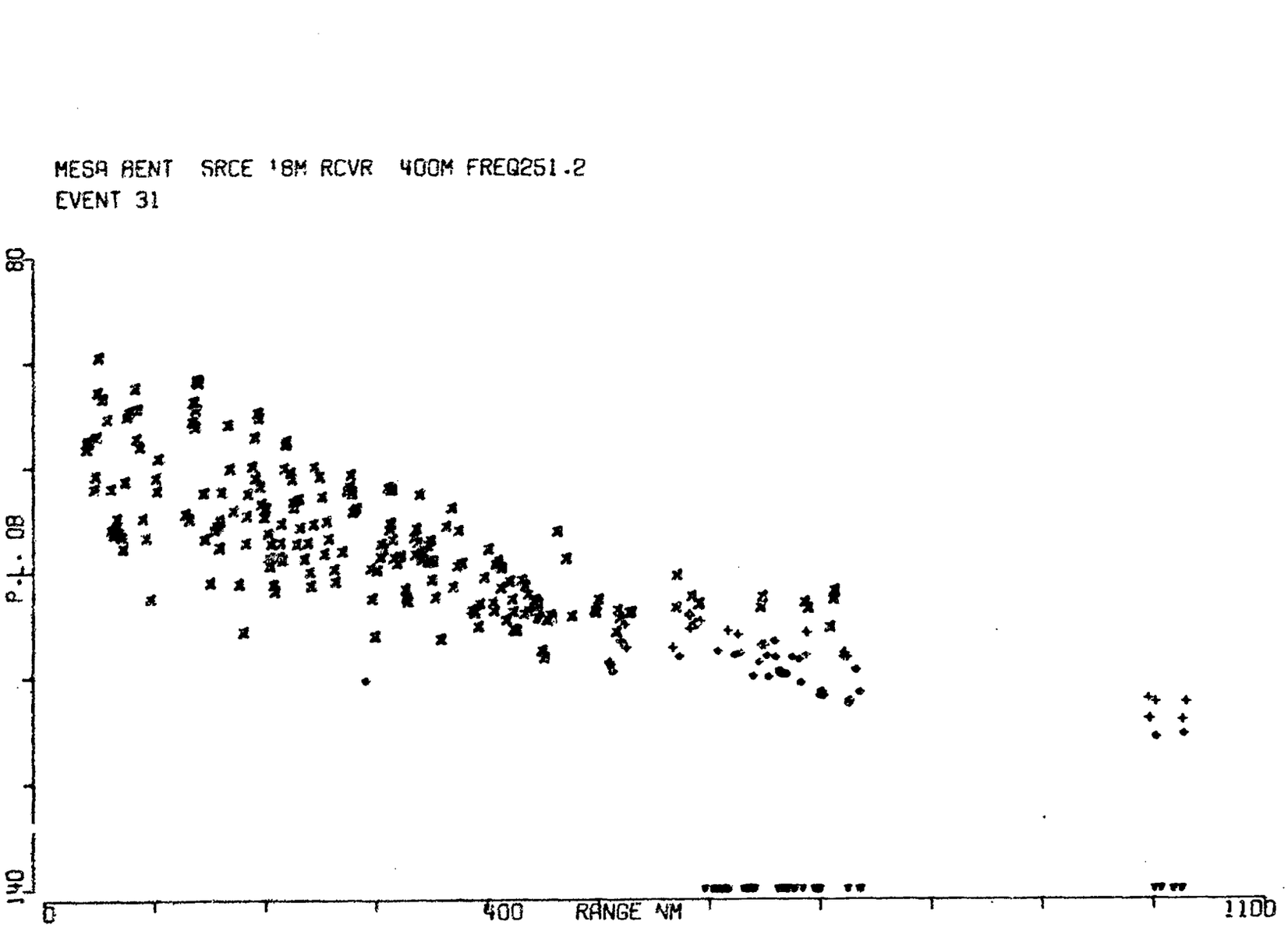
MESA BENT SRCE 18M RCVR 400M FREQ251.2
EVENT 31
80
P.L. DB
140
0
400
RANGE NM
1100

FIGURE B-9

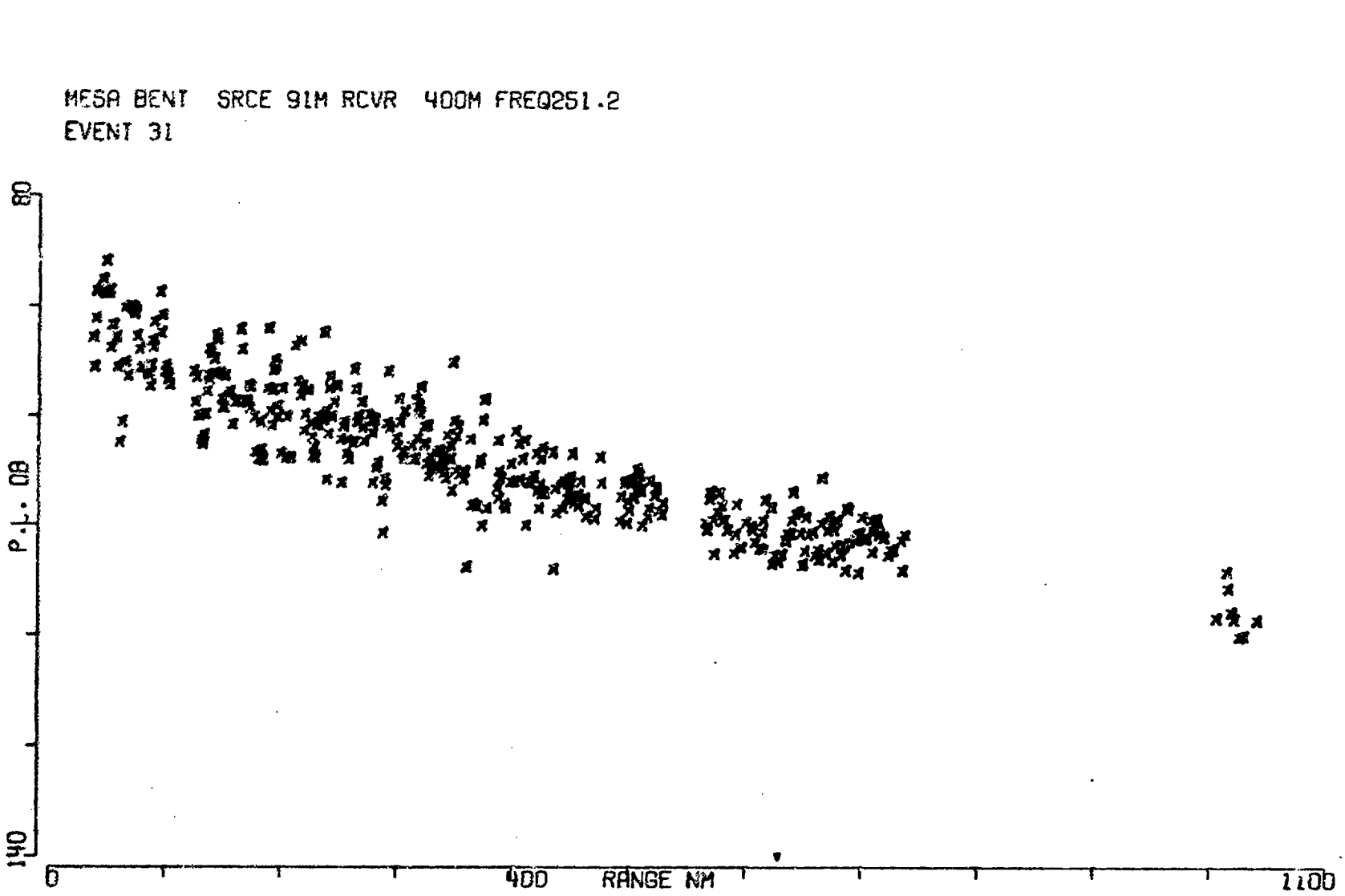
MESA BENT SRCE 91M RCVR 400M FREQ251.2
EVENT 31
80
P.L. dB
140
0
400
RANGE NM
1100

FIGURE B-10

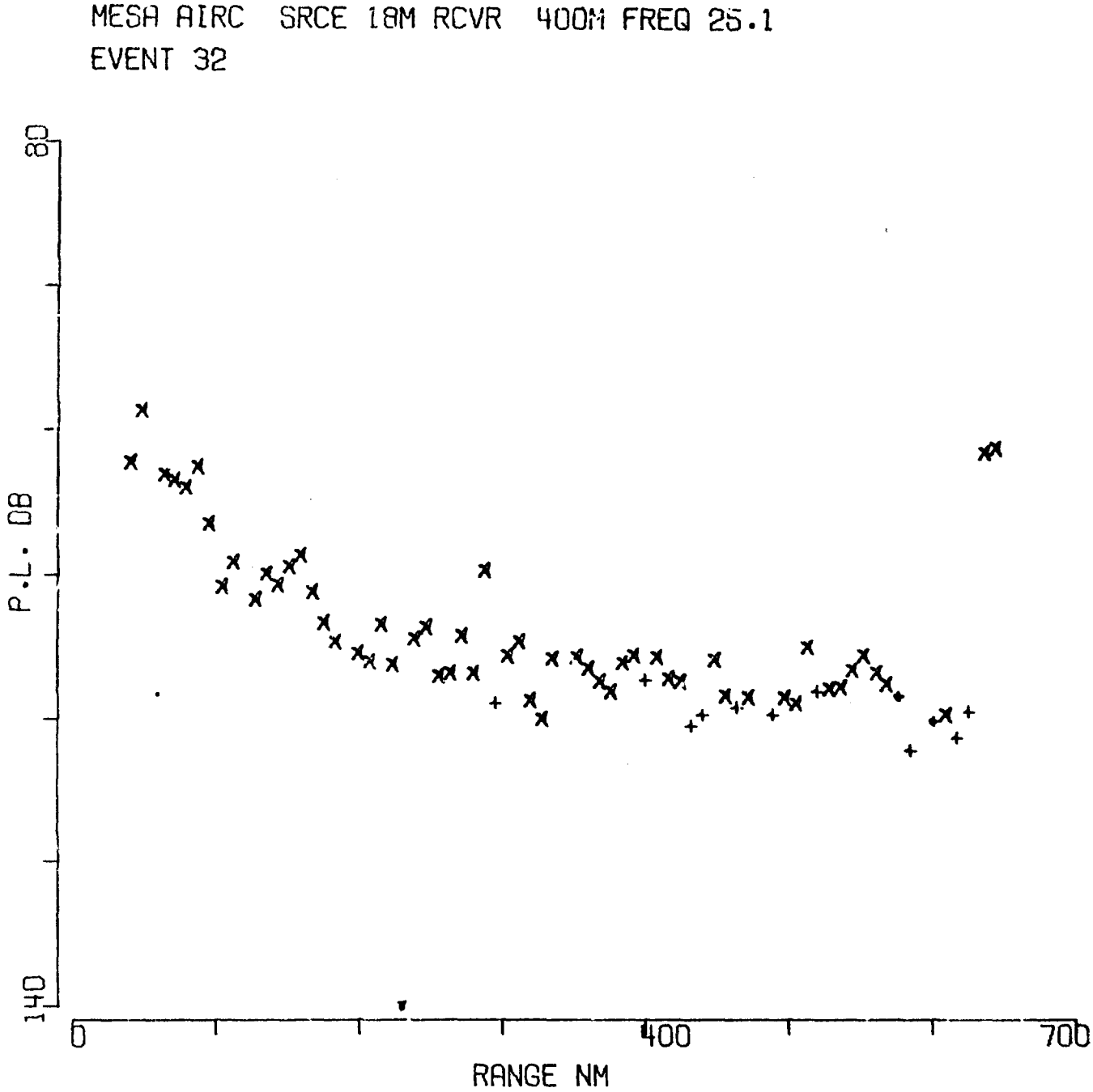
MESA AIRC SRCE 18M RCVR 400M FREQ 25.1
EVENT 32
80
140
P.L. DB
0
400
700
RANGE NM

FIGURE B-11

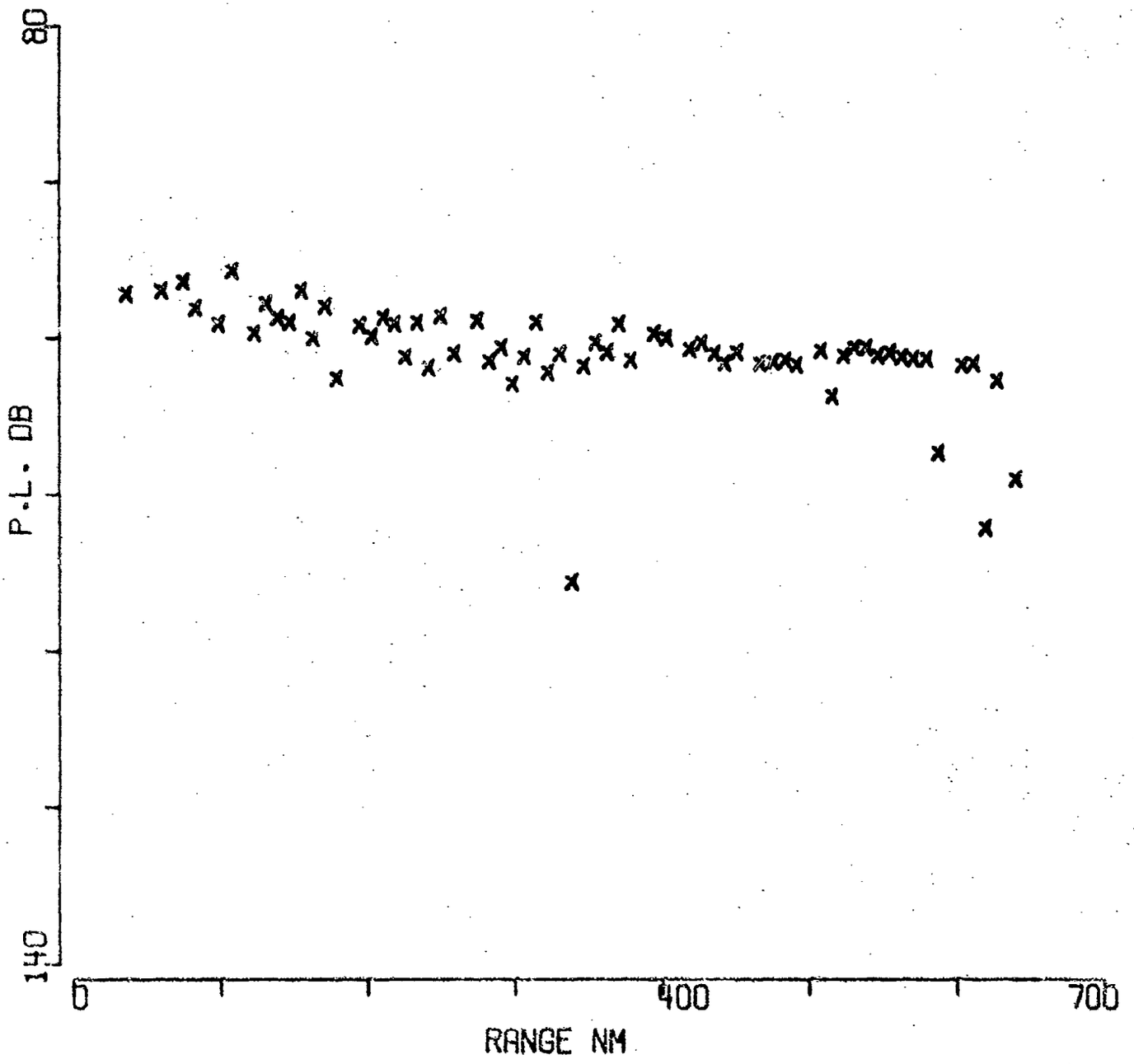
MESA AIRC SRCE 91M RCVR 400M FREQ 25.1
EVENT 32
80
140
P.L. DB
0
400
700
RANGE NM

FIGURE B-12

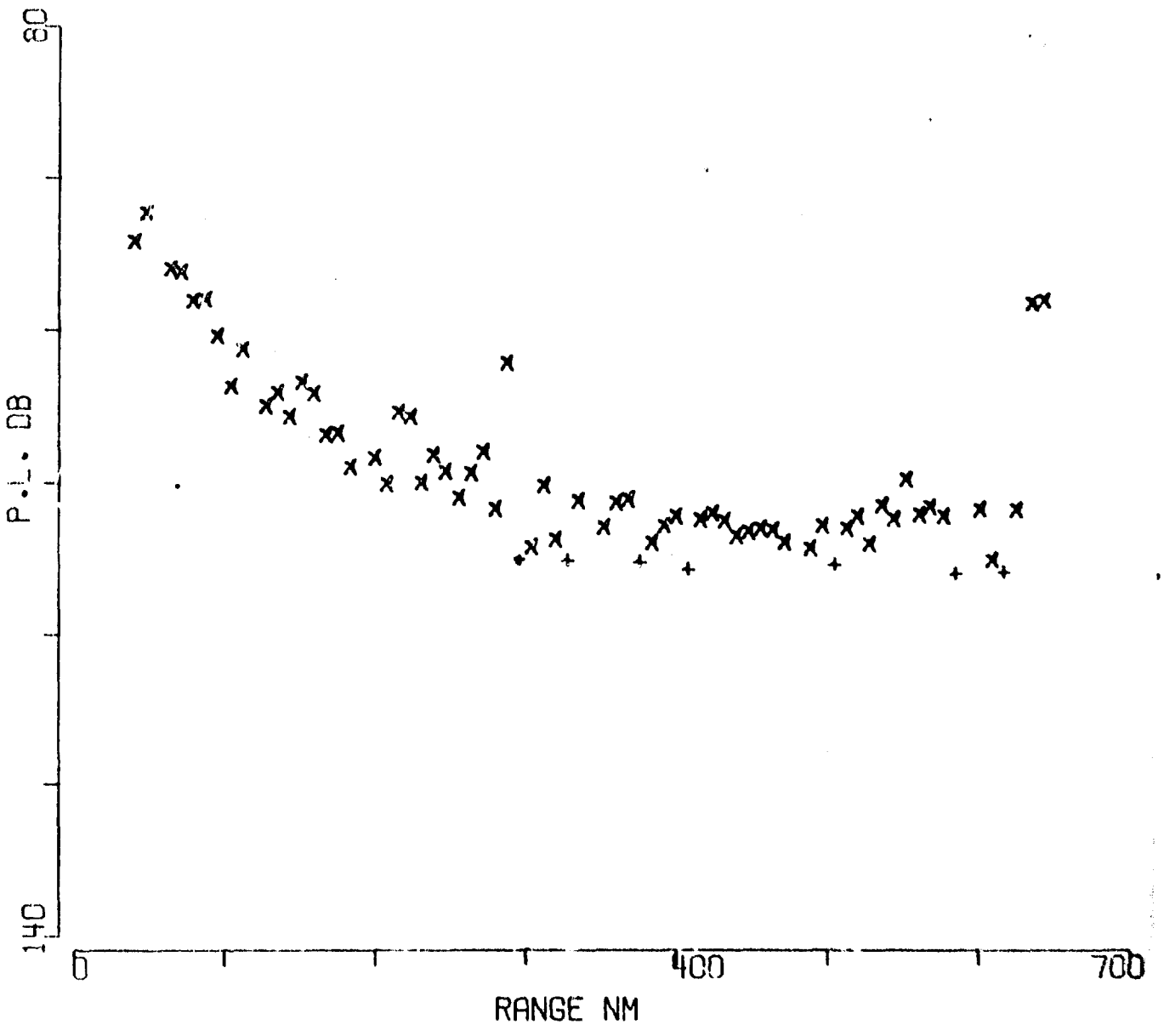
MESA AIRC SRCE 18M RCVR 400M FREQ 50.1
EVENT 32
80
140
P.L. DB
0
400
700
RANGE NM

FIGURE B-15

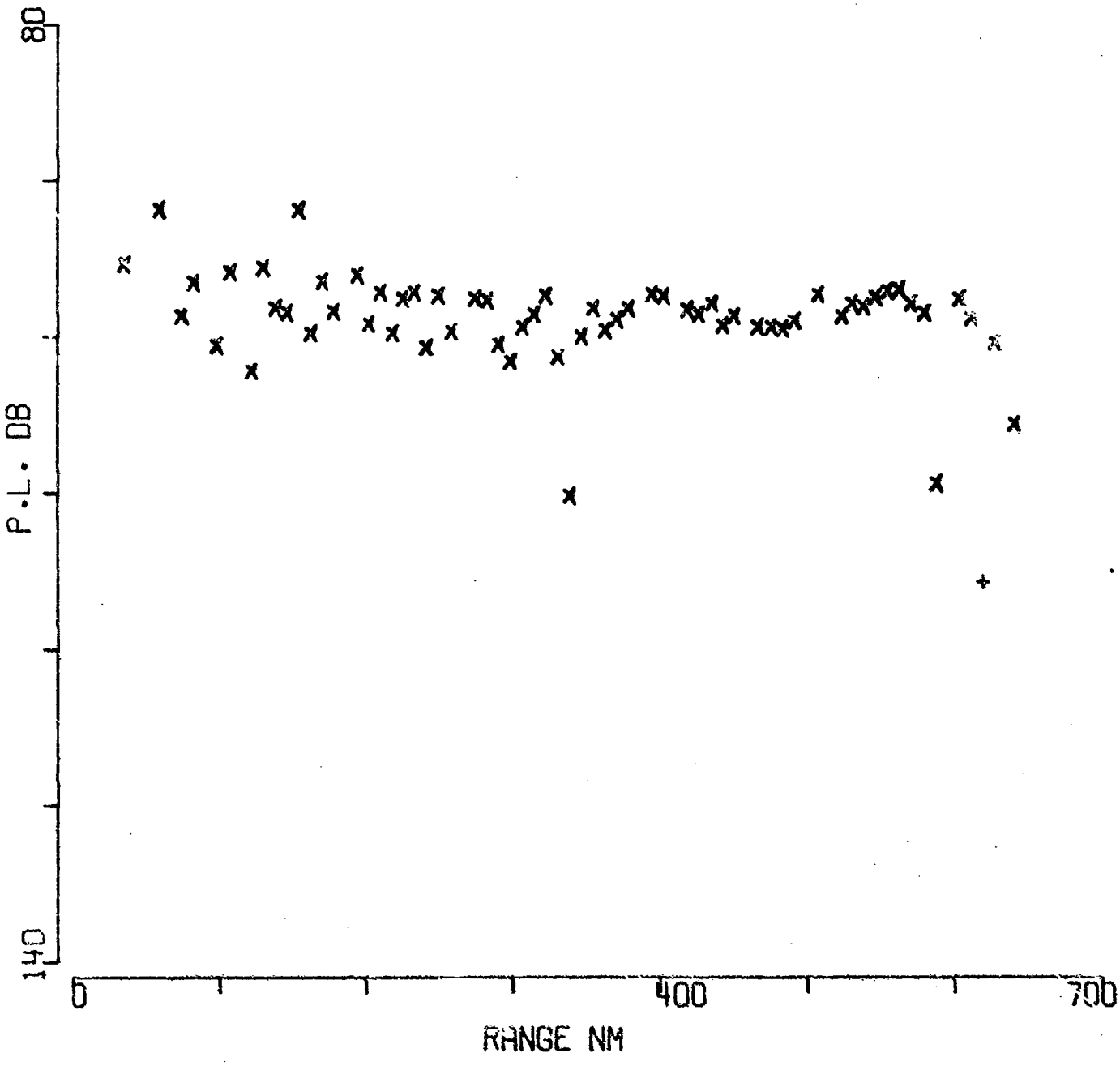
MESA AIRC SRCE 91M RCVR 400M FREQ 50.1
EVENT 32
80
140
P.L. DB
0
400
700
RANGE NM

FIGURE B-14

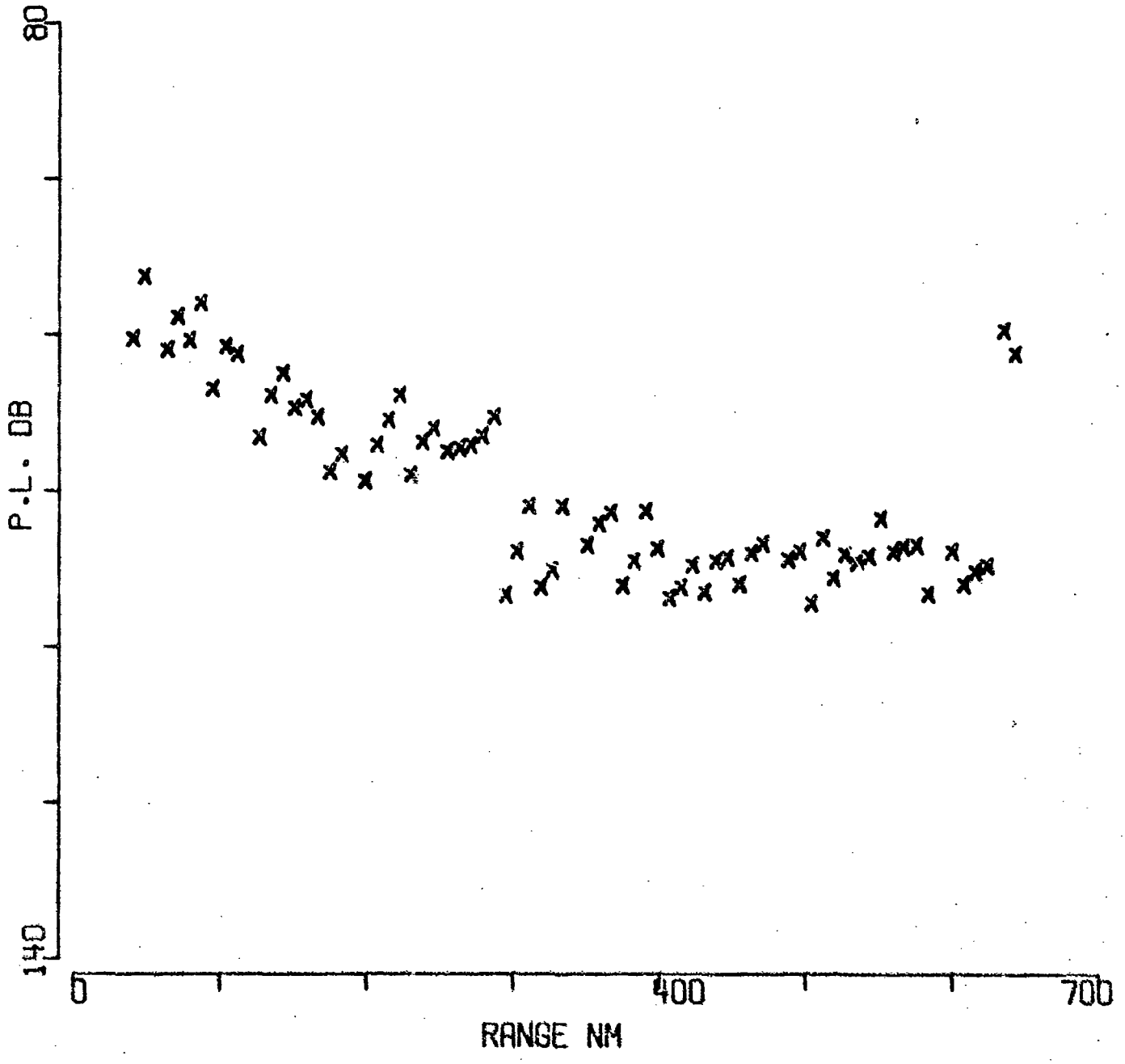
MESA AIRC SRCE 18M RCVR 400M FREQ100.0
EVENT 32
80
140
P.L. DB
0
400
700
RANGE NM

FIGURE B-15

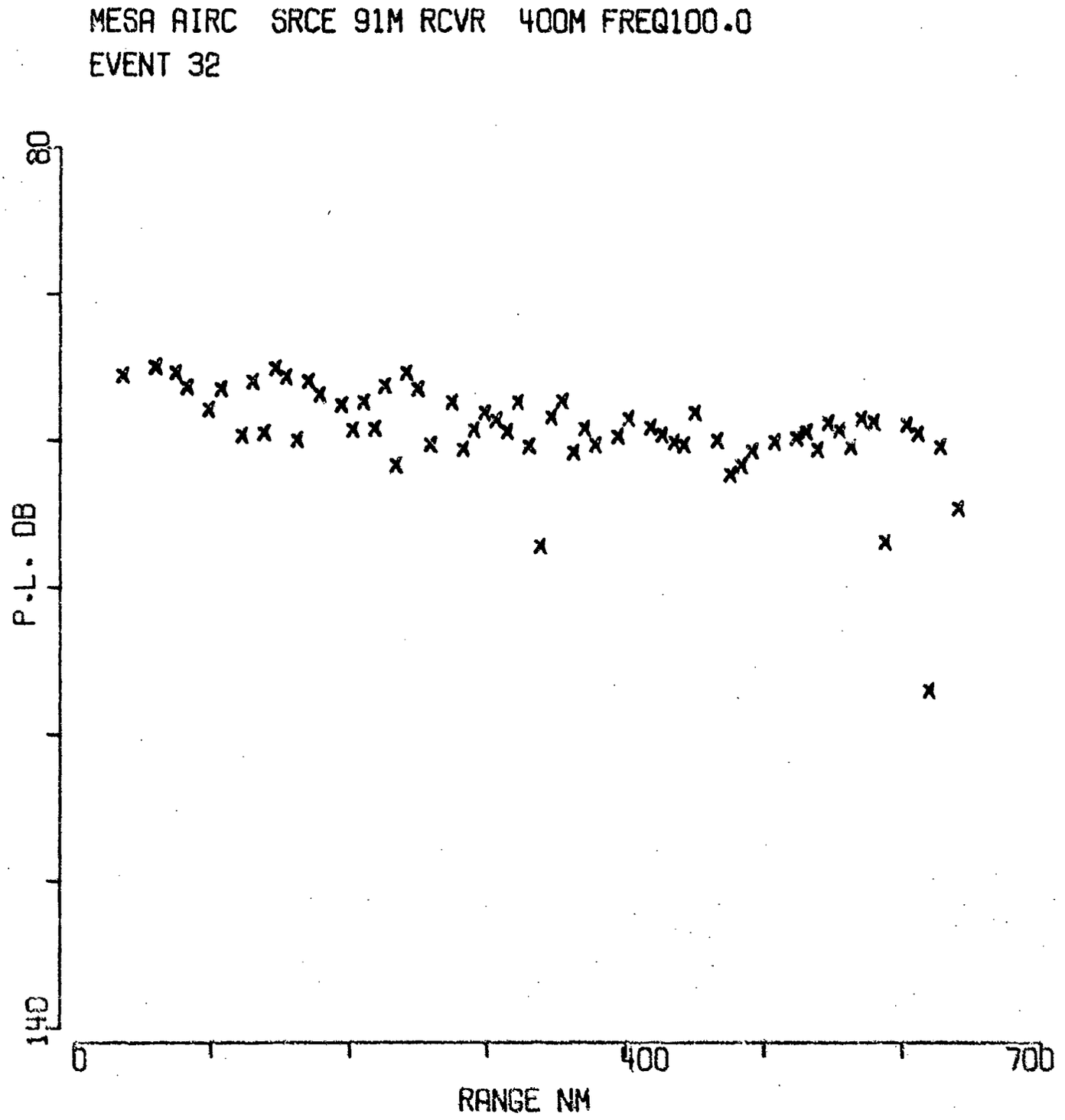
MESA AIRC SRCE 91M RCVR 400M FREQ100.0
EVENT 32
80
140
P.L. DB
0
400
700
RANGE NM

FIGURE B-16

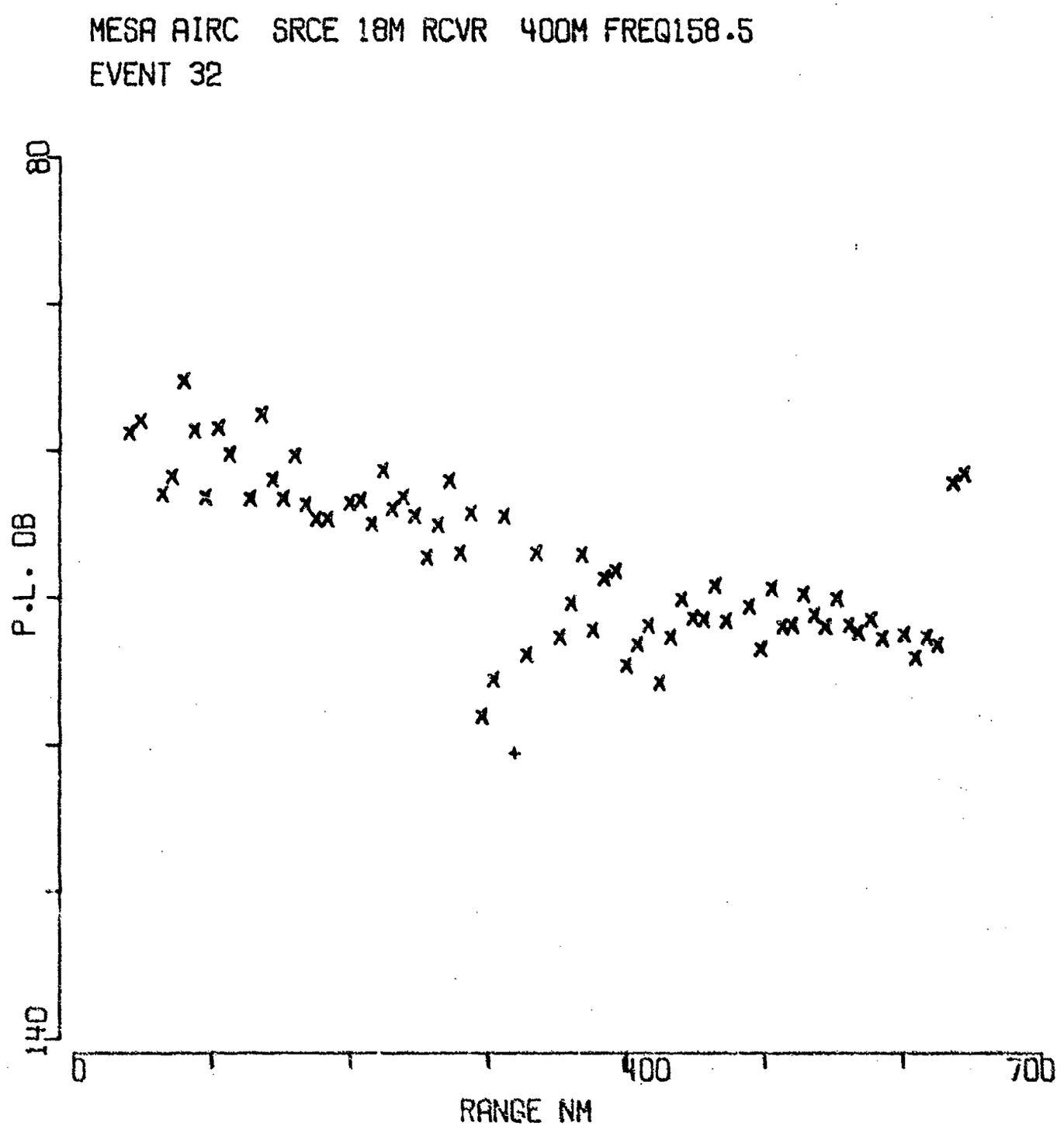
MESA AIRC SRCE 18M RCVR 400M FREQ158.5
EVENT 32
80
P.L. DB
140
0
400
700
RANGE NM

FIGURE B-17

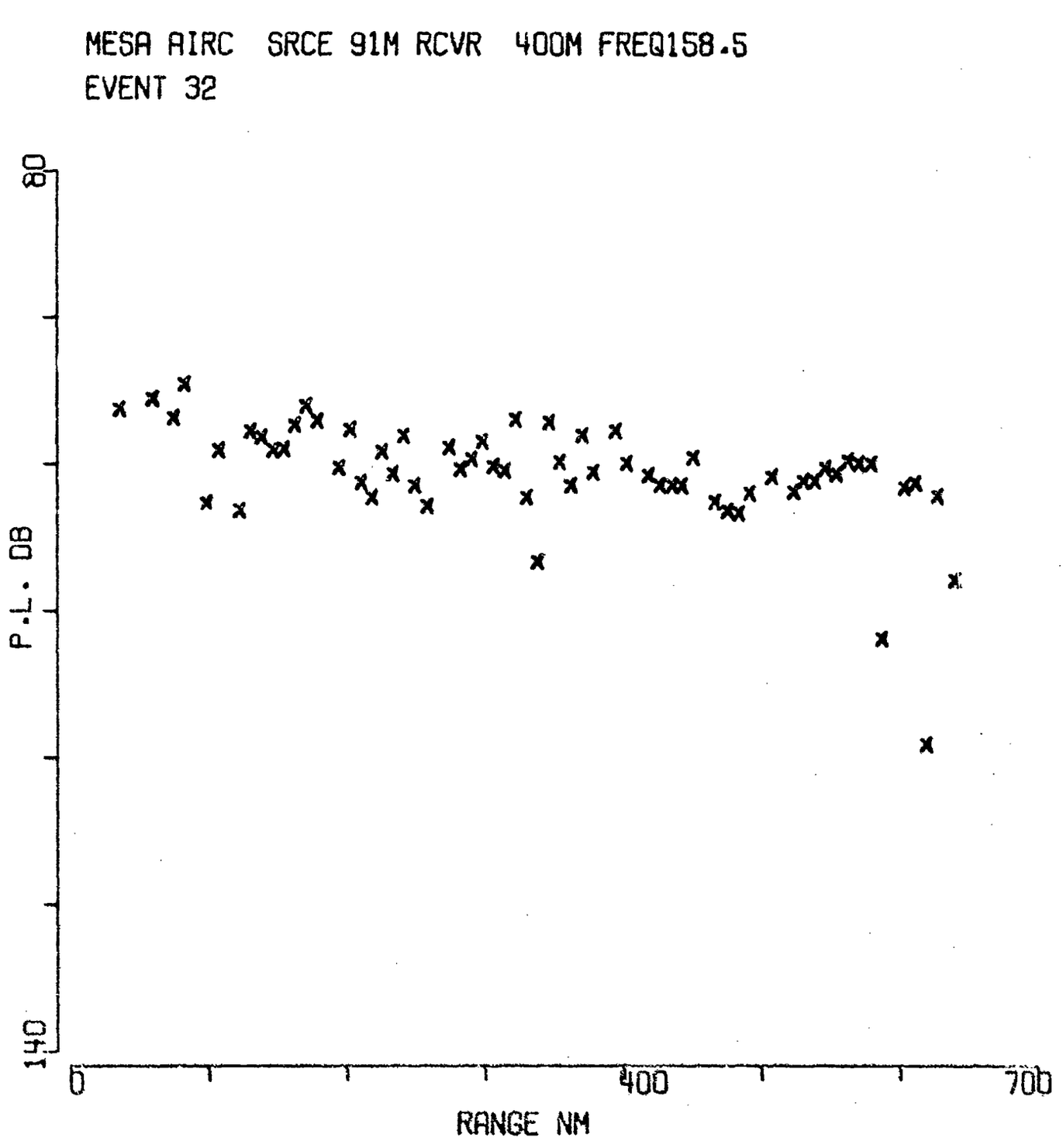
MESA AIRC SRCE 91M RCVR 400M FREQ158.5
EVENT 32
80
140
P.L. DB
0
400
700
RANGE NM

FIGURE B-18

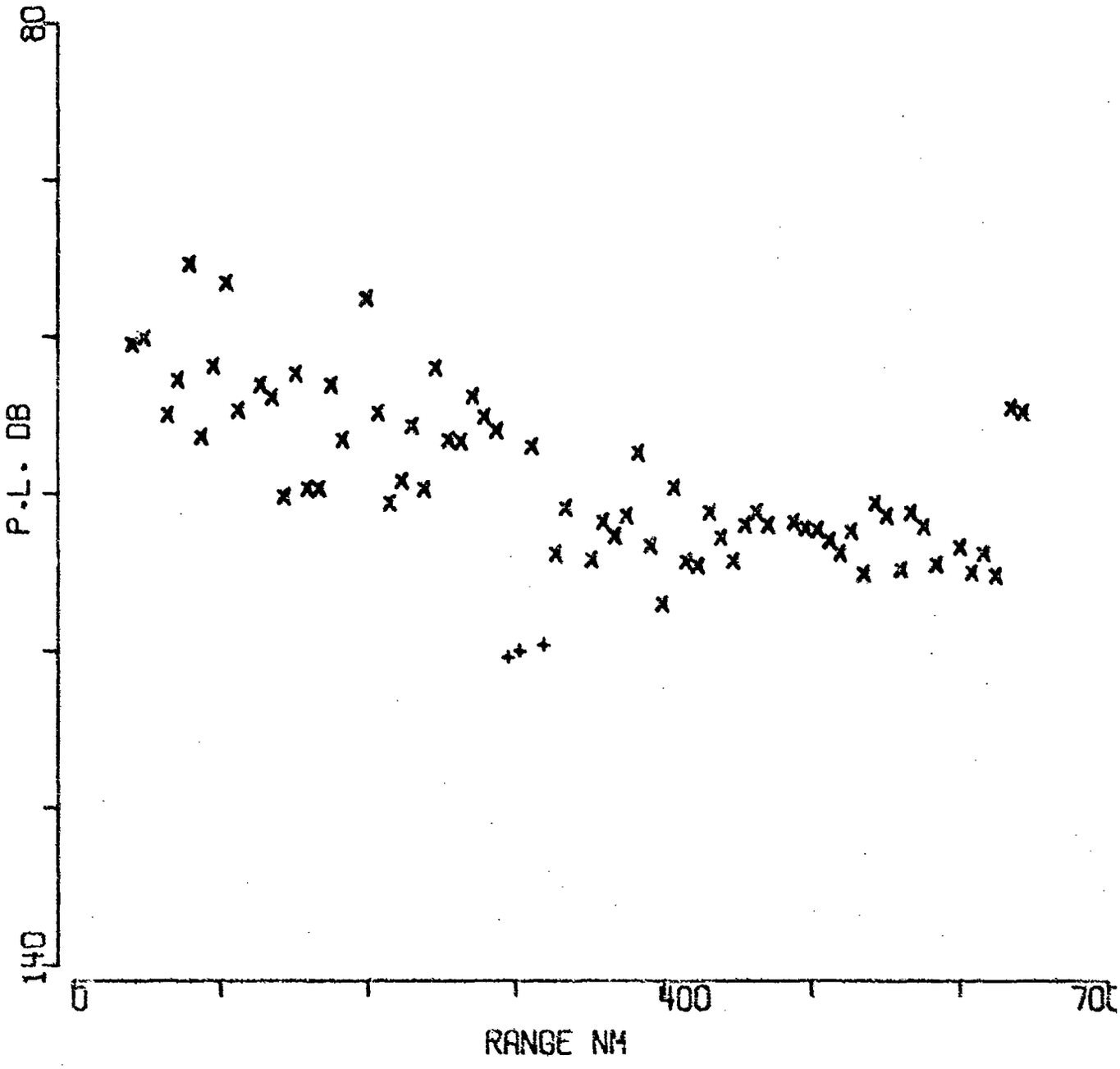
MESA AIRC SRCE 18M RCVR 400M FREQ251.2
EVENT 32
80
140
P.L. DB
0
400
700
RANGE NM

FIGURE B-19

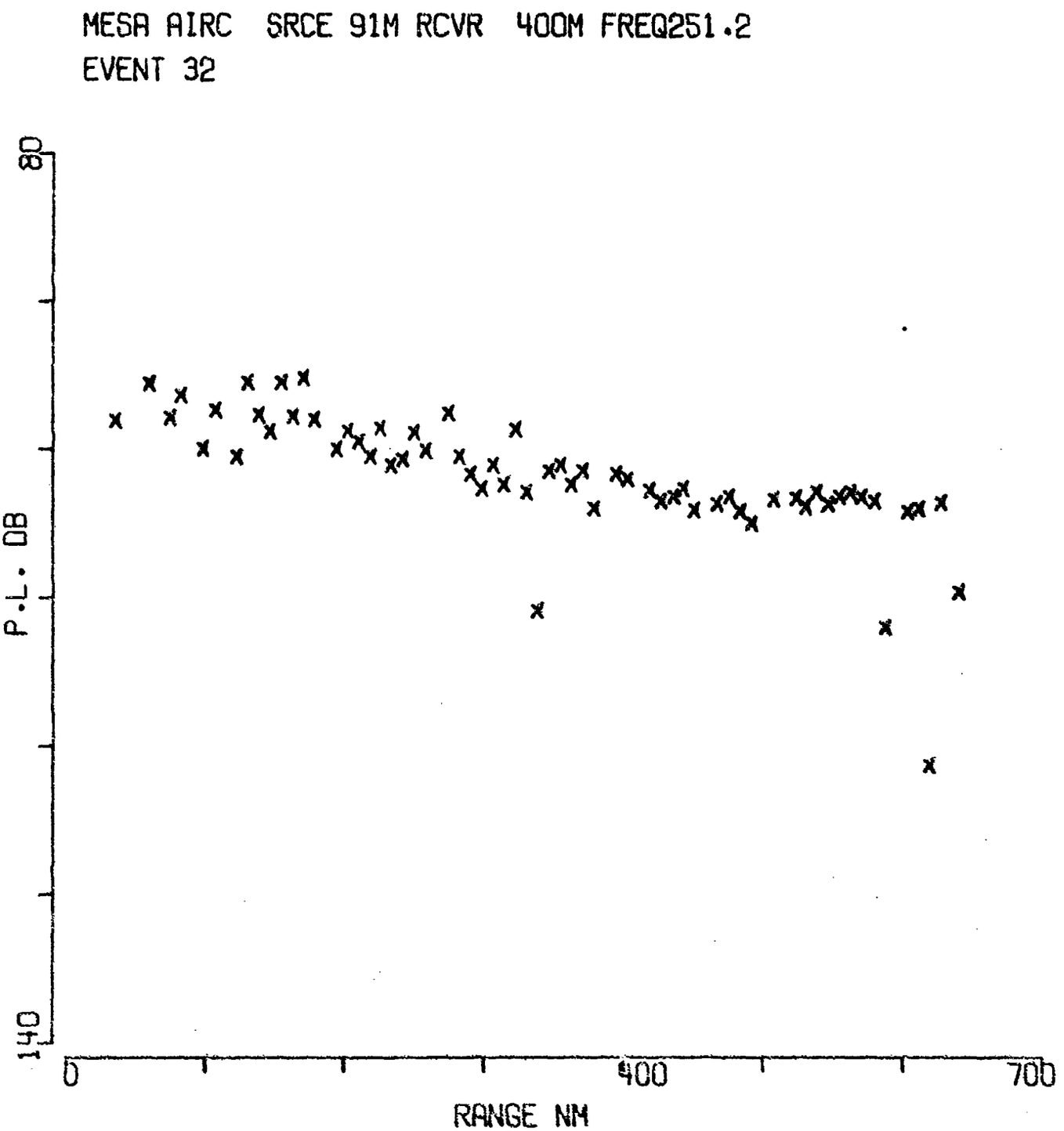
MESA AIRC SRCE 91M RCVR 400M FREQ251.2
EVENT 32
80
140
P.L. DB
0
400
700
RANGE NM

FIGURE B-20

APPENDIX C

QUALITY CONTROL OF THE ACODAC DATA ANALYSIS

(U) Meaningful interpretation of the experimental results requires that sufficient quality control be exercised during the data processing to minimize the errors introduced through the processing system and techniques. These errors must be small relative to the variations in shot-to-shot signal level that have been introduced by the transmission environment.

(U) Two studies were conducted at the Applied Research Laboratories of The University of Texas at Austin (ARL/UT) (Refs. 1 and 2) to determine repeatibility and compatibility of the digital SUS processor with analog processors. A summary of the results of these studies follows.

(U) 1. On a single ARL digitizing day, for repeated digitization, the energy in frequency bands for either shots or noise had standard deviations of 1% to 2%. The energy in the same bands of the calibration signal showed a similar spread.

(U) 2. The signal levels, as digitized, showed variations from day to day that yield 5% to 10% (5% ≅ 0.2 dB) deviations of energy in the selected bands before the calibration signal was used for compensation. Since the calibration signals associated with the data were similarly affected, adequate compensation can be made.

(U) 3. The times at which the automatic shot process (ARL/UT) detected a shot showed no fluctuations with repeated processing other than those to be expected from the temporal resolution imposed by the sampling rate (i.e., approximately 0.02 sec).

(U) 4. The standard deviations due to repeated processing of transmission loss for given frequency bands is of the order of 0.1 and 0.2 dB.

(U) 5. To prevent an introduction of frequency smearing due to mechanical variations in the analog record/playback procedures, a reference track should be used in any shot processor, whether analog or digital.

(U) 6. The stability of the ACODAC calibration signal analyzed showed a variation in power of only 1 dB over a 24 h period in data.

(U) 7. A comparison of two data segmentation techniques used in the digital calculation of total shot energy in a given frequency band and the shot energy calculated by the traditional analog method was performed using selected shots from the CHURCH GABBRO Exercise ACODAC data. The selected shots had different characteristics due to different propagation situations. To complete the study between the two digital techniques, a comparison was made with 700 shots from the CHURCH GABBRO shot runs.

(U) For the selected shots, which had a time duration of 25 to 40 sec, contiguous data blocks were transformed (FFT) and summed "coherently and incoherently" and compared to a digital simulation of an analog system (50 Hz at 1/3 octave). It was found that when equivalent integration times are used the incoherent summation gave the best comparison to the analog system (within 0.1 dB) for data segmentation from 27.2 to 0.85 sec blocks. The variance from the analog system using the coherent summation showed a maximum deviation of 1.4 dB with 0.85 sec data blocks. Using 6.8 sec data blocks (ARL/UT system), the variance for the coherent sum was 0.01 to 0.5 dB. It is apparent that on a shot-to-shot basis the difference between all three techniques are data independent.

(U) The comparison of the total energy calculations for the 700 shots for the coherent and incoherent summation techniques show that the ensemble mean of the difference between the two techniques is 0.1 dB or less, with an rms difference, that varied with frequency band and integration time, of less than 1.0 dB.

(U) 8. For the shot data from the SQUARE DEAL Exercise, the shot duration is on the order of 10 sec. Using a 6.8 sec data segment, a comparison between the coherent and incoherent techniques showed a mean of 0.02 dB and a rms value of 0.25 dB.

(U) 9. For the CHURCH ANCHOR Exercise, the majority of the shot durations fit into one data segment or FFT.

(U) 10. The choice that a shot processor makes on the two digital processing segmentation techniques is based on the hardware/software configuration of the processing system, length of data segments, shot duration, available funds and, of course, the accuracy required in the energy calculation relative to other sources of system error. For a software FFT implementation, for example, the computation economy (depending on the shot duration) favors the coherent summation by a factor of two or three. For a hardware FFT, this savings is not present.

(U) 11. A comparison of the ARL/UT shot processing system with systems at other facilities show the following results on a set of shots (70) from the SQUARE DEAL Exercise. The comparisons are for propagation loss in a 50 Hz 1/3-octave frequency band.

PROCESSOR	MEAN DIFFERENCE (dB)	STD. DEV. (dB)
ARL Digital/ARL Analog	0.07	0.51
ARL January/ARL June	0.02	0.14
ARL/WHOI	-0.99	1.45
ARL/NUSC	-0.47	0.51
ARL/WECO	1.20	1.20

(U) WHOI - Woods Hole Oceanographic Institution
NUSC - Naval Undersea Systems Center
WECO - Western Electric Co.

(U) Analysis of the total ACODAC measurement accuracy is the subject of Ref. 3, which accounts for all errors occurring from the explosive sources to the final digital processing of the SUS data. Thus, the error analysis of Ref. 1 is included in the study of Ref. 3. As an example the error estimates for the ACODAC system include those associated with the hydrophone and preamplifier, the transmission cable, the data amplifier, the tape recorder, and the calibration system. The conclusion reached in this study is that for SUS measurements an uncertainty of ±2.48 dB to ±2.60 dB can be expected in the propagation loss estimation, principally because of uncertainty in the SUS source levels.

References:

1) "Quality Control Analysis of SUS Processing from ACODAC Data," S. K. Mitchell and T. D. Plemons, Applied Research Laboratories Technical Memorandum No. 73-42 (ARL-TM-73-42), 20 December 1973.

2) Weinstein, M. S., and Ellis, G., "SUS Signal Data Processing (U), Final Report on Investigations Conducted Under the Diagnostic Plan for CHURCH ANCHOR and SQUARE DEAL Shot Data" (U), April 14, 1975, Underwater Systems. CONFIDENTIAL

3) "Analysis of ACODAC Measurement Accuracy," BK Dynamics, Inc., TR-3186, Rockville, Maryland, March 1974.

December 1974

DISTRIBUTION LIST FOR
ARL-TR-74-53
UNDER CONTRACT N00014-70-A-0156, Task 0023
CONFIDENTIAL, ~~EXEMPT 3~~ GDS

Copy No.

Chief of Naval Operations
Department of the Navy
Washington, DC 20350
1 Attn: OP-951
2 955F
3 981H

4 - 5 Commander
Third Fleet
FPO San Francisco, CA 96610

6 Commander
Submarine Forces
U. S. Pacific Fleet
FPO San Francisco, CA 96610

7 Commander,
Oceanographic Systems Pacific
Box 1390
FPO San Francisco, CA 96610

8 Commander
Naval Sea Systems Command
Department of the Navy
Washington, DC 20362
Attn: Code 06H

Project Manager
Antisubmarine Warfare Systems Project
Department of the Navy
Washington, DC 20360
9 Attn: ASW-11
10 111
11 13

Distribution List for ARL-TR-74-53, N00014-70-A-0166, Task 0023

Copy No.

Commander
Naval Electronic Systems Command
Department of the Navy
Washington, DC 20362
12 Attn: PME-124
13 124/TA
14 124/20
15 124/30
16 124/40
17 124/60

18 Oceanographer of the Navy
Hoffman Building
200 Stovall Street
Alexandria, VA 22332

Chief of Naval Research
Department of the Navy
Arlington, VA 22217
19 Attn: Code 102-08
20 - 22 102-08C
23 431
24 212
25 - 26 AESD

Commander
Naval Oceanographic Office
Department of the Navy
Washington, DC 20373
27 Attn: Commander
28 - 29 Code 6130
30 06

31 Director
Center for Naval Analysis
Arlington, VA 22217
Attn: CAPT C. Woods

32 - 33 Commander
Naval Undersea Center
San Diego, CA 92132

Officer-in-Charge
New London Laboratory
Naval Underwater Systems Center
New London, CT 06320
34 Attn: Officer-in-Charge
35 Code TA

Distribution List for ARL-TR-74-53, N00014-70-A-0166, Task 0023

Copy No.

Director
Naval Research Laboratory
Washington, DC 20390
36 Attn: Director
37 Code 2627
38 8160

Commander
Naval Surface Weapons Center
White Oak Laboratory
Silver Spring, MD 20910
39 Attn: Commander
40 Code 021

41 Commanding Officer
Fleet Numerical Weather Central
Monterey, CA 93940

42 Commander
Naval Ship Research and Development Center
Bethesda, MD 20034

Commander
Naval Air Development Center
Warminster, PA 18974
43 Attn: Commander
44 Code 205

45 - 46 Commanding Officer and Director
Defense Documentation Center
Defense Services Administration
Cameron Station, Building 5
5010 Duke Street
Alexandria, VA 22314

47 Arthur D. Little, Inc.
Acorn Park
Cambridge, MA 02140
Attn: Dr. G. Raisbeck

48 B-K Dynamics, Incorporated
15825 Shady Grove Road
Rockville, MD 20850
Attn: Mr. A. E. Fadness

Distribution List for ARL-TR-74-53, N00014-70-A-0166, Task 0023

Copy No.

Bell Telephone Laboratories
1 Whippany Road
Whippany, NJ 07981
49 Attn: Dr. G. Fox
50 Dr. T. Phillips

Hawaii Institute of Geophysics
2525 Correa Road
Honolulu, HI 96722
51 Attn: Mr. M. Odegard
52 Dr. G. Woollard

University of California, San Diego
Marine Physical Laboratory of the
Scripps Institution of Oceanography
San Diego, CA 92132
53 Attn: Director
54 Dr. G. B. Morris

55 Planning Systems, Inc.
7900 Westpark Drive, Suite 507
The Honeywell Center
McLean, VA 22101
Attn: Dr. L. P. Solomon

TRW Systems Group
7600 Coleshire Drive
McLean, VA 22101
56 Attn: Mr. C. C. Carter
57 Mr. R. T. Brown

58 Tetra Tech, Incorporated
Suite 601
1911 N. Ft. Myer Drive
Arlington, VA 22209
Attn: Mr. C. Dabney

59 Texas Instruments, Inc.
13500 North Central Expressway
Dallas, TX 75222
Attn: Mr. A. Kirst

60 Tracor, Inc. (Rockville Laboratory)
1601 Research Boulevard
Rockville, MD 20850
Attn: Mr. J. Gottwald
Ocean Technology Division

Distribution List for ARL-TR-74-53, N00014-70-A-0166, Task 0023

Copy No.

61 Underwater Systems, Inc.
World Building
8121 Georgia Avenue
Silver Spring, MD 20910
Attn: Dr. M. Weinstein

62 Woods Hole Oceanographic Institution
86-96 Water Street
Woods Hole, MA 02543
Attn: Dr. E. E. Hays

63 Marine Sciences Division, ARL/UT

64 Computer Science Division, ARL/UT

65 Library, ARL/UT

UNCLASSIFIED

SECURITY CLASSIFICATION OF THIS PAGE (When Data Entered)

REPORT DOCUMENTATION PAGE		READ INSTRUCTIONS BEFORE COMPLETING FORM
1. REPORT NUMBER ARL-TR-74-53	2. GOVT ACCESSION NO.	3. RECIPIENT'S CATALOG NUMBER
4. TITLE (and Subtitle) CHURCH ANCHOR EXPLOSIVE SOURCE (SUS) PROPAGATION MEASUREMENTS (U)		5. TYPE OF REPORT & PERIOD COVERED technical report 6. PERFORMING ORG. REPORT NUMBER
7. AUTHOR(s) Aubrey L. Anderson, ed.		8. CONTRACT OR GRANT NUMBER(s) N00014-70-A-0166
9. PERFORMING ORGANIZATION NAME AND ADDRESS Applied Research Laboratories The University of Texas at Austin Austin, Texas 78712		10. PROGRAM ELEMENT, PROJECT, TASK AREA & WORK UNIT NUMBERS Task 0023
11. CONTROLLING OFFICE NAME AND ADDRESS Office of Naval Research Department of the Navy Arlington, VA 22217		12. REPORT DATE December 1974 13. NUMBER OF PAGES 262
14. MONITORING AGENCY NAME & ADDRESS(if different from Controlling Office)		15. SECURITY CLASS. (of this report) CONFIDENTIAL 15a. DECLASSIFICATION/DOWNGRADING SCHEDULE ~~EXEMPT~~ GDS-1980

16. DISTRIBUTION STATEMENT (of this Report)

none

17. DISTRIBUTION STATEMENT (of the abstract entered in Block 20, if different from Report)

18. SUPPLEMENTARY NOTES

19. KEY WORDS (Continue on reverse side if necessary and identify by block number)

propagation
underwater sound propagation
low frequency propagation measurements

20. ABSTRACT (Continue on reverse side if necessary and identify by block number)

The received energy of sound waves generated by underwater explosive sources (SUS) was recorded during August and September 1973 as part of the CHURCH ANCHOR Exercise conducted in the central Northeastern Pacific Ocean. The analog and digital magnetic tape recordings of these data have been analyzed by digital hardware/software processing techniques including automatic shot detection, shot length estimation, and fast Fourier transform (FFT) spectrum analysis. Results of these analyses are plotted as

DD FORM 1 JAN 73 1473 EDITION OF 1 NOV 65 IS OBSOLETE

UNCLASSIFIED

SECURITY CLASSIFICATION OF THIS PAGE (When Data Entered)

propagation loss versus range, for ranges up to 1200 nm; for frequencies of 25, 50, and 158 Hz, with limited data for 100 and 250 Hz; for source depths of 18 m and 91 m; and for receiver depths near the sound channel axis, near the critical depth, and near the ocean bottom. Sound propagation characteristics were examined as a function of source-to-receiver range, source depth, receiver depth, frequency, and bathymetry. (U)

DEPARTMENT OF THE NAVY
OFFICE OF NAVAL RESEARCH
875 NORTH RANDOLPH STREET
SUITE 1425
ARLINGTON VA 22203-1995

IN REPLY REFER TO:

5510/1
Ser 321OA/011/06
31 Jan 06

MEMORANDUM FOR DISTRIBUTION LIST

Subj: DECLASSIFICATION OF LONG RANGE ACOUSTIC PROPAGATION PROJECT (LRAPP) DOCUMENTS

Ref: (a) SECNAVINST 5510.36

Encl: (1) List of DECLASSIFIED LRAPP Documents

1. In accordance with reference (a), a declassification review has been conducted on a number of classified LRAPP documents.

2. The LRAPP documents listed in enclosure (1) have been downgraded to UNCLASSIFIED and have been approved for public release. These documents should be remarked as follows:

   Classification changed to UNCLASSIFIED by authority of the Chief of Naval Operations (N772) letter N772A/6U875630, 20 January 2006.

   DISTRIBUTION STATEMENT A: Approved for Public Release; Distribution is unlimited.

3. Questions may be directed to the undersigned on (703) 696-4619, DSN 426-4619.

BRIAN LINK
By direction

Subj: DECLASSIFICATION OF LONG RANGE ACOUSTIC PROPAGATION PROJECT (LRAPP) DOCUMENTS

DISTRIBUTION LIST:

NAVOCEANO (Code N121LC – Jaime Ratliff)
NRL Washington (Code 5596.3 – Mary Templeman)
PEO LMW Det San Diego (PMS 181)
DTIC-OCQ (Larry Downing)
ARL, U of Texas
Blue Sea Corporation (Dr.Roy Gaul)
ONR 32B (CAPT Paul Stewart)
ONR 321OA (Dr. Ellen Livingston)
APL, U of Washington
APL, Johns Hopkins University
ARL, Penn State University
MPL of Scripps Institution of Oceanography
WHOI
NAVSEA
NAVAIR
NUWC
SAIC

Declassified LRAPP Documents

Report Number	Personal Author	Title	Publication Source (Originator)	Pub. Date	Current Availability	Class.
Unavailable	Beam, J. P., et al.	LONG-RANGE ACOUSTIC PROPAGATION LOSS MEASUREMENTS OF PROJECT TRANSLANT I IN THE ATLANTIC OCEAN EAST OF BERMUDA	Naval Underwater Systems Center	740612	ADC001521	U
Unavailable	Cornyn, J. J., et al.	AMBIENT-NOISE PREDICTION. VOLUME 2. MODEL EVALUATION WITH IOMEDEX DATA	Naval Research Laboratory	740701	AD0530983	U
Unavailable	Unavailable	COHERENCE OF HARMONICALLY RELATED CW SIGNALS	Naval Underwater Systems Center	740722	ADB181912	U
Unavailable	Banchero, L. A., et al.	IOMEDEX SOUND VELOCITY ANALYSIS AND ENVIRONMENTAL DATA SUMMARY	Naval Oceanographic Office	740801	ADC000419	U
3810	Unavailable	CONSTRUCTION AND CALIBRATION OF USRD TYPE F58 VIBROSEIS MONITORING HYDROPHONES SERIALS 1 THROUGH 7	Naval Research Laboratory	741002	ND	U
ARL-TM-73-11; ARL-TM-73-12	Ellis, G. E., et al.	ARL PRELIMINARY DATA ANALYSIS FROM ACODAC SYSTEM; ANALYSIS OF THE BLAKE TEST ACODAC DATA	University of Texas, Applied Research Laboratories	741015	ADA001738; ND	U
Unavailable	Mitchell, S. K., et al.	QUALITY CONTROL ANALYSIS OF SUS PROCESSING FROM ACODAC DATA	University of Texas, Applied Research Laboratories	741015	ADB000283	U
Unavailable	Unavailable	MEDEX PROCESSING SYSTEM. VOLUME II. SOFTWARE	Bunker-Ramo Corp. Electronic Systems Division	741021	ADB000363	U
Unavailable	Spofford, C. W.	FACT MODEL. VOLUME I	Maury Center for Ocean Science	741101	ADA078581	U
Unavailable	Bucca, P. J., et al.	SOUND VELOCITY STRUCTURE OF THE LABRADOR SEA, IRMINGER SEA, AND BAFFIN BAY DURING THE NORLANT-72 EXERCISE	Naval Oceanographic Office	741101	ADC000461	U
Unavailable	Anderson, V. C.	VERTICAL DIRECTIONALITY OF NOISE AND SIGNAL TRANSMISSIONS DURING OPERATION CHURCH ANCHOR	Scripps Institution of Oceanography Marine Physical Laboratory	741115	ADA011110	U
Unavailable	Baker, C. L., et al.	FACT MODEL. VOLUME II	Office of Naval Research	741201	ADA078539	U
ARL-TR-74-53	Anderson, A. L.	CHURCH ANCHOR EXPLOSIVE SOURCE (SUS) PROPAGATION MEASUREMENTS (U)	University of Texas, Applied Research Laboratories	741201	ADC002497; ND	U
MCR106	Cherkis, N. Z., et al.	THE NEAT 2 EXPERIMENT VOL 1 (U)	Maury Center for Ocean Science	741201	NS; ND	U
MCR107	Cherkis, N. Z., et al.	THE NEAT 2 EXPERIMENT VOL 2 - APPENDICES (U)	Maury Center for Ocean Science	741201	NS; ND	U
Unavailable	Mahler, J., et al.	INTERIM SHIPPING DISTRIBUTION	Tetra, Tech, BB&N, & PSI	741217	ND	U
75-9M7-VERAY-R1	Jones, C. H.	LRAPP VERTICAL ARRAY- PHASE IV	Westinghouse Electric Corp.	750113	ADA008427; ND	U
AESD-TN-75-01	Spofford, C. W.	ACOUSTIC AREA ASSESSMENT	Office of Naval Research	750201	ADA090109; ND	U